Synthesis and Characterization of Diazocines and their Incorporation in Polymers

DISSERTATION

Toward the Academic Degree
Doctor Rerum Naturalium (Dr. rer. nat.)

Submitted to the
Department of Biology and Chemistry
of the University of Bremen

by

Shuo Li

from Bremen
March, 2023

This work was carried out under the supervision of

Prof. Dr. Anne Staubitz

from January 2017 to March 2023 at the Institute of Organic Chemistry, Department of Chemistry of the Kiel University and at the Institute of Organic and Analytical Chemistry, Department of Biology and Chemistry of the University of Bremen.

Reviewers:

1. Prof. Dr. Peter Spiteller (University of Bremen)
2. Prof. Dr. Jens Beckmann (University of Bremen)

Date of the doctoral colloquium: 27.04.2023

List of Publications

1. Shuo Li, Nadi Eleya, and Anne Staubitz, Cross-Coupling Strategy for the Synthesis of Diazocines, *Org. Lett.* **2020**, *22*, 1624–1627.

2. Shuo Li, Ruchira Colaco, and Anne Staubitz, ARGET ATRP of Methyl Acrylate and Methyl Methacrylate with Diazocine-Derived Initiators, *ACS Appl. Polym. Mater.* **2022**, *4*, 6825–6833.

3. Shuo Li, Katrin Bamberg, Yuzhou Lu, Frank D. Sönnichsen and Anne Staubitz, Facile Synthesis of Light-Switchable Polymers with Diazocine Units in the Main Chain, *Polymers* **2023**, *15*, 1306.

Eigenständigkeitserklärung

Versicherung an Eides Statt

Ich, Shuo Li,

versichere an Eides Statt durch meine Unterschrift, dass ich die vorstehende Arbeit selbstständig und ohne fremde Hilfe angefertigt und alle Stellen, die ich wörtlich dem Sinne nach aus Veröffentlichungen entnommen habe, als solche kenntlich gemacht habe, mich auch keiner anderen als der angegebenen Literatur oder sonstiger Hilfsmittel bedient habe.

Ich versichere an Eides Statt, dass ich die vorgenannten Angaben nach bestem Wissen und Gewissen gemacht habe und dass die Angaben der Wahrheit entsprechen und ich nicht verschwiegen habe.

Die Strafbarkeit einer falschen eidesstattlichen Versicherung ist mir bekannt, namentlich die Strafandrohung gemäß § 156 StGB bis zu drei Jahren Freiheitsstrafe oder Geldstrafe bei vorsätzlicher Begehung der Tat bzw. gemäß § 161 Abs. 1 StGB bis zu einem Jahr Freiheitsstrafe oder Geldstrafe bei fahrlässiger Begehung.

Ort, Datum: _____

Unterschrift: _____

Dedicated to my family

"Sincerity at its most extreme, but details in crystal."

Jerzy Grotowski

Acknowledgments

First and foremost, I offer my sincerest gratitude to my supervisor Prof. Dr. Anne Staubitz who welcomed me to her group, entrusted me with a curious PhD topic and supported my work in discussions and group meetings. I deeply value the experience and knowledge I have gained during this time and will remember the advice she has given me as a student.

I greatly appreciate Prof. Dr. Peter Spiteller and Prof. Dr. Jens Beckmann for the review of this work.

My sincere thanks also go to Dr. Nadi Eleya, Ruchira Colaco, Katrin Bamberg, Yuzhou Lu and Prof. Dr. Frank D. Sönnichsen for their essential scientific input to complete our common research projects. I am glad to have accomplished results in a team with talented and experienced fellow scientists. I specifically appreciate the insight and diligence they bring to every issue and I wish I could learn much more from them.

Dr. Sindu Shree, Dr. Leonard Siebert and Prof. Dr. Adelung from the Technical Faculty in Kiel University deserve special thanks as inspiring collaboration partners who provided me insight into the world of material science. I would like to express my gratitude to Jasmin Richter, the very honorable technician of our group and essential to the everyday working conditions in the lab. Special thanks also go to the spectroscopic departments in Kiel and Bremen for their respectable and important work.

I feel indebted to Dr. Mathias Dowds as an overall helpful person and a valuable discussion partner in the years in Kiel. Together with Jan-Ole Springer, Dr. Jonas Hoffmann, Melanie Walther and Sven Schultzke, the Kiel group ensured a vibrant atmosphere without any dull moments. I will always particularly remember the weekly breakfast and lunchtime meals with Dr. Nils Preußke and Dr. Matthias Lipfert that were accompanied by a lot of hilarious small talk.

Furthermore, I would like to acknowledge all the group members in Bremen for a great time: Dr. Clement Appiah, Yannik Appiarius, Christoph Eschen, Philipp Gliese, Dr. Anne Heitmann, Waldemar Kipke, Dr. Souvik Ghosh, Dr. Isabel Ramirez y Medina, Laura Schumacher, Dr. Sara Urrego-Riveros and Jan Thayssen. The time we spent together was too short and I will miss the lively exchanges in and outside of science. I am grateful for the time and effort Dr. Arne Wittstock has devoted to each one of us as well as Petra Grundmann who has been a wonderful support to our activities.

Lastly, I would like to express gratitude and love for my friends and family, especially my sister Xinyi Li and my father Prof. Dr. Pu Li as enduring support in my life that I can always rely on. I cherish my girlfriend Dr. Lan Cheng above all else and I am deeply moved by her continuous kindness and support.

Kurzzusammenfassung

Eine nützliche Strategie, um Kontrolle über die Funktion von makromolekularen Systemen zu gewinnen, besteht aus dem gezielten Einsatz von konstruierten molekularen Schaltern, die nach externer Anregung reversible chemische Reaktionen eingehen. Die vorliegende Dissertation untersucht die Synthese und Charakterisierung von Ethylen-verbrückten Azobenzolen, den sogenannten Diazocinen, vor allem in ihrer Rolle als molekulare Photoschalter in Polymeren. Obwohl Diazocin seit über einem Jahrhundert bekannt ist, wurden außer der etablierten N–N Redoxkupplung keine alternativen Synthesewege berücksichtigt und seine Anwendung auf Makromoleküle nicht erforscht. Im Folgenden wurde eine Strategie verfolgt, bei der ausgehend von 2-Brombenzylbromiden zuerst 2,2'-Dihalogenbibenzyle erzeugt wurden, entweder auf direktem Wege in einer reduktiven Kupplung oder indirekt über das korrespondierende Stilben. Die Konstruktion des Diazocinheterozyklus wurde durch eine stufenförmige C–N Amidierungsreaktion mit einem Hydrazin-basierten Nukleophil ermöglicht, um danach über einfache Entschützungs- und Oxidationsreaktionen zu den gewünschten Produkten zu gelangen. Die hergestellten Diazocinderivate, die sich ursprünglich in der thermodynamisch begüngstigten (*Z*) Form befanden, wurden mit 385 nm Licht in die metastabile (*E*) Konfiguration photoisomerisiert und mit 565 nm Licht wieder zurückgeschaltet. Übereinstimmend mit dem unsubstituierten Diazocin konnte eine gute Auflösung der $n\pi^*$ Absorptionsbanden zwischen den jeweiligen Isomeren gefunden werden. Der Großteil der synthetisierten Derivate erreichte einen relativen (*E*) Isomeranteil von 77–87% im photostationären Gleichgewicht bei 385 nm Belichtung. Um Schalteinheiten kovalent in Polymere einzubauen, wurden primäre Alkohol- und Aminfunktionen in Alkylhalogenide umgewandelt, die als Initiatoren für Atom transfer radical polymerization (ATRP) zur Herstellung von Diazocin-dotierten Elastomerketten verwendet wurden. Die photochromen Eigenschaften der synthetisierten Polymere, also das Schalten zwischen den beiden Isomeren (*Z*) und (*E*), blieben sowohl in Lösung als auch im Festkörper erhalten. Für die Integration multipler Einheiten in Polymerketten wurden Diazocindiacrylate einer Michael-artigen Thiol-En-Polyaddition mit 1,6-Hexandithiol unterzogen und zu Poly(thioether)n verknüpft. Zudem wurde die zangenartige (*Z*)→(*E*) Schaltbewegung des Diazocins ausgenutzt, um einen Ausdehnungseffekt zu erreichen, gemessen an der Zunahme des hydrodyamischen Radius der einzelnen Polymerketten in Lösung mittels Größenausschluss-Chromatographie (GPC). Die vorliegende Arbeit ebnet den Weg für den Einsatz von Diazocinen in Materialien und insbesondere als photochrome Schalter, die starke Konformationsänderungen in Polymerketten hervorrufen können.

Abstract

A useful strategy to gain functional control over macromolecular systems involves the targeted use of carefully designed molecular switches that respond to external stimuli by reversible chemical reactions. The present thesis aims for the synthesis and characterization of ethylene-bridged azobenzenes, so-called diazocines, as molecular photoswitches and their incorporation in polymers. Although diazocine has been known for over a century, synthetic routes alternative to the established N–N redox coupling were not considered and applications in macromolecules have not been studied extensively. Herein, a new strategy was pursued towards diazocine compounds using 2-bromobenzyl bromides as starting materials, which were converted to 2,2'-dihalobibenzyls directly in a reductive coupling reaction or indirectly via the corresponding stilbene intermediate. The construction of the diazocine heterocycle was realized by cascade C–N amidations with a hydrazine-based nucleophile before simple deprotection and oxidation reactions delivered the desired products. Originally in the thermodynamically favored (*Z*) form, the diazocine derivatives were photoisomerized with 385 nm light to the metastable (*E*) configuration and switched back to the (*Z*) state with 565 nm light. The diazocine deriatives exhibited a good resolution of the $n\pi^*$ transition bands between the isomers in agreement with unsubstituted diazocine. The majority of synthesized derivatives attained 77–87% of relative (*E*) isomer content in the photostationary state at 385 nm light irradiation. For the covalent incorporation of switching units in polymers, primary alcohol and amine functions were transformed into alkyl halide initiators for the atom transfer radical polymerization to yield defined diazocine-doped elastomeric chains. The photochromic properties of the synthesized polymers were retained, efficiently switching between the (*Z*) and (*E*) forms both in solution and in the solid state. To integrate multiple units in a polymer chain, diazocine diacrylates were subjected to Michael-type thiol-ene polyaddition reactions with 1,6-hexanedithiol to produce poly(thioether)s. The (*Z*)→(*E*) pincer-type switching motion of the diazocine was further exploited to generate a size expansion effect, whereupon the individual polymer coils experienced a photoinduced increase in hydrodynamic radius in solution, as measured by gel permeation chromatography (GPC). This work paves the way for the use of diazocines in materials, especially as photochromic switches that can induce large conformational changes in polymer chains.

Contents

1 Introduction

1.1 Molecular Switches

Molecular switches interconvert between two or more metastable states by external stimuli including thermal and electrical energy, light, mechanical stress and chemicals such as protons or metal ions under thermodynamic or kinetic control.[1] In these bidirectional pathways, excitation of the molecular switch to an energetically higher electronic state is the first step upon which the nuclei experience different electronic forces. The electronic forces impart thermal motion (nonadiabatic) or enforce photon emission (adiabatic) until reaching the ground state of the product molecule. The geometrical rearrangements are accompanied by the formation or dissociation of covalent bonds during the transition and an alteration of the π-conjugation. In photochemistry, where chemical reactions are induced by light absorption, electrons are excited to higher energies with incoming photons at around 100–1000 $kJmol^{-1}$ in energy which relate to 1200–120 nm in wavelength.[2] Light as electromagnetic radiation has several major advantages such as the non-invasive manipulation of materials, the energetic modulation by intensity and wavelength and the excellent resolution by spatial and temporal control.[3]

In synthetic molecular photoswitches,[4] a large number of geometrical changes is induced by unimolecular isomerization reactions. As a result, the photogenerated isomers exhibit photochromism, *i.e.*, a change of the absorption characteristics upon switching with shifts to shorter (hypsochromic) or longer (bathochromic) wavelengths and higher (hyperchromic) or lower (hypochromic) intensities.[5] Photochromic molecules are characterized by their photophysical properties that are highly dependent on the chemical structure and on molecular interactions. In the absorption spectrum, the maximum absorption is reached at wavelength λ_{max}, while the photostationary state (PSS) is defined as the chemical equilibrium under a certain irradiation wavelength with a certain relative distribution of isomers. Thermally reversible (T-type) photoswitches are characterized by the thermal half-life $t_{1/2}$, stating the time after which half the amount of

the metastable state has been converted to the thermodynamic ground state by spontaneous relaxation. A good assessment of the efficiency of photochemical reactions is given by the quantum yield Φ which counts the number of photochemical events that occurred after the absorption of a certain number of photons (see Equation 1.1). The photofatigue resistance of a molecular switch is determined by the stability of the isomer concentrations after repeated cyclic irradiations.

$$\Phi = \frac{number\ of\ reacted\ molecules}{number\ of\ absorbed\ photons} \tag{1.1}$$

A number of synthetic photoswitches undergo $(Z)/(E)$ isomerization including stilbene and azobenzene as the simplest examples of diarylethylenes[6] and diaryldiazenes,[7] respectively (see Scheme 1.1). Starting from their π-conjugated, thermodynamically preferred (E) configuration with C_{2h} symmetry, the central double bond is photoexcited to set the phenyl rings in motion until reaching the metastable C_2-symmetric (Z) state. In the case of stilbene, conversion to the (Z) isomer provides access to dihydrophenanthrene by reversible photoinduced electrocyclization.[8] The photoinduced dimerization reaction of stilbene occurs in the (E) state, leading to the formation of stereoisomeric tetraphenylcyclobutane products.[9] While the stilbene dimerization is an irreversible process, the [4+4] cycloaddition reaction of two anthracene molecules can be reversed.[5] The photochromism of dithienylethene,[10] on the other hand, is solely based on 6π-electrocyclization (ring closing) since the central ethylene bond is locked in the (Z) form. The ring opening of the closed form of dithienylethene proceeds exclusively via light and is therefore classified as a P-type photoswitch. To further control the relative motion between molecular parts adjacent to the isomerizing double bond, asymmetry was introduced to generate restricted unidirectional rotation in overcrowded alkenes.[11] The two stereogenic methyl substituents of the first-generation molecular motor are preferentially in a pseudoaxial orientation due to steric crowding and dictate the rotation direction of the helical molecular switch.[12] The scientific advancement of molecular machines was honored with the Nobel Prize in 2016.[13]

1.2 Azobenzene

In 1834, Mitscherlich reported the first synthesis of azobenzene[14] before Hartley described its $(Z)/(E)$ photochromism in 1937.[15] The strong UV transition band of (E) at 320 nm corresponds to the $S_2(\pi\pi^*)$ transition while the weak band at 450 nm arises from the $S_1(n\pi^*)$ transition (see Figure 1.1).[16] Upon switching to the (Z) isomer, the $n\pi^*$ band absorbs more strongly and two weak $\pi\pi^*$ bands peaking at 250 and 270 nm replace the

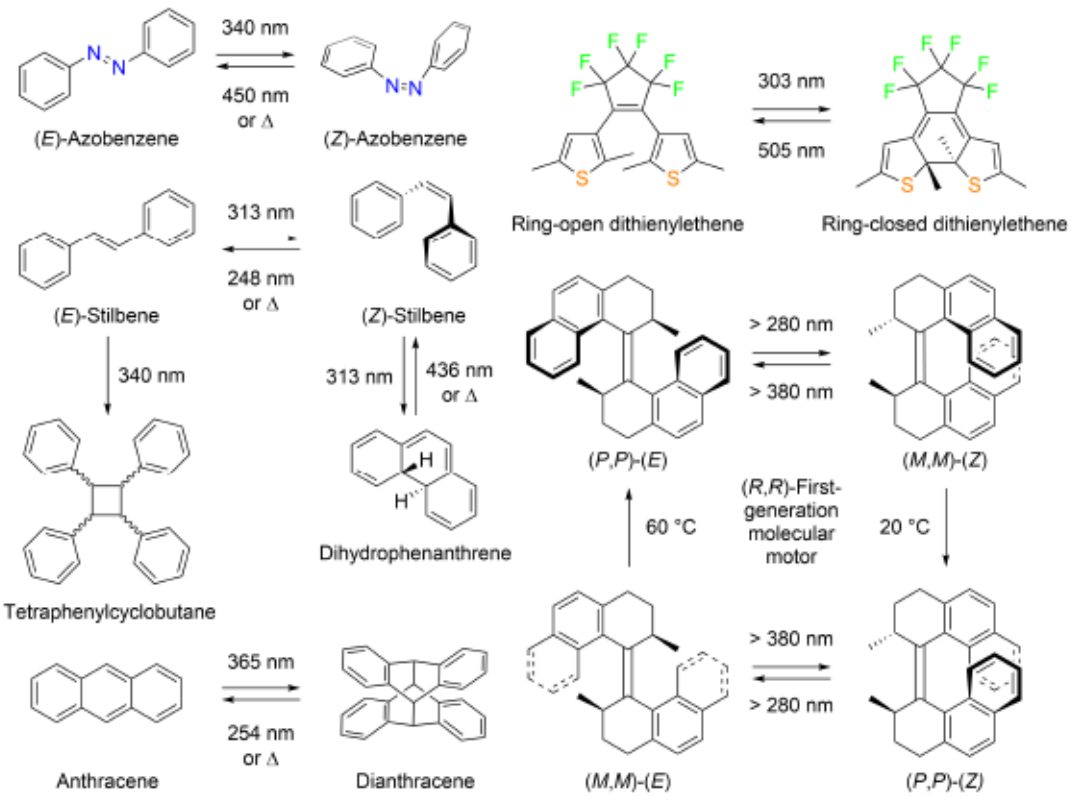

Scheme 1.1. Photoisomerization reactions of exemplary molecular photoswitches and their irradiation wavelengths.[5–7,10,12]

strong UV transition band of the (*E*) isomer.[17] Following (*E*)→(*Z*) photoisomerization, the (*Z*)→(*E*) backisomerization occurs spontaneously by thermal relaxation but can be triggered also by other external stimuli such as light irradiation (photochromism),[15] electrical energy (electrochromism)[18] and mechanical stress (mechanochromism).[19–21] The transition to the (*Z*) isomer leads to the geometrical distortion of the phenyl rings twisted by 53° and a CNNC dihedral angle of 8°.[22] As a result, the (*Z*) azobenzene structure is truncated from 9.0 to 5.5 Å, accompanied by the generation of a dipole moment of 3.2 D[23] and an overall increase in energy by 15.3 kcal mol^{-1}, as compared to the (*E*) isomer.[24] The photoisomerization quantum yields of azobenzene differ greatly between the excitations of the $n\pi^*$ and $\pi\pi^*$ transition bands. Measured at 20 °C in methanol solution, the $n\pi^*$ transition upon 436 nm light irradiation resulted in higher quantum yields ((*E*)→(*Z*) 0.315±0.002, (*Z*)→(*E*) 0.469±0.003) than the $\pi\pi^*$ transition caused by 313 nm light irradiation ((*E*)→(*Z*) 0.155±0.006, (*Z*)→(*E*) 0.388±0.053).[25] However, the azobenzene isomerization pathway is still under discussion, suggesting mechanisms between rotation by torsion around the N–N bond and inversion by an in-plane movement of the phenyl rings towards each other (see Figure 1.1).[26] The research on azobenzene as a functional molecular switch to perform a task is ongoing which covers the areas of photopharmacology,[27] photonics,[28] adhesive materials[29] and molecular machines[30] among others.[31,32]

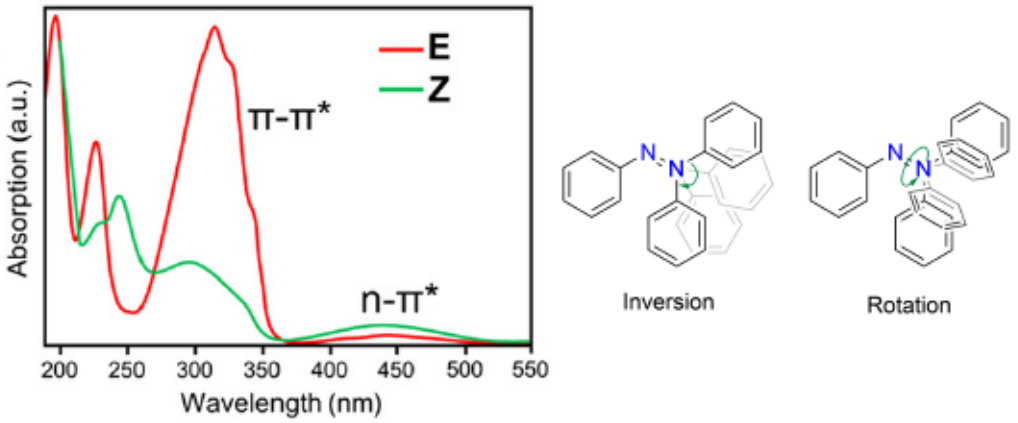

Figure 1.1. UV-Vis absorption spectrum of (*E*) and (*Z*) azobenzene in *n*-hexane (left). Published by John Wiley and Sons.[33] (*Z*)→(*E*) Photoisomerization mechanism of azobenzene including inversion and rotation (right).

Several external factors have a direct influence on the photoisomerization of azobenzene including the solvent,[34] temperature[35] and pressure.[36] Alteration and tuning of the physicochemical properties such as the operational wavelength range are effectively achieved by introducing substituents onto the phenyl rings (see Figure 1.2).[7] For example, the 4-amino-substituted azobenzene exhibits a red shift of the $\pi\pi^*$ transition that overlaps with the $n\pi^*$ transition band.[37] The increased electron density in the π^* orbital produced higher thermal relaxation rates with hydrogen bond formation and tautomerization. In push-pull azobenzenes (pseudostilbene, donor-acceptor), electron-donating and -withdrawing groups are located on the opposite para positions.[38] The large dipole moment and the strong intermolecular charge transfer of the molecule resulted in a red shift of the $\pi\pi^*$ transition band and an extremely fast thermal relaxation. Apart from substituents on the phenyl ring, the altered electronic system in heteroaryl azo dyes offers vast opportunities to add additional functions to photoswitching.[39] The arylazopyrazole in Figure 1.2 was switched quantitatively in both directions (*Z*) and (*E*) while the thermal stability of the (*Z*) isomer depended highly on the presence of substituents on the pyrazole.[40] Furthermore, the BF_2-coordinated azo compound with an extended conjugation of the diazo π-electrons accomplished a far red-shift of the $\pi\pi^*$ transition to the near-infrared region.[41] The synthetic accessibility and the high impact of substituents on azobenzene as a chromophore promote its use in dyes and indicators since over 70% of the world's commercial dyes are azobenzene-based.[42]

Distinct photochromism for the isolated enrichment of a particular isomer requires well-separated $n\pi^*$ transition bands of the (*Z*) and (*E*) isomers that are preferably located in the visual spectrum.[44] Visible-light driven azobenzenes extend the scope of future applications since UV light is only partially penetrable and can be chemically damaging.[2] In order for novel azobenzene molecules to be implemented in biological systems and

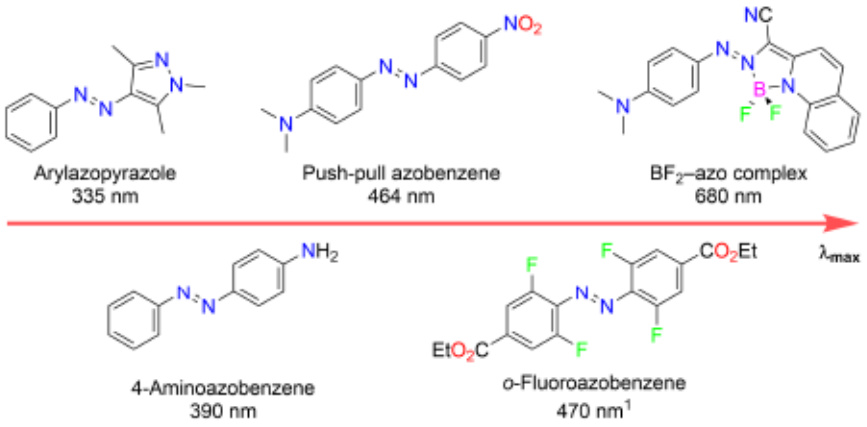

Figure 1.2. Molecular structures of modified azobenzenes in the order of increasing maximum absorption wavelengths $\lambda_{max}(E)$ of the $\pi\pi^*$ transition band. $^1\lambda_{max}(E)$ of the $n\pi^*$ transition band.[37,38,40,41,43]

advanced materials, high photoconversion efficiencies and good control over the molecular motion are very often required. A common feature of *tetraortho*-substituted azobenzenes with chloro,[45] fluoro[43] and methoxy[46] groups is the red-shifted $n\pi^*$ band in the absorption spectra compared to parent azobenzene. As in *o*-fluoroazobenzenes (see Figure 1.2), the fluorine atoms reduce the electron density of the nearby N=N bond, lowering the *n*-orbital energy. The $n\pi^*$ bands of the (*E*) and (*Z*) isomers are well separated to allow for the selective excitation of the two isomers in the visible range of the spectrum. The molecular motion during isomerization is restricted by the steric bulk of the *ortho*-substituents. Increasing steric bulk of tetraalkylated azobenzenes at the *ortho* positions led to a significant destabilization of the (*Z*) isomers but with slightly higher photoisomerization quantum yields for (*Z*)→(*E*) backswitching.[47]

1.3 Diazocine

11,12-Dihydrodibenzo[*c*,*g*][1,2]diazocine, commonly named diazocine after its central heterocycle, can be conceived as the ethylene-bridged cyclic congener of azobenzene. The first synthesis of diazocine was reported by Duval in 1910,[48] but it was not until 1995 that Tauer and Machinek discovered its photochromism with reversed thermal stability of the isomers compared to non-bridged azobenzene (see Scheme 1.2).[49] Theoretical calculations later confirmed the higher stability of the (*Z*) to the (*E*) form by 7.3 kcal mol^{-1}.[50] The mechanical strain on the (*E*) diazocine heterocycle accounts for an energy of about 17 kcal mol^{-1}.[51] In 2009, Siewertsen and co-workers observed superior switching properties such as very high photoconversion yields in both directions ((*Z*)→(*E*) 92±3%, (*E*)→(*Z*) >99%): Light irradiation at 405 nm wavelength triggers the

$n\pi^*$ excitation of the (*Z*) isomer leading to the (*E*) isomer, while quantitative backswitching is accomplished by thermal relaxation or via green light at 525 nm wavelength.[52] Hence, photochromism is achieved solely by visible light with a good resolution of the $n\pi^*$ transition bands between the isomeric states; their maximum wavelengths were found at 404 (*Z*) and 490 nm (*E*) which relate to energy barriers of 70.7 (*Z*) and 58.3 kcal mol^{-1} (*E*). Diazocine maintained a high photostability after repeated cyclic irradiation without showing photobleaching or fatigue but the thermal half-life measured in *n*-hexane is significantly shorter in diazocine (4.5 h at 28.5 °C)[52] than in azobenzene (2 days at 20 °C).[7]

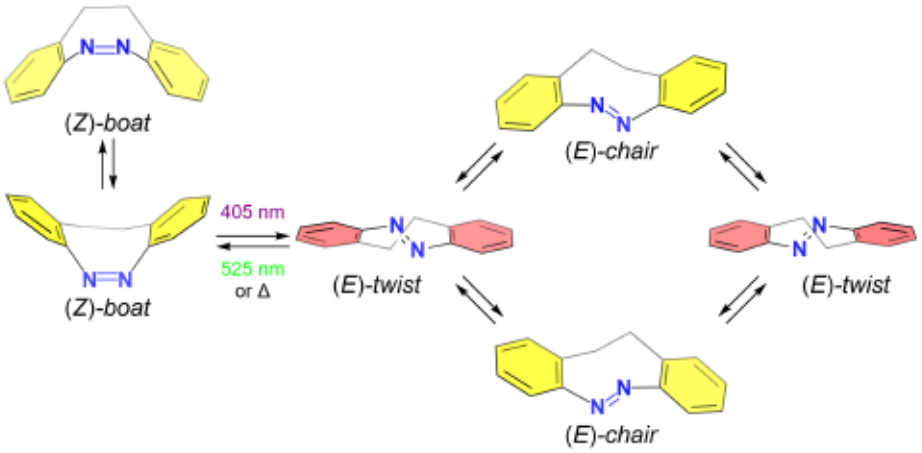

Scheme 1.2. Molecular structures of diazocine as a result of isomerization reactions between (*Z*)-*boat*, (*E*)-*twist* and (*E*)-*chair*.[4]

Crystal structures of (*Z*) and (*E*) configurations revealed that the ethylene bridge in diazocine imposes a geometrical constraint on the switching mechanism.[52,53] The central diazocine ring in (*Z*) form resembles the geometrical (*Z*) form of azobenzene and is therefore hardly affected by ring strain.[54] The (*Z*) isomer undergoes a boat inversion that has a calculated activation barrier of 33.3 kcal mol^{-1} (see Scheme 1.2). However, the (*E*) form displays a non-planar structure with a tilted CNNC torsion angle of 147° and does not attain full π-conjugation. The strong structural contrast between both isomers is particularly well reflected in the ^{15}N NMR spectrum where the (*Z*) to (*E*) transition led to a huge downfield shift of the sole signal from 542 to 601 ppm relative to NH_3.[53] Conformational movements of the (*E*) form consist of the crank-type motion of the central ring between the enantiomeric structures of the predominant *twist* rotamers and the *chair* rotamers which are less stable by 2.4 kcal mol^{-1} in energy. Besides, theoretical calculations revealed an almost isoenergetic $n\pi^*$ transition for the (*E*)-*chair* conformation and the (*Z*)-*boat* isomer. This fact could contribute to lower (*Z*)→(*E*) photoconversion yields in modified diazocines, particularly in cases where the *chair* conformation becomes more energetically stabilized compared to the *twist* conformation.[54]

Overall, the conformational changes of diazocine as a [6,8,6] condensed ring system originate largely from the central heterocycle that functions as a semi-rigid hinge between two rigid benzene rings. In comparison to tetrahydrodibenzo[*a*,*e*][8]annulene as a molecule with similar geometry,[55,56] the photoactivation of the thermodynamically favored boat (*Z*) to the twisted (*E*) diazocine resembles pincer motion, consisting of a straightening of the central eight-membered ring and an increase in overall molecular length.[52] Crystal structures of 3,8-diaminosubstituted diazocine (see **6**, Figure 1.4) showed an increase in molecular length measured by the distance between the amino nitrogen atoms from 8 (*Z*) to 11 Å (*E*).[57] Femtosecond time-resolved spectroscopy revealed higher quantum yields for (*Z*)→(*E*) in *n*-hexane ((*Z*)→(*E*) 0.72±0.04, (*E*)→(*Z*) 0.50±0.10) than from theoretical calculations in the gas phase ((*Z*)→(*E*) 0.44, (*E*)→(*Z*) 0.49),[50] because the cooling effect of the solvent on the vibrationally hot (*E*) isomer prevents the reformation of the (*Z*) isomer.[58] The (*Z*)→(*E*) isomerization also attains a high light conversion efficiency of 7.6% at 400 nm irradiation wavelength.[59]

Determined by ab initio nonadiabatic molecular photodynamic simulations, the $S_0 \rightarrow S_1$ photoexcitation of the (*Z*) isomer sets the CNNC moiety into pedal-like hula-twist motion and induces large changes to the orientation of the phenyl rings (see Figure 1.3).[60] The fast escape from the Franck-Condon region in the S_1 state (about 79 fs)[50] is facilitated by the favorable orientation of the phenyl rings and by the steric blockade of the deactivation pathways.[61] However, the electronic relaxation to the S_0 state (270±60 fs)[58] is slowed down by the rotational rearrangement of the ethylene bridge which is triggered by vibrational excitation.[50,62] Compared to the S_1 lifetime of (*Z*) diazocine as well as that of parent (*E*) azobenzene,[62] the relaxation dynamics of the (*E*) diazocine in the S_1 state is much faster with a lifetime of about 36 fs.[50] During the short S_1 period, the phenyl rings experience an out-of-plane distortion before the ensuing electronic relaxation to S_0 (320±100 fs).[58] Along the S_0 pathway, the vibrational relaxation to the final (*Z*) and (*E*) diazocine products is theoretically an ultrafast process[50] and completed within 5 ps, as observed by femtosecond time-resolved spectroscopy in *n*-hexane.[58]

1.4 Diazocine Synthesis

The molecular structure of diazocine comprises a bibenzyl component with a bridging diazo group or an azobenzene component with a bridging ethylene group. In this section, the common synthetic approaches to bibenzyl and azobezene are outlined before they are combined to accomplish the synthesis of diazocine. In terms of the chemical stability towards redox reagents, the ethylene group of bibenzyl is generally more

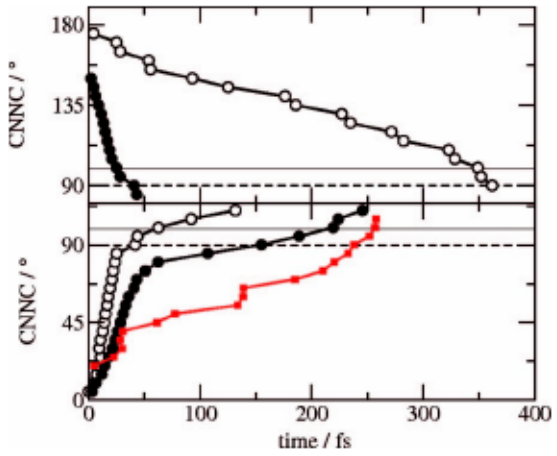

Figure 1.3. Ensemble averaged CNNC dihedral angle in the S_1 state after vertical $S_0 \rightarrow S_1$ photoexcitation at $t = 0$ as a function of time for (*E*) (top) and (*Z*) (bottom) isomers of diazocine (●) and parent azobenzene (○). In addition, respective data for the ethylene bridge CC_bC_bC (■) are shown for (*Z*) diazocine (bottom panel) to illustrate the cause for the slowdown of the CNNC changes. Reprinted,[62] with the permission from AIP Publishing.

stable and hence to be constructed before the prone diazo group. General procedures to synthesize bibenzyls include the oxidative coupling of toluene with bromine and potassium *tert*-butoxide, facilitated and activated by the strong electron-withdrawing nitro groups on the phenyl ring (see Scheme 1.3).[63] Bibenzyls can also be prepared by the Wurtz coupling of benzyl bromide and benzyllithium.[64] Alternatively, they are accessible through stilbene and tolane after the hydrogenation of the central double or triple bond, respectively. Stilbenes are accessible through many different chemical reactions.[65] A common method involves the coupling of a benzylphosphonium halide with benzaldehyde in a Wittig reaction.[66] The Sonogashira cross-coupling reaction between phenyl halide and phenylacetylene produces tolane.[67] In contrast to the straightforward but harsh redox coupling to obtain bibenzyl which usually requires bromine or *n*-butyllithium as reagents, the heterocoupling approach via tolanes or stilbenes is milder and ensures the generation of asymmetric bibenzyls, *i.e.*, with different functional groups on each phenyl ring.

The diazo group in azobenzene is established by carefully designed redox reactions between nitrogen atoms on two benzene rings (see Scheme 1.4).[68] With nitrogen atoms in the (-I) oxidation state, azobenzene is flanked by hydrazobenzene (-II) and azoxybenzene (+I/-I). Widely available anilines (-III) and nitrobenzenes (+III) are often used as starting materials to initiate the redox process that encounters nitrosobenzene (+I) and hydroxylaminobenzene (-I) as intermediates. Azobenzene formation is the result of a Baeyer-Mills condensation between nitroso and amino compounds,[69,70] or, after the condensation between nitroso and hydroxylamino groups, the reduction of the originated azoxybenzene.[71] Alternatively, the N–N coupling between anilines could be

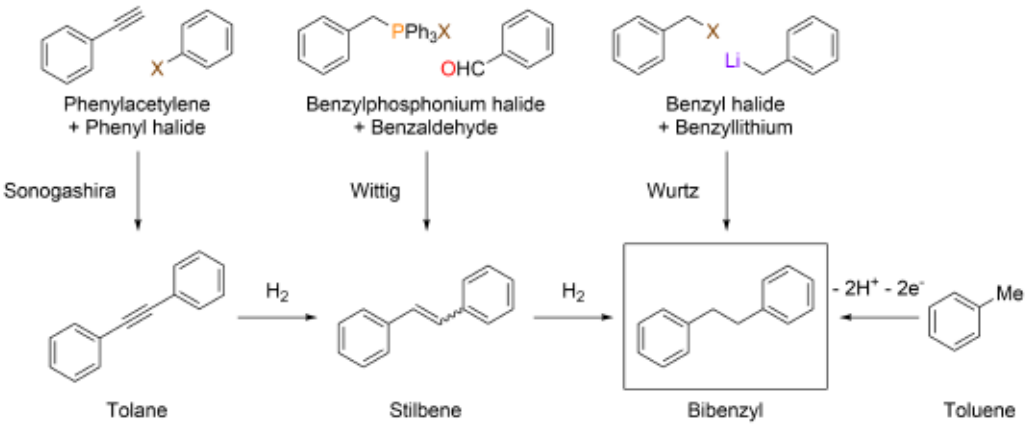

Scheme 1.3. Most common synthetic routes towards bibenzyl. X = Halogen.

directly achieved through a single electron transfer mechanism.[72] The diazo dioxide (+I) is unstable and tautomerizes with nitrosobenzene.[73] Low yields of azobenzene are often the result of the overreduction of nitrobenzene or the overoxidation of aniline that prevent effective condensation reactions. Therefore, maximizing the yield of azobenzene requires good kinetic control attained by the optimization of the reaction conditions and the appropriate choice of the redox agent.

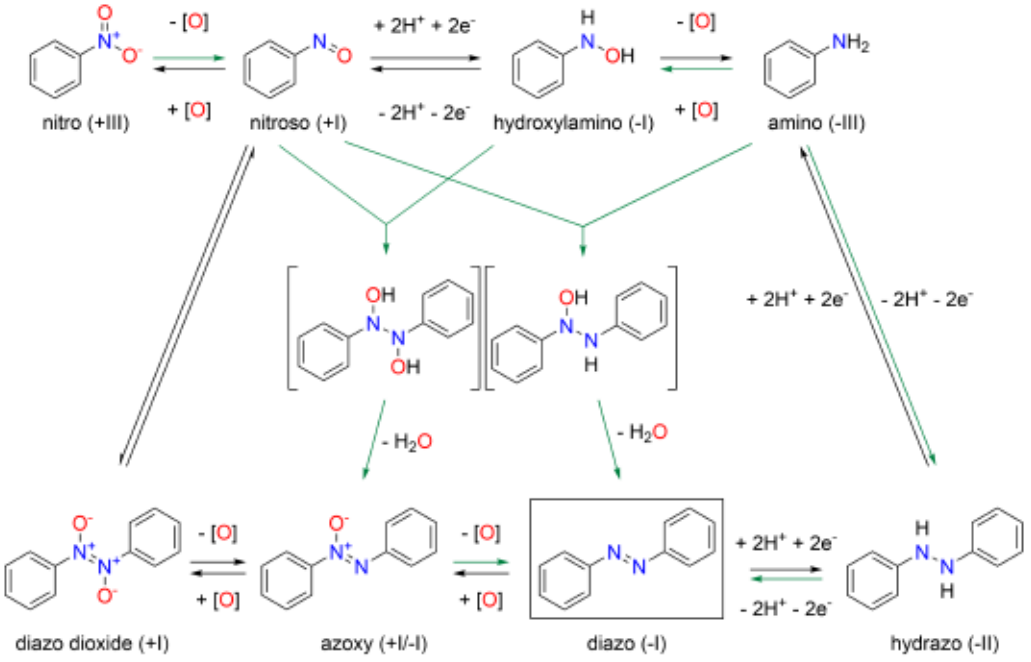

Scheme 1.4. Synthetic routes towards azobenzene based on redox pathways.

The general strategy of diazocine synthesis commences with the construction of 2,2′-disubstituted bibenzyl from 1,2-disubstituted benzenes as starting materials. In contrast to the bimolecular reaction towards azobenzene, the diazo group formation in diazocine is accomplished intramolecularly by the covalent connection of the 2,2′-positions,[74,75]

facilitated by the rotation about the C–C single bond of the ethylene group. Therefore, the diazocine ring formation is a highly conformation-dependent reaction that also competes with intermolecular reactions between bibenzyls. To selectively favor the diazocine product, a one-pot photoreduction method was developed to encapsulate 2,2′-dinitrobibenzyl in a metal-organic cage that acts as a microenvironment catalyst.[76] In combination with triisopropylamine as the electron donor, the yield of diazocine increased drastically to 85%, compared to 4% attained in 2009 (see Scheme 1.5).[52] To obtain diazocine products via the oxidative pathway, 2,2′-diaminobibenzyl was converted by the slow addition of *meta*-chloroperoxybenzoic acid as the oxidant in acidic media, thereby gaining better kinetic control over the intramolecular Mills reaction (85% yield).[75]

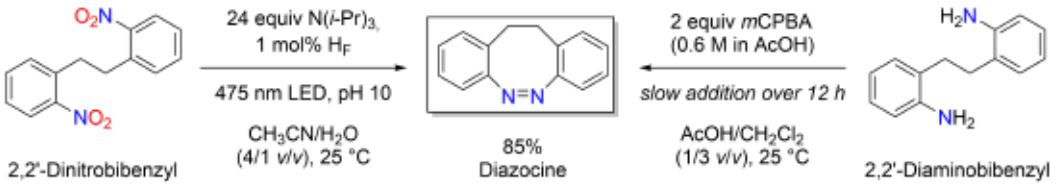

Scheme 1.5. N–N coupling of 2,2′-dinitro- and 2,2′-diaminobibenzyl under optimized reaction conditions.[75,76] H_F: dye-infused Co-based metal-coordination cage.

1.5 Diazocine Modifications

The use of diazocine in applications most often requires additional functional groups on the aromatic rings for the covalent connection to other entities such as macromolecules. Apart from additional substituents that preexist on 1,2-disubstituted benzenes as starting materials, functional groups can be introduced during the stages of diazocine formation or afterward in late-stage transformations. Specifically, the 2,9-positions on diazocine were functionalized by directed electrophilic aromatic substitutions with *N*-bromosuccinimide (NBS) under strongly acidic conditions,[77] while the iodination with *N*-iodosuccinimide (NIS) was achieved para to the amino groups in 2,2′-diaminobibenzyl (see Scheme 1.6).[75] Halogenated diazocines can serve as useful reactants like electrophiles in cross-coupling reactions.[78]

The photoswitching behavior of diazocine is affected by substituents on the benzene ring as well as modifications of the ethylene bridge with heteroatoms (heterodiazocines): Drastic changes in the thermal half-life of the (*E*) isomer were observed in the sulfur- (**1**, 3.5 days at 27 °C) and oxygen-substituted (**2**, 89 s at 20 °C) congeners.[51] The acetamido substituent (**3**) greatly enhances the solubility in water (see Figure 1.4).[79] The highest measured quantum yields (70–90%) and a high light conversion efficiency of 18.1% at 400 nm irradiation wavelength were obtained for the diindane diazocine derivative in

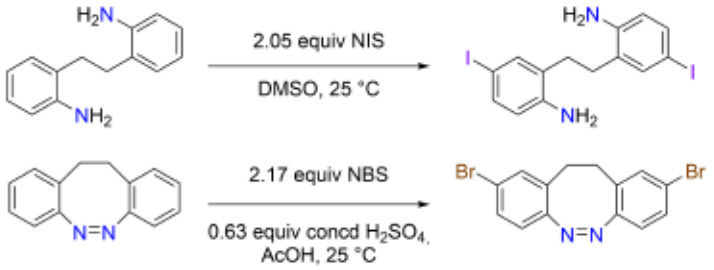

Scheme 1.6. Halogenation reactions of 2,2′-diaminobibenzyl and diazocine.[75,77]

which additional bridges reduced conformational movements and forced a directional switching motion to further prevent unproductive relaxational pathways.[59] The diindane of diazocine exists in two different diastereomers: *meso* (**4**) with a very short (*E*)→(*Z*) half-life (3 s in acetone at 27 °C) and *racemate* (**5**) with a much longer (*E*)→(*Z*) half-life (117 h in acetone at 27 °C) due to the drastic differences in ring strain of the (*E*) isomers.

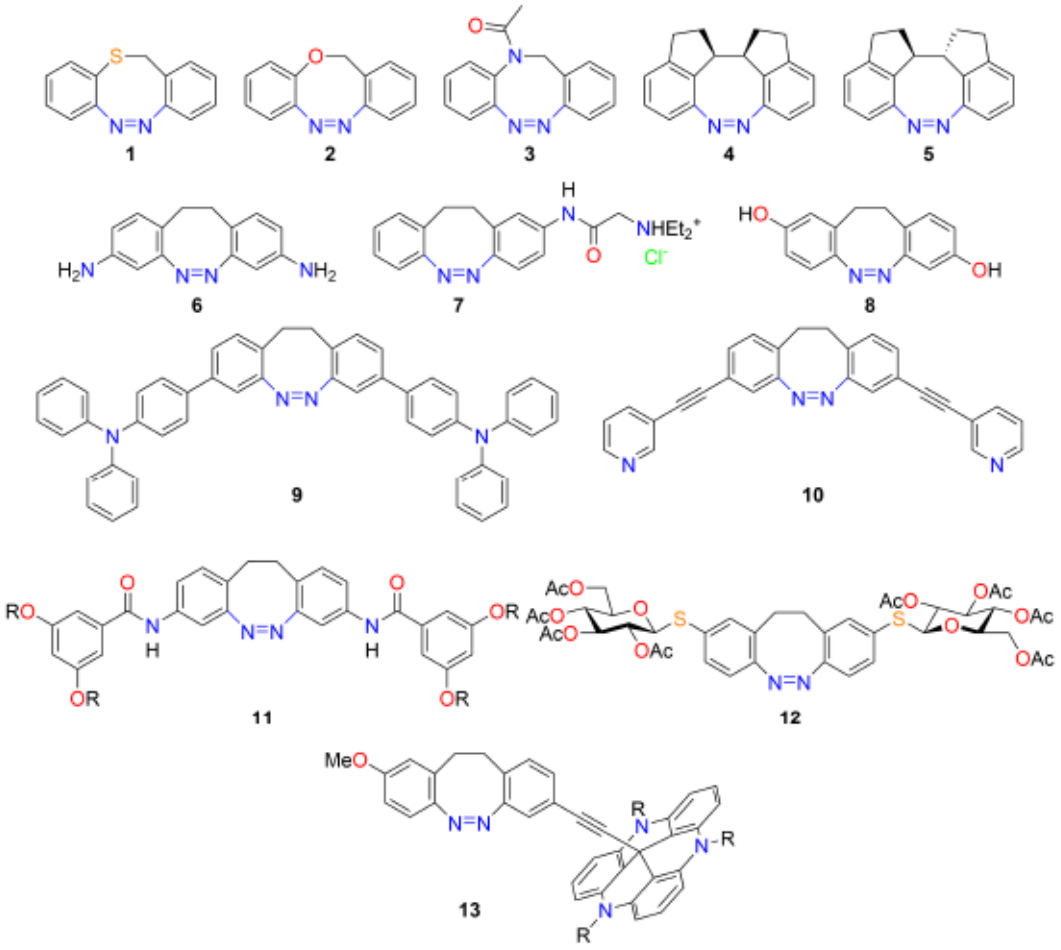

Figure 1.4. Diazocine modifications and substitutions for applications.[51,57,59,79–86] R = *n*-octyl.

Besides improving the photochromic properties and synthetic possibilities, the application potential of diazocine was explored to gain photoresponse and photocontrol in interactive systems. Since backswitching to the thermodynamically stable (*Z*) state is quantitative, the (*E*) isomer can serve as a turned-on photoswitch which can be completely deactivated with green light (525 nm).[82,84] Pharmacological ligands containing (*Z*) diazocine that are inactive in the dark were photoactivated to (*E*) diazocine to gain signaling control in cells,[82] for example to act as a potassium ion channel blocker (**7**) or as an estrogen receptor antagonist (**8**).[83] Diazocines linked to conjugated π-systems showed highly enhanced light emissions when switched to the (*E*) configuration (**9**).[84] Photocontrol of the geometrical structure of a Pd-mediated coordination cage was observed with the employment of diazocine-containing chelating ligands (**10**).[85] Under constant violet light irradiation, the transformed coordination cage was able to encapsulate a small ion. Diazocines are continuously exploited in various applicative fields, *e.g.*, as a building block in organogels (**11**),[86] conjugated to carbohydrates (**12**)[80] and as a linker to triazatriangulene platforms (**13**).[81]

1.6 Stimuli-Responsive Polymers

New challenges in the field of polymer and material science lie in the creation of materials with increasing complexity given by high spatial and temporal self-organization.[87] While the organization of passive, static matter depends only on space, the spatial complexity of a dynamic polymer out of its thermal equilibrium changes through time.[88] Adaptive polymers have the additional ability to respond to external stimuli, leading to a change in physicochemical properties. Therefore, an important part of the development of functional materials is the design, synthesis and analysis of those stimuli-responsive or smart polymers.[89] One way to enhance and gain control over the properties of polymers consists of the incorporation of molecular switches since their chemical reactions are reversible and non-destructive to most materials. The mutual influences between the molecular switching units and the polymer chains are studied to achieve the desired and optimized responses. Complex responses were generated from polymers by the integration of multiple chromophore types in a macromolecular system,[90] preferably with orthogonality, *i.e.*, a clear separation of reactivities between the individual chromophore types.[91] The use of multiple discrete wavelengths instead of monochromatic light, or multiple external stimuli in general,[92] allows the execution of stepwise processes along selectively activated disparate pathways. New morphologies and self-organized nanostructures arise through implementation of multiple monomers during polymerization to generate copolymers.[93,94] Combinatorial effects and additional

properties of stimuli-responsive polymers are obtained through the hybrid interconnection between inorganic[95] or biopolymers[96] with organic polymers and from the non-covalent interactions with other materials in composites.[97]

1.7 Azopolymers

In the case of azobenzene as a molecular switch, the large geometrical rearrangement during isomerization from the rod-like (*E*) to the bent (*Z*) shape is investigated to control the physicochemical properties of polymers.[7,98] An overview of the possibilities from the synthetic methodology to the stimuli-responsiveness of azobenzene-containing polymers, or azopolymers, is given in Table 1.1. This section provides a short introduction to the effects of the polymer structure and the incident light on the physicochemical changes in azopolymers. The following sections then deal with polymerization reactions and applications that are more specific to the present work. The dispersion of azobenzene molecules with isotropic distribution into an amorphous polymer matrix is the most straightforward way to create photoresponsive azopolymers. To achieve a stronger involvement in the dynamic processes of macromolecular systems, functionalized azobenzenes were covalently integrated into polymer systems with various topologies including linear,[99] cyclic,[100] dendritic,[101] ladder,[102] star-branched,[103] hyper-branched[104] and network architectures.[105] Hence, the classification of azopolymers is typically based on the location of the functional molecular switch in the polymer chain. Main-chain azopolymers contain single or multiple azobenzene units in the polymer backbone. The incorporation of single azobenzene units was accomplished via a cross-reaction between reactive sites on the polymer chain with functional azobenzene molecules.[106] To insert multiple switching units into the polymer backbone, mainly step-growth polymerization procedures were carried out, namely polyaddition[107] and polycondensation[108] reactions with azobenzene derivatives as monomers. In side-chain azopolymers, where azobenzene is part of the pendant group of a polymer chain, polymerization predominantly proceeded through chain-growth polymerization methods, for example ionic,[109,110] radical[29] or ring-opening polymerizations.[111]

The effect of azobenzene as a photoswitchable molecular building block in materials depends highly on the order in relation to the other azobenzene units and in relation to the surrounding environment.[112,113] Strong supramolecular interactions and a high chain regularity prevalent in semi- and liquid crystalline polymers provide a high degree of orientational order for the covalently linked azobenzene units.[114] Owing to the structural changes during molecular isomerization, collective (*E*)→(*Z*) switching of azobenzene units embedded into ordered hierarchical assemblies causes a transition

Table 1.1. Characterization of azopolymers based on the composition, polymerization, architecture and stimuli-responsiveness

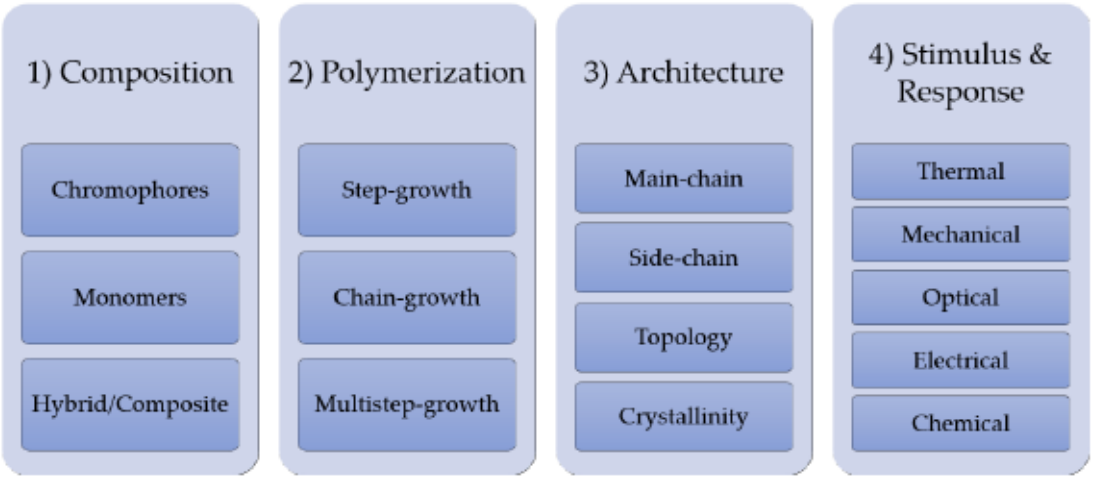

from an ordered to a disordered state.[115] In the case of liquid crystalline polymers, mesogenic azobenzene groups experience a reversible phase transition from the nematic to the isotropic state.[116] For example, azobenzene mesogens were utilized in lightly cross-linked elastomers to cause a photomechanical actuation of the material and high degrees of anisotropic mechanical deformation as a result.[105] The modulation of optical properties such as birefringence and Bragg diffraction allows the phototropic liquid crystalline azopolymers to be used as photonic materials.[28]

The photoisomerization of azopolymers is susceptible to the polarization of the incident light. The alignment of rod-like (*E*) azobenzenes along a common director to achieve uniaxial symmetry was induced externally by repeated cyclic (*E*)/(*Z*) photoisomerization with linearly polarized light,[117] known as the Weigert effect.[118] The molecules were reoriented orthogonal to the polarization direction. Photoirradiation with two polarized light sources that produce interference patterns induced a mass transport, resulting in the inscription of surface relief gratings into azopolymer films.[119,120] Photopatterning is considered a promising method to store optical data in holographic recording media.[121] Furthermore, the use of circularly polarized light enabled the chiroptical switching of aligned azobenzene units to impose a supramolecular chirality onto achiral azopolymer films.[122]

1.8 Azopolymers by ATRP

The preparation of well-defined polymers with novel architectures, compositions and functionalities is an ongoing challenge for chemists.[87] Since its discovery by Sawamoto[123] and Matyjaszewski[124] in 1995, atom transfer radical polymerization (ATRP) has

become the most widely used controlled radical polymerization technique and has been successfully employed for the synthesis of various functional materials.[125] Scheme 1.7 represents the general, Cu-catalyzed ATRP mechanism with ethyl α-bromoisobutyrate (EBiB) as the initiator and (meth)acrylates as monomers. The Cu-binding ligand L has a large impact on the ATRP activity and control and belongs to one of four structural classes: bipyridines, polydentate linear amines, tetradentate tripodal amines and picolylamines.[126] ATRP commences with the generation of primary radicals from the initiator (reaction **1a**) to react with the monomer (reaction **1b**) during initiation.[127] The first step involves the homolytic cleavage of the alkyl halide bond of the initiator by the activator complex $Cu(I)L^+$ via inner-sphere electron transfer to produce the oxidized $Br-Cu(II)L^+$ species and the corresponding alkyl radical.[128] The initiation in ATRP is usually much faster than in free radical polymerizations to ensure that chains start growing at the same time for a better control over the chain architecture. Propagation consists of the repetitive addition of the growing radical chain to the double bond of the monomer (reaction **2a**). In ATRP, the propagation is controlled by the kinetic equilibrium K_{ATRP} (reaction **2b**) under which the growing active radical chains are constantly deactivated by $Br-Cu(II)L^+$ to the dormant species in order to minimize the proportion of terminated chains (see Equation 1.2).

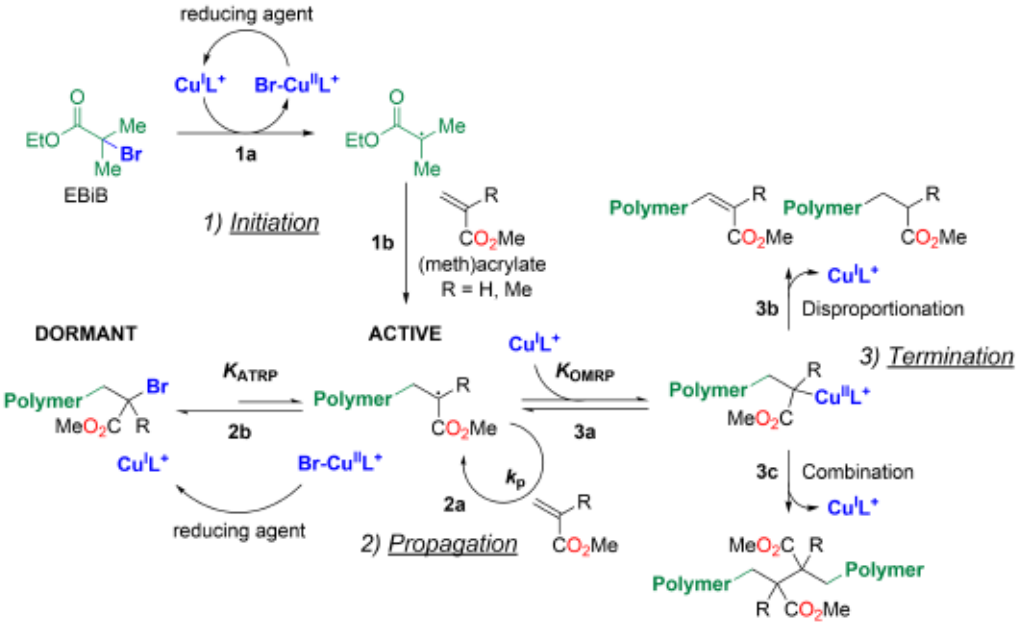

Scheme 1.7. The Cu-catalyzed ARGET ATRP mechanism from initiation to propagation and termination processes under the application of EBiB as the initiator and (meth)acrylate monomers.

$$K_{\mathrm{ATRP}} = \frac{k_{act}}{k_{deact}} \tag{1.2}$$

As a result, the lifetime of the growing chains is much higher than in free radical polymerizations due to a large amount of Br-capped dormant species. The maintenance of a kinetic balance between initiator reactivity and dormant species activation is crucial for a good control over ATRP and is realized by the structural similarity of the components. A much higher activity of the initiator than the polymer chain end would lead to a high instantaneous concentration of radicals and termination whereas a higher chain end reactivity would result in a higher dispersity.[127,129] In all radical polymerizations, termination events of active radical chains are inevitable and occur by the direct disproportionation (reaction 3b) or combination (reaction 3c) of free radicals or via the organocopper intermediate as a result of the organometallic mediated radical polymerization (OMRP) equilibrium (reaction 3a).[130] The radical electron on the polymer chain can be transferred irreversibly to another molecule (ligand, solvent, *etc.*)[131] or relocated to another atom of the same molecule (backbiting) which could lead to branching or cross-linking (see Scheme 1.8).[130] The effect of slow initiation and chain-breaking reactions on the overall molecular weight of the propagating polymer chains is depicted in Figure 1.5.

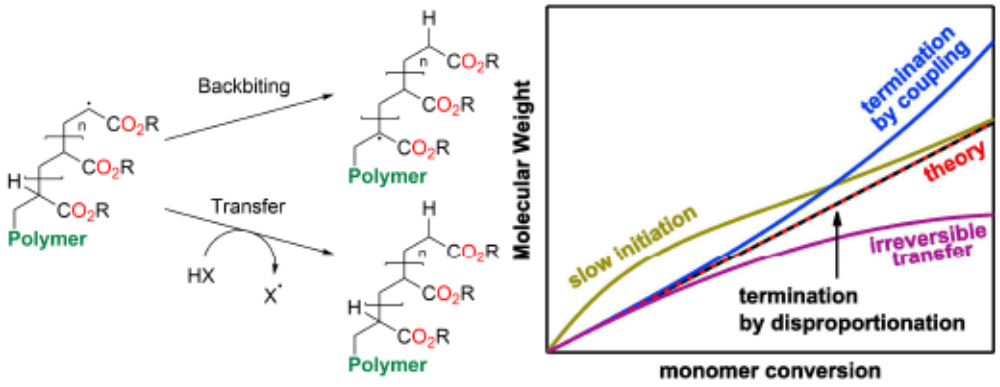

Scheme 1.8 & Figure 1.5. Termination of radical polymer chains by backbiting and transfer (left). Effect of slow initiation and chain-breaking reactions on the molecular weight (right). Reprinted,[129] with permission from Elsevier.

The deactivation of the propagating radicals by Br–Cu(II)L^+, which is determined by the rate constant of deactivation k_{deact} in the ATRP equilibrium, defines the control over chain growth, dispersity $Đ$ and the preservation of the chain-end functionality after the depletion of monomers.[127,129] Overall, the dispersity in ATRP depends on the degree of polymerization DP, the polymerization rate k_p, k_{deact}, the employed concentration of the alkyl halide initiator $[RX]_0$, the concentration of the catalyst $[Br–Cu(II)L^+]$ and the monomer conversion p (see Equation 1.3). In activators generated by electron transfer (AGET),[132] a reducing agent like ascorbic acid[133] is introduced to generate Cu(I)L^+ from Br–Cu(II)L^+. Some reducing agents like Cu(0) also showed the capability of directly activating the dormant species (supplemental activator and reducing agent,

SARA).[134] By keeping very low levels of Br–Cu(II)L^+ deactivator, the Cu(I)L^+ activator is continuously regenerated in a steady state equilibrium (activator regenerated by electron transfer, ARGET).[135] Under ARGET conditions, the polymerization rate becomes virtually independent from the catalyst loading and is largely determined by the reduction of Br–Cu(II)L^+ while also showing better oxygen tolerance.[129] Besides the use of reducing agents, the regeneration of the activator in ATRP can be achieved by thermal radical initiators,[136] light,[137] electrical energy[138] and ultrasound.[139]

$$Đ = 1 + \frac{1}{DP} + \left(\frac{k_p[\mathrm{RBr}]_0}{k_{deact}[\mathrm{Br{-}Cu(II)L^+}]}\right)\left(\frac{2}{p} - 1\right) \tag{1.3}$$

Functional polymers via ATRP are synthesized by the employment of functional monomers, functional initiators or through conversion of the chain-end functionality of the originated polymer.[125] To generate azobenzene-doped polymers, azobenzene was transformed into alkyl halide initiators that mimic the dormant species of the corresponding poly(methyl acrylate) (PMA) and poly(methyl methacrylate) (PMMA) chains.[19,140,141] After the synthesis of azobenzene-centered PMA and (*E*)→(*Z*) photoisomerization (see Scheme 1.9), ultrasonication of the azopolymer in THF solution transduced the generated mechanical force towards the central azobenzene unit in the polymer chain and led to its mechanochromic (*Z*)→(*E*) backswitching.[19]

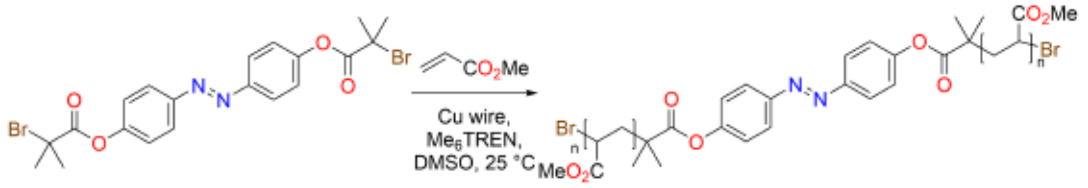

Scheme 1.9. SARA ATRP of methyl acrylate with a difunctional azobenzene-based initiator to diazocine-centered PMA.[19]

1.9 Azopolymer Examples

The most straightforward application of the azobenzene photoisomerization in polymers consists of the transfer of the anisotropic mechanical motion to enforce large conformational changes to the three-dimensional structure of polymer chains.[142,143] Using single-molecule force spectroscopy, individual main-chain azopolymer chains were found to contract against an external force applied by an atomic force microscopy (AFM) tip (up to 500 nN) along the polymer backbone due to optical (*E*)→(*Z*) switching, thus delivering mechanical work (see Figure 1.6).[144] When an external load was applied to the polymer in the original extended (*E*) configuration (I), it followed the force-extension curve up to point (II), where the system was photoswitched with 365 nm

light to its short (Z) configuration (III). The ensuing polymer contraction ΔL is related to the optomechanical work output of the system. The removal of the load resulted in the relaxation of the polymer (IV). From there it was switched back with 420 nm light to (E) to complete the force-extension cycle (I).

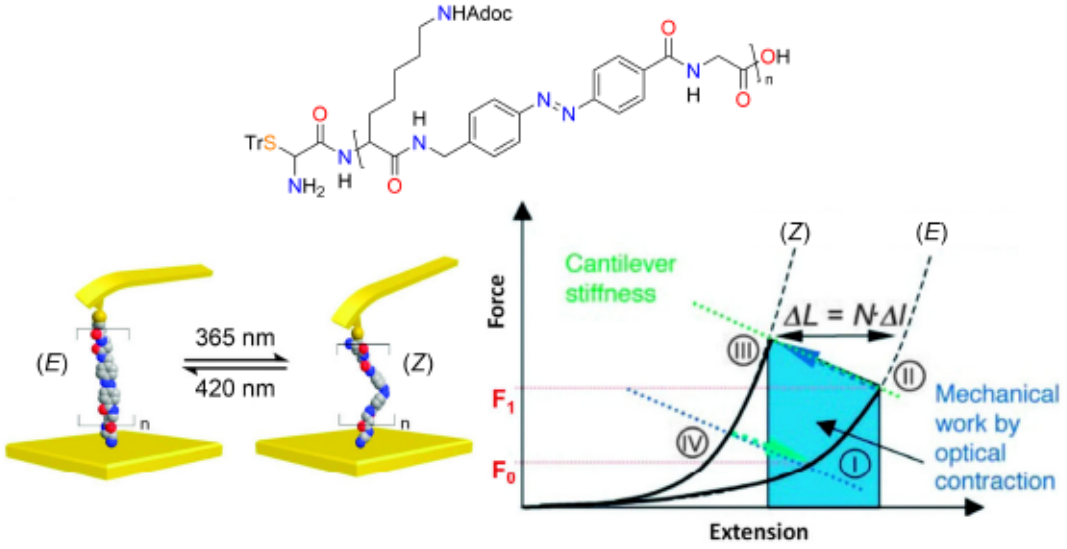

Figure 1.6. Chemical structure of the examined azopolymer by single-molecule force spectroscopy (above). Reversible photoinduced contraction of the azopolymer against the external force applied by the AFM tip (below left). Used with permission of Royal Society of Chemistry;[143] permission conveyed through Copyright Clearance Center, Inc. Force-extension cycle of the azopolymer (below right). Reprinted with permission from AAAS.[144] Tr = trityl. Adoc = adamantyl-oxycarbonyl.

In order to maximize the deformation of individual polymer chains, multiple azobenzene units were incorporated into the backbone of poly(*p*-phenylene) via polycondensation (see Figure 1.7).[145] (E)→(Z) photoisomerization resulted in a reversible shrinkage and compression of the extended rigid rod-like polymer chains. Likewise, individual linear hybrid polymer chains with alternating trisiloxane and azobenzene units exhibited a photoinduced hydrodynamic contraction in solution.[108]

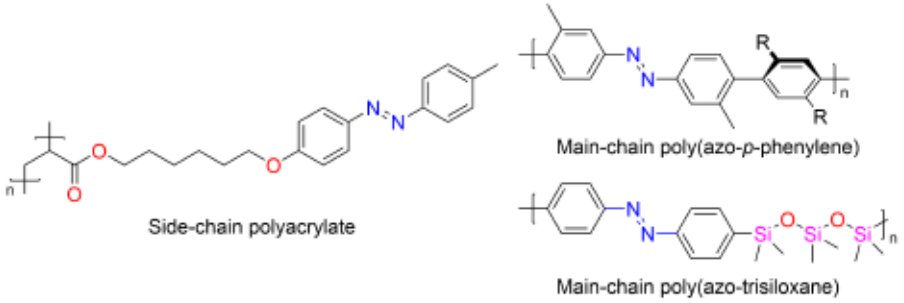

Figure 1.7. Azopolymer examples.[29,108,145] R = *n*-dodecanyl.

In general, research on azobenzene as a trigger in polymers focused on the photocontrol

of solubility, surface wettability, viscosity, electrical conductivity and mechanical properties.[146] Concomitant changes in free volume, chain stiffness and interchain cohesion influence the thermal properties of azopolymers, causing a shift in the glass transition temperature (T_g).[147,148] The T_g is the temperature region in which a polymer transitions from a hard, glassy state into a soft, rubbery state and is marked by a step change in the heat capacity and the coefficients of thermal expansion. At temperatures below T_g, the elastic modulus of polymers is strongly increased since the motion and reorientation of polymer chains are restricted. As a consequence, polymers with high T_g relative to room temperature (20 °C) often serve as hard coatings or as structural elements. On the other hand, polymers with low T_g are processable and healable by molding and extrusion due to a much higher elasticity and polymer chain flexibility. Reversible addition-fragmentation chain-transfer (RAFT) polymerization as a controlled radical polymerization technique was applied to prepare polyacrylate chains with pendant azobenzene groups.[29] The polymer side chains in the (*E*) configuration constituted a crystalline structure with higher relative density[147] that restricted segmental motion and provided less free volume in the matrix.[149] (*E*)→(*Z*) photoisomerization induced a higher flexibility to the polymer side chains and caused a large decrease in T_g from 48 °C to -10 °C, thus traversing room temperature and enabling the reversible photoinduced melting and recrystallization of the polymer. This photomelting effect has potential applications in healable hard coatings, fabrication of smooth surfaces and transfer printing. A similar effect was realized in a main-chain azopolymer in which an azobenzene diacrylate was subjected to the Michael-type thiol-ene polyaddition with 1,6-hexanedithiol to yield poly(azo-thioether).[107] (*E*)→(*Z*) photoisomerization led to the disintegration of its semi-crystalline structure followed by a decrease in T_g from 34 °C to -35 °C (see Figure 1.8).

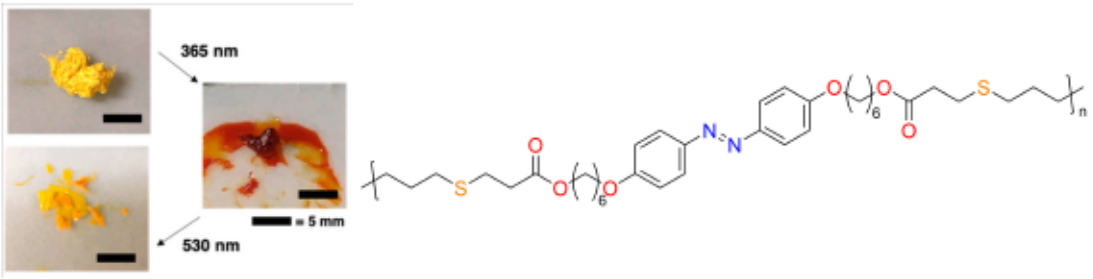

Figure 1.8. Photoinduced melting, recrystallization (left) and molecular structure (right) of the main-chain poly(azo-thioether). Reprinted with permission.[107] Copyright 2020 American Chemical Society.

1.10 Examples of Polymers Containing Diazocines

The photoresponsive properties of diazocine were examined in main-chain,[150] side-chain[151] and cross-linked polymers.[152,153] Initial research focused on its influential control over the functionality of biopolymers.[154] Diazocine substituted with two 2-chloroacetamide groups on the phenyl rings was implemented as a cross-linker into a peptide that contained two sulfhydryl groups from cysteine residues (see Figure 1.9). Intramolecular cross-linking resulted in a circular peptide in which the diazocine moiety functioned as a molecular clamp. The photoinduced unlocking of the clamp owing to its (*Z*)→(*E*) molecular expansion initiated conformational changes in the peptide and an increase in alpha-helical content as a consequence (see Figure 1.10). Therefore, a single diazocine unit can alter the conformation of a polymer chain substantially, in order to gain photocontrol over the three-dimensional structure and the functionality of macromolecules such as peptides. The inclusion of single diazocine units into the side chain of oligonucleotide strands was carried out by the phosphoramidite-based solid phase synthesis.[151] Diazocine accommodation led to a decrease in the stability of oligonucleotide duplexes, as evident by a decrease in the melting temperature. However, this destabilizing effect mitigated upon (*Z*)→(*E*) photoswitching, concluding that the (*E*) isomer was better accommodated than the (*Z*) isomer. The photocontrol over the temperature-dependent formation of oligonucleotide duplexes demonstrated the efficient application of diazocine photoisomerization to modulate supramolecular structures.

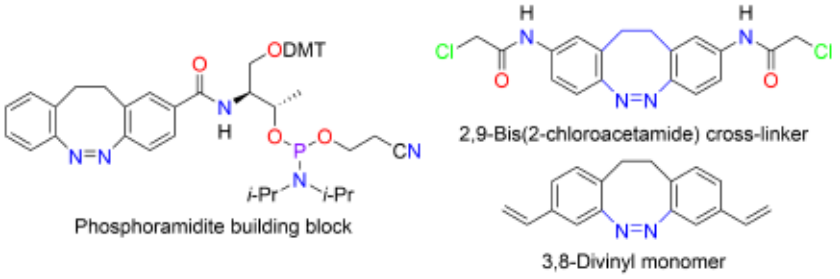

Figure 1.9. Diazocine derivatives as building blocks and linkers for the integration into polymers.[151,153,154] DMT = dimethoxytrityl.

Moreover, diazocine derivatives were transformed into difunctional monomers for the synthesis of linear chains containing multiple diazocine units.[150] For instance, the 3,8-diamine of diazocine was polymerized with hexamethylene diisocyanate and dibutyltin dilaurate as the catalyst in a polyaddition reaction to form polyurea (see Figure 1.10). The resulting linear polymer chains with a molecular weight of 5 kDa comprised multiple diazocine units and exhibited a dispersity of 1.05 as characterized by GPC. No thermal phase transitions could be detected by DSC measurements. After processing

the polymer to a thin film, 405 nm light irradiation resulted in the photoexpansion of the surface layer and the mechanical deformation of the film away from the light source. The photoactuation process was reversible with 532 nm light irradiation. The urea groups in the backbone presumably formed intermolecular hydrogen bonds that constructed a higher-ordered network microstructure. While the non-planarity of (*Z*) diazocine prevented π-π stacking interactions between the switching units, (*Z*)→(*E*) photoisomerization was believed to favor π-π stacking due to the nearly planar geometry of (*E*) diazocine resulting from an amorphous-to-crystalline transition.

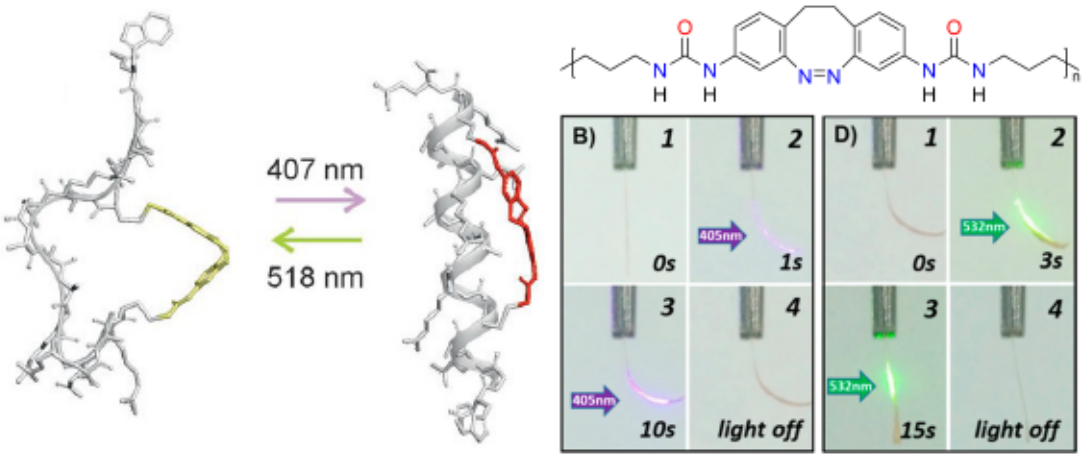

Figure 1.10. Photoinduced conformational change of the diazocine-crosslinked FK-11 peptide (left). Reprinted with permission.[154] Copyright 2012 John Wiley and Sons. Molecular structure and photomechanical bending of the diazocine-containing polyurea film (right). Reprinted with permission.[150] Copyright 2018 American Chemical Society.

To incorporate diazocine as a component in a cross-linked network, 3,8-divinylated diazocine was co-polymerized with 1,3,5-trivinyl-1,3,5-trimethylcyclotrisiloxane and di-*tert*-butyl peroxide as the radical initiator to produce photochromic thin films via initiated Chemical Vapor Deposition.[153] The same method was successfully employed to copolymerize monomers of different polarity, namely 3,8-divinylated diazocine with hydroxyethyl methacrylate.[152] Irradiation with blue light onto the obtained polymer film enabled reversible (*Z*)→(*E*) photopatterning after applying a mask and photolabeling using a laser pointer as the light source.

2 Objectives

Despite the early synthesis of diazocine in 1910 and the discovery of its unique photoswitching properties in 2009, the synthetic method to obtain diazocine remained unchanged and produced low yields. Therefore, it was necessary to overcome limitations of previous synthetic methods and provide better alternative solutions to higher and more predictable yields. **Project I** examines possible alternative pathways toward the synthesis of diazocines which is centered around the connection of 1,2-substituted arenes to bibenzyls, the formation of the eight-membered diazocine ring and the establishment of the diazo group. A new strategy could offer more flexibility in the handling of diazocines and its precursors under various chemical conditions and enable access to previously unknown products. Synthetically, the formation of the eight-membered heterocycle is considered the most challenging step after which the conversion to the desired diazocine product would proceed easily and in good yields. Instead of a condensation reaction between nitrogen atoms at 2,2'-positions of bibenzyl, connection via two consecutive C–N coupling reactions with a dinitrogen building block represents a different retrosynthetic approach to diazocine (see Scheme 2.1). To establish a synthetic pathway, the newly found method needs to be tested with equivalent starting materials containing substituent groups on the benzene rings for the synthesis of diazocine derivatives. Special emphasis is placed on electron-donating and -withdrawing groups to alter the photoswitching π-system as well as aromatic heterocycles as substituents for benzene. Finally, the photochromic properties of the newly synthesized diazocines are analyzed and compared spectroscopically in solution, with a focus on the photostationary states after the enrichment of the (*Z*) and (*E*) isomers.

Unlike azobenzene, the potential of diazocine as a novel molecular photoswitch has only been little explored in polymers. Inspired by the strategies to synthesize and characterize azopolymers, the substituents on the benzene rings of diazocine are designed and transformed into reactive functional groups for the covalent incorporation into polymers. By using diazocine-derived initiators in ATRP as a radical polymerization technique, diazocine-capped and diazocine-centered polymers are easily generated for the study of the photoisomerization behavior of single diazocine units in polymer chains

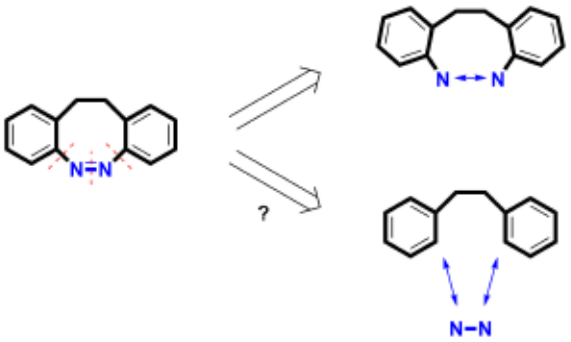

Scheme 2.1. Retrosynthetic considerations for diazocine.

(see Scheme 2.2). Although there has been much progress in the understanding of ATRP, the reactivity of functional alkyl halides during initiation has not been systematically studied. The radicals generated during radical polymerizations could potentially interfere with the functional groups on the initiator or the monomer. Therefore, the reaction conditions for the synthesis of functional polymers often need to be optimized to obtain the desired architecture and dispersity in good yields. Particularly for diazocine units in amorphous polymers with elastomeric properties, the isomerization efficiency of a novel photoswitch in a solid polymer matrix environment is highly dependent on the chemical composition of the polymer which determines the free volume and chain flexibility. In this context, the effect of the polymer matrix on the photochromism and on the (*E*)→(*Z*) thermal relaxation of diazocine is investigated for different substitution patterns on diazocine with PMA and PMMA as exemplary elastomers in **Project II**.

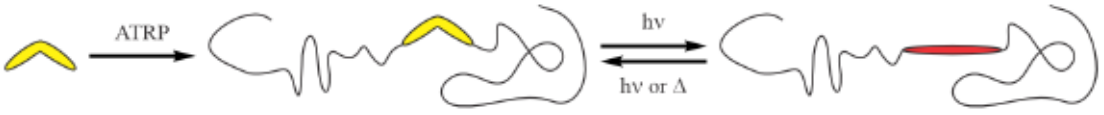

Scheme 2.2. Diazocine as an ATRP initiator to build diazocine-centered elastomeric chains. Yellow shape: (*Z*) diazocine. Red shape: (*E*) diazocine.

The utilization of molecular switches to induce changes in the macromolecular conformation and the physicochemical properties of polymers has been extensively explored for different kinds of azobenzenes. However, the (*Z*)→(*E*) pincer-type switching motion and the reversed stability of isomers compared to parent azobenzene are unique features of diazocine that could be exploited, *i.e.*, transferred to or enhanced on a macromolecular scale for future applications in novel smart materials. In terms of polymerization strategies, diazocines with a single vinyl group could act as monomers to build side-chain azopolymers while diazocines containing two vinyl groups qualify as cross-linkers or as monomers in polyadditions to build main-chain azopolymers. Acrylates are widely used as reactive functional groups not only for radical polymerizations but also as strong electron acceptors that readily react with nucleophiles such as thiols in a Michael-type thiol-ene reaction. In **Project III**, the inclusion and effect of multiple

molecular switching units in a linear polymer chain are investigated to alter the polymer backbone conformation and potentially enable cooperative switching in an organized superstructure. In addition to a higher chromophore load leading to higher absorption intensities, photoswitching of the diazocine units in the backbone would result in a correlated pincer-type motion of diazocines and an overall extension of the individual polymer chains (see Scheme 2.3).

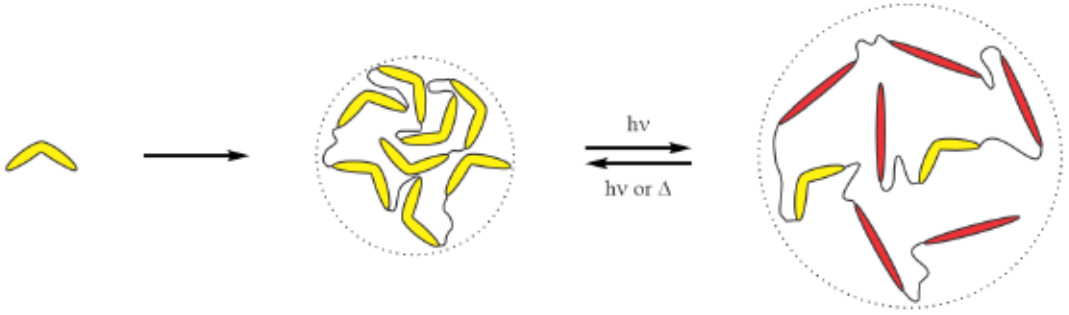

Scheme 2.3. Polymer with multiple diazocine units in the main chain and photoinduced size expansion. Yellow shape: (*Z*) diazocine. Red shape: (*E*) diazocine.

3 Results

3.1 A New Strategy for the Synthesis of Diazocines

Cross-Coupling Strategy for the Synthesis of Diazocines

Shuo Li, Nadi Eleya, and Anne Staubitz, *Org. Lett.* **2020**, *22*, 1624–1627.

DOI: 10.1021/acs.orglett.0c00122

Reprinted with permission from ACS Publications. Copyright 2020. Published by American Chemical Society. The supporting information includes all used materials and methods, experimental procedures, analytical data, images of spectra and is available free of charge online.

Abstract

Ethylene bridged azobenzenes are novel, promising molecular switches that are thermodynamically more stable in the (*Z*) than in the (*E*) configuration, contrary to the linear azobenzene. However, their previous synthetic routes were often not general, and yields were poorly reproducible, and sometimes very low. Here we present a new synthetic strategy that is both versatile and reliable. Starting from widely available 2-bromobenzyl bromides, the designated molecules can be obtained in three simple steps.

Scientific Contribution

After initial drafting and planning by Prof. Dr. Anne Staubitz, this project was planned, organized and conducted by me. The synthesis, purification and characterization of the compounds were carried out by me. The manuscript and the supporting information were written by me. Dr. Nadi Eleya supported me with the synthesis of two diazocine compounds. Prof. Dr. Anne Staubitz as the principal investigator was responsible for the funding and edited the article. All authors have read and edited the article and agreed to the published version of the manuscript.

Table 3.1. Contribution of the candidate in % of the total workload (up to 100% for each of the following categories)

Experimental concept and design	80%
Experimental work and/or acquisition of (experimental) data	90%
Data analysis and interpretation	100%
Preparation of Figures and Tables	100%
Drafting of the manuscript	80%

OL Organic Letters

pubs.acs.org/OrgLett Letter

Cross-Coupling Strategy for the Synthesis of Diazocines

Shuo Li, Nadi Eleya, and Anne Staubitz*

Cite This: Org. Lett. 2020, 22, 1624−1627 Read Online

ACCESS | Metrics & More | Article Recommendations | Supporting Information

ABSTRACT: Ethylene bridged azobenzenes are novel, promising molecular switches that are thermodynamically more stable in the (*Z*) than in the (*E*) configuration, contrary to the linear azobenzene. However, their previous synthetic routes were often not general, and yields were poorly reproducible, and sometimes very low. Here we present a new synthetic strategy that is both versatile and reliable. Starting from widely available 2-bromobenzyl bromides, the designated molecules can be obtained in three simple steps.

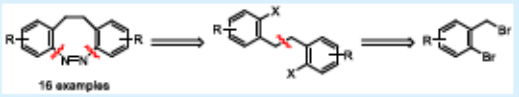

Downloaded via UNIV BREMEN on February 25, 2020 at 08:23:46 (UTC).
See https://pubs.acs.org/sharingguidelines for options on how to legitimately share published articles.

The development of molecular switches that isomerize by irradiation with light have gained much attraction in recent years due to their numerous applications.[1] In 2009, the ethylene-bridged cyclic congener of azobenzene, 11,12-dihydrodibenzo[*c*,*g*][1,2]diazocine (cAB, **1a**), was observed to have superior switching properties compared to linear azobenzene.[2] In particular, the high photoconversion ($Z \rightarrow E$ 92 ± 3%, $E \rightarrow Z$ 100%), the good resolution of absorption bands between isomeric states (*Z* to *E* isomer: 404 to 490 nm), and photoisomerization quantum yields ($Z \rightarrow E$ 72 ± 4%, $E \rightarrow Z$ 50 ± 10%) are much higher in cAB than in the nonbridged azobenzene. Furthermore, in cAB, photochromism is achieved solely by visible light: Blue light irradiation at 385 nm triggers the $n\pi^*$ excitation and transition to the (*E*) isomer, while backswitching is accomplished by thermal relaxation or via green light at a wavelength of 520 nm. In contrast to linear azobenzene, the (*Z*) isomer of cAB is thermodynamically favored over the (*E*) isomer by 37.08 kJ/mol.[3] The switching behavior of cAB has been examined in detail by quantummechanical simulations[4,5] and spectroscopic methods.[6,7] However, compared to linear azobenzenes,[8] diazocines have been used to a much lesser extent (examples are a photocontrolled switch in a peptide,[9] in polyurea,[10] on molecular platforms,[11] and in oligonucleotides).[12] The reason for this low level of exploitation of these favorable properties is that although syntheses exist, they tend to be low yielding and substrate specific.

Synthetically, cAB can be understood as two rigid benzene rings linked by a diazo and an ethylene group. These entities are formed successively from 1,2-disubstituted arenes as starting materials. Previous reports describe C−C coupling of *o*-nitrotoluene (**2**) to establish the ethylene bridge (**3**) first (Scheme 1).[13,14] Then, the nitro groups were joined in an intramolecular reduction step using lead as a reductant to generate the diazo group in cAB in 51% yield.[13,15] Very recent approaches to the diazocine ring formation involve an intramolecular oxidation of amino groups by Oxone[16] (40% yield) or by *m*-chloroperoxybenzoic acid (85% yield).[17]

Scheme 1. Comparison of Strategies for the Synthesis of cAB

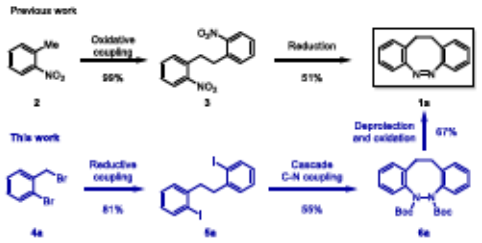

Commonly, arenes containing nitro groups are often less soluble in organic solvents. A further complication is that the success of the reduction depends on the addition of specific amounts of reductant or oxidant and the choice of defined reaction conditions.[13,17] To date, all procedures for cAB preparation rely on an intramolecular redox reaction between nitrogen-containing functional groups to establish the diazocine ring.

Herein, we follow a novel retrosynthetic disconnection: Instead of breaking the bond between the nitrogen atoms, we aimed for the insertion of a diazo unit via consecutive C−N cross-coupling reactions to construct the diazocine ring. Only a few studies described the synthesis of heterocycles containing diazo functions[18,19] and azobenzenes[20] via C−N bond formation. In this report, an alternative facile synthesis of functionalized cABs is presented.

Following the newly designed strategy, we started with formation of the C−C bond in cAB from an initial 1,2-disubstituted arene (Scheme 1). Thus, reduction of 2-

Received: January 15, 2020
Published: February 3, 2020

© 2020 American Chemical Society

https://dx.doi.org/10.1021/acs.orglett.0c00122
Org. Lett. 2020, 22, 1624−1627

bromobenzyl bromide (**4a**) with *n*-butyllithium (*n*-BuLi) constructed the ethylene bridge of bibenzyl.[21] Further addition of *n*-BuLi and quenching with iodine converted the aryl bromide into corresponding aryl iodide (**5a**) in an overall 81% yield. The resulting dielectrophile then underwent Cu-catalyzed cascade amidations with di-*tert*-butyl hydrazodicarboxylate ($DBADH_2$) as a dinucleophilic hydrazine substrate in which the second C–N coupling led to intramolecular cyclization (**6a**) in 55% yield. This step followed a protocol for diamine ligand-catalyzed Ullmann–Goldberg amidation reactions[22−24] except that a low-boiling solvent was used, i.e., acetonitrile. As the major byproduct of this reaction, we detected the amidation product having consumed two $DBADH_2$ substrates, one on each aryl halide position. Remaining *tert*-butyloxycarbonyl (Boc) groups on the diazocine heterocycle were cleaved via Lewis acid promoted hydrolysis using trimethylsilyl iodide (TMSI) before oxidation of the exposed hydrazo group with NBS/Py, furnishing the cAB product (**1a**) in 67% yield.

We sought to explore the scope of this new process by fabrication of novel cAB derivatives containing functional groups at convenient carbon positions 2, 3, 8, and 9. Consequently, an array of 2-bromobenzyl bromides including electron-donating and electron-withdrawing groups were prepared (Scheme 2). Subsequent homocoupling to the corresponding bibenzyls **5b**–**5n** occurred in 41–82% yields. Fusion of benzyl bromides containing reducible functional groups such as methyl ester and nitrile was achieved by employment of the reductive Zn/$[NiCl_2(PPh_3)_2]$ system.[25] Asymmetric cAB carrying different substitution patterns on each benzene ring of the molecule such as **1m** was prepared from the combination of a benzyl bromide with a benzaldehyde in a Wittig reaction. The resulting stilbene was then hydrogenated to the desired bibenzyl compound **5m**.[26] Alongside benzyl coupling, we also established ethylene bridges between heterocycles such as thiophene (**5o**) and pyridine (**5p**).

Subsequently, we focused on the cyclization of *ortho*-halogenated bibenzyl compounds using C–N coupling chemistry (Scheme 3). Both electron-rich and electron-deficient arenes were readily transformed to the desired diazocine products **6b**–**6n** with similar efficiencies (35–70%). However, when aryl bromides were used as electrophiles, the desired cyclization product was only obtained in comparable yields after addition of 1 equiv of CuI catalyst. Likewise, heterocycles could also be annulated, delivering novel condensed ring systems **6o** and **6p**. Deprotection of the Boc-protected diazocine species and oxidation of the exposed hydrazo to diazo furnished the cAB products **1b**–**1p** in all cases in good to excellent yields (33–92%). In the example of the *tert*-butyl ether (**6e**), concomitant cleavage of ether and carbamate groups finally resulted in the phenol (**1e**).

In all previous examples, the functional group substituents are already present in the corresponding starting materials. However, late-stage derivatization is extremely valuable in terms of versatility and synthetic efficiency. Therefore, capitalizing on the Cl functional group allowed the conversion to amines (**1q**, **1r**) using a Buchwald–Hartwig amination with lithium bis(trimethylsilyl)amide (LHMDS) as the nucleophilic cross-coupling partner in 51–58% yields (Scheme 4a).[27] The examples show that general cross-coupling chemistry is possible for chlorinated cABs. Treatment of the methyl ester functions such as basic hydrolysis and the reduction with diisobutylaluminum hydride (DIBAL) were accomplished to give cABs with carboxylic acid (**1s**, **1t**) and benzyl alcohol (**1u**) in good to excellent yields (70–91%) (Scheme 4b). Finally, the photochromic properties of cABs were examined by UV–

Scheme 2. Synthesis of Various Bibenzyls from Benzyl Bromides

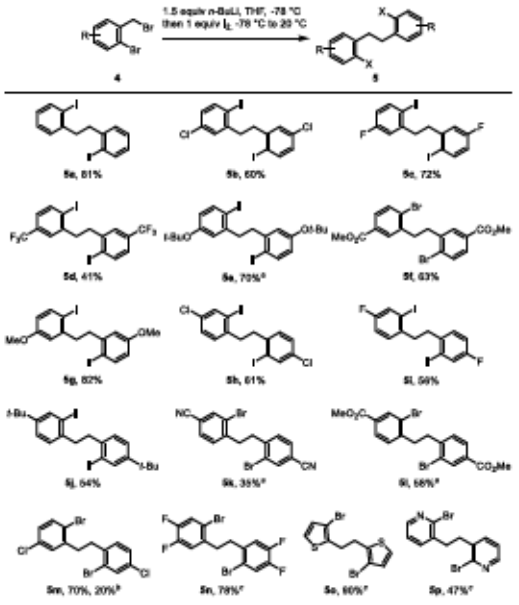

[a]1.5 equiv of Zn, 5 mol % $[NiCl_2(PPh_3)_2]$, 1 equiv of NEt_4I, MeCN/THF, 20 °C. [b]Via Wittig reaction and alkene reduction; see the Supporting Information. [c]0.5 equiv of *n*-BuLi, THF, −78 °C.

Scheme 3. Synthesis of Various cABs from Bibenzyls

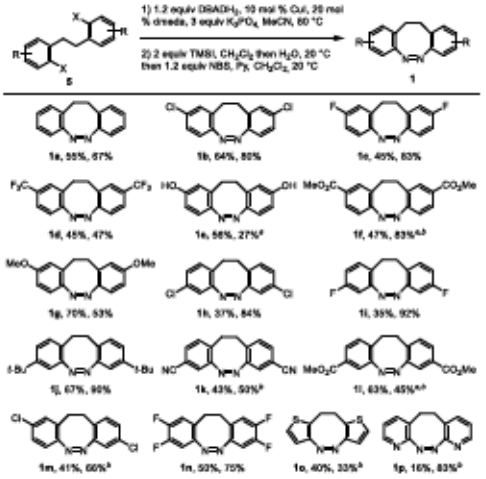

[a]4 equiv of TMSI used. [b]1 equiv of CuI used.

https://dx.doi.org/10.1021/acs.orglett.0c00122
Org. Lett. 2020, 22, 1624−1627

Scheme 4. Transformation of Reactive cABs

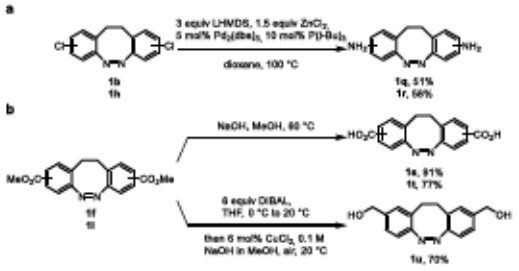

[a]$Pd_2(dba)_3$ = Tris(dibenzylideneacetone)dipalladium(0).

vis and NMR spectroscopy (see Supporting Information). Absorption maxima and photostationary states were determined after irradiation, with 385 and 565 nm wavelength light, of **1a**−**1u** in acetonitrile or DMSO. No significant deviations from parent cAB were found except for the products **1e**, **1q**, **1r**, and **1o** where the electronic coupling between the substituent and the aromatic system presumably causes rapid thermal relaxation of the (*E*) isomers.[28]

In conclusion, we show a new general route to functionalized ethylene bridged azobenzenes carrying a wide variety of functional groups. Additional derivatives could be prepared, in which the diazo group was flanked by the aromatic heterocycles thiophene and pyridine. Our strategy for the establishment of the diazocine ring consisted of building the ethylene bridge from 2-bromo benzyl bromides and inserting a hydrazine unit via cascade C−N coupling reactions. This method also provided products which could be further transformed into useful building blocks that may be used in materials chemistry,[29−32] in which higher amounts of ethylene bridged azobenzenes are required.

■ ASSOCIATED CONTENT

Supporting Information

The Supporting Information is available free of charge at https://pubs.acs.org/doi/10.1021/acs.orglett.0c00122.

Full experimental details, including synthetic procedures and characterization details (PDF)

■ AUTHOR INFORMATION

Corresponding Author

Anne Staubitz − *Otto-Diels-Institute for Organic Chemistry, University of Kiel, 24098 Kiel, Germany; Institute for Organic and Analytical Chemistry, University of Bremen, 28359 Bremen, Germany; University of Bremen, MAPEX Center for Materials and Processes, 28359 Bremen, Germany;* orcid.org/0000-0002-9040-3297; Email: staubitz@uni-bremen.de

Authors

Shuo Li − *Otto-Diels-Institute for Organic Chemistry, University of Kiel, 24098 Kiel, Germany;* orcid.org/0000-0002-6015-5659

Nadi Eleya − *Institute for Organic and Analytical Chemistry, University of Bremen, 28359 Bremen, Germany;* orcid.org/0000-0001-6409-6169

Complete contact information is available at: https://pubs.acs.org/10.1021/acs.orglett.0c00122

Notes

The authors declare no competing financial interest.

■ ACKNOWLEDGMENTS

This work has been supported by the German Research Foundation (DFG) within the Collaborative Research Center 677 "Function by Switching" (subproject C14). N.E. would like to thank the Philipp Schwartz Initiative of the Alexander von Humboldt foundation for their support. This research has been supported by the Institutional Strategy of the University of Bremen, funded by the German Excellence Initiative.

■ REFERENCES

(1) Bléger, D.; Hecht, S. *Angew. Chem., Int. Ed.* **2015**, *54*, 11338−11349.
(2) Siewertsen, R.; Neumann, H.; Buchheim-Stehn, B.; Herges, R.; Näther, C.; Renth, F.; Temps, F. *J. Am. Chem. Soc.* **2009**, *131*, 15594−15595.
(3) Carstensen, O.; Sielk, J.; Schönborn, J. B.; Granucci, G.; Hartke, B. *J. Chem. Phys.* **2010**, *133*, 124305.
(4) Böckmann, M.; Doltsinis, N. L.; Marx, D. *J. Chem. Phys.* **2012**, *137*, 22A505.
(5) Liu, L.; Wang, Y.; Fang, Q. *J. Chem. Phys.* **2017**, *146*, 064308.
(6) Siewertsen, R.; Schönborn, J. B.; Hartke, B.; Renth, F.; Temps, F. *Phys. Chem. Chem. Phys.* **2011**, *13*, 1054−1063.
(7) Jun, M.; Joshi, D. K.; Yalagala, R. S.; Vanloon, J.; Simionescu, R.; Lough, A. J.; Gordon, H. L.; Yan, H. *ChemistrySelect* **2018**, *3*, 2697−2701.
(8) Bandara, H. M. D.; Burdette, S. C. *Chem. Soc. Rev.* **2012**, *41*, 1809−1825.
(9) Samanta, S.; Qin, C.; Lough, A. J.; Woolley, G. A. *Angew. Chem., Int. Ed.* **2012**, *51*, 6452−6455.
(10) Li, S.; Han, G.; Zhang, W. *Macromolecules* **2018**, *51*, 4290−4297.
(11) Löw, R.; Rusch, T.; Röhricht, F.; Magnussen, O.; Herges, R. *Beilstein J. Org. Chem.* **2019**, *15*, 1485−1490.
(12) Eljabu, F.; Dhruval, J.; Yan, H. *Bioorg. Med. Chem. Lett.* **2015**, *25*, 5594−5596.
(13) Moormann, W.; Langbehn, D.; Herges, R. *Synthesis* **2017**, *49*, 3471−3475.
(14) Enyedy, I. J.; Huang, Y.; Long, Y. Q.; Roller, P. P.; Yang, D.; Wang, S.; Ling, Y.; Nacro, K.; Tomita, Y.; Wu, X.; et al. *J. Med. Chem.* **2001**, *44*, 4313−4324.
(15) Pauller, W. W.; Zeiler, A. G. *J. Org. Chem.* **1969**, *34*, 3237−3239.
(16) Cabré, G.; Garrido-Charles, A.; González-Lafont, À.; Moormann, W.; Langbehn, D.; Egea, D.; Lluch, J. M.; Herges, R.; Alibés, R.; Busqué, F.; et al. *Org. Lett.* **2019**, *21*, 3780−3784.
(17) Maier, M. S.; Hüll, K.; Reynders, M.; Matsuura, B. S.; Leippe, P.; Ko, T.; Schäffer, L.; Trauner, D. *J. Am. Chem. Soc.* **2019**, *141*, 17295−17304.
(18) Ball, C. J.; Gilmore, J.; Willis, M. C. *Angew. Chem., Int. Ed.* **2012**, *51*, 5718−5722.
(19) Martín, R.; Rivero, M. R.; Buchwald, S. L. *Angew. Chem., Int. Ed.* **2006**, *45*, 7079−7082.
(20) Kim, K. Y.; Shin, J. T.; Lee, K. S.; Cho, C. G. *Tetrahedron Lett.* **2004**, *45*, 117−120.
(21) Jensen, J.; Tejler, J.; Wärnmark, K. *J. Org. Chem.* **2002**, *67*, 6008−6014.
(22) Surry, D. S.; Buchwald, S. L. *Chem. Sci.* **2010**, *1*, 13.
(23) Klapars, A.; Antilla, J. C.; Huang, X.; Buchwald, S. L. *J. Am. Chem. Soc.* **2001**, *123*, 7727−7729.
(24) Klapars, A.; Huang, X.; Buchwald, S. L. *J. Am. Chem. Soc.* **2002**, *124*, 7421−7428.
(25) Iyoda, M.; Sakaitan, M.; Otsuka, H.; Oda, M. *Chem. Lett.* **1985**, *14*, 127−130.
(26) Zhao, P.; Beaudry, C. M. *Org. Lett.* **2013**, *15*, 402−405.

https://dx.doi.org/10.1021/acs.orglett.0c00122
Org. Lett. 2020, 22, 1624−1627

(27) Lee, D. Y.; Hartwig, J. F. *Org. Lett.* **2005**, *7*, 1169−1172.
(28) Moormann, W.; Langbehn, D.; Herges, R. *Beilstein J. Org. Chem.* **2019**, *15*, 727−732.
(29) Donovan, B. R.; Matavulj, V. M.; Ahn, S.-k.; Guin, T.; White, T. J. *Adv. Mater.* **2019**, *31*, 1805750.
(30) Chang, V. Y.; Fedele, C.; Priimagi, A.; Shishido, A.; Barrett, C. J. *Adv. Opt. Mater.* **2019**, *7*, 1900091.
(31) Wang, L.; Li, Q. *Chem. Soc. Rev.* **2018**, *47*, 1044−1097.
(32) Lancia, F.; Ryabchun, A.; Katsonis, N. *Nat. Rev. Chem.* **2019**, *3*, 536−551.

https://dx.doi.org/10.1021/acs.orglett.0c00122
Org. Lett. 2020, 22, 1624−1627

3.2 ATRP Optimization and Characterization of Diazocine-Doped Linear Elastomers

ARGET ATRP of Methyl Acrylate and Methyl Methacrylate with Diazocine-Derived Initiators

Shuo Li, Ruchira Colaco, and Anne Staubitz, *ACS Appl. Polym. Mater.* **2022**, *4*, 6825–6833.

DOI: 10.1021/acsapm.2c00769

Reprinted with permission from ACS Publications. Copyright 2022. Published by American Chemical Society. The supporting information includes all used materials and methods, experimental procedures, analytical data, images of spectra and is available free of charge online.

Abstract

Diazocine-functionalized initiators for atom transfer radical polymerization (ATRP) were synthesized and tested for their efficiency in controlled radical polymerizations of methyl acrylate and methacrylate under reaction conditions for activators regenerated by electron transfer (ARGET). The α-bromoisobutyl condensates of anilide and benzyloxycarbonate required high amounts of reducing agents and catalysts for the initiation. On the other hand, violet light irradiation during ATRP caused severe retardation or termination during initiation of the anilide compound, in contrast to the previously reported photoinduced initiation under otherwise very similar conditions. The final linear elastomers obtained from optimized polymerization kinetics responded to light irradiation of 405 and 525 nm wavelengths by $(Z)/(E)$ photoisomerization of diazocine in both solution and in the solid state. The $(E)\rightarrow(Z)$ thermal relaxation rate was highly influenced by electronic effects on the diazocine ring, the solvent, and the polymer matrix in the solid state. Our polymers find potential use as photonic materials in ultraviolet light sensors and optical waveguides.

Scientific Contribution

After initial drafting and planning by Prof. Dr. Anne Staubitz, this project was planned, organized and conducted by me. The synthesis, purification and characterization of the compounds were carried out by me. The manuscript and the supporting information were written by me. Ruchira Colaco synthesized the ligand Me_6TREN and prepared the solid thin films by drop-casting. Prof. Dr. Anne Staubitz as the principal investigator was responsible for the funding and edited the article. All authors have read and edited the article and agreed to the published version of the manuscript.

Table 3.2. Contribution of the candidate in % of the total workload (up to 100% for each of the following categories)

Experimental concept and design	70%
Experimental work and/or acquisition of (experimental) data	90%
Data analysis and interpretation	90%
Preparation of Figures and Tables	100%
Drafting of the manuscript	80%

ACS APPLIED POLYMER MATERIALS

pubs.acs.org/acsapm Article

ARGET ATRP of Methyl Acrylate and Methyl Methacrylate with Diazocine-Derived Initiators

Shuo Li, Ruchira Colaco, and Anne Staubitz*

Cite This: ACS Appl. Polym. Mater. 2022, 4, 6825−6833 Read Online

ACCESS | Metrics & More | Article Recommendations | Supporting Information

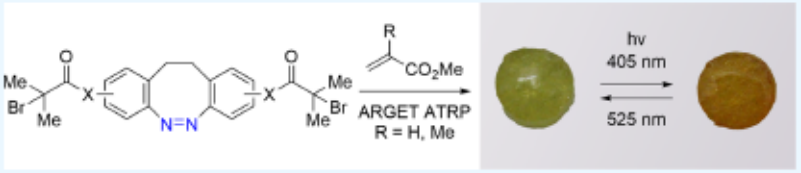

ABSTRACT: Diazocine-functionalized initiators for atom transfer radical polymerization (ATRP) were synthesized and tested for their efficiency in controlled radical polymerizations of methyl acrylate and methacrylate under reaction conditions for activators regenerated by electron transfer (ARGET). The α-bromoisobutyl condensates of anilide and benzyloxycarbonate required high amounts of reducing agents and catalysts for the initiation. On the other hand, violet light irradiation during ATRP caused severe retardation or termination during initiation of the anilide compound, in contrast to the previously reported photoinduced initiation under otherwise very similar conditions. The final linear elastomers obtained from optimized polymerization kinetics responded to light irradiation of 405 and 525 nm wavelengths by *Z*/*E* photoisomerization of diazocine in both solution and in the solid state. The $E \rightarrow Z$ thermal relaxation rate was highly influenced by electronic effects on the diazocine ring, the solvent, and the polymer matrix in the solid state. Our polymers find potential use as photonic materials in ultraviolet light sensors and optical waveguides.

KEYWORDS: *poly(methyl acrylate), poly(methyl methacrylate), atom transfer radical polymerization, diazocine, photochromism*

Downloaded via UNIV BREMEN on November 28, 2022 at 23:04:43 (UTC).
See https://pubs.acs.org/sharingguidelines for options on how to legitimately share published articles.

INTRODUCTION

Macromolecular systems can be modified and enhanced by the incorporation of molecular switches that change their molecular geometry and therefore physical properties upon irradiation with light.[1−3] Among these switches, the ethylene bridged azobenzene (diazocine) stands out as a photoresponsive molecule with interconvertible configurations where the bent (*Z*) form is energetically favored over the (*E*) isomer (Scheme 1).[4−6] The photoswitching of diazocine is accomplished by irradiation with violet (405 nm wavelength) and green light (525 nm wavelength) and is affected highly by the modifications of the ethylene bridge. Drastic changes in the thermal half-life of the (*E*) isomer (4.5 h, all carbon skeleton) were observed in the oxygen- (89 s) and sulfur-substituted (3.5 days) congeners,[7] while the acetamido substituent greatly enhanced the solubility in water.[8] A very high energy conversion efficiency of 18.1% was evaluated in the di-indane of diazocine compared to the original molecule (7.6%).[9]

Scheme 1. Photochemical Isomerization Reaction between (*Z*)- and (*E*)-Diazocine

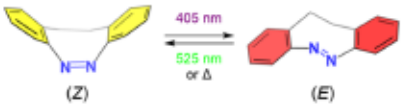

To date, there have been two reports on the use of diazocine as a comonomer: Li et al. applied the 3,8-diaminosubstituted diazocine in a polyaddition reaction to synthesize a polyurea polymer that could be photopatterned and also reported the photomechanical bending of a film.[10] Burk et al. fabricated photochromic thin films via initiated chemical vapor deposition from the radical polymerization of divinylated diazocine in the gas phase.[11] However, the incorporation of a single functional unit is often sufficient to accomplish an effective photocontrol of macromolecular systems. Diazocines have been utilized in biomolecules such as peptides,[12] oligonucleotides,[13] and carbohydrates[14] to induce a conformational change for functional control.

Atom transfer radical polymerization (ATRP) is a widely used radical polymerization technique that allows for good control over molar mass distribution, dispersity (*Đ*), and

Received: May 6, 2022
Accepted: August 23, 2022
Published: September 2, 2022

© 2022 American Chemical Society

https://doi.org/10.1021/acsapm.2c00769
ACS Appl. Polym. Mater. 2022, 4, 6825−6833

architecture of polymer chains.[15,16] The initiation of the polymerization[17] proceeds through a concerted inner-sphere electron transfer mechanism involving the C–X bond dissociation of an alkyl halide initiator and transfer of the halogen atom to produce X–Cu(II)L$^+$ from the Cu(I)L$^+$ catalyst complex.[18] Among various initiation systems for ATRP,[15] activators regenerated by electron transfer (ARGET) shows better oxygen tolerance and polymerization control via the dynamic ATRP equilibrium between the X–Cu(II)L$^+$ deactivator and the Cu(I)L$^+$ activator. The polymerization rate is determined particularly by the type and the amount of the employed reducing agent, which continuously regenerates the Cu(I)L$^+$ species.[19] The polymerization of acrylates was extensively studied by the groups of Haddleton[20] and Percec[21] who employed the highly reactive ethyl α-bromoisobutyrate (EBiB) initiator in combination with the Cu(0)/tris[2-(dimethylamino)ethyl]amine (Me_6TREN) catalytic system in dimethyl sulfoxide (DMSO). Cu(0) is considered the supplemental activation reducing agent (SARA), to regenerate Cu(I)L$^+$ from X–Cu(II)L$^+$ through comproportionation.[22] Hutchinson and co-workers demonstrated that the polymerization of methyl acrylate using ascorbic acid (AA) is very efficient after Cu(0)-mediated initiation.[23] In fact, some ATRP ligands such as Me_6TREN are capable of effectively reducing the X–Cu(II)L$^+$ complex especially when they are used in excess.[24,25] Anastasaki and co-workers achieved outstanding end-group fidelity and control of the polymerization of acrylates with photoinduced ATRP (photo-ATRP)[26−28] in which the photoexcited Me_6TREN ligand presumably becomes an electron donor to the initiator to induce C–Br bond homolysis.[29,30]

In this work, we report the polymerization of methyl acrylate and methyl methacrylate using the photochromic diazocine, functionalized with α-bromoisobutyryl initiating sites. The newly synthesized initiating system is compared to the established EBiB initiator with regard to its polymerization efficiency and the resulting molar mass distributions. With these studies, we could detect for the first time a strong inhibiting effect of violet light on the initiation process of ARGET ATRP. With optimized ATRP conditions for the diazocine-functionalized initiator, structural variations of that initiating system were tested for the synthesis of poly(methyl acrylate) and poly(methyl methacrylate) (PMMA). We further studied the photochromism of diazocine incorporated in high-molecular-weight acrylate and methacrylate polymer chains in both solution and in the solid state. Polymers containing photochromic units in the main chain serve in potential photonic applications[31] such as optical waveguides,[32] data storage,[33,34] and photopatterned surfaces.[10,35,36]

EXPERIMENTAL SECTION

Materials. α-Bromoisobutyryl bromide (BIBB, 98%, Sigma-Aldrich), *N,N,N′,N″,N″*-pentamethyldiethylenetriamine (PMDETA, Merck), tris[2-(dimethylamino)ethyl]amine (Me_6TREN, synthesized according to the procedure by Ciampolini and Nardi),[37] and triethylamine (anhydrous, Fluorochem) were degassed by three freeze–pump–thaw cycles and stored in the glovebox. Methyl acrylate (99%, Alfa Aesar) and methyl methacrylate (99%, J&K) were passed through aluminum oxide 90 basic (Macherey-Nagel, 50–200 μm particle size) before use. Tetrahydrofuran (THF) (>99%, Honeywell) was dried by a solvent purification system (SPS) from Inert Technologies. Ascorbic acid (>99%, Roth), anisole (>99%, Roth), and DMSO (99.7%, Acros) were employed without further purification. To conduct the polymerization with Cu(0), the copper wire (diameter: 0.4 mm, Knorr Prandell) was wrapped around a stirring bar, cleaned with concentrated HCl (12 M) for 10 min, rinsed with water and acetone, and transferred into the glovebox. The stirring bar was added to the reaction mixture to start the polymerization. To irradiate the reaction vial with light during the reaction, the light-emitting diode (LED) light source was switched on just before the stirring bar was added. A solution of $CuBr_2$ (99%, Stem Chemicals) in DMSO (67 mg/3 mL, 0.1 M) was prepared in the glovebox.

Instrumentation. NMR spectra were recorded on a Bruker Avance Neo 600 (Bruker BioSpin, Rheinstetten, Germany) (600 MHz (^{1}H), 151 MHz (^{13}C{^{1}H})) at 298 K. All ^{1}H NMR and ^{13}C{^{1}H} NMR spectra were referenced to the residual proton signals of the solvent (^{1}H) or the solvent itself (^{13}C{^{1}H}). The exact assignment of the peaks was performed by two-dimensional NMR spectroscopy such as ^{1}H correlated spectroscopy (COSY), ^{13}C{^{1}H} heteronuclear single quantum coherence (HSQC), and ^{1}H/^{13}C{^{1}H} heteronuclear multiple bond correlation (HMBC) when possible. The UV–vis absorption measurements were recorded in a PerkinElmer UV/vis near-infrared (NIR) spectrometer Lambda 900 and in a VWR UV-1600PC at 298 K. Quartz cuvettes of 10 mm optical path length were used. The irradiation experiments were carried out using LED light sources from Sahlmann Photochemical Solutions of 405 nm central wavelength (3× Nichia NVSU233A of 980 mW optical power) and 525 nm central wavelength (3× Nichia NCSG219B-V1 of 400 mW optical power) at a 2 cm distance from the cuvette or from the reaction vial. The photostationary states (PSSs) of compounds **2a–d** were determined by ^{1}H NMR spectroscopy (5 mM in MeCN-d_3) at 25 °C. The NMR tubes were irradiated with light at 405 and 525 nm wavelength for 2 min each before the NMR spectra were recorded. Absorption maxima at wavelengths $\lambda_{max}(E)$ and $\lambda_{max}(Z)$ of compounds **2–4** were determined by UV–vis spectroscopy (1 mM in THF for **2a–d**, 10 mg/mL in THF for **3a–d** and **4a–d**) at 25 °C. The cuvettes were irradiated with light at 405 and 525 nm wavelength for 2 min each before the absorption spectra were measured. The thermal relaxation kinetics of compounds **2–4** were monitored by UV–vis spectroscopy (1 mM in THF for **2a–d**, 10 mg/mL in THF and as drop-casted thin films for **3a–d** and **4a–d**) at 25 °C. After the photostationary state (PSS) at 405 nm was reached, 19 spectra were recorded in the dark in 10 min intervals. The absorptions at $\lambda_{max}(E)$ were plotted against the reaction time before the rate constant k and the half-life $t_{1/2}$ were determined via first-order kinetics. Kinetic measurements for every sample were conducted three times to determine the mean and the standard deviation of k and $t_{1/2}$. Gel permeation chromatography (GPC) was performed on a polymer standard service (PSS) SECurity GPC system at 308 K after a conventional calibration using polystyrene standards. The molar mass distribution of polymers was determined using refractive index detection (RID) in combination with light scattering (LS) detection and diode-array detection (DAD). The polymers were dissolved in THF (≈1 mg/mL; 5 mg/mL for the detection of absorption at 395 nm wavelength), and the GPC spectra were recorded at the 1 mg/mL elution flow rate. To prepare polymer thin films (0.03–0.04 mm thickness), 100 μL of a 60 mg/mL polymer solution in THF was drop-casted and distributed onto a Menzel-Gläser cover slip (18 mm × 18 mm) and dried on a glass plate at 60 °C for 24 h.

Chemical Synthesis. *Procedure for the Polymerization of Methyl Acrylates **3a–d**.* Methyl acrylate (1.72 g, 20.0 mmol, 1000 equiv), initiator **2a** (10.7 mg, 20.0 μmol, 1.00 equiv), and DMSO (1.9 mL) were added to a microwave vial and degassed by purging with argon for 10 min. The sealed vial was transferred into a glovebox, opened, and AA (35.0 mg, 22.2 μmol, 50.0 equiv), $CuBr_2$ solution in DMSO (40.0 μL, 4.00 μmol, 100 mM, 0.20 equiv), and Me_6TREN (6.40 μL, 24.0 μmol, 1.20 equiv) were added within 20 s. The vial was sealed, transferred out of the glovebox, and stirred at 20 °C for 2 h. Samples were taken periodically and conversions were measured using ^{1}H NMR spectroscopy. Then, the vial was opened and the reaction mixture was precipitated dropwise in stirring methanol (25 mL). The resulting solid was collected, redissolved in THF (2.5 mL), and re-precipitated in methanol (25 mL) twice before the solid residue was

https://doi.org/10.1021/acsapm.2c00769
ACS Appl. Polym. Mater. 2022, 4, 6825–6833

dried in vacuum (50 °C, 48 h) to furnish product **3a** (244 mg, 14%) as a yellow solid. This procedure was adopted for the synthesis of **3b** from **2b**, **3c** from **2c**, and **3d** from **2d** (see the SI).

Procedure for the Polymerization of Methyl Methacrylates ***4a–d***. Methyl methacrylate (2.00 g, 20.0 mmol, 1000 equiv), initiator **2a** (10.7 mg, 20.0 μmol, 1.00 equiv), and anisole (2.2 mL) were added to a microwave vial and degassed by purging with argon for 10 min. The sealed vial was transferred into the glovebox, opened, and AA (3.50 mg, 20.0 μmol, 1.00 equiv), $CuBr_2$ solution in DMSO (20.0 μL, 2.00 μmol, 100 mM, 0.10 equiv), and PMDETA (4.20 μL, 53.0 μmol, 1.00 equiv) were added within 20 s. The vial was sealed, transferred out of the glovebox, and stirred at 90 °C for the given time. Samples were taken periodically and conversions were measured using ^{1}H NMR spectroscopy. Then, the vial was opened and to the reaction mixture was added THF (2.5 mL) and precipitated dropwise in stirring methanol (25 mL). The resulting solid was collected, redissolved in THF (5 mL), and re-precipitated in methanol (25 mL) twice before the solid residue was dried in vacuum (50 °C, 48 h) to furnish product **4a** (986 mg, 49%) as a yellow solid. This procedure was adopted for the synthesis of **4b** from **2b**, **4c** from **2c**, and **4d** from **2d** (see the SI).

RESULTS AND DISCUSSION

Preparation of Diazocine-Functionalized ATRP Initiators. The syntheses of substituted diazocines have been established previously in a three-step process starting from functionalized 2-bromobenzyl bromides.[5] Treatment of dianilines **1a** and **1b** with α-bromoisobutyryl bromide (BIBB) generated the desired difunctional diazocine initiators **2a** and **2b** in 82 and 84% yields (Scheme 2). The easily accessible dihydroxymethyl derivative of diazocine **1c** was treated under the same conditions to deliver the difunctional initiator **2c** in a 92% yield. To obtain the monofunctional equivalent of initiator **2c**, benzyl bromide **5** and benzaldehyde **6** were first combined in a Wittig reaction to generate the stilbene **7** (see Scheme S2). The ensuing hydrogenation with Adams' catalyst

Scheme 2. Overview of Starting Materials 1a–d, Initiators 2a–d, Poly(methyl acrylate)s 3a–d, and Poly(methyl methacrylate)s 4a–d Containing Diazocine[a]

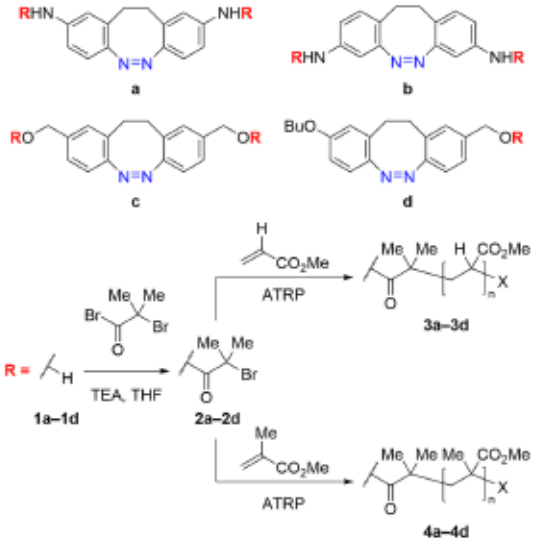

[a]X = end group.

to the bibenzyl compound paved the way for the synthesis of benzyl alcohol **1d** via the cascade Cu-catalyzed amidation reaction, in accordance with the previously reported synthesis of **1c**.[5] Condensation with BiBB finally provided the product **2d** in a 46% yield. Thus, the ATRP initiators **2a–d** were generated containing one or two α-bromoisobutyryl groups with different attachments to the diazocine core.

ATRP Optimization for Poly(methyl acrylate) with a Difunctional Diazocine Initiator. Throughout this study, the targeted degree of polymerization was set to 500 for each reactive initiating alkyl bromide site. Molecular weights M_n and M_w were obtained from the molar mass distribution by GPC analysis (calibrated from polystyrene standards, Figures S1–S8) and conversions were determined by ^{1}H NMR spectroscopy. Prior to the investigation of the diazocine-functionalized initiators, the polymerization of methyl acrylate was reproduced with the highly reactive initiator EBiB to compare the subsequent polymerization results (Table 1, entry 1). The use of the very effective catalyst system $CuBr_2$ and tris[2-(dimethylamino)ethyl]amine (Me_6TREN) in DMSO with Cu(0) as the reducing agent was adopted from Haddleton and co-workers.[20,38] The solvent to monomer ratio was set to 50:50 v/v DMSO/methyl acrylate and the reaction temperature of 20 °C was kept constant throughout the reaction. After 5 h, 91% of the monomer had converted to poly(methyl acrylate) with an M_n of 42 kDa and a dispersity of less than 1.1, in good agreement with the literature.

However, when the same conditions were applied to the diazocine initiator **2a**, conversion after 2 h was only at 4% (entry 2). Low conversion in combination with an excessively high M_n of 104 kDa and a dispersity of 1.8 strongly suggested that initiator **2a** was less reactive than EBiB. Increasing the length of the Cu(0) wire from 5 to 25 cm led to an increase in conversion to 63% and the targeted degree of polymerization was reached after only 2 h of reaction time (entry 3). The GPC result revealed a trimodal distribution of polymers, containing the major peak of the expected extension of the difunctionalized initiator on both reactive sites together with a minor peak consisting of single-extended polymer chains and a broad peak that was attributed to bimolecular radical terminations. Entry 3 illustrates that the amount of the available reducing agent and thus the rapid generation of the $Cu(I)L^+$ activator during the initial stage of polymerization are crucial in the case of **2a**. The decline in initiation efficiency from EBiB to **2a** also caused significantly more radical terminations at the nascent polymer chain end.

To evaluate whether the amount of the catalyst influences the outcome regarding molar mass distribution, the concentrations of $CuBr_2$ and Me_6TREN were increased 10-fold (entry 4).[39] Apart from a high conversion of 70%, which was reached after only 1 h, bimolecular radical termination events became more frequent as reflected by the high M_n shoulder in the molar mass distribution (Figure 1a). As a consequence, rapid polymer chain growth and bimolecular combinations generated a very high M_n of 123 kDa and a dispersity of 1.9 after 1 h of reaction time. The result is consistent with the observation made by Anastasaki and co-workers in which an increase in ligand concentration led to more termination events mediated by the ligand Me_6TREN.[40] Defunctionalization by chain transfer and ligand quaternization at the ω-chain end resulted in dead polymer chains. An increase in bimolecular radical termination events is explained by the accumulating amounts

https://doi.org/10.1021/acsapm.2c00769
ACS Appl. Polym. Mater. 2022, 4, 6825–6833

ACS Applied Polymer Materials pubs.acs.org/acsapm Article

Table 1. Comparison of ATRP Reaction Conditions and Results for 2a to 3a after 2 h of Reaction Time[a,b,f]

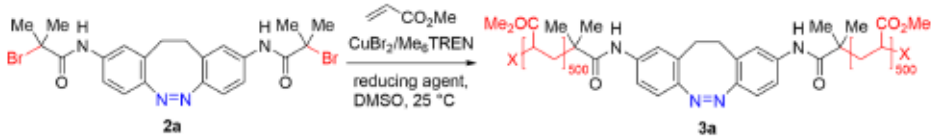

entry	initiator	$[CuBr_2]/[Me_6TREN]$	reducing agent	conversion (%)	$M_{n,GPC}$ (kDa)	$M_{n,theo}$ (kDa)	$Đ$
1[c]	EBiB	0.02:0.12	5 cm Cu(0)	91	42	40	<1.1
2	**2a**	0.02:0.12	5 cm Cu(0)	4	104	4	1.8
3	**2a**	0.02:0.12	25 cm Cu(0)	63	82	55	1.6
4[d]	**2a**	0.2:1.2	25 cm Cu(0)	70	123	61	1.9
5	**2a**	0.2:1.2 + *hν*[e]	25 cm Cu(0)	9	66	8	1.3
6	**2c**	0.2:1.2 + *hν*[e]	25 cm Cu(0)	46	66	40	1.3
7	**2a**	0.2:1.2	[AA] = 1	52	60	45	1.2
8	**2a**	0.2:1.2	[AA] = 10	68	87	59	1.4
9	**2a**	0.2:1.2 + *hν*[e]	[AA] = 10	43	152	38	3.1

[a]X = end group. [b]Monomers/alkyl bromide site = 500. [c]2 equiv of the initiator, reaction time 5 h. [d]Reaction time 1 h. [e]405 nm wavelength. [f]Bold values represent the following: 2a and 2c are the assigned names of the chemical initiators. Entries 4 and 8 are separately discussed in Figure 1.

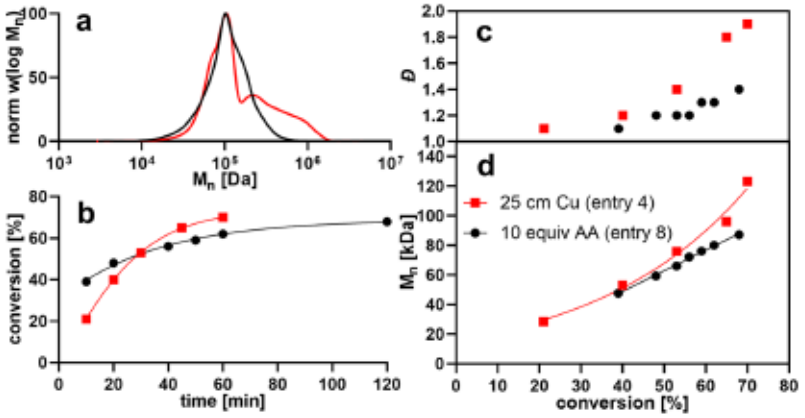

Figure 1. Comparison of the reducing environments 25 cm Cu(0) (entry 4, red) and 10 equiv AA (entry 8, black) in the ATRP to poly(methyl acrylate) **3a**. Normalized molar mass distributions of entry 4 (after 1 h) and entry 8 (after 2 h) (a), reaction kinetics (b), dispersities (c), and chain growths (d).

of $Cu(I)L^+$, which can mediate polymer chain ligations after its attachment to active radical chain ends.[29,41−43]

It is possible that the configurational states (*Z*) and (*E*) of the diazocine exert thermodynamic influence over the homolysis of the C−Br bond. Therefore, the reaction mixture was irradiated with light at 405 nm wavelength before and during polymerization (entry 5). Surprisingly, the conversion after 2 h of reaction time was only 9%, with a smaller than expected M_n of 66 kDa. No progress in polymerization was detected even after gradual thermal relaxation from (*E*) to (*Z*) isomers over 24 h, thereby preventing monomer addition during the initial stages by violet light. In photo-ATRP established by Anastasaki and co-workers, C−Br bond homolysis of the initiator and the (re)generation of the $Cu(I)L^+$ activator were accomplished by an external light source at 305−550 nm wavelengths in the absence of a reducing agent.[28,44] However, initiators **2a** and **2c** only underwent (*Z*) to (*E*) photoisomerization as evident by a color change from yellow to red and did not initiate polymerization under photo-ATRP conditions. In the presence of Cu(0), both initiators yielded polymers with constant M_n of 66 kDa and dispersities of 1.3. However, a substantial difference in conversion was detected, obtaining only 9% of poly(methyl acrylate) from initiator **2a** (entry 5), opposite to 46% from initiator **2c** (entry 6). Therefore, the photoisomerization of diazocine had no significant effect on the C−Br bond homolysis. On the other hand, the strong effect of violet light on the initiator **2a** but not on **2c** originated from competing side reactions involving the *α*-bromoamide group:[45] In the presence of a $Cu(I)L^+$-based catalyst, it could undergo reactions with methyl acrylate to form the corresponding iminolactone.[46] Heterocycle condensations usually require high temperatures but the photoactivation of the catalyst could further lower the activation barrier. As shown before for the catalytic amination of *α*-chloroisobutylamides, Cu(I) complexes can be photoactivated by blue light.[47]

Since the monomer conversion highly depends on the concentration of the reducing agent, Cu(0) wire was replaced by ascorbic acid (AA),[48] creating a homogeneous reaction environment independent from the surface area of Cu(0) (entry 7). After 2 h and a relative initial AA concentration of 1 to the initiator, 52% of the monomer was converted to

https://doi.org/10.1021/acsapm.2c00769
ACS Appl. Polym. Mater. 2022, 4, 6825−6833

poly(methyl acrylate) with a low dispersity of 1.2, but the propagation stopped at about an M_n of 60 kDa and the distribution remained trimodal. As a result, raising the relative amount of AA from 1 to 10 aimed for a faster conversion and sustained propagation (entry 8). Monomer conversion reached 68% after 2 h of reaction time (Figure 1b), comparable to the same conditions under Cu(0) in entry 4. Linear growth of the nascent polymer chains was observed, leading to well-defined poly(methyl acrylate) of close to ideal M_n of 87 kDa (Figure 1d). The good solubility of AA in DMSO contributed to a faster generation of the $Cu(I)L^+$ activator to accelerate the initiation. At the same time, the high concentration of AA suppressed catalyst deactivation, causing dispersities to grow slowly over the course of the reaction from 1.1 to 1.4 (Figure 1c).

Interestingly, violet light irradiation during the polymerization did not cause termination of the reaction (entry 9). Instead after 2 h, a slight decrease in conversion to 43%, a very high M_n of 152 kDa, and a dispersity of 3.1 confirm that violet light hampers the initiation process. However, the high concentration of AA enabled faster kinetics of initiation than the competing photoinduced termination processes while reducing the photocatalytic activity of free Me_6TREN through protonation.

Preparation of Diazocine-Centered Poly(methyl acrylate)s. Following the optimization of ARGET ATRP with initiator **2a**, the conditions from entry 8 were applied to the initiators **2b–d** (Table 2). Generation of poly(methyl acrylate) was successful in all cases with very similar results in conversion (64–73%), M_n (79–87 kDa in **3a–c** and 50 kDa in **3d**), and a dispersity of 1.4. Trace signals of the diazocine center were detectable in the aromatic region of the ^{1}H NMR spectra and were highlighted (see the SI). Most importantly, the measured M_n approached the targeted values of 87 and 44 kDa and the purified polymers were confirmed via ^{1}H NMR spectroscopy. Slightly lower theoretical M_n than obtained by GPC is attributed to the lower reactivity of diazocine-derived initiators. Nevertheless, the use of AA as the reducing agent combined with a high concentration of the catalyst ensured effective polymerization, thus establishing a general method for the syntheses of poly(methyl acrylate) from less efficient α-bromoisobutyryl-based initiators.

Table 2. Polymerization Results of Initiators 2a–d to Polymers 3a–d and 4a–dc[a]

entry	$[CuBr_2]$/[ligand]/[AA]	conversion (%)	$M_{n,GPC}$ (kDa)	$M_{n,theo}$ (kDa)	$Đ$
2a to 3a	0.2:1.2[b]:10	68	87	59	1.4
2b to 3b	0.2:1.2[b]:10	73	80	63	1.4
2c to 3c	0.2:1.2[b]:10	64	79	56	1.4
2d to 3d[c]	0.2:1.2[b]:10	65	50	28	1.4
2a to 4a	0.1:1[d]:1	63	97	64	1.5
2b to 4b	0.1:1[d]:1	65	113	66	1.8
2c to 4c[e]	0.1:1[d]:1	78	89	79	1.3
2d to 4d[c,e]	0.1:1[d]:1	75	52	38	1.4

[a]Monomers/alkyl bromide site = 500. [b]Ligand Me_6TREN. [c]2 equiv of the initiator. [d]Ligand PMDETA. [e]Reaction time 3 h.

Preparation of Diazocine-Centered Poly(methyl methacrylate)s. The polymerization of methyl methacrylate with functional initiators **2a–d** by ARGET ATRP (Table 2) followed similar conditions derived from a previous study,[49] except that tin(II) 2-ethylhexanoate was replaced by AA as the reducing agent. The catalyst system was chosen with relative concentrations of 0.1:1:1 for $[CuBr_2]$/[PMDETA]/[AA] (PMDETA = *N,N,N′,N″,N″*-pentamethyldiethylenetriamine) to the initiator and a solvent to monomer ratio of 50:50 v/v for anisole/methyl methacrylate. The targeted degree of polymerization was set to 500 for each reactive initiating alkyl bromide site. Purification after the reaction led to diazocine-centered poly(methyl methacrylate)s **4a–d** with M_n of 89–113 and 52 kDa near the targeted value of 101 and 51 kDa, as confirmed by ^{1}H NMR spectroscopy and GPC. Trace signals of diazocine in the aromatic region of the ^{1}H NMR spectra were highlighted (see the SI). While the dispersities remained constant for poly(methyl acrylate)s **3a–d**, deviating results between 1.3 and 1.8 were obtained from the poly(methyl methacrylate)s **4a–d**. The poor solubility of AA in anisole led to its agglomeration during the reaction. Although there was a lower activity resulting from the reduced surface area of AA, high conversions (63–78%) were reached within 2–3 h. Therefore, the chosen ARGET ATRP condition is very effective for the polymerization of methyl methacrylate from initiators **2a–d**.

To verify the covalent incorporation of diazocine in the poly(methyl acrylate) and methacrylate chains, the GPC analysis of the polymers **3a–d** and **4a–d** was repeated with both refractive index detection (RID) and diode-array detection (DAD) set at 395 nm wavelength absorption to detect the nπ^* absorption band of (*Z*)-diazocine. The results were compared to a linear poly(methyl methacrylate) sample without diazocine content as the negative control. While all polymers including the negative control showed a signal in the RID, which was applied for the determination of their molar mass distributions (Figure S9), an increased absorption of light at 395 nm wavelength in the DAD could only be detected in the diazocine-containing polymers **3a–d** and **4a–d**. Thus, the absence of an increased absorbance signal from the PMMA negative control during the GPC elution confirms the covalent incorporation of diazocine in the polymers.

Photochromism of Initiators and Diazocine-Centered Poly(methyl acrylate)s and Methacrylates. The UV–vis spectra of the initiators **2a–d** and the polymers **3a–d** and **4a–d** in THF were recorded at 25 °C (Figures S10–S15). Photoexcitation of the (*Z*) isomers with light at 405 nm enabled the isomerization to the metastable (*E*) configuration with good photoconversion yields of 55–69% for **2a–d** (Table S1). A complete $E \rightarrow Z$ conversion (>99%) was achieved with light at 525 nm wavelength. The photostationary states (PSSs) of the diazocine products were all reached within 1 min of irradiation time. The n–π^* transition maxima of the (*Z*) and (*E*) isomers were detected at around 405 and 490 nm, respectively (Table S2).

The spontaneous $E \rightarrow Z$ thermal relaxation of the initiators **2a–d** and polymer-linked diazocine **3a–d** and **4a–d** followed first-order reaction kinetics (Tables 3 and S3 and Figures S20–S22) and was measured by the decay of the absorption band of the (*E*)-isomer at its maximum wavelength λ_{max}. The determined thermal half-lives $t_{1/2}$ (Table 3) of the initiators show a high dependence on the substituents on the aromatic ring of diazocine; fast relaxation kinetics were found with the para-substituted strong electron-donating substituents NHR and OR in **2a** (143 min) and **2d** (69 min) in particular. The general half-life trend among the explored diazocine types **a–d** was maintained in the diazocine-centered polymers **3a–d** and

https://doi.org/10.1021/acsapm.2c00769
ACS Appl. Polym. Mater. 2022, 4, 6825–6833

Table 3. $E \rightarrow Z$ Thermal Relaxation Half-Lives $t_{1/2}$ of the Initiators 2a–d, Diazocine-Centered Polymers 3a–d and 4a–d in THF, and as Solid Films Determined from UV–Vis Spectroscopy

diazocine product	2a–d in THF (min)	3a–d in THF (min)	3a–d as the solid film (min)	4a–d in THF (min)
a	143 ± 12	113 ± 2	153 ± 17	105 ± 2
b	333 ± 11	306 ± 20	826 ± 27	447 ± 55
c	237 ± 1	173 ± 4	368 ± 19	225 ± 5
d	69 ± 0	75 ± 1	39 ± 5	50 ± 3

4a–d dissolved in THF. Thermal backisomerizations proceeded slightly faster in diazocines bound to poly(methyl acrylate) for **3b** (306 min) and **3c** (173 min) when compared to the initiators **2b** (333 min) and **2c** (237 min) but were again decelerated when bound to poly(methyl methacrylate)s **4b** (447 min) and **4c** (225 min) in relation to their poly(methyl acrylate) counterparts. The increased half-lives of **2b**/**4b** to **3b** and **2c**/**4c** to **3c** in THF are presumably caused by the vicinal substituents on the diazocine moiety. The heavy bromine atoms in **2b** and **2c** and the additional steric methyl group in the repeating unit in **4b** and **4c** restrain the conformational transitions of the diazocine heterocycle.

In the solid state, the polymers **3a–d** and **4a–d** underwent photochromism as evident from the color change between the yellow (*Z*) and red (*E*) configurations (Figure 2). Therefore, drop-casted thin films of the polymer samples were prepared to compare the photochromism (Figures S16–S19) and thermal behavior of polymer-bound (*E*)-diazocine in THF solution and in the solid state. At 25 °C, poly(methyl acrylate) is in a rubbery state (glass transition temperature, T_g: 16 °C)[50] compared to the glassy state of poly(methyl methacrylate) (T_g: 105 °C).[51] Strikingly, the solid-state samples of **4a–d** did not follow first-order kinetics since the regression functions deviate from straight lines (Figure S22, right), a common feature found in photochromes within polymer matrices below their T_g.[52−55] Based on the temperature-dependent Williams–Landel–Ferry model for relaxation rates in amorphous polymers,[56] the low chain segmental mobility in poly(methyl methacrylate) enforces a different environment on each photochromic unit, thereby causing thermal relaxation rates to depend on individual conditions and to be nonlinear.[57−59]

Solid thin films of diazocine types **b** and **c** exhibited large differences in half-lives when compared to the dissolved samples. In solid-state poly(methyl acrylate)s (826 min in **3b** and 368 min in **3c**), thermal relaxation is decelerated more than twice as much compared to the solutions in THF (306 min in **3b**, 173 min in **3c**). Due to the multiexponential decay of (*E*)-diazocine in solid-state poly(methyl methacrylate), thermal half-lives of **4b** and **4c** in solid thin films cannot be obtained and compared with the relaxation in THF (447 min in **4b**, 225 min in **4c**) via first-order kinetics (Figure 3). Nonetheless, the juxtaposition of reaction kinetics in the solid

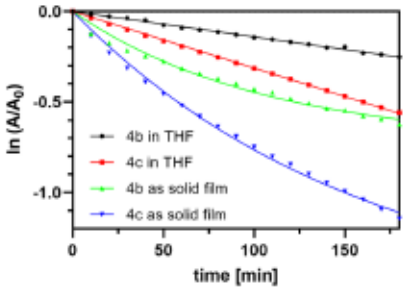

Figure 3. First-order thermal relaxation kinetic plot of poly(methyl methacrylate)s **4b** and **4c** in THF (black and red) and as solid thin films (green and blue) from the PSS (405 nm) at $\lambda_{max}(E)$. Unlike the polymer solutions, the solid-state samples did not follow first-order kinetics as the regressions deviate from straight lines.

state and solution in Figure 3 reveals a notable acceleration of the $E \rightarrow Z$ isomerization reaction from the solution to the solid state in both **4b** (black vs green dots) and **4c** (red vs blue dots). Similar to the pronounced solvent effect during the $E \rightarrow Z$ photoisomerization of parent diazocine where hexane extended the lifetime of the excited intermediate structure of the (*E*) form through steric hindrance,[60,61] THF presumably induces a stabilizing effect on the (*E*) isomer and thus lowers reaction rates for **4b** and **4c** than in the solid state. The contrary relaxation behavior of poly(methyl acrylate)s **3b** and **3c** in relation to poly(methyl methacrylate)s **4b** and **4c** with regard to the transition from solution to the solid state can be explained by the influence of the polymer matrix on the diazocine unit. Poly(methyl acrylate) acts as a viscous liquid that cools the excited states of (*E*)-diazocine through molecular vibration.[62,63] Poly(methyl methacrylate), on the other hand, is more rigid and provides less free volume for photochromic transitions.[64,65] The $Z \rightarrow E$ irradiation of diazocine units imposes a high internal strain on the stiff polymer matrix that needs to be resolved thermodynamically by diazocine backisomerization.[54,58,59] In the case of the diazocine types **a** and **d**, thermal relaxation is predominantly controlled by the strong electronic effects of the substituents,[66] so that solvents and polymer matrices exert less influence on the kinetic reaction rates.

CONCLUSIONS

Three structurally different difunctional initiators and a monofunctional diazocine-based initiator were prepared and utilized in the ATRP of methyl acrylate and methyl

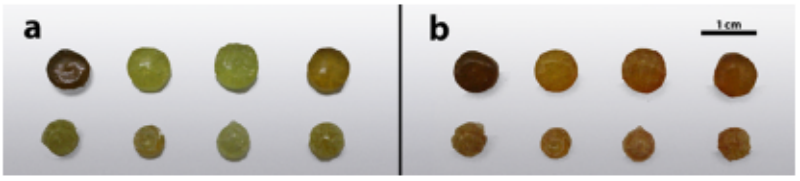

Figure 2. Polymer samples after light irradiation for 2 min at (a) 525 nm and (b) 405 nm wavelength (each from top left to right **3a–d** and from bottom left to right **4a–d**).

https://doi.org/10.1021/acsapm.2c00769
ACS Appl. Polym. Mater. 2022, 4, 6825–6833

methacrylate under generalized and optimized ARGET conditions. The initiators were less reactive than EBiB so high initial amounts of the catalyst and reducing agent were required to obtain poly(methyl acrylate) in high conversions and low dispersity. However, when the reaction was irradiated with violet light, ARGET ATRP of methyl acrylate with the α-bromoamide initiator was severely hampered or terminated. Therefore, with regard to the effectivity of ATRP initiators, α-bromoamides are less suitable than the corresponding α-bromoesters due to their potential reactivity and involvement in side reactions. To date, the influence of the initiator structure on ATRP is only poorly studied,[17,41] even though functional ATRP initiators are widely used for the preparation of advanced materials.[15,67,68] The final diazocine-centered poly(methyl acrylate)s and methacrylates were photochromic in both solution and solid states, effectively switching their colors between yellow and red by light irradiation at 405 and 525 nm wavelengths. The $E \rightarrow Z$ thermal relaxation kinetics of the diazocine-centered polymeric chains depended greatly on the presence of the solvent and on the polymer matrix (glassy/rubbery) in the solid state, especially when strong electronic effects from substituents on the diazocine aromatic ring were absent. Our diazocine-containing elastomers qualify as potential candidates for the use in optical waveguides,[32] data storage,[33,34] and photopatterning.[10,35,36]

■ ASSOCIATED CONTENT

Supporting Information

The Supporting Information is available free of charge at https://pubs.acs.org/doi/10.1021/acsapm.2c00769.

Full experimental details, including synthetic procedures and characterization details (PDF)

■ AUTHOR INFORMATION

Corresponding Author

Anne Staubitz – *Institute for Organic and Analytical Chemistry, University of Bremen, D-28359 Bremen, Germany; MAPEX Center for Materials and Processes, University of Bremen, D-28359 Bremen, Germany;* orcid.org/0000-0002-9040-3297; Email: staubitz@uni-bremen.de

Authors

Shuo Li – *Institute for Organic and Analytical Chemistry, University of Bremen, D-28359 Bremen, Germany; MAPEX Center for Materials and Processes, University of Bremen, D-28359 Bremen, Germany;* orcid.org/0000-0002-6015-5659

Ruchira Colaco – *Institute for Organic and Analytical Chemistry, University of Bremen, D-28359 Bremen, Germany; MAPEX Center for Materials and Processes, University of Bremen, D-28359 Bremen, Germany;* orcid.org/0000-0002-5317-9273

Complete contact information is available at: https://pubs.acs.org/10.1021/acsapm.2c00769

Notes

The authors declare no competing financial interest.

■ ACKNOWLEDGMENTS

This work has been supported by the German Research Foundation (DFG) within the Collaborative Research Center 677 "Function by Switching" (subproject C14) (S.L. and A.S.). R.C. and A.S. also thank the German Research Foundation (DFG) for support for the project STA1195/6-1 within SPP 2206: 40200687 (KOMMMA). This research has been supported by the Institutional Strategy of the University of Bremen, funded by the German Excellence Initiative.

■ REFERENCES

(1) Goulet-Hanssens, A.; Eisenreich, F.; Hecht, S. Enlightening Materials with Photoswitches. *Adv. Mater.* **2020**, *32*, No. 1905966.

(2) Dattler, D.; Fuks, G.; Heiser, J.; Moulin, E.; Perrot, A.; Yao, X.; Giuseppone, N. Design of Collective Motions from Synthetic Molecular Switches, Rotors, and Motors. *Chem. Rev.* **2020**, *120*, 310−433.

(3) Wang, L.; Li, Q. Photochromism into Nanosystems: Towards Lighting up the Future Nanoworld. *Chem. Soc. Rev.* **2018**, *47*, 1044−1097.

(4) Siewertsen, R.; Neumann, H.; Buchheim-Stehn, B.; Herges, R.; Näther, C.; Renth, F.; Temps, F. Highly Efficient Reversible Z-E Photoisomerization of a Bridged Azobenzene with Visible Light through Resolved S1(Nπ*) Absorption Bands. *J. Am. Chem. Soc.* **2009**, *131*, 15594−15595.

(5) Li, S.; Eleya, N.; Staubitz, A. Cross-Coupling Strategy for the Synthesis of Diazocines. *Org. Lett.* **2020**, *22*, 1624−1627.

(6) Maier, M. S.; Hüll, K.; Reynders, M.; Matsuura, B. S.; Leippe, P.; Ko, T.; Schäffer, L.; Trauner, D. Oxidative Approach Enables Efficient Access to Cyclic Azobenzenes. *J. Am. Chem. Soc.* **2019**, *141*, 17295−17304.

(7) Hammerich, M.; Schütt, C.; Stähler, C.; Lentes, P.; Röhricht, F.; Höppner, R.; Herges, R. Heterodiazocines: Synthesis and Photochromic Properties, Trans to Cis Switching within the Bio-Optical Window. *J. Am. Chem. Soc.* **2016**, *138*, 13111−13114.

(8) Lentes, P.; Stadler, E.; Röhricht, F.; Brahms, A.; Gröbner, J.; Sönnichsen, F. D.; Gescheidt, G.; Herges, R. Nitrogen Bridged Diazocines: Photochromes Switching within the Near-Infrared Region with High Quantum Yields in Organic Solvents and in Water. *J. Am. Chem. Soc.* **2019**, *141*, 13592−13600.

(9) Moormann, W.; Tellkamp, T.; Stadler, E.; Röhricht, F.; Näther, C.; Puttreddy, R.; Rissanen, K.; Gescheidt, G.; Herges, R. Efficient Conversion of Light to Chemical Energy: Directional, Chiral Photoswitches with Very High Quantum Yields. *Angew. Chem., Int. Ed.* **2020**, *59*, 15081−15086.

(10) Li, S.; Han, G.; Zhang, W. Concise Synthesis of Photoresponsive Polyureas Containing Bridged Azobenzenes as Visible-Light-Driven Actuators and Reversible Photopatterning. *Macromolecules* **2018**, *51*, 4290−4297.

(11) Burk, M. H.; Schröder, S.; Moormann, W.; Langbehn, D.; Strunskus, T.; Rehders, S.; Herges, R.; Faupel, F. Fabrication of Diazocine-Based Photochromic Organic Thin Films via Initiated Chemical Vapor Deposition. *Macromolecules* **2020**, *53*, 1164−1170.

(12) Samanta, S.; Qin, C.; Lough, A. J.; Woolley, G. A. Bidirectional Photocontrol of Peptide Conformation with a Bridged Azobenzene Derivative. *Angew. Chem., Int. Ed.* **2012**, *51*, 6452−6455.

(13) Wang, G. A.; Xu, J.; Traynor, S. M.; Chen, H.; Eljabu, F.; Wu, X.; Yan, H.; Li, F. DNA Balance for Native Characterization of Chemically Modified DNA. *J. Am. Chem. Soc.* **2021**, *143*, 13655−13663.

(14) Berry, J.; Lindhorst, T. K.; Despras, G. Sulfur and Azobenzenes, a Profitable Liaison: Straightforward Synthesis of Photoswitchable Thioglycosides with Tunable Properties. *Chem.—Eur. J.* **2022**, *28*, No. e202200354.

(15) Matyjaszewski, K. Advanced Materials by Atom Transfer Radical Polymerization. *Adv. Mater.* **2018**, *30*, No. 1706441.

(16) Ribelli, T. G.; Lorandi, F.; Fantin, M.; Matyjaszewski, K. Atom Transfer Radical Polymerization: Billion Times More Active Catalysts and New Initiation Systems. *Macromol. Rapid Commun.* **2019**, *40*, No. 1800616.

(17) Fang, C.; Fantin, M.; Pan, X.; De Fiebre, K.; Coote, M. L.; Matyjaszewski, K.; Liu, P. Mechanistically Guided Predictive Models for Ligand and Initiator Effects in Copper-Catalyzed Atom Transfer Radical Polymerization (Cu-ATRP). *J. Am. Chem. Soc.* **2019**, *141*, 7486−7497.
(18) Isse, A. A.; Gennaro, A.; Lin, C. Y.; Hodgson, J. L.; Coote, M. L.; Guliashvili, T. Mechanism of Carbon-Halogen Bond Reductive Cleavage in Activated Alkyl Halide Initiators Relevant to Living Radical Polymerization: Theoretical and Experimental Study. *J. Am. Chem. Soc.* **2011**, *133*, 6254−6264.
(19) Jakubowski, W.; Matyjaszewski, K. Activators Regenerated by Electron Transfer for Atom-Transfer Radical Polymerization of (Meth)Acrylates and Related Block Copolymers. *Angew. Chem., Int. Ed.* **2006**, *45*, 4482−4486.
(20) Anastasaki, A.; Nikolaou, V.; Nurumbetov, G.; Wilson, P.; Kempe, K.; Quinn, J. F.; Davis, T. P.; Whittaker, M. R.; Haddleton, D. M. Cu(0)-Mediated Living Radical Polymerization: A Versatile Tool for Materials Synthesis. *Chem. Rev.* **2016**, *116*, 835−877.
(21) Rosen, B. M.; Percec, V. Single-Electron Transfer and Single-Electron Transfer Degenerative Chain Transfer Living Radical Polymerization. *Chem. Rev.* **2009**, *109*, 5069−5119.
(22) Konkolewicz, D.; Wang, Y.; Krys, P.; Zhong, M.; Isse, A. A.; Gennaro, A.; Matyjaszewski, K. SARA ATRP or SET-LRP. End of Controversy? *Polym. Chem.* **2014**, *5*, 4396−4417.
(23) Chan, N.; Cunningham, M. F.; Hutchinson, R. A. Copper Mediated Controlled Radical Polymerization of Methyl Acrylate in the Presence of Ascorbic Acid in a Continuous Tubular Reactor. *Polym. Chem.* **2012**, *3*, 1322−1333.
(24) Wang, Y. ATRP of Methyl Acrylate by Continuous Feeding of Activators Giving Polymers with Predictable End-Group Fidelity. *Polymers* **2019**, *11*, No. 1238.
(25) Yu, Y. H.; Liu, X. H.; Jia, D.; Cheng, B. W.; Zhang, F. J.; Chen, P.; Xie, S. CuBr2/Me6TREN-Mediated Living Radical Polymerization of Methyl Methacrylate at Ambient Temperature. *Polymer* **2013**, *54*, 148−154.
(26) Frick, E.; Anastasaki, A.; Haddleton, D. M.; Barner-Kowollik, C. Enlightening the Mechanism of Copper Mediated PhotoRDRP via High-Resolution Mass Spectrometry. *J. Am. Chem. Soc.* **2015**, *137*, 6889−6896.
(27) Anastasaki, A.; Nikolaou, V.; Simula, A.; Godfrey, J.; Li, M.; Nurumbetov, G.; Wilson, P.; Haddleton, D. M. Expanding the Scope of the Photoinduced Living Radical Polymerization of Acrylates in the Presence of CuBr2 and Me6-Tren. *Macromolecules* **2014**, *47*, 3852−3859.
(28) Anastasaki, A.; Nikolaou, V.; Zhang, Q.; Burns, J.; Samanta, S. R.; Waldron, C.; Haddleton, A. J.; McHale, R.; Fox, D.; Percec, V.; Wilson, P.; Haddleton, D. M. Copper(II)/Tertiary Amine Synergy in Photoinduced Living Radical Polymerization: Accelerated Synthesis of ω-Functional and α,ω-Heterofunctional Poly(Acrylates. *J. Am. Chem. Soc.* **2014**, *136*, 1141−1149.
(29) Ribelli, T. G.; Konkolewicz, D.; Bernhard, S.; Matyjaszewski, K. How Are Radicals (Re)Generated in Photochemical ATRP? *J. Am. Chem. Soc.* **2014**, *136*, 13303−13312.
(30) Dadashi-Silab, S.; Lee, I. H.; Anastasaki, A.; Lorandi, F.; Narupai, B.; Dolinski, N. D.; Allegrezza, M. L.; Fantin, M.; Konkolewicz, D.; Hawker, C. J.; Matyjaszewski, K. Investigating Temporal Control in Photoinduced Atom Transfer Radical Polymerization. *Macromolecules* **2020**, *53*, 5280−5288.
(31) De Martino, S.; Mauro, F.; Netti, P. A. Photonic Applications of Azobenzene Molecules Embedded in Amorphous Polymer. *Riv. Nuovo Cimento* **2020**, *43*, 599−629.
(32) Liu, Z.; Srisanit, N.; Ke, X.; Wu, P.; Song, S.; Yang, J. J.; Wang, M. R. An Azobenzene Functionalized Polymer for Laser Direct Writing Waveguide Fabrication. *Opt. Commun.* **2007**, *273*, 94−98.
(33) Hvilsted, S.; Sánchez, C.; Alcalá, R. The Volume Holographic Optical Storage Potential in Azobenzene Containing Polymers. *J. Mater. Chem.* **2009**, *19*, 6641−6648.
(34) Brown, D.; Natansohn, A.; Rochon, P. Azo Polymers for Reversible Optical Storage. 5. Orientation and Dipolar Interactions of Azobenzene Side Groups in Copolymers and Blends Containing Methyl Methacrylate Structural Units. *Macromolecules* **1995**, *28*, 6116−6123.
(35) Burk, M. H.; Langbehn, D.; Hernández Rodríguez, G.; Reichstein, W.; Drewes, J.; Schröder, S.; Rehders, S.; Strunskus, T.; Herges, R.; Faupel, F. Synthesis and Investigation of a Photoswitchable Copolymer Deposited via Initiated Chemical Vapor Deposition for Application in Organic Smart Surfaces. *ACS Appl. Polym. Mater.* **2021**, *3*, 1445−1456.
(36) Viswanathan, N. K.; Kim, D. Y.; Bian, S.; Williams, J.; Liu, W.; Li, L.; Samuelson, L.; Kumar, J.; Tripathy, S. K. Surface Relief Structures on Azo Polymer Films. *J. Mater. Chem.* **1999**, *9*, 1941−1955.
(37) Ciampolini, M.; Nardi, N. Five-Coordinated High-Spin Complexes of Bivalent Cobalt, Nickel, and Copper with Tris(2-Dimethylaminoethyl)Amine. *Inorg. Chem.* **1966**, *5*, 41−44.
(38) Nyström, F.; Soeriyadi, A. H.; Boyer, C.; Zetterlund, P. B.; Whittaker, M. R. End-Group Fidelity of Copper(0)-Meditated Radical Polymerization at High Monomer Conversion: An ESI-MS Investigation. *J. Polym. Sci., Part A: Polym. Chem.* **2011**, *49*, 5313−5321.
(39) Min, K.; Gao, H.; Matyjaszewski, K. Preparation of Homopolymers and Block Copolymers in Miniemulsion by ATRP Using Activators Generated by Electron Transfer (AGET. *J. Am. Chem. Soc.* **2005**, *127*, 3825−3830.
(40) Anastasaki, A.; Waldron, C.; Wilson, P.; McHale, R.; Haddleton, D. M. The Importance of Ligand Reactions in Cu(0)-Mediated Living Radical Polymerisation of Acrylates. *Polym. Chem.* **2013**, *4*, 2672−2675.
(41) Tang, W.; Kwak, Y.; Braunecker, W.; Tsarevsky, N. V.; Coote, M. L.; Matyjaszewski, K. Understanding Atom Transfer Radical Polymerization: Effect of Ligand and Initiator Structures on the Equilibrium Constants. *J. Am. Chem. Soc.* **2008**, *130*, 10702−10713.
(42) Allan, L. E. N.; Perry, M. R.; Shaver, M. P. Organometallic Mediated Radical Polymerization. *Prog. Polym. Sci.* **2012**, *37*, 127−156.
(43) Ribelli, T. G.; Augustine, K. F.; Fantin, M.; Krys, P.; Poli, R.; Matyjaszewski, K. Disproportionation or Combination? The Termination of Acrylate Radicals in ATRP. *Macromolecules* **2017**, *50*, 7920−7929.
(44) Nardi, M.; Blasco, E.; Barner-Kowollik, C. Wavelength-Resolved PhotoATRP. *J. Am. Chem. Soc.* **2022**, *144*, 1094−1098.
(45) Fantinati, A.; Zanirato, V.; Marchetti, P.; Trapella, C. The Fascinating Chemistry of α-Haloamides. *ChemistryOpen* **2020**, *9*, 100−170.
(46) Yamane, Y.; Miyazaki, K.; Nishikata, T. Different Behaviors of a Cu Catalyst in Amine Solvents: Controlling N and O Reactivities of Amide. *ACS Catal.* **2016**, *6*, 7418−7425.
(47) Kainz, Q. M.; Matier, C. D.; Bartoszewicz, A.; Zultanski, S. L.; Peters, J. C.; Fu, G. C. Asymmetric Copper-Catalyzed C-N Cross-Couplings Induced by Visible Light. *Science* **2016**, *351*, 681−684.
(48) Min, K.; Gao, H.; Matyjaszewski, K. Use of Ascorbic Acid as Reducing Agent for Synthesis of Well-Defined Polymers by ARGET ATRP. *Macromolecules* **2007**, *40*, 1789−1791.
(49) Jeon, H. J.; Youk, J. H.; Cho, K. S.; Ahn, S. H.; Choi, J. H. Synthesis of High Molecular Weight 3-Arm Star PMMA by ARGET ATRP. *Macromol. Res.* **2009**, *17*, 240−244.
(50) Maiti, P.; Dikshit, A. K.; Nandi, A. K. Glass-Transition Temperature of Poly(Vinylidene Fluoride)-Poly(Methyl Acrylate) Blends: Influence of Aging and Chain Structure. *J. Appl. Polym. Sci.* **2001**, *79*, 1541−1548.
(51) Olabisi, O.; Simha, R. Pressure-Volume-Temperature Studies of Amorphous and Crystallizable Polymers. I. Experimental. *Macromolecules* **1974**, *8*, 206−210.
(52) Paik, C. S.; Morawetz, H. Photochemical and Thermal Isomerization of Azoaromatic Residues in the Side Chains and the Backbone of Polymers in Bulk. *Macromolecules* **1972**, *5*, 171−177.

https://doi.org/10.1021/acsapm.2c00769
ACS Appl. Polym. Mater. 2022, 4, 6825−6833

(53) Barrett, C.; Natansohn, A.; Rochon, P. Cis-Trans Thermal Isomerization Rates of Bound and Doped Azobenzenes in a Series of Polymers. *Chem. Mater.* **1995**, *7*, 899−903.
(54) Munakata, Y.; Tsutsumi, T.; Saito, S. The Matrix Effect on the Thermal Reactions of Spirooxazine in Polymer Matrices. *Polym. J.* **1990**, *22*, 843−848.
(55) Mita, I.; Horie, K.; Hirao, K. Photochemistry in Polymer Solids. 9. Photoisomerization of Azobenzene in a Polycarbonate Film. *Macromolecules* **1989**, *22*, 558−563.
(56) Williams, M. L.; Landel, R. F.; Ferry, J. D. The Temperature Dependence of Relaxation Mechanisms in Amorphous Polymers and Other Glass-Forming Liquids. *J. Am. Chem. Soc.* **1955**, *77*, 3701−3707.
(57) Eisenbach, C. D. Effect of Polymer Matrix on the Cis-Trans Isomerization of Azobenzene Residues in Bulk Polymers. *Makromol. Chem.* **1978**, *179*, 2489−2506.
(58) Such, G.; Evans, R. A.; Yee, L. H.; Davis, T. P. Factors Influencing Photochromism of Spiro-Compounds Within Polymeric Matrices. *J. Macromol. Sci., Polym. Rev.* **2003**, *43*, 547−579.
(59) Eisenbach, C. D. Relation between Photochromism of Chromophores and Free Volume Theory in Bulk Polymers. *Ber. Bunsen-Ges. Phys. Chem.* **1980**, *84*, 680−690.
(60) Carstensen, N. O. QM/MM Surface-Hopping Dynamics of a Bridged Azobenzene Derivative. *Phys. Chem. Chem. Phys.* **2013**, *15*, 15017−15026.
(61) Siewertsen, R.; Schönborn, J. B.; Hartke, B.; Renth, F.; Temps, F. Superior Z → e and e → Z Photoswitching Dynamics of Dihydrodibenzodiazocine, a Bridged Azobenzene, by S1($N\pi^*$) Excitation at λ = 387 and 490 Nm. *Phys. Chem. Chem. Phys.* **2011**, *13*, 1054−1063.
(62) Hamm, P.; Ohline, S. M.; Zinth, W. Vibrational Cooling after Ultrafast Photoisomerization of Azobenzene Measured by Femtosecond Infrared Spectroscopy. *J. Chem. Phys.* **1997**, *106*, 519−529.
(63) Tamai, N.; Miyasaka, H. Ultrafast Dynamics of Photochromic Systems. *Chem. Rev.* **2000**, *100*, 1875−1890.
(64) Shen, Y. Q.; Rau, H. The Environmentally Controlled Photoisomerization of Probe Molecules Containing Azobenzene Moieties in Solid Poly(Methyl Methacrylate). *Makromol. Chem.* **1991**, *192*, 945−957.
(65) Barrett, C.; Natansohn, A.; Rochen, P. Thermal Cis-Trans Isomerization Rates of Azobenzenes Bound in the Side Chain of Some Copolymers and Blends. *Macromolecules* **1994**, *27*, 4781−4786.
(66) Bandara, H. M. D.; Burdette, S. C. Photoisomerization in Different Classes of Azobenzene. *Chem. Soc. Rev.* **2012**, *41*, 1809−1825.
(67) Lutz, J. F.; Lehn, J. M.; Meijer, E. W.; Matyjaszewski, K. From Precision Polymers to Complex Materials and Systems. *Nat. Rev. Mater.* **2016**, *1*, No. 16024.
(68) Colaco, R.; Shree, S.; Siebert, L.; Appiah, C.; Dowds, M.; Schultzke, S.; Adelung, R.; Staubitz, A. Mechanochromic Microfibers Stabilized by Polymer Blending. *ACS Appl. Polym. Mater.* **2020**, *2*, 2055−2062.

Recommended by ACS

Miniemulsion SI-ATRP by Interfacial and Ion-Pair Catalysis for the Synthesis of Nanoparticle Brushes
Rongguan Yin, Krzysztof Matyjaszewski, *et al.*
JULY 22, 2022
MACROMOLECULES
READ

Red-Light-Induced, Copper-Catalyzed Atom Transfer Radical Polymerization
Sajjad Dadashi-Silab, Krzysztof Matyjaszewski, *et al.*
FEBRUARY 28, 2022
ACS MACRO LETTERS
READ

Ultrafast Visible-Light-Induced ATRP in Aqueous Media with Carbon Quantum Dots as the Catalyst and Its Application for 3D Printing
Liang Qiao, Xinchang Pang, *et al.*
MAY 26, 2022
JOURNAL OF THE AMERICAN CHEMICAL SOCIETY
READ

PET-RAFT Enables Efficient and Automated Multiblock Star Synthesis
Henry Foster, Robert Chapman, *et al.*
JULY 06, 2022
MACROMOLECULES
READ

Get More Suggestions >

https://doi.org/10.1021/acsapm.2c00769
ACS Appl. Polym. Mater. 2022, 4, 6825−6833

3.3 Synthesis and Characterization of Polymers with Diazocine Repeating Units in the Main Chain

3.3.1 Part A

Facile Synthesis of Light-Switchable Polymers with Diazocine Units in the Main Chain

Shuo Li, Katrin Bamberg, Yuzhou Lu, Frank D. Sönnichsen and Anne Staubitz, *Polymers* **2023**, *15*, 1306.

DOI: 10.3390/polym15051306

Published by MDPI. The supporting information includes all used materials and methods, experimental procedures, analytical data, images of spectra and is available free of charge online.

Abstract

Unlike azobenzene, the photoisomerization behavior of its ethylene-bridged derivative, diazo-cine, has hardly been explored in synthetic polymers. In this communication, linear photore-sponsive poly(thioether)s containing diazocine moieties in the polymer backbone with different spacer lengths are reported. They were synthesized in thiol-ene polyadditions between a diazocine diacrylate and 1,6-hexanedithiol. The diazocine units could be reversibly photoswitched between the (*Z*) and (*E*) configurations, with light at 405 nm and 525 nm, respectively. Based on the chemical structure of the diazocine diacrylates, the resulting polymer chains differed in their thermal relaxation kinetics and molecular weights (7.4 vs. 43 kDa) but maintained a clearly visible photoswitchability in the solid state. Gel permeation chromatography (GPC) measurements indicated a hydrodynamic size expansion of the individual polymer coils as a result of the (*Z*)→(*E*) pincer-like diazocine switching motion on a molecular scale. Our work establishes diazocine as an elongating actuator that can be used in macromolecular systems and smart materials.

Scientific Contribution (including Part B)

After initial drafting and planning by Prof. Dr. Anne Staubitz, this project was planned, organized and conducted by me. The synthesis, purification and characterization of the compounds were carried out by me. The manuscript and the supporting information were written by me. Katrin Bamberg and Prof. Dr. Frank D. Sönnichsen measured and analyzed the ^{1}H DOSY NMR spectra. Yuzhou Lu supported me with the synthesis, purification and characterization of polymer **P2** during his F-Praktikum at the University of Bremen under my supervision. Prof. Dr. Anne Staubitz as the principal investigator was responsible for the funding and edited the article. All authors have read and edited the article and agreed to the published version of the manuscript. In order to ensure the reproducibility of the GPC data for polymer **P2**, Jasmin Richter helped with the execution of the experiment under my guidance.

Table 3.6. Contribution of the candidate in % of the total workload (up to 100% for each of the following categories)

Experimental concept and design	80%
Experimental work and/or acquisition of (experimental) data	70%
Data analysis and interpretation	70%
Preparation of Figures and Tables	80%
Drafting of the manuscript	80%

polymers

MDPI

Communication

Facile Synthesis of Light-Switchable Polymers with Diazocine Units in the Main Chain

Shuo Li [1,2], Katrin Bamberg [3], Yuzhou Lu [1,2], Frank D. Sönnichsen [3] and Anne Staubitz [1,2,*]

[1] University of Bremen, Institute for Organic and Analytical Chemistry, Leobener Strasse 7, D-28359 Bremen, Germany
[2] University of Bremen, MAPEX Center for Materials and Processes, Bibliothekstraße 1, D-28359 Bremen, Germany
[3] Kiel University, Otto-Diels-Institute for Organic Chemistry, Otto-Hahn-Platz 4, D-24098 Kiel, Germany
* Correspondence: staubitz@uni-bremen.de

Abstract: Unlike azobenzene, the photoisomerization behavior of its ethylene-bridged derivative, diazocine, has hardly been explored in synthetic polymers. In this communication, linear photoresponsive poly(thioether)s containing diazocine moieties in the polymer backbone with different spacer lengths are reported. They were synthesized in thiol-ene polyadditions between a diazocine diacrylate and 1,6-hexanedithiol. The diazocine units could be reversibly photoswitched between the (*Z*)- and (*E*)-configurations with light at 405 nm and 525 nm, respectively. Based on the chemical structure of the diazocine diacrylates, the resulting polymer chains differed in their thermal relaxation kinetics and molecular weights (7.4 vs. 43 kDa) but maintained a clearly visible photoswitchability in the solid state. Gel permeation chromatography (GPC) measurements indicated a hydrodynamic size expansion of the individual polymer coils as a result of the $Z \rightarrow E$ pincer-like diazocine switching motion on a molecular scale. Our work establishes diazocine as an elongating actuator that can be used in macromolecular systems and smart materials.

Keywords: photoswitch; thiol-ene; main-chain diazocine polymer; photochromism; hydrodynamic size expansion; DOSY NMR

check for updates

Citation: Li, S.; Bamberg, K.; Lu, Y.; Sönnichsen, F.D.; Staubitz, A. Facile Synthesis of Light-Switchable Polymers with Diazocine Units in the Main Chain. *Polymers* **2023**, *15*, 1306. https://doi.org/10.3390/polym15051306

Academic Editor: Ivan Gitsov

Received: 25 January 2023
Revised: 26 February 2023
Accepted: 1 March 2023
Published: 5 March 2023

Copyright: © 2023 by the authors. Licensee MDPI, Basel, Switzerland. This article is an open access article distributed under the terms and conditions of the Creative Commons Attribution (CC BY) license (https://creativecommons.org/licenses/by/4.0/).

1. Introduction

Photoswitching of molecular systems is a powerful tool to modulate their chemical and physical properties with spatiotemporal control [1]. The most prominent photoswitch, azobenzene, acts as a photochromic molecule with two interconvertible configurations, the planar C_{2h}-symmetrical (*E*) isomer and the bent (*Z*) isomer in which the phenyl rings are twisted by 30° [2]. Azobenzene and its derivatives have been applied in many advanced materials [3,4], molecular machines [5] and biological systems [6]. The photoisomerization of synthetic polymers that contain azobenzene groups in the main chain leads to conformational changes of the polymer backbone, often resulting in the contraction and expansion of the polymer chains [7,8]. Particularly in polymers with semi-rigid backbones, the collective motion of azobenzene groups can induce reversible helical folding [9–11], show aggregation behavior for an amplified photoresponse and alter the electrochemical conductivity in π-conjugated chains [12]. Recent advances in main-chain type azobenzene-containing polymers also focused on the photocontrol of semi-crystalline and liquid crystalline properties [13–15]. The resulting photoinduced phase transitions enabled reversible photomelting [15,16], photomechanical actuation of thin films [17–20], as well as surface relief gratings after polarized light illumination with interference patterns [21,22].

Among azobenzene modifications, so-called diazocines enjoy special attention because the relative thermodynamical stability of their photoswitchable isomers is reversed compared to the parent azobenzene: the bent (*Z*) isomer is thermodynamically favored,

Polymers 2023, *15*, 1306

Among azobenzene modifications, so-called diazocines enjoy special attention because the relative thermodynamical stability of their photoswitchable isomers is reversed compared to the parent azobenzene: the bent (*Z*) isomer is thermodynamically favored, and the elongated (*E*) form is metastable [23]. Synthetic procedures to obtain functionalized diazocines include the reduction of 2,2′-dinitrobibenzyl [24], oxidation of 2,2′-diaminobibenzyl [25] and the cascade amidation reaction of 2,2′-dihalobibenzyl compounds via Boc-protected diazocines [26]. The photoconversion of the yellow (*Z*) to the red (*E*) isomer occurs at an irradiation wavelength of 405 nm, resulting in an energetic increase of 37.08 kJ/mol (Scheme 1) [27]. The photochromism of diazocine is reversible with green light with a wavelength of 525 nm or via thermal relaxation with a half-life in hexane of 4.5 h at 28.5 °C [23]. According to the X-ray crystal structures of the 3,3′-diaminosubstituted diazocine provided by Sell and co-workers, the amino nitrogen atoms were further apart upon switching from *Z* (8 Å) to *E* (11 Å) configuration [28]. This molecular pincer motion was exploited to gain photocontrol over macromolecular systems such as peptides [29] and oligonucleotides [30]. Li and co-workers prepared diazocine-inserted polyurea in which photoisomerization triggered an amorphous-to-crystalline transition of the material [31]. Photomechanical thin films were produced; however, probably due to complex intermolecular interactions, no thermal phase transitions were detected. Although the photoinduced shrinking of polymers with integrated azobenzene moieties in the main chain has been studied with various kinds of polymers [18,32,33], the potential of size switching of linear polymers containing multiple diazocine groups has not been reported yet.

Scheme 1. Photochemical isomerization reaction between (*Z*)- and (*E*)-diazocine.

In this communication, we explore the possibilities of photoinduced hydrodynamic size expansion by insertion of multiple diazocine groups into the polymer backbone as a result of their collective pincer-type switching motions. Based on our synthetic cross-coupling strategy towards substituted diazocines, we recently generated diazocines as alkyl halide initiators for their incorporation into polymeric chains via atom transfer radical polymerization [34]. Herein, we focus on diazocine diacrylates as monomers in thiol-ene polyadditions to form photochromic units in the polymer main chain with different alkyl spacer lengths. In contrast to the previously reported polyurea where the microstructure is stabilized by hydrogen bonds [31], poly(thioether)s create much weaker interactive forces and hydrogen bonds are absent. Until now, the properties and possibilities of diazocine in synthetic polymers have hardly been explored. We report on the synthesis, photochromism, thermal analysis and hydrodynamic size-switching of diazocine-containing poly(thioether)s. The expected photoinduced size expansions of the polymer coils were quantified using gel permeation chromatography (GPC) and ^{1}H diffusion-ordered nuclear magnetic resonance spectroscopy (^{1}H DOSY NMR).

2. Materials and Methods

2.1. Materials

Syntheses under Schlenk conditions or in a glovebox (Pure LabHE from Inert, Amesbury, MA, USA) were performed with nitrogen as the protection gas. All glassware was dried in an oven at 200 °C for at least 2 h prior to use. Syringes that were used to transfer anhydrous solvents or reagents were purged with nitrogen three times. Microwave vials were used as sealed tubes and equipped with a septum cap from Biotage (Uppsala, Sweden). CH_2Cl_2 (ACS grade, ≥99.9%), $CHCl_3$ (≥99.0–99.4%), Diethyl ether (>99.8%, contained butylated hydroxytoluene), ethyl acetate (ACS grade, >99.5%) and toluene (ACS grade, >99.7%) were purchased from Sigma-Aldrich (St. Louis, MO, USA). Cyclohexane (ACS grade, >99.5%) and THF (reagent grade, >99% contained 250 ppm butylated hydroxytoluene) were purchased from Honeywell (Morristown, NJ, USA). All

solvents for purification and extraction were used as received. Solvents used for synthesis under inert conditions (CH_2Cl_2, THF, toluene) were dried using a solvent purification system (SPS) from Inert Corporation (Amesbury, MA, USA). 1,9-Nonanediol (98%, from TCI, Tokyo, Japan) and acryloyl chloride (96%, stabilized with 400 ppm phenothiazine, from Alfa Aesar, Ward Hill, MA, USA), Na_2SO_4 (ACS grade, 99.0%, from Merck, Darmstadt, Germany), NaCl (>99%, from T.H. Geyer, Renningen, Germany), $NaHCO_3$ (analytical reagent grade, from Fisher Scientific, Pittsburgh, PA, USA), NaOH (pellets, from VWR, Radnor, PA, USA), NH_4Cl (>99.7% p.a., from Roth, Karlsruhe, Germany), pyridine (99.5%, from Grüssing, Filsum, Germany) and thionyl chloride (99.7%, from Fisher Scientific, Pittsburgh, PA, USA) were used as received. 1,6-Hexanedithiol (HDT, 97+%, from Apollo, Cheshire, UK), dimethylphenylphosphine (DMPP, 97%, from Alfa Aesar, Ward Hill, MA, USA), dimethylformamide (DMF, 99.8%, extra dry, from Fisher Scientific, Pittsburgh, PA, USA) and triethylamine (TEA, anhydrous, from Fluorochem, Hadfield, UK) were stored in the glovebox. Spin-coating was performed with polymer solutions (3 mg/mL) on Menzel-Gläser coverslips (Thermo Fischer Scientific, Waltham, MA, USA) (18 mm × 18 mm) at 150 rps for 1 min.

2.2. Methods

NMR spectra were recorded on a Bruker Avance Neo 600 (Bruker BioSpin, Rheinstetten, Germany) (600 MHz (^{1}H), 151 MHz (^{13}C{^{1}H})) at 298 K. ^{1}H DOSY NMR spectra were recorded on a Bruker Avance II HD 600 (Bruker BioSpin, Rheinstetten, Germany) (600 MHz (^{1}H)) at 298 K with 32 increments, 8 scans, 14 ppm spectral width, 2.5 s delay time and 130 ms diffusion delay time and analyzed with MestReNova 11.0.4 (Metrelab Research, Santiago de Compostela, Spain) and Bruker TopSpin 4.0.6 (Bruker Biospin, Rheinstetten, Germany) software. All ^{1}H NMR and ^{13}C{^{1}H} NMR spectra were referenced to the residual proton signals of the solvent (^{1}H) or the solvent itself (^{13}C{^{1}H}). The exact assignment of the peaks was performed using two-dimensional NMR spectroscopy such as ^{1}H,^{1}H-COSY; ^{1}H,^{13}C-HSQC; and ^{1}H,^{13}C-HMBC when possible. Photostationary states (PSS) of compounds **M1**, **M2**, **P1**, **P2** were determined using ^{1}H NMR spectroscopy (1 mM in for monomers **M1** and **M2**, 3 mg/mL for polymers **P1** and **P2** in THF-d_8) at 25 °C. Compound irradiations were performed directly on sample solutions in the NMR tubes with light at 405 nm or 525 nm wavelength for 2 min before the NMR spectra were recorded.

High-resolution EI mass spectra were recorded on a MAT 95XL double-focusing mass spectrometer from Finnigan MAT (Thermo Fisher Scientific, Waltham, MA, USA) at an ionization energy of 70 eV. Samples were measured using a direct or indirect inlet method with a source temperature of 200 °C. High-resolution ESI and APCI mass spectra were measured using a direct inlet method on an Impact II mass spectrometer from Bruker (Bruker Daltonics, Bremen, Germany). ESI mass spectra were recorded in the positive ion collection mode.

IR spectra were recorded on a Nicolet i510 FT-IR spectrometer from Thermo Fisher Scientific (Thermo Fisher Scientific, Waltham, MA, USA) with a diamond window in an area from 500 to 4000 cm^{-1} with a resolution of 4 cm^{-1}. All samples were measured 16 times against a background scan.

Melting points were recorded on a Büchi Melting Point M-560 (Büchi, Essen, Germany) and are reported corrected.

Thin layer chromatography (TLC) was performed using TLC Silica gel 60 F254 from Merck (Merck, Darmstadt, Germany) and compounds were visualized using exposure to UV light at a wavelength of 254 nm. Column chromatography was performed by using SiO_2 (0.040–0.063 mm, 230–400 mesh ASTM) from Merck.

Irradiation experiments were carried out using LED light sources of 405 nm central wavelength (optical power = 680 mW; intensity = 2.2 mW/cm^2) and 525 nm central wavelength (optical power = 20 W; intensity = 64 mW/cm^2) at a 2 cm distance from the object.

UV-vis absorption measurements were recorded on a Perkin Elmer UV/VIS NIR Spectrometer Lambda (PerkinElmer, Waltham, MA, USA) 900 at 298 K. Quartz cuvettes

of 10 mm optical path length were used. The absorption maxima at wavelengths λ_{max} and thermal relaxation kinetics were determined using UV-vis spectroscopy (1 mM in for monomers **M1** and **M2** in THF, 0.5 mg/mL for polymers **P1** and **P2** in THF) at 25 °C. The cuvettes and the spin-coated films were irradiated with light at 405 nm or 525 nm wavelength for 2 min before the absorption spectra were measured. The thermal relaxation kinetics were recorded three times using UV-vis spectroscopy (1 mM in for monomers **M1** and **M2** in THF, 3 mg/mL for polymers **P1** and **P2** in THF) at 25 °C. The cuvettes were irradiated with light at 405 nm wavelength for 2 min before 37 spectra were recorded in the dark in 5 min intervals. The absorption at λ_{max} (*E*) was plotted against the reaction time before the rate constant k and the half-life $t_{1/2}$ were determined via first-order reaction kinetics.

Diffusion coefficients *D* of compounds **M1**, **M2**, **P1**, **P2** were determined using ^{1}H DOSY NMR spectroscopy (1 mM for monomers **M1** and **M2** in THF-d_8, 3 mg/mL for polymers **P1** and **P2** in THF-d_8) at 25 °C under the same irradiation conditions as above. The average over the three aromatic diazocine signals and the resulting standard error were determined. Due to the fast relaxation kinetics of the (*E*)-diazocines in **M1** and **P1**, the DOSY signal intensities were corrected and normalized. For the (*Z*)-isomer, a time offset *f* was necessary to describe the hypothetical time at which I(*Z*) = 1:

$$1 - (I(Z)/I_0(Z)) = e^{-k\,(t+f)} \quad (1)$$

This time *f* was calculated with the following equation:

$$I(Z) = (\text{amount of } E \text{ at } t = 0) \times e^{-kf} = 1 \quad (2)$$

In addition to the experimental time of the DOSY, the period between irradiation and the start of the DOSY experiment must also be considered. The time of each data point of the DOSY results from the quotient of the experimental time and the number of intervals between the data points, which is successively added to the start time of the DOSY after the irradiation. The corrected and normalized intensity I′ results from the following equation:

$$I' = n \times I_0 \quad (3)$$

The normalization factor *n* was chosen so that the intensities of the first data point, both in the measured and in the corrected data set, stay identical. These corrected and normalized intensities were plotted as a function of the gradient strength *G* and fitted with the Stejskal–Tanner equation [35]:

$$I' = e^{\wedge}(-D \times 4\pi^2\gamma^2\delta^2G^2((\Delta - \delta)/2)) \times I_0 \quad (4)$$

D: diffusion coefficient in cm^2 s^{-1}, γ: gyromagnetic ratio, δ: pulse width, Δ: diffusion delay time, *G*: gradient strength. The hydrodynamic radii were determined using the Stokes–Einstein equation:

$$r = k \times T/(6\pi \times \eta \times D) \quad (5)$$

with k: Boltzmann constant, T: temperature, and *D*: diffusion coefficient. The dynamic viscosity η of THF-d_8 at 298 K was adopted from Dowds and co-workers [32]:

$$\eta = 4.84 \times 10^{-4}\ \text{Pa}\times\text{s} \quad (6)$$

Gel permeation chromatography (GPC) was performed using a PSS (polymer standard service) SECurity GPC system with a conventional calibration using polystyrene standards. The polymers were dissolved in THF (1 mg/mL) and the GPC elugrams were recorded at an elution flow rate of 1 mL/min. Molecular weights M_n and M_w were obtained from the molar mass distribution via GPC analysis using PSS WinGPC® UniChrom 8.20 (PSS GmbH, Mainz, Germany) software. Apparent molecular weights of the polymers **P1** and **P2** (1 mg/mL in THF) were calculated from molar mass distributions using GPC at 35 °C. The open vials were irradiated from above with light at 405 nm or 525 nm wavelength

with k: Boltzmann constant, T: temperature, and D: diffusion coefficient. The dynam
viscosity η of THF-d_8 at 298 K was adopted from Dowds and co-workers [32]:

$$\eta = 4.84\times10^{-4}\ \text{Pa}\times\text{s}$$

Gel permeation chromatography (GPC) was performed using a PSS (polymer stan
ard service) SECurity GPC system with a conventional calibration using polystyre
standards. The polymers were dissolved in THF (1 mg/mL) and the GPC elugrams we
recorded at an elution flow rate of 1 mL/min. Molecular weights M_n and M_w were obtain
from the molar mass distribution via GPC analysis using PSS WinGPC® UniChrom 8
(PSS GmbH, Mainz, Germany) software. Apparent molecular weights of the polymers
and **P2** (1 mg/mL in THF) were calculated from molar mass distributions using GPC at
°C. The open vials were irradiated from above with light at 405 nm or 525 nm wavelen
for 2 min and capped before the polymer solution was injected into the GPC system. T
dispersity $Đ$ was calculated from GPC data and is defined as the ratio between weig
average (M_w) and number average molar mass (M_n):

$$Đ = M_w / M_n \qquad (7)$$

Differential scanning calorimetry measurements (DSC) were performed on a Mettler
Toledo DSC3+ instrument in aluminum crucibles (100 µL) at a heating rate of 10 K/min
under N_2 with a flow rate of 20 mL/min. The first heating and cooling curves were
used. Glass transition temperatures T_g of compounds **P1** (sample weight: 6.96 mg) and
P2 (sample weight: 8.79 mg) were determined as the inflection points between onset and
endpoint temperatures of the DSC plot. The polymer-coated aluminum crucibles were
irradiated from above with light at 405 nm or 525 nm wavelength for 2 min before the DSC
plots were recorded in the dark.

2.3. Synthetic Procedures

9-Hydroxynonyl acrylate

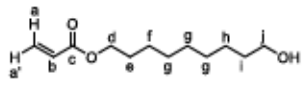

A dry, nitrogen-flushed Schlenk-flask equipped with a magnetic stirring bar and a septum was charged with 9-nonen-1-ol (3.0 g, 21.24 mmol), anhydrous THF (25 mL), and triethylamine (3.2 mL, 22.08 mmol), and the flask was cooled to 0 °C prior to the dropwise addition of acryloyl chloride (1.66 mL, 20.4 mmol) over a course of 30 min. The reaction mixture was stirred at 0 °C for 4 h before allowing the reaction mixture to warm slowly to 20 °C, at which temperature it was stirred for a further 12 h. The reaction mixture was quenched with saturated aq $NaHCO_3$ (30 mL), extracted with ethyl acetate (3 × 30 mL), washed with brine (30 mL) and dried over Na_2SO_4. After filtration, the organic phase was concentrated under reduced pressure and the crude residue was purified using silica gel column chromatography (cyclohexane/ethyl acetate 50/50) to furnish the product **9-hydroxynonyl acrylate** as a colorless oil (1.107 g, 5.17 mmol, 25%).

^{1}H NMR (601 MHz, $CDCl_3$): δ = 6.39 (dd, J = 17.3, 1.5 Hz, 1H, H-a), 6.11 (dd, J = 17.3, 10.4 Hz, 1H, H-p), 5.81 (dd, J = 10.4, 1.5 Hz, 1H, H-a'), 4.14 (t, J = 6.7 Hz, 2H, H-d), 3.63 (t, J = 6.6 Hz, 2H, H-j), 1.70 – 1.62 (m, 2H, H-e), 1.60–1.52 (m, 2H, H-i), 1.38 – 1.28 (m, 10H, H-f, H-g, H-h) ppm.

^{13}C{^{1}H} NMR (151 MHz, $CDCl_3$): δ = 166.5 (C-c), 130.6 (C-a), 128.8 (C-b), 64.8 (C-d), 63.2 (C-j), 32.9 (C-i), 29.6 (C-g), 29.4 (C-g), 29.3 (C-g), 28.7 (C-e), 26.0 (C-f), 25.8 (C-h) ppm.

HRMS (ESI) m/z for $C_{12}H_{22}O_3$ [M+H]$^+$: calcd 215.16417, found: 215.16415.

IR (ATR): $\tilde{\nu}$ = 3351 (w), 2927 (m), 2855 (m), 1723 (s), 1636 (w), 1465 (w), 1408 (m), 1295 (m), 1272 (m), 1188 (s), 1056 (w), 983 (m), 810 (m), 754 (s) cm^{-1}.

R_f: 0.30 (cyclohexane/ethyl acetate = 80/20)

Bis(9-(acryloyloxy)nonyl) (Z)-11,12-dihydrodibenzo[c,g][1,2]diazocine-2,9-dicarboxylate (M1)

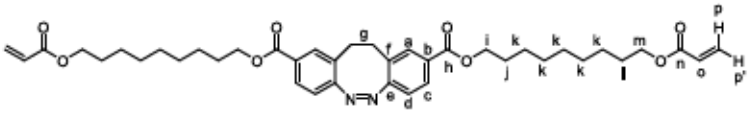

A nitrogen-flushed Schlenk-flask equipped with a magnetic stirring bar and a reflux condenser was charged with compound **1** (325 mg, 1.10 mmol, reference [29]) and thionyl chloride (3.2 mL, 44.00 mmol). The reaction mixture was stirred under nitrogen at 76 °C for 3 h before it was cooled to 20 °C. Then, low-boiling compounds were removed using vacuum distillation (35 °C, 100 mbar) and the solid residue was washed with dry DCM (3 × 5 mL) before it was stored under a nitrogen atmosphere.

In a glovebox, a sealed tube was charged with the solid residue, dry toluene (11 mL), pyridine (370 µL, 4.53 mmol) and 9-hydroxynonyl acrylate (551 mg, 2.57 mmol). The vial was capped, transferred out of the glovebox and stirred at 100 °C for 3 h. After cooling to 20 °C, the reaction mixture was quenched with water (50 mL), extracted with ethyl acetate (3 x 30 mL), washed with saturated aq NH_4Cl (30 mL) and brine (30 mL), and dried over Na_2SO_4. After filtration, the organic phase was concentrated under reduced pressure and the crude residue was purified using silica gel column chromatography (cyclohexane to cyclohexane/ethyl acetate 75/25) to furnish the product **M1** as a yellow solid (481 mg, 700 µmol, 63%).

^{1}H NMR (601 MHz, $CDCl_3$): δ = 7.79 (dd, J = 8.2, 1.7 Hz, 2H, H-c), 7.67 (d, J = 1.7 Hz, 2H, H-a), 6.88 (d, J = 8.2 Hz, 2H, H-d), 6.39 (dd, J = 17.3, 1.5 Hz, 2H, H-p), 6.11 (dd, J = 17.3,

R_f: 0.30 (cyclohexane/ethyl acetate = 80/20)

Bis(9-(acryloyloxy)nonyl) (Z)-11,12-dihydrodibenzo[*c*,*g*][1,2]diazocine-2,9-dicarboxylate (M1)

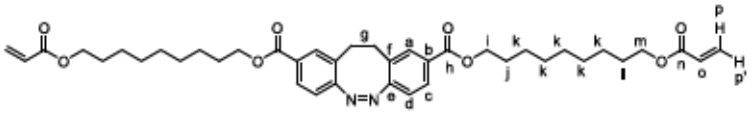

A nitrogen-flushed Schlenk-flask equipped with a magnetic stirring bar and a reflux condenser was charged with compound **1** (325 mg, 1.10 mmol, reference [26]) and thionyl chloride (3.2 mL, 44.00 mmol). The reaction mixture was stirred under nitrogen at 76 °C for 3 h before it was cooled to 20 °C. Then, low-boiling compounds were removed using vacuum distillation (55 °C, 100 mbar) and the solid residue was washed with dry DCM (2 × 5 mL) before it was stored under a nitrogen atmosphere.

vacuum distillation (55 °C, 100 mbar) and the solid residue was washed with dry DCM (2 × 5 mL) before it was stored under a nitrogen atmosphere.

In a glovebox, a sealed tube was charged with the solid residue, dry toluene (11 mL), pyridine (370 µL, 4.53 mmol) and 9-hydroxynonyl acrylate (551 mg, 2.57 mmol). The vial was capped, transferred out of the glovebox and stirred at 100 °C for 3 h. After cooling to 20 °C, the reaction mixture was quenched with water (50 mL), extracted with ethyl acetate (3 × 30 mL), washed with saturated aq NH_4Cl (30 mL) and brine (30 mL), and dried over Na_2SO_4. After filtration, the organic phase was concentrated under reduced pressure and the crude residue was purified using silica gel column chromatography (cyclohexane to cyclohexane/ethyl acetate 75/25) to furnish the product **M1** as a yellow solid (481 mg, 700 µmol, 63%).

In a glovebox, a sealed tube was charged with the solid residue, dry toluene (11 mL), pyridine (370 µL, 4.53 mmol) and 9-hydroxynonyl acrylate (551 mg, 2.57 mmol). The vial was capped, transferred out of the glovebox and stirred at 100 °C for 3 h. After cooling to 20 °C, the reaction mixture was quenched with water (50 mL), extracted with ethyl acetate (3 × 30 mL), washed with saturated aq NH_4Cl (30 mL) and brine (30 mL), and dried over Na_2SO_4. After filtration, the organic phase was concentrated under reduced pressure and the crude residue was purified using silica gel column chromatography (cyclohexane to cyclohexane/ethyl acetate 75/25) to furnish the product **M1** as a yellow solid (481 mg, 700 µmol, 63%).

^{1}H NMR (601 MHz, $CDCl_3$): δ = 7.79 (dd, J = 8.2, 1.7 Hz, 2H, H-c), 7.67 (d, J = 1.7 Hz, 2H, H-a), 6.88 (d, J = 8.2 Hz, 2H, H-d), 6.39 (dd, J = 17.3, 1.5 Hz, 2H, H-p), 6.11 (dd, J = 17.3, 10.4 Hz, 2H, H-o), 5.81 (dd, J = 10.4, 1.5 Hz, 2H, H-p'), 4.23 (td, J = 6.8, 2.2 Hz, 4H, H-i), 4.14 (t, J = 6.7 Hz, 4H, H-m), 3.06 – 2.84 (m, 4H, H-g), 1.75 – 1.67 (m, 4H, H-l), 1.68 – 1.63 (m, 4H, H-j), 1.45–1.28 (m, 20H, H-k) ppm.

^{1}H NMR (601 MHz, $CDCl_3$): δ = 7.79 (dd, J = 8.2, 1.7 Hz, 2H, H-c), 7.67 (d, J = 1.7 Hz, 2H, H-a), 6.88 (d, J = 8.2 Hz, 2H, H-d), 6.39 (dd, J = 17.3, 1.5 Hz, 2H, H-p), 6.11 (dd, J = 17.3, 10.4 Hz, 2H, H-o), 5.81 (dd, J = 10.4, 1.5 Hz, 2H, H-p'), 4.23 (td, J = 6.8, 2.2 Hz, 4H, H-i), 4.14 (t, J = 6.7 Hz, 4H, H-m), 3.06 – 2.84 (m, 4H, H-g), 1.75 – 1.67 (m, 4H, H-l), 1.68–1.63 (m, 4H, H-j), 1.45–1.28 (m, 20H, H-k) ppm.

^{1}H NMR (600 MHz, THF): δ = 7.77 (dd, J = 8.2, 1.7 Hz, 2H), 7.70 (d, J = 1.7 Hz, 2H), 6.88 (d, J = 8.2 Hz, 2H), 6.31 (dd, J = 17.3, 1.7 Hz, 2H), 6.10 (dd, J = 17.3, 10.4 Hz, 2H), 5.78 (dd, J = 10.4, 1.7 Hz, 2H), 4.19 (dt, J = 10.9, 6.7 Hz, 4H), 4.10 (t, J = 6.7 Hz, 4H), 3.01 – 2.91 (m, 4H), 1.71–1.67 (m, 4H), 1.64 (p, J = 6.7 Hz, 4H), 1.46 – 1.29 (m, 20H) ppm.

^{1}H NMR (600 MHz, THF): δ = 7.77 (dd, J = 8.2, 1.7 Hz, 2H), 7.70 (d, J = 1.7 Hz, 2H), 6.88 (d, J = 8.2 Hz, 2H), 6.31 (dd, J = 17.3, 1.7 Hz, 2H), 6.10 (dd, J = 17.3, 10.4 Hz, 2H), 5.78 (dd, J = 10.4, 1.7 Hz, 2H), 4.19 (dt, J = 10.9, 6.7 Hz, 4H), 4.10 (t, J = 6.7 Hz, 4H), 3.01 – 2.91 (m, 4H), 1.71–1.67 (m, 4H), 1.64 (p, J = 6.7 Hz, 4H), 1.46 – 1.29 (m, 20H) ppm.

^{13}C{^{1}H} NMR (151 MHz, $CDCl_3$): δ = 166.5 (C-n), 165.8 (C-h), 158.8 (C-e), 131.5 (C-a), 130.6 (C-p), 129.5 (C-b), 128.8 (C-c), 128.2 (C-f), 126.7 (C-d), 65.5 (C-i), 64.8 (C-m), 31.4 (C-g), 29.5 (C-k), 29.3 (C-k), 28.8 (C-l2), 28.7 (C-j), 26.1 (C-k), 26.0 (C-k) ppm.

^{13}C{^{1}H} NMR (151 MHz, $CDCl_3$): δ = 166.5 (C-n), 165.8 (C-h), 158.8 (C-e), 131.5 (C-a), 130.6 (C-p), 129.5 (C-b), 128.8 (C-c), 128.2 (C-f), 126.7 (C-d), 65.5 (C-i), 64.8 (C-m), 31.4 (C-g), 29.5 (C-k), 29.3 (C-k), 28.8 (C-l2), 28.7 (C-j), 26.1 (C-k), 26.0 (C-k) ppm.

HRMS (ESI) *m/z* for $C_{41}H_{57}NO_8$ [M + H]$^+$: calcd 689.37964, found: 689.37890.

IR (ATR): $\tilde{\nu}$ = 2930 (w), 2853 (w), 1712 (s), 1633 (w), 1476 (s), 1408 (m), 1276 (m), 1252 (m), 1190 (s), 1134 (m), 1012 (m), 959 (m), 892 (w), 809 (m), 758 (m), 723 (w) cm^{-1}.

mp: 58 °C.

R_f: 0.52 (cyclohexane/ethyl acetate = 80/20)

(Z)-(11,12-dihydrodibenzo[*c*,*g*][1,2]diazocine-2,9-diyl)bis(methylene) diacrylate (M2)

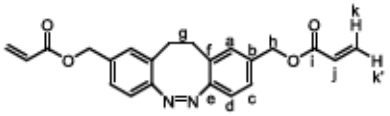

In a glovebox, compound **2** (268 mg, 1.00 mmol, reference [26]), dry DMF (5 mL) and dry TEA (550 µL, 4.00 mmol) were added to a sealed tube. The tube was capped with a crimp cap equipped with a PTFE septum, transferred out of the glovebox and cooled down to 0 °C. Acryloyl chloride (200 µL, 2.00 mmol) was dissolved in dry DMF (2.5 mL) and added dropwise within 5 min. The mixture was stirred at 0 °C for 1 h, then warmed up to 20 °C and stirred for a further 24 h. The solution was diluted and extracted with DCM (50 mL), washed with H_2O (2 × 15 mL) and brine (10 mL), and dried over Na_2SO_4. After filtration, the organic phase was concentrated under reduced pressure and the crude residue was purified using silica gel column chromatography (cyclohexane/ethyl acetate 70/30) to furnish product **M2** as a yellow solid (140 mg, 370 µmol, 37%).

In a glovebox, compound **2** (268 mg, 1.00 mmol, reference [26]), dry DMF (5 mL) and dry TEA (550 µL, 4.00 mmol) were added to a sealed tube. The tube was capped with a crimp cap equipped with a PTFE septum, transferred out of the glovebox and cooled down to 0 °C. Acryloyl chloride (200 µL, 2.00 mmol) was dissolved in dry DMF (2.5 mL) and added dropwise within 5 min. The mixture was stirred at 0 °C for 1 h, then warmed up to 20 °C and stirred for a further 24 h. The solution was diluted and extracted with DCM (50 mL), washed with H_2O (2 × 15 mL) and brine (10 mL), and dried over Na_2SO_4. After filtration, the organic phase was concentrated under reduced pressure and the crude residue was purified using silica gel column chromatography (cyclohexane/ethyl acetate 70/30) to furnish product **M2** as a yellow solid (140 mg, 370 µmol, 37%).

^{1}H NMR (601 MHz, $CDCl_3$): δ = 7.16 (dd, J = 8.1, 1.8 Hz, 2H, H-c), 7.00 (d, J = 1.8 Hz, 2H, H-a), 6.86 (d, J = 8.1 Hz, 2H, H-d), 6.43 (dd, J = 17.3, 1.3 Hz, 2H, H-k), 6.14 (dd, J = 17.3, 10.5 Hz, 2H, H-j), 5.85 (dd, J = 10.4, 1.3 Hz, 2H, H-k'), 5.06 (s, 4H, H-h), 2.88 (m, 4H, H-g) ppm.

^{1}H NMR (600 MHz, THF): δ = 7.16 (dd, J = 8.0, 1.6 Hz, 2H), 7.05 (d, J = 1.4 Hz, 2H), 6.79 (d, J = 8.0 Hz, 2H), 6.34 (dd, J = 17.3, 1.6 Hz, 2H), 6.12 (dd, J = 17.3, 10.4 Hz, 2H), 5.81 (dd, J = 10.4, 1.6 Hz, 2H), 5.02 (d, J = 8.9 Hz, 4H), 2.97–2.76 (m, 4H) ppm.

^{13}C{^{1}H} NMR (151 MHz, $CDCl_3$): δ = 166.0 (C-i), 155.3 (C-e), 134.9 (C-b), 131.5 (C-k), 129.6 (C-a), 128.3 (C-f, C-j), 126.8 (C-c), 119.5 (C-d), 65.7 (C-h), 31.8 (C-g) ppm.

Results

DCM (50 mL), washed with H_2O (2 × 15 mL) and brine (10 mL) and dried over Na_2SO_4. After filtration through a glass frit, the solvent was removed under reduced pressure and the crude residue was purified using silica gel column chromatography (cyclohexane/ethyl acetate 70/30) to furnish product M2 as a yellow solid (140 mg, 37%).

¹H NMR (600 MHz, $CDCl_3$): δ = 7.16 (dd, J = 8.1, 1.8 Hz, 2H, H-c), 7.00 (d, J = 1.8 Hz, 2H, H-a), 6.86 (d, J = 8.2 Hz, 2H, H-d), 6.43 (dd, J = 17.3, 1.5 Hz, 2H, H-j), 6.14 (dd, J = 17.3, 10.5 Hz, 2H, H-i), 5.85 (dd, J = 10.5, 1.5 Hz, 2H, H-k), 5.06 (s, 4H, H-h), 2.88 (m, 4H, H-g) ppm.

¹H NMR (600 MHz, THF): δ = 7.16 (dd, J = 8.0, 1.6 Hz, 2H), 7.05 (d, J = 1.4 Hz, 2H), 6.79 (d, J = 8.0 Hz, 2H), 6.34 (dd, J = 17.3, 1.6 Hz, 2H), 6.12 (dd, J = 17.3, 10.4 Hz, 2H), 5.81 (dd, J = 10.4, 1.6 Hz, 2H), 5.02 (s, 4H), 2.96 (m, 4H) ppm.

¹³C{¹H} NMR (151 MHz, $CDCl_3$): δ = 166.0 (C-i), 155.3 (C-e), 134.9 (C-b), 131.5 (C-k), 129.6 (C-a), 128.3 (C-j), 128.0 (C-c), 119.5 (C-d), 66.1 (C-h), 31.8 (C-g) ppm.

HRMS (EI) m/z for $C_{22}H_{20}N_2O_4$ $[M]^+$: calcd 376.1423, found: 376.14203 (30), 55 (100).

IR (ATR): $\tilde{\nu}$ = 2961 (w), 1718 (s), 1633 (w), 1404 (s), 1294 (m), 1265 (m), 1174 (s), 1046 (m), 967 (m), 807 (s), 755 (w), 657 (w) cm^{-1}.

mp: 62 °C.

R_f: 0.55 (cyclohexane/ethyl acetate = 67/33)

Poly[3,3′-hexane-1,6-diylbis(sulfanediyl) bis(propionyloxynonyl) (Z)-(11,12-dihydrodibenzo[c,g][1,2]diazocine-2,9-dicarboxylate] (P1)

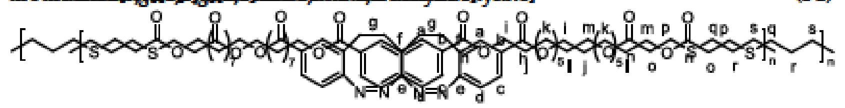

In a glovebox, a sealed tube was charged with compound M1 (400 mg, 580 µmol), THF (1 mL) and 1,6-hexanedithiol (84.0 µL, 550 µmol). Dimethylphenylphosphine (0.80 µL, 5.80 µmol) was added, the tube was capped with a crimp cap equipped with a PTFE septum and the reaction mixture was stirred at 20 °C for 40 min. Then, the tube was transferred out of the glovebox and the reaction mixture was precipitated dropwise in methanol (5 mL). The resulting solid was collected, redissolved in THF (1 mL) and re-precipitated in methanol (10 mL). The resulting solid was collected, redissolved in THF (1 mL) and re-precipitated in diethyl ether (10 mL) before the solid residue was dried in vacuum (50 °C, 48 h) to furnish the product **P1** (322 mg, 67%) as a yellow solid.

¹H NMR (600 MHz, THF): δ = 7.77 (dd, J = 8.2, 1.7 Hz, 2H, H-c), 7.70 (d, J = 1.7 Hz, 2H, H-a), 6.89 (d, J = 8.2 Hz, 2H, H-d), 4.28–4.14 (m, 4H, H-i), 4.12–4.01 (m, 4H, H-m), 3.05–2.90 (m, 4H, H-g), 2.79–2.68 (m, 4H, H-p), 2.54 (t, J = 7.4 Hz, 4H, H-o), 2.51 (t, J = 7.4 Hz, 4H, H-q), 1.72–1.65 (m, 4H, H-j), 1.65–1.53 (m, 8H, H-l, H-r), 1.45–1.37 (m, 8H, H-k, H-s), 1.37–1.30 (m, 16H, H-k) ppm.

¹³C{¹H} NMR (151 MHz, THF): δ = 172.2 (C-n), 165.9 (C-h), 160.3 (C-e), 132.2 (C-a), 130.4 (C-b), 129.5 (C-c), 129.1 (C-f), 119.5 (C-d), 65.8 (C-i), 65.1 (C-m), 35.8 (C-o), 32.7 (C-q), 32.1 (C-g), 30.8 (C-k), 30.6 (C-k), 30.5 (C-k), 30.3 (C-k), 30.3, (C-l) 29.8 (C-j), 29.5 (C-s), 27.9 (C-p), 27.1 (C-k), 27.0 (C-k) ppm.

IR (ATR): $\tilde{\nu}$ = 2918 (m), 2850 (m), 1715 (s), 1605 (w), 1463 (m), 1347 (m), 1285 (s), 1247 (s), 1163 (s), 1110 (s), 1000 (m), 961 (m), 756 (s), 722 (w) cm^{-1}.

Poly[(Z)-(11,12-dihydrodibenzo[c,g][1,2]diazocine-2,9-dimethyl-3,3′-(hexane-1,6-diylbis(sulfanediyl))dipropionate] (P2)

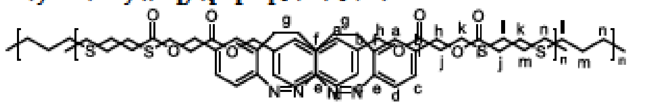

In a glovebox, a sealed tube was charged with compound M2 (217 mg, 580 µmol), THF (1 mL) and 1,6-hexanedithiol (84.0 µL, 550 µmol). Dimethylphenylphosphine (0.80 µL, 5.80 µmol) was added, the tube was capped with a crimp cap equipped with a PTFE septum and the reaction mixture was stirred at 20 °C for 40 min. Then, the tube was transferred out of the glovebox and reaction mixture was precipitated dropwise in methanol (5 mL). The resulting solid was collected, redissolved in THF (2.5 mL) and re-precipitated in methanol (10 mL). The resulting solid was collected, redissolved in THF (2.5 mL) and re-precipitated in diethyl ether (10 mL) before the solid residue was dried in vacuum (50 °C, 48 h) to furnish the product **P2** (168 mg, 56%) as a yellow solid.

¹H NMR (600 MHz, THF): δ = 7.19–7.10 (m, 2H, H-c), 7.08–7.01 (m, 2H, H-a), 6.84–6.76 (m, 2H, H-d), 5.03–4.90 (m, 4H, H-h), 2.98–2.75 (m, 4H, H-g), 2.75–2.68 (m, 4H, H-k), 2.56 (m, 4H, H-j), 2.53–2.46 (m, 4H, H-l), 1.62–1.48 (m, 4H, H-m), 1.48–1.34 (m, 4H, H-n) ppm.

¹³C{¹H} NMR (151 MHz, THF): δ = 172.1 (C-i), 156.6 (C-e), 136.3 (C-b), 130.4 (C-a), 129.1 (C-f), 127.5 (C-c), 120.0 (C-d), 66.2 (C-h), 35.8 (C-j), 32.7 (C-l), 32.5 (C-g), 30.6 (C-m), 29.5 (C-n), 27.8 (C-k) ppm.

ferred out of the glovebox and reaction mixture was precipitated dropwise in methanol (5 mL). The resulting solid was collected, redissolved in THF (2.5 mL) and re-precipitated in methanol (10 mL). The resulting solid was collected, redissolved in THF (2.5 mL) and re-precipitated in diethyl ether (10 mL) before the solid residue was dried in vacuum (50 °C, 48 h) to furnish the product **P2** (168 mg, 56%) as a yellow solid.

^{1}H NMR (600 MHz, THF): δ = 7.19 – 7.10 (m, 2H, H-c), 7.08 – 7.01 (m, 2H, H-a), 6.84 – 6.76 (m, 2H, H-d), 5.03 – 4.90 (m, 4H, H-h), 2.98 – 2.75 (m, 4H, H-g), 2.75 – 2.68 (m, 4H, H-k), 2.56 (m, 4H, H-j), 2.53 – 2.46 (m, 4H, H-l), 1.62 – 1.48 (m, 4H, H-m), 1.48 – 1.34 (m, 4H, H-n) ppm.

^{13}C{^{1}H} NMR (151 MHz, THF): δ = 172.1 (C-i), 156.6 (C-e), 136.3 (C-b), 130.4 (C-a), 129.1 (C-f), 127.5 (C-c), 120.0 (C-d), 66.2 (C-h), 35.8 (C-j), 32.7 (C-l), 32.5 (C-g), 30.6 (C-m), 29.5 (C-n), 27.8 (C-k) ppm.

IR (ATR): $\tilde{\nu}$ = 2924 (m), 2851 (w), 1729 (s), 1414 (w), 1376 (w), 1343 (m), 1239 (s), 1143 (s), 962 (m), 891 (m), 827 (m), 803 (m), 734 (m), 672 (m) cm^{-1}.

3. Results and Discussion

Previous work enabled the access to functionalized diazocine compounds [26], among which carboxylic acid (**1**) and dihydroxymethyl (**2**) compounds (Scheme 2) were easily formed from methyl ester as the common starting material. Acylation of the dihydroxymethyl derivative of diazocine **2** with acryloyl chloride provided the short diazocine diacrylate **M2** in a 37% yield. For the synthesis of the diacrylate comprising nonanyl alkyl spacers **M1**, the carboxylic acid functions in **1** were activated to reactive acyl chlorides before esterification with 9-hydroxynonyl acrylate established product **M1** in an overall 63% yield. Finally, the monomers **M1** and **M2** were subjected to the Michael-type thiol-ene polyaddition reaction [36] with 1,6-hexanedithiol (HDT) as the nucleophile in a 1.05:1 stoichiometric ratio to ensure acrylate groups at the polymer chain ends and to prevent disulfide links. By employing 1 mol% of dimethylphenylphosphine (DMPP) as the catalyst, the desired polymers **P1** and **P2** were formed in good yields (67% and 56%, respectively) after purification by precipitation.

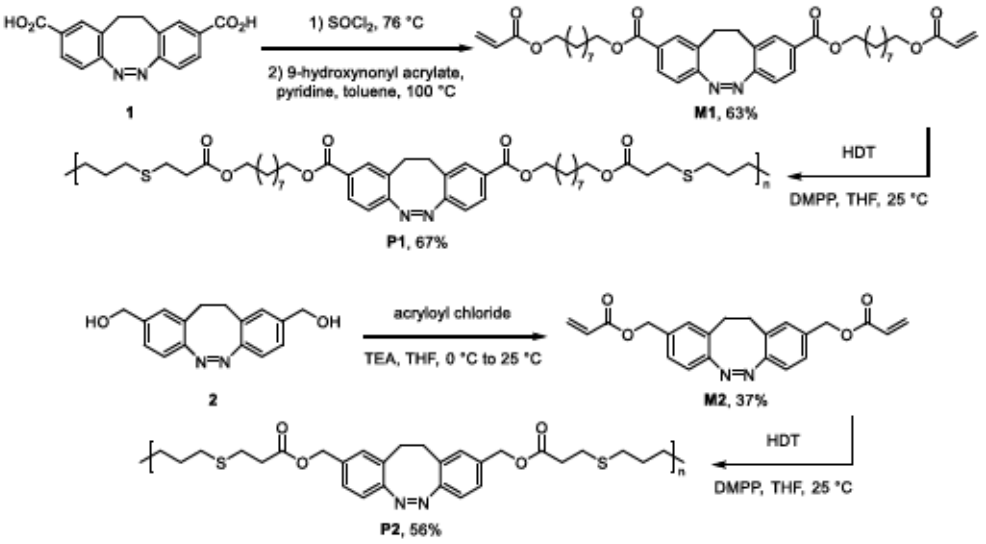

Scheme 2. Synthesis of the monomers and polymerization. Compounds **1** and **2** were synthesized according to previously published procedures [26].

The photochromism of the diazocine monomers and polymers was investigated using UV-vis spectroscopy at 25 °C (Table 1). The π–π^* transition maxima of the (*Z*) and (*E*) isomers were detected at around 400 and 452 nm, in agreement with existing diazocine compounds (Figures 1a,b and S1). No signs of photodegradation were observed for the polymers **P1** and **P2** after ten cyclic irradiation measurements (Figure S2). The spontaneous *E*→*Z* thermal relaxation of the diazocine units followed first-order reaction kinetics (Figures S3 and S4). Since the relaxation rates are predominantly influenced by the electronic effects of the proximal substituents on the aromatic rings of diazocines [25], a large difference in thermal half-lives was determined between the polymers **P1** and **P2** (39 min and 350 min) but without significant differences compared to the respective monomers **M1** and **M2** (42 min and 358 min). In the solid state, the polymers **P1** and **P2** underwent photochromism in bulk, as evident from the color change between the yellow (*Z*) and red (*E*) configurations

isomers were detected at around 400 and 492 nm, in agreement with existing diazocine compounds (Figures 1a, 1b and S1). No signs of photodegradation were observed for the polymers **P1** and **P2** after ten cyclic irradiation measurements (Figure S2). The spontaneous $E \rightarrow Z$ thermal relaxation of the diazocine units followed first-order reaction kinetics (Figure S3 and S4). Since the relaxation rates are predominantly influenced by the electronic effects of the proximal substituents on the aromatic rings of diazocines [25], a large difference in thermal half-lives was determined between the polymers **P1** and **P2** (39 min and 350 min) but without significant differences compared to the respective monomers **M1** and **M2** (42 min and 358 min). In the solid state, the polymers **P1** and **P2** underwent photochromism in bulk, as evident from the color change between the yellow (*Z*) and red (*E*) configurations (Figure 2). To compare the photochromism of the polymers **P1** and **P2** in the solid state with the dissolved samples, thin films were produced using spin-coating of the polymer solutions on glass slides. The photostationary states at 405 and 525 nm light irradiation wavelengths were equally reached within 1 min as no spectral changes could be detected after longer irradiation times. The absorption spectra of the thin films resemble the polymer solutions in THF, thereby showing equal photochromic efficiencies in the solid state (Figure S5).

(Figure 2). To compare the photochromism of the polymers P1 and P2 in the solid state with the dissolved samples, thin films were produced using spin-coating of the polymer solutions on glass slides. The photostationary states at 405 and 525 nm light irradiation wavelengths were equally reached within 1 min as no spectral changes could be detected after longer irradiation times. The absorption spectra of the thin films resemble the polymer solutions in THF, thereby showing equal photochromic efficiencies in the solid state (Figure S5).

Table 1. Diazocine photoswitching data obtained from UV-vis and NMR spectroscopy.

	PSS (405 nm)				PSS (525 nm)				
	$\Gamma_{Z\rightarrow E}$ (%) E	λ_{max} (E) (nm)	D (10^{-6} cm^2 s^{-1})[1]	$\Gamma_{E\rightarrow Z}$ (%) Z	λ_{max} (Z) (nm)	D (10^{-6} cm^2 s^{-1})[1]	k ($E\rightarrow Z$) (10^{-3} min^{-1})	$t_{1/2}$ (min)
M1	60%	491	7.45 ± 0.14 (Z) 7.39 ± 0.07 (E)	>99%	399	7.46 ± 0.11	26.73 ± 0.84	26 ± 1
P1	60%	496	1.90 ± 0.03 (Z) 1.94 ± 0.02 (E)	>99%	402	1.96 ± 0.05	28.56 ± 0.37	24 ± 0
M2	64%	488	10.4 ± 0.16 (Z) 11.0 ± 0.26 (E)	>99%	402	10.6 ± 0.09	1.90 ± 0.04	366 ± 7
P2	64%	492	2.72 ± 0.21 (Z) 2.75 ± 0.07 (E)	>99%	405	2.84 ± 0.08	1.90 ± 0.05	366 ± 9

[1] After application of correction factors and Stejskal–Tanner fitting.

PSS (405 nm) PSS (525 nm)
$\Gamma_{Z\rightarrow E}$ (%) E λ_{max} (E) (nm) D (10^{-6} cm^2 s^{-1})[1] $\Gamma_{E\rightarrow Z}$ (%) Z λ_{max} (Z) (nm) D (10^{-6} cm^2 s^{-1})[1] k ($E\rightarrow Z$) (10^{-3} min^{-1}) $t_{1/2}$ (min)
M1 60% 491 7.45 ± 0.14 (Z) 7.39 ± 0.07 (E) >99% 399 7.46 ± 0.11 26.73 ± 0.84 26 ± 1
P1 60% 496 1.90 ± 0.03 (Z) 1.94 ± 0.02 (E) >99% 402 1.96 ± 0.05 28.56 ± 0.37 24 ± 0
M2 64% 488 10.4 ± 0.16 (Z) 11.0 ± 0.26 (E) >99% 402 10.6 ± 0.09 1.90 ± 0.04 366 ± 7
P2 64% 492 2.72 ± 0.21 (Z) 2.75 ± 0.07 (E) >99% 405 2.84 ± 0.08 1.90 ± 0.05 366 ± 9
[1] After application of correction factors and Stejskal–Tanner fitting.

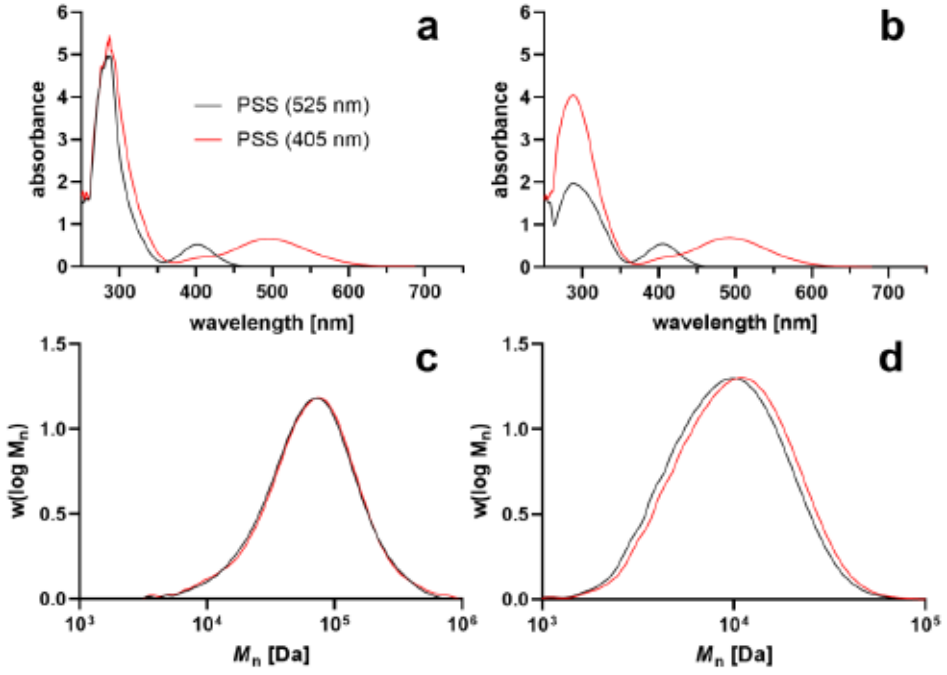

Figure 1. UV-vis spectra of polymers **P1** (**a**) and **P2** (**b**) at PSS (405 nm, red) and PSS (525 nm, black) at a concentration of 0.5 mg/mL in THF; and molar mass distribution of polymers **P1** (**c**) and **P2** (**d**).

at a concentration of 0.5 mg/mL in THF; and molar mass distribution of polymers **P1** (c) and **P2** (d).

The diazocine products were further analyzed using ^{1}H NMR spectroscopy, initially showing the (*Z*) isomer in **M1**, **M2**, **P1** and **P2** (see the SI). For the polymers **P1** and **P2**, depletion of the acrylate signals of the monomer and the emergence of broad alkyl signals confirmed the incorporation of 1,6-hexanedithiol and thus the success of the thiol-ene step-growth polymerization. Furthermore, the ^{1}H NMR spectrum of polymer **P2** contained end-group acrylate signals which allowed the determination of a DP of 17 using the integration of the signals between the acrylate protons and aromatic protons of the diazocine repeating units. Upon photoexcitation of the (*Z*) isomers at a wavelength of 405 nm, the photostationary states (PSS) of all diazocine products were reached within 1 min with an accumulation of the downfield-shifted (*E*) isomer in good photoconversion yields ($\Gamma_{Z\rightarrow E}$) for **M1** (60%) and **M2** (64%) (Table 1). In comparison to the monomers **M1** and **M2**, the *E*/*Z* ratios of the respective polymers **P1** and **P2** remained constant, thereby showing no signs of restraint with regard to the switching ability of the integrated diazocine units in the polymer chain. Complete conversion ($\Gamma_{E\rightarrow Z} > 99\%$) to the (*Z*) isomers was reached within 1 min of light irradiation at 525 nm wavelength for all diazocine compounds **M1**, **M2**, **P1** and **P2**.

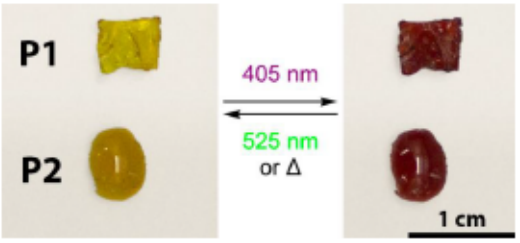

Figure 2. Polymer samples of **P1** and **P2** at PSS (525 nm) and PSS (405 nm).

To analyze the molecular weights of the polymers, the molecular mass distributions were determined using gel permeation chromatography (GPC) in THF (Figure 1c,d). In the case of polymer **P1**, long polymer chains were obtained, with a number average molecular weight (M_n) of 43 kDa and a dispersity ($Đ$) of 2.5, corresponding to a degree of polymerization (DP) of 51 (Table 2). Polymer **P2** had much shorter polymer chains than **P1** with an M_n of 7.4 kDa and a dispersity of 1.6, corresponding to a DP of 14. Since the GPC was calibrated from polystyrene standards, the DP of 17 obtained from the NMR integral measurement was expected to be more accurate. After irradiation of polymer **P2** with light at 405 nm wavelength, the apparent M_n measured using GPC increased to 8.1 kDa. In comparison to the measurement under ambient conditions, the apparent increase in M_n by 0.7 kDa reflects the collective photoisomerization of the main-chain diazocine groups which caused hydrodynamic size expansion of the individual polymer coils in THF. However, no change in the apparent M_n could be detected after light irradiation at 405 nm wavelength for **P1**, possibly due to the fast $E\rightarrow Z$ thermal relaxation of the diazocine units during the GPC elution process or because the change is small.

Table 2. GPC and DSC data for polymers **P1** and **P2**.

		$M_{n,GPC}$ (kDa)	$Đ$	T_g (°C)
P1	**PSS (525 nm)**	43	2.5	−11.3
	PSS (405 nm)	43	2.5	−10.9
P2	**PSS (525 nm)**	7.4	1.6	12.3
	PSS (405 nm)	8.1	1.6	10.3

To study the thermal properties and potential transitions of the polymer materials **P1** and **P2**, the photoinduced enthalpic changes of the polymers **P1** and **P2** were measured as a function of temperature using differential scanning calorimetry (DSC). The long alkyl

spacers between the diazocine units in polymer **P1** led to a low glass transition temperature (T_g) of −11.3 °C under ambient conditions (Figures S6 and S7). The shorter polymer **P2** exhibited a T_g at 12.3 °C without further phase transitions at higher temperatures. Apart from the glass transitions, no other thermal phase transitions could be detected. After irradiation of the polymer samples with light at 405 nm wavelength, the changes in T_g as a result of the $Z \rightarrow E$ photoisomerization of the diazocine groups were negligible (0.4–2 °C). Therefore, the configurations of diazocine did not have a strong impact on the rigidity of the polymer chains and did not suggest a higher crystalline order upon photoinduced $Z \rightarrow E$ switching. In comparison to the amorphous-to-crystalline transition in diazocine-containing polyurea proposed by Li and co-workers [31], the poly(thioether) chains **P1** and **P2** did not form an intermolecular network and allowed an isotropic movement of the diazocine units. The polymers remained in a soft, rubbery state at room temperature (25 °C) due to the low T_g of **P1** and **P2**. Sufficient free volume in the polymer matrix provided a similar photochromic behavior compared to the polymer solutions in THF.

^{1}H DOSY NMR spectroscopy provided useful information about the size of individual polymer coils. For polymers containing molecular switches that undergo substantial geometric changes such as the diazocine, the collective isomerization of the switching units is expected to lead to an alteration of the measured diffusion coefficients (D). The hydrodynamic radius (r) of an individual polymer coil is inversely proportional to the diffusion coefficient and dependent on the dynamic viscosity of the solvent given by the Stokes–Einstein equation (Equation 9). In order to detect the hydrodynamic size expansion of the polymer coils in solution, DOSY experiments at PSS of 405 and 525 nm light irradiation wavelengths were conducted in THF-d_8, focusing on the aromatic signals of diazocine. The dynamic viscosity of THF-d_8 at 25 °C was adopted from previous work by Dowds and co-workers (Equation 10) [32]. As expected at PSS (525 nm), single diffusion coefficients of the diazocine products **M1**, **M2**, **P1** and **P2** in (*Z*) configuration were obtained (for **M2** and **P2**, see the SI).

The (*E*) isomers of **M1** and in **P1** relaxed noticeably during the DOSY measurements, as the experiment duration (~20 min) was of the order of the compound half-lives (~25 min), see also Figure S8 The associated increase or decrease in concentration of (*Z*) and (*E*) species, respectively, influenced the integrals of the DOSY peaks, which in turn affected the fit quality and led to erroneous diffusion coefficients D for both species. In order to correct this error in the measured data, the $E \rightarrow Z$ thermal relaxation kinetics must be taken into account. Therefore, the intensities were corrected and normalized with a normalization factor n, and a time offset f was included in the calculation of the (*Z*) isomer intensities (Table S1). Finally, the corrected and normalized intensities I′ were plotted as a function of the gradient strength G and fitted with the Stejskal–Tanner equation (Figure S9) [35]. A detailed procedure can be found in the *Methods* section.

Photoswitching of the diazocine **M1** with 405 nm violet light gave rise to a new and slightly decreased diffusion coefficient of $7.39 \pm 0.07 \times 10^{-6}$ cm^2 s^{-1} that corresponded to the (*E*) isomer compared to the steady (*Z*) isomer at $7.45 \pm 0.14 \times 10^{-6}$ cm^2 s^{-1}. In addition, the DOSY spectra of the polymers **P1** and **P2** reflected the molar mass distributions obtained using GPC analysis: Firstly, the diffusion coefficients showed higher statistical deviation attributed to the polydispersity of the polymers (see Table S1). Secondly, the higher M_n of **P1** compared to **P2** was confirmed by the lower diffusion coefficient of **P1** ($1.96 \pm 0.05 \times 10^{-6}$ cm^2 s^{-1}) compared to **P2** ($2.84 \pm 0.08 \times 10^{-6}$ cm^2 s^{-1}). Since each individual polymer chain in **P1** and **P2** contains multiple diazocine units, photoswitching with light at 405 nm wavelength resulted in a distribution of the (*Z*)- and (*E*)-diazocine isomers within a macromolecule. As a consequence, the diffusion behavior of the polymers in THF-d_8 upon photoswitching to PSS (405 nm) is expected to shift collectively for both isomeric forms. In this case, the mean value of the diffusion coefficient of **P1** decreased from $1.96 \pm 0.05 \times 10^{-6}$ to $1.91 \pm 0.02 \times 10^{-6}$ (*Z*) and $1.90 \pm 0.03 \times 10^{-6}$ (*E*) cm^2 s^{-1}, and the diffusion coefficient of **P2** decreased from $2.84 \pm 0.08 \times 10^{-6}$ cm^2 s^{-1} to $2.72 \pm 0.21 \times 10^{-6}$ (*Z*) and $2.75 \pm 0.07 \times 10^{-6}$ (*E*) cm^2 s^{-1}, which corresponded to an increase in hydrodynamic

radius from 2.30 nm (*Z*) to about 2.36 nm (*E*), and from 1.59 nm (*Z*) to about 1.64 nm (*E*), respectively. The observed changes in size, however, are small compared to the experimental error of the DOSY NMR measurements and the distribution of the diffusion coefficients resulting from the polymer dispersity. Because of these error margins, DOSY experiments are not by themselves sufficient to prove a size change. While the photoswitching of the diazocine units is expected to alter the conformation of the polymer backbone, the overall size of the polymer coil remained largely unaffected. This was presumably caused by the conformational freedom of the interconnecting alkyl chain linkers that simultaneously ensured a non-restrained photoswitching of the diazocine units.

4. Conclusions

Based on our synthetic strategy for the synthesis of functionalized diazocines, diacrylates with two different alkyl spacer lengths were generated and employed as monomers in the thiol-ene polyaddition reaction with 1,6-hexanedithiol. The resulting linear polymers with diazocine moieties in the polymer backbone differed in molecular weight and glass transition temperature while closely mimicking the photochromic behavior of the respective monomers. Owing to the $Z \rightarrow E$ pincer-like motion of the diazocine switch, the flexible polymer coils experienced a photoinduced hydrodynamic size expansion of the polymer with shorter alkyl chain linkers as confirmed by an increase in the apparent molecular weight from analytical GPC measurements in THF. However, the diffusion coefficients obtained from ^{1}H DOSY NMR only decreased minimally at PSS (405 nm), probably due to the conformational freedom of the interconnecting alkyl chain linkers. Our results clearly show the potential of diazocine with its favorable properties as a photoswitch in the main chain of polymers. The reactive acrylate end groups of the polymers can be further exploited in post-polymerization modifications and cross-linking reactions. Future work includes the implementation and incorporation of diazocines in more complex polymeric architectures and higher crystalline environments such as micelles, where photoinduced size-switching can be instrumentalized for targeted drug delivery [37].

Supplementary Materials: The following supporting information can be downloaded at: https://www.mdpi.com/article/10.3390/polym15051306/s1, Figure S1: UV-vis spectra of compounds M1 (left) and M2 (right) after light irradiation at 405 nm (red) and 525 nm wavelength (black) at a concentration of 1 mM in THF; Figure S2. Cyclic UV-vis measurements of polymers P1 (left) and P2 (right) after light irradiation at 405 nm (red) and 525 nm wavelength (black) at a concentration of 0.5 mg/mL in THF; Figure S3. First-order thermal relaxation kinetics of M1 (left) and M2 (right) from PSS (405 nm wavelength) at $\lambda_{max}(E)$ at a concentration of 3 mg/mL in THF; Figure S4. First-order thermal relaxation kinetics of P1 (left) and P2 (right) from PSS (405 nm wavelength) at $\lambda_{max}(E)$ at a concentration of 3 mg/mL in THF; Figure S5. UV-vis spectra of polymers P1 (left) and P2 (right) after light irradiation at 405 (red) and 525 nm wavelength (black) as spin-coated thin films; Figure S6. DSC plots of polymer P1 at PSS (525 nm) (black) and PSS (405 nm) (red) indicating the glass transition temperature T_g. The DSC measurements were cycled between −70 and 150 °C and −40 and 40 °C, respectively; Figure S7. DSC plots of polymer P2 at PSS (525 nm) (black) and PSS (405 nm) (red) indicating the glass transition temperature T_g. The DSC measurements were cycled between −70 and 150 °C and −40 and 40 °C, respectively; Figure S8. Stacked plot of the 1D ^{1}H NMR spectra of M1 from 8.5 to −0.5 ppm at T = 298 K. Bottom: before irradiation, center: after irradiation at t = 0 min and top: after irradiation and the DOSY experiment at t = 27.3 min; Figure S9. Example graphs are presented to highlight the effect of data intensity correction of one peak of the (*E*) (top) and (*Z*) isomer (bottom) after light irradiation at 405 nm wavelength of M1. Fit statistics are shown for the individual fits of these resonances; Figure S10. Stacked plot of the 1D ^{1}H NMR spectra of polymer P1 from 8.5 to −0.5 ppm at T = 298 K. Bottom: before irradiation, center: after irradiation at t = 0 min and top: after irradiation and the DOSY experiment at t = 26.5 min; Table S1. Corrected diffusion coefficients D [10^{-6} cm^2 s^{-1}] of the (*Z*) and (*E*) isomers of M1, P1, M2, P2 after light irradiation at 405 and 525 nm wavelength from ^{1}H DOSY NMR measurements.; ^{1}H and ^{13}C{^{1}H} NMR spectra of the products.; ^{1}H DOSY NMR spectra of M2 and P2. Ref [38] is cited in Supplementary Materials.

Author Contributions: Conceptualization, A.S.; methodology, S.L., K.B. and F.D.S.; validation, S.L. and K.B.; formal analysis, S.L., K.B., Y.L. and F.D.S.; investigation, S.L., K.B. and Y.L.; resources, S.L.; data curation, S.L.; writing—original draft preparation, S.L.; writing—review and editing, S.L., K.B., F.D.S., Y.L. and A.S.; visualization, S.L., K.B.; supervision, A.S. and F.D.S.; project administration, A.S. All authors have read and agreed to the published version of the manuscript.

Funding: This research received funding from the University of Bremen and the German Research Foundation (DFG) within the Collaborative Research Center 677 "Function by Switching".

Data Availability Statement: The raw /processed data are available upon reasonable request.

Acknowledgments: This work has been supported by the German Research Foundation (DFG) within the Collaborative Research Center 677 "Function by Switching" (S.L., F.S. and A.S.).

Conflicts of Interest: The authors declare no conflict of interest.

References

1. Pianowski, Z.L. (Ed.) *Molecular Photoswitches*; Wiley: Hoboken, NJ, USA, 2022; ISBN 9783527351046.
2. Bandara, H.M.D.; Burdette, S.C. Photoisomerization in Different Classes of Azobenzene. *Chem. Soc. Rev.* **2012**, *41*, 1809–1825. [CrossRef]
3. Kizilkan, E.; Strueben, J.; Staubitz, A.; Gorb, S.N. Bioinspired Photocontrollable Microstructured Transport Device. *Sci. Robot.* **2017**, *2*, 9454. [CrossRef] [PubMed]
4. Oscurato, S.L.; Salvatore, M.; Maddalena, P.; Ambrosio, A. From Nanoscopic to Macroscopic Photo-Driven Motion in Azobenzene-Containing Materials. *Nanophotonics* **2018**, *7*, 1387–1422. [CrossRef]
5. Erbas-Cakmak, S.; Leigh, D.A.; McTernan, C.T.; Nussbaumer, A.L. Artificial Molecular Machines. *Chem. Rev.* **2015**, *115*, 10081–10206. [CrossRef]
6. Beharry, A.A.; Woolley, G.A. Azobenzene Photoswitches for Biomolecules. *Chem. Soc. Rev.* **2011**, *40*, 4422. [CrossRef] [PubMed]
7. Dattler, D.; Fuks, G.; Heiser, J.; Moulin, E.; Perrot, A.; Yao, X.; Giuseppone, N. Design of Collective Motions from Synthetic Molecular Switches, Rotors, and Motors. *Chem. Rev.* **2020**, *120*, 310–433. [CrossRef]
8. Bléger, D.; Liebig, T.; Thiermann, R.; Maskos, M.; Rabe, J.P.; Hecht, S. Light-Orchestrated Macromolecular "Accordions": Reversible Photoinduced Shrinking of Rigid-Rod Polymers. *Angew. Chemie Int. Ed.* **2011**, *50*, 12559–12563. [CrossRef]
9. Sogawa, H.; Shiotsuki, M.; Sanda, F. Synthesis and Photoresponse of Helically Folded Poly(Phenyleneethynylene)s Bearing Azobenzene Moieties in the Main Chains. *Macromolecules* **2013**, *46*, 4378–4387. [CrossRef]
10. Yu, Z.; Hecht, S. Reversible and Quantitative Denaturation of Amphiphilic Oligo(Azobenzene) Foldamers. *Angew. Chem. Int. Ed.* **2011**, *50*, 1640–1643. [CrossRef] [PubMed]
11. Tie, C.; Gallucci, J.C.; Parquette, J.R. Helical Conformational Dynamics and Photoisomerism of Alternating Pyridinedicarboxamide/m-(Phenylazo)Azobenzene Oligomers. *J. Am. Chem. Soc.* **2006**, *128*, 1162–1171. [CrossRef]
12. Izumi, A.; Nomura, R.; Masuda, T. Design and Synthesis of Stimuli-Responsive Conjugated Polymers Having Azobenzene Units in the Main Chain. *Macromolecules* **2001**, *34*, 4342–4347. [CrossRef]
13. Zhong, H.-Y.; Chen, L.; Yang, R.; Meng, Z.-Y.; Ding, X.-M.; Liu, X.-F.; Wang, Y.-Z. Azobenzene-Containing Liquid Crystalline Polyester with π–π Interactions: Diverse Thermo- and Photo-Responsive Behaviours. *J. Mater. Chem. C* **2017**, *5*, 3306–3314. [CrossRef]
14. Appiah, C.; Woltersdorf, G.; Pérez-Camargo, R.A.; Müller, A.J.; Binder, W.H. Crystallization Behavior of Precision Polymers Containing Azobenzene Defects. *Eur. Polym. J.* **2017**, *97*, 299–307. [CrossRef]
15. Kuenstler, A.S.; Clark, K.D.; Read de Alaniz, J.; Hayward, R.C. Reversible Actuation via Photoisomerization-Induced Melting of a Semicrystalline Poly(Azobenzene). *ACS Macro Lett.* **2020**, *9*, 902–909. [CrossRef] [PubMed]
16. Shen, D.; Yao, Y.; Zhuang, Q.; Lin, S. Mainchain Alternating Azopolymers with Fast Photo-Induced Reversible Transition Behavior. *Macromolecules* **2021**, *54*, 10040–10048. [CrossRef]
17. Carstensen, N.O. QM/MM Surface-Hopping Dynamics of a Bridged Azobenzene Derivative. *Phys. Chem. Chem. Phys.* **2013**, *15*, 15017–15026. [CrossRef] [PubMed]
18. Lee, K.M.; Wang, D.H.; Koerner, H.; Vaia, R.A.; Tan, L.-S.; White, T.J. Enhancement of Photogenerated Mechanical Force in Azobenzene-Functionalized Polyimides. *Angew. Chem. Int. Ed.* **2012**, *51*, 4117–4121. [CrossRef]
19. Fang, L.; Zhang, H.; Li, Z.; Zhang, Y.; Zhang, Y.; Zhang, H. Synthesis of Reactive Azobenzene Main-Chain Liquid Crystalline Polymers via Michael Addition Polymerization and Photomechanical Effects of Their Supramolecular Hydrogen-Bonded Fibers. *Macromolecules* **2013**, *46*, 7650–7660. [CrossRef]
20. Wang, D.H.; Lee, K.M.; Lee, D.H.; Baczkowski, M.; Park, H.; McConney, M.E.; Tan, L.-S. Role of Alicyclic Conformation-Isomerization in the Photomechanical Performance of Azobenzene-Functionalized Cross-Linked Polyimides Containing Tetra-Substituted Cyclohexane Moieties. *ACS Macro Lett.* **2021**, *10*, 278–283. [CrossRef]
21. Xue, X.; Zhu, J.; Zhang, Z.; Zhou, N.; Tu, Y.; Zhu, X. Soluble Main-Chain Azobenzene Polymers via Thermal 1,3-Dipolar Cycloaddition: Preparation and Photoresponsive Behavior. *Macromolecules* **2010**, *43*, 2704–2712. [CrossRef]

22. Wu, Y.; Natansohn, A.; Rochon, P. Photoinduced Birefringence and Surface Relief Gratings in Polyurethane Elastomers with Azobenzene Chromophore in the Hard Segment. *Macromolecules* **2004**, *37*, 6090–6095. [CrossRef]
23. Siewertsen, R.; Neumann, H.; Buchheim-Stehn, B.; Herges, R.; Näther, C.; Renth, F.; Temps, F. Highly Efficient Reversible Z−E Photoisomerization of a Bridged Azobenzene with Visible Light through Resolved S 1 (Nπ*) Absorption Bands. *J. Am. Chem. Soc.* **2009**, *131*, 15594–15595. [CrossRef] [PubMed]
24. Yang, Y.; Jing, X.; Zhang, J.; Yang, F.; Duan, C. Modifying Electron Injection Kinetics for Selective Photoreduction of Nitroarenes into Cyclic and Asymmetric Azo Compounds. *Nat. Commun.* **2022**, *13*, 1940. [CrossRef] [PubMed]
25. Maier, M.S.; Hüll, K.; Reynders, M.; Matsuura, B.S.; Leippe, P.; Ko, T.; Schäffer, L.; Trauner, D. Oxidative Approach Enables Efficient Access to Cyclic Azobenzenes. *J. Am. Chem. Soc.* **2019**, *141*, 17295–17304. [CrossRef] [PubMed]
26. Li, S.; Eleya, N.; Staubitz, A. Cross-Coupling Strategy for the Synthesis of Diazocines. *Org. Lett.* **2020**, *22*, 1624–1627. [CrossRef] [PubMed]
27. Carstensen, O.; Sielk, J.; Schönborn, J.B.; Granucci, G.; Hartke, B. Unusual Photochemical Dynamics of a Bridged Azobenzene Derivative. *J. Chem. Phys.* **2010**, *133*, 124305. [CrossRef]
28. Sell, H.; Näther, C.; Herges, R. Amino-Substituted Diazocines as Pincer-Type Photochromic Switches. *Beilstein J. Org. Chem.* **2013**, *9*, 1–7. [CrossRef]
29. Samanta, S.; Qin, C.; Lough, A.J.; Woolley, G.A. Bidirectional Photocontrol of Peptide Conformation with a Bridged Azobenzene Derivative. *Angew. Chemie Int. Ed.* **2012**, *51*, 6452–6455. [CrossRef]
30. Wang, G.A.; Xu, J.; Traynor, S.M.; Chen, H.; Eljabu, F.; Wu, X.; Yan, H.; Li, F. DNA Balance for Native Characterization of Chemically Modified DNA. *J. Am. Chem. Soc.* **2021**, *143*, 13655–13663. [CrossRef]
31. Li, S.; Han, G.; Zhang, W. Concise Synthesis of Photoresponsive Polyureas Containing Bridged Azobenzenes as Visible-Light-Driven Actuators and Reversible Photopatterning. *Macromolecules* **2018**, *51*, 4290–4297. [CrossRef]
32. Dowds, M.; Bank, D.; Strueben, J.; Soto, D.P.; Sönnichsen, F.D.; Renth, F.; Temps, F.; Staubitz, A. Efficient Reversible Photoisomerisation with Large Solvodynamic Size-Switching of a Main Chain Poly(Azobenzene-Alt-Trisiloxane). *J. Mater. Chem. C* **2020**, *8*, 1835–1845. [CrossRef]
33. Izumi, A.; Teraguchi, M.; Nomura, R.; Masuda, T. Synthesis of Poly(p-Phenylene)-Based Photoresponsive Conjugated Polymers Having Azobenzene Units in the Main Chain. *Macromolecules* **2000**, *33*, 5347–5352. [CrossRef]
34. Li, S.; Colaco, R.; Staubitz, A. ARGET ATRP of Methyl Acrylate and Methyl Methacrylate with Diazocine-Derived Initiators. *ACS Appl. Polym. Mater.* **2022**, *4*, 6825–6833. [CrossRef]
35. Stejskal, E.O.; Tanner, J.E. Spin Diffusion Measurements: Spin Echoes in the Presence of a Time-Dependent Field Gradient. *J. Chem. Phys.* **1965**, *42*, 288–292. [CrossRef]
36. Nair, D.P.; Podgórski, M.; Chatani, S.; Gong, T.; Xi, W.; Fenoli, C.R.; Bowman, C.N. The Thiol-Michael Addition Click Reaction: A Powerful and Widely Used Tool in Materials Chemistry. *Chem. Mater.* **2014**, *26*, 724–744. [CrossRef]
37. Wang, G.; Tong, X.; Zhao, Y. Preparation of Azobenzene-Containing Amphiphilic Diblock Copolymers for Light-Responsive Micellar Aggregates. *Macromolecules* **2004**, *37*, 8911–8917. [CrossRef]
38. Coghill, A.M.; Garson, L.R.; American Chemical Society (Eds.) *The ACS Style Guide: Effective Communication of Scientific Information*, 3rd ed.; American Chemical Society; Oxford University Press: Washington, DC, USA; Oxford, UK; New York, NY, USA, 2006; ISBN 9780841239999/9780841274006.

Disclaimer/Publisher's Note: The statements, opinions and data contained in all publications are solely those of the individual author(s) and contributor(s) and not of MDPI and/or the editor(s). MDPI and/or the editor(s) disclaim responsibility for any injury to people or property resulting from any ideas, methods, instructions or products referred to in the content.

3.3.2 Part B

The reversible photoinduced size-expansion effect of polymer **P2** was confirmed by repeated GPC measurements of the respective crude polymer product **P2a** without undergoing purification by precipitation. The molar mass distribution of **P2a** revealed the presence of low molar mass species, presumably involving cyclic oligomers as side products during the polymerization reaction (see Figure 3.6). Overall, the molar mass distributions at PSS (405 nm) slightly shifted to higher apparent molecular weights compared to the molar mass distributions at PSS (565 nm). (*Z*)→(*E*) photoswitching of the inherent diazocine units in the polymer backbone resulted in an increase in M_n from 5.14 to 5.51 kDa and an increase in M_w from 7.82 to 8.69 kDa (in average numbers, see Figure 3.7 & Table 3.9), thereby confirming the size-switching effect of polymer **P2**.

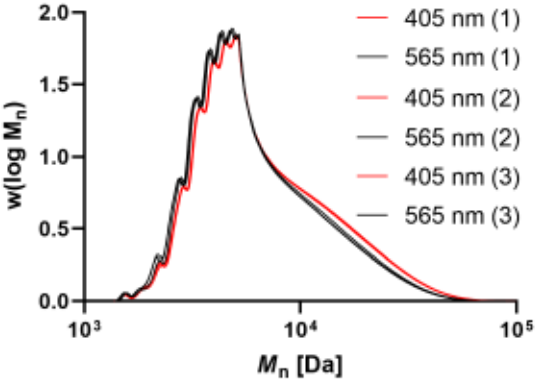

Figure 3.6. Molar mass distributions of polymer **P2a** after light irradiation at 405 nm (red) and 565 nm wavelength (black).

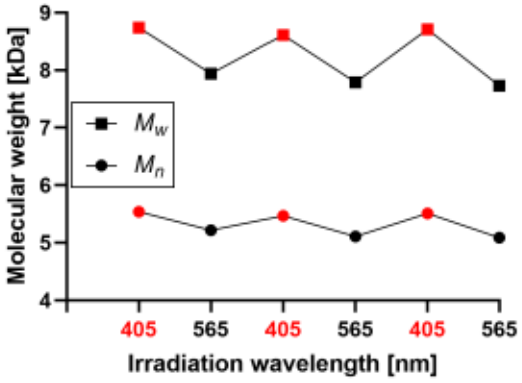

PSS	M_n [kDa]	M_w [kDa]
405 nm (1)	5.54	8.74
525 nm (1)	5.22	7.94
405 nm (2)	5.47	8.61
525 nm (2)	5.11	7.79
405 nm (3)	5.51	8.71
525 nm (3)	5.09	7.73

Figure 3.7 & Table 3.9. Apparent molecular weights M_n and M_w of polymer **P2a** after cyclic light irradiation at 405 nm (red) and 565 nm wavelength (black)

The synthetic strategy towards functionalized diazocines developed in **Project I** was applied to gain access to more diazocine-containing building blocks for the purpose of polymerization. Side-chain azopolymers generally achieve a high alignment of the pendant azobenzene groups in the polymer matrix[29] but diazocine as a photoswtichable pendant group has only been little studied.[151] To synthesize a diazocine-derived

monoacrylate, compound **1d** from **Project II** was subjected to acylation with acryloyl chloride to obtain **M3** in 28% yield (see Scheme 3.9).

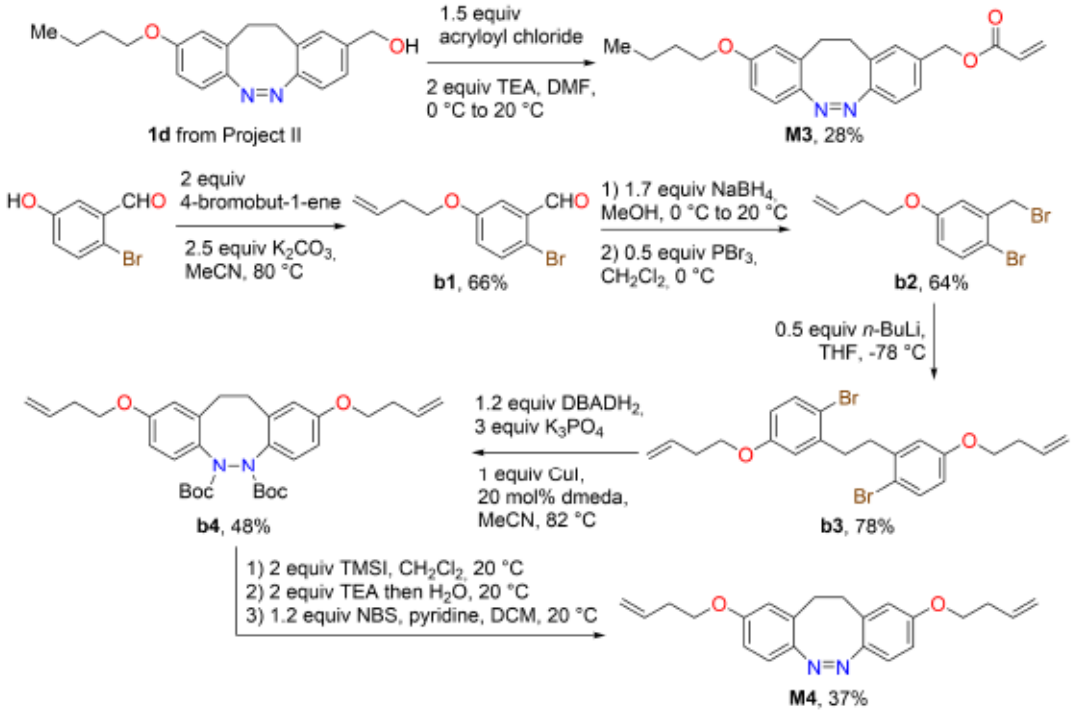

Scheme 3.9. Synthetic route towards diazocine monoacrylate **M3** and diazocine diolefin **M4**.

The interconnection of diazocine monomers linked by linear alkyl chains could also provide a polymer matrix with high crystalline content[155] as the more polar and bulkier ester or amide linkages could interfere with the alignment or crystallization process. The diolefin monomer **M4** was synthesized by applying the typical procedure towards diazocines developed in **Project I** to the 2-bromobenzyl bromide derivative **b2** (see Scheme 3.9). **b2** was prepared from 2-bromo-5-hydroxybenzaldehyde by Williamson ether synthesis with 4-bromobut-1-ene (66% yield), followed by the transformation of the benzaldehyde to the benzyl bromide in two steps and in overall 64% yield. The photochromism of the potential monomers **M3** and **M4** was characterized by UV-Vis and NMR spectroscopy (see Table 3.10 and Figure 3.8).

Table 3.10. Diazocine photoswitching data of **M3** and **M4** obtained from UV-Vis and NMR spectroscopy in acetonitrile

Diazocine Monomer	$\lambda_{max}(Z)$ [nm]	PSS (525 nm) % (*Z*)	$\lambda_{max}(E)$ [nm]	PSS (405 nm) % (*E*)
M3	407	>99%	491	69%
M4	405	>99%	488	65%

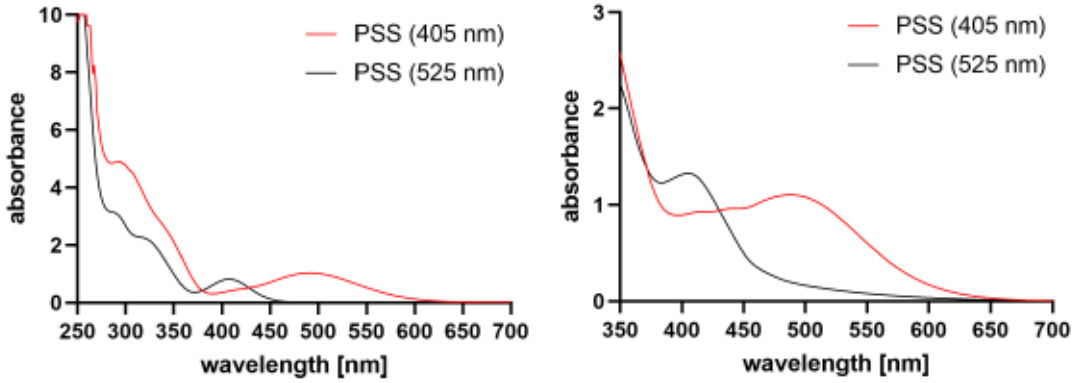

Figure 3.8. UV–Vis spectra of compounds **M3** (left) and **M4** (right) after light irradiation at 405 nm (red) and 525 nm wavelength (black) in acetonitrile.

4 Summary and Outlook

The present thesis deals with an alternative synthetic method towards ethylene-bridged azobenzenes, so-called diazocines (**Project I**), the optimization of ATRP conditions to generate diazocine-doped elastomers via ATRP (**Project II**) and the concatenation of diazocine monomers to build linear main-chain azopolymers (**Project III**). With a focus on the photochromism of diazocine as a molecular switch, the final products were characterized by UV-Vis and ^{1}H NMR spectroscopy for their potential application in functional materials.

In **Project I**, a new synthetic method for the synthesis of diazocines was established. Common strategies commence with 1,2-substituted benzenes for the construction of the ethylene bridge to yield 2,2′-bibenzyls, either by the base-promoted oxidation of toluene[63] or the hydrogenation of tolanes.[75] The present work utilized benzyl bromides as starting materials for diazocine syntheses (see Scheme 4.1) which were readily obtained from the Wohl-Ziegler radical bromination of toluenes or from the conversion of benzyl alcohols with phosphorus tribromide. 2,2′-Dibromobibenzyl compounds were easily generated by the Wurtz-type reduction of 2-bromobenzyl bromides with *n*-butyllithium without a need for activation. The bromine atoms on the phenyl rings were converted to iodine atoms by further lithiation with *n*-butyllithium and quenching with iodine. To integrate functional groups such as nitrile and methyl ester which are sensitive to organolithium reagents, benzyl bromides were metalated with zinc to undergo a Negishi-type coupling with $[NiCl_2(PPh_3)_2]$ as the catalyst.[156]

Distinctive coupling between different 1,2-substituted benzenes enables access to asymmetric bibenzyls for the generation of asymmetric diazocines. In an approach conducted by Trauner and co-workers, the transformation of an acetylene derivative by two successive Sonogashira reactions to the tolane and subsequent hydrogenation yielded the asymmetric bibenzyl compound.[75] However, this approach could not be applied in the present strategy because bromine or iodine substituents on the benzene rings were reserved for the ensuing C–N coupling reactions. For this reason, asymmetric stilbenes were synthesized in a Wittig reaction between a benzaldehyde and a phosphonium ylide. Phosphonium ylides were obtained from the phosphorylation of benzyl bromides

with triphenylphosphine followed by the deprotonation with potassium *tert*-butoxide or sodium methoxide. Subsequent hydrogenation of the central double bond of stilbene with Adams' catalyst provided the asymmetric bibenzyl compounds. Hydrogenation with in situ-generated diimide from the thermal degradation of tosyl hydrazide only provided the bibenzyl product in incomplete conversion and lower yield.

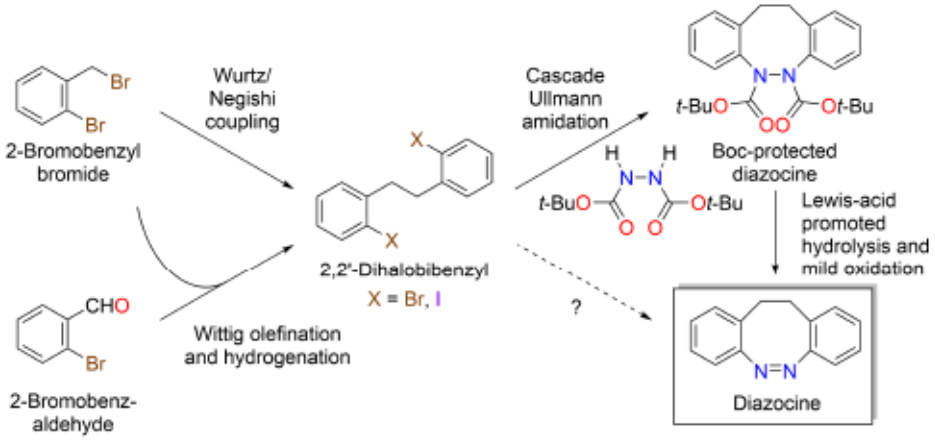

Scheme 4.1. Three-step synthetic method towards substituted diazocine products from 2-bromobenzyl bromides as starting materials.

The construction of the diazocine heterocycle had proceeded through the intramolecular coupling of the bibenzyl compounds with nitrogen-based functional groups at the 2,2′-positions. By using a dinitrogen building block to connect the 2,2′-dibromo or 2,2′-diiodo positions of bibenzyl compounds in two consecutive C–N coupling reactions, the diazocine heterocycle was established without traversing multiple redox intermediates and different nitrogen species. Di-*tert*-butyl hydrazine-1,2-dicarboxylate ($DBADH_2$) was chosen as the dinucleophile for cascade Ullmann-Goldberg amidation reactions with 2,2′-dibromo- or 2,2′-diiodobibenzyl electrophiles due to the very efficient deprotection of *tert*-butyloxycarbonyl (Boc) protecting groups and the high nucleophilicity of the nitrogen atoms. The reaction follows the conditions optimized by Buchwald and co-workers, employing the Cu(I)-dmeda complex as the catalyst and the auxiliary inorganic base K_3PO_4 to quench the originating hydrogen halide acid.[157] This one-pot reaction was carried out in acetonitrile instead of DMF as the solvent and the amount of CuI catalyst had to be increased for the conversion of the less reactive 2,2′-dibromobibenzyls in order to obtain higher product yields. This finding suggests the requirement of an iodide source for the reaction involving the less reactive aryl bromide electrophiles.

The attached Boc protecting groups on the heterocycle are generally easy to cleave under acidic environments but the resulting exposed diazocine ring could further undergo an acid-promoted benzidine rearrangement, leading to undesired products. Therefore, the hydrolytic deprotection of Boc groups was carried out under the promotion of the Lewis acid trimethylsilyl iodide and in the presence of triethylamine as the base. After

deprotection, the exposed hydrazo group was readily oxidized to the diazo group with *N*-bromosuccinimide/pyridine under mild conditions. Future work should include different dinitrogen building blocks for the synthesis of diazocines, containing carbamate groups to be deprotected under basic conditions or the direct implementation of hydrazine to carry out cascade Buchwald-Hartwig aminations on 2,2′-dihalobibenzyls. In the proposed scenarios, oxidation to the diazo group could directly follow the carbamate deprotection or the C–N coupling reactions in the same reaction mixture.

The photostationary states at 385 and 565 nm wavelength of the synthesized diazocine compounds were captured by UV-Vis and ^{1}H NMR spectroscopy in acetonitrile, except for the carboxylic acids which were measured in DMSO (see Figure 4.1). The majority of diazocine compounds accumulated 77–87% of the (*E*) isomer after photoirradiation at 385 nm wavelength. The electron-poor pyridine species attained the highest (87%) and the electron-rich thiophene species the lowest (18%) (*E*)/(*Z*) ratio. Amino and hydroxy groups on the diazocine caused rapid (*E*)→(*Z*) thermal relaxation which prevented accurate PSS measurements. All diazocine samples were switched back quantitatively to the (*Z*) state after 565 nm irradiation within 2 min. Therefore, light sources at 385 and 565 nm irradiation wavelengths are highly suitable for efficient diazocine photoswitching. However, the photoconversion yields for the (*E*) isomer are expected to shift with slightly different irradiation wavelengths according to the different absorption spectra of each diazocine derivative.

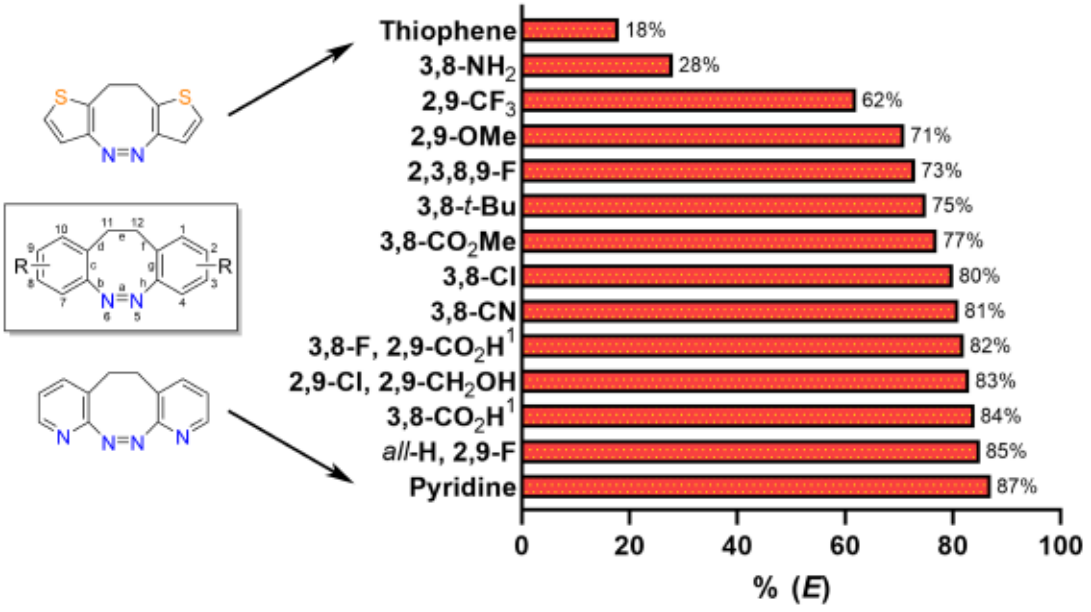

Figure 4.1. (*E*) isomer content of diazocine derivatives at PSS (385 nm) in acetonitrile. [1]In DMSO. For 2,9-OH and 2,9-NH_2, the thermal relaxation to the (*Z*) isomer was faster than data acquisition of the (*E*) isomer.

Generally, the acylation of primary amines and alcohol functions to form amide and ester groups is a facile assembling method to create reactive alkyl halide initiators for ATRP and vinyl monomers for radical and addition polymerizations. Diazocine diamines were synthesized from the dichlorides via Buchwald-Hartwig amination and the hydroxymethyl derivatives were obtained after reducing the methyl ester functions on diazocine with diisobutylaluminium hydride, followed by the re-oxidation of the hydrazo to the diazo group with $CuCl_2$/air.[63] For the realization of **Projects II** and **III**, the primary amines and alcohols of diazocine were acylated with α-bromoisobutyryl bromide (BIBB) and acryloyl chloride to obtain appending alkyl halide and acrylate functions (see Figure 4.2). Additionally, a diazocine diacrylate was prepared containing long alkyl spacer chains as spacers between molecular switch and acrylate groups. Aliphatic terminal olefins on diazocine could fulfill the role of a crosslinker or monomer in transition metal-catalyzed polymerization reactions.

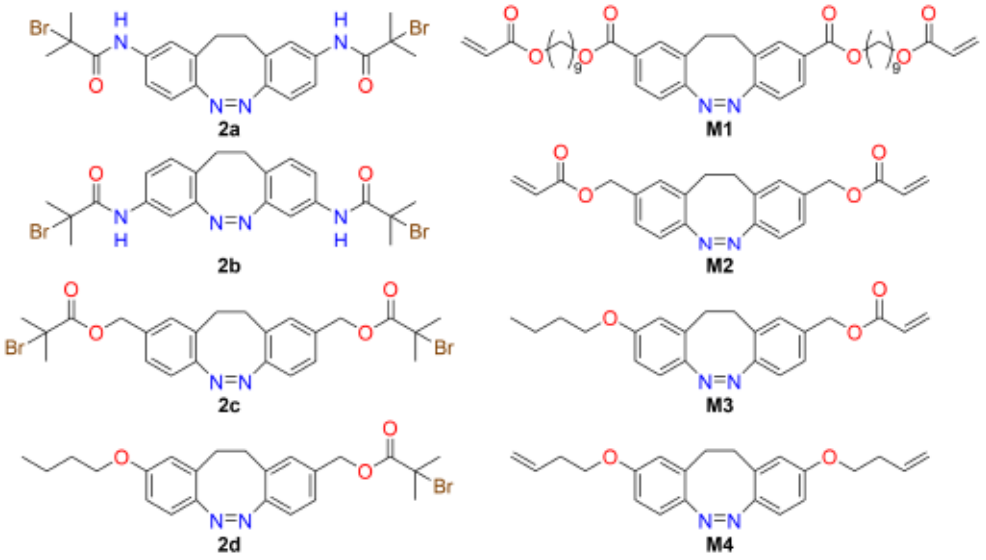

Figure 4.2. Synthesized diazocine-based ATRP initiators (left) and monomers (right) for polymerization.

In **Project II**, four diazocine-functionalized alkyl halide initiators were synthesized for the polymerization of methyl acrylate and methyl methacrylate via ARGET ATRP. The reaction conditions for the synthesis of poly(methyl acrylate) were optimized, especially comparing the reducing agents Cu(0) with ascorbic acid. In comparison to the commercially available initiator EBiB, ATRP initiation decelerated when diazocine-based ATRP initiators were used. Therefore, the catalyst and reducing agent concentrations were increased to ensure a higher initial availability of $Cu(I)L^+$ activator for a more efficient initiation. However, high activator concentrations resulted in lower deactivation rates and less control over the propagation, so that dispersity increased from less than 1.1 for

EBiB to 1.4 for the diazocine-based initiators **2a–2d**. The dependency on the catalyst concentration indicated that the initiation process was decelerated by the diazocine-based ATRP initiators, hence producing higher dispersities and more radical terminations under ARGET ATRP conditions.[129] The heterogenous reaction environment with Cu(0) wire as the reducing agent proved to be inferior to the highly soluble ascorbic acid which was required to accelerate the initiation process. Especially for the polymerization of acrylates, the OMRP equilibrium is shifted towards the organometallic species which can lead to increased termination events including chain-end coupling. In conclusion, slow initiations did not only affect the polymer conversion and dispersity but also increased radical chain terminations. In fact, 405 nm photoirradiation led to the rapid termination during the initial stages of ATRP. The $Cu(I)L^+$ complex was presumably photoactivated, catalyzing the reaction between the diazocine-based initiator **2a** and methyl acrylate to the corresponding iminolactone. The same photoactivated $Cu(I)L^+$ catalyst has been employed by Anastasaki and co-workers to gain photocontrol over the ATRP equilibrium (photoATRP),[158] thus further reiterating the crucial importance of fast initiations during controlled radical polymerizations.

The photochromism of the resulting diazocine-centered and diazocine-capped PMA and PMMA chains was analyzed by UV-Vis spectroscopy in THF solution and in the solid state. All samples exhibited efficient photochromism without notable differences from the initiators. At room temperature (20 °C), PMA is in a rubbery state due to its low T_g of 16 °C[159] while PMMA is in a glassy state with a significantly higher T_g of 105 °C.[160] For this reason, the solid PMMA matrix imposed individual conditions for the switching units and higher internal strain, so that the $(E)\rightarrow(Z)$ thermal relaxation of diazocine did not follow first-order kinetics. Furthermore, a notable solvent effect was observed for the diazocine-centered PMA samples. Compared to the solid-state samples of PMA, THF as the solvent presumably cooled down the excited states of (E) diazocine and decelerated the $(E)\rightarrow(Z)$ thermal backswitching process. Future work should include the potential $(Z)\rightarrow(E)$ mechanochromic switching of diazocine in polymers since the $(Z)\rightarrow(E)$ diazocine isomerization is accompanied by molecular elongation. Elastomers like PMA possess high moduli suitable for the transfer of mechanical force toward the polymer chain center.[161]

In **Project III**, the two synthesized diazocine diacrylates were subjected to the Michael-type thiol-ene polyaddition reaction with 1,6-hexanedithiol, catalyzed by dimethylphenylphosphine to yield main-chain diazocine-based polymers (see Scheme 4.2). The resulting short and linear polymer chains with multiple diazocine units in the backbone were characterized by UV-Vis and NMR spectroscopy as well as GPC and DSC. Apart from the photochromic effect upon 405 nm photoirradiation, the polymer chains showed a reversible photoinduced size expansion in THF solution, as a result of the

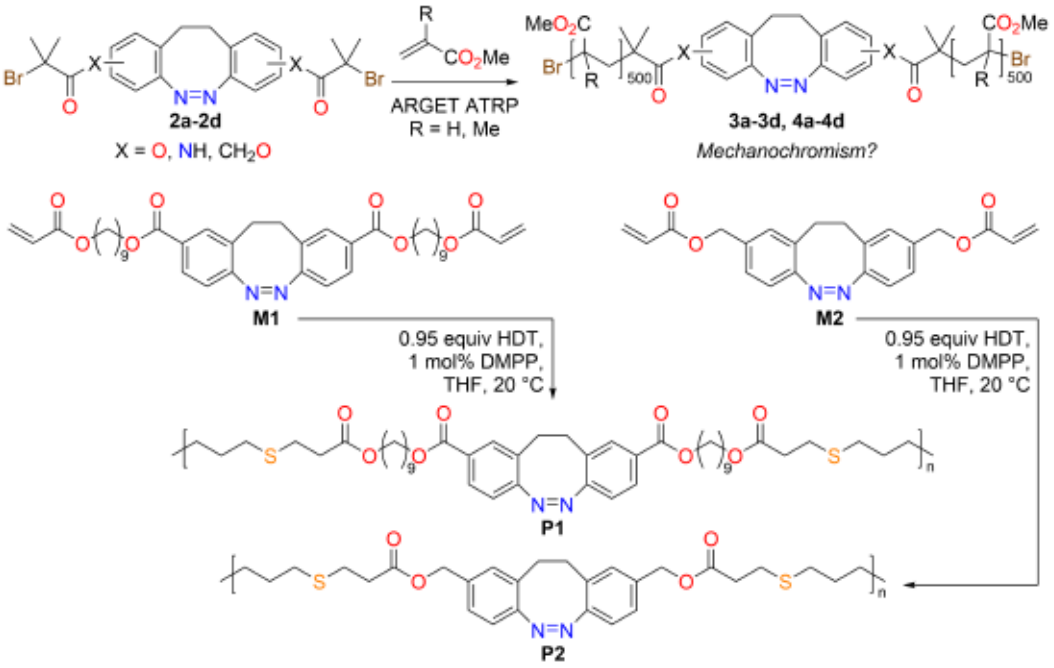

Scheme 4.2. Summary of the polymerization reactions in **Project II** and **III**. HDT = 1,6-hexanedithiol. DMPP = dimethylphenylphosphine.

(*Z*)→(*E*) pincer-type motion of the individual diazocine units. The hydrodynamic size-switching effect was captured by GPC, as evident from the higher apparent molecular weight upon 405 nm photoirradiation. The diazocine polymer with longer alkyl spacers between two diazocine units of the polymer chain typically provided less diazocine content and more conformational freedom, so that the observed size-switching effect was more pronounced in the case of polymer **P2**. This work outlined the unique switching properties of diazocine through the incorporation into synthetic polymers. Acrylate functions on diazocine can be used in many ways, not only in thiol-ene reactions but also for radical polymerization. Therefore, the diacrylate monomer as well as the acrylate-capped polymer chain could be useful for cross-linking, either with polythiol curing agents or with a radical photoinitiator to produce diazocine-containing networks. The monoacrylate **M3** contains diazocine as a pendant group and could be employed in radical polymerizations such as ATRP[125] or RAFT[29] to generate side-chain azopolymer **P3** (see Scheme 4.3). The diazocine-containing α,ω-diene **M4** could be treated as a cross-linker in Pt-catalyzed hydrosilylation reactions to produce silicone polymers.[162] Alternatively, **M4** could undergo Ru-catalyzed acyclic diene metathesis polymerization[163] as a monomer, followed by the hydrogenation of the resulting polyene to yield alkyl chain-linked main-chain azopolymer **P4**.[155]

Future work should include the examination of curing processes including the drawing of fibers from the melt or the manufacture of a thin film. Switching of the diazocine

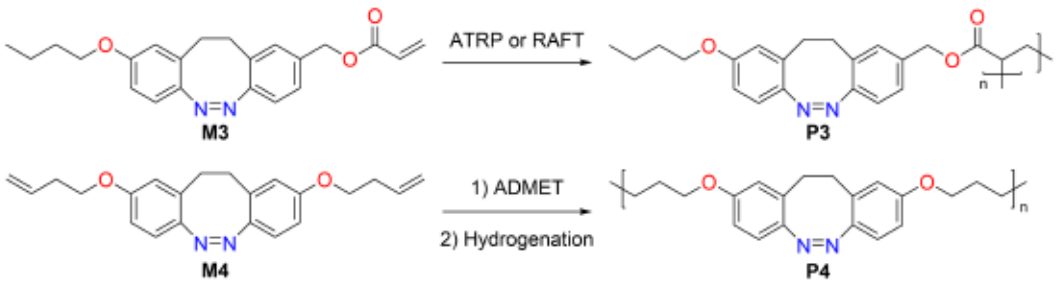

Scheme 4.3. Possible polymerization reactions involving monomers **M3** and **M4**.

units within a polymer network could lead to more pronounced changes in the physicochemical properties and to the photomechanical deformation of the material. It remains unclear whether a phase transition can be invoked by the photoisomerization of diazocine units in a polymer, suggesting a transition from an isotropic (*Z*) to a crystalline (*E*) configuration due to the near-planarity of the (*E*) isomer.[150] The (*Z*) isomer, however, possesses C_2 symmetry[52] and could contribute to polymer chain alignment and crystalline ordering. Therefore, the chemical composition and the polymer topology are crucial factors for the design of novel functional diazocine-based polymers.

Bibliography

[1] In *Molecular Switches*, (Eds.: B. L. Feringa, W. R. Browne), Wiley-VCH Verlag GmbH & Co. KGaA, Weinheim, Germany, **2011**.

[2] L. Buglioni, F. Raymenants, A. Slattery, S. D. Zondag, T. Noël, *Chem. Rev.* **2022**, *122*, 2752–2906.

[3] S. Aubert, M. Bezagu, A. C. Spivey, S. Arseniyadis, *Nat. Rev. Chem.* **2019**, *3*, 706–722.

[4] *Molecular Photoswitches*, 1st ed., (Ed.: Z. L. Pianowski), Wiley, **2022**.

[5] H. Bouas-Laurent, A. Castellan, J. P. Desvergne, R. Lapouyade, *Chem. Soc. Rev.* **2001**, *30*, 248–263.

[6] M. Irie, T. Fukaminato, K. Matsuda, S. Kobatake, *Chem. Rev.* **2014**, *114*, 12174–12277.

[7] H. M. D. Bandara, S. C. Burdette, *Chem. Soc. Rev.* **2012**, *41*, 1809–1825.

[8] F. B. Mallory, C. S. Wood, J. T. Gordon, *J. Am. Chem. Soc.* **1964**, *86*, 3094–3102.

[9] T. Doi, H. Kashida, H. Asanuma, *Org. Biomol. Chem.* **2015**, *13*, 4430–4437.

[10] S. Kobatake, T. Yamada, K. Uchida, N. Kato, M. Irie, *J. Am. Chem. Soc.* **1999**, *121*, 2380–2386.

[11] D. Roke, S. J. Wezenberg, B. L. Feringa, *Proc. Natl. Acad. Sci. U. S. A.* **2018**, *115*, 9423–9431.

[12] N. Koumura, R. W. J. Zijlstra, R. A. van Delden, N. Harada, B. L. Feringa, *Nature* **1999**, *401*, 152–155.

[13] B. L. Feringa, *Angew. Chemie Int. Ed.* **2017**, *56*, 11060–11078.

[14] E. Mitscherlich, *Ann. der Phys. und Chemie* **1834**, *108*, 225–227.

[15] G. S. Hartley, *Nature* **1937**, *140*, 281–281.

[16] I. Lednev, T.-Q. Ye, P. Matousek, M. Towrie, P. Foggi, F. Neuwahl, S. Umapathy, R. Hester, J. Moore, *Chem. Phys. Lett.* **1998**, *290*, 68–74.

[17] C. L. Forber, E. C. Kelusky, N. J. Bunce, M. C. Zerner, *J. Am. Chem. Soc.* **1985**, *107*, 5884–5890.

[18] X. Tong, M. Pelletier, A. Lasia, Y. Zhao, *Angew. Chemie Int. Ed.* **2008**, *47*, 3596–3599.

[19] S. K. Surampudi, H. R. Patel, G. Nagarjuna, D. Venkataraman, *Chem. Commun.* **2013**, *49*, 7519–7521.

[20] Y. Lin, H. R. Hansen, W. J. Brittain, S. L. Craig, *J. Phys. Chem. B* **2019**, *123*, 8492–8498.

[21] E.-h. Cho, K. Luu, S.-y. Park, *Macromolecules* **2021**, *54*, 5397–5409.

[22] N. Biswas, S. Umapathy, *J. Phys. Chem. A* **1997**, *101*, 5555–5566.

[23] G. S. Hartley, R. J. W. Le Fèvre, *J. Chem. Soc.* **1939**, 531–535.

[24] A. Dias, M. Minas Da Piedade, J. Martinho Simões, J. Simoni, C. Teixeira, H. Diogo, Y. Meng-Yan, G. Pilcher, *J. Chem. Thermodyn.* **1992**, *24*, 439–447.

[25] V. Ladányi, P. Dvořák, J. Al Anshori, L. Vetráková, J. Wirz, D. Heger, *Photochem. Photobiol. Sci.* **2017**, *16*, 1757–1761.

[26] I. C. D. Merritt, D. Jacquemin, M. Vacher, *Phys. Chem. Chem. Phys.* **2021**, *23*, 19155–19165.

[27] M. M. Lerch, M. J. Hansen, G. M. van Dam, W. Szymanski, B. L. Feringa, *Angew. Chemie Int. Ed.* **2016**, *55*, 10978–10999.

[28] S. Kim, T. Ogata, S. Kurihara, *Polym. J.* **2017**, *49*, 407–412.

[29] H. Zhou, C. Xue, P. Weis, Y. Suzuki, S. Huang, K. Koynov, G. K. Auernhammer, R. Berger, H.-J. Butt, S. Wu, *Nat. Chem.* **2017**, *9*, 145–151.

[30] S. Corra, M. Curcio, M. Baroncini, S. Silvi, A. Credi, *Adv. Mater.* **2020**, *32*, 1–22.

[31] C. Fedele, T.-P. Ruoko, K. Kuntze, M. Virkki, A. Priimagi, *Photochem. Photobiol. Sci.* **2022**, *21*, 1719–1734.

[32] F. A. Jerca, V. V. Jerca, R. Hoogenboom, *Nat. Rev. Chem.* **2022**, *6*, 51–69.

[33] M. Gao, D. Kwaria, Y. Norikane, Y. Yue, *Nat. Sci.* **2022**, 1–45.

[34] P. Bortolus, S. Monti, *J. Phys. Chem.* **1979**, *83*, 648–652.

[35] E. Fischer, *J. Am. Chem. Soc.* **1960**, *82*, 3249–3252.

[36] T. Asano, T. Yano, T. Okada, *J. Am. Chem. Soc.* **1982**, *104*, 4900–4904.

[37] Y. Hirose, H. Yui, T. Sawada, *J. Phys. Chem. A* **2002**, *106*, 3067–3071.

[38] B. Schmidt, C. Sobotta, S. Malkmus, S. Laimgruber, M. Braun, W. Zinth, P. Gilch, *J. Phys. Chem. A* **2004**, *108*, 4399–4404.

[39] S. Crespi, N. A. Simeth, B. König, *Nat. Rev. Chem.* **2019**, *3*, 133–146.

[40] C. E. Weston, R. D. Richardson, P. R. Haycock, A. J. P. White, M. J. Fuchter, *J. Am. Chem. Soc.* **2014**, *136*, 11878–11881.

[41] Y. Yang, R. P. Hughes, I. Aprahamian, *J. Am. Chem. Soc.* **2014**, *136*, 13190–13193.

[42] V. Gupta, Suhas, *J. Environ. Manage.* **2009**, *90*, 2313–2342.

[43] D. Bléger, J. Schwarz, A. M. Brouwer, S. Hecht, *J. Am. Chem. Soc.* **2012**, *134*, 20597–20600.

[44] D. Bléger, S. Hecht, *Angew. Chemie Int. Ed.* **2015**, *54*, 11338–11349.

[45] S. Samanta, A. A. Beharry, O. Sadovski, T. M. McCormick, A. Babalhavaeji, V. Tropepe, G. A. Woolley, *J. Am. Chem. Soc.* **2013**, *135*, 9777–9784.

[46] A. A. Beharry, O. Sadovski, G. A. Woolley, *J. Am. Chem. Soc.* **2011**, *133*, 19684–19687.

[47] H. Rau, S. Yu-Quan, *J. Photochem. Photobiol. A Chem.* **1988**, *42*, 321–327.

[48] H. Duval, *Bull Soc Chim Fr* **1910**, *7*, 727–732.

[49] E. Tauer, R. Machinek, *Liebigs Ann.* **2006**, *1996*, 1213–1216.

[50] L. Liu, Y. Wang, Q. Fang, *J. Chem. Phys.* **2017**, *146*, 064308.

[51] M. Hammerich, C. Schütt, C. Stähler, P. Lentes, F. Röhricht, R. Höppner, R. Herges, *J. Am. Chem. Soc.* **2016**, *138*, 13111–13114.

[52] R. Siewertsen, H. Neumann, B. Buchheim-Stehn, R. Herges, C. Näther, F. Renth, F. Temps, *J. Am. Chem. Soc.* **2009**, *131*, 15594–15595.

[53] M. Jun, D. K. Joshi, R. S. Yalagala, J. Vanloon, R. Simionescu, A. J. Lough, H. L. Gordon, H. Yan, *ChemistrySelect* **2018**, *3*, 2697–2701.

[54] F. Röhricht, PhD thesis, Kiel University, **2021**.

[55] X. Shen, C. Viney, E. R. Johnson, C. Wang, J. Q. Lu, *Nat. Chem.* **2013**, *5*, 1035–1041.

[56] T. Yamakado, K. Otsubo, A. Osuka, S. Saito, *J. Am. Chem. Soc.* **2018**, *140*, 6245–6248.

[57] H. Sell, C. Näther, R. Herges, *Beilstein J. Org. Chem.* **2013**, *9*, 1–7.

[58] R. Siewertsen, J. B. Schönborn, B. Hartke, F. Renth, F. Temps, *Phys. Chem. Chem. Phys.* **2011**, *13*, 1054–1063.

[59] W. Moormann, T. Tellkamp, E. Stadler, F. Röhricht, C. Näther, R. Puttreddy, K. Rissanen, G. Gescheidt, R. Herges, *Angew. Chemie Int. Ed.* **2020**, *59*, 15081–15086.

[60] O. Carstensen, J. Sielk, J. B. Schönborn, G. Granucci, B. Hartke, *J. Chem. Phys.* **2010**, *133*, 124305.

[61] I. Conti, M. Garavelli, G. Orlandi, *J. Am. Chem. Soc.* **2008**, *130*, 5216–5230.

[62] M. Böckmann, N. L. Doltsinis, D. Marx, *J. Chem. Phys.* **2012**, *137*, 22A505.

[63] W. Moormann, D. Langbehn, R. Herges, *Synthesis* **2017**, *49*, 3471–3475.

[64] T. D. Harris, G. P. Roth, *J. Org. Chem.* **1979**, *44*, 2004–2007.

[65] Z. A. Khan, A. Iqbal, S. A. Shahzad, *Mol. Divers.* **2017**, *21*, 483–509.

[66] B. E. Maryanoff, A. B. Reitz, *Chem. Rev.* **1989**, *89*, 863–927.

[67] K. Sonogashira, *J. Organomet. Chem.* **2002**, *653*, 46–49.

[68] E. Merino, *Chem. Soc. Rev.* **2011**, *40*, 3835–3853.

[69] C. Mills, *J. Chem. Soc. Trans.* **1895**, *67*, 925–933.

[70] K. Ueno, S. Akiyoshi, *J. Am. Chem. Soc.* **1954**, *76*, 3670–3672.

[71] M. G. Pizzolatti, R. A. Yunes, *J. Chem. Soc. Perkin Trans. 2* **1990**, 759–764.

[72] K. Orito, T. Hatakeyama, M. Takeo, S. Uchiito, M. Tokuda, H. Suginome, *Tetrahedron* **1998**, *54*, 8403–8410.

[73] R. Glaser, R. K. Murmann, C. L. Barnes, *J. Org. Chem.* **1996**, *61*, 1047–1058.

[74] F. Klockmann, C. Fangmann, E. Zender, T. Schanz, C. Catapano, A. Terfort, *ACS Omega* **2021**, *6*, 18434–18441.

[75] M. S. Maier, K. Hüll, M. Reynders, B. S. Matsuura, P. Leippe, T. Ko, L. Schäffer, D. Trauner, *J. Am. Chem. Soc.* **2019**, *141*, 17295–17304.

[76] Y. Yang, X. Jing, J. Zhang, F. Yang, C. Duan, *Nat. Commun.* **2022**, *13*, 1940.

[77] J. Deng, X. Wu, G. Guo, X. Zhao, Z. Yu, *Org. Biomol. Chem.* **2020**, *18*, 5602–5607.

[78] M. Walther, W. Kipke, S. Schultzke, S. Ghosh, A. Staubitz, *Synthesis* **2021**, *53*, 1213–1228.

[79] P. Lentes, E. Stadler, F. Röhricht, A. Brahms, J. Gröbner, F. D. Sönnichsen, G. Gescheidt, R. Herges, *J. Am. Chem. Soc.* **2019**, *141*, 13592–13600.

[80] J. Berry, T. K. Lindhorst, G. Despras, *Chem. – A Eur. J.* **2022**, *28*, DOI 10.1002/chem.202200354.

[81] R. Löw, T. Rusch, F. Röhricht, O. Magnussen, R. Herges, *Beilstein J. Org. Chem.* **2019**, *15*, 1485–1490.

[82] J. B. Trads, K. Hüll, B. S. Matsuura, L. Laprell, T. Fehrentz, N. Görldt, K. A. Kozek, C. D. Weaver, N. Klöcker, D. M. Barber, D. Trauner, *Angew. Chemie Int. Ed.* **2019**, *58*, 15421–15428.

[83] J. Ewert, L. Heintze, M. Jordà-Redondo, J. S. Von Glasenapp, S. Nonell, G. Bucher, C. Peifer, R. Herges, *J. Am. Chem. Soc.* **2022**, *144*, 15059–15071.

[84] Q. Zhu, S. Wang, P. Chen, *Org. Lett.* **2019**, *21*, 4025–4029.

[85] H. Lee, J. Tessarolo, D. Langbehn, A. Baksi, R. Herges, G. H. Clever, *J. Am. Chem. Soc.* **2022**, *144*, 3099–3105.

[86] Y. Wang, M. Li, C. Yan, N. Ma, Y. Chen, *CCS Chem.* **2022**, *4*, 704–712.

[87] J.-F. Lutz, J.-M. Lehn, E. W. Meijer, K. Matyjaszewski, *Nat. Rev. Mater.* **2016**, *1*, 16024.

[88] J.-M. Lehn, *Angew. Chemie Int. Ed.* **2013**, *52*, 2836–2850.

[89] D. Roy, J. N. Cambre, B. S. Sumerlin, *Prog. Polym. Sci.* **2010**, *35*, 278–301.

[90] P. Lu, D. Ahn, R. Yunis, L. Delafresnaye, N. Corrigan, C. Boyer, C. Barner-Kowollik, Z. A. Page, *Matter* **2021**, *4*, 2172–2229.

[91] N. Corrigan, M. Ciftci, K. Jung, C. Boyer, *Angew. Chemie Int. Ed.* **2021**, *60*, 1748–1781.

[92] P. Schattling, F. D. Jochum, P. Theato, *Polym. Chem.* **2014**, *5*, 25–36.

[93] Y. Zhao, J. He, *Soft Matter* **2009**, *5*, 2686–2693.

[94] H. Feng, X. Lu, W. Wang, N.-G. Kang, J. Mays, *Polymers* **2017**, *9*, 494.

[95] A.-M. Caminade, E. Hey-Hawkins, I. Manners, *Chem. Soc. Rev.* **2016**, *45*, 5144–5146.

[96] I. Cobo, M. Li, B. S. Sumerlin, S. Perrier, *Nat. Mater.* **2015**, *14*, 143–159.

[97] R. Hsissou, R. Seghiri, Z. Benzekri, M. Hilali, M. Rafik, A. Elharfi, *Compos. Struct.* **2021**, *262*, 113640.

[98] R. H. El Halabieh, O. Mermut, C. J. Barrett, *Pure Appl. Chem.* **2004**, *76*, 1445–1465.

[99] A. A. Berlin, V. I. Liogon'Kii, V. P. Parini, *J. Polym. Sci.* **1961**, *55*, 675–682.

[100] X. Xu, N. Zhou, J. Zhu, Y. Tu, Z. Zhang, Z. Cheng, X. Zhu, *Macromol. Rapid Commun.* **2010**, *31*, 1791–1797.

[101] R. Deloncle, A. M. Caminade, *J. Photochem. Photobiol. C Photochem. Rev.* **2010**, *11*, 25–45.

[102] L. Ding, T. Li, J. Li, W. Song, *Macromol. Chem. Phys.* **2017**, *218*, 1700245.

[103] E. Blasco, B. V. K. J. Schmidt, C. Barner-Kowollik, M. Piñol, L. Oriol, *Macromolecules* **2014**, *47*, 3693–3700.

[104] L. Sun, F. Gao, D. Shen, Z. Liu, Y. Yao, S. Lin, *Polym. Chem.* **2018**, *9*, 2977–2983.

[105] T. Ikeda, M. Nakano, Y. Yu, O. Tsutsumi, A. Kanazawa, *Adv. Mater.* **2003**, *15*, 201–205.

[106] J. Bredenbeck, J. Helbing, J. R. Kumita, G. A. Woolley, P. Hamm, *Proc. Natl. Acad. Sci. U. S. A.* **2005**, *102*, 2379–2384.

[107] A. S. Kuenstler, K. D. Clark, J. Read de Alaniz, R. C. Hayward, *ACS Macro Lett.* **2020**, *9*, 902–909.

[108] M. Dowds, D. Bank, J. Strueben, D. P. Soto, F. D. Sönnichsen, F. Renth, F. Temps, A. Staubitz, *J. Mater. Chem. C* **2020**, *8*, 1835–1845.

[109] S. Peris, B. Tylkowski, J. Carles Ronda, R. Garcia-Valls, J. A. Reina, M. Giamberini, *J. Polym. Sci. Part A Polym. Chem.* **2009**, *47*, 5426–5436.

[110] T. Yoshida, S. Kanaoka, S. Aoshima, *J. Polym. Sci. Part A Polym. Chem.* **2005**, *43*, 5138–5146.

[111] J.-a. Lv, Y. Liu, J. Wei, E. Chen, L. Qin, Y. Yu, *Nature* **2016**, *537*, 179–184.

[112] A. Goulet-Hanssens, F. Eisenreich, S. Hecht, *Adv. Mater.* **2020**, *32*, 1905966.

[113] Z. Hassan, Y. Matt, S. Begum, M. Tsotsalas, S. Bräse, *Adv. Funct. Mater.* **2020**, *30*, 1907625.

[114] H. K. Bisoyi, Q. Li, *Chem. Rev.* **2016**, *116*, 15089–15166.

[115] C. D. Eisenbach, *Polymer* **1980**, *21*, 1175–1179.

[116] T. Ikeda, O. Tsutsumi, *Science* **1995**, *268*, 1873–1875.

[117] T. Todorov, L. Nikolova, N. Tomova, *Appl. Opt.* **1984**, *23*, 4309–4312.

[118] F. Weigert, *Zeitschrift für Phys.* **1921**, *5*, 410–427.

[119] D. Y. Kim, S. K. Tripathy, L. Li, J. Kumar, *Appl. Phys. Lett.* **1995**, *66*, 1166–1168.

[120] P. Rochon, E. Batalla, A. Natansohn, *Appl. Phys. Lett.* **1995**, *66*, 136–138.

[121] A. S. Matharu, S. Jeeva, P. S. Ramanujam, *Chem. Soc. Rev.* **2007**, *36*, 1868–1880.

[122] S. W. Choi, S. Kawauchi, N. Y. Ha, H. Takezoe, *Phys. Chem. Chem. Phys.* **2007**, *9*, 3671–3681.

[123] M. Kato, M. Kamigaito, M. Sawamoto, T. Higashimura, *Macromolecules* **1995**, *28*, 1721–1723.

[124] J.-S. Wang, K. Matyjaszewski, *J. Am. Chem. Soc.* **1995**, *117*, 5614–5615.

[125] K. Matyjaszewski, *Adv. Mater.* **2018**, *30*, 1–22.

[126] T. G. Ribelli, F. Lorandi, M. Fantin, K. Matyjaszewski, *Macromol. Rapid Commun.* **2019**, *40*, 1–44.

[127] F. Lorandi, M. Fantin, K. Matyjaszewski, *J. Am. Chem. Soc.* **2022**, *144*, 15413–15430.

[128] Y. L. Ching, M. L. Coote, A. Gennaro, K. Matyjaszewski, *J. Am. Chem. Soc.* **2008**, *130*, 12762–12774.

[129] P. Krys, K. Matyjaszewski, *Eur. Polym. J.* **2017**, *89*, 482–523.

[130] T. G. Ribelli, K. F. Augustine, M. Fantin, P. Krys, R. Poli, K. Matyjaszewski, *Macromolecules* **2017**, *50*, 7920–7929.

[131] L. Thevenin, C. Fliedel, K. Matyjaszewski, R. Poli, *Eur. J. Inorg. Chem.* **2019**, *2019*, 4489–4499.

[132] K. Min, H. Gao, K. Matyjaszewski, *J. Am. Chem. Soc.* **2005**, *127*, 3825–3830.

[133] K. Min, H. Gao, K. Matyjaszewski, *Macromolecules* **2007**, *40*, 1789–1791.

[134] A. Anastasaki, V. Nikolaou, G. Nurumbetov, P. Wilson, K. Kempe, J. F. Quinn, T. P. Davis, M. R. Whittaker, D. M. Haddleton, *Chem. Rev.* **2016**, *116*, 835–877.

[135] W. Jakubowski, K. Matyjaszewski, *Angew. Chemie Int. Ed.* **2006**, *45*, 4482–4486.

[136] K. Matyjaszewski, W. Jakubowski, K. Min, W. Tang, J. Huang, W. A. Braunecker, N. V. Tsarevsky, *Proc. Natl. Acad. Sci.* **2006**, *103*, 15309–15314.

[137] D. Konkolewicz, K. Schröder, J. Buback, S. Bernhard, K. Matyjaszewski, *ACS Macro Lett.* **2012**, *1*, 1219–1223.

[138] A. J. D. Magenau, N. C. Strandwitz, A. Gennaro, K. Matyjaszewski, *Science* **2011**, *332*, 81–84.

[139] H. Mohapatra, M. Kleiman, A. P. Esser-Kahn, *Nat. Chem.* **2017**, *9*, 135–139.

[140] G. Wang, X. Zhu, C. Zhenping, J. Zhu, *J. Polym. Sci. Part A Polym. Chem.* **2005**, *43*, 2358–2367.

[141] W. Xu, X. Zhu, Z. Cheng, J. Zhu, *J. Macromol. Sci. Part A* **2006**, *43*, 393–403.

[142] R. Lovrien, *Proc. Natl. Acad. Sci.* **1967**, *57*, 236–242.

[143] D. Bléger, Z. Yu, S. Hecht, *Chem. Commun.* **2011**, *47*, 12260.

[144] T. Hugel, N. B. Holland, A. Cattani, L. Moroder, M. Seitz, H. E. Gaub, *Science* **2002**, *296*, 1103–1106.

[145] D. Bléger, T. Liebig, R. Thiermann, M. Maskos, J. P. Rabe, S. Hecht, *Angew. Chemie Int. Ed.* **2011**, *50*, 12559–12563.

[146] G. S. Kumar, D. C. Neckers, *Chem. Rev.* **1989**, *89*, 1915–1925.

[147] G. Groeninckx, H. Berghmans, G. Smets, *J. Polym. Sci. Polym. Phys. Ed.* **1976**, *14*, 591–602.

[148] J. E. Mark, A. C. Society, A. Eisenberg, W. W. Graessley, *Physical Properties of Polymers*, American Chemical Society, **1993**.

[149] C. D. Eisenbach, *Berichte der Bunsengesellschaft für Phys. Chemie* **1980**, *84*, 680–690.

[150] S. Li, G. Han, W. Zhang, *Macromolecules* **2018**, *51*, 4290–4297.

[151] F. Eljabu, J. Dhruval, H. Yan, *Bioorg. Med. Chem. Lett.* **2015**, *25*, 5594–5596.

[152] M. H. Burk, D. Langbehn, G. Hernández Rodríguez, W. Reichstein, J. Drewes, S. Schröder, S. Rehders, T. Strunskus, R. Herges, F. Faupel, *ACS Appl. Polym. Mater.* **2021**, *3*, 1445–1456.

[153] M. H. Burk, S. Schröder, W. Moormann, D. Langbehn, T. Strunskus, S. Rehders, R. Herges, F. Faupel, *Macromolecules* **2020**, *53*, 1164–1170.

[154] S. Samanta, C. Qin, A. J. Lough, G. A. Woolley, *Angew. Chemie Int. Ed.* **2012**, *51*, 6452–6455.

[155] C. Appiah, G. Woltersdorf, R. A. Pérez-Camargo, A. J. Müller, W. H. Binder, *Eur. Polym. J.* **2017**, *97*, 299–307.

[156] M. Iyoda, M. Sakaitan, H. Otsuka, M. Oda, *Chem. Lett.* **1985**, *14*, 127–130.

[157] A. Klapars, X. Huang, S. L. Buchwald, *J. Am. Chem. Soc.* **2002**, *124*, 7421–7428.

[158] A. Anastasaki, V. Nikolaou, Q. Zhang, J. Burns, S. R. Samanta, C. Waldron, A. J. Haddleton, R. McHale, D. Fox, V. Percec, P. Wilson, D. M. Haddleton, *J. Am. Chem. Soc.* **2014**, *136*, 1141–1149.

[159] P. Maiti, A. K. Dikshit, A. K. Nandi, *J. Appl. Polym. Sci.* **2001**, *79*, 1541–1548.

[160] O. Olabisi, R. Simha, *Macromolecules* **1975**, *8*, 206–210.

[161] D. A. Davis, A. Hamilton, J. Yang, L. D. Cremar, D. Van Gough, S. L. Potisek, M. T. Ong, P. V. Braun, T. J. Martínez, S. R. White, J. S. Moore, N. R. Sottos, *Nature* **2009**, *459*, 68–72.

[162] R. Y. Lukin, A. M. Kuchkaev, A. V. Sukhov, G. E. Bekmukhamedov, D. G. Yakhvarov, *Polymers* **2020**, *12*, 2174.

[163] L. Caire da Silva, G. Rojas, M. D. Schulz, K. B. Wagener, *Prog. Polym. Sci.* **2017**, *69*, 79–107.

A Supporting Information

Supporting Information

for

Cross-Coupling Strategy for the Synthesis of Diazocines

-Experimental Data-

Shuo Li,[†] Nadi Eleya,[‡] Anne Staubitz*[,†,‡,‖]

[†]*Otto-Diels-Institute for Organic Chemistry, University of Kiel, Otto-Hahn-Platz 4, 24098 Kiel, Germany*

[‡]*University of Bremen, Institute for Organic and Analytical Chemistry, Leobener Str. 7, 28359 Bremen, Germany*

[‖]*University of Bremen, MAPEX Center for Materials and Processes, Bibliothekstr. 1, 28359 Bremen, Germany*

*staubitz@uni-bremen.de

Table of Contents

General Information

Syntheses under Schlenk conditions or in a glovebox were performed with nitrogen as protection gas. All glassware were dried in an oven at 200 °C for at least 2 h prior to use. Syringes that were used to transfer anhydrous solvents or reagents were purged with nitrogen prior to use.

^{1}H NMR, ^{13}C{^{1}H} NMR and ^{19}F NMR spectra were recorded on a Bruker DRX 500 (^{1}H NMR at 500 MHz, ^{13}C{^{1}H} NMR spectra at 126 MHz and ^{19}F NMR at 471 MHz) at 298.15 K. NMR spectra for the determination of photostationary states of cyclic azobenzenes were recorded on a Bruker AV 600 (^{1}H NMR: 600 MHz). All ^{1}H NMR and ^{13}C{^{1}H} NMR spectra were referenced to the residual proton signals of the solvent (^{1}H), the solvent itself (^{13}C{^{1}H}) or against TMS. ^{19}F NMR spectra were externally referenced to CCl_3F. The exact assignment of the peaks was performed by two-dimensional NMR spectroscopy when possible. The ^{13}C{^{1}H} NMR spectra for compounds **6a-6o** could not be reported because the signals were too small and dispersed probably due to sluggish conformational changes.

High-resolution EI mass spectra were recorded on a JEOL ACCUTOF GCV JMS-T100GCV at 70 eV ionization energy. High-resolution ESI mass spectra were recorded on a ThermoFisher Orbitrap.

IR spectra were recorded on a Perkin Elmer Paragon 1000 FT-IR spectrometer with an A531-G Golden-Gate-ATR-unit.

Melting points were recorded on an electrothermal melting point apparatus Gallenkamp MPD350.BM2.5 and are uncorrected.

Column chromatography was performed using SiO_2 (0.040–0.063 mm, 230–400 mesh ASTM) from Merck.

Thin layer chromatography was performed using POLYGRAM SIL G/UV$_{254}$ pre-coated polyester sheets from Macherey-Nagel and compounds were visualized by exposure to UV light at 254 nm wavelength.

UV–vis spectra were measured with a Lambda 650 spectrophotometer (Perkin-Elmer) at 298.15 K from 700 nm to 250 nm. Quartz cuvettes of 10 mm optical path length were used.

Light irradiation was performed with LED light sources [365 nm: Nichia: NC-4U122E, 300 mW; 385 nm: Nichia NC-SU034A, 340 mW; 565 nm: Luxeon LXML-PX02 350 mW], Sahlmann Photochemical Solutions.

All solvents were freshly distilled prior to use. Dry solvents were stored over 3 Å molecular sieves and degassed by freeze-pump-thaw cycling.

The use of abbreviations follows the conventions from the ACS Style guide.

Reagents

Reagent	Supplier	Purity
(2-Bromo-5-(trifluoromethyl)phenyl)methanol	Apollo Scientific	95%
1,2-Dimethylethylenediamine	abcr	95%
1-(*tert*-Butyl)-4-methylbenzene	Alfa Aesar	95%
1-Bromo-2-(bromomethyl)-4-methoxybenzene	Acros	97%
1-Bromo-2-(bromomethyl)benzene	abcr	98%
1-Bromo-4,5-difluoro-2-methylbenzene	TCI	98%
1-Bromo-4-chloro-2-methylbenzene	abcr	98%
1-Bromo-4-fluoro-2-methylbenzene	TCI	>98.0%
2-Bromo-3-methylpyridine	abcr	95%
2-Bromo-4-chloro-1-methylbenzene	abcr	98.0%
2-Bromo-4-fluoro-1-methylbenzene	abcr	98%
2-Bromo-5-chlorobenzaldehyde	abcr	97%
3-Bromo-4-methylbenzoic acid	abcr	98%
3-Bromo-4-methylbenzonitrile	abcr	97%
3-Bromothiophene-2-carboxaldehyde	TCI	>95.0%
3-Methylphenol	TCI	>98%
4-Bromo-3-methylbenzoic acid	abcr	≥95%
Benzoyl peroxide	Sigma-Aldrich	75%, remainder water
Bromine	Merck	≥99.0%
CuI	Sigma-Aldrich	≥99.5%
$CuCl_2$ dihydrate	Sigma-Aldrich	ACS, ≥99.0%
Di-*tert*-butyl dicarbonate	TCI	>95.0%
Di-*tert*-butyl hydrazine-1,2-dicarboxylate	abcr	98%
Diisobutylaluminum hydride	Acros	1.2 M in toluene
DMSO	Grüssing	99.5%
H_2SO_4	VWR	95%
Hexamethyldisilane	abcr	97%
HBr	Acros	48% in water
Iodine	TCI	>98%
K_3PO_4	abcr	97%, anhydrous
Lithium hexamethyldisilazide	Acros	95%
$Mg(ClO_4)_2$	Alfa Aesar	ACS, anhydrous
$Na_2S_2O_3$	Grüssing	97%
Na_2SO_4	Grüssing	98%
$NaBH_4$	TCI	>95%
NaCl	Grüssing	99.5%

$NaHCO_3$	Grüssing	99.5%
NaOH	Grüssing	99%
NBS	Alfa Aesar	99%
NH_4Cl	Grüssing	99.5%
PBr_3	Acros	99%
Potassium *tert*-butoxide	abcr	95-99%
Pyridine	Grüssing	99.5%
Sodium acetate	Grüssing	99%
Tetraethylammonium iodide	Sigma-Aldrich	98%
Tri-*tert*-butylphosphine	abcr	99%
Triethylamine	Grüssing	99%
Triphenylphosphine	Alfa Aesar	99+%
Tris(dibenzylideneacetone)dipalladium(0)	abcr	20-23% Pd
Zinc	Sigma-Aldrich	dust, <10 µm, ≥98%
$ZnCl_2$	Alfa Aesar	98+%
$[NiCl_2(PPh_3)_2]$	TCI	>96%
m-Chloroperoxybenzoic acid	Merck	4% *m*-chlorobenzoic acid, 41% water
n-Butyllithium	Acros	2.5 M in hexanes
p-Toluenesulfonylhydrazide	abcr	98%

Solvents

CH_2Cl_2	BCD Inc	dried with a PS-MD-5 by Innovation Technology
$CHCl_3$	BCD Inc	technical grade
DMF	VWR	water <150 ppm
HCl	Grüssing	37% in water
NH_3	Grüssing	25% in water
THF	VWR	dried with a PS-MD-5 by Innovation Technology
Acetonitrile	VWR	dried over CaH_2 and degassed
Benzene	BCD Inc	technical grade
Diethyl ether	BCD Inc	dried with a PS-MD-5 by Innovation Technology
Dioxane	Sigma-Aldrich	anhydrous, 99.8%
Ethyl Acetate	BCD Inc	technical grade
Heptane	BCD Inc	technical grade
Hexane	Walter CMP	technical grade
Methanol	BCD Inc	technical grade
Pentane	BCD Inc	technical grade
Toluene	VWR	technical grade
Water		doubly-distilled

Experimental Procedures and Characterization Data

Preparation of Trimethylsilyl Iodide

In a glovebox, Iodine (4.442 g, 17.5 mmol) and hexamethyldisilane (3.58 mL, 17.5 mmol) were added to a round-bottomed flask equipped with a magnetic stirring bar. The reaction mixture was stirred in the glovebox at 20 °C for 30'min and at 60 °C for 1'h before it was cooled down and stored at -30 °C in the glovebox to give trimethylsilyl iodide (35.0 mmol) as a darkbrown oil.

Preparation of Anhydrous $ZnCl_2$

A Schlenk flask was charged with $ZnCl_2$ (20.442 g, 150 mmol) and dried at 150 °C for 6 h at high vacuum (0.01 mbar) under stirring. After cooling to 20 °C, the flask was purged with nitrogen and transferred into a glovebox for use.

Synthesis of 2-Bromobenzyl Bromides and Precursors (S1-S19)

1-Bromo-2-(bromomethyl)-4-chlorobenzene (S1)

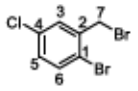

1-Bromo-4-chloro-2-methylbenzene (2.055 g, 10.00 mmol), acetonitrile (20 mL), benzoyl peroxide (484 mg, 2 mmol) and NBS (1.958 g, 11 mmol) were added sequentially to a round-bottomed flask equipped with a reflux condenser. The reaction mixture was stirred at 82 °C for 12 h. After cooling to 20 °C, the reaction mixture was quenched with water (30 mL), extracted with $CHCl_3$ (3 x 50 mL), washed with brine (30 mL) and dried over Na_2SO_4. After filtration, the organic phase was concentrated under reduced pressure followed by silica gel column chromatography (pentane) to furnish the product **S1** as a colorless solid (1.730 g, 6.08 mmol, 61%, lit. 85%[1]).

^{1}H NMR (500 MHz, $CDCl_3$) δ 7.50 (d, *J* = 8.5 Hz, 1H, H-6), 7.45 (d, *J* = 2.5 Hz, 1H, H-3), 7.15 (dd, *J* = 8.5, 2.5 Hz, 1H, H-5), 4.53 (s, 2H, H-7) ppm.

^{13}C{^{1}H} NMR (126 MHz, $CDCl_3$) δ 138.8 (C-2), 134.5 (C-6), 133.9 (C-4), 131.2 (C-3), 130.3 (C-5), 122.4 (C-1), 32.4 (C-7) ppm.

HRMS (EI) *m/z* for $C_7H_5{}^{79}Br^{81}Br^{35}Cl$ $[M]^+$: calcd 283.84261, found: 283.84221 (10); 204.92 (100).

IR (ATR): $\tilde{\nu}$ = 3080 (w), 3056 (w), 0338 (w), 1902 (w), 1764 (w), 1642 (w), 1556 (w), 1460 (s), 1384 (m), 1270 (m), 1217 (s), 1094 (s), 1032 (s), 894 (s), 884 (s), 820 (s), 719 (m), 622 (m), 568 (s), 512 (s) cm^{-1}.

mp: 65 °C.

Rf: 0.61 (hexane)

1-Bromo-2-(bromomethyl)-4-fluorobenzene (S2)

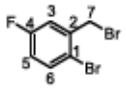

1-Bromo-4-fluoro-2-methylbenzene (9.451 g, 50.00 mmol), acetonitrile (100 mL), benzoyl peroxide (2.422 g, 10 mmol) and NBS (9.789 g, 55 mmol) were added sequentially to a round-bottomed flask equipped with a reflux condenser. The reaction mixture was stirred at 82 °C for 12 h. After cooling to 20 °C, the reaction mixture was quenched with water (50 mL), extracted with $CHCl_3$ (3 x 50 mL), washed with brine (50 mL) and dried over Na_2SO_4. After filtration, the organic phase was concentrated under reduced pressure followed by silica gel column chromatography (pentane) to furnish the product **S2** as a colorless solid (7.209 g, 26.91 mmol, 54%, lit. 99%[2]).

^{1}H NMR (500 MHz, $CDCl_3$) δ 7.53 (dd, *J* = 8.8, 5.2 Hz, 1H, H-3), 7.20 (dd, *J* = 8.8, 3.0 Hz, 1H, H-6), 6.95 – 6.87 (m, 1H, H-5), 4.54 (s, 2H, H-7) ppm.

^{13}C{^{1}H} NMR (126 MHz, $CDCl_3$) δ 162.0 (d, *J* = 248.1 Hz, C-4), 139.0 (d, *J* = 7.7 Hz, C-2), 134.7 (d, *J* = 8.0 Hz, C-3), 118.6 (d, *J* = 3.4 Hz, C-1), 118.3 (d, *J* = 23.4 Hz, C-6), 117.5 (d, *J* = 22.4 Hz, C-5), 32.6 (d, *J* = 1.6 Hz, C-7) ppm.

^{19}F NMR (471 MHz, $CDCl_3$) δ -114.27 (dd, *J* = 13.5, 8.2 Hz) ppm.

HRMS (EI) *m/z* for $C_7H_5{}^{79}Br^{81}BrF$ $[M]^+$: calcd 267.87216, found: 267.87190 (10); 186.96 (100).

IR (ATR): ϑ = 3101 (w), 3078 (w), 3035 (w), 2978 (w), 1894 (w), 1746 (w), 1576 (m), 1471 (s), 1436 (m), 1407 (m), 1271 (m), 1234 (s), 1158 (m), 1125 (m), 1030 (m), 960 (m), 873 (s), 817 (s), 711 (m), 635 (m), 589 (s), 568 (s), 524 (s) cm^{-1}.

mp: 33 °C.

Rf: 0.57 (hexane)

1-Bromo-2-(bromomethyl)-4-(trifluoromethyl)benzene (S3)

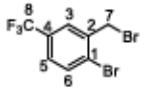

A dry, nitrogen flushed Schlenk-flask equipped with a magnetic stirring bar and a septum was charged with (2-bromo-5-(trifluoromethyl)phenyl)methanol (1.270 g, 5.00 mmol), anhydrous CH_2Cl_2 (25 mL) and the flask was cooled to 0 °C prior to the dropwise addition of PBr_3 (220 µL, 2.5 mmol) over the course of 30 s. The reaction mixture was stirred at 0 °C for 2 h. Then, the reaction mixture was allowed to warm slowly to 20 °C and quenched by dropwise addition of saturated aq $NaHCO_3$ (30 mL), extracted with $CHCl_3$ (3 x 30 mL), washed with brine (30 mL) and dried over Na_2SO_4. After filtration, the organic phase was concentrated under reduced pressure and the crude residue was purified by silica gel column chromatography (pentane) to furnish the product **S3** as a colorless oil (1.250 g, 3.93 mmol, 79%, lit. 79%[3]).

^{1}H NMR (500 MHz, $CDCl_3$) δ 7.74 – 7.68 (m, 2H, H-5,6), 7.45 – 7.39 (m, 1H, H-3), 4.61 (s, 2H, H-7) ppm.

^{13}C{^{1}H} NMR (126 MHz, $CDCl_3$) δ 138.1 (C-1), 134.0 (C-6), 130.5 (q, *J* = 33.3 Hz, C-4), 128.3 (q, *J* = 1.5 Hz, C-2), 127.9 (q, *J* = 3.8 Hz, C-3), 126.6 (q, *J* = 3.7 Hz, C-5), 123.4 (q, *J* = 272.4 Hz, C-8), 32.0 (C-7) ppm.

^{19}F NMR (471 MHz, $CDCl_3$) δ -62.82 ppm.

HRMS (EI) *m/z* for $C_8H_5{}^{79}Br_2F_3$ $[M]^+$: calcd 315.87101, found: 315.87046 (6); 237 (100).

IR (ATR): ϑ = 1605 (w), 1579 (w), 1479 (w), 1438 (w), 1409 (w), 1327 (s), 1274 (s), 1215 (m), 1168 (s), 1122 (s), 1077 (s), 1029 (s), 906 (w), 895 (w), 869 (w), 826 (s), 747 (m), 727 (m), 677 (w) cm^{-1}.

Rf: 0.38 (pentane)

1-Bromo-4-(*tert*-butoxy)-2-methylbenzene (S4)

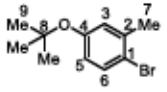

3-Methylphenol (5.407 g, 50.00 mmol), ethyl acetate (100 mL) and DMSO (3.9 mL, 55 mmol) were added sequentially to a round-bottomed flask. The reaction mixture was heated to 60 °C and treated with dropwise addition of aq HBr (6.26 mL, 55 mmol, 48% in water) over the course of 2 min before it was stirred at 60 °C for 15 min. After cooling to 20 °C, the reaction mixture was quenched with saturated aq $NaHCO_3$ (20 mL) and washed with brine (20 mL). The organic phase was concentrated under reduced pressure. The crude residue was directly used in the next step. Adapted from lit.[4]

A dry, nitrogen flushed two-necked round-bottomed flask equipped with a reflux condenser and a magnetic stirring bar was charged with the crude product, di-*tert*-butyl dicarbonate (25.100 g, 115 mmol) and $Mg(ClO_4)_2$ (1.116 g, 5 mmol). The reaction mixture was stirred at 40 °C for 3 h under nitrogen atmosphere. After cooling to 20 °C, the reaction mixture was quenched with water (50 mL), extracted with $CHCl_3$ (3 x 50 mL), washed with brine (20 mL) and dried over Na_2SO_4. After filtration, the organic phase was concentrated under reduced pressure and the crude residue was purified by silica gel column chromatography (pentane/CH_2Cl_2 = 50/50) to furnish the product **S4** as a colorless oil (6.756 g, 27.79 mmol, 56%). Adapted from lit.[5]

^{1}H NMR (500 MHz, $CDCl_3$) δ 7.38 (d, *J* = 8.6 Hz, 1H, H-6), 6.87 (d, *J* = 2.5 Hz, 1H, H-3), 6.72 – 6.68 (m, 1H, H-5), 2.35 (s, 3H, H-7), 1.33 (s, 9H, H-9) ppm.

^{13}C{^{1}H} NMR (126 MHz, $CDCl_3$) δ 154.7 (C-4), 138.4 (C-1), 132.5 (C-6), 126.8 (C-3), 123.2 (C-5), 118.8 (C-2), 78.9 (C-8), 28.9 (C-9), 23.2 (C-7) ppm.

HRMS (EI) *m/z* for $C_{11}H_{15}{}^{81}BrO$ $[M]^+$: calcd 242.03063, found: 242.03099 (2); 185.97 (100).

IR (ATR): ϑ = 2977 (m), 2931 (w), 1593 (w), 1569 (w), 1473 (s), 1392 (m), 1365 (s), 1282 (m), 1263 (m), 1239 (s), 1180 (m), 1153 (s), 1122 (m), 1029 (s), 960 (m), 889 (m), 851 (m), 818 (w), 765 (w), 696 (m), 642 (m), 567 (w) cm^{-1}.

Rf: 0.82 ($CHCl_3$)

1-Bromo-2-(bromomethyl)-4-(*tert*-butoxy)benzene (S5)

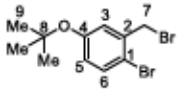

Compound **S4** (1.470 g, 6.05 mmol), benzene (30 mL), benzoyl peroxide (268 mg, 1.11 mmol) and NBS (1.184 g, 6.65 mmol) were added sequentially to a round-bottomed flask equipped with a reflux condenser. The reaction mixture was stirred at 82 °C for 6 h. After cooling to 20 °C, the reaction mixture was quenched with water (30 mL), extracted with $CHCl_3$ (3 x 30 mL), washed with brine (20 mL) and dried over Na_2SO_4. After filtration, the organic phase was concentrated under reduced pressure followed by silica gel column chromatography (pentane/CH_2Cl_2 = 50/50) to furnish the product **S5** as a colorless oil (1.669 g, 5.18 mmol, 86%).

^{1}H NMR (500 MHz, $CDCl_3$) δ 7.44 (d, *J* = 8.6 Hz, 1H, H-6), 7.09 (d, *J* = 2.8 Hz, 1H, H-3), 6.82 (dd, *J* = 8.6, 2.8 Hz, 1H, H-5), 4.54 (s, 2H, H-7), 1.35 (s, 9H, H-9) ppm.

^{13}C{^{1}H} NMR (126 MHz, $CDCl_3$) δ 155.2 (C-4), 137.6 (C-2), 133.6 (C-6), 126.9 (C-3), 125.9 (C-5), 118.0 (C-1), 79.5 (C-8), 33.5 (C-7), 28.9 (C-9) ppm.

HRMS (EI) *m/z* for $C_{11}H_{14}{}^{79}Br^{81}BrO$ $[M]^+$: calcd 321.93909, found 321.93895 (2); 184.96 (100).

IR (ATR): ϑ = 2976 (m), 2932 (w), 2869 (w), 1593 (w), 1568 (w), 1471 (s), 1394 (m), 1366 (s), 1284 (m), 1242 (s), 1153 (s), 1029 (m), 973 (m), 897 (m), 853 (m), 822 (m), 771 (w), 708 (w), 673 (w), 611 (w), 573 (s), 536 (m) cm^{-1}.

R$_f$ 0.82 ($CHCl_3$)

Methyl 4-bromo-3-methylbenzoate (S6)

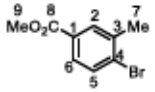

Methanol (80 mL), concd H_2SO_4 (2 mL, 36 mmol, 18 M) and 4-bromo-3-methylbenzoic acid (13.118 g, 61.00 mmol) were added sequentially to a round-bottomed flask equipped with a reflux condenser. The reaction mixture was stirred at 65 °C for 12 h. After cooling to 20 °C, the reaction mixture was quenched with saturated aq $NaHCO_3$ (30 mL), extracted with $CHCl_3$ (3 x 30 mL), washed with brine (30 mL) and dried over Na_2SO_4. After filtration, the organic phase was concentrated under reduced pressure and dried under vacuum (0.1 mbar) to yield the analytically pure product **S6** as a red solid[1] (12.457 g, 54.38 mmol, 89%, lit. 95%[6]).

^{1}H NMR (500 MHz, $CDCl_3$) δ 7.90 (d, *J* = 2.0 Hz, 1H, H-2), 7.69 (dd, 1H, H-6), 7.60 (d, *J* = 8.3 Hz, 1H, H-5), 3.91 (s, 3H, H-9), 2.44 (s, 3H, H-7) ppm.

^{13}C{^{1}H} NMR (126 MHz, $CDCl_3$) δ 166.7 (C-8), 138.4 (C-4), 132.7 (C-5), 131.8 (C-2), 130.6 (C-3), 129.4 (C-1), 128.4 (C-6), 52.4 (C-9), 23.0 (C-7) ppm.

HRMS (EI) *m/z* for $C_9H_9{}^{79}BrO_2$ $[M]^+$: calcd 227.97859, found: 227.97865 (40); 196.96 (100).

[1] The red color is likely due to trace impurities that were already present in the starting material.

IR (ATR): ϑ = 3417 (w), 3018 (w), 2990 (w), 2958 (w), 2841 (w), 1714 (s), 1593 (m), 1571 (m), 1473 (w), 1429 (s), 1380 (m), 1301 (s), 1256 (s), 1198 (s), 1104 (s), 1027 (s), 966 (m), 896 (m), 845 (m), 758 (s), 683 (w), 553 (m), 506 (w) cm^{-1}.

mp: 42 °C.

R$_f$ 0.53 (hexane/ethyl acetate = 80/20)

Methyl 4-bromo-3-(bromomethyl)benzoate (S7)

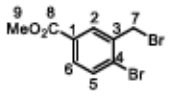

Compound **S6** (12.805 g, 55.90 mmol), acetonitrile (60 mL), benzoyl peroxide (2.700 g, 11.12 mmol) and NBS (10.946 g, 61.50 mmol) were added sequentially to a round-bottomed flask equipped with a reflux condenser. The reaction mixture was stirred at 82 °C for 12 h. After cooling to 20 °C, the reaction mixture was quenched with water (50 mL), extracted with $CHCl_3$ (3 x 30 mL), washed with brine (20 mL) and dried over Na_2SO_4. After filtration, the organic phase was concentrated under reduced pressure followed by silica gel column chromatography (applied gradient from pentane to CH_2Cl_2) to furnish the product **S7** as a colorless solid (12.767 g, 41.46 mmol, 74%, lit. 91%[7]).

^{1}H NMR (500 MHz, $CDCl_3$) δ 8.12 (d, *J* = 2.1 Hz, 1H, H-2), 7.81 (dd, *J* = 8.3, 2.1 Hz, 1H, H-1), 7.66 (d, *J* = 8.3 Hz, 1H, H-5), 4.62 (s, 2H, H-7), 3.93 (s, 3H, H-9) ppm.

^{13}C{^{1}H} NMR (126 MHz, $CDCl_3$) δ 166.0 (C-8), 137.7 (C-3), 133.8 (C-5), 132.3 (C-2), 130.9 (C-6), 130.2 (C-1), 129.9 (C-4), 52.6 (C-9), 32.7 (C-7) ppm.

HRMS (EI) *m/z* for $C_9H_8{}^{79}Br^{81}BrO_2$ $[M]^+$: calcd 307.88706, found: 307.88655 (10); 226.97 (100).

IR (ATR): ϑ = 3421 (w), 3043 (w), 2994 (w), 2945 (w), 1715 (s), 1592 (w), 1430 (m), 1291 (s), 1258 (s), 1224 (s), 1202 (s), 1151 (w), 1108 (m), 1027 (m), 994 (m), 926 (w), 874 (w), 835 (m), 796 (w), 759 (s), 613 (s), 565 (s), 516 (m) cm^{-1}.

mp: 95 °C.

R$_f$ 0.71 ($CHCl_3$)

2-Bromo-1-(bromomethyl)-4-chlorobenzene (S8)

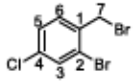

2-Bromo-4-chloro-1-methylbenzene (20.548 g, 100.00 mmol), acetonitrile (150 mL), benzoyl peroxide (4.845 g, 20 mmol) and NBS (19.578 g, 110 mmol) were added sequentially to a round-bottomed flask equipped with a reflux condenser. The reaction mixture was stirred at 82 °C for 12 h. After cooling to 20 °C, the reaction mixture was quenched with water (50 mL), extracted with $CHCl_3$ (3 x 30 mL), washed with brine (30 mL) and dried over Na_2SO_4. After filtration, the organic phase was concentrated under reduced pressure followed by silica gel column chromatography (pentane) to furnish the product **S8** as a colorless oil (19.188 g, 67.47 mmol, 67%, lit. 71%[8]).

^{1}H NMR (500 MHz, $CDCl_3$) δ 7.59 (d, *J* = 2.1 Hz, 1H, H-3), 7.39 (d, *J* = 8.3 Hz, 1H, H-6), 7.28 (dd, *J* = 8.3, 2.1 Hz, 1H, H-5), 4.56 (s, 2H, H-7) ppm.

^{13}C{^{1}H} NMR (126 MHz, $CDCl_3$) δ 135.8 (C-1), 135.3 (C-4), 133.1 (C-3), 132.0 (C-6), 128.4 (C-5), 124.9 (C-2), 32.4 (C-7) ppm.

HRMS (EI) *m/z* for $C_7H_5{}^{79}Br^{81}Br^{35}Cl$ [M]$^+$: calcd 283.84261, found: 283.84221 (10); 204.92 (100).

IR (ATR): ϑ = 3085 (w), 2976 (w), 1783 (w), 1583 (s), 1558 (m), 1466 (s), 1437 (m), 1379 (s), 1223 (s), 1202 (m), 1113 (m), 1096 (m), 1040 (s), 870 (s), 817 (s), 723 (m), 694 (s), 604 (s), 533 (m) cm^{-1}.

Rf: 0.67 (hexane)

2-Bromo-1-(bromomethyl)-4-fluorobenzene (S9)

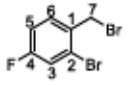

2-Bromo-4-fluoro-1-methylbenzene (11.342 g, 60.00 mmol), acetonitrile (120 mL), benzoyl peroxide (2.907 g, 12 mmol) and NBS (11.747 g, 66 mmol) were added sequentially to a round-bottomed flask equipped with a reflux condenser. The reaction mixture was stirred at 82 °C for 12 h. After cooling to 20 °C, the reaction mixture was quenched with water (50 mL), extracted with $CHCl_3$ (3 x 50 mL), washed with brine (50 mL) and dried over Na_2SO_4. After filtration, the organic phase was concentrated under reduced pressure followed by silica gel column chromatography (pentane) to furnish the product **S9** as a colorless solid (11.344 g, 42.34 mmol, 71%, lit. 87%[9]).

^{1}H NMR (500 MHz, $CDCl_3$) δ 7.44 (dd, *J* = 8.6, 5.9 Hz, 1H, H-6), 7.33 (dd, *J* = 8.1, 2.6 Hz, 1H, H-3), 7.03 (td, 1H, H-5), 4.58 (s, 2H, H-7) ppm.

^{13}C{^{1}H} NMR (126 MHz, $CDCl_3$) δ 162.3 (d, *J* = 253.0 Hz, C-4), 133.3 (d, *J* = 3.7 Hz, C-1), 132.4 (d, *J* = 8.8 Hz, C-6), 124.9 (d, *J* = 9.8 Hz, C-2), 120.8 (d, *J* = 24.6 Hz, C-3), 115.4 (d, *J* = 21.3 Hz, C-5), 32.6 (s, C-7) ppm.

^{19}F NMR (471 MHz, $CDCl_3$) δ -110.86 (dd, *J* = 14.5, 7.3 Hz) ppm.

HRMS (EI) *m/z* for $C_7H_5{}^{79}Br^{81}BrF$ [M]$^+$: calcd 267.87216, found: 267.87222 (5); 186.96 (100).

IR (ATR): ϑ = 3099 (w), 3072 (w), 1887 (w), 1722 (w), 1588 (s), 1483 (s), 1433 (m), 1397 (m), 1260 (w), 1232 (s), 1182 (m), 1134 (m), 1031 (m), 946 (w), 883 (s), 863 (s), 818 (s), 764 (m), 716 (w), 675 (m), 602 (s), 551 (s), 480 (s) cm^{-1}.

mp: 51 °C.

Rf: 0.60 (hexane)

2-Bromo-4-(*tert*-butyl)-1-methylbenzene (S10)

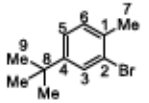

1-(*tert*-Butyl)-4-methylbenzene (889 mg, 6.00 mmol) and $CHCl_3$ (3 mL) were added into a round-bottomed flask. The flask was cooled to 0 °C prior to the dropwise addition of bromine (320 µL, 6.06 mmol) over the course of 1 min. Evolving gas was quenched in an aq NaOH (6 M) solution. The reaction mixture was allowed to warm slowly to 20 °C while stirring for 18 h before it was quenched by dropwise addition of aq $Na_2S_2O_3$ (2 mL, 2 M) and saturated aq $NaHCO_3$ (20 mL), extracted with $CHCl_3$ (3 x 30 mL), washed with brine (30 mL) and dried over Na_2SO_4. After filtration, the organic phase was concentrated under reduced pressure followed by silica gel column chromatography (pentane) to furnish the product **S10** as a colorless oil (1.144 g, 5.04 mmol, 84%, lit. 70%[10]).

^{1}H NMR (500 MHz, $CDCl_3$) δ 7.53 (d, *J* = 2.0 Hz, 1H, H-3), 7.22 (dd, *J* = 8.0, 2.0 Hz, 1H, H-5), 7.15 (d, *J* = 8.0 Hz, 1H, H-6), 2.35 (s, 3H, H-7), 1.29 (s, 9H, H-9) ppm.

^{13}C{^{1}H} NMR (126 MHz, $CDCl_3$) δ 151.0 (C-4), 134.8 (C-1), 130.5 (C-6), 129.5 (C-3), 124.9 (C-2), 124.5 (C-), 34.6 (C-8), 31.4 (C-9), 22.5 (C-7) ppm.

HRMS (EI) *m/z* for $C_{11}H_{15}{}^{79}Br$ [M]$^+$: calcd 226.03571, found: 226.03536 (20); 211.01 (100).

IR (ATR): ϑ = 3076 (w), 2963 (s), 2907 (m), 2872 (m), 1897 (w), 1753 (w), 1606 (w), 1560 (w), 1496 (s), 1480 (m), 1464 (m), 1383 (m), 1362 (m), 1260 (s), 1203 (w), 1115 (m), 1037 (s), 993 (w), 878 (m), 862 (m), 818 (s), 709 (m), 692 (m), 598 (m) cm^{-1}.

Rf: 0.75 (hexane)

2-Bromo-1-(bromomethyl)-4-(*tert*-butyl)benzene (S11)

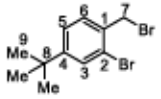

Compound **S10** (3.065 g, 13.50 mmol), acetonitrile (15 mL), benzoyl peroxide (654 mg, 2.70 mmol) and NBS (2.642 g, 14.84 mmol) were added sequentially to a round-bottomed flask equipped with a reflux condenser. The reaction mixture was stirred at 82 °C for 7 h. After cooling to 20 °C, the reaction mixture was quenched with water (50 mL), extracted with $CHCl_3$ (3 x 30 mL), washed with brine (30 mL) and dried over Na_2SO_4. After filtration, the organic phase was concentrated under reduced pressure followed by silica gel column chromatography (pentane) to furnish the product **S11** as a colorless oil (2.787 g, 9.11 mmol, 67%, lit. 86%[10]).

^{1}H NMR (500 MHz, $CDCl_3$) δ 7.57 (d, *J* = 1.9 Hz, 1H, H-3), 7.38 (d, *J* = 8.1 Hz, 1H, H-6), 7.31 (dd, *J* = 8.1, 1.9 Hz, 1H, H-5), 4.59 (s, 2H, H-7), 1.30 (s, 9H, H-9) ppm.

^{13}C{^{1}H} NMR (126 MHz, $CDCl_3$) δ 154.1 (C-4), 134.1 (C-1), 131.0 (C-6), 130.6 (C-3), 125.3 (C-5), 124.5 (C-2), 34.9 (C-8), 33.6 (C-7), 31.2 (C-9) ppm.

HRMS (EI) *m/z* for $C_{11}H_{14}{}^{79}Br^{81}Br$ [M]$^+$: calcd 305.94418, found: 305.94507 (10); 225.03 (100).

IR (ATR): $\tilde{\nu}$ = 2964 (s), 2906 (w), 2871 (w), 1697 (w), 1601 (m), 1552 (w), 1491 (m), 1436 (w), 1387 (s), 1363 (m), 1261 (m), 1231 (s), 1206 (m), 1118 (w), 1039 (s), 874 (m), 830 (m), 699 (m), 663 (m), 632 (s), 570 (m), 518 (w) cm^{-1}.

Rf 0.37 (hexane)

3-Bromo-4-(bromomethyl)benzonitrile (S12)

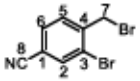

3-Bromo-4-methylbenzonitrile (11.763 g, 60.00 mmol), acetonitrile (60 mL), benzoyl peroxide (2.907 g, 12 mmol) and NBS (11.747 g, 66 mmol) were added sequentially to a round-bottomed flask equipped with a reflux condenser. The reaction mixture was stirred at 82 °C for 12 h. After cooling to 20 °C, the reaction mixture was quenched with water (50 mL), extracted with $CHCl_3$ (3 x 30 mL), washed with brine (30 mL) and dried over Na_2SO_4. After filtration, the organic phase was concentrated under reduced pressure followed by silica gel column chromatography (pentane/ethyl acetate = 90/10) to furnish the product **S12** as a colorless solid (7.839 g, 28.51 mmol, 48%).

^{1}H NMR (500 MHz, $CDCl_3$) δ 7.88 (d, *J* = 1.4 Hz, 1H, H-2), 7.60 (dd, *J* = 8.0, 1.5 Hz, 1H, H-6), 7.57 (d, *J* = 8.0 Hz, 1H, H-5), 4.58 (s, 2H, H-7) ppm.

^{13}C{^{1}H} NMR (126 MHz, $CDCl_3$) δ 142.5 (C-4), 136.6 (C-2), 131.8 (C-5), 131.6 (C-6), 124.9 (C-3), 117.0 (C-8), 114.0 (C-1), 31.7 (C-7) ppm.

HRMS (EI) *m/z* for $C_8H_5{}^{79}Br{}^{81}BrN$ $[M]^+$: calcd 274.87683, found: 274.87699 (10); 193.96 (100).

IR (ATR): $\tilde{\nu}$ = 3095 (w), 3063 (w), 3041 (w), 2231 (m), 1924 (w), 1791 (w), 1739 (w), 1597 (w), 1551 (w), 1482 (m), 1440 (w), 1385 (m), 1271 (w), 1224 (m), 1206 (m), 1188 (m), 1044 (m), 964 (), 881 (m), 837 (s), 746 (m), 717 (m), 673 (w), 619 (s), 572 (m), 462 (m) cm^{-1}.

mp: 83 °C.

Rf 0.37 (hexane/ethyl acetate = 80/20)

Methyl 3-bromo-4-methylbenzoate (S13)

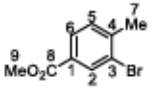

Methanol (50 mL), concd H_2SO_4 (1.5 mL, 27 mmol, 18 M) and 3-bromo-4-methylbenzoic acid (8.602 g, 40.00 mmol) were added sequentially to a round-bottomed flask equipped with a reflux condenser. The reaction mixture was stirred at 65 °C for 12 h. After cooling to 20 °C, the reaction mixture was quenched with saturated aq $NaHCO_3$ (30 mL), extracted with ethyl acetate (3 x 30 mL), washed with brine (30 mL) and dried over Na_2SO_4. After filtration, the organic phase was concentrated under reduced pressure and

dried under vacuum (0.1 mbar) to yield the analytically pure product **S13** as an orange oil[2] (9.006 g, 39.32 mmol, 98%, lit. 86%[11]).

^{1}H NMR (500 MHz, $CDCl_3$) δ 8.20 (d, *J* = 1.5 Hz, 1H, H-2), 7.86 (dd, *J* = 7.9, 1.5 Hz, 1H, H-6), 7.29 (d, *J* = 7.9 Hz, 1H, H-5), 3.91 (s, 3H, H-9), 2.45 (s, 3H, H-7) ppm.

^{13}C{^{1}H} NMR (126 MHz, $CDCl_3$) δ 166.0 (C-8), 143.5 (C-4), 133.6 (C-2), 130.8 (C-5), 129.6 (C-1), 128.5 (C-6), 124.9 (C-3), 52.4 (C-9), 23.3 (C-7) ppm.

HRMS (EI) *m/z* for $C_9H_9{}^{79}BrO_2$ $[M]^+$: calcd 227.97859, found: 227.97818 (40); 196.95 (100).

IR (ATR): $\tilde{\nu}$ = 2951 (w), 2845 (w), 1720 (s), 1603 (w), 1562 (w), 1489 (w), 1434 (m), 1380 (m), 1282 (s), 1250 (s), 1192 (m), 1110 (s), 1041 (m), 973 (m), 901 (w), 850 (w), 756 (s), 679 (m), 628 (w), 503 (w) cm^{-1}.

Rf 0.53 (hexane/ethyl acetate = 80/20)

Methyl 3-bromo-4-(bromomethyl)benzoate (S14)

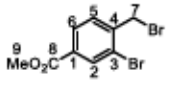

Compound **S13** (8.970 g, 39.17 mmol), acetonitrile (100 mL), benzoyl peroxide (1.841 g, 7.6 mmol) and NBS (7.440 g, 41.8 mmol) were added sequentially to a round-bottomed flask equipped with a reflux condenser. The reaction mixture was stirred at 82 °C for 12 h. After cooling to 20 °C, the reaction mixture was quenched with water (50 mL), extracted with $CHCl_3$ (3 x 30 mL), washed with brine (30 mL) and dried over Na_2SO_4. After filtration, the organic phase was concentrated under reduced pressure followed by silica gel column chromatography (applied gradient from pentane to CH_2Cl_2) to furnish the product **S14** as a colorless solid (6.830 g, 22.18 mmol, 56%, lit. 77%[11]).

^{1}H NMR (500 MHz, $CDCl_3$) δ 8.24 (d, *J* = 1.6 Hz, 1H, H-2), 7.95 (dd, *J* = 8.0, 1.7 Hz, 1H, H-6), 7.53 (d, *J* = 8.0 Hz, 1H, H-5), 4.61 (s, 2H, H-7), 3.93 (s, 3H, H-9) ppm.

^{13}C{^{1}H} NMR (126 MHz, $CDCl_3$) δ 165.4 (C-8), 141.9 (C-3), 134.5 (C-2), 131.9 (C-1), 131.3 (C-5), 129.1 (C-6), 124.4 (C-4), 52.7 (C-9), 32.4 (C-7) ppm.

HRMS (EI) *m/z* for $C_9H_8{}^{79}Br{}^{81}BrO_2$ $[M]^+$: calcd 307.88706, found: 307.88440 (10); 226.98 (100).

IR (ATR): $\tilde{\nu}$ = 3064 (w), 3000 (w), 2948 (w), 2842 (w), 1713 (s), 1601 (w), 1560 (w), 1432 (m), 1392 (m), 1284 (s), 1261 (s), 1226 (m), 1189 (m), 1117 (m), 1041 (w), 964 (m), 929 (w), 843 (w), 799 (m), 768 (s), 721 (m), 682 (m), 637 (m), 605 (m), 523 (m) cm^{-1}.

mp: 61 °C.

Rf 0.71 ($CHCl_3$)

[2] The orange color is likely due to trace impurities that were already present in the starting material.

1-Bromo-2-(bromomethyl)-4,5-difluorobenzene (S15)

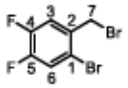

1-Bromo-4,5-difluoro-2-methylbenzene (1.000 g, 4.83 mmol), CH_2Cl_2 (50 mL), benzoyl peroxide (11 mg, 50 µmol) and NBS (860 mg, 4.83 mmol) were added sequentially to a round-bottomed flask equipped with a reflux condenser. The reaction mixture was stirred at 40 °C for 4 h. After cooling to 20 °C, the reaction mixture was quenched with water (20 mL), extracted with $CHCl_3$ (3 x 30 mL) and dried over Na_2SO_4. After filtration, the organic phase was concentrated under reduced pressure followed by silica gel column chromatography (pentane) to furnish the product **S15** as a colorless solid (878 mg, 3.07 mmol, 63%).

^{1}H NMR (500 MHz, $CDCl_3$) δ 7.42 (dd, *J* = 9.5, 7.4 Hz, 1H, H-6), 7.31 (dd, *J* = 10.4, 8.0 Hz, 1H, H-3), 4.51 (s, 2H, H-7) ppm.

^{13}C{^{1}H} NMR (126 MHz, $CDCl_3$) δ 150.0 (q, *J* = 255.3 Hz, C-4), 149.5 (q, *J* = 250.8 Hz, C-5), 133.9 (q, *J* = 5.6 Hz, C-2), 122.2 (q, *J* = 20.1 Hz, C-6), 119.5 (q, *J* = 18.8 Hz, C-3), 118.0 (q, *J* = 7.4 Hz, C-1), 31.7 (d, *J* = 1.1 Hz, C-7) ppm.

^{19}F NMR (471 MHz, $CDCl_3$) δ -134.4, -137.6 ppm.

HRMS (EI) *m/z* for $C_7H_4{}^{79}Br_2F_2$ $[M]^+$: calcd 283.86478, found: 283.86423 (10); 205 (100).

IR (ATR): ϑ = 3047 (w), 2941 (w), 1731 (w), 1584 (m),1506 (m), 1486 (s), 1453 (s), 1388 (m), 1282 (m), 1266 (s), 1185 (s), 1161 (m), 1144 (m), 1015 (w), 969 (m), 876 (m), 839 (m), 796 (s), 704 (w) cm^{-1}.

mp: 103 °C.

Rf: 0.37 (pentane)

(3-Bromothiophen-2-yl)methanol (S16)

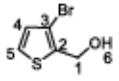

A dry, nitrogen flushed Schlenk-flask equipped with a magnetic stirring bar and septa was charged with 3-bromothiophene-2-carboxaldehyde (3.210 g, 16.80 mmol) and anhydrous methanol (60 mL). After cooling to 0 °C, $NaBH_4$ (1.094 g, 28.91 mmol) was portionwise over the course of 1 min added and the reaction mixture was stirred at 0 °C for 2 h. Then, the reaction mixture was allowed to warm slowly to 20 °C and quenched by dropwise addition of saturated aq NH_4Cl (30 mL), extracted with ethyl acetate (3 x 30 mL), washed with brine (30 mL) and dried over Na_2SO_4. After filtration, the organic phase was concentrated under reduced pressure and the crude residue was purified by silica gel column chromatography (applied gradient from pentane to pentane/ethyl acetate = 50/50) to furnish the product **S16** as a colorless oil (2.955 g, 15.31 mmol, 91%, lit. 90%[12]).

^{1}H NMR (500 MHz, $CDCl_3$) δ 7.26 (d, *J* = 5.3 Hz, 1H, H-4), 6.96 (d, *J* = 5.3 Hz, 1H, H-5), 4.79 (s, 2H, H-1), 2.01 (s, 1H, H-6) ppm.

^{13}C{^{1}H} NMR (126 MHz, $CDCl_3$) δ 138.2 (C-2), 130.3 (C-5), 125.6 (C-4), 109.2 (C-3), 59.2 (C-1) ppm.

HRMS (EI) *m/z* for $C_5H_5{}^{79}BrOS$ $[M]^+$: calcd 191.92445, found: 191.92436 (100).

IR (ATR): ϑ = 3308 (m), 3108 (w), 2928 (w), 2872 (w), 1738 (w), 1520 (m), 1430 (m), 1347 (m), 1231 (w), 1154 (m), 1081 (w), 1007 (s), 968 (s), 856 (s), 789 (m), 698 (s), 641 (m), 584 (s), 501 (m) cm^{-1}.

Rf: 0.21 ($CHCl_3$)

3-Bromo-2-(bromomethyl)thiophene (S17)

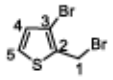

A dry, nitrogen flushed two-necked Schlenk-flask equipped with a magnetic stirring bar and a septum was charged with compound **S16** (75 mg, 40.00 mmol) and anhydrous diethyl ether (60 mL). After cooling to 0 °C, PBr_3 (1.9 mL, 20 mmol) was added dropwise over the course of 1 min and the reaction mixture was stirred at 0 °C for 2 h. Then, the reaction mixture was warmed slowly to 20 °C and quenched by dropwise addition of saturated aq $NaHCO_3$ (30 mL), extracted with $CHCl_3$ (3 x 30 mL), washed with brine (30 mL) and dried over Na_2SO_4. After filtration, the organic phase was concentrated under reduced pressure and the crude residue was purified by silica gel column chromatography (pentane) to furnish the product **S17** as a colorless solid (8.407 g, 32.85 mmol, 82%).

^{1}H NMR (500 MHz, $CDCl_3$) δ 7.32 (d, *J* = 5.4 Hz, 1H, H-4), 6.95 (d, *J* = 5.4 Hz, 1H, H-5), 4.68 (s, 2H, H-1) ppm.

^{13}C{^{1}H} NMR (126 MHz, $CDCl_3$) δ 134.8 (C-2), 130.7 (C-5), 126.9 (C-4), 112.9 (C-3), 25.3 (C-1) ppm.

HRMS (EI) *m/z* for $C_5H_4{}^{79}Br{}^{81}BrS$ $[M]^+$: calcd 255.83800, found: 255.83411 (10); 174.93 (100).

IR (ATR): ϑ = 3104 (w), 3026 (w), 2971 (w), 1749 (w), 1599 (w), 1514 (m), 1413 (s), 1347 (s), 1219 (s), 1186 (s), 1168 (s), 1101 (m), 971 (m), 900 (s), 849 (s), 773 (w), 722 (s), 636 (w), 555 (s) cm^{-1}.

mp: 37 °C.

Rf: 0.46 (hexane)

2-Bromo-3-(bromomethyl)pyridine (S18)

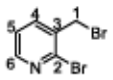

2-Bromo-3-methylpyridine (8.601 g, 50.0 mmol), benzene (50 mL), benzoyl peroxide (2.422 g, 10 mmol) and NBS (10.679 g, 60 mmol) were added sequentially to a round-bottomed flask equipped with a reflux condenser. The reaction mixture was stirred at 80 °C for 12 h. After cooling to 20 °C, the reaction mixture was quenched with water (50 mL), extracted with $CHCl_3$ (3 x 30 mL), washed with brine (30 mL) and dried over Na_2SO_4. After filtration, the organic phase was concentrated under reduced pressure followed by silica gel column chromatography (CH_2Cl_2) to furnish the product **S18** as a colorless solid (6.600 g, 26.30 mmol, 53%, lit. 64%[13]).

^{1}H NMR (500 MHz, $CDCl_3$) δ 8.32 (dd, *J* = 4.7, 1.9 Hz, 1H, H-6), 7.78 (dd, *J* = 7.6, 1.9 Hz, 1H, H-4), 7.29 (dd, *J* = 7.6, 4.7 Hz, 1H, H-5), 4.56 (s, 2H, H-1) ppm.

$^{13}C\{^1H\}$ NMR (126 MHz, $CDCl_3$) δ 149.9 (C-6), 143.8 (C-2), 139.4 (C-4), 134.8 (C-3), 123.4 (C-5), 31.6 (C-1) ppm.

HRMS (EI) *m/z* for $C_8H_8{}^{79}Br^{81}BrN$ [M]$^+$: calcd 250.87683, found: 250.87705 (10); 169.95 (100).

IR (ATR): ϑ = 3050 (w), 3026 (w), 2972 (w), 2924 (w), 2851 (w), 1577 (m), 1558 (m), 1445 (w), 1401 (s), 1275 (m), 1215 (m), 1104 (m), 1063 (m), 1048 (s), 868 (m), 827 (m), 801 (s), 736 (s), 662 (s), 614 (s), 568 (m), 490 (m) cm^{-1}.

mp: 35 °C.

Rf: 0.48 ($CHCl_3$)

(*Z*)-1-Bromo-2-(2-bromo-4-chlorostyryl)-4-chlorobenzene (S19)

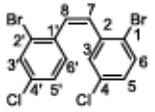

Compound **S8** (5.688 g, 20.00 mmol) and DMF (10 mL) were added to a two-necked round-bottomed flask. Triphenylphosphine (5.246 g, 20.00 mmol) was added and the reaction mixture was stirred at 20 °C for 10 h in a nitrogen atmosphere. Then, the reaction mixture was diluted with toluene (10 mL) and filtered through a Büchner funnel. The remaining solid was washed by solvation in CH_2Cl_2 (15 mL) and addition of diethyl ether (30 mL). The resulting precipitation was collected in a Büchner funnel and dried under vacuum (0.1 mbar).

A dry, nitrogen flushed two-necked Schlenk-flask equipped with a magnetic stirring bar and a septum was charged with the crude product and anhydrous THF (100 mL). The reaction mixture was cooled to 0 °C before potassium *tert*-butoxide (2.618 g, 23.33 mmol) was added and stirred at 0 °C for 30 min. Then, the reaction mixture was treated with 2-bromo-5-chlorobenzaldehyde (3.658 g, 16.67 mmol), allowed to warm to 20 °C and stirred for 12 h. The reaction mixture was quenched with water (50 mL), extracted with $CHCl_3$ (3 x 30 mL), washed with brine (30 mL) and dried over Na_2SO_4. After filtration, the organic phase was concentrated under reduced pressure and the crude residue was purified by silica gel column chromatography (pentane) to furnish the product **S19** as a colorless oil (5.665 g, 13.92 mmol, 70%).

^1H NMR (500 MHz, $CDCl_3$) δ 7.61 (d, *J* = 2.1 Hz, 1H, H-3'), 7.50 (d, *J* = 8.5 Hz, 1H, H-6), 7.08 – 7.02 (m, 2H, H-5,5'), 6.94 (d, *J* = 2.5 Hz, 1H, H-3), 6.88 (d, *J* = 8.4 Hz, 1H, H-6'), 6.76 (d, *J* = 11.9 Hz, 1H, H-8), 6.70 (d, *J* = 11.9 Hz, 1H, H-7) ppm.

$^{13}C\{^1H\}$ NMR (126 MHz, $CDCl_3$) δ 138.5 (C-2), 134.9 (C-1'), 134.2 (C-4'), 134.0 (C-6), 133.2 (C-4), 132.7 (C-3'), 131.4 (C-6'), 131.00 (C-8), 130.5 (C-3), 130.5 (C-7), 129.2 (C-5), 127.6 (C-5'), 124.5 (C-2'), 121.9 (C-1) ppm.

HRMS (EI) *m/z* for $C_{14}H_8{}^{79}Br^{81}Br^{35}Cl_2$ [M]$^+$: calcd 405.83493, found: 405.83415 (30); 246.00 (100).

IR (ATR): ϑ = 3088 (w), 3058 (w), 1888 (w), 1736 (w), 1581 (s), 1547 (m), 1470 (m), 1450 (s), 1374 (m), 1256 (w), 1200 (w), 1159 (w), 1094 (s), 1026 (s), 953 (m), 909 (m), 868 (s), 809 (s), 780 (m), 752 (s), 678 (w), 626 (m), 587 (m), 550 (m), 480 (m) cm^{-1}.

Rf: 0.57 (hexane)

Synthesis of Bibenzyl Derivatives (5a-5p)

Typical procedure for the preparation of bibenzyl derivatives (5a-5e, 5g-5j) by the reaction of benzyl bromides (1-bromo-2-(bromomethyl)benzene, S1-S3, S5, 1-bromo-2-(bromomethyl)-4-methoxybenzene, S8, S9, S11) with *n*-butyllithium and iodine (TP1):

A dry, nitrogen flushed two-necked Schlenk-flask equipped with a magnetic stirring bar and a septum was charged with the benzyl bromide derivative (1.0 equiv) and anhydrous THF (3 mL/mmol). The reaction mixture was cooled to -78 °C and *n*-butyllithium (1.5 equiv, 2.5 M in hexanes) was added dropwise (3 mL/min) under stirring. After completion of the addition and stirring at -78 °C for 5 min, iodine (1.0 equiv) was added. Then, the reaction mixture was warmed to 20 °C before it was quenched with aq $Na_2S_2O_3$ (0.2 mL/mmol, 2 M) and water (3 mL/mmol), followed by an extraction with $CHCl_3$ (3 x 3 mL/mmol). The organic phase was washed with brine (3 mL/mmol) and dried over Na_2SO_4. After filtration, the organic phase was concentrated under reduced pressure and the residue was washed with hexane (5 mL/mmol) and dried under vacuum (0.1 mbar) to furnish the bibenzyl derivative product.

1,2-Bis(2-iodophenyl)ethane (5a)

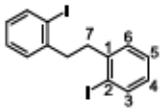

The reaction was performed according to the typical procedure (TP1) using the reagent 1-bromo-2-(bromomethyl)benzene (12.497 g, 50.00 mmol), leading to the corresponding product **5a** (8.838 g, 20.36 mmol, 81%, lit. 25% over two steps[14]) as a colorless solid.

^1H NMR (500 MHz, $CDCl_3$) δ 7.83 (dd, *J* = 7.9, 0.9 Hz, 2H, H-3), 7.28 – 7.20 (m, 4H, H-4,6), 6.92 – 6.88 (m, 2H, H-5), 2.99 (s, 4H, H-7) ppm.

$^{13}C\{^1H\}$ NMR (126 MHz, $CDCl_3$) δ 143.8 (C-2), 139.6 (C-3), 129.9 (C-6), 128.5 (C-4), 128.1 (C-5), 100.7 (C-1), 41.4 (C-7) ppm.

HRMS (EI) *m/z* for $C_{14}H_{12}I_2$ [M]$^+$: calcd 433.90284, found: 433.90215 (40); 216.95 (100).

IR (ATR): ϑ = 3044 (w), 2944 (w), 2858 (w), 1738 (w), 1559 (w), 1462 (s), 1451 (m), 1430 (m), 1295 (w), 1150 (m), 1088 (w), 1005 (s), 863 (w), 748 (s), 717 (s), 643 (m), 538 (m) cm^{-1}.

mp: 100 °C.

Rf: 0.53 (hexane)

1,2-Bis(5-chloro-2-iodophenyl)ethane (5b)

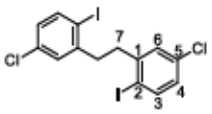

The reaction was performed according to the typical procedure (TP1) using the reagent **S2** (12.279 g, 43.18 mmol), leading to the corresponding product **5b** (6.568 g, 13.06 mmol, 60%) as a colorless solid.

^{1}H NMR (500 MHz, $CDCl_3$) δ 7.74 (d, *J* = 8.4 Hz, 2H, H-3), 7.20 (d, *J* = 2.5 Hz, 2H, H-6), 6.93 (dd, *J* = 8.4, 2.5 Hz, 2H, H-4), 2.94 (s, 4H, H-7) ppm.

^{13}C{^{1}H} NMR (126 MHz, $CDCl_3$) δ 145.2 (C-5), 140.6 (C-3), 134.8 (C-2), 129.7 (C-6), 128.5 (C-4), 97.6 (C-1), 41.0 (C-7) ppm.

HRMS (EI) *m/z* for $C_{14}H_{10}{}^{35}Cl_2I_2$ [M]$^+$: calcd 501.82489, found: 501.82315 (30); 250.93 (100).

IR (ATR): ṽ = 2955 (w), 2934 (w), 2863 (w), 1893 (w), 1736 (w), 1577 (m), 1546 (m), 1457 (s), 1382 (s), 1275 (m), 1198 (m), 1152 (w), 1091 (s), 1012 (s), 948 (m), 869 (s), 815 (s), 767 (m), 710 (w), 540 (w), 491 (m) cm^{-1}.

mp: 124 °C.

Rf 0.53 (hexane)

1,2-Bis(5-fluoro-2-iodophenyl)ethane (5c)

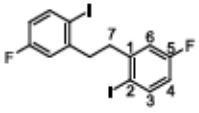

The reaction was performed according to the typical procedure (TP1) using the reagent **S2** (6.104 g, 22.78 mmol), leading to the corresponding product **5c** (3.876 g, 8.25 mmol, 72%) as a colorless solid.

^{1}H NMR (500 MHz, $CDCl_3$) δ 7.77 (dd, *J* = 8.7, 5.7 Hz, 2H, H-3), 6.95 (dd, *J* = 9.5, 3.0 Hz, 2H, H-6), 6.70 (td, 2H, H-4), 2.96 (s, 4H, H-7) ppm.

^{13}C{^{1}H} NMR (126 MHz, $CDCl_3$) δ 163.2 (d, *J* = 247.7 Hz, C-5), 145.6 (d, *J* = 7.2 Hz, C-2), 140.7 (d, *J* = 7.8 Hz, C-3), 116.9 (d, *J* = 21.9 Hz, C-6), 115.8 (d, *J* = 21.8 Hz, C-4), 93.3 (d, *J* = 3.1 Hz, C-1), 41.1 (d, *J* = 0.9 Hz, C-7) ppm.

^{19}F NMR (471 MHz, $CDCl_3$) δ -114.57 (ddd, *J* = 9.2, 8.2, 5.7 Hz) ppm.

HRMS (EI) *m/z* for $C_{14}H_{10}F_2I_2$ [M]$^+$: calcd 469.88399, found: 469.88501 (20); 216.08 (100).

IR (ATR): ṽ = 3072 (w), 2954 (w), 2930 (w), 2861 (w), 1878 (w), 1742 (w), 1598 (w), 1570 (m), 1461 (s), 1452 (s), 1398 (m), 1276 (m), 1230 (s), 1159 (m), 1089 (m), 1012 (m), 948 (m), 873 (s), 806 (s), 706 (w), 572 (s), 540 (w) cm^{-1}.

mp: 116 °C.

Rf 0.67 (hexane)

1,2-Bis(2-iodo-5-(trifluoromethyl)phenyl)ethane (5d)

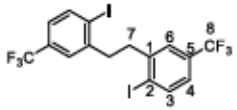

The reaction was performed according to the typical procedure (TP1) using the reagent **S3** (500 mg, 1.57 mmol), leading to the corresponding product **5d** (370 mg, 650 µmol, 41%) as a colorless solid.

^{1}H NMR (500 MHz, $CDCl_3$) δ 7.97 (d, *J* = 8.2 Hz, 2H, H-3), 7.29 (d, *J* = 1.9 Hz, 2H, H-6), 7.16 (dd, *J* = 8.2, 2.1 Hz, 2H, H-4), 3.80 (s, 4H, H-7) ppm.

^{13}C{^{1}H} NMR (126 MHz, $CDCl_3$) δ 144.0 (C-1), 140.2 (C-3), 131.0 (q, *J* = 32.7 Hz, C-5), 126.1 (q, *J* = 3.8 Hz, C-6), 124.7 (q, *J* = 3.2 Hz, C-4), 124.3 (q, *J* = 299.2 Hz, C-8), 104.7 (C-2), 40.8 (C-7) ppm.

^{19}F NMR (471 MHz, $CDCl_3$) δ -63.46 ppm.

HRMS (EI) *m/z* for $C_{16}H_{10}F_6I_2$ [M]$^+$: calcd 569.87761, found: 569.87786 (40); 285 (100).

IR (ATR): ṽ = 2649 (w), 2162 (w), 1790 (w), 1498 (m), 1471 (s), 1456 (w), 1410 (w), 1384 (w), 1350 (w), 1264 (w), 1248 (m), 1233 (s), 1172 (w), 1127 (m), 1106 (m), 929 (s), 901 (m), 874 (s), 764 (s), 722 (s), 671 (m).

mp: 156 °C.

Rf 0.25 (heptane/ethyl acetate = 90/10)

1,2-Bis(5-(*tert*-butoxy)-2-iodophenyl)ethane (5e)

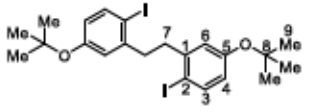

A dry, nitrogen flushed two-necked Schlenk-flask equipped with a magnetic stirring bar and a septum was charged with compound **S5** (1.610 g, 5.00 mmol) and anhydrous THF (20 mL). The reaction mixture was cooled to -78 °C and *n*-butyllithium (3 mL, 7.5 mmol, 2.5 M in hexanes) was added dropwise over the course of 1 min under stirring. After completion of the addition and stirring at -78 °C for 5 min, iodine (1.269 g, 5.0 mmol) was added. Then, the reaction mixture was warmed to 20 °C before it was quenched with aq $Na_2S_2O_3$ (5 mL, 2 M), water (30 mL) extracted with $CHCl_3$ (3 x 30 mL), washed with brine (30 mL) and dried over Na_2SO_4. After filtration, the organic phase was concentrated under reduced pressure followed by silica gel column chromatography (applied gradient from pentane to CH_2Cl_2) to furnish the product **5e** as a colorless solid (1.007 g, 1.74 mmol, 70%).

^{1}H NMR (500 MHz, $CDCl_3$) δ 7.66 (d, *J* = 8.5 Hz, 2H, H-3), 6.86 (d, *J* = 2.8 Hz, 2H, H-6), 6.57 (dd, *J* = 8.5, 2.8 Hz, 2H, H-4), 2.94 (s, 4H, H-7), 1.30 (s, 18H, H-9) ppm.

$^{13}C\{^1H\}$ NMR (126 MHz, $CDCl_3$) δ 156.1 (C-5), 144.3 (C-2), 139.5 (C-3), 125.8 (C-6), 124.0 (C-4), 93.2 (C-1), 79.0 (C-8), 41.2 (C-7), 28.9 (C-9) ppm.

HRMS (EI) *m/z* for $C_{22}H_{28}I_2O_2$ $[M]^+$: calcd 578.01787, found: 578.01765 (1); 212.07 (100).

IR (ATR): ϑ = 2975 (m), 2930 (w), 2864 (w), 1761 (w), 1587 (w), 1559 (w), 1463 (s), 1390 (m), 1365 (s), 1283 (m), 1261 (m), 1236 (s), 1154 (s), 1143 (s), 1103 (m), 1010 (m), 968 (m), 892 (m), 851 (m), 818 (m), 765 (w), 706 (w), 658 (m), 583 (w), 547 (w) cm^{-1}.

mp: 101 °C.

Rf: 0.72 ($CHCl_3$)

Dimethyl 3,3'-(ethane-1,2-diyl)bis(4-bromobenzoate) (5f)

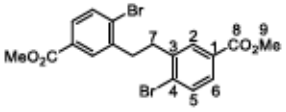

In a glovebox, compound **S7** (1.540 g, 5.00 mmol), anhydrous acetonitrile (7.5 mL), $[NiCl_2(PPh_3)_2]$ (164 mg, 250 µmol), tetraethylammonium iodide (1.286 g, 5.0 mmol) and zinc (490 mg, 7.5 mmol) were added sequentially to a round-bottomed flask equipped with a magnetic stirring bar. The flask was capped with a septum and the reaction mixture was stirred in the glovebox at 20 °C for 18 h before it was transferred out of the glovebox and filtered through a pad of celite. Then, the resulting filtrate was washed with water (30 mL), extracted with $CHCl_3$ (3 x 30 mL), washed with brine (30 mL) and dried over Na_2SO_4. After filtration, the organic phase was concentrated under reduced pressure followed by washing with hexane (20 mL) and ethyl acetate (10 mL) to furnish the product **5f** (718 g, 1.57 mmol, 63%, lit. 64%[14]) as a colorless solid. Adapted from lit.[15]

^1H NMR (500 MHz, $CDCl_3$) δ 7.88 (d, *J* = 2.1 Hz, 2H, H-2), 7.74 (dd, *J* = 8.3, 2.1 Hz, 2H, H-6), 7.63 (d, *J* = 8.3 Hz, 2H, H-2), 3.91 (s, 6H, H-9), 3.09 (s, 4H, H-7) ppm.

$^{13}C\{^1H\}$ NMR (126 MHz, $CDCl_3$) δ 166.6 (C-8), 140.8 (C-4), 133.2 (C-5), 131.6 (C-2), 130.1 (C-3), 129.7 (C-1), 129.0 (C-6), 52.4 (C-9), 36.4 (C-7) ppm.

HRMS (EI) *m/z* for $C_{18}H_{16}{}^{79}Br^{81}BrO_4$ $[M]^+$: calcd 455.93949, found: 455.93962 (10); 226 98 (100).

IR (ATR): ϑ = 3083 (w), 3006 (w), 2956 (w), 2849 (w), 1714 (s), 1595 (w), 1575 (w), 1439 (m), 1398 (w), 1303 (m), 1260 (s), 1204 (m), 1188 (m), 1155 (w), 1106 (s), 1022 (m), 977 (w), 904 (m), 842 (m), 760 (s), 684 (w), 551 (w), 524 (w) cm^{-1}.

mp: 170 °C.

Rf: 0.64 ($CHCl_3$)

1,2-Bis(2-iodo-5-methoxyphenyl)ethane (5g)

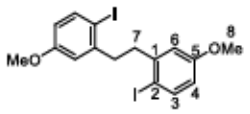

The reaction was performed according to the typical procedure (TP1) using the reagent 1-bromo-2-(bromomethyl)-4-methoxybenzene (5.600 g, 20.00 mmol), leading to the corresponding product **5g** (4.060 g, 8.22 mmol, 82%) as a colorless solid.

^1H NMR (500 MHz, $CDCl_3$) δ 7.68 (d, *J* = 8.7 Hz, 2H, H-3), 6.79 (d, *J* = 3.0 Hz, 2H, H-6), 6.53 (dd, *J* = 8.7, 3.0 Hz, 2H, H-4), 3.75 (s, 6H, H-8), 2.94 (s, 4H, H-7) ppm.

$^{13}C\{^1H\}$ NMR (126 MHz, $CDCl_3$) δ 159.9 (C-5), 139.7 (C-1), 115.6 (C-3), 114.0 (C-6), 89.0 (C-4), 77.2 (C-2), 55.2 (C-8), 41.2 (C-7) ppm.

HRMS (EI) *m/z* for $C_{16}H_{16}I_2O_2$ $[M]^+$: calcd 493.92397, found: 493.92411 (10); 240 (100).

IR (ATR): ϑ = 2923 (w), 1587 (w), 1438 (m), 1312 (w), 1235 (w), 1172 (w), 1001 (m), 848 (w) 756 (s), 719 (s), 682 (s) cm^{-1}.

mp: 112 °C

Rf: 0.48 (hexane/$CHCl_3$ = 50/50)

1,2-Bis(4-chloro-2-iodophenyl)ethane (5h)

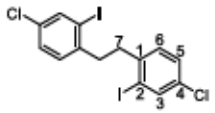

The reaction was performed according to the typical procedure (TP1) using the reagent **S8** (8.531 g, 30.00 mmol), leading to the corresponding bibenzyl **5h** (4.577 g, 9.10 mmol, 61%) as a colorless solid.

^1H NMR (500 MHz, $CDCl_3$) δ 7.82 (d, *J* = 2.2 Hz, 2H, H-3), 7.23 (dd, *J* = 8.2, 2.2 Hz, 2H, H-5), 7.05 (d, *J* = 8.2 Hz, 2H, H-6), 2.94 (s, 4H, H-7) ppm.

$^{13}C\{^1H\}$ NMR (126 MHz, $CDCl_3$) δ 141.9 (C-2), 138.8 (C-3), 132.7 (C-4), 130.3 (C-6), 128.7 (C-5), 100.4 (C-1), 40.5 (C-7) ppm.

HRMS (EI) *m/z* for $C_{14}H_{10}{}^{35}Cl_2I_2$ $[M]^+$: calcd 501.82489, found: 501.82123 (20); 250.92 (100).

IR (ATR): ϑ = 3079 (w), 3043 (w), 2956 (w), 2933 (w), 1886 (w), 1739 (w), 1575 (w), 1552 (w), 1462 (s), 1376 (s), 1152 (m), 1083 (m), 1025 (s), 875 (m), 816 (s), 670 (s), 549 (s) cm^{-1}.

mp: 141 °C.

Rf: 0.68 (hexane)

1,2-Bis(4-fluoro-2-iodophenyl)ethane (5i)

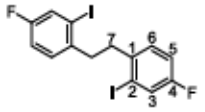

The reaction was performed according to the typical procedure (TP1) using the reagent **S9** (4.673 g, 17.44 mmol), leading to the corresponding product **5i** (2.300 g, 4.89 mmol, 56%) as a colorless solid.

^{1}H NMR (500 MHz, $CDCl_3$) δ 7.54 (dd, *J* = 8.1, 2.6 Hz, 2H, H-3), 7.08 (dd, *J* = 8.5, 5.9 Hz, 2H, H-6), 6.98 (td, *J* = 8.3, 2.7 Hz, 2H, H-5), 2.95 (s, 4H, H-7) ppm.

^{13}C{^{1}H} NMR (126 MHz, $CDCl_3$) δ 160.7 (d, *J* = 249.9 Hz, C-4), 139.4 (d, *J* = 3.4 Hz, C-2), 130.3 (d, *J* = 7.9 Hz, C-6), 126.3 (d, *J* = 23.5 Hz, C-3), 115.5 (d, *J* = 20.7 Hz, C-4), 99.5 (d, *J* = 8.1 Hz, C-1), 40.4 (d, *J* = 1.3 Hz, C-7) ppm.

^{19}F NMR (471 MHz, $CDCl_3$) δ -115.69 (td, *J* = 8.1, 6.0 Hz) ppm.

HRMS (EI) *m/z* for $C_{14}H_{10}F_2I_2$ [M]$^+$: calcd 469.88399, found: 469.87954 (40); 234.95 (100).

IR (ATR): ϑ = 3059 (w), 2955 (w), 2934 (w), 2863 (w), 1888 (w), 1740 (w), 1592 (m), 1579 (m), 1478 (s), 1296 (w), 1254 (w), 1219 (s), 1181 (m), 1149 (w), 1025 (m), 858 (s), 819 (s), 743 (s), 665 (m), 569 (s) cm^{-1}.

mp: 109 °C.

Rf 0.67 (hexane)

1,2-Bis(4-(*tert*-butyl)-2-iodophenyl)ethane (5j)

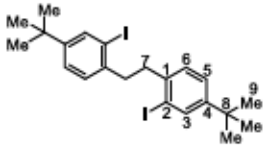

The reaction was performed according to the typical procedure (TP1) using the reagent **S11** (7.650 g, 25.00 mmol), leading to the corresponding product **5j** (3.690 g, 6.75 mmol, 54%) as a colorless solid.

^{1}H NMR (500 MHz, $CDCl_3$) δ 7.82 (d, *J* = 2.0 Hz, 2H, H-3), 7.31 (dd, *J* = 8.0, 2.0 Hz, 2H, H-5), 7.22 (d, *J* = 8.0 Hz, 2H, H-6), 2.93 (s, 4H, H-7), 1.30 (s, 18H, H-9) ppm.

^{13}C{^{1}H} NMR (126 MHz, $CDCl_3$) δ 151.4 (C-4), 141.1 (C-1), 136.6 (C-3), 129.2 (C-6), 125.8 (C-5), 100.9 (C-2), 41.1 (C-7), 34.4 (C-8), 31.4 (C-9) ppm.

HRMS (EI) *m/z* for $C_{22}H_{28}I_2$ [M]$^+$: calcd 546.02804, found: 546.02759 (10); 273.03 (100).

IR (ATR): ϑ = 3007 (w), 2951 (s), 2902 (w), 2865 (w), 1758 (w), 1595 (w), 1543 (w), 1479 (m), 1452 (m), 1384 (m), 1362 (m), 1301 (w), 1259 (m), 1205 (w), 1119 (w), 1030 (m), 881 (m), 857 (m), 835 (s), 764 (w), 732 (w), 680 (m), 610 (s) cm^{-1}.

mp: 116 °C.

Rf 0.69 (hexane)

4,4'-(Ethane-1,2-diyl)bis(3-bromobenzonitrile) (5k)

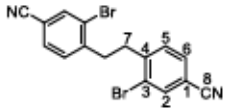

In a glovebox, compound **S12** (200 mg, 730 µmol), anhydrous acetonitrile (1.2 mL), [$NiCl_2(PPh_3)_2$] (24 mg, 40 µmol), tetraethylammonium iodide (187 mg, 730 µmol) and zinc (71 mg, 1.09 mmol) were added sequentially to a round-bottomed flask equipped with a magnetic stirring bar. The flask was capped with a septum and the reaction mixture was stirred in the glovebox at 20 °C for 18 h before it was transferred out of the glovebox and filtered through a pad of celite. Then, the resulting filtrate was washed with water (30 mL), extracted with $CHCl_3$ (3 x 30 mL), washed with brine (30 mL) and dried over Na_2SO_4. After filtration, the organic phase was concentrated under reduced pressure followed by washing with hexane (10 mL) and silica gel column chromatography (CH_2Cl_2) to furnish the bibenzyl derivative product **5k** (50 mg, 130 µmol, 35%) as a colorless solid. Adapted from lit.[15]

^{1}H NMR (500 MHz, $CDCl_3$) δ 7.86 (d, *J* = 1.6 Hz, 2H, H-2), 7.52 (dd, *J* = 7.9, 1.7 Hz, 2H, H-6), 7.23 (d, *J* = 7.9 Hz, 2H, H-5), 3.11 (s, 4H, H-7) ppm.

^{13}C{^{1}H} NMR (126 MHz, $CDCl_3$) δ 145.5 (C-3), 136.3 (C-2), 131.2 (C-6), 131.2 (C-5), 124.9 (C-4), 117.3 (C-8), 112.4 (C-1), 36.2 (C-7) ppm.

HRMS (EI) *m/z* for $C_{16}H_{10}{}^{79}Br^{81}BrN_2$ [M]$^+$: calcd 389.91903, found: 389.91896 (20); 273.03 (100).

IR (ATR): ϑ = 3055 (w), 2960 (w), 2938 (w), 2869 (w), 2229 (m), 1812 (w), 1718 (w), 1598 (w), 1544 (w), 1482 (m), 1454 (m), 1387 (m), 1274 (w), 1191 (m), 1114 (w), 1041 (m), 967 (w), 909 (s), 836 (s), 771 (w), 712 (m), 672 (w), 599 (s) cm^{-1}.

mp: 221 °C.

Rf 0.23 (hexane/ethyl acetate = 80/20)

Dimethyl 4,4'-(ethane-1,2-diyl)bis(3-bromobenzoate) (5l)

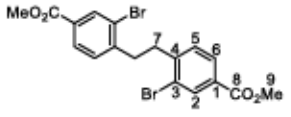

In a glovebox, compound **S14** (780 mg, 2.53 mmol), anhydrous acetonitrile (4 mL), [$NiCl_2(PPh_3)_2$] (83 mg, 130 µmol), tetraethylammonium iodide (651 mg, 2.53 mmol) and zinc (248 mg, 3.80 mmol) were added sequentially to a round-bottomed flask equipped with a magnetic stirring bar. The flask was capped with a septum and the reaction mixture was stirred in the glovebox at 20 °C for 18 h before it was transferred out of the glovebox and filtered through a pad of celite. Then, the resulting filtrate was washed with water (50 mL), extracted with $CHCl_3$ (3 x 30 mL), washed with brine (30 mL) and dried over

Na_2SO_4. After filtration, the organic phase was concentrated under reduced pressure followed by washing with hexane (20 mL) and ethyl acetate (10 mL) to furnish product **5l** (336 mg, 740 µmol, 58%) as a colorless solid. Adapted from lit.[15]

^{1}H NMR (500 MHz, $CDCl_3$) δ 8.22 (d, *J* = 1.7 Hz, 2H, H-2), 7.85 (dd, *J* = 7.9, 1.7 Hz, 2H, H-6), 7.17 (d, *J* = 7.9 Hz, 2H, H-5), 3.92 (s, 6H, H-9), 3.11 (s, 4H, H-7) ppm.

^{13}C{^{1}H} NMR (126 MHz, $CDCl_3$) δ 165.9 (C-8), 145.3 (C-1), 134.1 (C-2), 130.7 (C-5), 130.2 (C-3), 128.7 (C-6), 124.5 (C-4), 52.5 (C-9), 36.2 (C-7) ppm.

HRMS (EI) *m/z* for $C_{18}H_{16}{}^{79}Br^{81}BrO_4$ [M]$^+$: calcd 455.93949, found: 455.93449 (10); 226.98 (100).

IR (ATR): ϑ = 3065 (w), 3026 (w), 2955 (w), 2934 (w), 2865 (w), 1720 (s), 1599 (w), 1563 (w), 1450 (w), 1432 (m), 1392 (m), 1283 (s), 1267 (s), 1252 (s), 1190 (m), 1123 (m), 1039 (w), 966 (m), 911 (w), 845 (m), 761 (s), 717 (m), 681 (m), 627 (w), 512 (w) cm^{-1}.

mp: 186 °C.

Rf. 0.64 ($CHCl_3$)

1-Bromo-2-(2-bromo-4-chlorophenethyl)-4-chlorobenzene (5m)

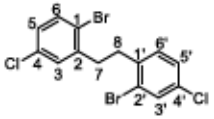

Compound **S19** (5.178 g, 12.77 mmol), THF (75 mL) and *p*-toluenesulfonylhydrazide (17.506 g, 128 mmol) were added sequentially to a two-necked round-bottomed flask equipped with a reflux condenser. The reaction mixture was heated to 65 °C and continuously stirred while an aq sodium acetate solution (15.714 g dissolved in 75 mL water, 191.55 mmol) was added over the course of 24 h under a nitrogen atmosphere. After cooling to 20 °C, the reaction mixture was diluted with water (50 mL), extracted with $CHCl_3$ (3 x 30 mL), washed with brine (30 mL) and dried over Na_2SO_4. After filtration, the organic phase was concentrated under reduced pressure. To the residue was added hexane (200 mL), the suspension was filtered through a Büchner funnel and the resulting filtrate was concentrated under reduced pressure. CH_2Cl_2 (75 mL) and *m*-chloroperoxybenzoic acid (6.611 mg, 38.31 mmol) were added sequentially to the residue. The reaction mixture was stirred at 20 °C for 12°h before it was illuminated with UV light at 365 nm wavelength for 30°min. The reaction mixture was again stirred at 20°C for 24°h and quenched with aq $Na_2S_2O_3$ (20 mL, 2 M), washed with aq HCl (10 mL, 1°M) and saturated aq $NaHCO_3$ (10 mL), extracted with $CHCl_3$ (3 x 30 mL), washed with brine (30 mL) and dried over Na_2SO_4. After filtration, the organic phase was concentrated under reduced pressure followed by silica gel column chromatography (pentane). The crude product was dissolved in hexane (30 mL) and the solid residue was removed by filtration. The resulting solution was concentrated under reduced pressure and dried under vacuum (0.1 mbar) to furnish the product **5m** as a colorless solid (1.042 g, 2.55 mmol, 20%). Adapted from lit.[16]

^{1}H NMR (500 MHz, $CDCl_3$) δ 7.57 (d, *J* = 2.1 Hz, 1H, H-3''), 7.46 (d, *J* = 8.5 Hz, 1H, H-6), 7.20 (dd, *J* = 8.2, 2.1 Hz, 1H, H-5''), 7.16 (d, *J* = 2.5 Hz, 1H, H-3), 7.09 (d, *J* = 8.2 Hz, 1H, H-6''), 7.07 (dd, *J* = 8.5, 2.6 Hz, 1H, H-5), 3.00 – 2.95 (m, 4H, H-7,8) ppm.

^{13}C{^{1}H} NMR (126 MHz, $CDCl_3$) δ 142.1 (C-2), 138.8 (C-1''), 134.0 (C-6), 133.5 (C-4), 133.0 (C-4''), 132.6 (C-3''), 131.4 (C-6''), 130.6 (C-3), 128.2 (C-5), 127.9 (C-5''), 124.8 (C-2''), 122.4 (C-1), 36.3 (C-7), 35.8 (C-8) ppm.

HRMS (EI) *m/z* for $C_{14}H_{10}{}^{79}Br^{81}Br^{35}Cl_2$ [M]$^+$: calcd 407.85058, found: 407.85078 (20); 204.93 (100).

IR (ATR): ϑ = 3084 (w), 3051 (w), 2972 (w), 2941 (w), 2866 (w), 1893 (w), 1736 (w), 1584 (m), 1555 (w), 1458 (s), 1379 (m), 1285 (w), 1201 (m), 1088 (s), 1025 (s), 872 (s), 816 (s), 742 (m), 687 (m), 567 (w), 537 (m), 503 (m) cm^{-1}.

mp: 52 °C.

Rf. 0.68 (hexane)

1,2-Bis(2-bromo-4,5-difluorophenyl)ethane (5n)

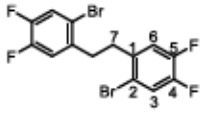

Compound **S15** (500 mg, 1.75 mmol) and THF (10 mL) were added into a pre-dried two-necked Schlenk flask. After cooling to -78 °C, *n*-butyllithium (350 µL, 870 µmol, 2.5 M in hexanes) was added dropwise over the course of 30 s under stirring. After completion of the addition and stirring at -78 °C for 5 min, the reaction mixture was warmed to 20 °C. The reaction mixture was quenched with water (30 mL), extracted with $CHCl_3$ (3 x 30 mL) and washed with brine (30 mL) and dried over Na_2SO_4. After filtration, the organic phase was concentrated under reduced pressure and the crude residue was washed with hexane (20 mL) and dried under vacuum (0.1 mbar) to furnish the product **5n** as a colorless solid (280 mg, 680 µmol, 78%).

^{1}H NMR (500 MHz, $CDCl_3$) δ 7.39 (dd, *J* = 9.6, 7.5 Hz, 2H, H-3), 6.98 (dd, *J* = 10.8, 8.2 Hz, 2H, H-6), 2.95 (s, 4H, H-7) ppm.

^{13}C{^{1}H} NMR (126 MHz, $CDCl_3$) δ 149.5 (q, *J* = 250.2 Hz, C-5), 148.7 (q, *J* = 250.9 Hz, C-4), 136.7 (q, *J* = 5.4 Hz, C-1), 121.6 (q, *J* = 19.7 Hz, C-2), 118.6 (q, *J* = 18.0 Hz, C-6), 117.5 (q, *J* = 7.2 Hz, C-2), 35.6 (C-7) ppm.

^{19}F NMR (471 MHz, CDCl3) δ -138.2, -138.7.

IR (ATR): ϑ = 3051 (w), 2946 (w), 2875 (w), 1735 (w), 1712 (w), 1600 (m), 1513 (m), 1489 (s), 1456 (s), 1395 (s), 1342 (m), 1297 (m), 1284 (m), 1266 (m), 1228 (m), 1192 (s), 1145 (s), 1128 (m), 983 (w), 877 (s), 856 (s), 799 (s), 696 (m), 654 (m) cm^{-1}.

HRMS (EI) *m/z* for $C_{14}H_8{}^{79}Br_2BrF_4$ [M]$^+$: calcd 409.89289, found: 409.89245 (5); 205 (100).

mp: 123 °C

Rf. 0.27 (heptane/ethyl acetate = 90/10)

1,2-Bis(3-bromothiophen-2-yl)ethane (5o)

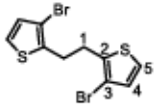

Compound **S17** (6.399 g, 25.00 mmol) and THF (60 mL) were added into a pre-dried two-necked Schlenk flask. After cooling to -78 °C, *n*-butyllithium (5 mL, 12.5 mmol, 2.5 M in hexanes) was added dropwise over the course of 2 min under stirring. After completion of the addition and stirring at -78 °C for 5 min, the reaction mixture was warmed to 20 °C. The reaction mixture was quenched with water (50 mL), extracted with $CHCl_3$ (3 x 30 mL) and washed with brine (30 mL) and dried over Na_2SO_4. After filtration, the organic phase was concentrated under reduced pressure and the crude residue was purified by silica gel column chromatography (pentane) to furnish the product **5o** as a colorless oil (3.967 g, 11.27 mmol, 90%).

^{1}H NMR (500 MHz, $CDCl_3$) δ 7.13 (d, *J* = 5.3 Hz, 2H, H-5), 6.92 (d, *J* = 5.3 Hz, 2H, H-4), 3.12 (s, 4H, H-1) ppm.

^{13}C{^{1}H} NMR (126 MHz, $CDCl_3$) δ 137.2 (C-3), 130.1 (C-4), 123.8 (C-5), 109.7 (C-2), 30.1 (C-1) ppm.

HRMS (EI) *m/z* for $C_{10}H_8{}^{79}Br^{81}BrS_2$ [M]$^+$: calcd 351.84137, found: 351.83925 (30); 176.93 (100).

IR (ATR): ϑ = 3108 (w), 2915 (w), 2847 (w), 1740 (w), 1520 (m), 1439 (m), 1346 (m), 1264 (w), 1216 (w), 1155 (w), 1107 (w), 1001 (w), 904 (w), 863 (s), 757 (w), 697 (s), 611 (m), 575 (w), 505 (m) cm^{-1}.

R_f: 0.54 (hexane)

1,2-Bis(2-bromopyridin-3-yl)ethane (5p)

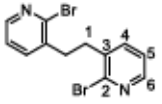

Compound **S18** (5.018 g, 20.00 mmol) and THF (60 mL) were added into a pre-dried two-necked Schlenk flask. After cooling to -78 °C, *n*-butyllithium (4 mL, 10 mmol, 2.5 M in hexanes) was added dropwise over the course of 2 min under stirring. After completion of the addition and stirring at -78 °C for 5 min, the reaction mixture was warmed to 20 °C. The reaction mixture was quenched with water (50 mL), extracted with $CHCl_3$ (3 x 20 mL) and washed with brine (5 mL) and dried over Na_2SO_4. After filtration, the organic phase was concentrated under reduced pressure and the crude residue was purified by silica gel column chromatography (applied gradient from CH_2Cl_2 to CH_2Cl_2/ethyl acetate = 50/50) to furnish the product **5p** as a colorless solid (1.620 g, 4.74 mmol, 47%)

^{1}H NMR (500 MHz, $CDCl_3$) δ 8.26 (dd, *J* = 4.7, 1.9 Hz, 2H, H-6), 7.43 (dd, *J* = 7.5, 1.9 Hz, 2H, H-4), 7.19 (dd, *J* = 7.5, 4.7 Hz, 2H, H-5), 3.07 (s, 4H, H-1) ppm.

^{13}C{^{1}H} NMR (126 MHz, $CDCl_3$) δ 148.3 (C-6), 144.3 (C-3), 139.0 (C-4), 137.3 (C-2), 123.1 (C-5), 35.0 (C-1) ppm.

HRMS (EI) *m/z* for $C_{12}H_{10}{}^{79}Br^{81}BrN_2$ [M]$^+$: calcd 341.91903, found: 341.92061 (60); 169.96 (100).

IR (ATR): ϑ = 3063 (w), 2924 (w), 2898 (w), 1577 (w), 1562 (m), 1430 (m), 1394 (s), 1280 (m), 1230 (w), 1174 (m), 1115 (m), 1045 (s), 812 (s), 765 (m), 708 (m), 668 (s), 560 (w), 482 (s) cm^{-1}.

mp: 146 °C.

R_f: 0.32 ($CHCl_3$)

Synthesis of Bis-*tert*-Butyloxycarbonyl Protected Diazocines (6a-6p)

Typical procedure for the preparation of the functionalized bis-*tert*-butyloxycarbonyl protected diazocines (6a-6e, 6g-6j, 6n) by the reaction of bis-functionalized bibenzyls (5a-5e, 5g-5j, 5n) with di-*tert*-butyl hydrazine-1,2-dicarboxylate in a Cu-catalyzed C-N coupling reaction (TP2):

In a glovebox, the bis-functionalized bibenzyl derivative (1.0 equiv), di-*tert*-butyl hydrazine-1,2-dicarboxylate (1.2 equiv), CuI (10 mol %), K_3PO_4 (3.0 equiv), acetonitrile (5 mL/mmol) and 1,2-dimethylethylenediamine (20 mol %) were added sequentially to a microwave vial. The vial was capped with a crimp cap equipped with a PTFE septum, transferred out of the glovebox and stirred at 82 °C for 18 h. After cooling to 20 °C, the reaction mixture was quenched with water (3 mL/mmol), washed with aq NH_3 (3 mL/mmol, 25%), extracted with $CHCl_3$ (3 x 5 mL/mmol), washed with brine (3 mL/mmol) and dried over Na_2SO_4. After filtration, the organic phase was concentrated under reduced pressure and the crude residue was purified by silica gel column chromatography to furnish the bis-*tert*-butyloxycarbonyl protected diazocine product. Adapted from lit.[17]

Typical procedure for the preparation of the functionalized bis-*tert*-butyloxycarbonyl protected diazocines (6f, 6k-6m, 6o, 6p) by the reaction of bis-functionalized bibenzyls (5f, 5k-5m, 5o, 5p) with di-*tert*-butyl hydrazine-1,2-dicarboxylate in a Cu-catalyzed C-N coupling reaction (TP3):

In a glovebox, the bis-functionalized bibenzyl derivative (1.0 equiv), di-*tert*-butyl hydrazine-1,2-dicarboxylate (1.2 equiv), CuI (1.0 equiv), K_3PO_4 (3.0 equiv), acetonitrile (5 mL/mmol) and 1,2-dimethylethylenediamine (0.2 equiv) were added sequentially to a microwave vial. The vial was capped with a crimp cap equipped with a PTFE septum, transferred out of the glovebox and stirred at 82 °C for 18 h. After cooling to 20 °C, the reaction mixture was quenched with water (3 mL/mmol), washed with aq NH_3 (10 mL/mmol, 25%), extracted with $CHCl_3$ (3 x 5 mL/mmol), washed with brine (3 mL/mmol) and dried over Na_2SO_4. After filtration, the organic phase was concentrated under reduced pressure and the crude residue was purified by silica gel column chromatography to furnish the bis-*tert*-butyloxycarbonyl protected diazocine product. Adapted from lit.[17]

Di-*tert*-butyl 11,12-dihydrodibenzo[*c*,*g*][1,2]diazocine-5,6-dicarboxylate (6a)

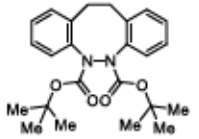

The reaction was performed according to the typical procedure (TP2) using the reagent **5a** (434 g, 1.00 mmol), leading to the corresponding product **6a** (226 mg, 550 µmol, 55%) after silica gel column chromatography (applied gradient from pentane to CH_2Cl_2) as a colorless solid.

^{1}H NMR (500 MHz, $CDCl_3$) δ 7.86 – 7.01 (m, 8H), 3.16 – 2.71 (m, 4H), 1.60 – 1.30 (m, 18H) ppm.

HRMS (ESI) *m/z* for $C_{24}H_{30}N_2O_4$ [M+Na]$^+$: calcd 433.20978, found: 433.20956.

IR (ATR): ϑ = 2978 (w), 2927 (w), 2857 (w), 1710 (s), 1494 (w), 1442 (w), 1395 (w), 1370 (m), 1340 (s), 1318 (s), 1256 (w), 1233 (w), 1152 (s), 1047 (m), 1006 (m), 914 (w), 853 (w), 763 (s), 722 (m), 627 (w), 577 (w) cm^{-1}.

mp: 178 °C.

Rf 0.52 (CHCl3)

Di-*tert*-butyl 2,9-dichloro-11,12-dihydrodibenzo[*c*,*g*][1,2]diazocine-5,6-dicarboxylate (6b)

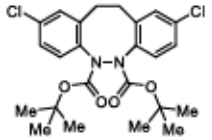

The reaction was performed according to the typical procedure (TP2) using the reagent **5b** (5.812 g, 11.56 mmol), leading to the corresponding product **6b** (3.547 g, 7.40 mmol, 64%) after silica gel column chromatography (applied gradient from pentane to CH_2Cl_2) as a colorless solid.

^{1}H NMR (500 MHz, $CDCl_3$) δ 7.77 – 7.12 (m, 6H), 3.12 – 2.64 (m, 4H), 1.61 – 1.32 (m, 18H) ppm.

HRMS (ESI) *m/z* for $C_{24}H_{28}N_2O_4{}^{35}Cl_2$ $[M+Na]^+$: calcd 501.13183, found: 501.13213.

IR (ATR): ϑ = 2997 (w), 2973 (w), 2935 (w), 2867 (w), 1726 (s), 1597 (w), 1490 (m), 1366 (m), 1329 (s), 1302 (s), 1245 (m), 1151 (s), 1094 (m), 1007 (m), 916 (w), 882 (w), 823 (w), 769 (w), 568 (w), 518 (w) cm^{-1}.

mp: 196 °C.

Rf 0.70 (CHCl3)

Di-*tert*-butyl 2,9-difluoro-11,12-dihydrodibenzo[*c*,*g*][1,2]diazocine-5,6-dicarboxylate (6c)

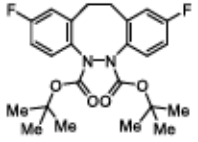

The reaction was performed according to the typical procedure (TP2) using the reagent **5c** (3.800 g, 8.08 mmol), leading to the corresponding product **6c** (1.610 g, 3.61 mmol, 45%) after silica gel column chromatography (applied gradient from pentane to CH_2Cl_2) as a colorless solid.

^{1}H NMR (500 MHz, $CDCl_3$) δ 7.83 – 7.04 (m, 6H), 3.16 – 2.59 (m, 4H), 1.62 – 1.32 (m, 18H) ppm.

^{19}F NMR (471 MHz, $CDCl_3$) δ -114.51, -114.79, -115.13, -115.28, -118.01 ppm.

HRMS (ESI) *m/z* for $C_{24}H_{28}N_2O_4F_2$ $[M+Na]^+$: calcd 469.19093, found: 469.19097.

IR (ATR): ϑ = 3011 (w), 2971 (w), 2932 (w), 1720 (s), 1614 (w), 1596 (w), 1495 (m), 1453 (w), 1368 (m), 1338 (s), 1309 (s), 1251 (s), 1220 (m), 1153 (s), 1111 (w), 1051 (w), 1010 (m), 943 (m), 888 (m), 824 (m), 771 (m), 690 (w), 630 (w), 597 (w), 556 (w), 518 (w), 489 (w) cm^{-1}.

mp: 177 °C.

Rf 0.59 (CHCl3)

Di-*tert*-butyl 2,9-bis(trifluoromethyl)-11,12-dihydrodibenzo[*c*,*g*][1,2]diazocine-5,6-dicarboxylate (6d)

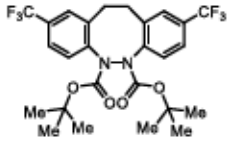

The reaction was performed according to the typical procedure (TP2) using the reagent **5d** (250 mg, 440 µmol), leading to the corresponding product **6d** (109 mg, 200 µmol, 45%) after silica gel column chromatography (applied gradient from pentane to CH_2Cl_2) as a colorless solid.

^{1}H NMR (500 MHz, $CDCl_3$) δ 7.97 – 7.43 (m, 6H), 3.26 – 2.73 (m, 4H), 1.62 – 1.31 (m, 18H) ppm.

^{19}F NMR (471 MHz, $CDCl_3$) δ -61.61, -61.64, -62.28, -62.31, -62.35, -62.47, -62.52 ppm.

HRMS (EI) *m/z* for $C_{26}H_{28}FeN_2O_4$ $[M]^+$: calcd 546.19533, found: 546.19669 (5); 57 (100).

IR (ATR): ϑ = 3075 (w), 2982 (w), 2937 (w), 2162(w), 1980 (w), 1720 (m), 1592 (w), 1496 (m), 1458 (w), 1430 (m), 1411 (w), 1349 (w), 1368 (w), 13018 (w), 1280 (m), 1265 (w), 1239 (w), 1111 (s), 1076 (w), 1047 (w), 1024 (w), 1004 (w), 961 (m), 896 (m), 915 (w), 878 (w), 790 (m), 764 (m), 748 (m), 712 (m), 700 (s), 692 (w), 658 (w) cm^{-1}.

mp: 141 °C

Rf 0.10 (heptane/ethyl acetate = 90/10)

Di-*tert*-butyl 2,9-di-*tert*-butoxy-11,12-dihydrodibenzo[*c*,*g*][1,2]diazocine-5,6-dicarboxylate (6e)

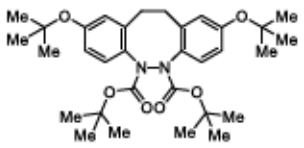

The reaction was performed according to the typical procedure (TP2) using the reagent **5e** (289 mg, 500 µmol) and the crude residue was purified by silica gel column chromatography (applied gradient from pentane to pentane/ethyl acetate = 70/30) leading to the corresponding product **6e** (154 mg, 280 µmol, 56%) as a colorless solid.

^{1}H NMR (500 MHz, $CDCl_3$) δ 7.72 – 6.69 (m, 6H), 3.04 – 2.63 (m, 4H), 1.62 – 1.24 (m, 38H) ppm.

HRMS (ESI) *m/z* for $C_{32}H_{46}N_2O_6$ $[M]^+$: calcd 554.33504, found: 554.33516.

IR (ATR): ϑ = 2977 (m), 2933 (w), 1715 (s), 1604 (w), 1497 (m), 1366 (s), 1308 (m), 1249 (m), 1151 (s), 1050 (m), 1010 (w), 969 (m), 895 (w), 855 (w), 763 (w) cm^{-1}.

mp: 90 °C.

*R*f: 0.35 (hexane/ethyl acetate = 80/20)

5,6-Di-*tert*-butyl 2,9-dimethyl 11,12-dihydrodibenzo[*c*,*g*][1,2]diazocine-2,5,6,9-tetracarboxylate (6f)

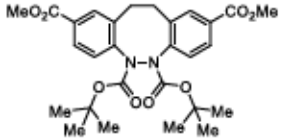

The reaction was performed according to the typical procedure (TP3) using the reagent **5f** (912 mg, 2.00 mmol), leading to the corresponding product **6f** (493 mg, 940 µmol, 47%) after silica gel column chromatography (CH_2Cl_2/ethyl acetate = 98/2) as a colorless solid.

^{1}H NMR (500 MHz, $CDCl_3$) δ 7.99 – 7.49 (m, 6H), 3.92 (m, 6H), 3.30 – 2.69 (m, 4H), 1.45 (m, 18H) ppm.

HRMS (ESI) *m/z* for $C_{28}H_{34}N_2O_8$ [M+Na]$^+$: calcd 549.22074, found: 549.22100.

IR (ATR): $\tilde{\nu}$ = 2983 (w), 2950 (w), 1719 (s), 1609 (w), 1498 (w), 1431 (m), 1371 (m), 1310 (m), 1277 (s), 1251 (s), 1152 (s), 1106 (m), 1048 (w), 993 (w), 911 (w), 843 (m), 813 (w), 758 (s), 491 (w) cm^{-1}.

mp: 197 °C.[3]

*R*f: 0.21 (hexane/ethyl acetate = 80/20)

Di-*tert*-butyl 2,9-dimethoxy-11,12-dihydrodibenzo[*c*,*g*][1,2]diazocine-5,6-dicarboxylate (6g)

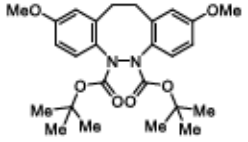

The reaction was performed according to the typical procedure (TP2) using the reagent **5g** (3.000 g, 6.38 mmol), leading to the corresponding product **6g** (2.090 g, 4.44 mmol, 70%) after silica gel column chromatography (pentane/ethyl acetate = 90/10) as a colorless solid.

^{1}H NMR (500 MHz, $CDCl_3$) δ 7.74 – 6.64 (m, 6H), 3.86 – 3.71 (m, 6H), 3.06 – 2.68 (m, 4H), 1.60 – 1.31 (m, 18H) ppm.

IR (ATR): $\tilde{\nu}$ = 2976 (w), 1711 (s), 1607 (w), 1502 (m), 1238 (s), 1151 (s), 1005 (m), 772 (w) cm^{-1}.

HRMS (EI) *m/z* for $C_{26}H_{34}N_2O_6$ [M]$^+$: calcd 470.24169, found: 470.24166 (5); 136.07 (100).

mp: 171 °C

*R*f: 0.24 (hexane/ethyl acetate = 80/20)

[3] Visually, it appeared as if the compound decomposed at this temperature.

Di-*tert*-butyl 3,8-dichloro-11,12-dihydrodibenzo[*c*,*g*][1,2]diazocine-5,6-dicarboxylate (6h)

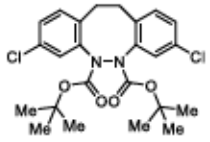

The reaction was performed according to the typical procedure (TP2) using the reagent **5h** (4.426 g, 8.80 mmol), leading to the corresponding product **6h** (1.536 g, 3.20 mmol, 37%) after silica gel column chromatography (applied gradient from pentane to CH_2Cl_2) as a colorless solid.

^{1}H NMR (500 MHz, $CDCl_3$) δ 7.83 – 7.04 (m, 6H), 3.16 – 2.59 (m, 4H), 1.62 – 1.32 (m, 18H) ppm.

HRMS (ESI) *m/z* for $C_{24}H_{28}{}^{35}Cl_2N_2O_4$ [M+Na]$^+$: calcd 501.13183, found: 501.13169.

IR (ATR): $\tilde{\nu}$ = 3014 (w), 2976 (w), 2950 (w), 1724 (s), 1596 (w), 1576 (w), 1488 (m), 1436 (w), 1368 (m), 1331 (s), 1304 (s), 1279 (m), 1260 (m), 1227 (m), 1153 (s), 1132 (m), 1098 (w), 1045 (m), 1022 (m), 949 (m), 858 (m), 815 (m), 795 (m), 773 (m), 656 (m), 577 (m), 534 (w), 492 (w) cm^{-1}.

mp: 171 °C.

*R*f: 0.67 ($CHCl_3$)

Di-*tert*-butyl 3,8-difluoro-11,12-dihydrodibenzo[*c*,*g*][1,2]diazocine-5,6-dicarboxylate (6i)

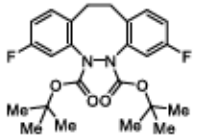

The reaction was performed according to the typical procedure (TP2) using the reagent **5i** (2.530 g, 5.38 mmol), leading to the corresponding product **6i** (832 mg, 1.86 mmol, 35%) after silica gel column chromatography (applied gradient from pentane to CH_2Cl_2) as a colorless solid.

^{1}H NMR (500 MHz, $CDCl_3$) δ 7.60 – 6.76 (m, 6H), 3.14 – 2.60 (m, 4H), 1.62 – 1.34 (m, 18H) ppm.

^{19}F NMR (471 MHz, $CDCl_3$) δ -116.16, -116.97, -117.12, -117.44, -117.89 ppm.

HRMS (ESI) *m/z* for $C_{24}H_{28}F_2N_2O_4$ [M+Na]$^+$: calcd 469.19093, found: 469.19113.

IR (ATR): $\tilde{\nu}$ = 3008 (w), 2979 (w), 2926 (w), 1716 (s), 1596 (m), 1499 (m), 1454 (w), 1422 (w), 1393 (w), 1369 (m), 1336 (s), 1314 (m), 1247 (m), 1146 (s), 1045 (w), 1023 (m), 984 (m), 879 (m), 863 (m), 841 (s), 773 (m), 732 (m), 643 (w), 598 (w), 533 (w), 472 (w) cm^{-1}.

mp: 165 °C.

*R*f: 0.70 ($CHCl_3$)

Di-*tert*-butyl 3,8-di-*tert*-butyl-11,12-dihydrodibenzo[*c*,*g*][1,2]diazocine-5,6-dicarboxylate (6j)

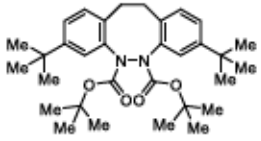

The reaction was performed according to the typical procedure (TP2) using the reagent **5j** (546 mg, 1.00 mmol), leading to the corresponding product **6j** (352 mg, 670 µmol, 67%) after silica gel column chromatography (applied gradient from pentane to CH_2Cl_2) as a colorless solid.

^{1}H NMR (500 MHz, $CDCl_3$) δ 7.87 – 7.02 (m, 6H), 3.12 – 2.62 (m, 4H), 1.66 – 1.31 (m, 36H) ppm.

HRMS (ESI) *m/z* for $C_{32}H_{46}N_2O_4$ [M+H]$^+$: calcd 523.35303, found: 523.35372.

IR (ATR): ϑ = 2965 (m), 2869 (w), 1719 (s), 1614 (w), 1572 (w), 1504 (w), 1458 (w), 1395 (w), 1366 (m), 1305 (s), 1253 (m), 1156 (s), 1107 (w), 1049 (w), 1028 (w), 972 (w), 936 (w), 866 (w), 828 (m), 751 (w), 657 (w), 625 (w), 534 (w) cm^{-1}.

mp: 90 °C.

Rf: 0.74 ($CHCl_3$)

Di-*tert*-butyl 3,8-dicyano-11,12-dihydrodibenzo[*c*,*g*][1,2]diazocine-5,6-dicarboxylate (6k)

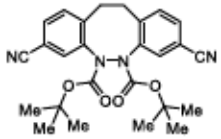

The reaction was performed according to the typical procedure (TP3) using the reagent **5k** (300 mg, 770 µmol), leading to the corresponding product **6k** (151 mg, 330 µmol, 43%) after silica gel column chromatography (applied gradient from pentane to pentane/ethyl acetate = 50/50) as a colorless solid.

^{1}H NMR (500 MHz, $CDCl_3$) δ 8.16 – 7.27 (m, 6H), 3.26 – 2.71 (m, 4H), 1.65 – 1.34 (m, 18H) ppm.

HRMS (ESI) *m/z* for $C_{26}H_{28}N_4O_4$ [M+H]$^+$: calcd 461.21833, found: 461.21868.

IR (ATR): ϑ = 3001 (w), 2982 (w), 2931 (w), 2230 (w), 1736 (m), 1708 (s), 1568 (w), 1499 (w), 1456 (w), 1414 (w), 1368 (m), 1333 (m), 1307 (s), 1296 (s), 1255 (m), 1153 (s), 1053 (m), 989 (w), 944 (w), 843 (m), 788 (m), 654 (w), 597 (w), 526 (w), 474 (w) cm^{-1}.

mp: 206 °C.[4]

Rf: 0.44 ($CHCl_3$)

[4] Visually, it appeared as if the compound decomposed at this temperature.

5,6-Di-*tert*-butyl 3,8-dimethyl 11,12-dihydrodibenzo[*c*,*g*][1,2]diazocine-3,5,6,8-tetracarboxylate (6l)

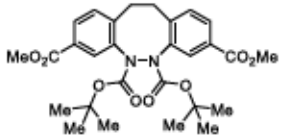

The reaction was performed according to the typical procedure (TP3) using the reagent **5l** (209 mg, 460 µmol), leading to the corresponding product **6l** (152 mg, 290 µmol, 63%) after silica gel column chromatography (CH_2Cl_2/ethyl acetate = 98/2) as a colorless solid.

^{1}H NMR (500 MHz, $CDCl_3$) δ 8.45 – 7.24 (m, 6H), 3.97 – 3.87 (m, 6H), 3.23 – 2.72 (m, 4H), 1.64 – 1.33 (m, 18H) ppm.

HRMS (ESI) *m/z* for $C_{28}H_{34}N_2O_8$ [M+NH_4]$^+$: calcd 544.26534, found: 544.2651.

IR (ATR): ϑ = 2983 (w), 2955 (w), 1713 (s), 1611 (w), 1578 (w), 1438 (m), 1418 (m), 1371 (m), 1337 (m), 1313 (m), 1282 (s), 1257 (m), 1219 (s), 1151 (s), 1139 (s), 1107 (m), 1026 (m), 995 (m), 932 (w), 847 (m), 768 (s), 717 (m), 642 (m), 571 (w), 524 (w) cm^{-1}.

mp: 177 °C.[5]

Rf: 0.21 (hexane/ethyl acetate = 80/20)

Di-*tert*-butyl 2,8-dichloro-11,12-dihydrodibenzo[*c*,*g*][1,2]diazocine-5,6-dicarboxylate (6m)

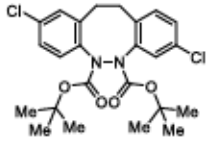

The reaction was performed according to the typical procedure (TP3) using the reagent **5m** (818 mg, 2.00 mmol), leading to the corresponding product **6m** (389 mg, 810 µmol, 41%) after silica gel column chromatography (applied gradient from pentane to CH_2Cl_2) as a colorless solid.

^{1}H NMR (500 MHz, $CDCl_3$) δ 7.82 – 7.03 (m, 6H), 3.18 – 2.61 (m, 4H), 1.62 – 1.30 (m, 18H) ppm.

HRMS (ESI) *m/z* for $C_{24}H_{28}{}^{35}Cl_2N_2O_4$ [M+Na]$^+$: calcd 501.13183, found: 501.13163.

IR (ATR): ϑ = 2980 (w), 2937 (w), 1713 (s), 1597 (w), 1490 (m), 1453 (w), 1406 (w), 1368 (m), 1338 (s), 1311 (s), 1233 (m), 1151 (s), 1093 (m), 1048 (m), 1013 (s), 932 (w), 883 (m), 817 (m), 787 (m), 717 (w), 661 (m), 585 (m), 510 (m), 460 (m) cm^{-1}.

mp: 145 °C.

Rf: 0.74 ($CHCl_3$)

[5] Visually, it appeared as if the compound decomposed at this temperature.

Di-*tert*-butyl 2,3,8,9-tetrafluoro-11,12-dihydrodibenzo[*c,g*][1,2]diazocine-5,6-dicarboxylate (6n)

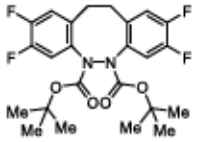

The reaction was performed according to the typical procedure (TP2) using the reagent **5n** (600 mg, 1.45 mmol), leading to the corresponding product **6n** (350 mg, 730 µmol, 50%) after silica gel column chromatography (applied gradient from pentane to CH_2Cl_2) as a colorless solid.

^{1}H NMR (500 MHz, $CDCl_3$) δ 7.70 –6.92 (m, 4H), 3.10 – 2.62 (m, 4H), 1.65 – 1.31 (m, 18H) ppm.

^{19}F NMR (471 MHz, $CDCl_3$) δ -138.14 (dt, *J* = 18.7, 9.4 Hz), -138.48 (dt, *J* = 18.7, 9.8 Hz), -138.79 (dt, *J* = 18.5, 9.9 Hz), -138.98 (dt, *J* = 18.6, 10.3 Hz), -139.73 (dt, *J* = 20.5, 9.8 Hz), -140.48 (dq, *J* = 19.5, 8.2 Hz), -140.79, -141.20 (dt, *J* = 20.8, 10.1 Hz), -141.64 ppm.

IR (ATR): ϑ = 2979 (w), 1719 (s), 1614 (w), 1506 (s), 1477 (w), 1455 (w), 1418 (w), 1394 (w), 1372 (m), 1352 (s), 1333 (m), 1317 (m), 1285 (s), 1254 (s), 1211 (m), 1172 (s), 1149 (s), 1118 (s), 1047 (m), 990 (w), 947 (w), 913 (w), 879 (s), 841 (s), 787 (s), 772 (s), 758 (m), 136 (w), 714 (w), 690 (w) cm^{-1}.

HRMS (EI) *m/z* for $C_{24}H_{26}F_2N_2O_4$ [M]$^+$: calcd 482.18287, found: 482.18232 (2); 57 (100).

mp: 176 °C

Rf: 0.25 (heptane/ethyl acetate = 90/10)

Di-*tert*-butyl 9,10-dihydrodithieno[*3,2-c:2',3'-g*][1,2]diazocine-4,5-dicarboxylate (6o)

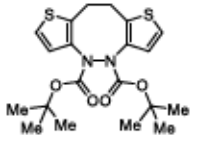

The reaction was performed according to the typical procedure (TP3) using the reagent **5o** (826 mg, 1.85 mmol), leading to the corresponding product **6o** (316 mg, 750 µmol, 40%) after silica gel column chromatography (applied gradient from pentane to pentane/ethyl acetate = 85/15) as a light-yellow solid.

^{1}H NMR (500 MHz, $CDCl_3$) δ 7.40 – 6.90 (m, 4H), 3.19 – 2.99 (m, 4H), 1.48 (s, 18H) ppm.

HRMS (ESI) *m/z* for $C_{20}H_{26}N_2O_4S_2$ [M+Na]$^+$: calcd 445.12262, found: 445.12260.

IR (ATR): ϑ = 3101 (w), 3016 (w), 2977 (w), 2933 (w), 1714 (s), 1555 (w), 1480 (w), 1455 (w), 1395 (m), 1370 (m), 1341 (s), 1309 (s), 1254 (m), 1160 (s), 1143 (s), 1093 (m), 1070 (m), 998 (w), 911 (m), 858 (m), 834 (m), 753 (s), 707 (m), 627 (w), 584 (w), 481 (w) cm^{-1}.

mp: 68 °C.

Rf: 0.60 (CHCl$_3$)

Di-*tert*-butyl 5,6-dihydrodipyrido[*2,3-c:3',2'-g*][1,2]diazocine-11,12-dicarboxylate (6p)

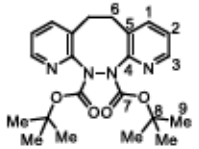

The reaction was performed according to the typical procedure (TP3) using the reagent **5p** (179 mg, 520 µmol), leading to the corresponding product **6p** (34 mg, 80 µmol, 16%) after silica gel column chromatography (CH_2Cl_2/ethyl acetate = 95/5) as a colorless solid.

^{1}H NMR (500 MHz, $CDCl_3$) δ 8.50 (s, 2H, H-3), 7.58 (d, *J* = 7.0 Hz, 2H, H-1), 7.13 (s, 2H, H-2), 3.18 – 2.96 (m, 4H, H-6), 1.37 (d, *J* = 43.1 Hz, 18H, H-9) ppm.

^{13}C{^{1}H} NMR (126 MHz, $CDCl_3$) δ 151.8 (C-4), 146.0 (C-3), 139.9 (C-1), 130.6 (C-5), 121.3 (C-2), 83.3 (C-8), 30.2 (C-6), 28.2 (C-9) ppm.[6]

HRMS (ESI) *m/z* for $C_{22}H_{28}N_4O_4$ [M+H]$^+$: calcd 413.21833, found: 413.21845.

IR (ATR): ϑ = 3045 (w), 3006 (w), 2974 (w), 2922 (w), 1746 (s), 1728 (s), 1572 (m), 1459 (m), 1430 (m), 1369 (m), 1302 (s), 1252 (m), 1153 (s), 1118 (m), 1054 (m), 1031 (m), 960 (w), 920 (w), 846 (w), 820 (m), 763 (m), 664 (m), 642 (w), 519 (s) cm^{-1}.

mp: 203 °C.[7]

Rf: 0.12 (CHCl$_3$)

Synthesis of Cyclic Azobenzenes (1a-1u)

Typical procedure for the preparation of the cyclic azobenzenes (1a-1d, 1g-1k, 1m-1o) by the trimethylsilyl iodide-promoted hydrolysis of bis-*tert*-butyloxycarbonyl protected diazocines (6a-6d, 6g-6k, 6m-6o) and subsequent oxidation with NBS (TP4):

In a glovebox, the bis-*tert*-butyloxycarbonyl protected diazocine derivative (1.0 equiv), CH_2Cl_2 (5 mL/mmol) and trimethylsilyl iodide (2.0 equiv) were added sequentially to a round-bottomed flask equipped with a magnetic stirring bar. The reaction mixture was stirred at 20 °C for 10 min before it was treated with triethylamine (2.0 equiv). The flask was capped, transferred out of the glovebox where the reaction mixture was quenched with water (5 mL/mmol), extracted with $CHCl_3$ (3 x 5 mL/mmol), washed with brine (5 mL/mmol) and dried over Na_2SO_4. After filtration, the organic phase was concentrated under reduced pressure. The resulting residue, CH_2Cl_2 (10 mL/mmol) and pyridine (0.1 mL/mmol, 1.24 equiv) were added sequentially to a round-bottomed flask. NBS (1.2 equiv) was added portionwise over the course of 2 min under stirring and the reaction mixture was stirred at 20 °C for 30 min. The reaction mixture was concentrated under reduced pressure and the residue was purified by silica gel column chromatography to furnish the cyclic azobenzene product.

[6] The ^{13}C{^{1}H} NMR signal C-7 for compound **6p** could not be detected.
[7] Visually, it appeared as if the compound decomposed at this temperature.

(*Z*)-11,12-Dihydrodibenzo[*c*,*g*][1,2]diazocine (1a)

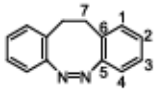

The reaction was performed according to the typical procedure (TP4) using the reagent **6a** (103 mg, 250 µmol), leading to the corresponding product **1a** (35 mg, 170 µmol, 67%) after silica gel column chromatography (applied gradient from pentane to CH_2Cl_2) as a yellow solid.

^{1}H NMR (500 MHz, $CDCl_3$) δ 7.12 (td, *J* = 7.7, 1.6 Hz, 2H, H-2), 7.00 (td, *J* = 7.4, 1.2 Hz, 2H, H-3), 6.97 (dd, *J* = 7.6, 1.5 Hz, 2H, H-1), 6.82 (dd, *J* = 7.8, 0.9 Hz, 2H, H-4), 2.88 (s, 4H, H-7) ppm.

^{13}C{^{1}H} NMR (126 MHz, $CDCl_3$) δ 155.6 (C-5), 129.7 (C-1), 128.2 (C-6), 127.2 (C-3), 126.8 (C-2), 118.8 (C-4), 31.8 (C-7) ppm.

HRMS (EI) *m/z* for $C_{14}H_{12}N_2$ [M]$^+$: calcd 208.10005, found: 208.10028 (20); 178.08 (100).

IR (ATR): ϑ = 3058 (w), 2948 (w), 2895 (w), 1712 (w), 1479 (m), 1436 (m), 1152 (w), 1038 (w), 949 (w), 870 (w), 763 (s), 748 (s), 535 (m), 481 (m) cm^{-1}.

mp: 109 °C.

R$_f$: 0.64 (CHCl$_3$)

(*Z*)-2,9-Dichloro-11,12-dihydrodibenzo[*c*,*g*][1,2]diazocine (1b)

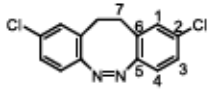

The reaction was performed according to the typical procedure (TP4) using the reagent **6b** (2.077 g, 4.33 mmol), leading to the corresponding product **1b** (960 mg, 3.46 mmol, 80%) after silica gel column chromatography (applied gradient from pentane to CH_2Cl_2) as a yellow solid.

^{1}H NMR (500 MHz, $CDCl_3$) δ 7.13 (dd, *J* = 8.4, 2.2 Hz, 2H, H-3), 7.00 (d, *J* = 2.1 Hz, 2H, H-1), 6.78 (d, *J* = 8.4 Hz, 2H, H-4), 2.84 (d, *J* = 102.8 Hz, 4H, H-7) ppm.

^{13}C{^{1}H} NMR (126 MHz, $CDCl_3$) δ 153.7 (C-5), 132.8 (C-2), 129.8 (C-6), 129.7 (C-1), 127.2 (C-3), 120.5 (C-4), 31.5 (C-7) ppm.

HRMS (EI) *m/z* for $C_{14}H_{10}{}^{35}Cl_2N_2$ [M]$^+$: calcd 276.02210, found: 276.02310 (10); 178.08 (100).

IR (ATR): ϑ = 3084 (w), 3022 (w), 2960 (w), 2913 (w), 2845 (w), 1906 (w), 1755 (w), 1587 (w), 1469 (s), 1392 (m), 1160 (m), 1107 (m), 992 (m), 922 (m), 891 (s), 877 (s), 824 (s), 806 (s), 684 (m), 631 (m), 575 (w), 524 (s), 478 (m) cm^{-1}.

mp: 153 °C.

R$_f$: 0.56 (CHCl$_3$)

(*Z*)-2,9-Difluoro-11,12-dihydrodibenzo[*c*,*g*][1,2]diazocine (1c)

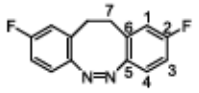

The reaction was performed according to the typical procedure (TP4) using the reagent **6c** (1.540 g, 3.45 mmol), leading to the corresponding product **1c** (695 mg, 2.87 mmol, 83%) after silica gel column chromatography (applied gradient from pentane to CH_2Cl_2) as a yellow solid.

^{1}H NMR (500 MHz, $CDCl_3$) δ 6.85 (td, *J* = 8.3, 2.5 Hz, 2H, H-3), 6.81 (dd, *J* = 8.6, 5.4 Hz, 2H, H-4), 6.72 (dd, *J* = 9.2, 2.5 Hz, 2H, H-1), 2.85 (s, 4H, H-7) ppm.

^{13}C{^{1}H} NMR (126 MHz, $CDCl_3$) δ 161.2 (d, *J* = 246.6 Hz, C-2), 151.4 (d, *J* = 2.9 Hz, C-5), 130.3 (d, *J* = 7.7 Hz, C-6), 121.0 (d, *J* = 8.8 Hz, C-4), 116.3 (d, *J* = 22.4 Hz, C-1), 114.0 (d, *J* = 22.6 Hz, C-3), 31.7 (d, *J* = 1.4 Hz, C-7) ppm.

^{19}F NMR (471 MHz, $CDCl_3$) δ -115.84 (ddd, *J* = 9.1, 8.0, 5.4 Hz) ppm.

HRMS (EI) *m/z* for $C_{14}H_{10}F_2N_2$ [M]$^+$: calcd 244.08120, found: 244.08103 (40); 215.06 (100).

IR (ATR): ϑ = 3061 (w), 2956 (w), 2903 (w), 1612 (w), 1581 (m), 1516 (w), 1479 (s), 1409 (w), 1274 (w), 1236 (s), 1155 (m), 1097 (w), 1001 (w), 957 (w), 911 (m), 883 (s), 818 (s), 800 (s), 704 (m), 592 (w), 544 (m), 504 (m) cm^{-1}.

mp: 132 °C.

R$_f$: 0.60 (CHCl$_3$)

(*Z*)-2,9-Bis(trifluoromethyl)-11,12-dihydrodibenzo[*c*,*g*][1,2]diazocine (1d)

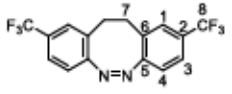

The reaction was performed according to the typical procedure (TP4) using the reagent **6d** (400 mg, 730 µmol), leading to the corresponding product **1d** (118 mg, 340 µmol, 47%) after silica gel column chromatography (applied gradient from pentane to CH_2Cl_2) as a yellow solid.

^{1}H NMR (500 MHz, $CDCl_3$) δ 7.43 (dd, *J* = 8.2, 1.1 Hz, 2H, H-3), 7.29 (s, 2H, H-1), 6.96 (d, *J* = 8.2 Hz, 2H, H-4), 3.50 – 2.50 (m, 4H, H-7) ppm.

^{13}C{^{1}H} NMR (126 MHz, $CDCl_3$) δ 157.4 (C-5), 129.6 (d, *J* = 32.8 Hz, C-2), 128.3 (C-6), 127.03 (q, *J* = 3.8 Hz, C-1), 124.32 (d, *J* = 3.7 Hz, C-3), 122.4 (q, *J* = 270 Hz, C-8), 119.2 (C-4), 31.3 (C-7) ppm.

^{19}F NMR (471 MHz, $CDCl_3$) δ -62.9 ppm.

HRMS (EI) *m/z* for $C_{16}H_{10}F_6N_2$ [M]$^+$: calcd 344.07482, found: 344.07595 (30); 178 (100).

IR (ATR): ϑ = 2932 (w), 1615 (w), 1577 (w), 1465 (w), 1413 (w), 1323 (s), 1276 (m), 1200 (m), 1151 (m), 1101 (m), 1068 (s), 995 (m), 961 (w), 930 (w), 898 (s), 823 (m), 810 (m), 733 (m), 691 (m), 663 (w) cm^{-1}.

mp: 119 °C.

Rf: 0.28 (heptane/ethyl acetate = 90/10)

(*Z*)-11,12-Dihydrodibenzo[*c*,*g*][1,2]diazocine-2,9-diol (1e)

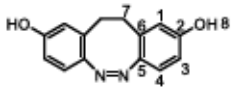

In a glovebox, compound **6e** (111 mg, 200 µmol), CH_2Cl_2 (1 mL) and trimethylsilyl iodide (114 µL, 800 µmol) were added sequentially to a round-bottomed flask equipped with a magnetic stirring bar. The reaction mixture was stirred at 20 °C for 10 min before it was treated with triethylamine (111 µL, 800 µmol). The flask was capped, transferred out of the glovebox where the reaction mixture was quenched with water (5 mL), extracted with $CHCl_3$ (3 x 20 mL), washed with brine (5 mL) and dried over Na_2SO_4. After filtration, the organic phase was concentrated under reduced pressure. The resulting residue, CH_2Cl_2 (5 mL) and pyridine (20 µL, 240 µmol) were added sequentially to a round-bottomed flask. NBS (43 mg, 240 µmol) was added portion wise over the course of 2 min under stirring and the reaction mixture was stirred at 20 °C for 30 min. The reaction mixture was concentrated under reduced pressure and the residue was purified by silica gel column chromatography (applied gradient from pentane to ethyl acetate) to furnish the product **1e** (13 mg, 50 µmol, 27%) as a red solid.

^{1}H NMR (500 MHz, MeOD) δ 6.66 (d, *J* = 8.5 Hz, 2H, H-4), 6.59 (dd, *J* = 8.5, 2.5 Hz, 2H, H-3), 6.47 (d, *J* = 2.5 Hz, 2H, H-1), 2.74 (s, 4H, H-7) ppm.

^{13}C{^{1}H} NMR (126 MHz, MeOD) δ 157.7 (C-2), 149.0 (C-5), 131.5 (C-6), 122.0 (C-4), 116.7 (C-1), 114.5 (C-3), 32.8 (C-7) ppm.

HRMS (EI) *m/z* for $C_{14}H_{12}N_2O_2$ [M]$^+$: calcd 240.08988, found: 240.08954 (100).

IR (ATR): ϑ = 3325 (w), 2924 (w), 2476 (w), 1604 (s), 1579 (m), 1504 (m), 1483 (m), 1433 (m), 1352 (w), 1290 (s), 1251 (m), 1210 (s), 1174 (m), 1155 (m), 1093 (w), 1011 (w), 959 (m), 905 (w), 874 (w), 831 (m), 802 (s), 691 (w) cm^{-1}.

mp: 165 °C.[8]

Rf: 0.59 (pentane/ethyl acetate = 20/80)

Dimethyl (*Z*)-11,12-dihydrodibenzo[*c*,*g*][1,2]diazocine-2,9-dicarboxylate (1f)

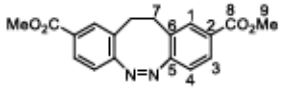

In a glovebox, compound **6f** (400 mg, 760 µmol), CH_2Cl_2 (4 mL) and trimethylsilyl iodide (432 µL, 3.04 mmol) were added sequentially to a round-bottomed flask equipped with a magnetic stirring bar. The reaction mixture was stirred at 20 °C for 10 min before it was treated with triethylamine (421 µL, 3.04 mmol). The flask was capped, transferred out of the glovebox where the reaction mixture was

[8] Visually, it appeared as if the compound decomposed at this temperature.

quenched with water (5 mL), extracted with $CHCl_3$ (3 x 5 mL), washed with brine (5 mL) and dried over Na_2SO_4. After filtration, the organic phase was concentrated under reduced pressure. The resulting residue, CH_2Cl_2 (10 mL) and pyridine (100 µL, 940 µmol) were added sequentially to a round-bottomed flask. NBS (162 mg, 910 µmol) was added portionwise over the course of 2 min under stirring and the reaction mixture was stirred at 20 °C for 30 min. The reaction mixture was concentrated under reduced pressure and the residue was purified by silica gel column chromatography (applied gradient from pentane to pentane/ethyl acetate = 80/20) to furnish the product **1f** (204 mg, 630 µmol, 83%) as a yellow solid.

^{1}H NMR (500 MHz, $CDCl_3$) δ 7.80 (dd, *J* = 8.2, 1.5 Hz, 2H, H-3), 7.68 (d, *J* = 1.2 Hz, 2H, H-1), 6.88 (d, *J* = 8.2 Hz, 2H, H-4), 3.85 (s, 6H, H-9), 2.95 (d, *J* = 67.5 Hz, 4H, H-7) ppm.

^{13}C{^{1}H} NMR (126 MHz, $CDCl_3$) δ 166.2 (C-8), 158.9 (C-5), 131.5 (C-1), 129.2 (C-2), 128.6 (C-3), 128.3 (C-6), 118.7 (C-4), 52.3 (C-9), 31.4 (C-7) ppm.

HRMS (EI) *m/z* for $C_{18}H_{16}N_2O_4$ [M]$^+$: calcd 324.11101, found: 324.11096 (30); 178.08 (100).

IR (ATR): ϑ = 3037 (w), 2947 (w), 2899 (w), 2835 (w), 1713 (s), 1603 (w), 1433 (s), 1282 (s), 1258 (s), 1189 (s), 1161 (m), 1113 (s), 1004 (m), 964 (w), 914 (w), 868 (w), 767(m), 756 (s), 527 (w), 509 (w) cm^{-1}.

mp: 169 °C.

Rf: 0.48 ($CHCl_3$)

(*Z*)-2,9-Dimethoxy-11,12-dihydrodibenzo[*c*,*g*][1,2]diazocine (1g)

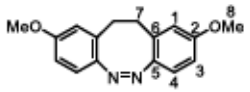

The reaction was performed according to the typical procedure (TP4) using the reagent **6g** (200 mg, 430 µmol), leading to the corresponding product **1g** (61 mg, 230 µmol, 53%) after silica gel column chromatography (pentane/ethyl acetate = 90/10) as an orange solid.

^{1}H NMR (500 MHz, $CDCl_3$) δ 6.81 (d, *J* = 8.6 Hz, 2H, H-4), 6.67 (dd, *J* = 8.6, 2.6 Hz, 2H, H-3), 6.52 (d, *J* = 2.6 Hz, 2H, H-1). 3.72 (s, 6H, H-8), 2.82 (s, 4H, H-7) ppm.

^{13}C{^{1}H} NMR (126 MHz, $CDCl_3$) δ 158.1 (C-2), 149.0 (C-5), 129.7 (C-6), 121.0 (C-1), 114.5 (C-4), 111.9 (C-3), 55.2 (C-8), 32.1 (C-7) ppm.

HRMS (EI) *m/z* for $C_{16}H_{16}N_2O_2$ [M]$^+$: calcd 268.12118, found: 268.12057 (70); 225 (100).

IR (ATR): ϑ = 2940 (w), 1597 (m), 1481 (m), 1316 (m) 1240 (s), 1170 (m), 1090 (m), 1028 (s), 942 (w), 806 (s), 702 (w) cm^{-1}.

mp: 108 °C.

Rf: 0.27 (hexane/ethyl acetate = 80/20)

(*Z*)-3,8-Dichloro-11,12-dihydrodibenzo[*c*,*g*][1,2]diazocine (1h)

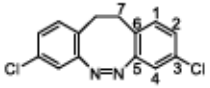

The reaction was performed according to the typical procedure (TP4) using the reagent **6h** (1.438 g, 3.00 mmol), leading to the corresponding product **1h** (700 mg, 2.53 mmol, 84%) after silica gel column chromatography (applied gradient from pentane to CH_2Cl_2) as a yellow solid.

^{1}H NMR (500 MHz, CDCl$_3$) δ 7.01 (dd, *J* = 8.2, 2.2 Hz, 2H, H-2), 6.92 (d, *J* = 8.2 Hz, 2H, H-1), 6.85 (d, *J* = 2.1 Hz, 2H, H-4), 2.98 – 2.68 (m, *J* = 84.9 Hz, 4H, H-7) ppm.

^{13}C{^{1}H} NMR (126 MHz, CDCl$_3$) δ 155.9 (C-5), 132.7 (C-3), 131.1 (C-1), 127.6 (C-2), 126.5 (C-6), 119.1 (C-4), 31.2 (C-7) ppm.

HRMS (EI) *m/z* for $C_{14}H_{10}{}^{35}Cl_2N_2$ [M]$^+$: calcd 276.02210, found: 276.02192 (10); 178.07 (100).

IR (ATR): ϑ = 3046 (w), 2957 (w), 2925 (w), 2862 (w) 1592 (m), 1562 (m), 1468 (s), 1390 (w), 1260 (w), 1161 (m), 1104 (s), 983 (w), 946 (w), 877 (s), 821 (s), 798 (s), 726 (w), 670 (w), 633 (m), 567 (w), 519 (w), 471 (s) cm^{-1}.

mp: 161 °C.

Rf. 0.77 (CHCl$_3$)

(*Z*)-3,8-Difluoro-11,12-dihydrodibenzo[*c*,*g*][1,2]diazocine (1i)

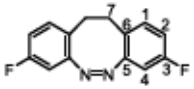

The reaction was performed according to the typical procedure (TP4) using the reagent **6i** (849 mg, 1.90 mmol), leading to the corresponding product **1i** (426 mg, 1.74 mmol, 92%) after silica gel column chromatography (applied gradient from pentane to CH_2Cl_2) as a yellow solid.

^{1}H NMR (500 MHz, CDCl$_3$) δ 6.94 (dd, *J* = 8.5, 5.5 Hz, 2H, H-1), 6.74 (td, *J* = 8.4, 2.7 Hz, 2H, H-2), 6.57 (dd, *J* = 8.5, 2.6 Hz, 2H, H-4), 2.97 – 2.68 (m, 4H, H-7) ppm.

^{13}C{^{1}H} NMR (126 MHz, CDCl$_3$) δ 161.3 (d, *J* = 247.4 Hz, C-3), 156.1 (d, *J* = 7.8 Hz, C-5), 131.3 (d, *J* = 8.3 Hz, C-1), 123.9 (d, *J* = 3.5 Hz, C-6), 114.4 (d, *J* = 21.2 Hz, C-2), 106.3 (d, *J* = 24.6 Hz, C-4), 31.0 (d, *J* = 0.9 Hz, C-7) ppm.

^{19}F NMR (471 MHz, CDCl$_3$) δ -115.08 (td, *J* = 8.3, 5.7 Hz) ppm.

HRMS (EI) *m/z* for $C_{14}H_{10}F_2N_2$ [M]$^+$: calcd 244.08120, found: 244.07985 (40); 215.07 (100).

IR (ATR): ϑ = 3059 (w), 2967 (w), 2907 (w), 1760 (w), 1605 (m), 1586 (s), 1482 (s), 1406 (w), 1241 (s), 1129 (m), 1087 (w), 928 (s), 906 (s), 879 (m), 817 (s), 803 (s), 737 (w), 692 (m), 621 (w), 526 (w), 478 (s) cm^{-1}.

mp: 147 °C.

Rf. 0.68 (CHCl$_3$)

(*Z*)-3,8-Di-*tert*-butyl-11,12-dihydrodibenzo[*c*,*g*][1,2]diazocine (1j)

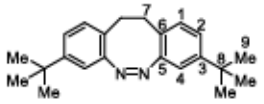

The reaction was performed according to the typical procedure (TP4) using the reagent **6j** (514 mg, 980 µmol), leading to the corresponding product **1j** (282 mg, 880 µmol, 90%) after silica gel column chromatography (applied gradient from pentane to CH_2Cl_2) as a yellow solid.

^{1}H NMR (500 MHz, CDCl$_3$) δ 6.99 (dd, *J* = 8.0, 2.0 Hz, 2H, H-2), 6.87 (d, *J* = 8.0 Hz, 2H, H-1), 6.79 (d, *J* = 2.0 Hz, 2H, H-4), 2.82 (d, *J* = 89.4 Hz, 4H, H-7), 1.19 (s, 18H, H-9) ppm.

^{13}C{^{1}H} NMR (126 MHz, CDCl$_3$) δ 155.6 (C-5), 150.0 (C-3), 129.3 (C-1), 125.5 (C-6), 123.9 (C-2), 115.8 (C-4), 34.6 (C-8), 31.3 (C-7), 31.3 (C-9) ppm.

HRMS (EI) *m/z* for $C_{22}H_{28}N_2$ [M]$^+$: calcd 320.22525, found: 320.22530 (20); 277.19 (100).

IR (ATR): ϑ = 3072 (w), 2964 (s), 2900 (w), 2869 (w), 1739 (w), 1608 (w), 1555 (w), 1494 (m), 1458 (m), 1391 (w), 1361 (m), 1258 (m), 1201 (w), 1117 (w), 982 (w), 927 (w), 903 (w), 889 (m), 828 (s), 735 (w), 636 (m), 587 (w), 520 (w), 464 (m) cm^{-1}.

mp: 116 °C.

Rf. 0.68 (CHCl$_3$)

(*Z*)-11,12-Dihydrodibenzo[*c*,*g*][1,2]diazocine-3,8-dicarbonitrile (1k)

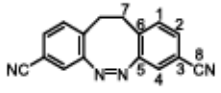

The reaction was performed according to the typical procedure (TP4) using the reagent **6k** (244 mg, 530 µmol), leading to the corresponding product **1k** (68 mg, 260 µmol, 50%) after silica gel column chromatography (applied gradient from pentane to ethyl acetate) as a yellow solid.

^{1}H NMR (500 MHz, CDCl$_3$) δ 7.36 (dd, *J* = 7.9, 1.6 Hz, 2H, H-2), 7.15 (d, *J* = 8.9 Hz, 2H, H-4), 7.14 (d, *J* = 15.2 Hz, 2H, H-1), 3.12 – 2.83 (m, 4H, H-7) ppm.

^{13}C{^{1}H} NMR (126 MHz, CDCl$_3$) δ 155.2 (C-5), 133.1 (C-6), 131.3 (C-2), 131.0 (C-1), 122.6 (C-4), 117.7 (C-8), 111.7 (C-3), 31.7 (C-7) ppm.

HRMS (EI) *m/z* for $C_{16}H_{10}N_4$ [M]$^+$: calcd 258.09055, found: 258.09053 (20); 229.07 (100).

IR (ATR): ϑ = 3055 (w), 2952 (w), 2911 (w), 2228 (s), 1738 (w), 1601 (w), 1554 (w), 1484 (m), 1460 (m), 1431 (m), 1393 (m), 1268 (w), 1209 (m), 1089 (w), 983 (w), 915 (m), 901 (m), 839 (s), 815 (s), 752 (m), 626 (s), 566 (m), 516 (m), 466 (m) cm^{-1}.

mp: 238 °C.[9]

Rf: 0.36 (CHCl3)

Dimethyl (*Z*)-11,12-dihydrodibenzo[*c*,*g*][1,2]diazocine-3,8-dicarboxylate (1l)

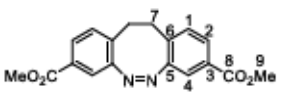

In a glovebox, compound **6l** (100 mg, 190 µmol), CH_2Cl_2 (1 mL) and trimethylsilyl iodide (108 µL, 760 µmol) were added sequentially to a round-bottomed flask equipped with a magnetic stirring bar. The reaction mixture was stirred at 20 °C for 10 min before it was treated with triethylamine (105 µL, 760 µmol). The flask was capped, transferred out of the glovebox where the reaction mixture was quenched with water (5 mL), extracted with $CHCl_3$ (3 x 5 mL), washed with brine (5 mL) and dried over Na_2SO_4. After filtration, the organic phase was concentrated under reduced pressure. The resulting residue, CH_2Cl_2 (2 mL) and pyridine (20 µL, 240 µmol) were added sequentially to a round-bottomed flask. NBS (41 mg, 230 µmol) was added portionwise over the course of 2 min under stirring and the reaction mixture was stirred at 20 °C for 30 min. The reaction mixture was concentrated under reduced pressure and the residue was purified by silica gel column chromatography (applied gradient from pentane to pentane/ethyl acetate = 70/30) to furnish the product **1l** (28 mg, 90 µmol, 45%) as a yellow solid.

^{1}H NMR (500 MHz, $CDCl_3$) δ 7.69 (dd, *J* = 8.0, 1.6 Hz, 2H, H-2), 7.51 (d, *J* = 1.6 Hz, 2H, H-4), 7.06 (d, *J* = 8.0 Hz, 2H, H-1), 3.86 (s, 6H, H-9), 2.95 (d, *J* = 89.1 Hz, 4H, H-7) ppm.

^{13}C{^{1}H} NMR (126 MHz, $CDCl_3$) δ 166.1 (C-8), 155.2 (C-5), 133.1 (C-6), 130.0 (C-1), 129.3 (C-3), 128.5 (C-2), 120.2 (C-4), 52.4 (C-9), 31.7 (C-7) ppm.

HRMS (EI) *m/z* for $C_{18}H_{16}N_2O_4$ [M]$^+$: calcd 324.11101, found: 324.11088 (10); 178.08 (100).

IR (ATR): ϑ = 3000 (w), 2953 (w), 2850 (w), 1715 (s), 1607 (w), 1571 (w), 1442 (m), 1298 (s), 1261 (s), 1201 (m), 1161 (m), 1108 (s), 973 (m), 904 (w), 852 (m), 754 (s), 697 (w), 668 (w), 624 (w), 558 (w) cm^{-1}.

mp: 229 °C.

Rf: 0.30 (CHCl3)

(*Z*)-2,8-Dichloro-11,12-dihydrodibenzo[*c*,*g*][1,2]diazocine (1m)

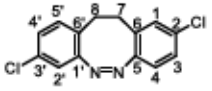

The reaction was performed according to the typical procedure (TP4) using the reagent **6m** (144 mg, 300 µmol), leading to the corresponding product **1m** (55 mg, 200 µmol, 66%) after silica gel column chromatography (applied gradient from pentane to CH_2Cl_2) as a yellow solid.

[9] Visually, it appeared as if the compound decomposed at this temperature.

^{1}H NMR (500 MHz, $CDCl_3$) δ 7.14 (dd, *J* = 8.4, 2.1 Hz, 1H, H-3), 7.02 (dd, *J* = 8.2, 2.1 Hz, 1H, H-4''), 6.98 (d, *J* = 2.1 Hz, 1H, H-1), 6.94 (d, *J* = 8.2 Hz, 1H, H-5''), 6.83 (d, *J* = 2.1 Hz, 1H, H-2''), 6.80 (d, *J* = 8.4 Hz, 1H, H-4), 2.99 – 2.68 (m, 4H, H-7,8) ppm.

^{13}C{^{1}H} NMR (126 MHz, $CDCl_3$) δ 132.8 (C-2), 132.7 (C-3''), 131.1 (C-5''), 129.8 (C-6), 129.7 (C-1), 127.6 (C-4''), 127.2 (C-3), 126.5 (C-6''), 120.6 (C-4), 119.0 (C-2''), 31.6 (C-7), 31.0 (C-8) ppm.[10]

HRMS (EI) *m/z* for $C_{14}H_{10}{}^{35}Cl_2N_2$ [M]$^+$: calcd 276.02210, found: 276.02163 (10); 178.08 (100).

IR (ATR): ϑ = 3059 (w), 2894 (w), 2851 (w), 1748 (w), 1590 (m), 1561 (m), 1473 (s), 1392 (w), 1191 (w), 1155 (w), 1105 (s), 1080 (m), 995 (w), 952 (w), 878 (m), 853 (s), 834 (s), 801 (s), 762 (m), 699 (w), 620 (m), 562 (m), 511 (m), 478 (m) cm^{-1}.

mp: 128 °C.

Rf: 0.73 (CHCl3)

(*Z*)-2,3,8,9-Tetrafluoro-11,12-dihydrodibenzo[*c*,*g*][1,2]diazocine (1n)

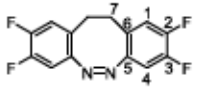

The reaction was performed according to the typical procedure (TP4) using the reagent **6n** (300 mg, 620 µmol), leading to the corresponding product **1n** (131 mg, 470 µmol, 75%) after silica gel column chromatography (applied gradient from pentane to CH_2Cl_2) as a yellow solid.

^{1}H NMR (500 MHz, $CDCl_3$) δ 6.84 (dd, *J* = 10.5, 7.6 Hz, 2H, H-4), 6.71 (dd, *J* = 10.5, 7.6 Hz, 2H, H-1), 2.93-2.68 (m, 4H, H-7) ppm.

^{13}C{^{1}H} NMR (126 MHz, $CDCl_3$) δ 150.6 (q, *J* = 5.6 Hz, C-5), 148.7 (q, *J* = 247.5 Hz, C-2), 148.6 (q, *J* = 249.6 Hz, C-3), 124.5 (q, *J* = 5.6 Hz, C-6), 118.2 (q, *J* = 18.2 Hz, C-1), 108.7 (q, *J* = 20.0 Hz, C-4), 30.9 (C-7) ppm.

^{19}F NMR (471 MHz, $CDCl_3$) δ -138.51 (ddd, *J* = 21.4, 9.8, 7.6 Hz), -139.13 (ddd, *J* = 21.3, 10.5, 7.3 Hz) ppm.

HRMS (EI) *m/z* for $C_{14}H_8F_4N_2$ [M]$^+$: calcd 280.06236, found: 280.06145 (73); 250 (100).

IR (ATR): ϑ = 3056 (w), 2925 (w), 1739 (w), 1605 (m), 1499 (s), 1460 (w), 1404 (w), 1343 (w), 1289 (s), 1236 (w), 1211 (s), 1153 (m), 1067 (m), 996 (w), 962 (w), 913 (m), 875 (s), 858 (m), 841 (s), 809 (s), 726 (w), 689 (w), 673 (w), 657 (w) cm^{-1}.

mp: 195 °C.

Rf: 0.27 (heptane/ethyl acetate = 90/10)

[10] The ^{13}C{^{1}H} NMR signals C-1' and C-5 for compound **1m** could not be detected.

(*Z*)-9,10-Dihydrodithieno[3,2-*c*:2',3'-*g*][1,2]diazocine (1o)

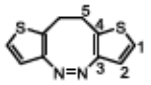

The reaction was performed according to the typical procedure (TP4) using the reagent **6o** (576 mg, 1.36 mmol), leading to the corresponding product **1o** (100 mg, 450 µmol, 33%) after silica gel column chromatography (applied gradient from pentane to pentane/ethyl acetate = 85/15) as a yellow solid.

^{1}H NMR (500 MHz, $CDCl_3$) δ 7.09 (d, *J* = 5.4 Hz, 2H, H-1 or H-2), 7.00 (d, *J* = 5.4 Hz, 2H, H-1 or H-2), 2.97 (s, 4H, H-5) ppm.

^{13}C{^{1}H} NMR (126 MHz, $CDCl_3$) δ 151.9 (C-3), 127.4 (C-4), 125.2 (C-1 or C-2), 122.8 (C-1 or C-2), 27.4 (C-5) ppm.

HRMS (EI) *m/z* for $C_{10}H_8N_2S_2$ [M]$^+$: calcd 220.01289, found: 220.01301 (60); 147.02 (100).

IR (ATR): ϑ = 3119 (w), 3061 (w), 2949 (w), 2923 (w), 2866 (w), 1737 (w), 1519 (w), 1431 (m), 1378 (w), 1355 (w), 1193 (w), 1160 (m), 1067 (w), 1042 (w), 972 (w), 913 (m), 833 (m), 804 (w), 733 (s), 706 (s), 649 (s), 625 (m), 529 (s), 481 (m) cm^{-1}.

mp: 98 °C.[11]

Rf: 0.44 (CHCl$_3$)

(*Z*)-5,6-Dihydrodipyrido[2,3-*c*:3',2'-*g*][1,2]diazocine (1p)

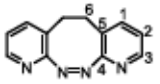

In a glovebox, compound **6p** (100 mg, 240 µmol), CH_2Cl_2 (1.2 mL) and trimethylsilyl iodide (69 µL, 490 µmol) were added sequentially to a round-bottomed flask equipped with a magnetic stirring bar. The reaction mixture was stirred at 20 °C for 10 min before it was treated with triethylamine (67 µL, 490 µmol). The flask was capped, transferred out of the glovebox where the reaction mixture was quenched with water (5 mL), extracted with $CHCl_3$ (5 x 5 mL), washed with brine (10 mL) and dried over Na_2SO_4. After filtration, the organic phase was concentrated under reduced pressure. The resulting residue, CH_2Cl_2 (2.4 mL) and pyridine (24 µL, 300 µmol) were added sequentially to a round-bottomed flask. NBS (52 mg, 290 µmol) was added portionwise over the course of 2 min under stirring and the reaction mixture was stirred at 20 °C for 30 min. The reaction mixture was washed with water (30 mL), extracted with $CHCl_3$ (3 x 20 mL), washed with brine (20 mL) and dried over Na_2SO_4. After filtration, the organic phase was concentrated under reduced pressure and the residue was purified by silica gel column chromatography (applied gradient from pentane to ethyl acetate) to furnish the product **1p** as a yellow solid (42 mg, 200 µmol, 83%).

^{1}H NMR (500 MHz, $CDCl_3$) δ 8.26 (d, *J* = 4.1 Hz, 2H, H-3), 7.36 (dd, *J* = 7.6, 1.5 Hz, 2H, H-1), 6.99 (dd, *J* = 7.6, 4.7 Hz, 2H, H-2), 3.13 – 2.72 (m, 4H, H-6) ppm.

[11] Visually, it appeared as if the compound decomposed at this temperature.

^{13}C{^{1}H} NMR (126 MHz, $CDCl_3$) δ 164.1 (C-4), 147.3 (C-3), 138.9 (C-1), 123.2 (C-5), 122.8 (C-2), 29.6 (C-6) ppm.

HRMS (EI) *m/z* for $C_{12}H_{10}N_4$ [M]$^+$: calcd 210.09055, found: 210.09067 (2); 181.07 (100).

IR (ATR): ϑ = 3043 (w), 2921 (w), 2870 (w), 1750 (w), 1566 (s), 1438 (m), 1417 (s), 1227 (w), 1190 (w), 1119 (w), 1087 (s), 981 (m), 873 (w), 804 (s), 785 (s), 771 (s), 731 (m), 698 (s), 688 (s), 565 (m) cm^{-1}.

mp: 190 °C.

Rf: 0.41 (ethyl acetate)

Buchwald-Hartwig amination (**1q, 1r**)

(*Z*)-11,12-Dihydrodibenzo[*c*,*g*][1,2]diazocine-2,9-diamine (1q)

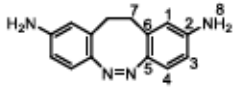

In a glovebox, compound **1b** (798 mg, 2.88 mmol), tris(dibenzylideneacetone)dipalladium(0) (132 mg, 140 µmol), lithium hexamethyldisilazide (1.445 g, 8.64 mmol), $ZnCl_2$ (589 mg, 4.32 mmol), dioxane (6 mL) and tri-*tert*-butylphosphine (106 mg, 290 µmol) were added sequentially into a microwave vial equipped with a magnetic stirring bar. The vial was capped with a crimp cap equipped with a PTFE septum, transferred out of the glovebox and stirred at 100 °C for 48 h. After cooling to 20 °C, the reaction mixture was diluted with diethyl ether (20 mL) and quenched with an aq HCl (10 mL, 1 M). Aq NaOH (50 mL, 1 M) was added and the reaction mixture was extracted with diethyl ether (10 x 30 mL) and dried over Na_2SO_4. After filtration, the organic phase was concentrated under reduced pressure and the crude product was purified by silica gel column chromatography (applied gradient from pentane to ethyl acetate) to furnish the product **1q** as a yellow solid (350 mg, 1.47 mmol, 51%). Adapted from lit.[18]

^{1}H NMR (500 MHz, MeOD) δ 6.61 (d, *J* = 8.4 Hz, 2H, H-4), 6.50 (dd, *J* = 8.4, 2.3 Hz, 2H, H-3), 6.38 (d, *J* = 2.2 Hz, 2H, H-1), 2.70 (s, 4H, H-7) ppm.

^{13}C{^{1}H} NMR (126 MHz, MeOD) δ 148.4 (C-5), 147.8 (C-6), 131.3 (C-2), 122.4 (C-4), 116.2 (C-1), 114.3 (C-3), 32.9 (C-7) ppm.

HRMS (EI) *m/z* for $C_{14}H_{14}N_4$ [M]$^+$: calcd 238.12185, found: 238.12159 (100).

IR (ATR): ϑ = 3417 (w), 3311 (w), 3194 (w), 2940 (w), 2893 (w), 2840 (w), 1738 (w), 1602 (s), 1574 (m), 1497 (s), 1310 (m), 1253 (s), 1158 (w), 1106 (w), 1083 (w), 958 (w), 869 (s), 810 (s), 735 (m), 666 (s), 599 (s), 547 (s), 469 (s) cm^{-1}.

mp: 195 °C (dec).

Rf: 0.48 (ethyl acetate)

(*Z*)-11,12-Dihydrodibenzo[*c*,*g*][1,2]diazocine-3,8-diamine (1r)

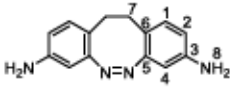

In a glovebox, compound **1h** (610 mg, 2.20 mmol), tris(dibenzylideneacetone)dipalladium(0) (101 mg, 110 µmol), lithium hexamethyldisilazide (1.104 g, 6.6 mmol), $ZnCl_2$ (450 mg, 3.3 mmol), dioxane (5 mL) and tri-*tert*-butylphosphine (81 mg, 220 µmol) were added sequentially into a microwave vial equipped with a magnetic stirring bar. The vial was capped with a crimp cap equipped with a PTFE septum, transferred out of the glovebox and stirred at 100 °C for 60 h. After cooling to 20 °C, the reaction mixture was diluted with diethyl ether (20 mL) and quenched with aq HCl (10 mL, 1 M). Aq NaOH (50 mL, 1 M) was added and the reaction mixture was extracted with diethyl ether (10 x 30 mL) and dried over Na_2SO_4. After filtration, the organic phase was concentrated under reduced pressure and the crude product was purified by silica gel column chromatography (applied gradient from pentane to ethyl acetate) to furnish the product **1r** as a yellow solid (305 mg, 1.28 mmol, 58%). Adapted from lit.[16]

^{1}H NMR (500 MHz, MeOD) δ 6.72 (d, *J* = 8.2 Hz, 2H, H-1), 6.39 (dd, *J* = 8.2, 2.4 Hz, 2H, H-2), 6.14 (d, *J* = 2.4 Hz, 2H, H-4), 2.74 – 2.57 (m, 4H, H-7) ppm.

^{13}C NMR (126 MHz, MeOD) δ 157.2 (C-5), 147.5 (C-3), 131.5 (C-1), 119.2 (C-6), 115.5 (C-2), 105.9 (C-4), 31.9 (C-7) ppm.

HRMS (EI) *m/z* for $C_{14}H_{14}N_4$ [M]$^+$: calcd 238.12185, found: 238.12148 (60); 209.11 (100).

IR (ATR): ϑ = 3466 (w), 3428 (w), 3374 (m), 3341 (w), 3198 (w), 3035 (w), 2926 (w), 2842 (w), 1738 (w), 1621 (s), 1496 (s), 1309 (m), 1274 (m), 1174 (m), 1140 (m), 897 (m), 850 (s), 811 (s), 658 (s), 618 (s), 590 (s), 519 (s), 487 (s) cm^{-1}.

mp: 190 °C (dec).

Rf: 0.48 (ethyl acetate)

Saponification (**1s**, **1t**)

(*Z*)-11,12-Dihydrodibenzo[*c*,*g*][1,2]diazocine-2,9-dicarboxylic acid (1s)

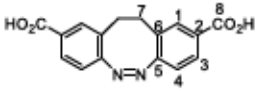

Compound **1f** (150 mg, 460 µmol) and methanol (10 mL) were added into a round-bottomed flask. NaOH (370 mg, 9.24 mmol) was added and the reaction mixture was stirred at 50 °C for 12 h. The reaction mixture was allowed to cool to 20 °C and quenched with aq HCl (20 mL, 1 M). The residue was filtered, the remaining precipitation was washed with water (20 mL), ethyl acetate (20 mL) and dried under vacuum (0.1 mbar) to furnish the product **1s** as a yellow solid (125 mg, 420 µmol, 91%).

^{1}H NMR (500 MHz, DMSO) δ 7.73 (dd, *J* = 8.1, 1.6 Hz, 2H, H-3), 7.67 (d, *J* = 1.5 Hz, 2H, H-1), 6.99 (d, *J* = 8.1 Hz, 2H, H-4), 3.02 – 2.83 (m, 4H, H-7) ppm.

^{13}C{^{1}H} NMR (126 MHz, DMSO) δ 166.4 (C-8), 158.3 (C-2), 131.2 (C-1), 129.6 (C-5), 128.4 (C-6), 128.1 (C-3), 118.6 (C-4), 30.4 (C-7) ppm.

HRMS (EI) *m/z* for $C_{16}H_{12}N_2O_4$ [M]$^+$: calcd 296.07971, found: 296.07966 (10); 178.08 (100).

IR (ATR): ϑ = 2949 (w), 2826 (w), 2662 (w), 2547 (w), 1681 (s), 1605 (m), 1435 (m), 1293 (s), 1189 (m), 1123 (w), 1084 (w), 913 (m), 842 (w), 755 (s), 681 (w), 548 (m), 511 (m) cm^{-1}.

mp: 290 °C (dec).

(*Z*)-11,12-Dihydrodibenzo[*c*,*g*][1,2]diazocine-3,8-dicarboxylic acid (1t)

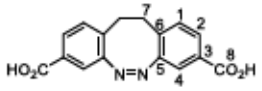

Compound **1l** (40 mg, 120 µmol) and methanol (3 mL) were added into a round-bottomed flask. NaOH (100 mg, 2.47 mmol) was added and the reaction mixture was stirred at 50 °C for 12 h. The reaction mixture was allowed to cool to 20 °C and quenched with aq HCl (15 mL, 1 M). The residue was filtered, washed with water (10 mL), ethyl acetate (10 mL) and dried under vacuum (0.1 mbar) to furnish the product **1t** as a yellow solid (28 mg, 100 µmol, 77%).

^{1}H NMR (500 MHz, DMSO) δ 7.61 (dd, *J* = 7.9, 1.4 Hz, 2H, H-2), 7.38 (d, *J* = 1.1 Hz, 2H, H-4), 7.22 (d, *J* = 7.9 Hz, 2H, H-1), 2.91 (s, 4H, H-7) ppm.

^{13}C{^{1}H} NMR (126 MHz, DMSO) δ 166.5 (C-8), 154.7 (C-5), 132.8 (C-6), 130.3 (C-1), 130.2 (C-3), 128.1 (C-2), 119.2 (C-4), 30.7 (C-7) ppm.

HRMS (EI) *m/z* for $C_{16}H_{12}N_2O_4$ [M]$^+$: calcd 296.07971, found: 296.07969 (10); 179.08 (100).

IR (ATR): ϑ = 3084 (w), 2948 (w), 2827 (w), 2661 (w), 2536 (w), 1683 (s), 1607 (m), 1558 (w), 1495 (w), 1423 (m), 1301 (s), 1255 (s), 1120 (w), 1082 (w), 942 (m), 901 (m), 853 (w), 759 (s), 652 (w), 623 (w), 549 (m) cm^{-1}.

mp: 300 °C (dec).

Reduction (**1u**)

(*Z*)-(11,12-Dihydrodibenzo[*c*,*g*][1,2]diazocine-2,9-diyl)dimethanol (1u)

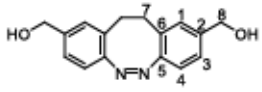

A dry, nitrogen flushed two-necked Schlenk-flask equipped with a magnetic stirring bar and a septum was charged with compound **1f** (621 mg, 1.92 mmol) and anhydrous THF (40 mL). The reaction mixture was cooled to 0 °C and diisobutylaluminium hydride (9.6 mL, 1.2 M in toluene) was added dropwise (3 mL/min) under stirring. After completion of the addition, the reaction mixture was warmed to 20 °C and stirred at 20 °C for 1 h. The reaction mixture was quenched with aq. Rochelle salt (50 mL, 0.2 M),

followed by an extraction with ethyl acetate (3 x 20 mL). The organic phase was washed with brine (30 mL) and dried over Na_2SO_4. After filtration, the organic phase was concentrated under reduced pressure and to the residue was added methanol (200 mL), NaOH (800 mg, 20 mmol) and $CuCl_2$ dihydrate (20 mg, 0.12 mmol). The reaction mixture was stirred while air was bubbled through the solution at 20 °C for 30 min. The reaction mixture was quenched with saturated aq NH_4Cl (20 mL) and water (20 mL), followed by an extraction with ethyl acetate (3 x 20 mL). The organic phase was washed with brine (30 mL) and dried over Na_2SO_4. After filtration, the organic phase was concentrated under reduced pressure and the residue was stirred in minimal amounts of ethanol at 78 °C. Hexane was added dropwise to the solution until a precipitate formed. The resulting precipitate was collected in a Büchner funnel, washed with additional hexane and dried under vacuum (0.1 mbar) to furnish the product **1u** as a yellow solid (362 mg, 1.35 mmol, 70%). Adapted from lit.[19]

^{1}H NMR (500 MHz, MeOD) δ 7.12 (dd, *J* = 8.0, 1.7 Hz, 2H, H-3), 7.02 (d, *J* = 1.3 Hz, 2H, H-1), 6.77 (d, *J* = 8.0 Hz, 2H, H-4), 4.44 (s, 4H, H-8), 2.87 (s, 4H, H-7) ppm.

^{13}C{^{1}H} NMR (126 MHz, MeOD) δ 155.8 (C-5), 142.0 (C-2), 129.7 (C-6), 129.4 (C-1), 126.4 (C-3), 119.8 (C-4), 64.5 (C-8), 32.6 (C-7) ppm.

HRMS (EI) *m/z* for $C_{16}H_{16}N_2O_2$ [M]$^+$: calcd 268.12118, found: 268.12100 (40); 179.08 (100).

IR (ATR): $\tilde{\nu}$ = 3286 (m), 2932 (w), 2875 (w), 2446 (w), 1524 (w), 1484 (w), 1457 (m), 1414 (m), 1366 (m), 1151 (m), 1023 (s), 995 (s), 915 (m), 838 (m), 814 (s), 752 (m), 675 (m) cm^{-1}.

mp: 150 °C.

Rf: 0.38 (ethyl acetate)

Synthetic Method Example (1c)

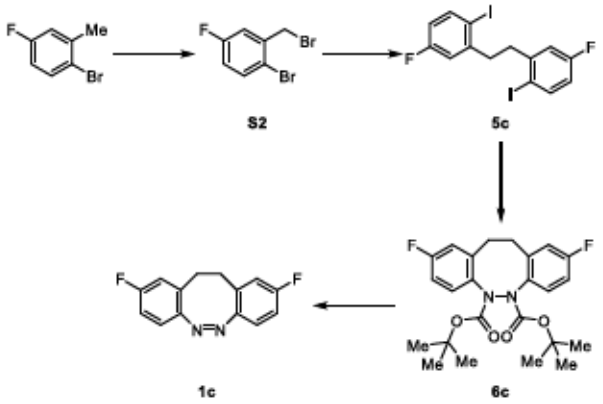

1-Bromo-2-(bromomethyl)-4-fluorobenzene (S2)

1-Bromo-4-fluoro-2-methylbenzene (9.451 g, 50.00 mmol), acetonitrile (100 mL), benzoyl peroxide (2.422 g, 10 mmol) and NBS (9.789 g, 55 mmol) were added sequentially to a round-bottomed flask equipped with a reflux condenser. The reaction mixture was stirred at 82 °C for 12 h. After cooling to 20 °C, the reaction mixture was quenched with water (50 mL), extracted with $CHCl_3$ (3 x 50 mL), washed with brine (50 mL) and dried over Na_2SO_4. After filtration, the organic phase was concentrated under reduced pressure followed by silica gel column chromatography (pentane) to furnish the product **S2** as a colorless solid (7.209 g, 26.91 mmol, 54%, lit. 99%[2]).

1,2-Bis(5-fluoro-2-iodophenyl)ethane (5c)

A dry, nitrogen flushed two-necked Schlenk-flask equipped with a magnetic stirring bar and a septum was charged with reagent **S2** (6.104 g, 22.78 mmol) and anhydrous THF (70 mL). The reaction mixture was cooled to -78 °C and *n*-butyllithium (13.67 mL, 34.17 mmol, 2.5 M in hexanes) was added dropwise (3 mL/min) under stirring. After completion of the addition and stirring at -78 °C for 5 min, iodine (5.782 g, 22.78 mmol) was added. Then, the reaction mixture was warmed to 20 °C before it was quenched with aq $Na_2S_2O_3$ (5 mL, 2 M) and water (70 mL), followed by an extraction with $CHCl_3$ (3 x 70 mL). The organic phase was washed with brine (70 mL) and dried over Na_2SO_4. After filtration, the organic phase was concentrated under reduced pressure and the residue was washed with hexane (110 mL) and dried under vacuum (0.1 mbar) to furnish product **5c** (3.876 g, 8.25 mmol, 72%) as a colorless solid.

Di-*tert*-butyl 2,9-difluoro-11,12-dihydrodibenzo[*c*,*g*][1,2]diazocine-5,6-dicarboxylate (6c)

In a glovebox, reagent **5c** (3.800 g, 8.08 mmol), di-*tert*-butyl hydrazine-1,2-dicarboxylate (1.2 equiv), CuI (10 mol%), K_3PO_4 (3.0 equiv), acetonitrile (5 mL/mmol) and 1,2-dimethylethylenediamine (20 mol%) were added sequentially to a microwave vial. The vial was capped with a crimp cap equipped with a PTFE septum, transferred out of the glovebox and stirred at 82 °C for 18 h. After cooling to 20 °C, the

reaction mixture was quenched with water (3 mL/mmol), washed with aq NH_3 (3 mL/mmol, 25%), extracted with $CHCl_3$ (3 x 5 mL/mmol), washed with brine (3 mL/mmol) and dried over Na_2SO_4. After filtration, the organic phase was concentrated under reduced pressure and the crude residue was purified by silica gel column chromatography (applied gradient from pentane to CH_2Cl_2) to furnish product **6c** (1.610 g, 3.61 mmol, 45%) as a colorless solid.

(*Z*)-2,9-Difluoro-11,12-dihydrodibenzo[*c*,*g*][1,2]diazocine (1c)

In a glovebox, reagent **6c** (1.540 g, 3.45 mmol), CH_2Cl_2 (17 mL) and trimethylsilyl iodide (1 mL, 6.9 mmol) were added sequentially to a round-bottomed flask equipped with a magnetic stirring bar. The reaction mixture was stirred at 20 °C for 10 min before it was treated with triethylamine (1 mL, 6.9 mmol). The flask was capped, transferred out of the glovebox where the reaction mixture was quenched with water (17 mL), extracted with $CHCl_3$ (3 x 17 mL), washed with brine (17 mL) and dried over Na_2SO_4. After filtration, the organic phase was concentrated under reduced pressure. The resulting residue, CH_2Cl_2 (35 mL) and pyridine (0.4 mL, 4.28 mmol) were added sequentially to a round-bottomed flask. NBS (737 mg, 4.14 mmol) was added portionwise over the course of 2 min under stirring and the reaction mixture was stirred at 20 °C for 30 min. The reaction mixture was concentrated under reduced pressure and the residue was purified by silica gel column chromatography (applied gradient from pentane to CH_2Cl_2) to furnish product **1c** (695 mg, 2.87 mmol, 83%) as a yellow solid.

Absorption Maxima and Photostationary States of Cyclic Azobenzenes (1a-1u)

Absorption maxima at wavelength λ_{max} were determined by ^{1}H NMR spectroscopy (5 mM in MeCN-d_3) at 298.15 K. The NMR tubes were irradiated with light at 385 nm and 565 nm wavelength for 2 min each before the NMR spectra were recorded. Photostationary states (PSS) were determined by UV–vis spectroscopy (1 mM in acetonitrile) at 298.15 K. The cuvettes were irradiated with light at 385 nm and 565 nm wavelength for 10 min each before the absorption spectra were measured. Cyclic azobenzenes **1s** and **1t** were dissolved in DMSO-d_6 and DMSO respectively.

Cyclic azobenzene	PSS (385 nm) [%] (*E*)	PSS (565 nm) [%] (*Z*)	λ_{max} (*E*) [nm]	λ_{max} (*Z*) [nm]
1a	85	>99	486	401
1b	83	>99	488	401
1c	85	>99	486	401
1d	62	>99	486	396
1e[12]	-	>99	489	409
1f	77	>99	491	399
1g	71	>99	492	405
1h	80	>99	486	399
1i	82	>99	484	398
1j	75	>99	486	300
1k	81	>99	484	397
1l	80	>99	486	399
1m	82	>99	486	400
1n	73	>99	484	399
1o	18	>99	490	406
1p	87	>99	492	405
1q[12]	-	>99	-	416
1r	28	>99	483	400
1s	82	>99	494	401
1t	84	>99	488	400
1u	83	>99	489	403

[12] Thermal relaxation to the (*Z*) isomer was faster than data acquisition of the (*E*) isomer.

References

(1) Hsieh, J. C.; Cheng, A. Y.; Fu, J. H.; Kang, T. W. *Org. Biomol. Chem.* **2012**, *10*, 6404–6409.

(2) Bradshaw, B.; Evans, P.; Fletcher, J.; Lee, A. T. L.; Mwashimba, P. G.; Oehlrich, D.; Thomas, E. J.; Davies, R. H.; Allen, B. C. P.; Broadley, K. J.; et al. *Org. Biomol. Chem.* **2008**, *6*, 2138–2157.

(3) Doye, S.; Severin, R.; Mujahidin, D.; Reimer, J. *Heterocycles* **2007**, *74*, 683.

(4) Song, S.; Sun, X.; Li, X.; Yuan, Y.; Jiao, N. *Org. Lett.* **2015**, *17*, 2886–2889.

(5) Bartoli, G.; Bosco, M.; Locatelli, M.; Marcantoni, E.; Melchiorre, P.; Sambri, L. *Org. Lett.* **2005**, *7*, 427–430.

(6) Burrows, A. D.; Frost, C. G.; Mahon, M. F.; Richardson, C. *Angew. Chemie - Int. Ed.* **2008**, *47*, 8482–8486.

(7) Quattropani, A.; Sauer, W. H. B.; Crosignani, S.; Dorbais, J.; Gerber, P.; Gonzalez, J.; Marin, D.; Muzerelle, M.; Beltran, F.; Nichols, A.; et al. *ChemMedChem* **2015**, *10*, 688–714.

(8) Rousseaux, S.; Garcia-Fortanet, J.; Del Agulla Sanchez, M. A.; Buchwald, S. L. *J. Am. Chem. Soc.* **2011**, *133*, 9282–9285.

(9) Kukosha, T.; Truflikina, N.; Katkevics, M. *Synlett* **2011**, *2011*, 2525–2528.

(10) Patchett, R.; Magpantay, I.; Saudan, L.; Schotes, C.; Mezzetti, A.; Santoro, F. *Angew. Chemie - Int. Ed.* **2013**, *52*, 10352–10355.

(11) Curran, D. P.; Yang, F.; Cheong, J. ho. *J. Am. Chem. Soc.* **2002**, *124*, 14993–15000.

(12) Levine, D. R.; Siegler, M. A.; Tovar, J. D. *J. Am. Chem. Soc.* **2014**, *136*, 7132–7139.

(13) Šámal, M.; Chercheja, S.; Rybáček, J.; Vacek Chocholoušová, J.; Vacek, J.; Bednárová, L.; Šaman, D.; Stará, I. G.; Starý, I. *J. Am. Chem. Soc.* **2015**, *137*, 8469–8474.

(14) Mboyi, C. D.; Gaillard, S.; Mabaye, M. D.; Pannetier, N.; Renaud, J. L. *Tetrahedron* **2013**, *69*, 4875–4882.

(15) Iyoda, M.; Sakaitan, M.; Otsuka, H.; Oda, M. *Chem. Lett.* **1985**, *14*, 127–130.

(16) Zhao, P.; Beaudry, C. M. *Org. Lett.* **2013**, *15*, 402–405.

(17) Klapars, A.; Antilla, J. C.; Huang, X.; Buchwald, S. L. *J. Am. Chem. Soc.* **2001**, *123*, 7727–7729.

(18) Lee, D. Y.; Hartwig, J. F. *Org. Lett.* **2005**, *7*, 1169–1172.

(19) Moormann, W.; Langbehn, D.; Herges, R. *Synthesis (Stuttg).* **2017**, *49*, 3471–3475.

UV–vis Spectra of Cyclic Azobenzenes (**1a-1u**)

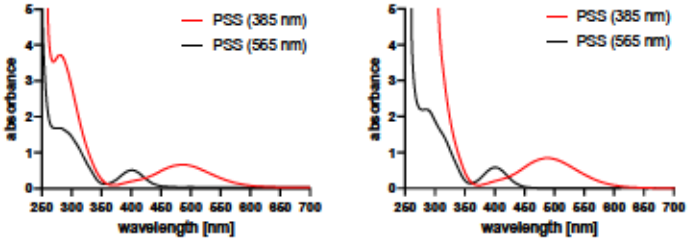

Figure S1. UV–vis spectra of compounds **1a** (left) and **1b** (right) after light irradiation at 385 nm wavelength (red) and 565 nm wavelength (black) in acetonitrile.

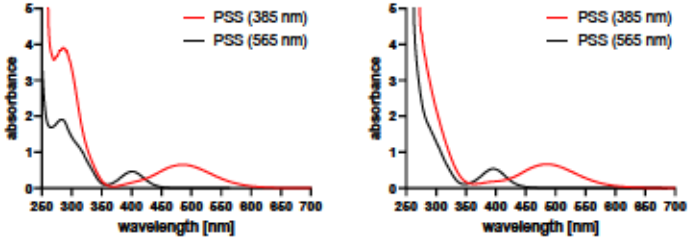

Figure S2. UV–vis spectra of compounds **1c** (left) and **1d** (right) after light irradiation at 385 nm wavelength (red) and 565 nm wavelength (black) in acetonitrile.

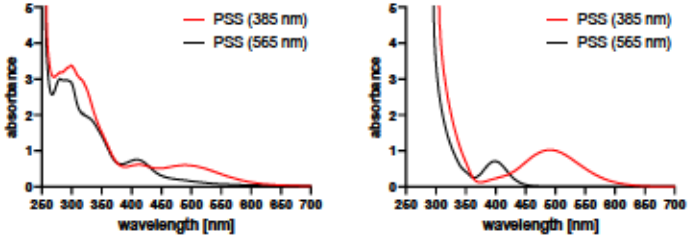

Figure S3. UV–vis spectra of compounds **1e** (left) and **1f** (right) after light irradiation at 385 nm wavelength (red) and 565 nm wavelength (black) in acetonitrile.

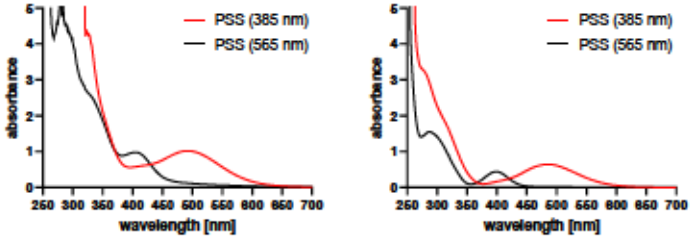

Figure S4. UV–vis spectra of compounds **1g** (left) and **1h** (right) after light irradiation at 385 nm wavelength (red) and 565 nm wavelength (black) in acetonitrile.

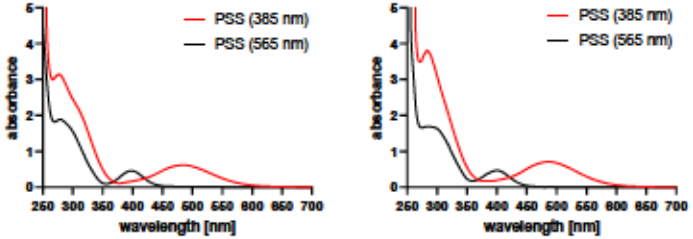

Figure S5. UV-vis spectra of compounds **1i** (left) and **1j** (right) after light irradiation at 385 nm wavelength (red) and 565 nm wavelength (black) in acetonitrile.

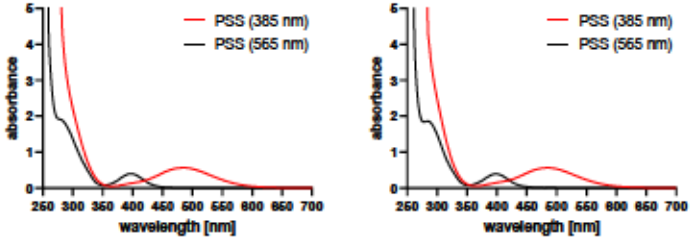

Figure S6. UV–vis spectra of compounds **1k** (left) and **1l** (right) after light irradiation at 385 nm wavelength (red) and 565 nm wavelength (black) in acetonitrile.

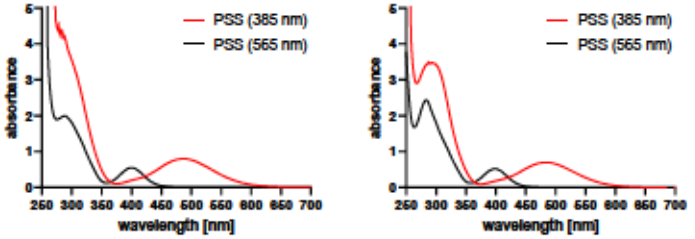

Figure S7. UV–vis spectra of compounds **1m** (left) and **1n** (right) after light irradiation at 385 nm wavelength (red) and 565 nm wavelength (black) in acetonitrile.

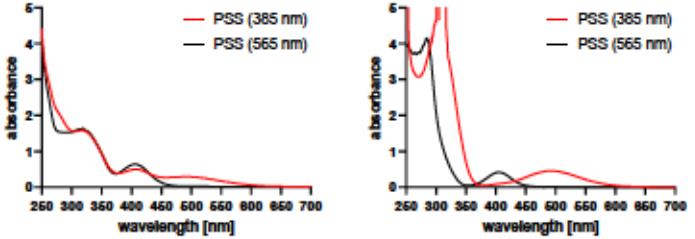

Figure S8. UV–vis spectra of compounds **1o** (left) and **1p** (right) after light irradiation at 385 nm wavelength (red) and 565 nm wavelength (black) in acetonitrile.

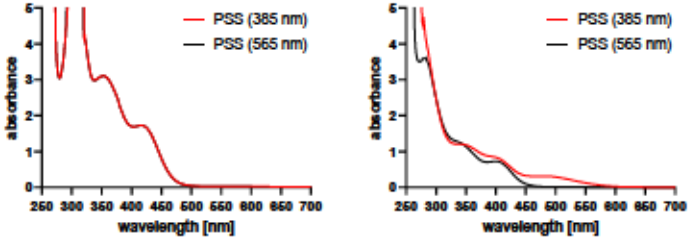

Figure S9. UV–vis spectra of compounds **1q** (left) and **1r** (right) after light irradiation at 385 nm wavelength (red) and 565 nm wavelength (black) in acetonitrile.

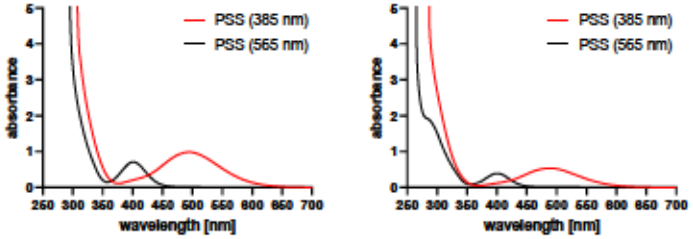

Figure S10. UV–vis spectra of compounds **1s** (left) and **1t** (right) after light irradiation at 385 nm wavelength (red) and 565 nm wavelength (black) in DMSO.

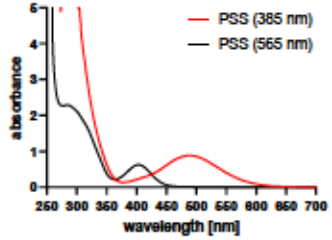

Figure S11. UV–vis spectra of compound **1u** after light irradiation at 385 nm wavelength (red) and 565 nm wavelength (black) in acetonitrile.

^{1}H, $^{13}C\{^{1}H\}$ and ^{19}F NMR Spectra of the Products

1-Bromo-2-(bromomethyl)-4-chlorobenzene (S1)

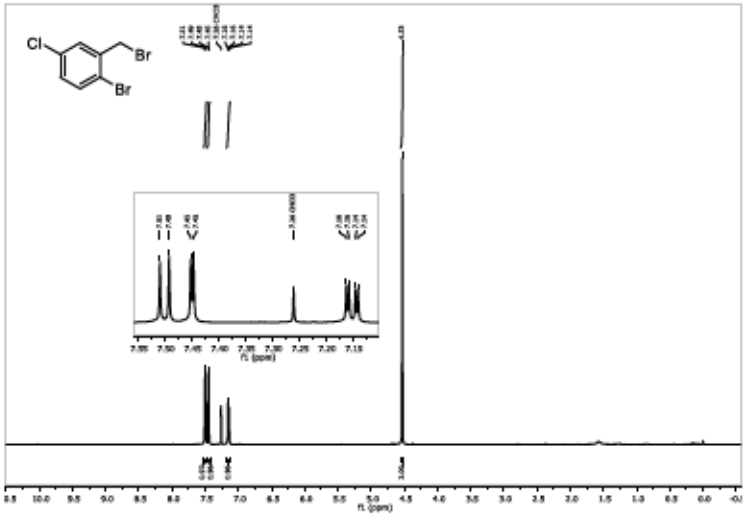

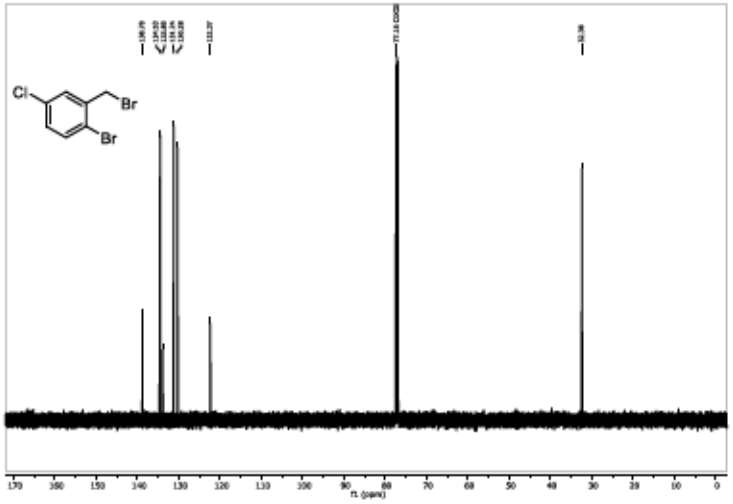

1-Bromo-2-(bromomethyl)-4-fluorobenzene (S2)

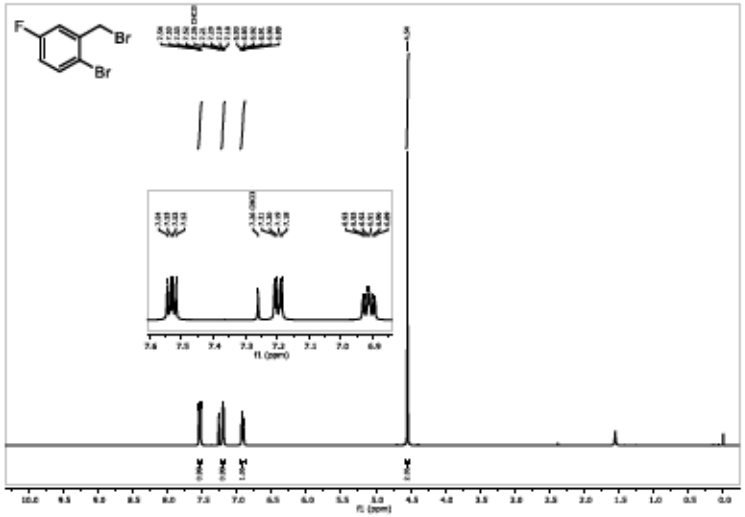

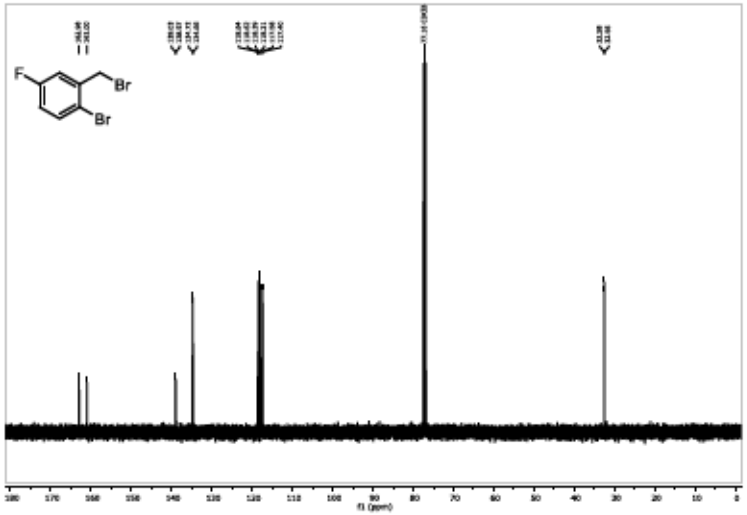

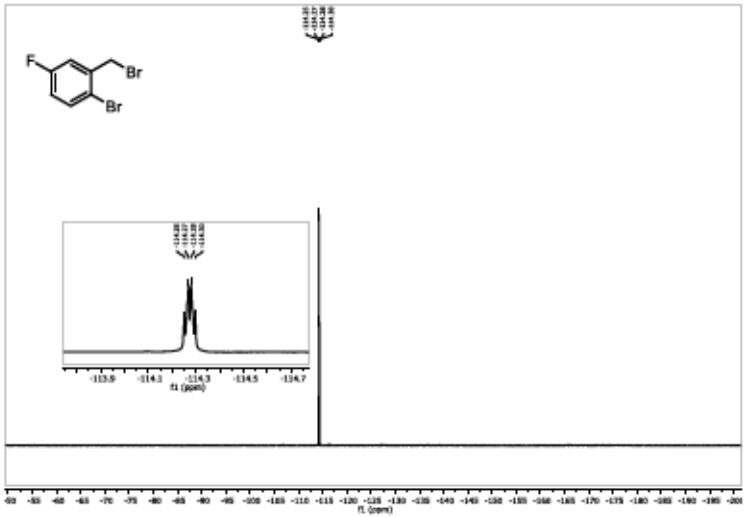

1-Bromo-2-(bromomethyl)-4-(trifluoromethyl)benzene (S3)

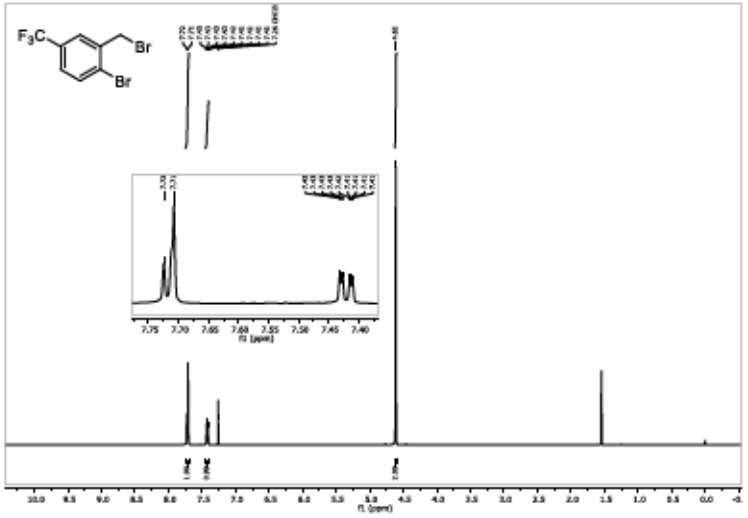

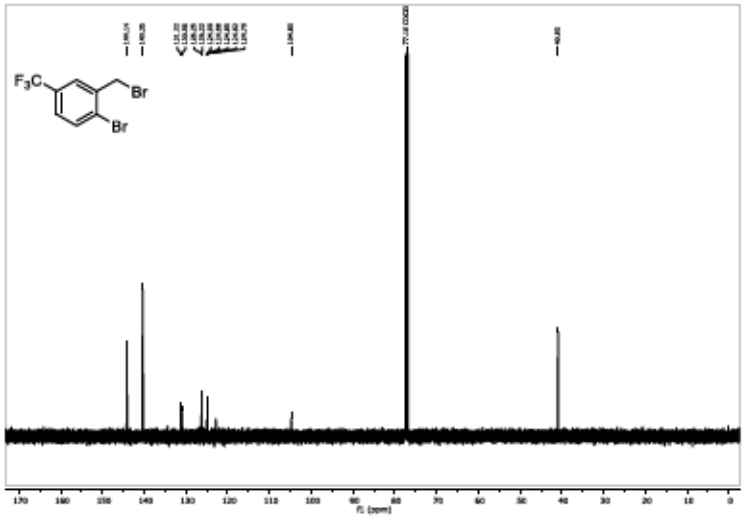

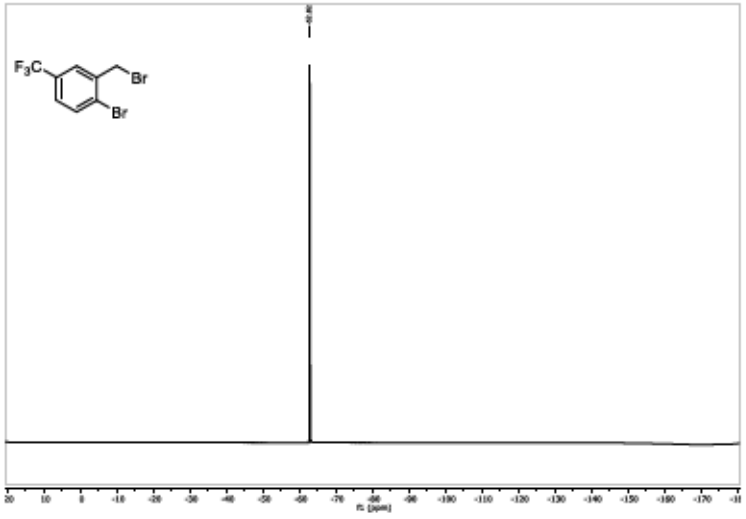

1-Bromo-4-(*tert*-butoxy)-2-methylbenzene (S4)

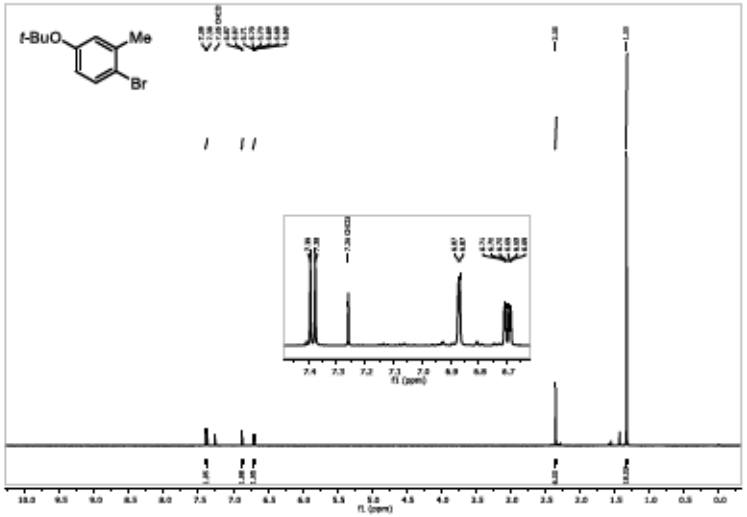

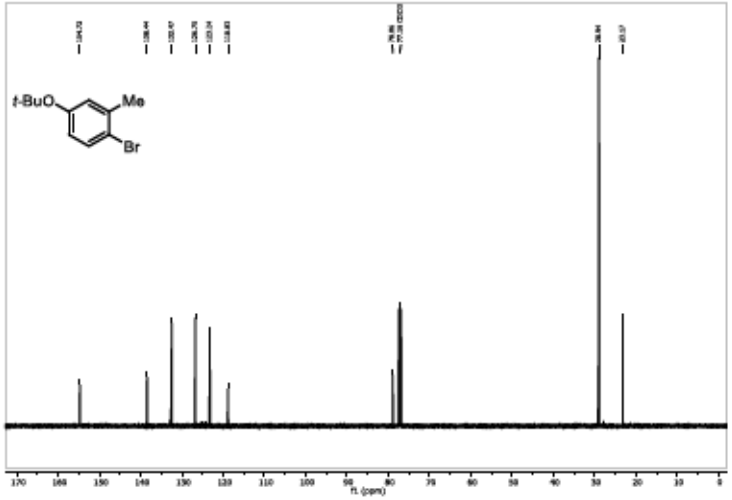

1-Bromo-2-(bromomethyl)-4-(*tert*-butoxy)benzene (S5)

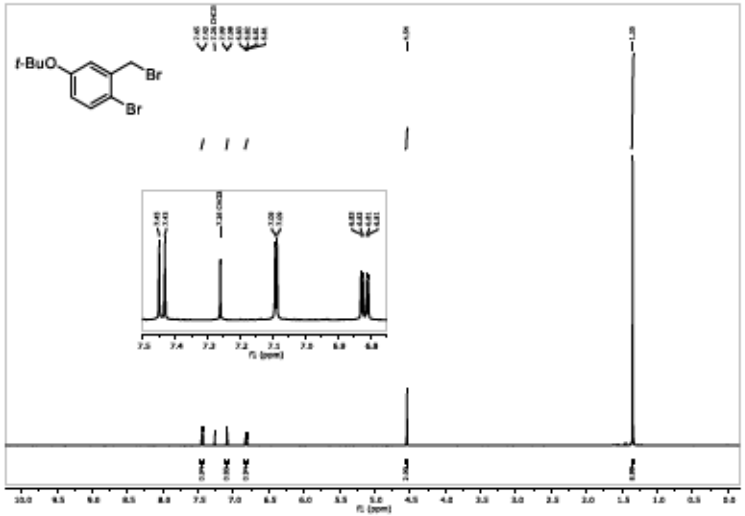

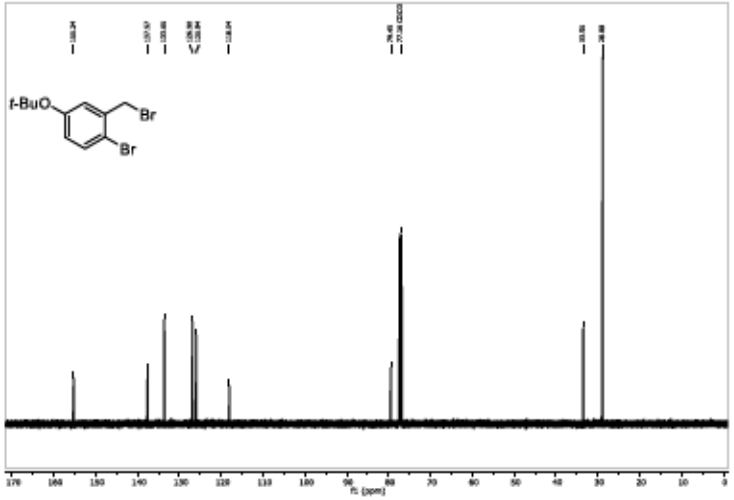

Methyl 4-bromo-3-methylbenzoate (S6)

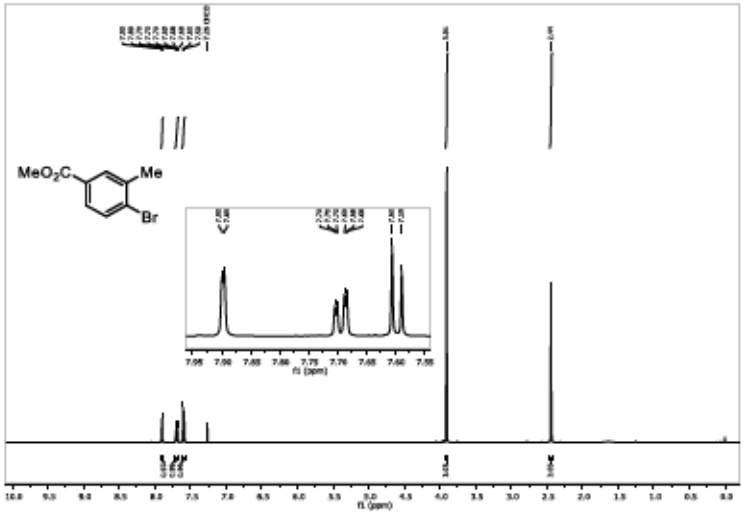

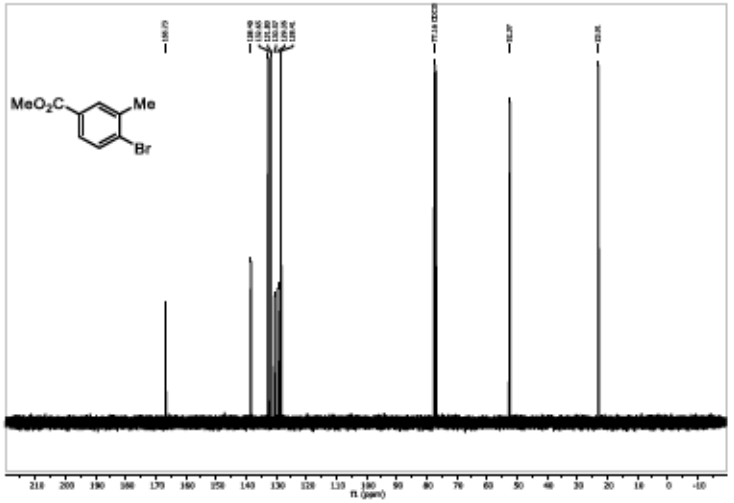

Methyl 4-bromo-3-(bromomethyl)benzoate (S7)

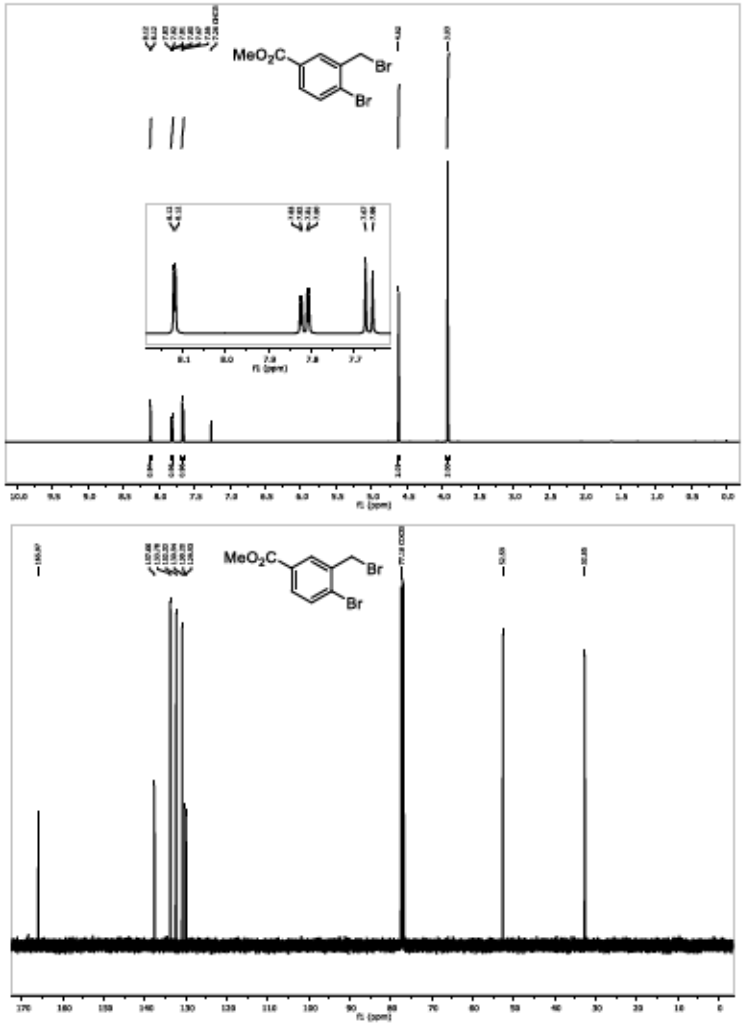

2-Bromo-1-(bromomethyl)-4-chlorobenzene (S8)

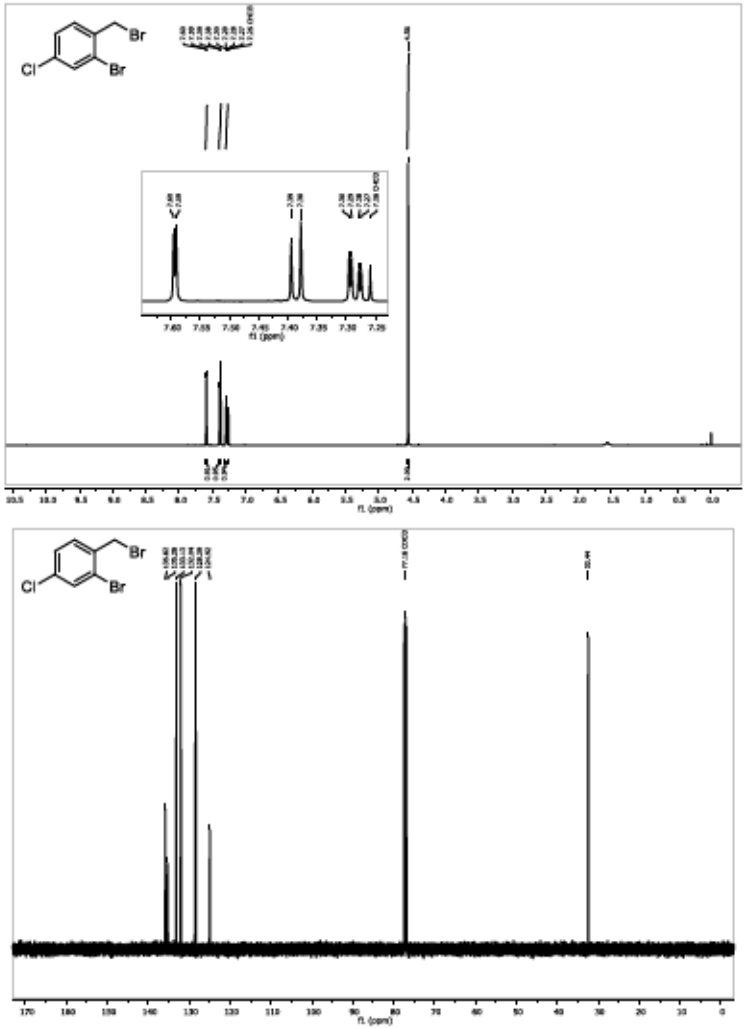

2-Bromo-1-(bromomethyl)-4-fluorobenzene (S9)

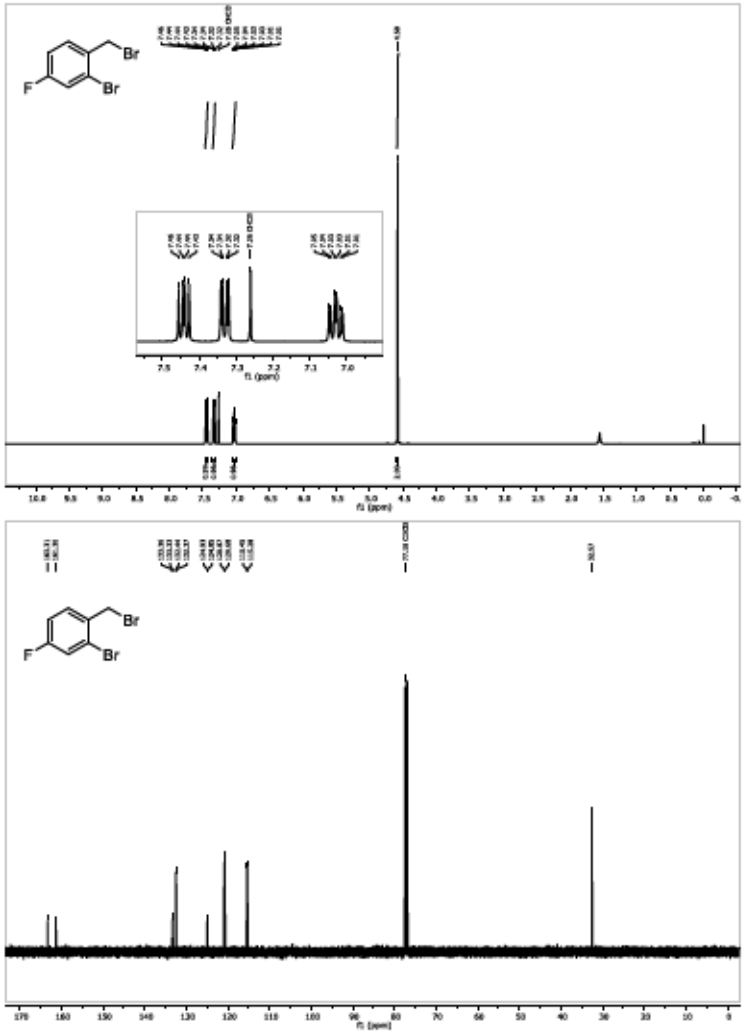

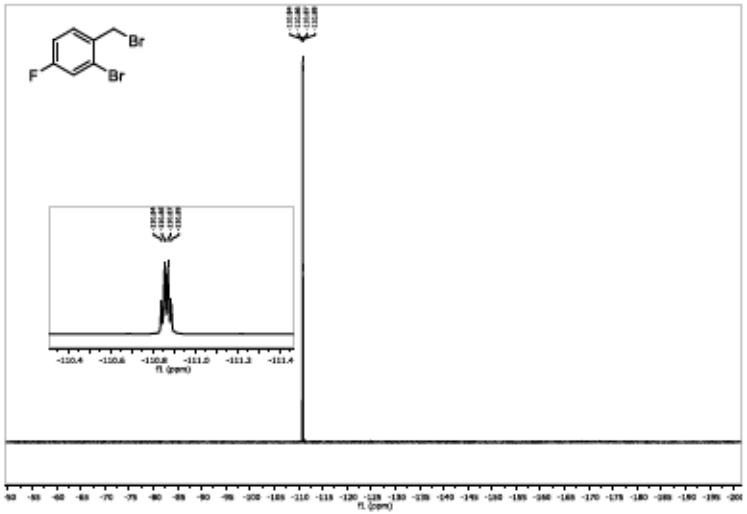

2-Bromo-4-(*tert*-butyl)-1-methylbenzene (S10)

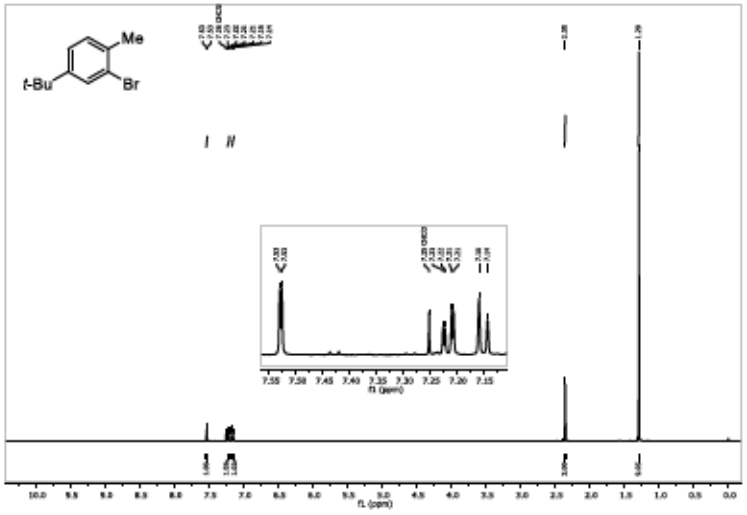

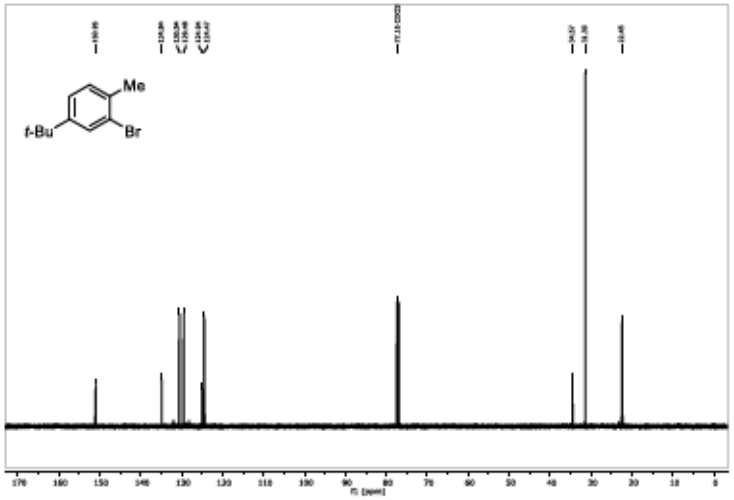

2-Bromo-1-(bromomethyl)-4-(*tert*-butyl)benzene (S11)

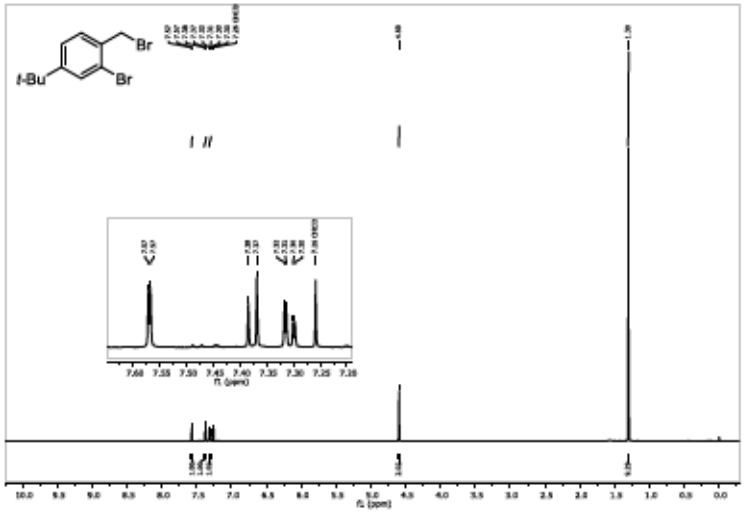

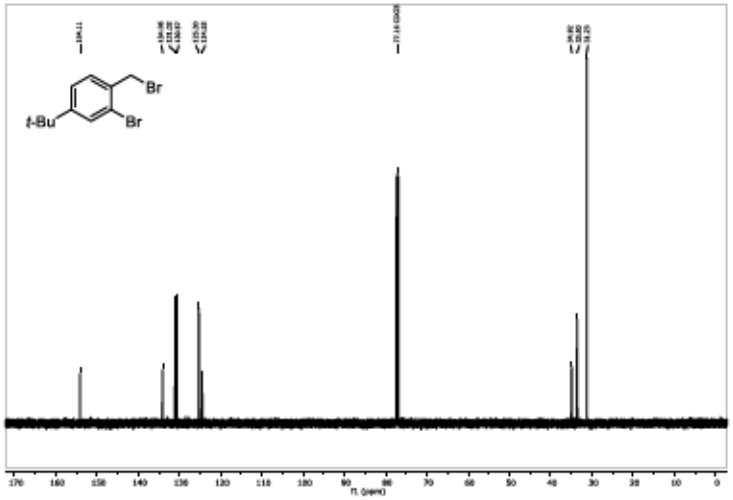

3-Bromo-4-(bromomethyl)benzonitrile (S12)

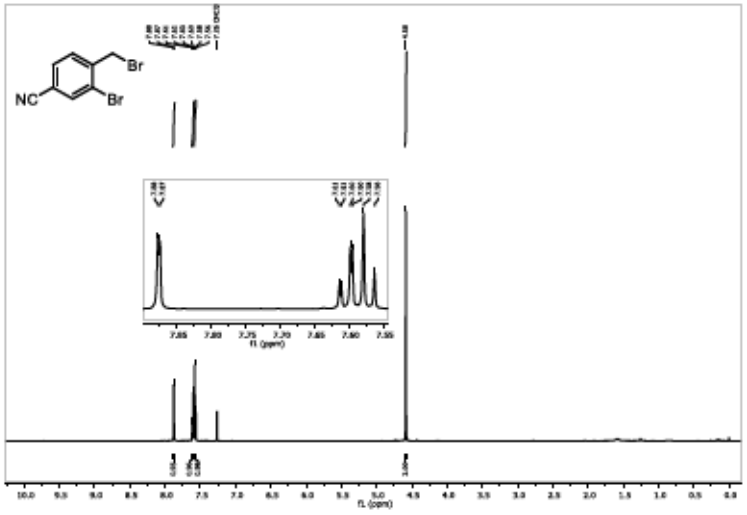

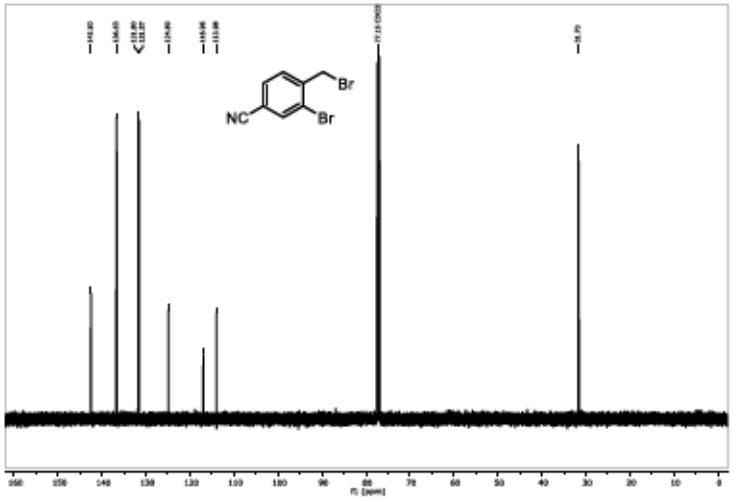

Methyl 3-bromo-4-methylbenzoate (S13)

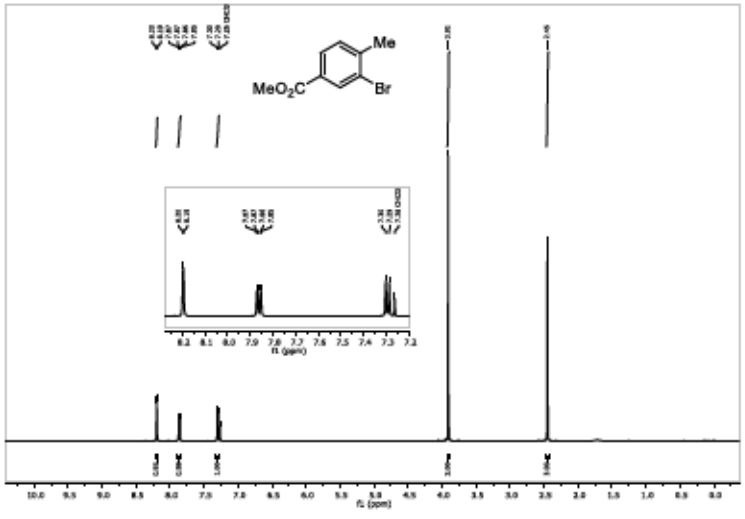

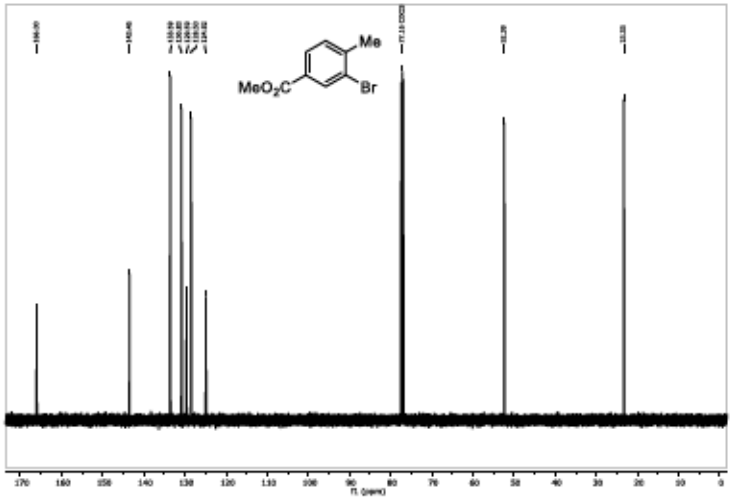

Methyl 3-bromo-4-(bromomethyl)benzoate (S14)

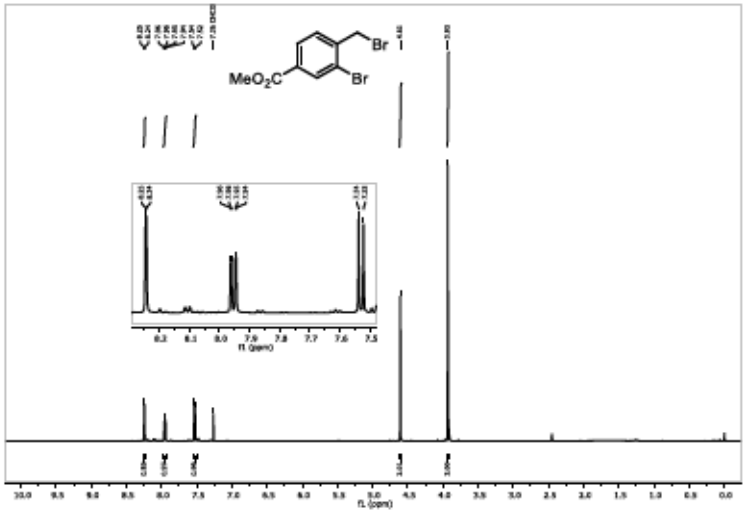

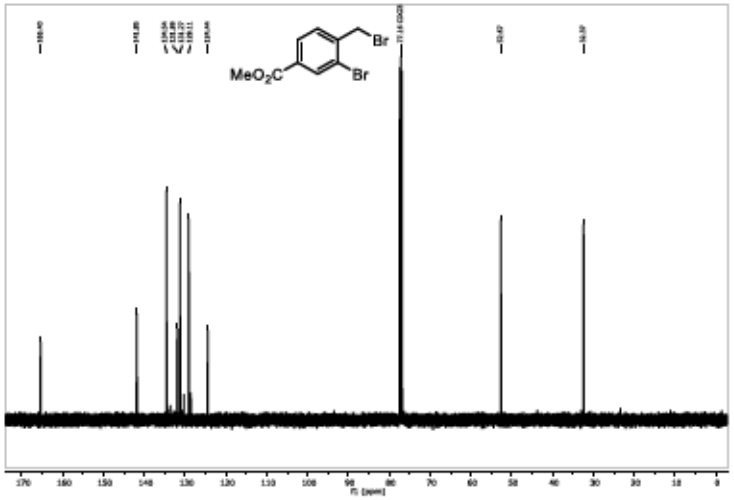

1-Bromo-2-(bromomethyl)-4,5-difluorobenzene (S15)

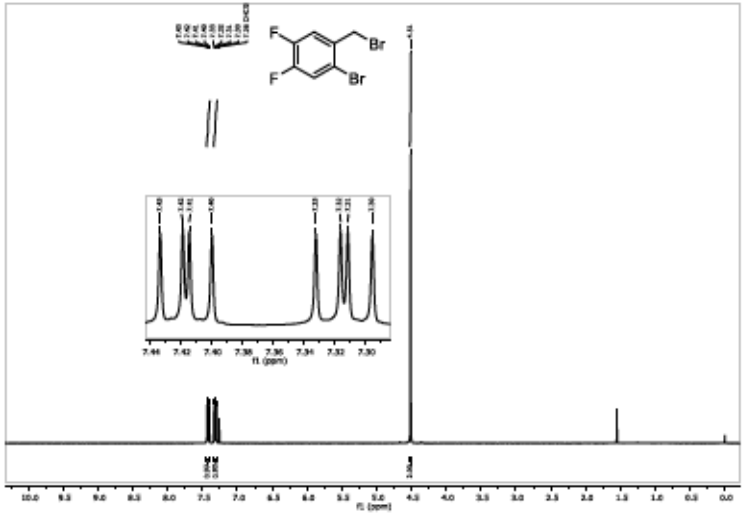

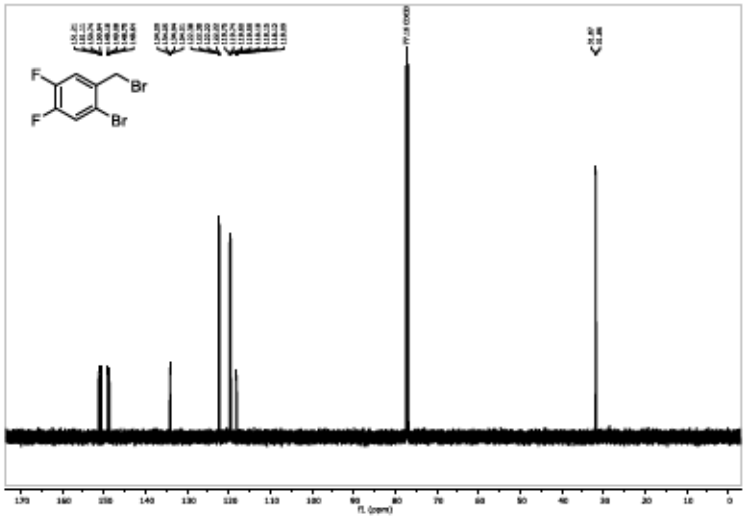

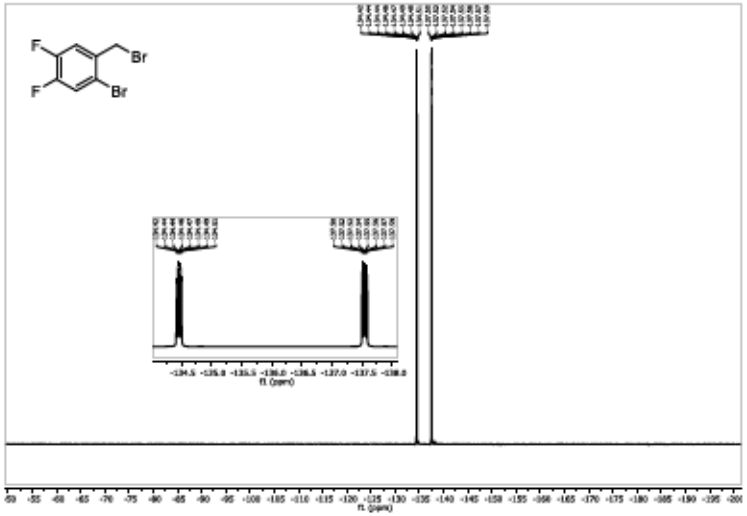

(3-Bromothiophen-2-yl)methanol (S16)

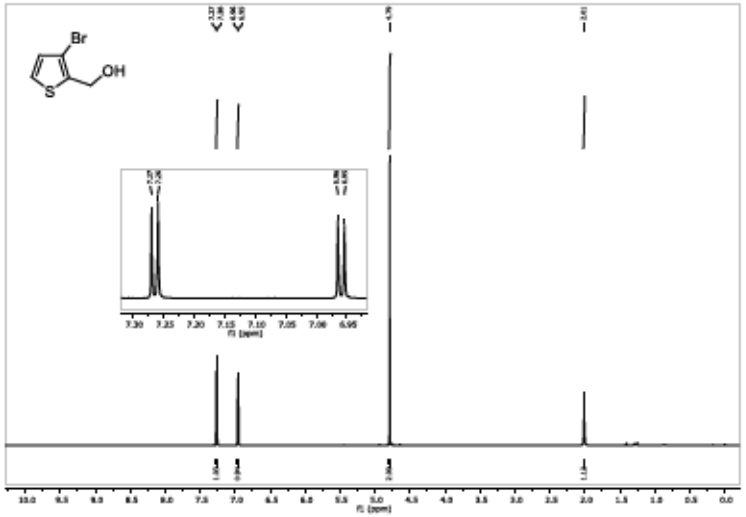

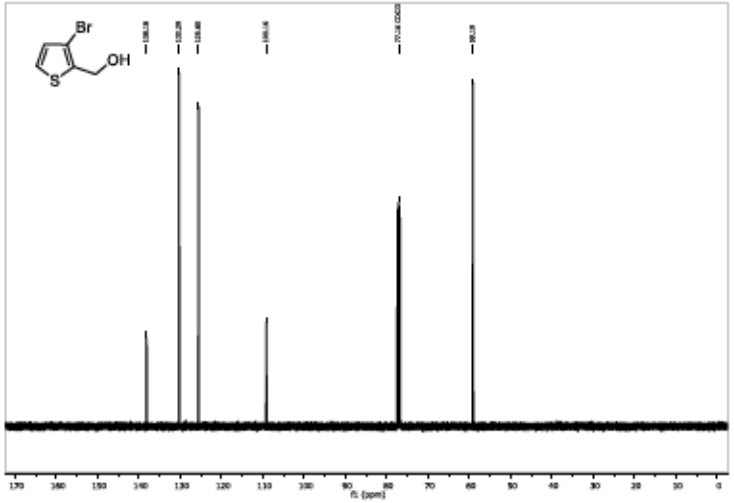

3-Bromo-2-(bromomethyl)thiophene (S17)

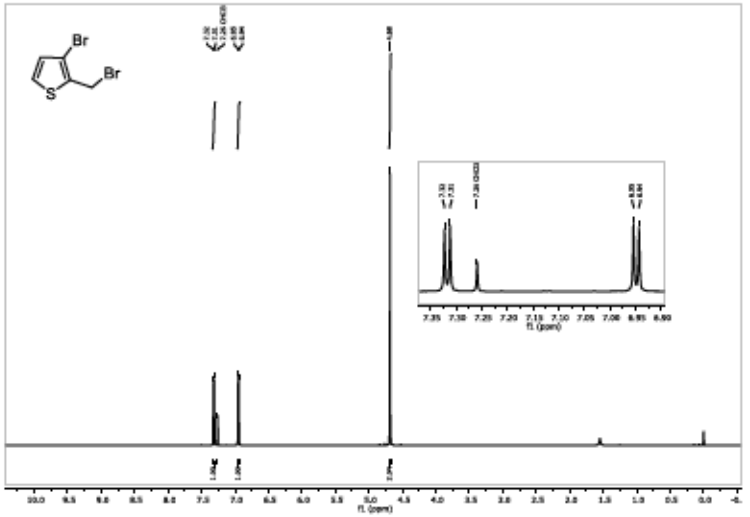

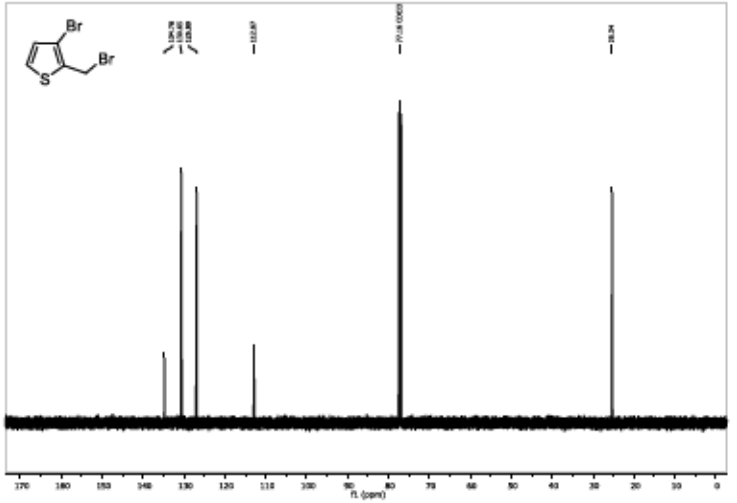

2-Bromo-3-(bromomethyl)pyridine (S18)

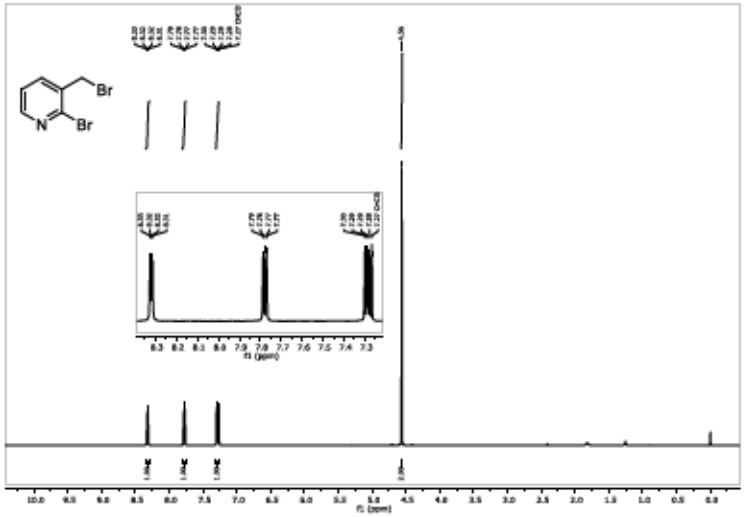

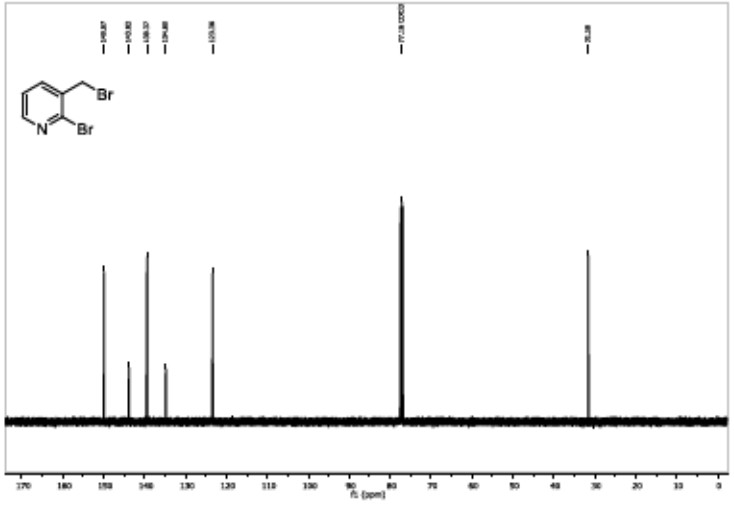

(Z)-1-Bromo-2-(2-bromo-4-chlorostyryl)-4-chlorobenzene (S19)

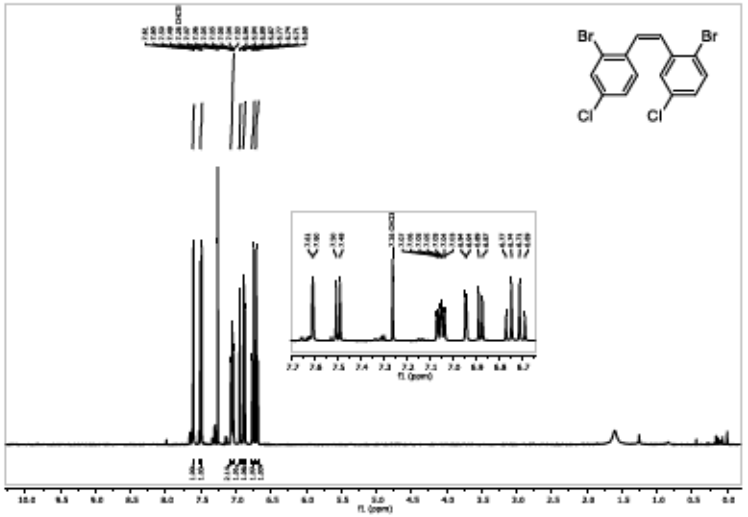

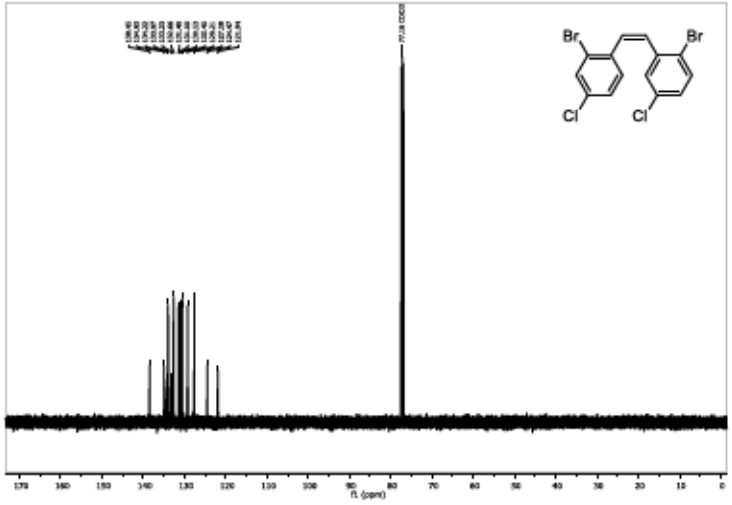

1,2-Bis(2-iodophenyl)ethane (5a)

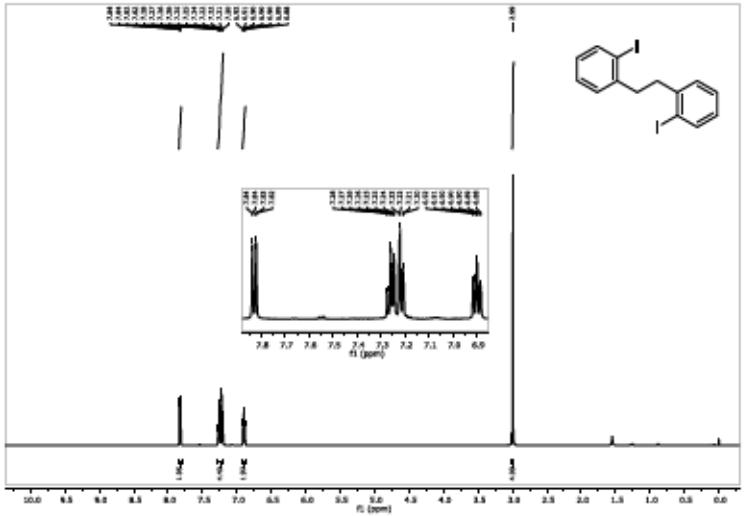

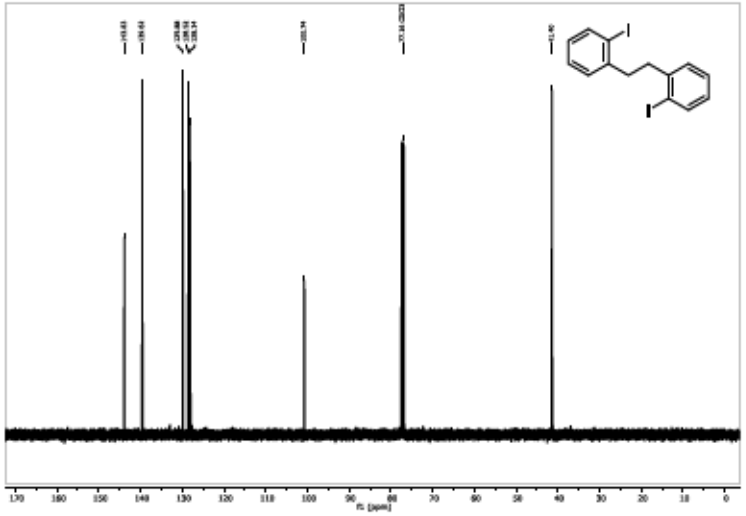

1,2-Bis(5-chloro-2-iodophenyl)ethane (5b)

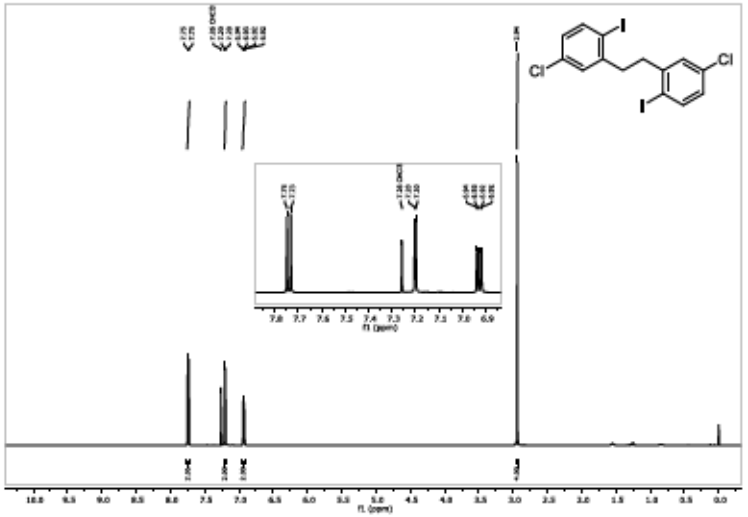

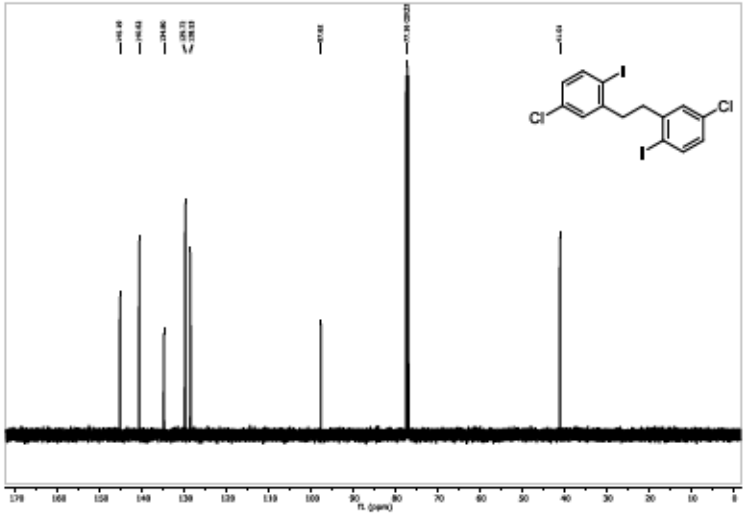

1,2-Bis(5-fluoro-2-iodophenyl)ethane (5c)

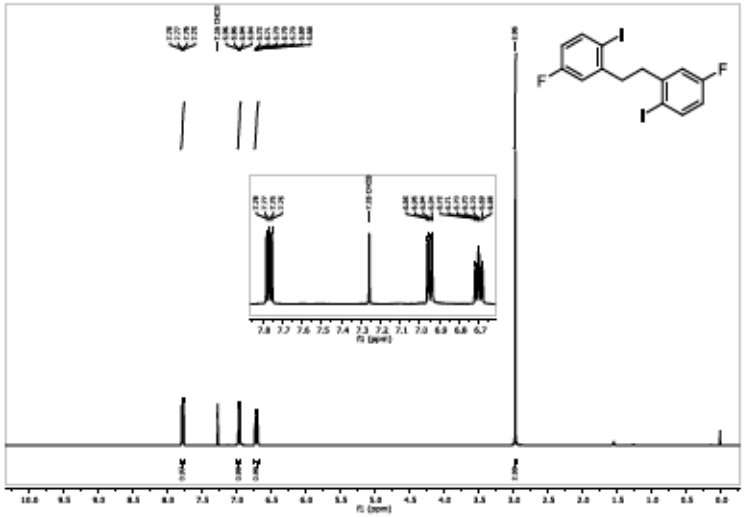

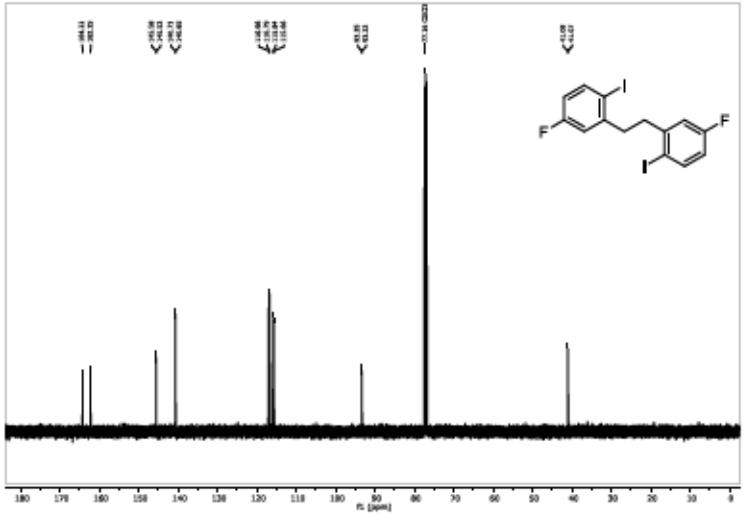

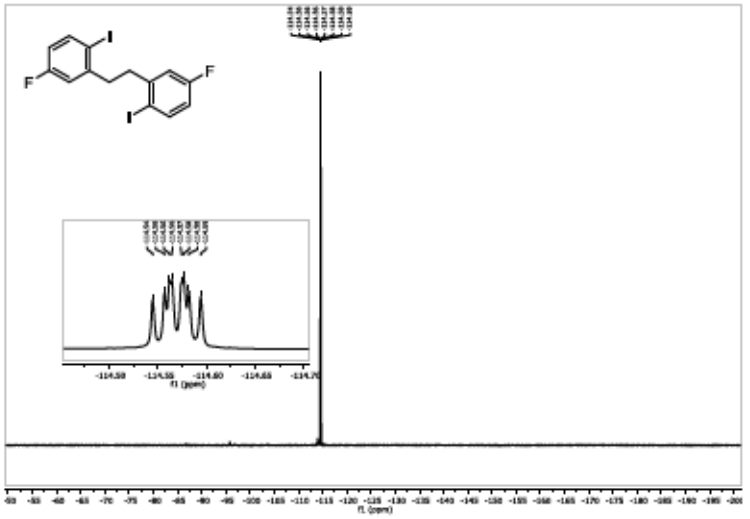

1,2-Bis(2-iodo-5-(trifluoromethyl)phenyl)ethane (5d)

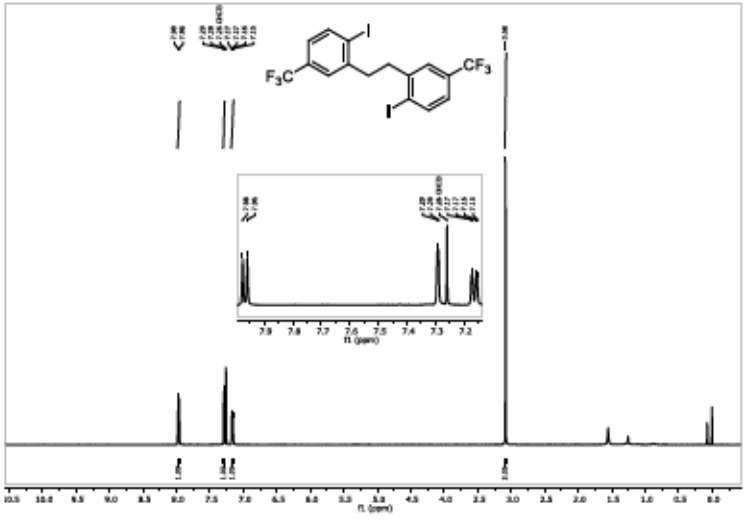

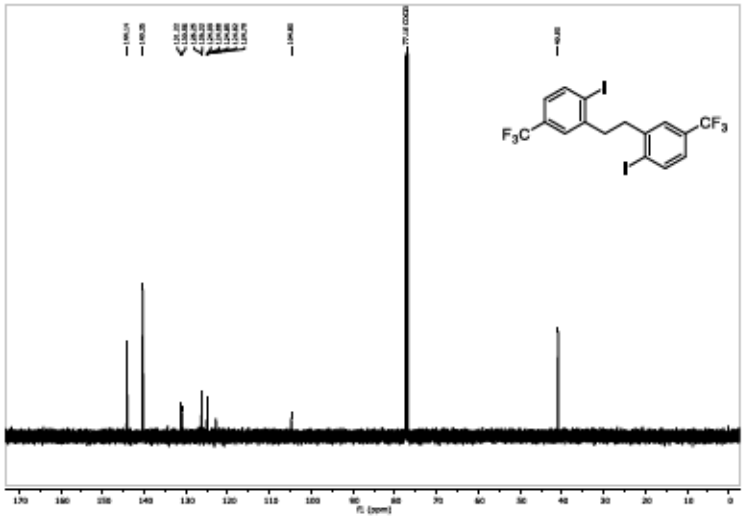

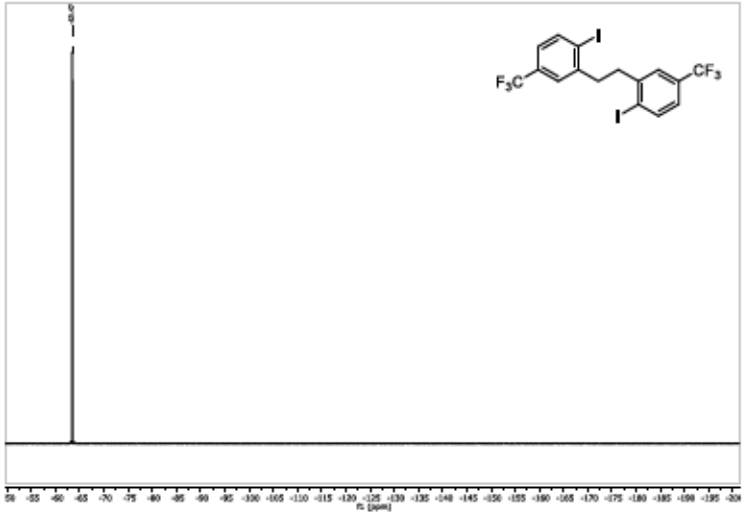

1,2-Bis(5-(*tert*-butoxy)-2-iodophenyl)ethane (5e)

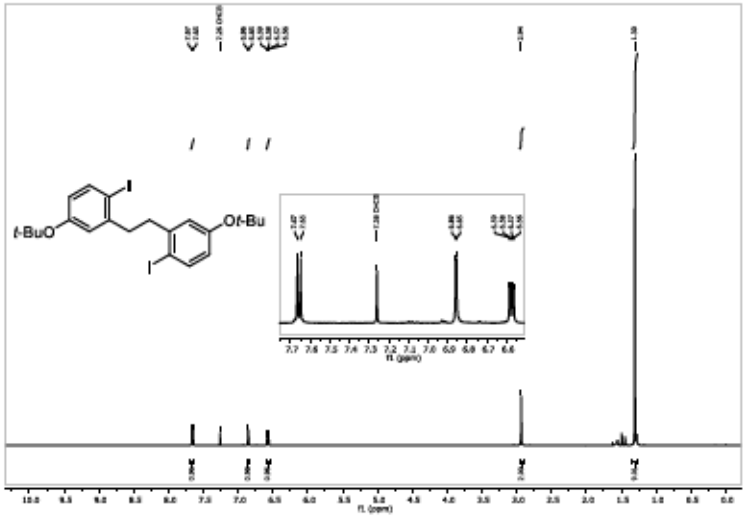

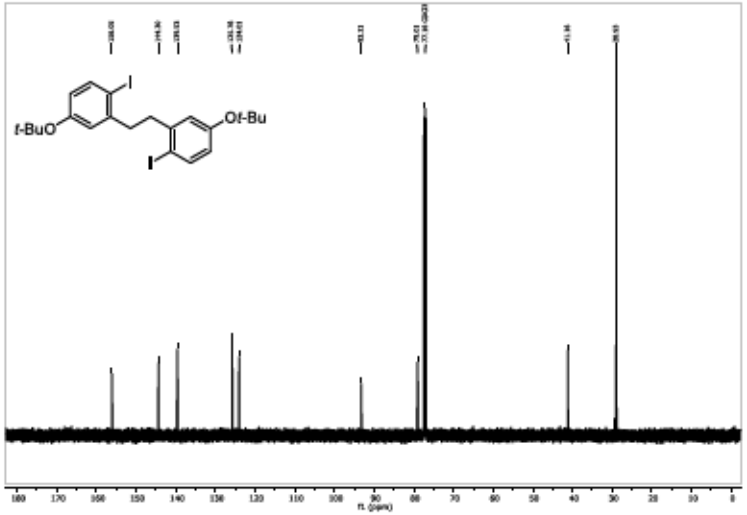

Dimethyl 3,3'-(ethane-1,2-diyl)bis(4-bromobenzoate) (5f)

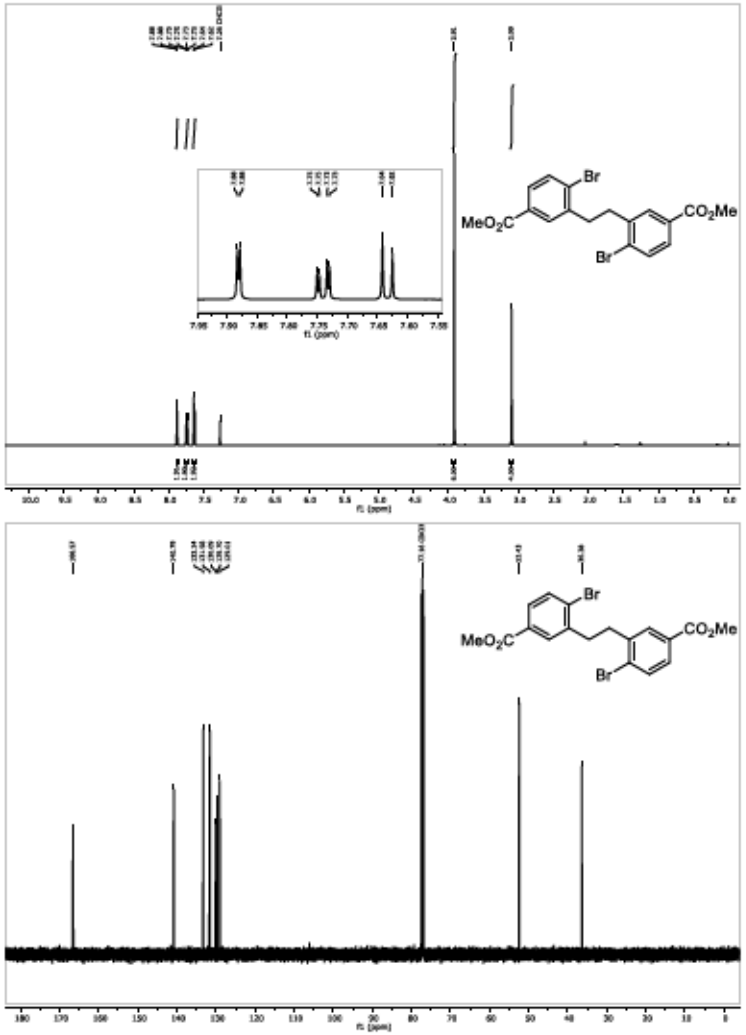

1,2-Bis(2-iodo-5-methoxyphenyl)ethane (5g)

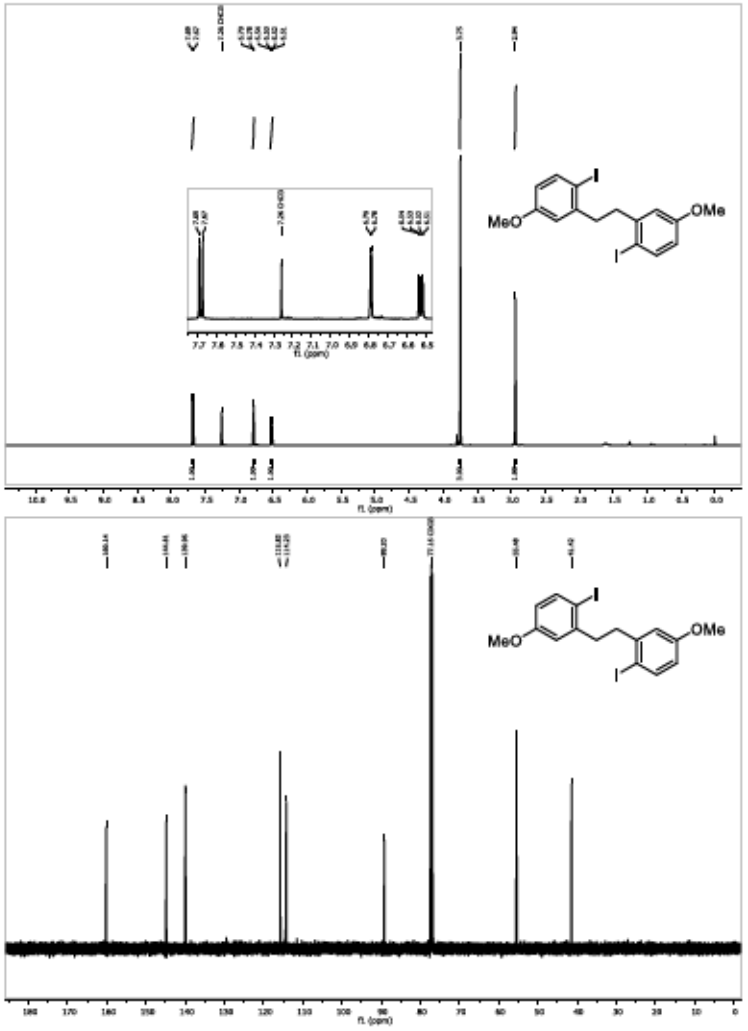

1,2-Bis(4-chloro-2-iodophenyl)ethane (5h)

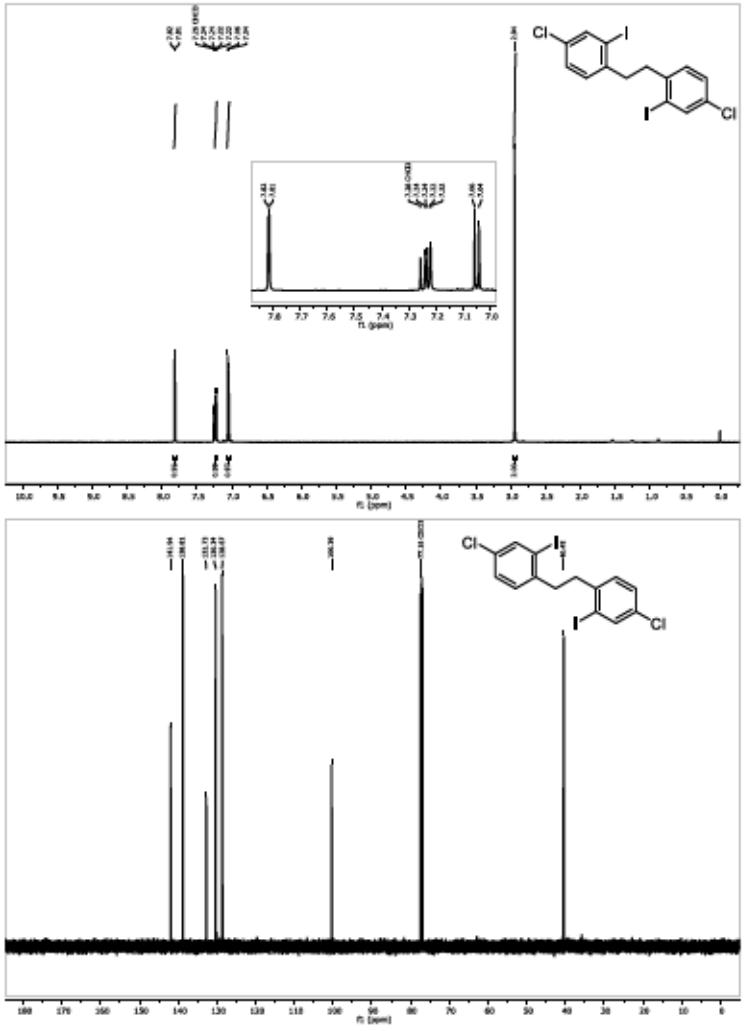

1,2-Bis(4-fluoro-2-iodophenyl)ethane (5l)

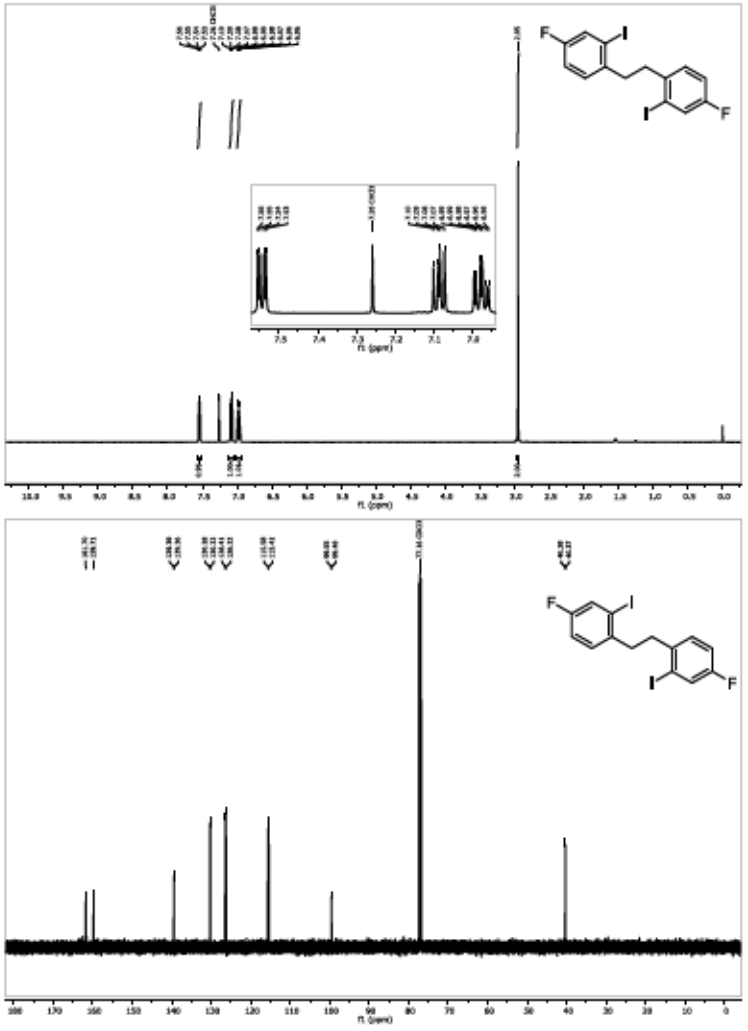

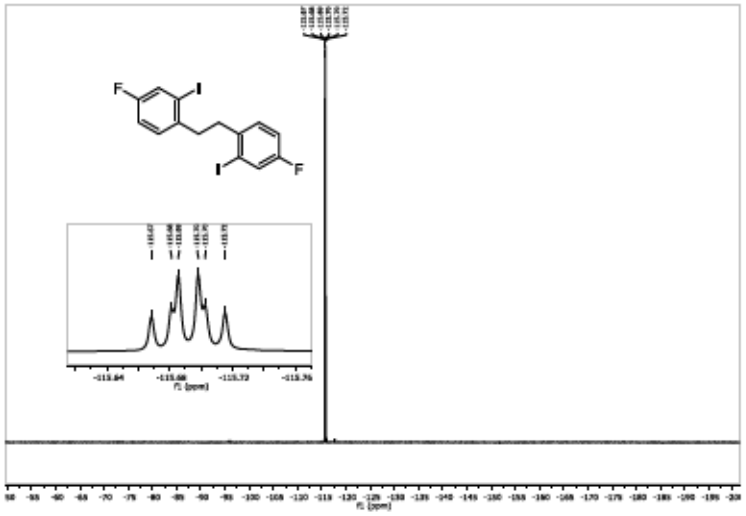

1,2-Bis(4-(tert-butyl)-2-iodophenyl)ethane (5j)

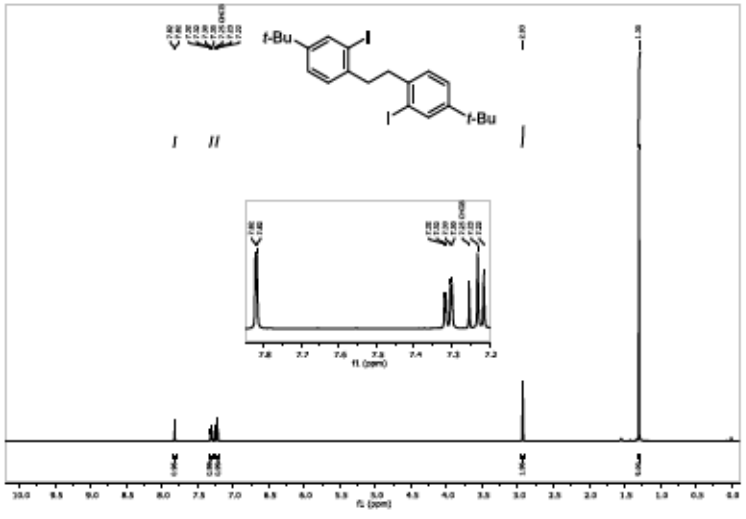

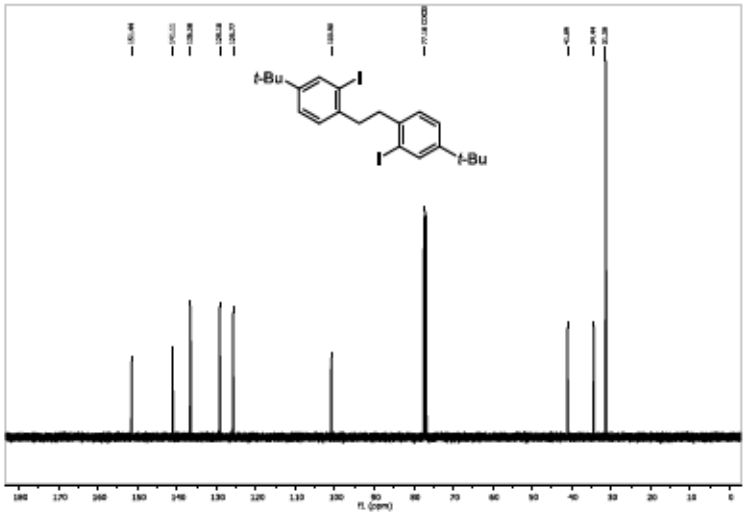

4,4'-(Ethane-1,2-diyl)bis(3-bromobenzonitrile) (5k)

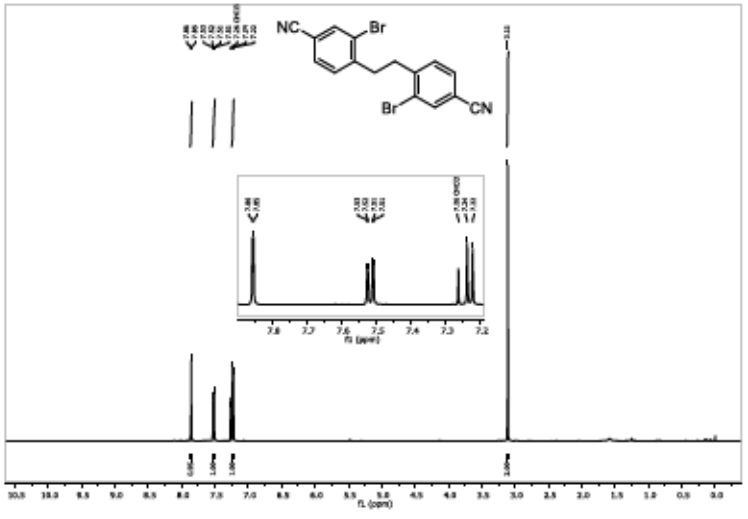

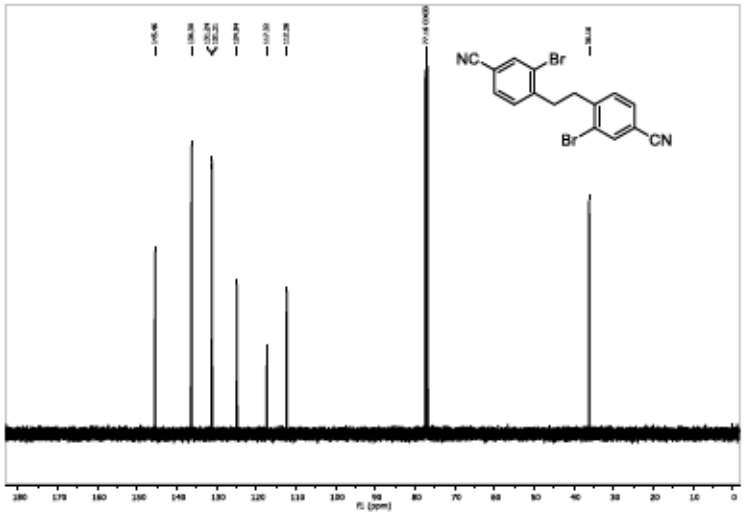

Dimethyl 4,4'-(ethane-1,2-diyl)bis(3-bromobenzoate) (5l)

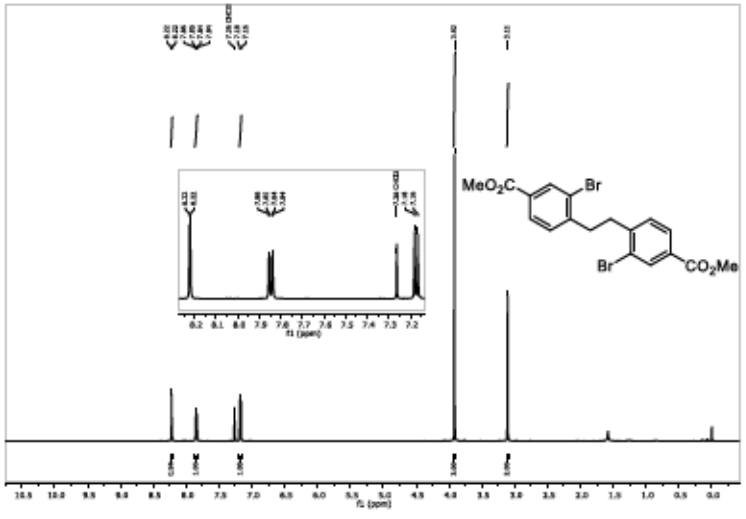

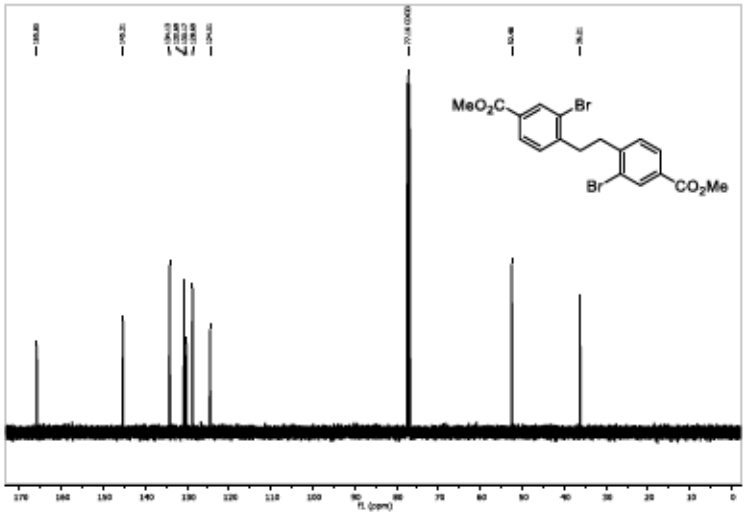

1-Bromo-2-(2-bromo-4-chlorophenethyl)-4-chlorobenzene (5m)

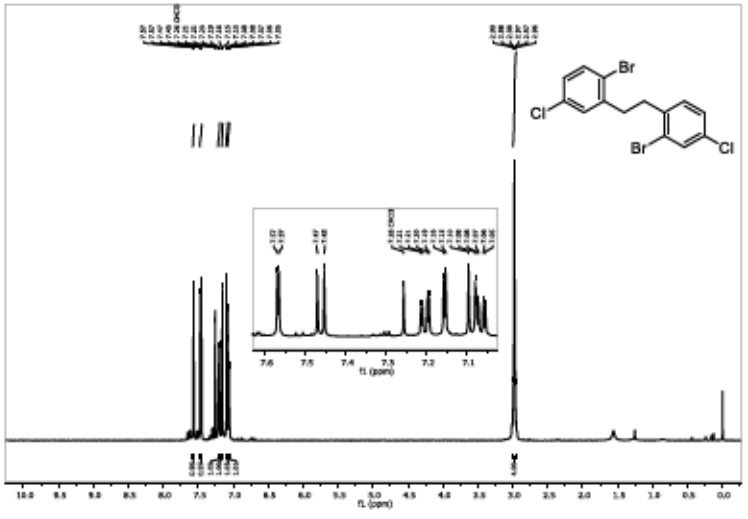

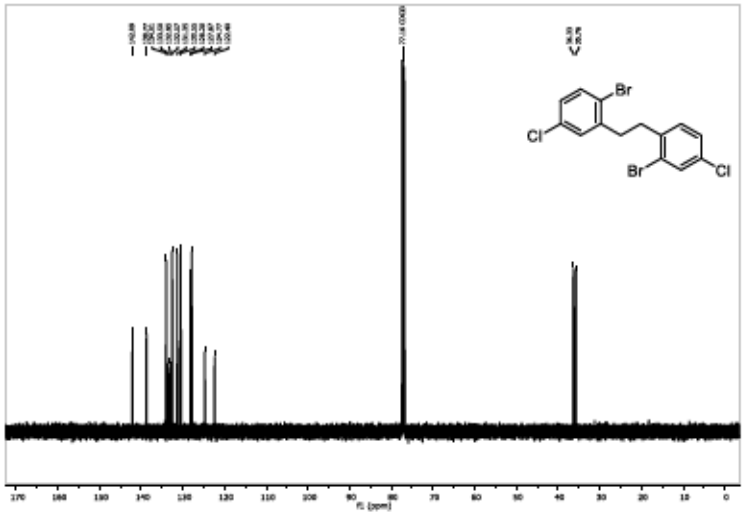

1,2-Bis(4,5-difluoro-2-iodophenyl)ethane (5n)

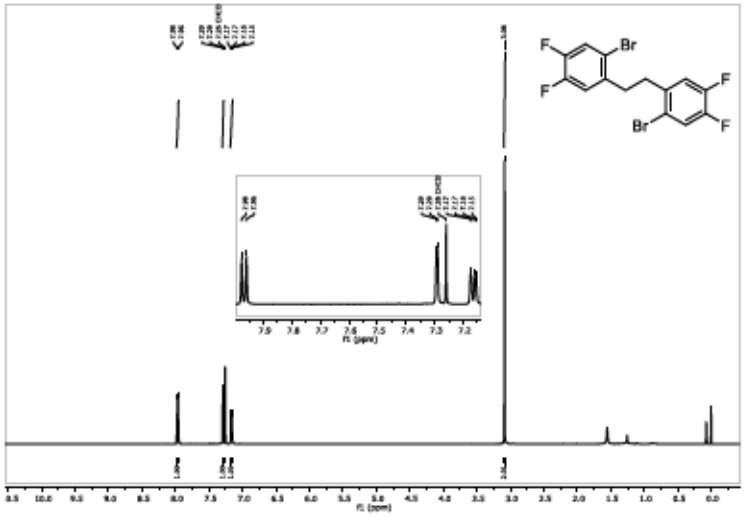

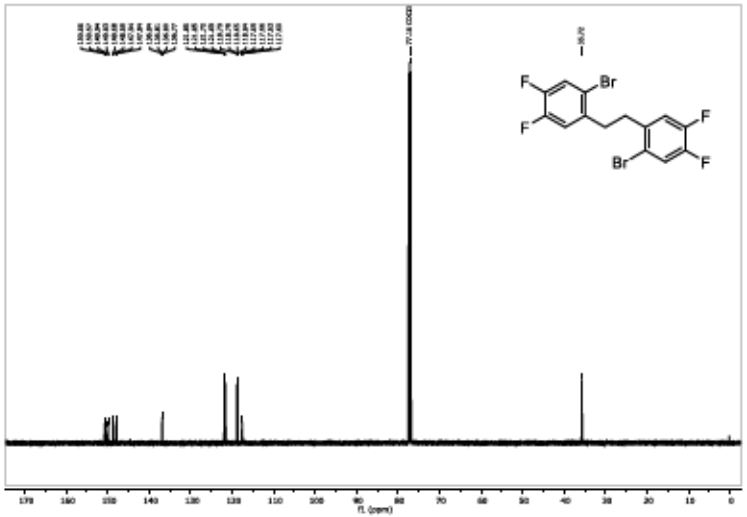

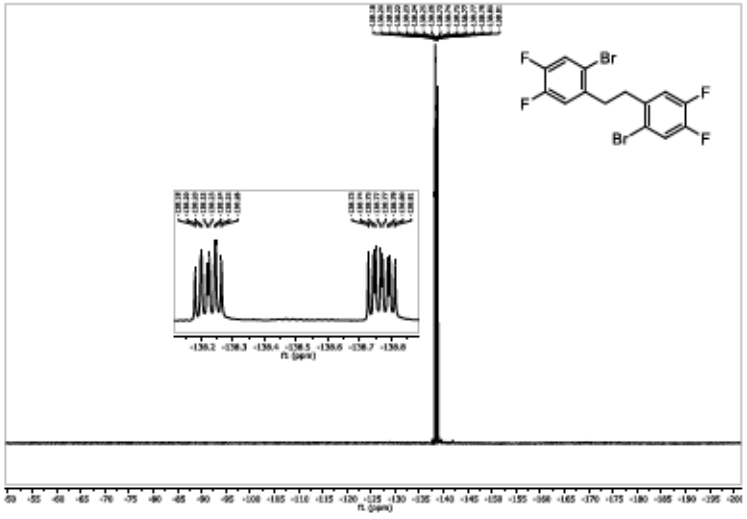

1,2-Bis(3-bromothiophen-2-yl)ethane (5o)

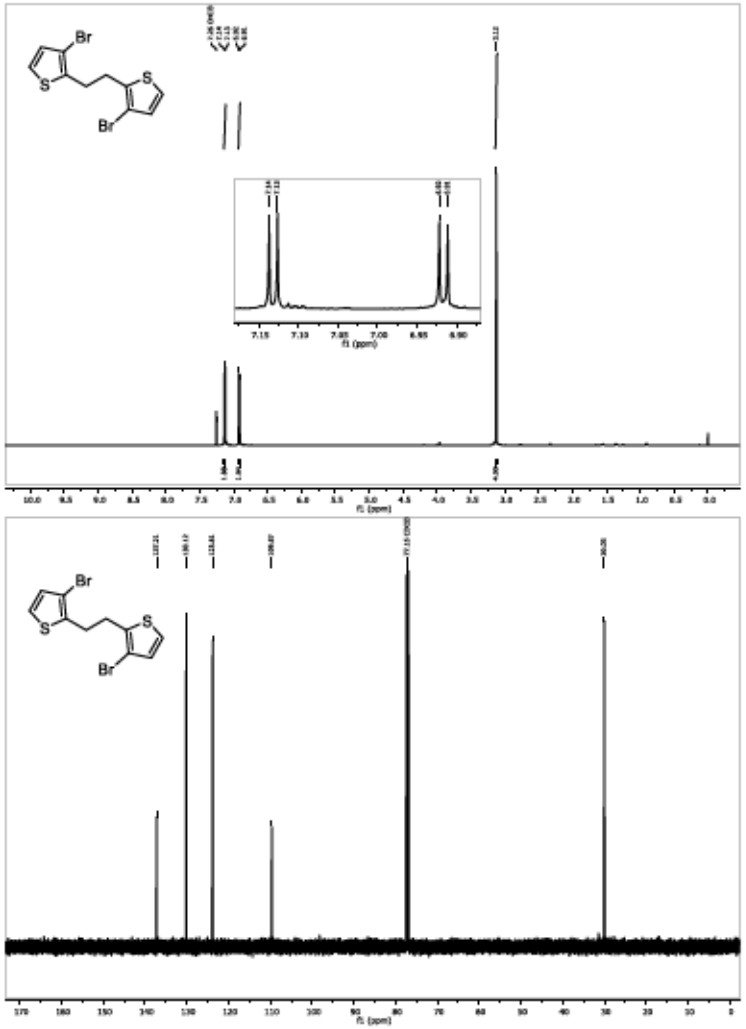

1,2-Bis(2-bromopyridin-3-yl)ethane (5p)

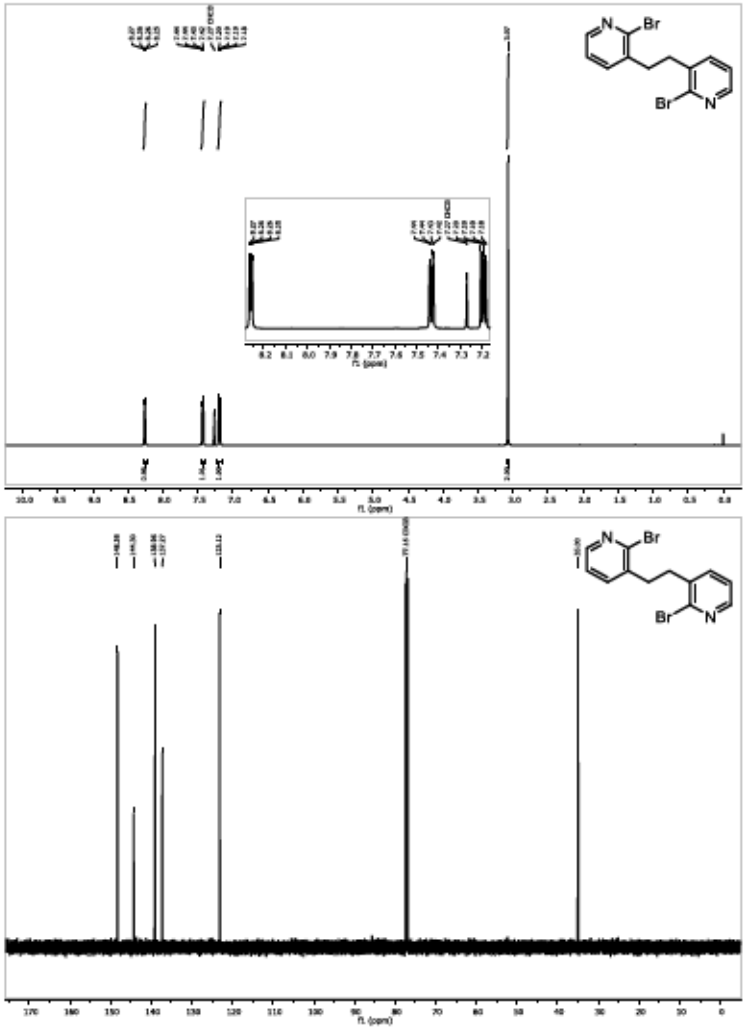

Di-*tert*-butyl 11,12-dihydrodibenzo[*c*,*g*][1,2]diazocine-5,6-dicarboxylate (6a)

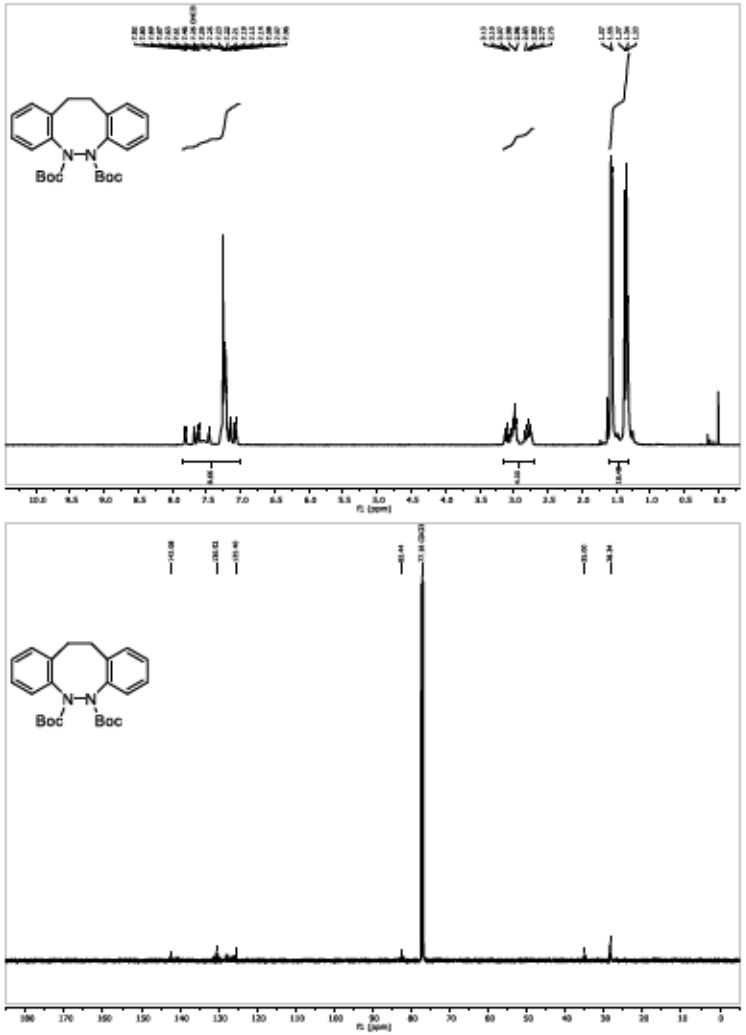

Di-*tert*-butyl 2,9-dichloro-11,12-dihydrodibenzo[*c*,*g*][1,2]diazocine-5,6-dicarboxylate (6b)

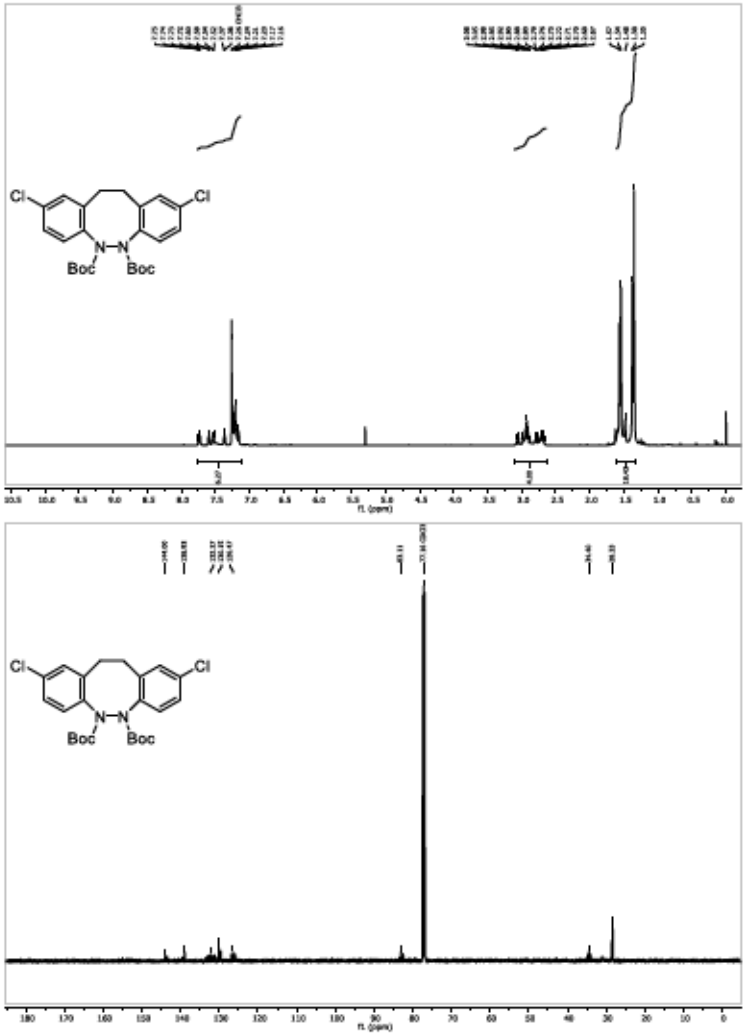

Di-*tert*-butyl 2,9-difluoro-11,12-dihydrodibenzo[*c*,*g*][1,2]diazocine-5,6-dicarboxylate (6c)

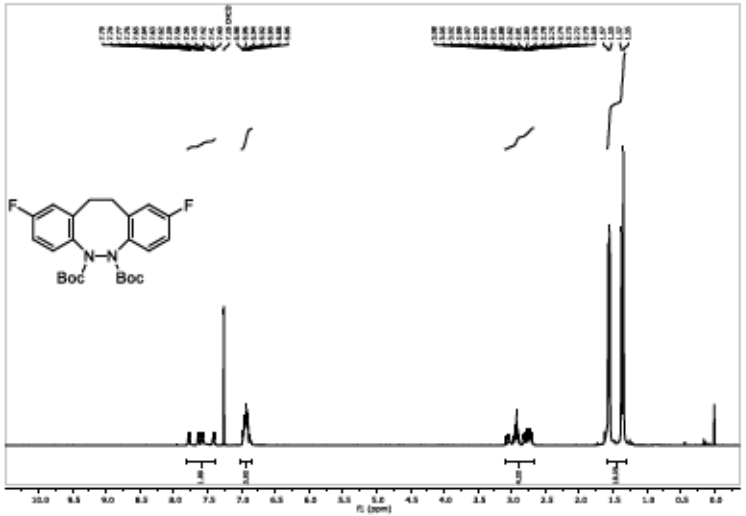

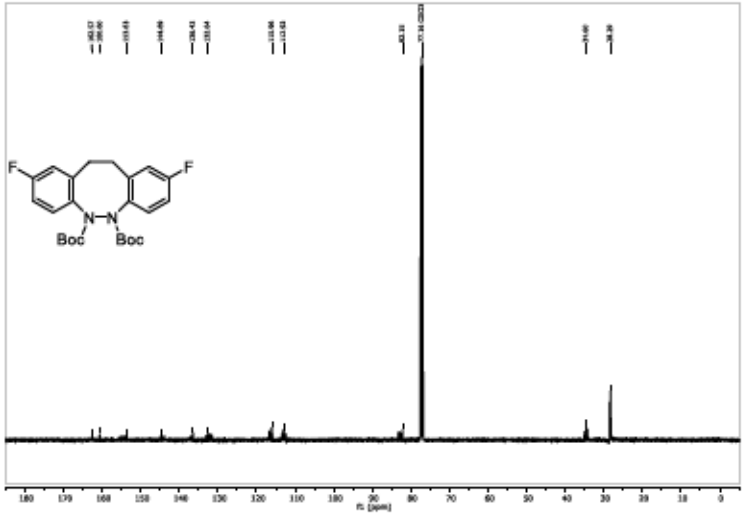

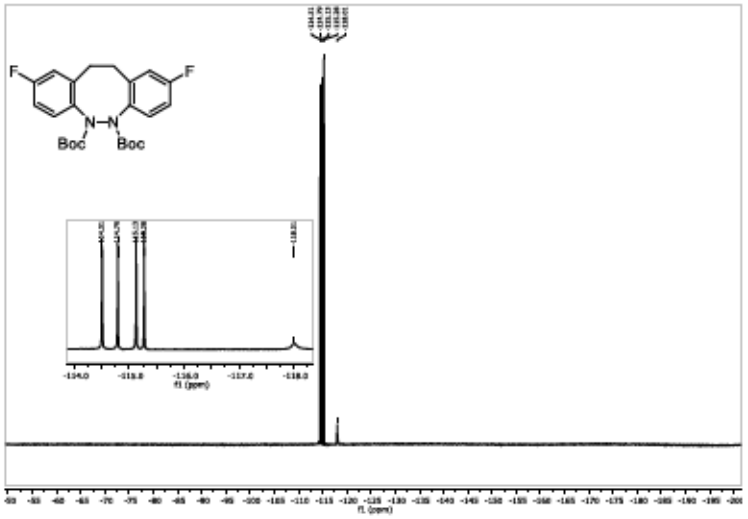

Di-*tert*-butyl 2,9-bis(trifluoromethyl)-11,12-dihydrodibenzo[*c*,*g*][1,2]diazocine-5,6-dicarboxylate (6d)

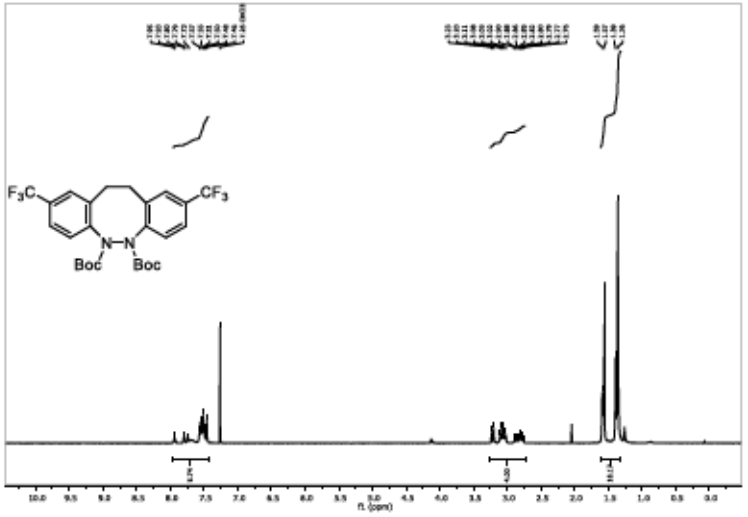

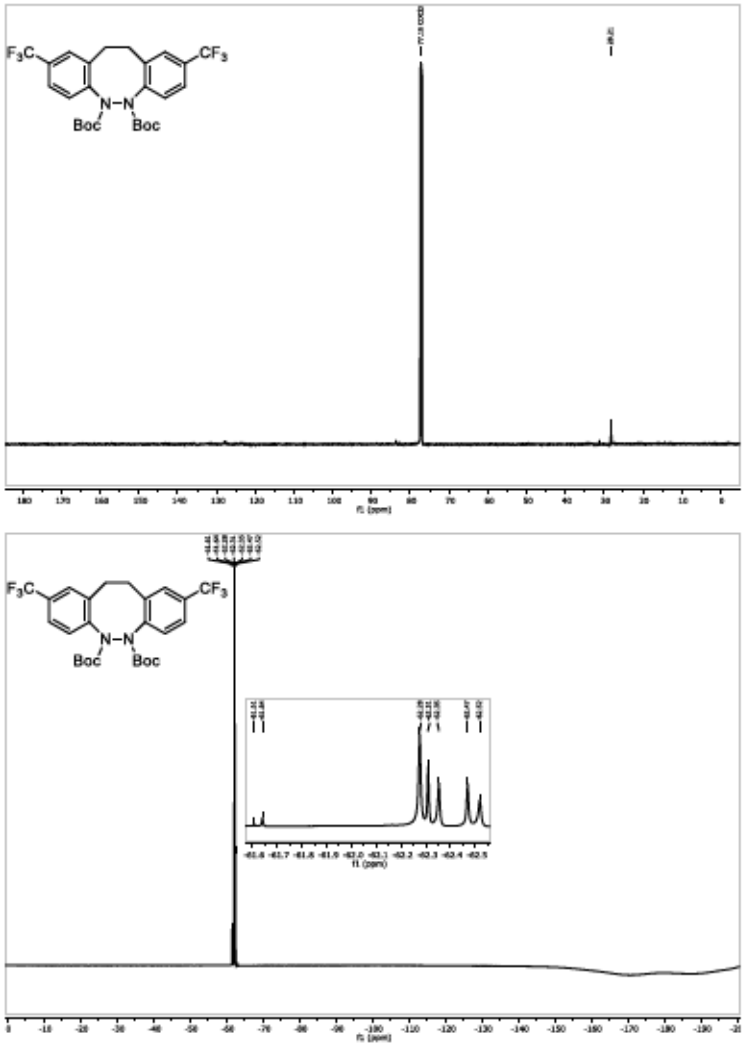

Di-*tert*-butyl 2,9-di-*tert*-butoxy-11,12-dihydrodibenzo[*c*,*g*][1,2]diazocine-5,6-dicarboxylate (6e)

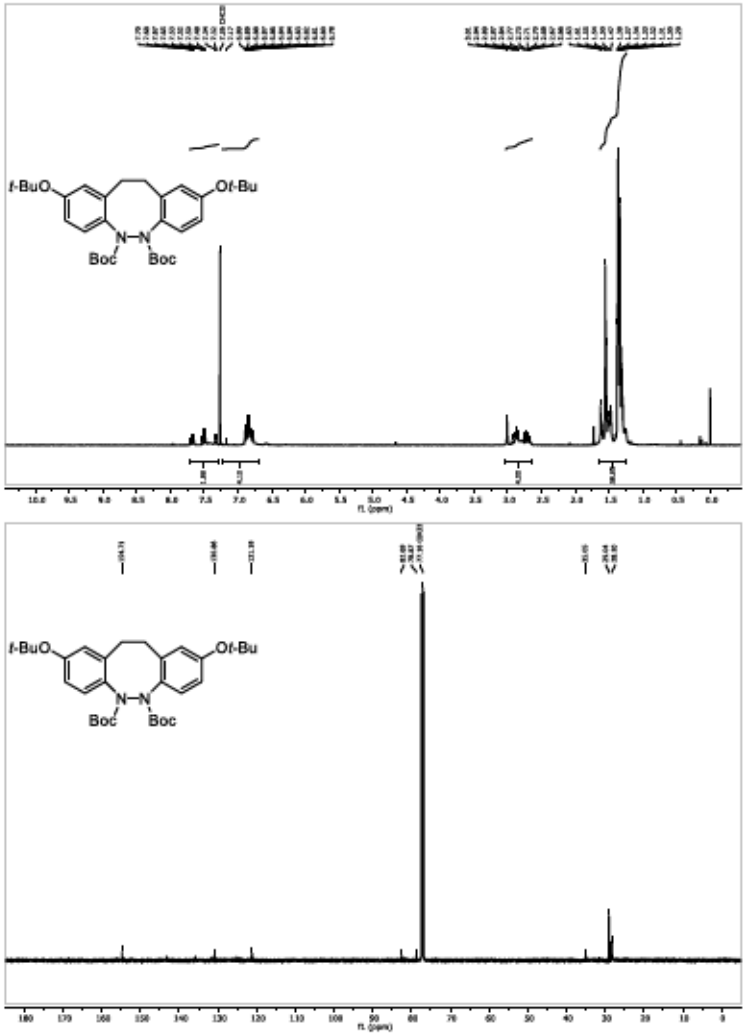

5,6-Di-*tert*-butyl 2,9-dimethyl 11,12-dihydrodibenzo[*c,g*][1,2]diazocine-2,5,6,9-tetracarboxylate (6f)

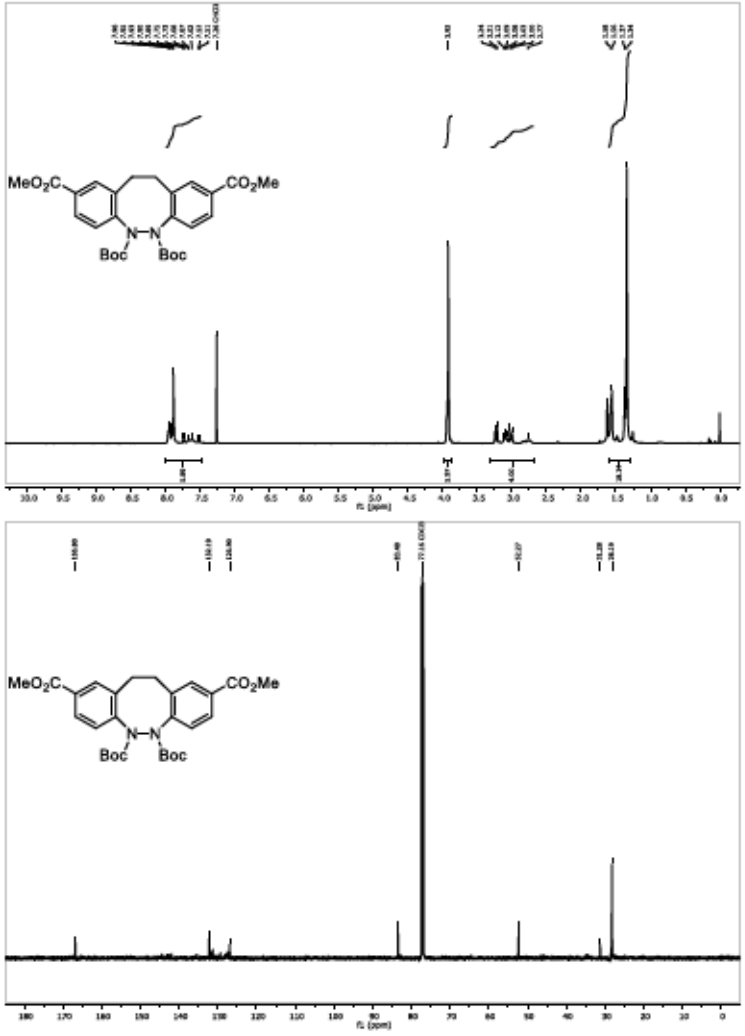

Di-*tert*-butyl 2,9-dimethoxy-11,12-dihydrodibenzo[*c,g*][1,2]diazocine-5,6-dicarboxylate (6g)

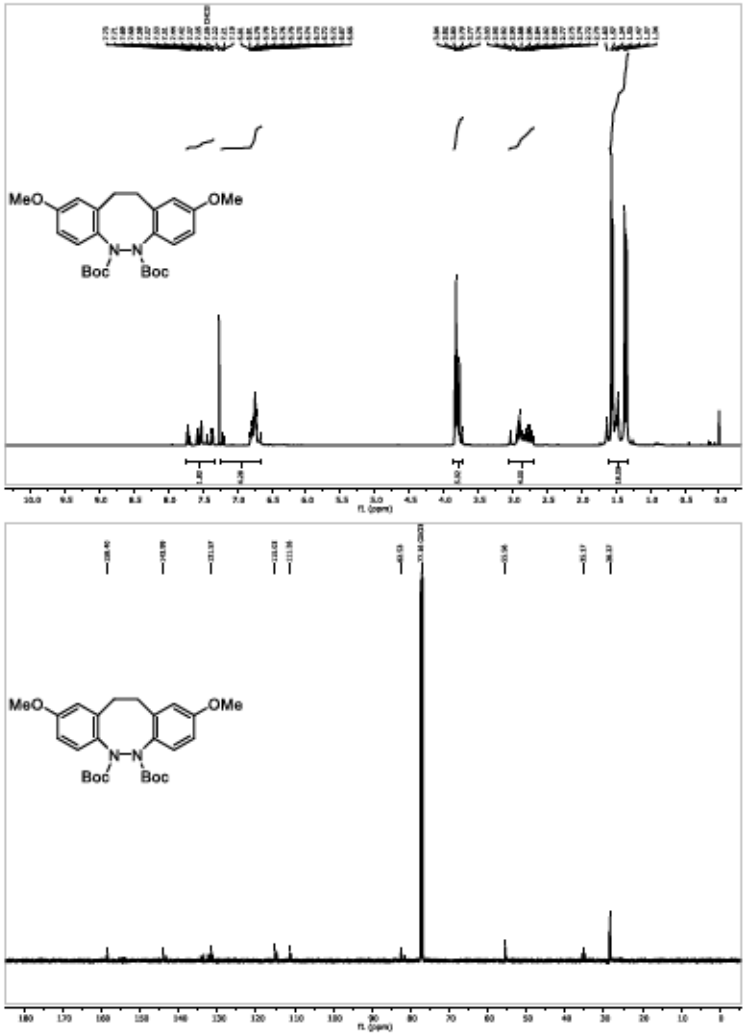

Di-tert-butyl 3,8-dichloro-11,12-dihydrodibenzo[c,g][1,2]diazocine-5,6-dicarboxylate (6h)

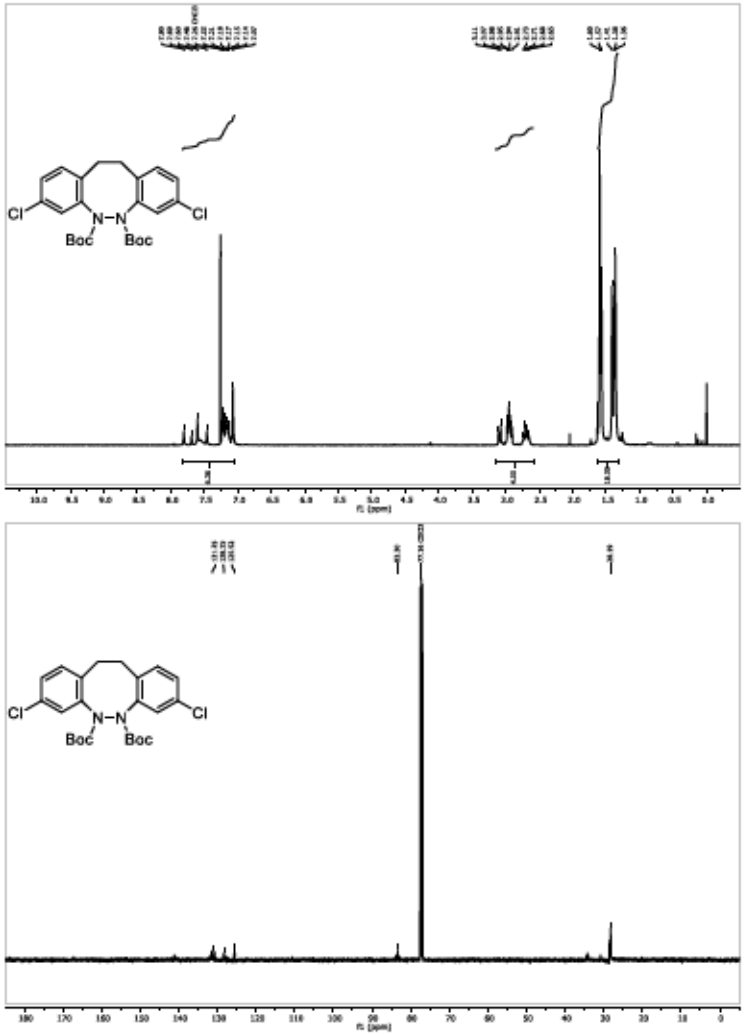

Di-tert-butyl 3,8-difluoro-11,12-dihydrodibenzo[c,g][1,2]diazocine-5,6-dicarboxylate (6l)

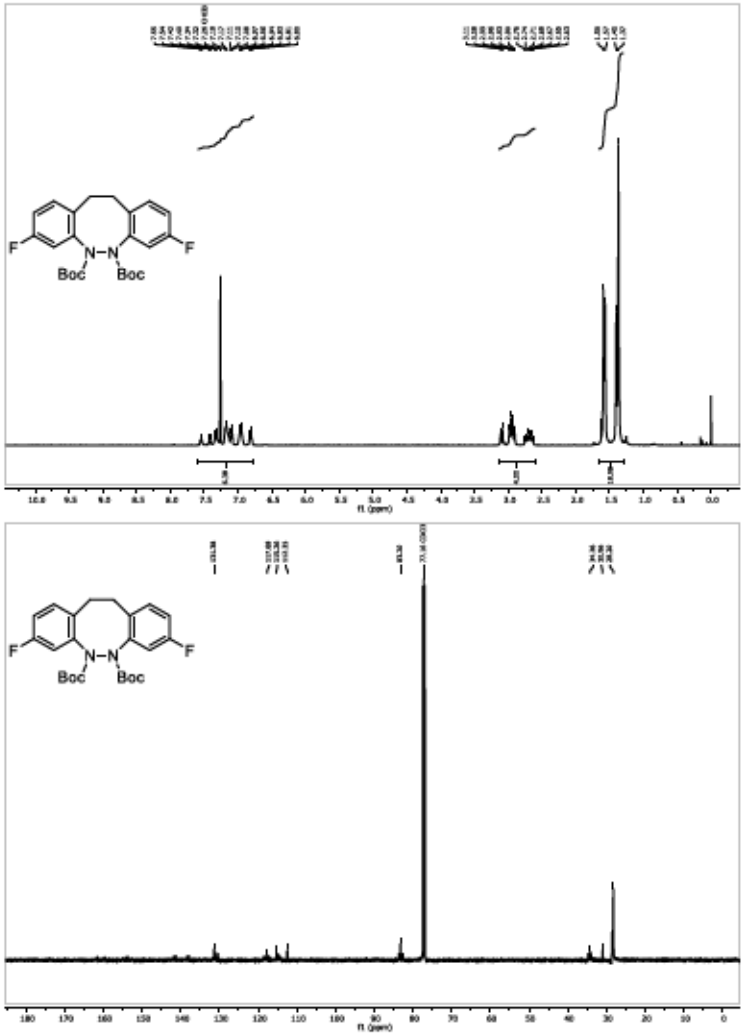

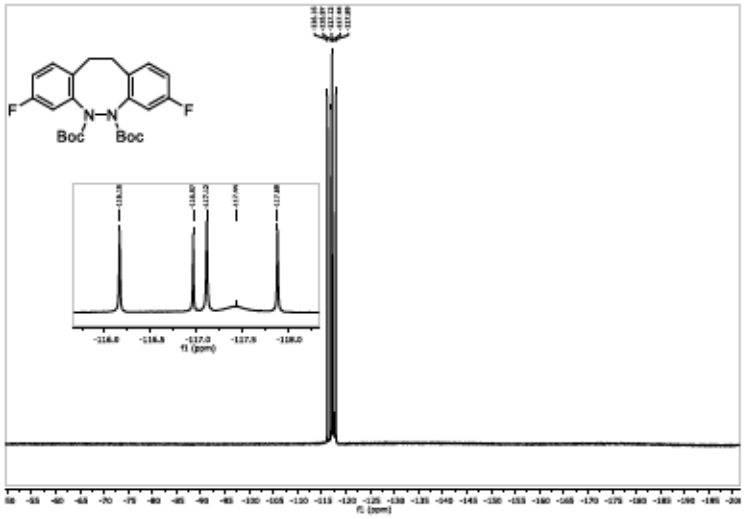

Di-*tert*-butyl 3,8-di-*tert*-butyl-11,12-dihydrodibenzo[*c*,*g*][1,2]diazocine-5,6-dicarboxylate (6j)

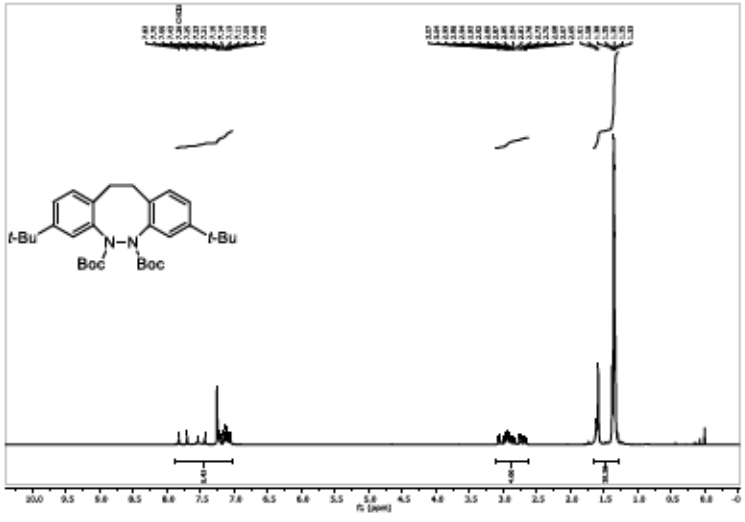

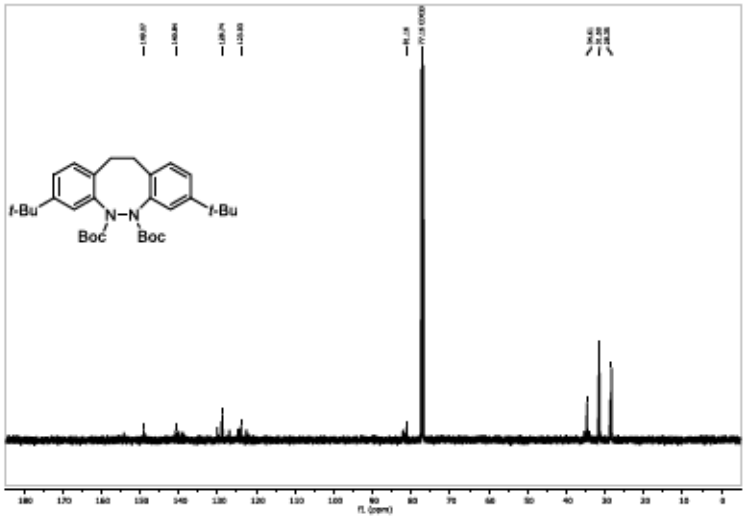

Di-*tert*-butyl 3,8-dicyano-11,12-dihydrodibenzo[*c*,*g*][1,2]diazocine-5,6-dicarboxylate (6k)

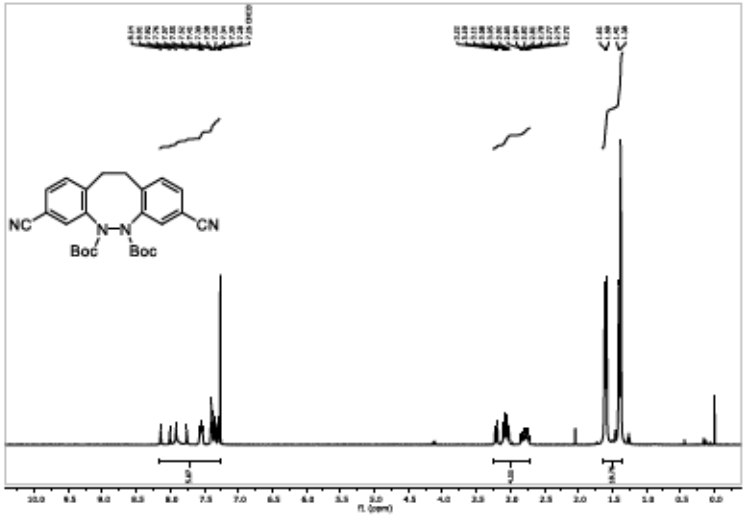

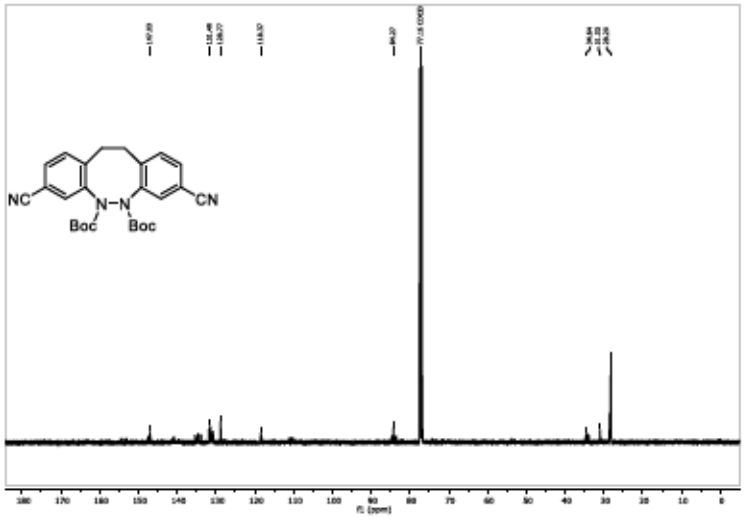

5,6-Di-*tert*-butyl 3,8-dimethyl 11,12-dihydrodibenzo[*c*,*g*][1,2]diazocine-3,5,6,8-tetracarboxylate (6l)

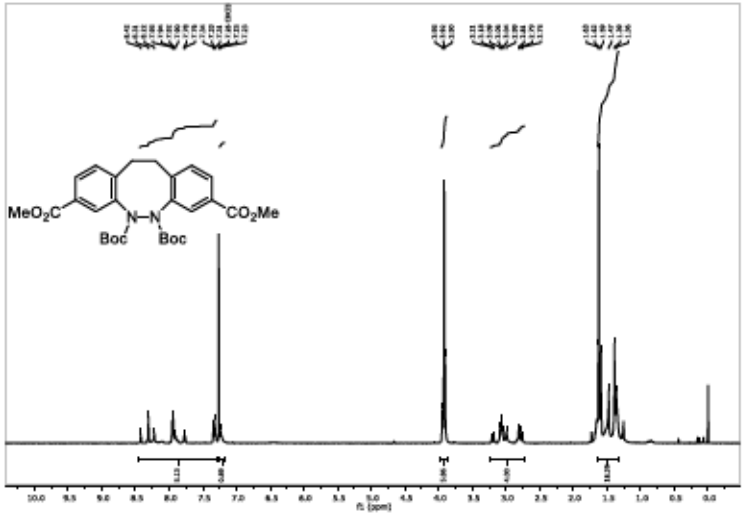

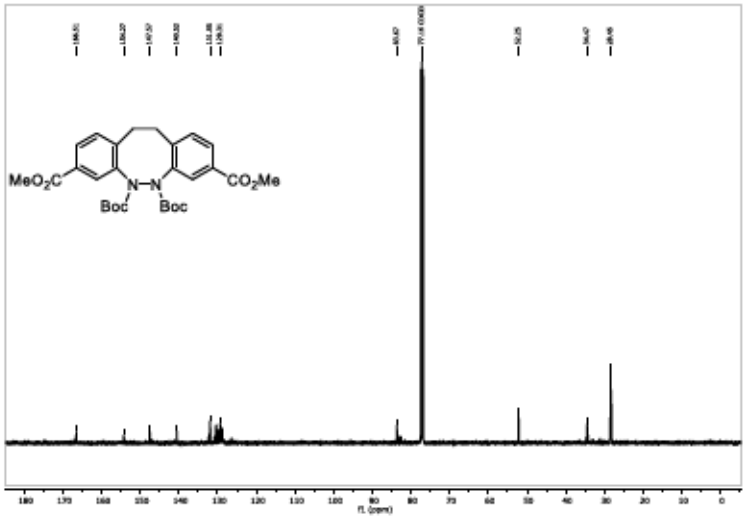

Di-*tert*-butyl 2,8-dichloro-11,12-dihydrodibenzo[*c*,*g*][1,2]diazocine-5,6-dicarboxylate (6m)

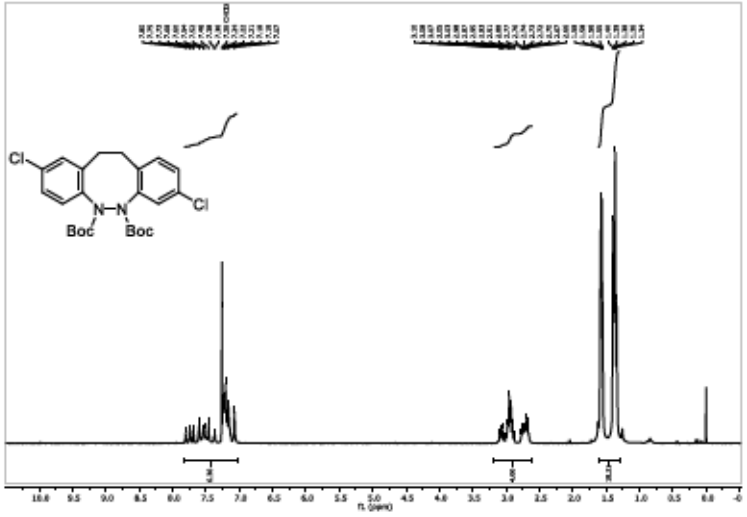

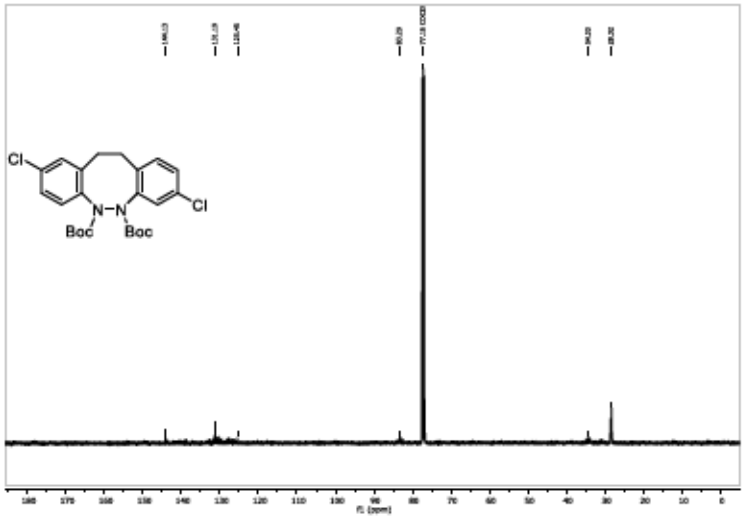

Di-*tert*-butyl 2,3,8,9-tetrafluoro-11,12-dihydrodibenzo[*c*,*g*][1,2]diazocine-5,6-dicarboxylate (6n)

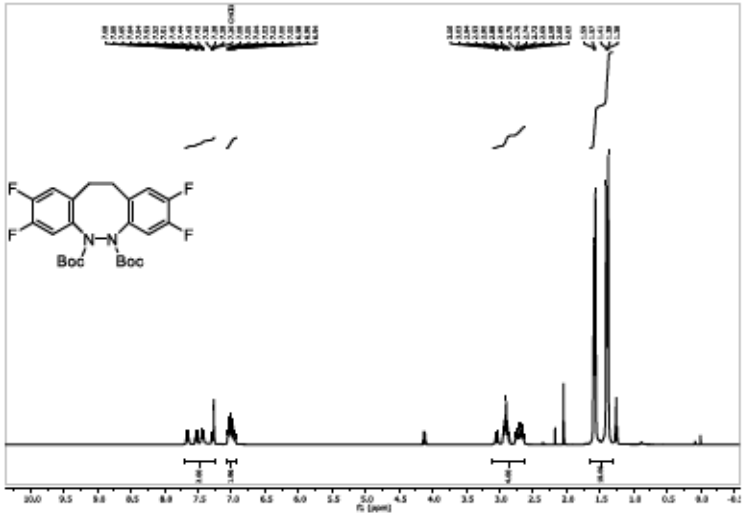

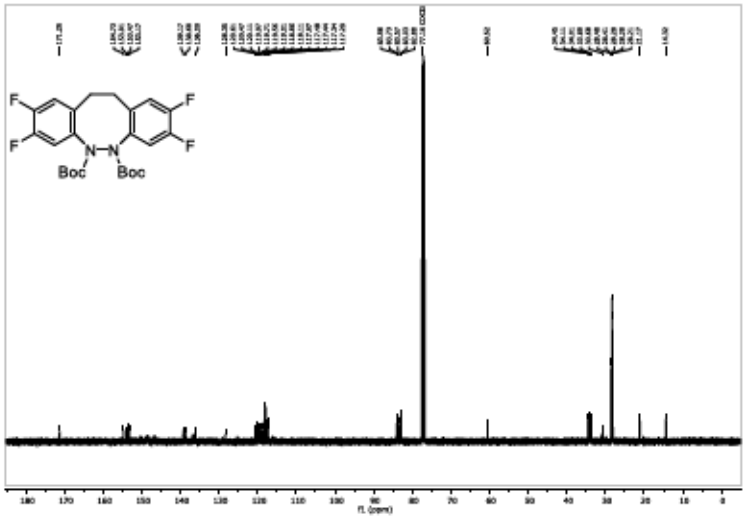

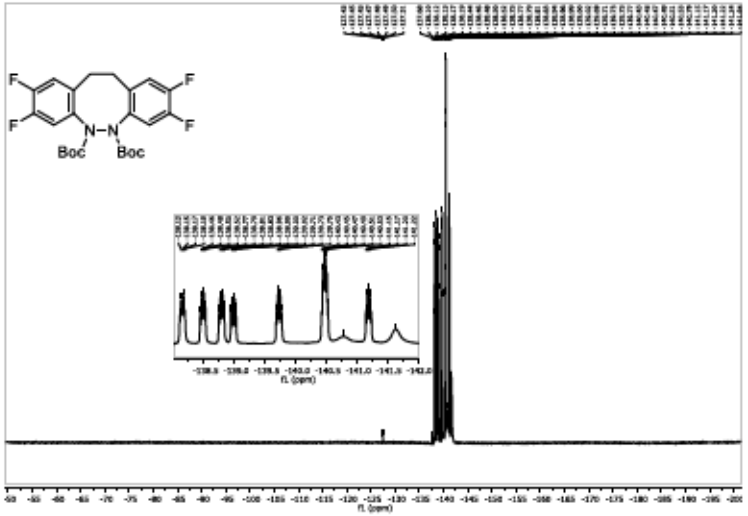

Di-*tert*-butyl 9,10-dihydrodithieno[3,2-*c*:2',3'-*g*][1,2]diazocine-4,5-dicarboxylate (6o)

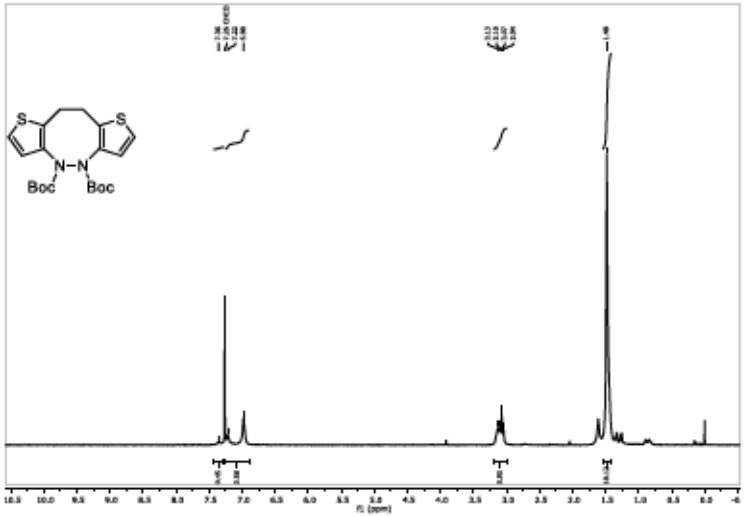

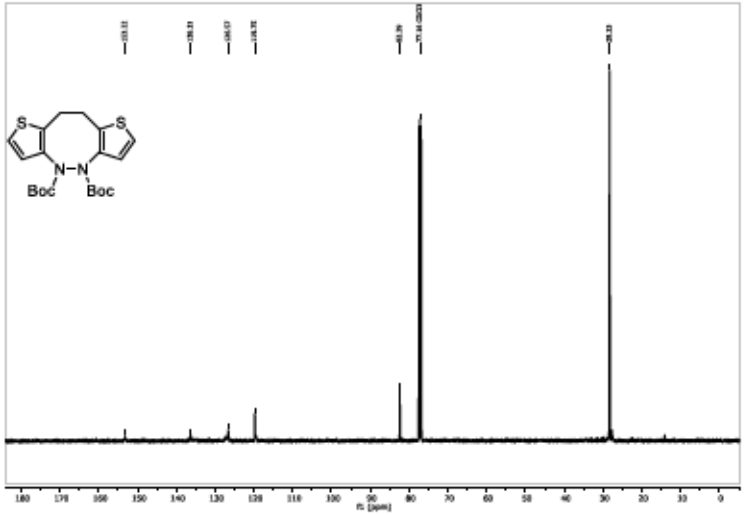

Di-*tert*-butyl 5,6-dihydrodipyrido[2,3-*c*:3',2'-*g*][1,2]diazocine-11,12-dicarboxylate (6p)

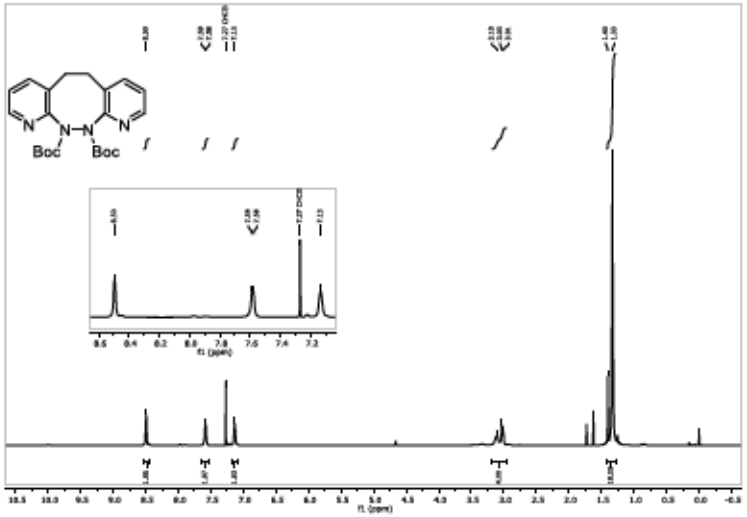

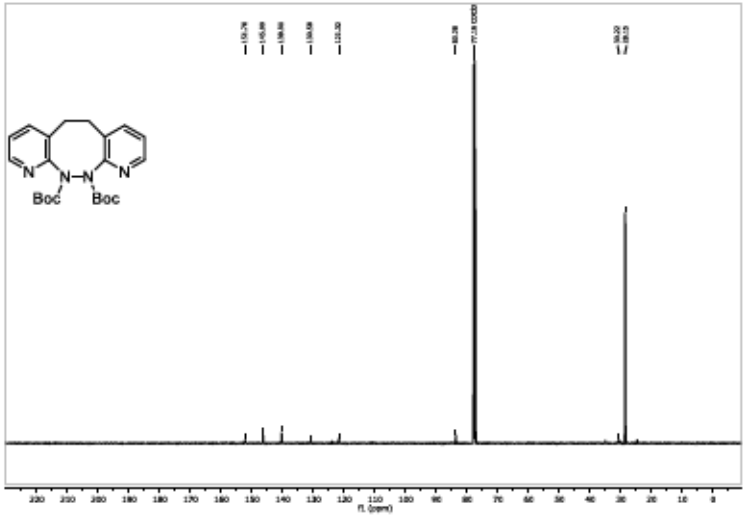

(Z)-11,12-Dihydrodibenzo[*c*,*g*][1,2]diazocine (1a)

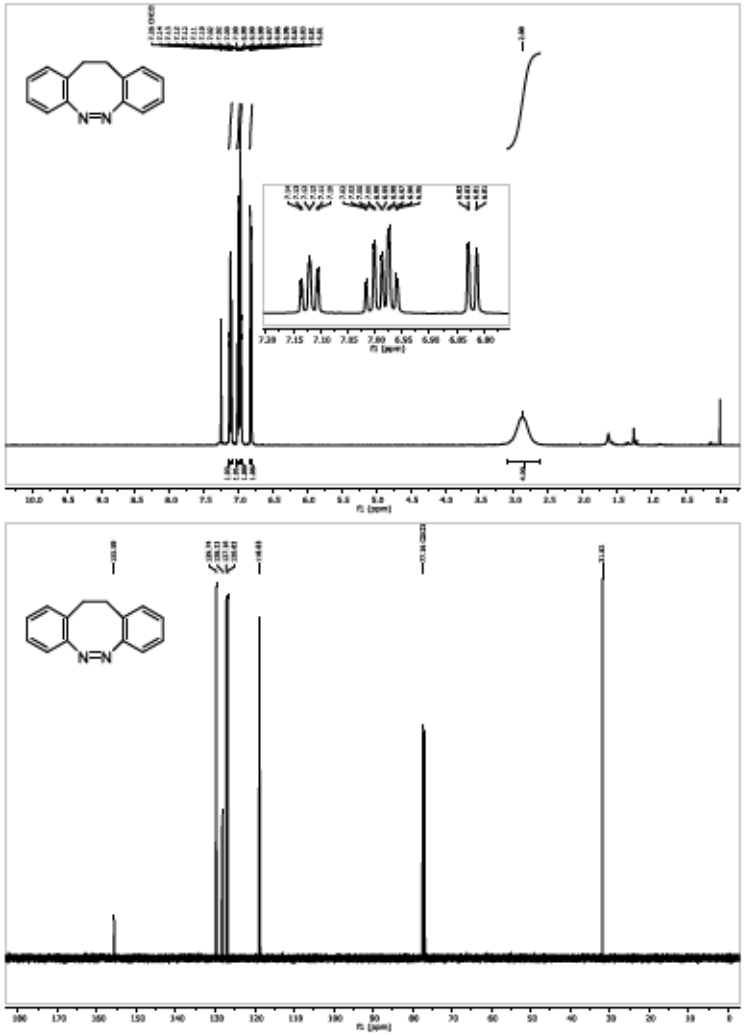

(Z)-2,9-Dichloro-11,12-dihydrodibenzo[*c*,*g*][1,2]diazocine (1b)

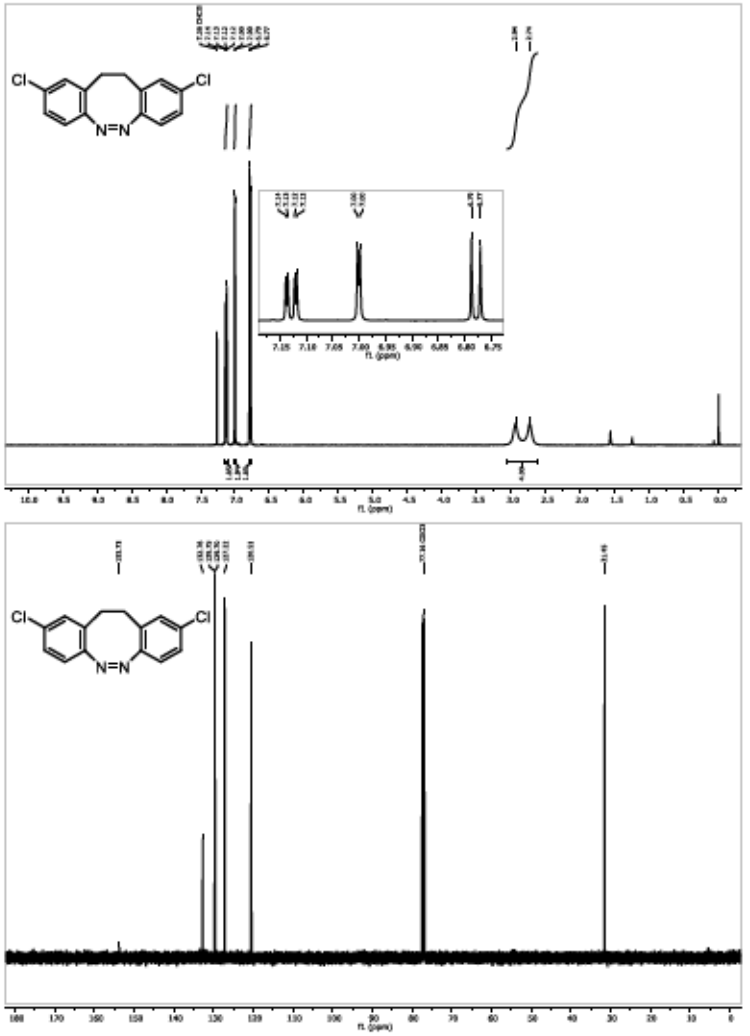

(Z)-2,9-Difluoro-11,12-dihydrodibenzo[*c*,*g*][1,2]diazocine (1c)

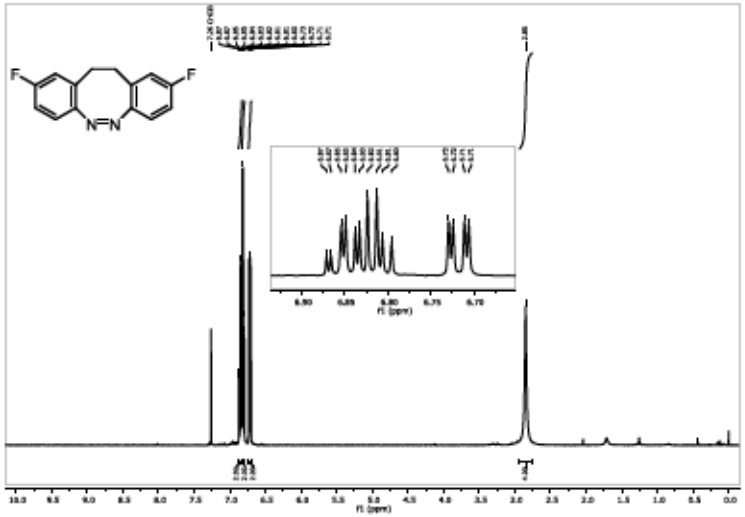

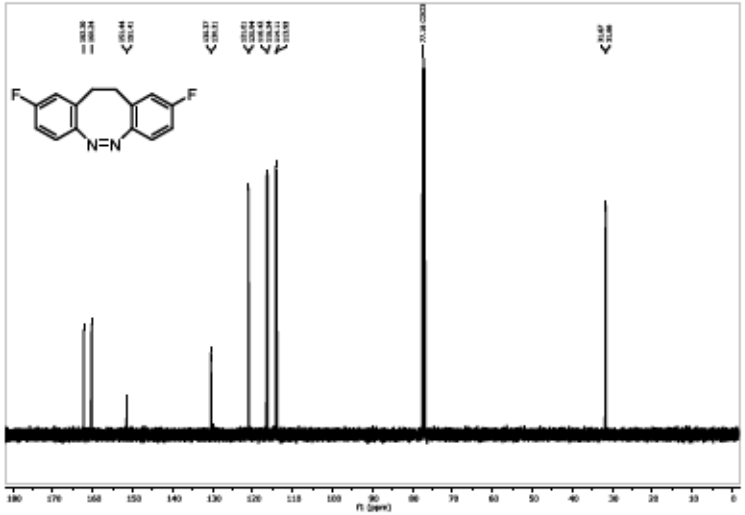

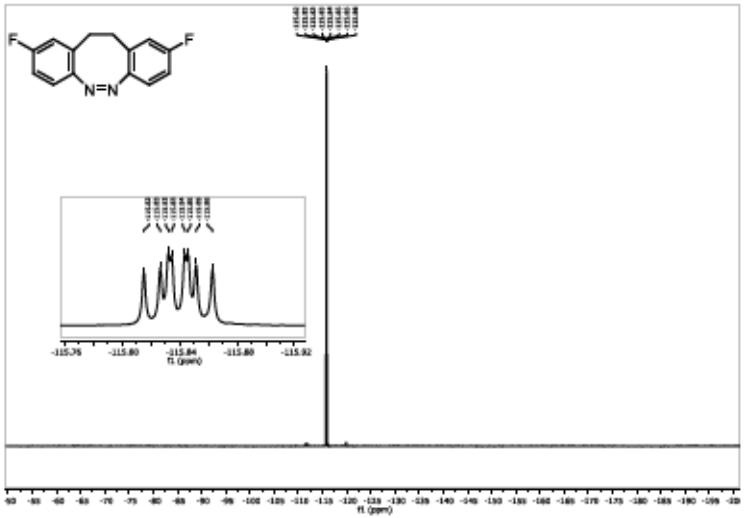

(Z)-2,9-Bis(trifluoromethyl)-11,12-dihydrodibenzo[*c*,*g*][1,2]diazocine (1d)

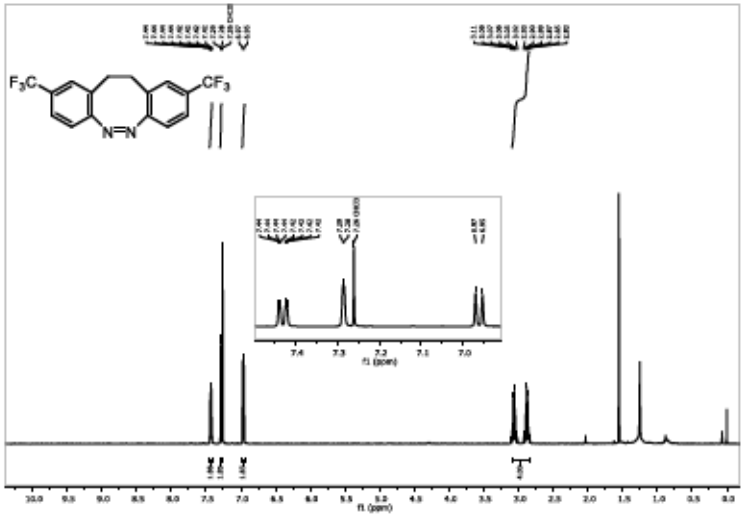

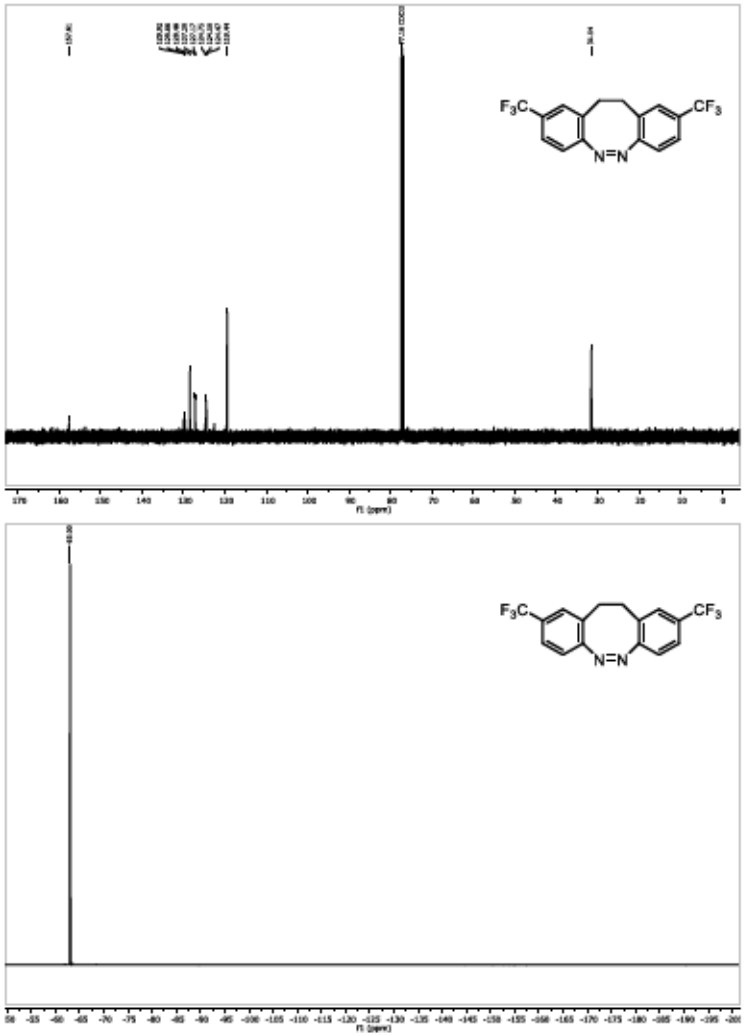

(Z)-11,12-Dihydrodibenzo[*c*,*g*][1,2]diazocine-2,9-diol (1e)

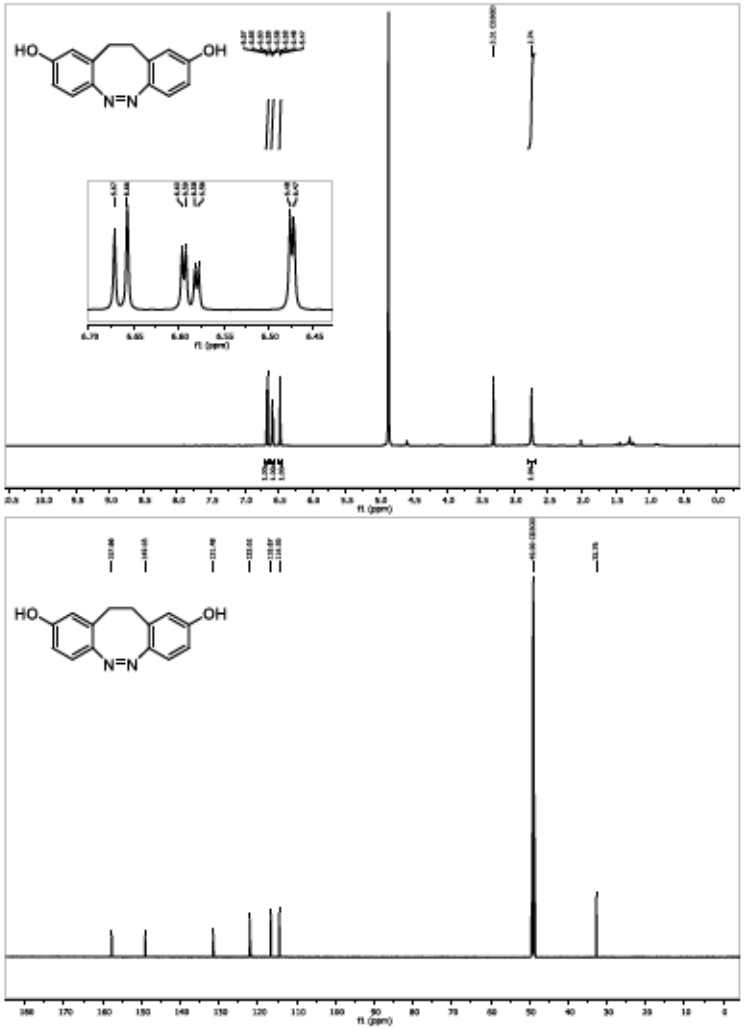

Dimethyl (Z)-11,12-dihydrodibenzo[c,g][1,2]diazocine-2,9-dicarboxylate (1f)

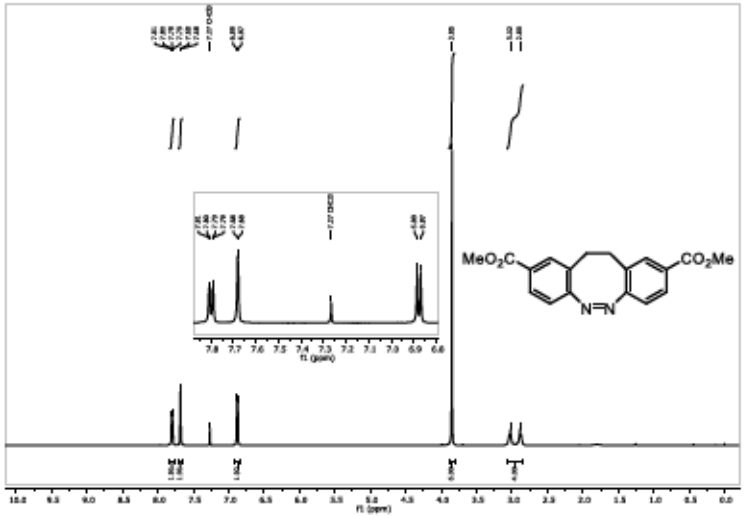

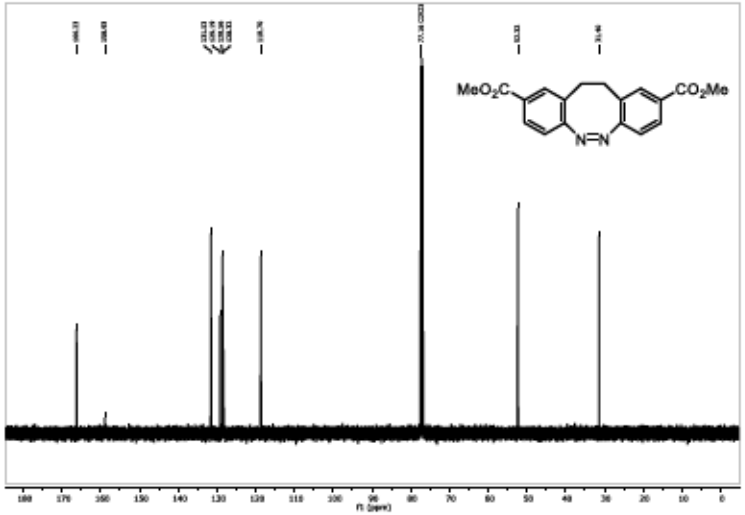

(Z)-2,9-Dimethoxy-11,12-dihydrodibenzo[c,g][1,2]diazocine (1g)

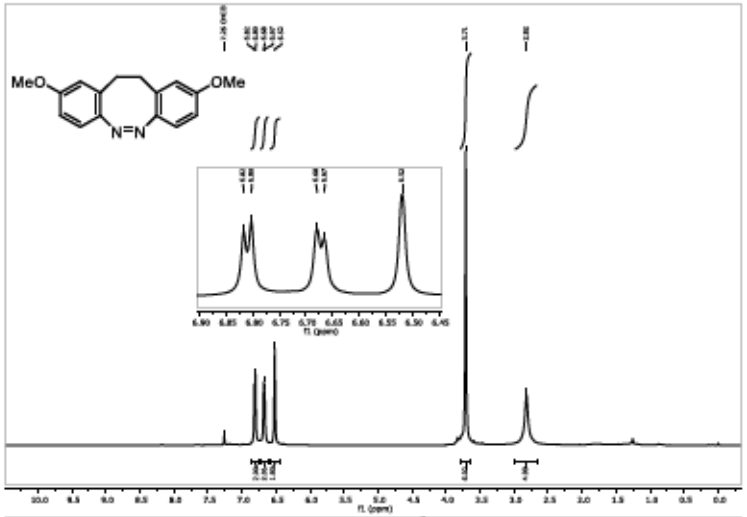

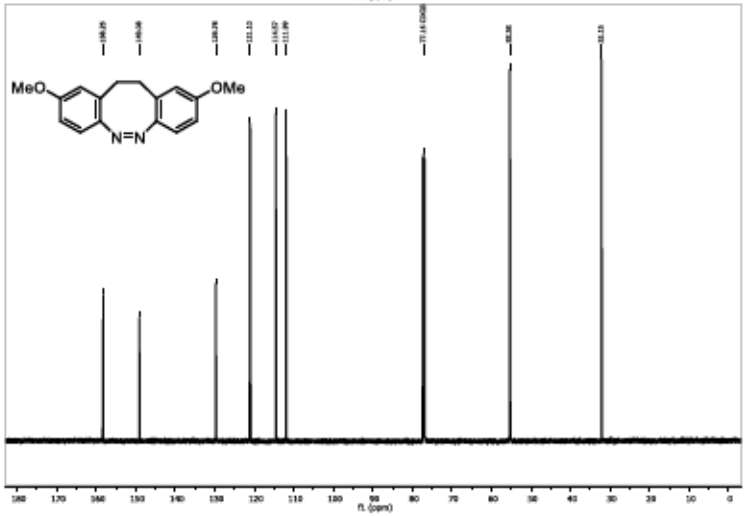

(Z)-3,8-Dichloro-11,12-dihydrodibenzo[*c*,*g*][1,2]diazocine (1h)

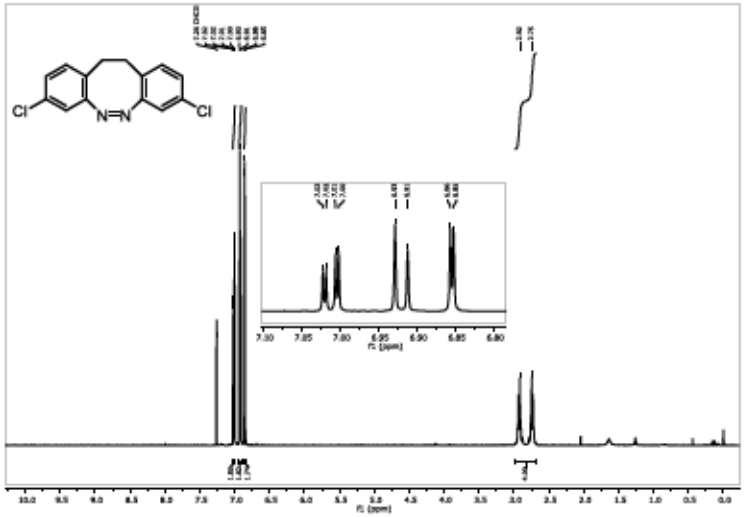

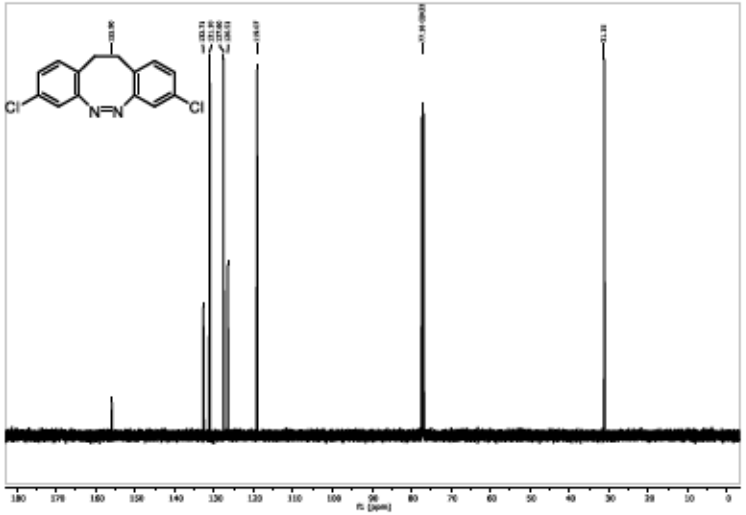

(Z)-3,8-Difluoro-11,12-dihydrodibenzo[*c*,*g*][1,2]diazocine (1i)

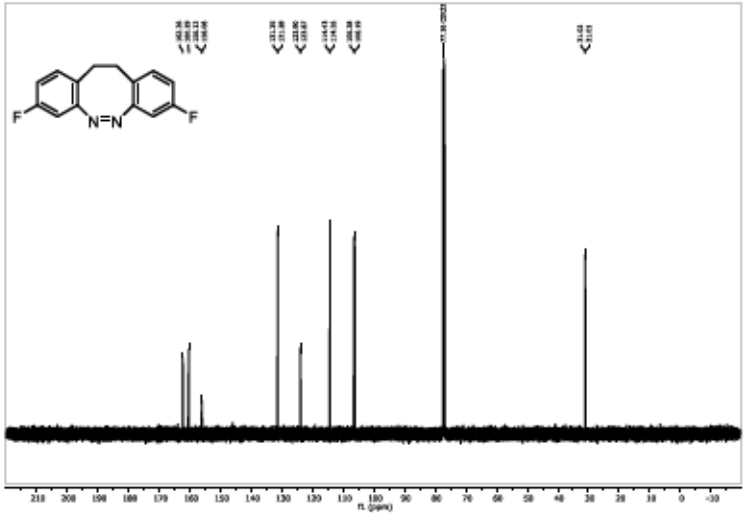

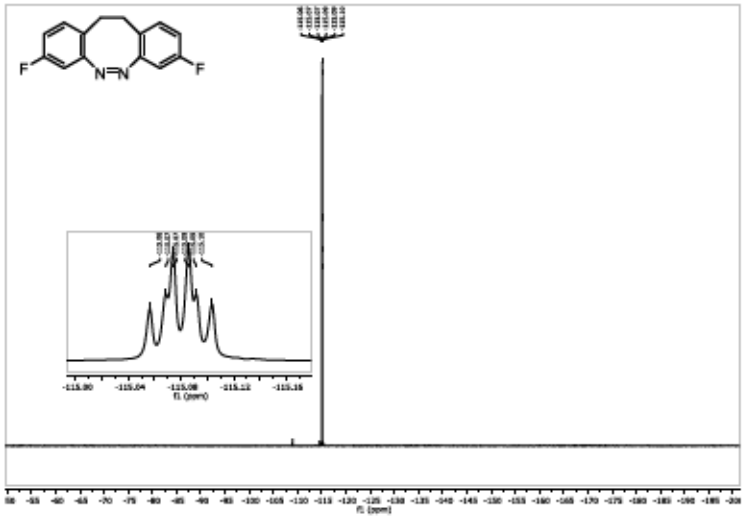

(*Z*)-3,8-Di-*tert*-butyl-11,12-dihydrodibenzo[*c*,*g*][1,2]diazocine (1j)

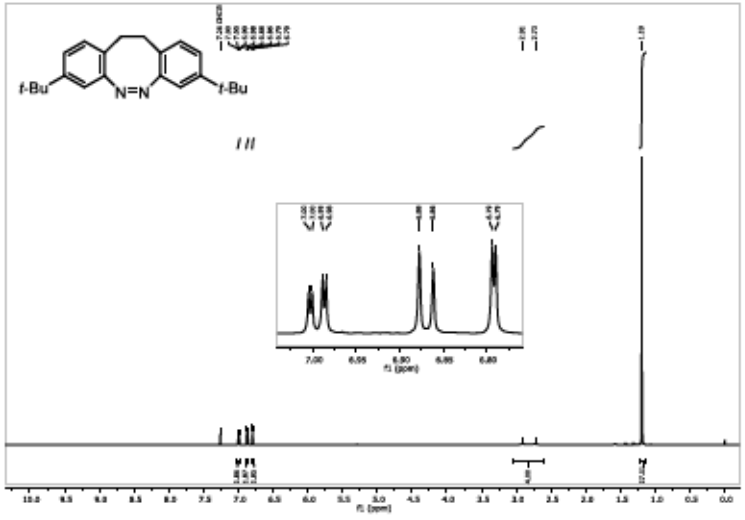

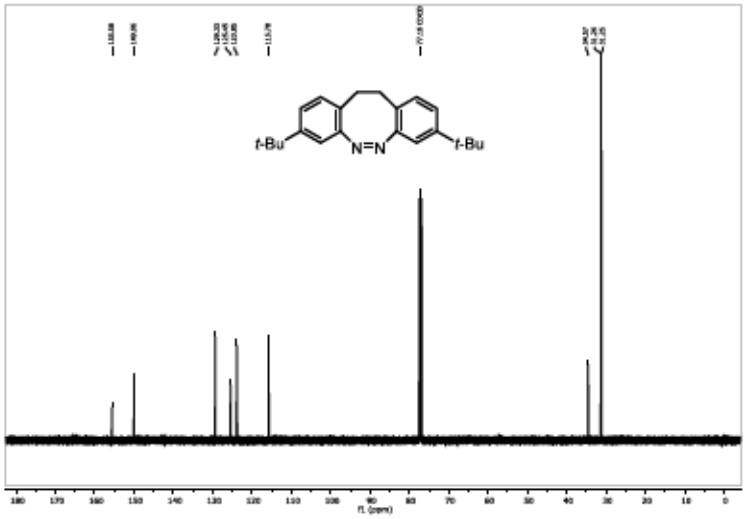

(*Z*)-11,12-Dihydrodibenzo[*c*,*g*][1,2]diazocine-3,8-dicarbonitrile (1k)

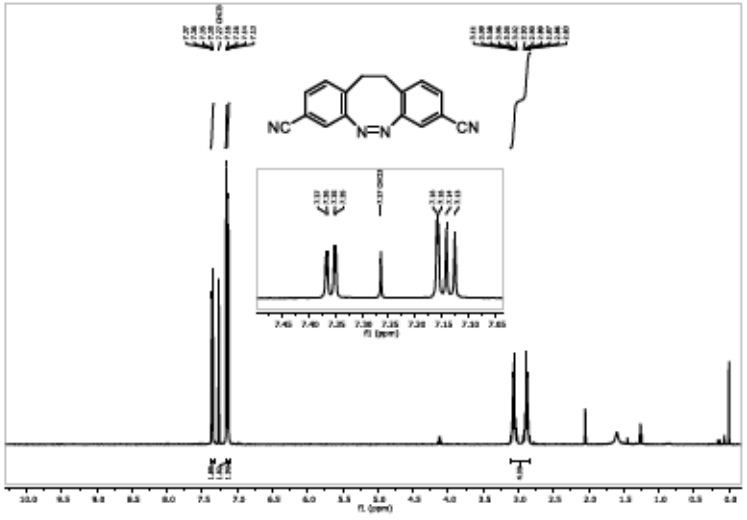

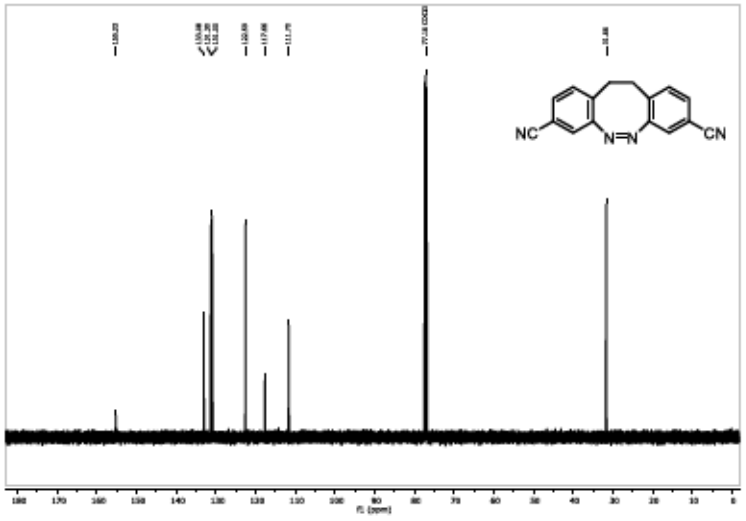

Dimethyl (Z)-11,12-dihydrodibenzo[*c*,*g*][1,2]diazocine-3,8-dicarboxylate (1l)

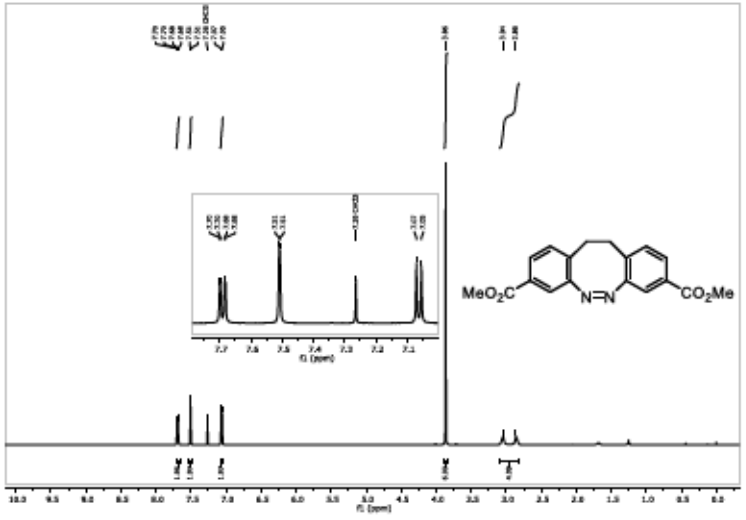

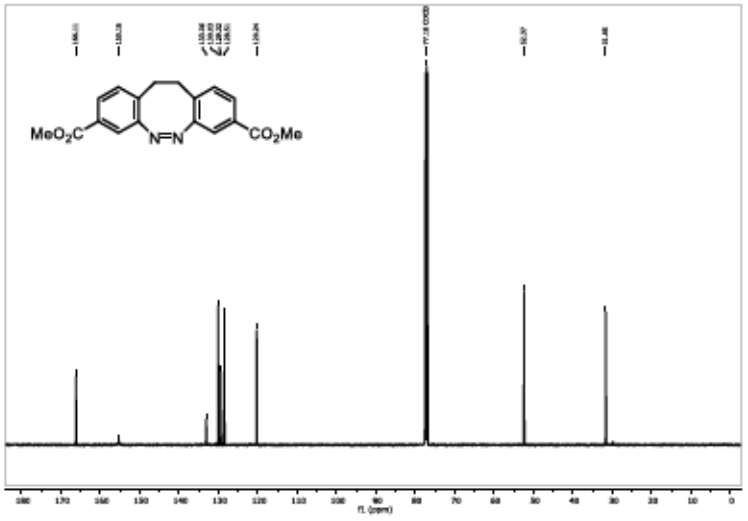

(Z)-2,8-Dichloro-11,12-dihydrodibenzo[*c*,*g*][1,2]diazocine (1m)

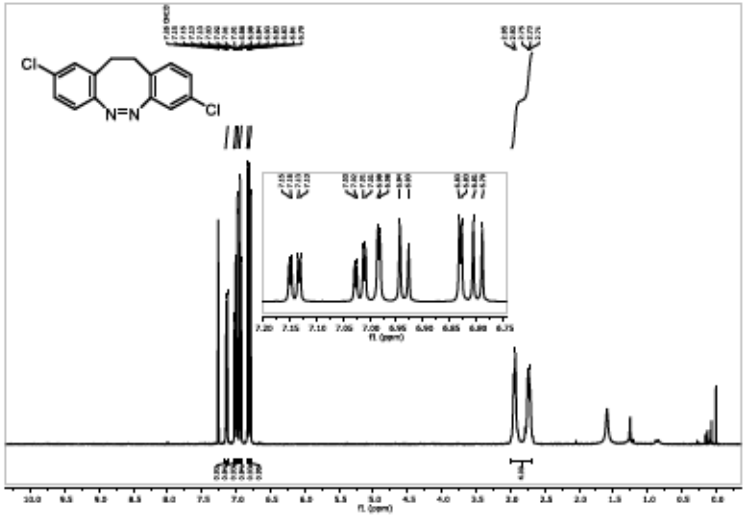

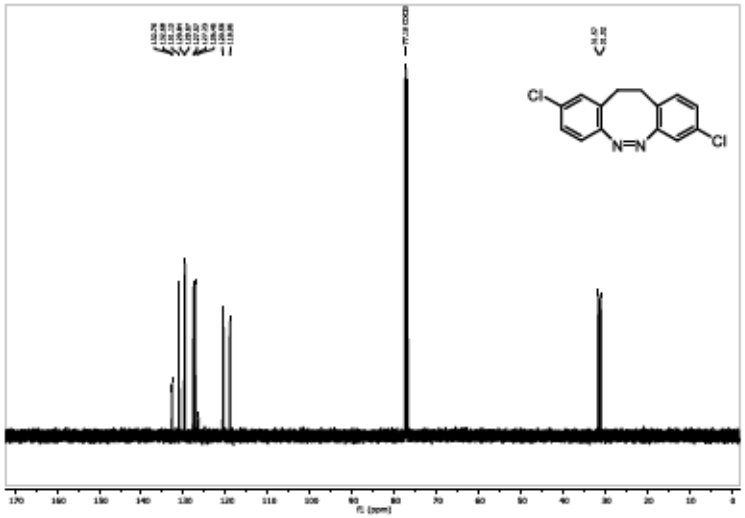

(Z)-2,3,8,9-Tetrafluoro-11,12-dihydrodibenzo[c,g][1,2]diazocine (1n)

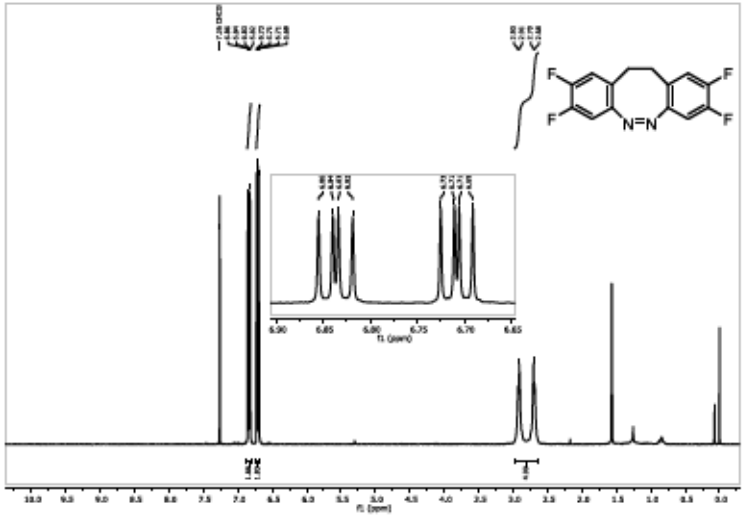

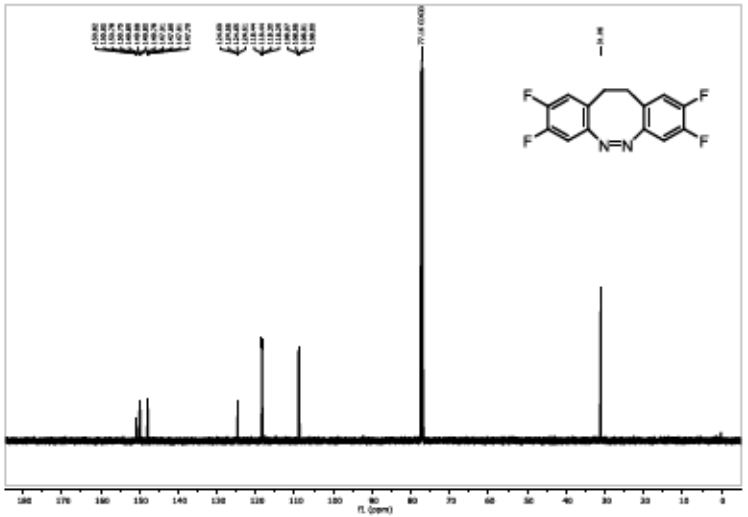

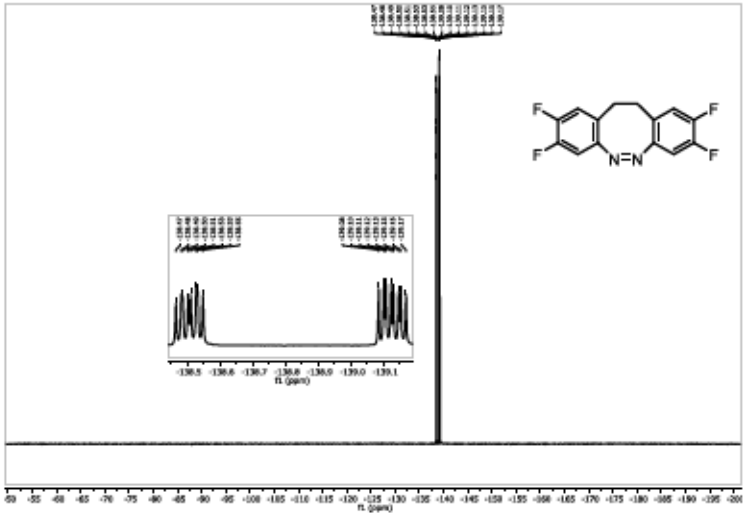

(Z)-9,10-Dihydrodithieno[3,2-c:2',3'-g][1,2]diazocine (1o)

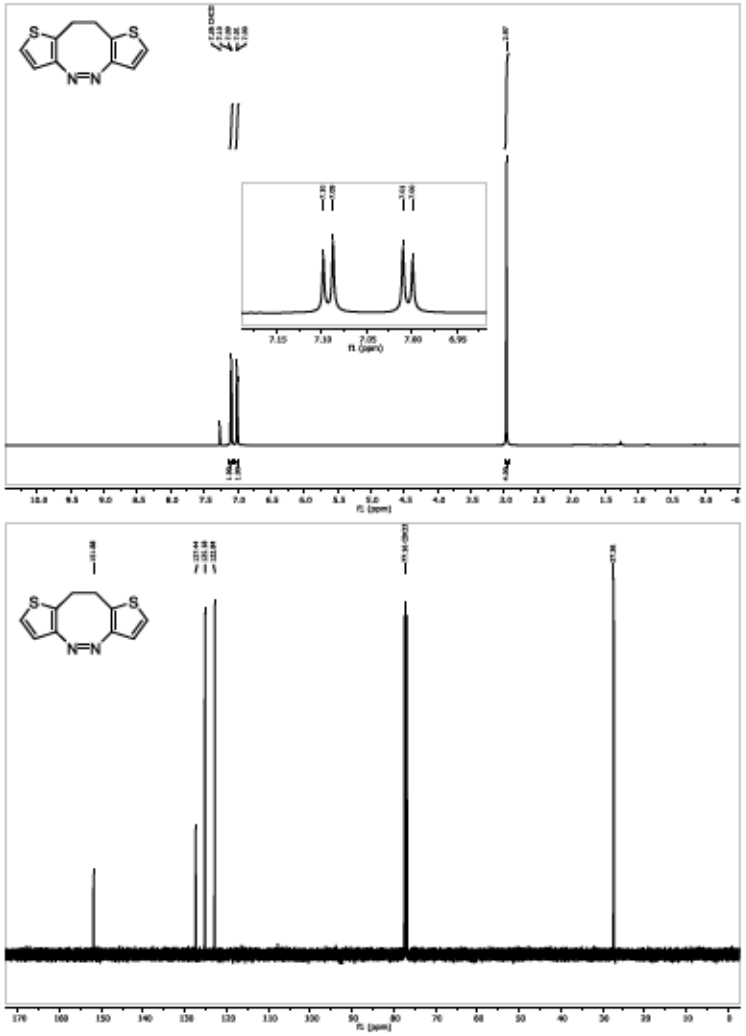

(Z)-5,6-Dihydrodipyrido[2,3-c:3',2'-g][1,2]diazocine (1p)

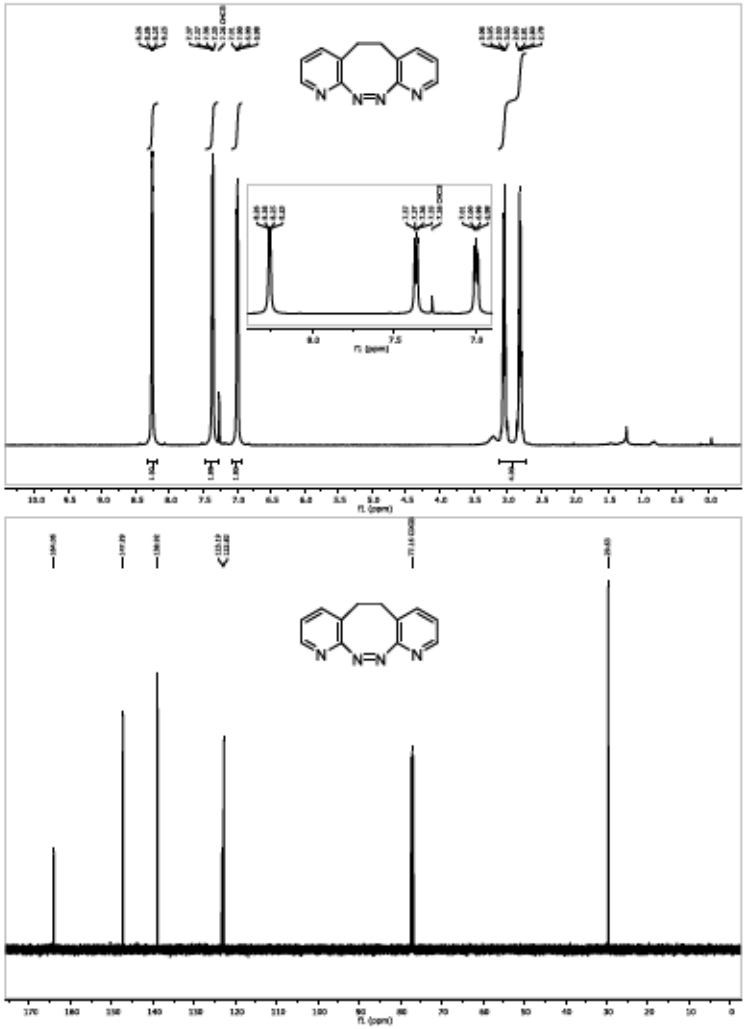

(Z)-11,12-Dihydrodibenzo[*c*,*g*][1,2]diazocine-2,9-diamine (1q)

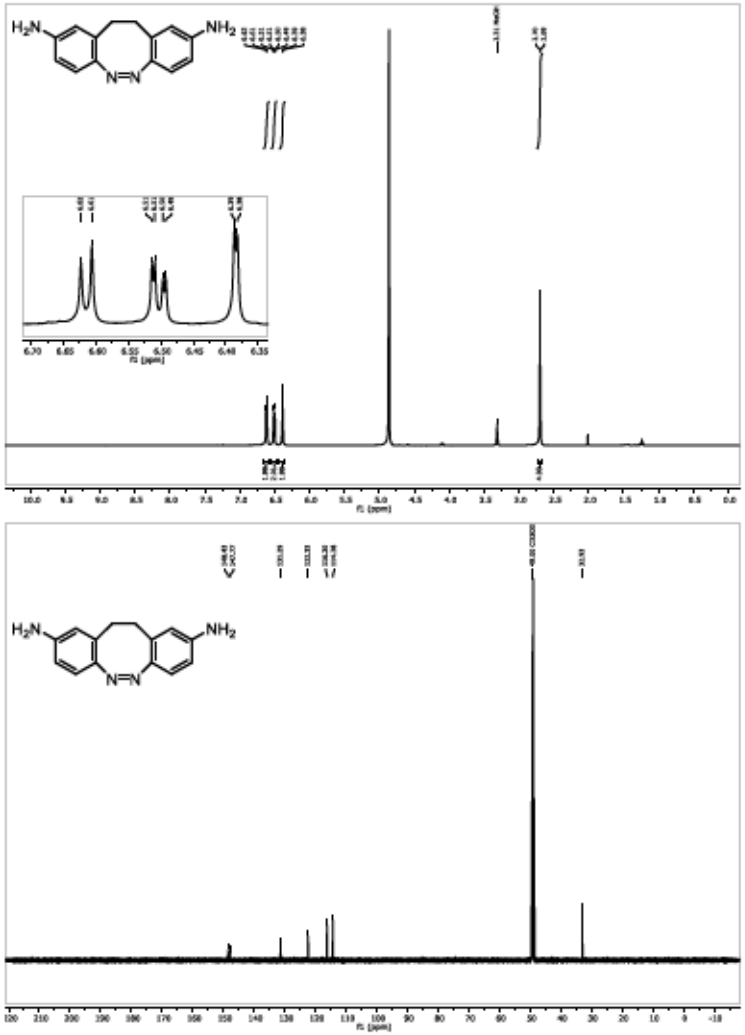

(Z)-11,12-Dihydrodibenzo[*c*,*g*][1,2]diazocine-3,8-diamine (1r)

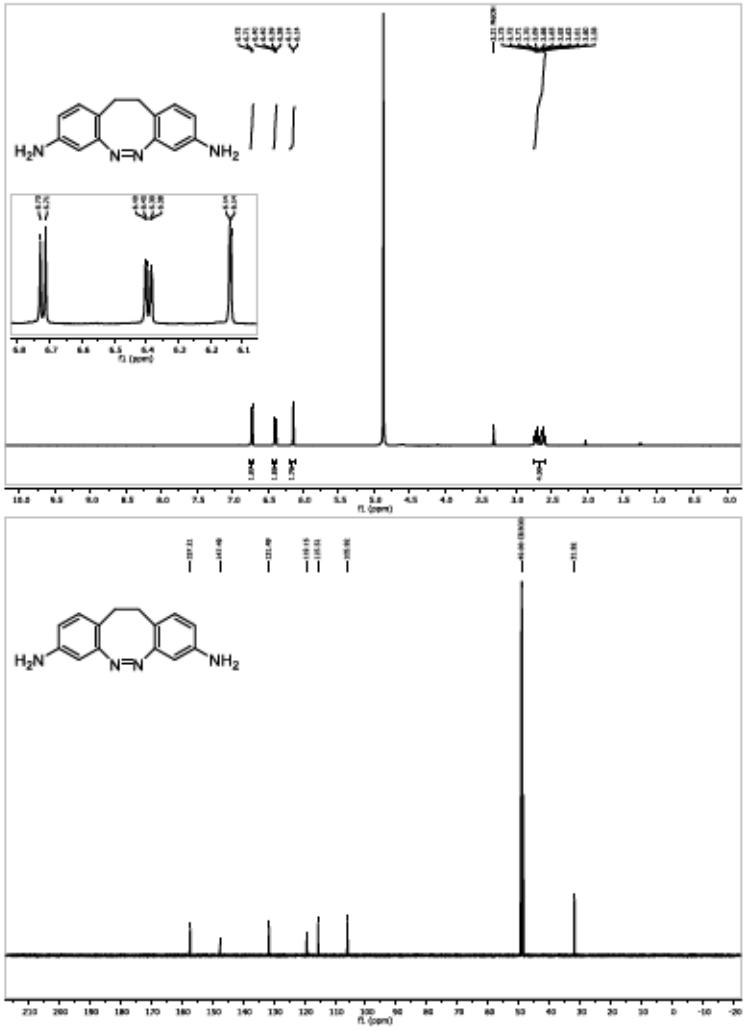

(Z)-11,12-Dihydrodibenzo[*c*,*g*][1,2]diazocine-2,9-dicarboxylic acid (1s)

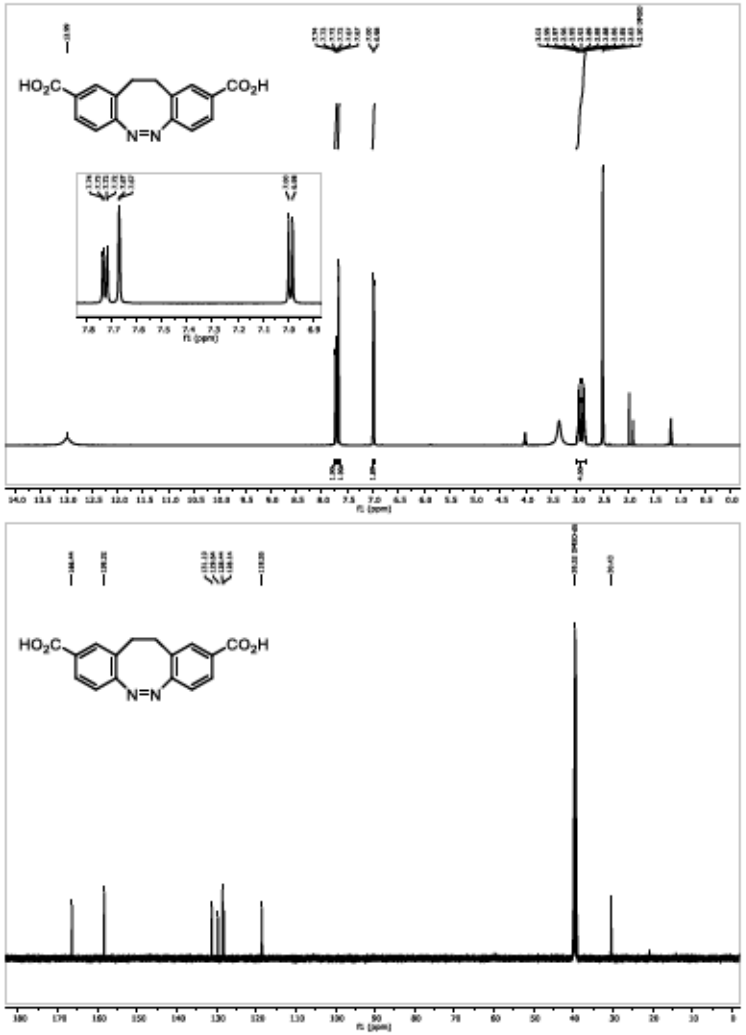

(Z)-11,12-Dihydrodibenzo[*c*,*g*][1,2]diazocine-3,8-dicarboxylic acid (1t)

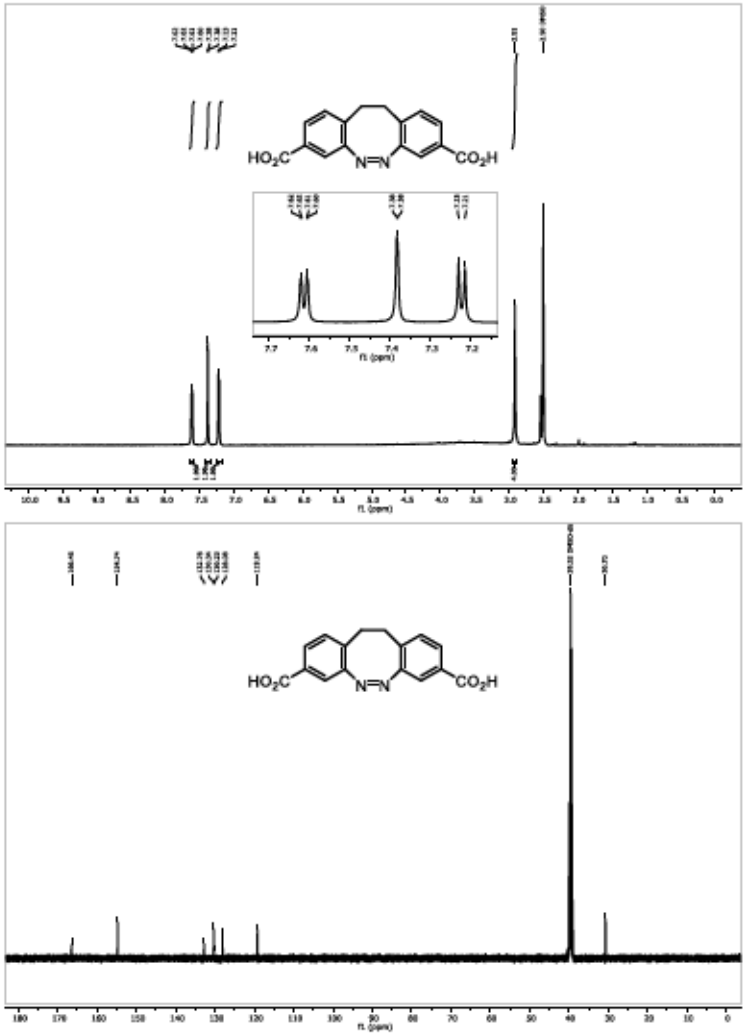

(Z)-(11,12-dihydrodibenzo[c,g][1,2]diazocine-2,9-diyl)dimethanol (1u)

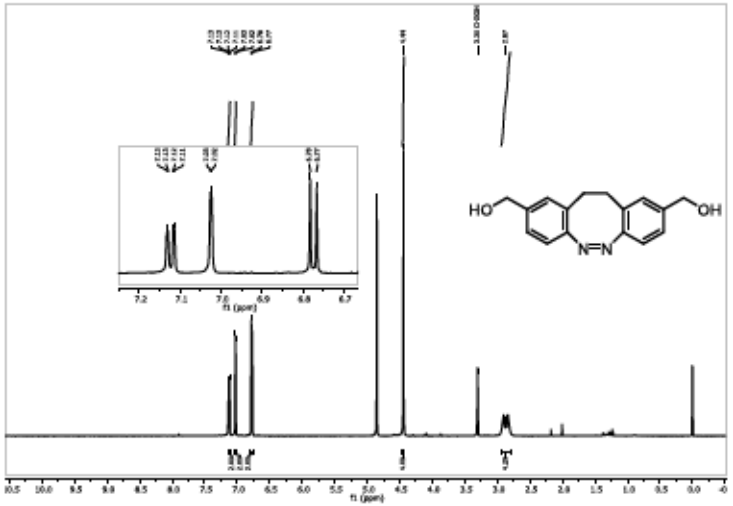

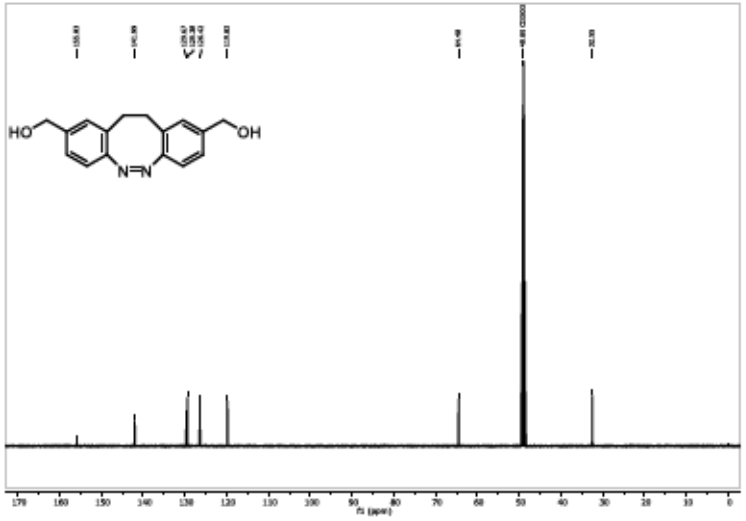

Supporting Information

for

ARGET ATRP of Methyl Acrylate and Methyl Methacrylate with Diazocine-Derived Initiators

-Experimental Data-

Shuo Li,[†,‡] Ruchira Colaco,[†,‡] Anne Staubitz*[,†,‡]

[†]*University of Bremen, Institute for Organic and Analytical Chemistry, Leobener Str. 7, 28359 Bremen, Germany*

[‡]*University of Bremen, MAPEX Center for Materials and Processes, Bibliothekstr. 1, 28359 Bremen, Germany*

*staubitz@uni-bremen.de

Table of Contents

General Information

Syntheses under Schlenk conditions or in a glovebox (Pure LabHE from Inert, Amesbury, MA, USA) were performed with nitrogen as protection gas. All glassware was dried in an oven at 200 °C for at least 2 h prior to use. Syringes that were used to transfer anhydrous solvents or reagents were purged with nitrogen prior to use. Microwave reaction vials were sealed with a septum cap from Biotage (Biotage, Uppsala, Sweden). All solvents for purification and extraction were used as received. α-Bromoisobutyryl bromide (BIBB), *N,N,N',N'',N''*-pentamethyldiethylenetriamine (PMDETA), tris[2-(dimethylamino)ethyl]amine (Me_6TREN) and triethylamine were degassed by three freeze-pump-thaw cycles and stored in the glovebox. Methyl acrylate and methyl methacrylate were passed through aluminum oxide 90 basic (Macherey-Nagel, 50–200 µm particle size) before use. Solvents used for synthesis under inert conditions (THF, acetonitrile, CH_2Cl_2) were dried by a solvent purification system (SPS) from Inert Technologies. All polymer samples were passed through a 0.45 µm PTFE filter before analysis.

NMR spectra were recorded on a Bruker Avance Neo 600 (Bruker BioSpin, Rheinstetten, Germany) (600 MHz (^{1}H), 151 MHz (^{13}C{^{1}H}) at 298 K. All ^{1}H NMR and ^{13}C{^{1}H} NMR spectra were referenced to the residual proton signals of the solvent (^{1}H) or the solvent itself (^{13}C{^{1}H}). The exact assignment of the peaks was performed by two-dimensional NMR spectroscopy such as ^{1}H COSY, ^{13}C{^{1}H} HSQC and ^{1}H/^{13}C{^{1}H} HMBC when possible. High-resolution EI mass spectra were recorded on a MAT 95XL double-focusing mass spectrometer from Finnigan MAT (Thermo Fisher Scientific, Waltham, MA, USA) at an ionization energy of 70 eV. Samples were measured by a direct or indirect inlet method with a source temperature of 200 °C. High-resolution ESI and APCI mass spectra were measured by a direct inlet method on an Impact II mass spectrometer from Bruker Daltonics (Bruker Daltonics, Bremen, Germany). ESI mass spectra were recorded in the positive ion collection mode. IR spectra were recorded on a Nicolet i510 FT-IR spectrometer from Thermo Fisher Scientific (Thermo Fisher Scientific, Waltham, MA, USA) with a diamond window in an area from 500–4000 cm^{-1} with a resolution of 4 cm^{-1}. All samples were measured 16 times against a background scan. Melting points were recorded on a Büchi Melting Point M-560 (Büchi, Essen, Germany) and are reported corrected. Thin layer chromatography (TLC) was performed using TLC Silica gel 60 F254 from Merck (Merck, Darmstadt, Germany) and compounds were visualized by exposure to UV light at a wavelength of 254 nm. Column chromatography was performed by using SiO_2 (0.040–0.063 mm, 230–400 mesh ASTM) from Merck. The UV-vis absorption measurements were recorded in a Perkin Elmer UV/VIS NIR Spectrometer Lambda 900 and in a VWR UV-1600PC at 298 K. Quartz cuvettes of 10 mm optical path length were used. The irradiation experiments were carried out using LED light sources from Sahlmann Photochemical Solutions of 405 nm central wavelength (3x Nichia NVSU233A of 980 mW optical power) and of 525 nm central wavelength (3x Nichia NCSG219B-V1 of 400 mW optical power) at a 2 cm distance from the cuvette or from the reaction vial. Gel permeation chromatography (GPC) was performed on a PSS (polymer standard service) SECurity GPC system at 308 K after a conventional calibration using polystyrene standards. The molar mass distribution of polymers was determined using refractive index detection (RID) in combination with light scattering detection (LS) and diode-array detection (DAD). The polymers were dissolved in THF (≈ 1 mg/mL; 5 mg/mL for the detection of absorption at 395 nm wavelength) and the GPC spectra were recorded at 1 mg/mL elution flow rate. To prepare polymer thin films (0.03 to 0.04 mm thickness), 100 µL of a 60 mg/mL polymer solution in THF was drop-casted and distributed onto a Menzel-Gläser cover slip (18 mm x 18 mm) and dried on a glass plate at 60 °C for 24 h.

The use of abbreviations follows the conventions from the ACS Style guide.

Reagents

Reagent	Supplier	Purity
1-Bromobutane	Acros	99%
2-Bromo-5-hydroxybenzaldehyde	Apollo	
1,2-Dimethylethylenediamine	Apollo	
Ascorbic acid	Roth	>99%
α-Bromoisobutyryl bromide	Sigma-Aldrich	98%
Cu(0)	KnorrPrandell	wire, diameter: 0.4 mm
CuI	Sigma-Aldrich	≥99.5%
$CuCl_2$	Merck	for synthesis
$CuBr_2$	Stem Chemicals	99%
Di-*tert*-butyl hydrazine-1,2-dicarboxylate	Apollo	
Diisobutylaluminum hydride	Acros	1.2 M in toluene
Ethyl α-bromoisobutyrate	J&K	98%
Formaldehyde	Sigma-Aldrich	aq 37% ACS, 10–15% methanol
Formic acid	Sigma-Aldrich	97%
HCl in 2-propanol	Acros	5–6 M
H_2SO_4	VWR	95%
KOH	Sigma-Aldrich	>85%
K_3PO_4	abcr	97%, anhydrous
Methyl acrylate	Alfa Aesar	99%, 15 ppm 4-methoxy-phenol
Methyl methacrylate	J&K	99%
Na_2SO_4	Merck	ACS grade, 99.0%
NaCl	T.H. Geyer	>99%
$NaHCO_3$	Fischer	Analytical reagent grade
NaOH	VWR	pellets
NBS	Alfa Aesar	99%
NH_4Cl	Roth	>99.7% p.a.
N,N'-Dimethylethylenediamine	Apollo	
N,N,N',N'',N''-Pentamethyldiethylenetriamine	Merck	for synthesis
Platinum(IV) oxide	TCI	>85.0%
Potassium sodium tartrate tetrahydrate	Roth	>99%
Pyridine	Grüssing	99.5%
Sodium methoxide	TCI	>96%
Thionylchloride	Acros	99.7%
Triethylamine	Fluorochem	anhydrous

Trimethylsilyl iodide	Apollo	
Triphenylphosphine	Alfa Aesar	99+%
Tris(2-aminoethyl)amine	Alfa Aesar	97%

Solvents

Acetonitrile	Fischer	analytical grade, >99.5%
Anisole	Roth	>99%, for synthesis
CH_2Cl_2	Sigma-Aldrich	ACS grade, >99.9%
$CHCl_3$	Sigma-Aldrich	p.a. 99.0–99.4%
Cyclohexane	Honeywell	ACS grade, >99.5%
Diethyl ether	Sigma-Aldrich	>99.8%, contains butylated hydroxytoluene
Ethyl Acetate	Sigma-Aldrich	ACS grade, >99.5%
DMF	Acros	99.8%, extra dry
DMSO	Acros	99.7%
HCl	Merck	ACS, fuming >37%
Methanol	VWR	ACS grade
NH_3	Fischer	25% in water, sp gr 0.91
THF	Honeywell	reagent grade, >99% contains 250 ppm butylated hydroxytoluene
Toluene	Sigma-Aldrich	ACS grade, >99.7%
Water		deionized

Experimental Procedures and Characterization Data

Compounds **5**, **1a**, **1b**, **1c** were synthesized according to previously published procedures.[1]

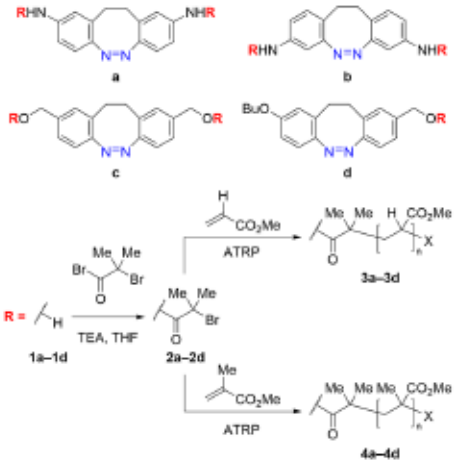

Scheme S1. Overview of starting materials **1a–1d**, initiators **2a–2d**, polymethyl acrylates **3a–3d** and polymethyl methacrylates **4a–4d** containing diazocine. (X = endgroup)

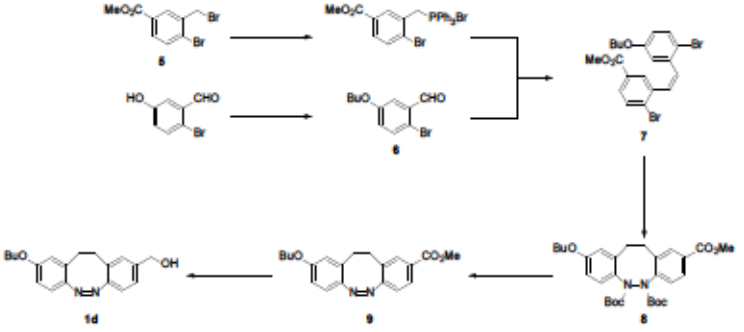

Scheme S2. Synthetic route to **1d**.

Initiator Synthesis

(*Z*)-*N*,*N*'-(11,12-Dihydrodibenzo[*c*,*g*][1,2]diazocine-2,9-diyl)bis(2-bromo-2-methylpropanamide) (2a)

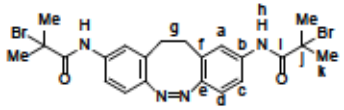

In a glovebox, a microwave vial was charged with compound **1a** (412 mg, 1.73 mmol), THF (17 mL) and TEA (1.20 mL, 8.65 mmol), sealed and transferred out of the glovebox. After cooling to 0 °C, a solution of BIBB (1.00 mL, 4.32 mmol) in THF (17 mL) was prepared in the glovebox, transferred into a syringe and out of the glovebox and added dropwise to the reaction mixture over the course of 30 min. Then, the reaction mixture was warmed slowly to 20 °C and stirred for 24 h. The reaction mixture was diluted with ethyl acetate (50 mL), quenched with aq. HCl (10 mL, 0.1 M), washed with saturated aq. $NaHCO_3$ (30 mL), brine (30 mL) and dried over Na_2SO_4. After filtration, the organic phase was concentrated under reduced pressure and the crude residue was purified by silica gel column chromatography (applied gradient from cyclohexane to cyclohexane/ethyl acetate 80/20) to furnish the product **2a** (761 mg, 1.42 mmol, 82%) as a yellow solid.

^{1}H NMR (500 MHz, $CDCl_3$): δ = 8.37 (s, 2H, H-h), 7.32 – 7.27 (m, 4H, H-a, H-c), 6.85 (d, *J* = 8.3 Hz, 2H, H-d), 3.15 – 2.62 (m, 4H, H-g), 2.00 (s, 12H, H-k) ppm.

^{1}H NMR (600 MHz, CD_3CN): δ = 8.42 (s, 2H), 7.36 (dd, *J* = 6.6, 2.2 Hz, 4H), 6.83 – 6.79 (m, 2H), 2.97 – 2.66 (m, 4H), 1.95 (s, 12H) ppm.

^{13}C{^{1}H} NMR (126 MHz, $CDCl_3$): δ = 170.1 (C-l), 152.3 (C-e), 136.4 (C-b), 129.2 (C-f), 120.7 (C-a), 120.2 (C-d), 118.3 (C-c), 63.1 (C-j), 32.6 (C-k), 31.9 (C-g) ppm.

HRMS (EI) *m/z* for $C_{22}H_{24}{}^{79}Br_2N_4O_2$ [M]$^+$: calcd 534.02660, found: 534.02609 (10); 41 (100).

IR (ATR): $\tilde{\nu}$ = 3315 (w), 2931 (w), 1735 (m), 1663 (s), 1584 (s), 1526 (s), 1483 (m), 1414 (m), 1234 (m), 1108 (s), 1007 (w), 918 (m), 820 (s), 762 (w) cm^{-1}.

mp: 170 °C (decomp.).

Rf: 0.42 (cyclohexane/ethyl acetate = 67/33)

(*Z*)-*N*,*N*'-(11,12-Dihydrodibenzo[*c*,*g*][1,2]diazocine-3,8-diyl)bis(2-bromo-2-methylpropanamide) (2b)

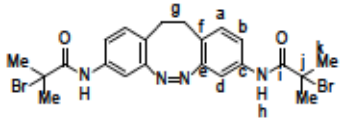

In a glovebox, a microwave vial was charged with compound **1b** (238 mg, 1.00 mmol), THF (10 mL) and TEA (700 µL, 5.00 mmol), sealed and transferred out of the glovebox. After cooling to 0 °C, a solution of BIBB (300 µL, 2.50 mmol) in THF (10 mL) was prepared in the glovebox, transferred into a syringe

and out of the glovebox and added dropwise to the reaction mixture over the course of 30 min. Then, the reaction mixture was warmed slowly to 20 °C and stirred for 24 h. The reaction mixture was diluted with ethyl acetate (50 mL), quenched with aq HCl (10 mL, 0.1 M), washed with saturated aq $NaHCO_3$ (30 mL), brine (30 mL) and dried over Na_2SO_4. After filtration, the organic phase was concentrated under reduced pressure and the crude residue was purified by silica gel column chromatography (applied gradient from cyclohexane to cyclohexane/ethyl acetate 80/20) to furnish the product **2b** (450 mg, 840 µmol, 84%) as a yellow solid.

^{1}H NMR (500 MHz, $CDCl_3$): δ = 8.39 (s, 2H, H-h), 7.26 (dd, *J* = 8.3, 2.3 Hz, 2H, H-b), 7.09 (d, *J* = 2.3 Hz, 2H, H-d), 6.97 (d, *J* = 8.3 Hz, 2H, H-a), 3.01 – 2.68 (m, 4H, H-g), 2.01 (d, *J* = 1.1 Hz, 12H, H-k) ppm.

^{1}H NMR (600 MHz, CD_3CN): δ = 8.47 (s, 2H), 7.22 (dd, *J* = 8.3, 2.1 Hz, 2H), 7.19 (d, *J* = 2.1 Hz, 2H), 7.03 (d, *J* = 8.3 Hz, 2H), 2.90 – 2.74 (m, 4H), 1.96 (s, 12H) ppm.

^{13}C{^{1}H} NMR (126 MHz, $CDCl_3$): δ = 170.1 (C-l), 155.6 (C-e), 136.2 (C-c), 130.5 (C-a), 124.6 (C-f), 118.6 (C-b), 110.3 (C-d), 63.0 (C-j), 32.7 (C-k), 32.6 (C-k), 31.4 (C-g) ppm.

HRMS (EI) *m/z* for $C_{22}H_{24}{}^{79}Br_2N_4O_2$ [M]$^+$: calcd 534.02660, found: 534.02605 (10); 41 (100).

IR (ATR): $\tilde{\nu}$ = 3320 (w), 2931 (w), 1734 (w), 1664 (s), 1593 (s), 1515 (s), 1496 (s), 1386 (s), 1301 (m), 1245 (m), 1159 (m), 1112 (s), 948 (w), 888 (m), 828 (s), 814 (s) cm^{-1}.

mp: 170 °C (decomp.).

Rf: 0.48 (cyclohexane/ethyl acetate = 67/33)

(*Z*)-(11,12-Dihydrodibenzo[*c*,*g*][1,2]diazocine-2,9-diyl)bis(methylene) bis(2-bromo-2-methylpropanoate) (2c)

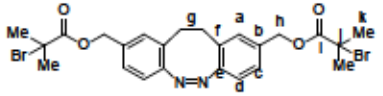

In a glovebox, a microwave vial was charged with compound **1c** (268 mg, 1.00 mmol), THF (10 mL) and TEA (690 µL, 4.98 mmol), sealed and transferred out of the glovebox. After cooling to 0 °C, a solution of BIBB (310 µL, 2.51 mmol) in THF (12 mL) was prepared in the glovebox, transferred into a syringe and out of the glovebox and added dropwise to the reaction mixture over the course of 30 min. Then, the reaction mixture was warmed slowly to 20 °C and stirred for 24 h. The reaction mixture was diluted with ethyl acetate (40 mL), quenched with saturated aq NH_4Cl (10 mL), washed with saturated aq $NaHCO_3$ (10 mL), brine (30 mL) and dried over Na_2SO_4. After filtration, the organic phase was concentrated under reduced pressure and the crude residue was purified by silica gel column chromatography (applied gradient from cyclohexane to cyclohexane/ethyl acetate 80/20) to furnish the product **2c** (530 mg, 920 µmol, 92%) as a yellow solid.

^{1}H NMR (500 MHz, $CDCl_3$): δ = 7.15 (dd, *J* = 8.0, 1.7 Hz, 2H, H-c), 6.99 (d, *J* = 1.7 Hz, 2H, H-a), 6.85 (d, *J* = 8.0 Hz, 2H, H-d), 5.07 (s, 4H, H-h), 3.06 – 2.71 (m, 4H, H-g), 1.91 (s, 12H, H-k) ppm.

^{1}H NMR (600 MHz, CD_3CN): δ = 7.21 (dd, *J* = 8.0, 1.4 Hz, 2H), 7.09 (s, 2H), 6.87 (d, *J* = 8.1 Hz, 2H), 5.06 (s, 4H), 2.98 – 2.76 (m, 4H), 1.89 (s, 12H) ppm.

^{13}C{^{1}H} NMR (126 MHz, $CDCl_3$): δ = 171.5 (C-l), 155.4 (C-e), 134.4 (C-b), 129.3 (C-a), 128.4 (C-f), 126.5 (C-c), 119.4 (C-d), 66.9 (C-h), 55.7 (C-g), 31.8 (C-k), 30.8 (C-k) ppm.

HRMS (ESI) *m/z* for $C_{24}H_{27}{}^{79}Br_2N_2O_4$ $[M+H]^+$: calcd 565.03321, found: 565.03283.

IR (ATR): $\tilde{\nu}$ = 2934 (w), 1732 (s), 1518 (w), 1461 (m), 1373 (m), 1272 (s), 1166 (s), 1149 (s), 1114 (m), 1098 (m), 1005 (m), 959 (m), 897 (m), 825 (m), 763 (w), 685 (w) cm^{-1}.

mp: 104 °C.

Rf: 0.53 (cyclohexane/ethyl acetate = 80/20)

2-Bromo-5-butoxybenzaldehyde (6)

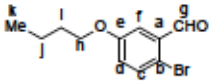

2-Bromobenzaldehyde (9.451 g, 50.00 mmol), K_2CO_3 (9.674 g, 70.00 mmol), DMF (70 mL) and butyl bromide (5.755 g, 42.00 mmol) were added to a round-bottomed flask. The reaction mixture was stirred at 80 °C for 12 h before it was concentrated under reduced pressure. Water (30 mL) and diethyl ether (100 mL) was added and the mixture was washed with aq NaOH (2 x 30 mL, 1 M) and dried over Na_2SO_4. After filtration, the organic phase was concentrated under reduced pressure and the residue was dried in vacuum to furnish the product **6** (8.84 mg, 34.4 mmol, 98%) as a yellow oil.

^{1}H NMR (601 MHz, $CDCl_3$): δ = 10.30 (s, 1H, H-g), 7.51 (d, J = 8.8 Hz, 1H, H-c), 7.40 (d, J = 3.2 Hz, 1H, H-f), 7.02 (dd, J = 8.8, 3.2 Hz, 1H, H-d), 3.99 (t, J = 6.5 Hz, 2H, H-h), 1.77 (dt, J = 14.3, 6.5 Hz, 2H, H-i), 1.52 – 1.44 (m, 2H, H-j), 0.97 (t, J = 7.4 Hz, 3H, H-k) ppm.

^{13}C{^{1}H} NMR (151 MHz, $CDCl_3$): δ = 192.0 (C-g), 158.9 (C-a), 134.6 (C-c), 134.0 (C-e), 123.6 (C-d), 117.8 (C-b), 113.5 (C-f), 68.4 (C-h), 31.2 (C-i), 19.3 (C-j), 13.9 (C-k) ppm.

HRMS (EI) *m/z* for $C_{11}H_{13}{}^{79}BrO_2$ $[M]^+$: calcd 256.00989, found: 256.00963 (10); 41 (100).

IR (ATR): $\tilde{\nu}$ = 2957 (w), 2933 (w), 2871 (w), 1691 (s), 1591 (m), 1567 (w), 1464 (s), 1386 (s), 1310 (s), 1273 (s), 1229 (s), 1165 (s), 1108 (m), 1068 (w), 1006 (w), 937 (w), 867 (w), 821 (m), 754 (m), 659 (w) cm^{-1}.

Rf: 0.76 (cyclohexane/ethyl acetate = 80/20)

Methyl (Z)-4-bromo-3-(2-bromo-5-butoxystyryl)benzoate (7)

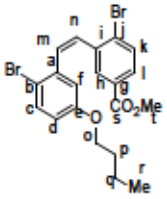

A dry, nitrogen flushed two-necked Schlenk-flask equipped with a magnetic stirring bar and a septum was charged with methyl 4-bromo-3-(bromomethyl)benzoate (compound **5**, 9.24 g, 30.00 mmol), PPh_3 (7.87 g, 30.00 mmol) and DMF (30 mL). The reaction mixture was stirred at 20 °C for 20 h under a

nitrogen atmosphere before the solid residue washed with toluene (30 mL), cyclohexane (30 mL) and concentrated under reduced pressure.

A dry, nitrogen flushed two-necked Schlenk-flask equipped with a magnetic stirring bar and a septum was charged with the crude product and THF (150 mL). The reaction mixture was cooled to 0 °C before NaOMe (2.43 g, 45.00 mmol) was added and stirred at 0 °C for 30 min. Then, the reaction mixture was treated with compound **6** (7.31 g, 28.42 mmol), allowed to warm to 20 °C and stirred for 21 h. The reaction mixture was quenched with water (100 mL), extracted with ethyl acetate (2 x 50 mL), washed with brine (30 mL) and dried over Na_2SO_4. After filtration, the organic phase was concentrated under reduced pressure.

Methanol (40 mL), concd H_2SO_4 (1.2 mL, 21.6 mmol, 18 M) and the organic residue were added sequentially to a round-bottomed flask equipped with a reflux condenser. The reaction mixture was stirred at 65 °C for 12 h. After cooling to 20 °C, the reaction mixture was quenched with saturated aq $NaHCO_3$ (30 mL), extracted with ethyl acetate (3 x 30 mL), washed with brine (30 mL) and dried over Na_2SO_4. After filtration, the organic phase was concentrated under reduced pressure and the crude residue was purified by silica gel column chromatography (cyclohexane/ethyl acetate 90/10) to furnish the product **7** as a colorless solid (8.96 g, 19.1 mmol, 64%). Adapted from lit.[1]

^{1}H NMR (601 MHz, $CDCl_3$): δ = 7.73 – 7.68 (m, 2H, H-h, H-l), 7.67 – 7.62 (m, 1H, H-k), 7.42 (d, J = 8.8 Hz, 1H, H-c), 6.84 (d, J = 11.9 Hz, 1H, H-m), 6.74 (d, J = 11.9 Hz, 1H, H-n), 6.62 (dd, J = 8.8, 3.0 Hz, 1H, H-d), 6.46 (d, J = 3.0 Hz, 1H, H-f), 3.79 (s, 3H, H-t), 3.56 (t, J = 6.6 Hz, 2H, H-o), 1.56 – 1.50 (m, 2H, H-p), 1.36 – 1.26 (m, 2H, H-q), 0.86 (t, J = 7.4 Hz, 3H, H-r) ppm.

^{13}C{^{1}H} NMR (151 MHz, $CDCl_3$): δ = 166.2 (C-s), 158.0 (C-e), 137.7 (C-l), 137.0 (C-a), 133.4 (C-c), 133.0 (C-k), 132.3 (C-m), 132.0 (C-h), 130.0 (C-k), 129.5 (C-l), 129.4 (C-j), 129.3 (C-g), 116.8 (C-d), 115.9 (C-f), 114.4 (C-b), 67.9 (C-o), 52.3 (C-t), 31.0 (C-p), 19.1 (C-q), 13.8 (C-r) ppm.

HRMS (EI) *m/z* for $C_{20}H_{20}{}^{79}Br_2O_3$ $[M]^+$: calcd 465.97792, found: 465.97755 (10); 252 (100).

IR (ATR): $\tilde{\nu}$ = 2955 (w), 2871 (w), 1722 (s), 1590 (m), 1564 (m), 1456 (m), 1435 (m), 1289 (s), 1236 (s), 1181 (m), 1105 (s), 1026 (s), 813 (m), 758 (s), 675 (w) cm^{-1}.

mp: 55 °C.

Rf: 0.68 (cyclohexane/ethyl acetate = 80/20)

5,6-Di-tert-butyl 2-methyl 9-butoxy-11,12-dihydrodibenzo[*c*,*g*][1,2]diazocine-2,5,6-tricarboxylate (8)[1]

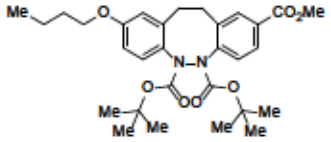

Compound **7** (12.122 g, 25.89 mmol), ethyl acetate (400 mL) and methanol (100 mL) were added sequentially to a round-bottomed flask and purged with nitrogen for 5 min. Platinum(IV) oxide (294 mg, 1.29 mmol) was added and the reaction mixture was purged with hydrogen for 10 min before stirring

[1] The ^{13}C{^{1}H} NMR spectrum for compound **8** could not be reported because the signal intensities were too low and broadened, probably due to sluggish conformational changes.

under a hydrogen atmosphere (1 atm) at 20 °C for 24 h. The reaction mixture was filtered through a pad of celite before the organic phase was concentrated under reduced pressure.

The crude product was transferred to a pressure vial, to which was added di-tert-butyl hydrazine-1,2-dicarboxylate (6.00 g, 25.89 mmol), CuI (4.93 g, 25.89 mmol), K_3PO_4 (16.49 g, 77.67 mmol). The vial was transferred into a glovebox before acetonitrile (125 mL) and 1,2-dimethylethylenediamine (560 µL, 5.72 mmol) were added. The vial was sealed, transferred out of the glovebox and stirred at 82 °C for 40 h. After cooling to 20 °C, the reaction mixture was quenched with water (50 mL), washed with aq NH_3 (50 mL), extracted with $CHCl_3$ (3 x 50 mL), washed with brine (50 mL) and dried over Na_2SO_4. After filtration, the organic phase was concentrated under reduced pressure and the crude residue was purified by silica gel column chromatography (applied gradient from cyclohexane to cyclohexane/ethyl acetate = 80/20) to furnish product **8** (6.321 g, 11.69 mmol, 45%) as a colorless solid. Adapted from lit.[1]

^{1}H NMR (601 MHz, $CDCl_3$): δ = 8.05 – 7.35 (m, 4H), 6.86 – 6.65 (m, 2H), 4.09 – 3.87 (m, 5H), 3.25 – 2.67 (m, 4H), 1.85 – 1.71 (m, 2H), 1.65 – 1.26 (m, 20H), 1.07 – 0.94 (m, 3H) ppm.

HRMS (EI) *m/z* for $C_{30}H_{40}N_2O_7$ $[M]^+$: calcd 540.28355, found: 540.28382 (10); 57 (100).

IR (ATR): $\tilde{\nu}$ = 2970 (w), 1717 (s), 1606 (w), 1501 (w), 1436 (w), 1367 (m), 1288 (m), 1246 (m), 1151 (s), 1109 (m), 1005 (w), 908 (w), 850 (w), 764 (m) cm^{-1}.

mp: 84 °C.

R_f: 0.56 (cyclohexane/ethyl acetate = 80/20)

Methyl (*Z*)-9-butoxy-11,12-dihydrodibenzo[*c*,*g*][1,2]diazocine-2-carboxylate (9)

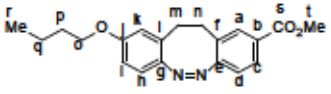

In a glovebox, compound **8** (2.90 g, 5.37 mmol), CH_2Cl_2 (30 mL) and trimethylsilyl iodide (3.8 mL, 21.46 mmol) were added sequentially to a round-bottomed flask equipped with a magnetic stirring bar. The reaction mixture was stirred at 20 °C for 10 min before it was treated with triethylamine (3.7 mL, 21.46 mmol). The flask was capped, transferred out of the glovebox where the reaction mixture was quenched by dropwise addition of water (25 mL), extracted with ethyl acetate (3 x 30 mL), washed with brine (30 mL) and dried over Na_2SO_4. After filtration, the organic phase was concentrated under reduced pressure. The resulting residue, CH_2Cl_2 (60 mL) and pyridine (500 µL, 6.4 mmol) were added sequentially to a round-bottomed flask. NBS (1.146 g, 6.44 mmol) was added portion wise over the course of 2 min under stirring and the reaction mixture was stirred at 20 °C for 30 min. The reaction mixture was concentrated under reduced pressure and the residue was purified by silica gel column chromatography (applied gradient from cyclohexane to cyclohexane/ethyl acetate = 80/20) to furnish product **9** (1.07 g, 3.17 mmol, 59%) as a yellow solid. Adapted from lit.[1]

^{1}H NMR (601 MHz, $CDCl_3$): δ = 7.79 (dd, J = 8.2, 1.7 Hz, 1H, H-c), 7.71 (d, J = 1.7 Hz, 1H, H-a), 6.85 (d, J = 8.2 Hz, 1H, H-d), 6.81 (d, J = 8.6 Hz, 1H, H-h), 6.65 (dd, J = 8.6, 2.6 Hz, 1H, H-i), 6.46 (d, J = 2.6 Hz, 1H, H-k), 3.85 (s, 3H, H-t), 3.83 (t, J = 6.5 Hz, 2H, H-o), 3.08 – 2.63 (m, 4H, H-m, H-n), 1.71 – 1.65 (m, 2H, H-p), 1.46 – 1.39 (m, 2H, H-q), 0.93 (t, J = 7.4 Hz, 3H, H-r) ppm.

^{13}C{^{1}H} NMR (151 MHz, $CDCl_3$): δ = 166.5 (C-s), 159.4 (C-e), 158.2 (C-j), 149.0 (C-g), 131.2 (C-a), 129.0 (C-i), 129.0 (C-f), 128.7 (C-b), 128.3 (C-c), 120.9 (C-h), 118.9 (C-d), 115.5 (C-k), 112.7 (C-l), 67.8 (C-o), 52.3 (C-t), 32.3 (C-m), 31.4 (C-n), 31.3 (C-p), 19.3 (C-q), 14.0 (C-r) ppm.

HRMS (EI) *m/z* for $C_{20}H_{22}N_2O_3$ $[M]^+$: calcd 338.16304, found: 338.16175 (40); 254 (100).

IR (ATR): $\tilde{\nu}$ = 2947 (w), 2867 (w), 1716 (s), 1599 (w), 1465 (w), 1431 (m), 1292 (s), 1263 (m), 1235 (m), 1198 (m), 1116 (m), 1025 (w), 969 (w), 817 (w), 762 (s), 680 (w) cm^{-1}.

mp: 90 °C.

R_f: 0.59 (cyclohexane/ethyl acetate = 80/20)

(*Z*)-(9-Butoxy-11,12-dihydrodibenzo[*c*,*g*][1,2]diazocin-2-yl)methanol (1d)

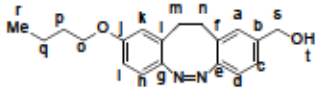

A dry, nitrogen flushed two-necked Schlenk-flask equipped with a magnetic stirring bar and a septum was charged with compound **9** (100 mg, 300 µmol) and anhydrous THF (6 mL). The reaction mixture was cooled to 0 °C and diisobutylaluminum hydride (1.0 mL, 1.20 mmol, 1.2 M in toluene) was added dropwise (3 mL/min) under stirring. After completion of the addition, the reaction mixture was warmed to 20 °C and stirred at 20 °C for 1 h. The reaction mixture was quenched by adding aq Rochelle salt (50 mL, 0.2 M) and stirring at 20 °C for 1 h, followed by an extraction with ethyl acetate (3 x 20 mL). The organic phase was washed with brine (20 mL) and dried over Na_2SO_4. After filtration, the organic phase was concentrated under reduced pressure and to the residue was added methanol (30 mL), NaOH (120 mg, 3 mmol) and $CuCl_2$ (3 mg, 20 µmol). The reaction mixture was stirred while air was bubbled through the solution at 20 °C for 30 min. The reaction mixture was quenched with saturated aq NH_4Cl (20 mL) and water (20 mL), followed by an extraction with $CHCl_3$ (3 x 20 mL). The organic phase was washed with brine (20 mL) and dried over Na_2SO_4. After filtration, the organic phase was concentrated under reduced pressure and the crude residue was purified by silica gel column chromatography (applied gradient from cyclohexane to cyclohexane/ethyl acetate 70/30) to furnish the product **1d** (60.0 mg, 190 µmol, 64%) as a yellow solid. Adapted from lit.[1]

^{1}H NMR (601 MHz, $CDCl_3$): δ = 7.08 (dd, J = 8.0, 1.3 Hz, 1H, H-c), 7.00 – 6.97 (m, 1H, H-a), 6.79 (d, J = 8.6 Hz, 1H, H-h), 6.79 (d, J = 8.0 Hz, 1H, H-d), 6.64 (dd, J = 8.6, 2.6 Hz, 1H, H-i), 6.48 (d, J = 2.6 Hz, 1H, H-k), 4.53 (s, 2H, H-s), 3.82 (t, J = 6.5 Hz, 2H, H-o), 3.05 – 2.55 (m, 4H, H-m, H-n), 2.10 (s, 1H, H-t), 1.72 – 1.64 (m, 2H, H-p), 1.46 – 1.39 (m, 2H, H-q), 0.93 (t, J = 7.4 Hz, 3H, H-r) ppm.

^{13}C{^{1}H} NMR (151 MHz, $CDCl_3$): δ = 158.0 (C-j), 154.8 (C-e), 148.9 (C-g), 139.7 (C-l), 129.5 (C-f), 128.5 (C-b), 128.1 (C-a), 125.3 (C-c), 121.0 (C-h), 119.4 (C-d), 115.3 (C-k), 112.5 (C-i), 67.8 (C-o), 64.7 (C-s), 32.3 (C-m/n), 31.7 (C-m/n),[2] 31.4 (C-p), 19.3 (C-q), 13.9 (C-r) ppm.

HRMS (EI) *m/z* for $C_{19}H_{22}N_2O_2$ $[M]^+$: calcd 310.16813, found: 310.16741 (40); 195 (100).

IR (ATR): $\tilde{\nu}$ = 3419 (w), 2949 (w), 2925 (w), 2866 (w), 2360 (w), 1715 (w), 1605 (w), 1570 (w), 1508 (w), 1465 (m), 1389 (w), 1281 (m), 1254 (s), 1171 (w), 1108 (m), 1021 (m), 890 (w), 815 (m), 796 (s), 745 (m) cm^{-1}.

mp: 78 °C.

R_f: 0.29 (cyclohexane/ethyl acetate = 67/33)Δ

[2] not resolvable due to close vicinity in chemical shifts

(*Z*)-(9-Butoxy-11,12-dihydrodibenzo[*c*,*g*][1,2]diazocin-2-yl)methyl 2-bromo-2-methylpropanoate (2d)

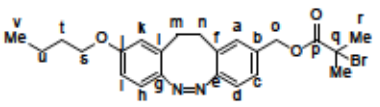

In a glovebox, a microwave vial was charged with compound **1d** (273 mg, 880 µmol), THF (9 mL) and TEA (1.20 mL, 8.65 mmol), sealed and transferred out of the glovebox. After cooling to 0 °C, a solution of BIBB (220 µL, 1.76 mmol) in THF (9 mL) was prepared in the glovebox, transferred into a syringe and out of the glovebox and added dropwise to the reaction mixture over the course of 30 min. Then, the reaction mixture was warmed slowly to 20 °C and stirred for 24 h. The reaction mixture was diluted with ethyl acetate (50 mL), quenched with aq NH_4Cl (10 mL), washed with saturated aq $NaHCO_3$ (30 mL), brine (30 mL) and dried over Na_2SO_4. After filtration, the organic phase was concentrated under reduced pressure and the crude residue was purified by silica gel column chromatography (applied gradient from cyclohexane to cyclohexane/ethyl acetate 80/20) to furnish the product **2d** (228 mg, 400 µmol, 46%) as an orange solid.

^{1}H NMR (601 MHz, $CDCl_3$): δ = 7.15 (dd, *J* = 8.1, 1.7 Hz, 1H, H-c), 7.01 (d, *J* = 1.7 Hz, 1H, H-a), 6.83 (d, *J* = 8.1 Hz, 1H, H-d), 6.81 (d, *J* = 8.6 Hz, 1H, H-h), 6.66 (dd, *J* = 8.6, 2.6 Hz, 1H, H-l), 6.49 (d, *J* = 2.6 Hz, 1H, H-**k**), 5.08 (s, 2H, H-o), 3.84 (t, *J* = 6.5 Hz, 2H, H-s), 2.88 – 2.80 (m, 4H, H-m, H-n), 1.91 (s, 6H, H-r), 1.72 – 1.66 (m, 2H, H-t), 1.48 – 1.39 (m, 2H, H-u), 0.94 (t, *J* = 7.4 Hz, 3H, H-v) ppm.

^{1}H NMR (600 MHz, CD_3CN): δ = 7.19 (d, *J* = 8.0 Hz, 1H), 7.10 (s, 1H), 6.81 (d, *J* = 8.0 Hz, 1H), 6.79 (d, *J* = 8.6 Hz, 1H), 6.70 (dd, *J* = 8.6, 2.6 Hz, 1H), 6.58 (d, *J* = 2.5 Hz, 1H), 5.07 (s, 2H), 3.86 (t, *J* = 6.5 Hz, 2H), 3.00 – 2.64 (m, 4H), 1.89 (s, 6H), 1.66 (dt, *J* = 14.4, 6.6 Hz, 2H), 1.45 – 1.37 (m, 2H), 0.92 (t, *J* = 7.4 Hz, 3H) ppm.

^{13}C{^{1}H} NMR (151 MHz, $CDCl_3$): δ = 171.5 (C-p), 158.0 (C-j), 155.5 (C-e), 149.0 (C-g), 134.2 (C-b), 129.4 (C-f), 129.2 (C-a), 128.8 (C-l), 126.4 (C-c), 121.1 (C-h), 119.4 (C-d), 115.3 (C-**k**), 112.6 (C-l), 67.9 (C-s), 67.0 (C-o), 55.7 (C-q), 32.3 (C-m/n), 31.7 (C-m/n),[3] 31.4 (C-t), 30.8 (C-r), 19.3 (C-u), 14.0 (C-v) ppm.

HRMS (EI) *m/z* for $C_{23}H_{27}{}^{79}BrN_2O_3$ [M]$^+$: calcd 458.12051, found: 458.12021 (10); 209 (100).

IR (ATR): $\tilde{\nu}$ = 2957 (w), 2872 (w), 1735 (s), 1599 (w), 1460 (m), 1388 (w), 1272 (m), 1242 (m), 1152 (s), 1105 (s), 1010 (w), 891 (w), 825 (m), 804 (m) cm^{-1}.

mp: 45 °C.

R_f: 0.47 (cyclohexane/ethyl acetate = 80/20)

[3] not resolvable due to close vicinity in chemical shifts

Tris[2-(dimethylamino)ethyl]amine (10)[4]

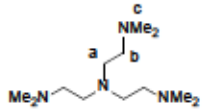

Tris(2-aminoethyl)amine (TREN) was dissolved in dry methanol (150 mL). Then, hydrochloric acid in 2-propanol (21.0 mL, 5-6 M) was added over the course of 25 min using a syringe pump. The reaction mixture was stirred for 1 h at 24 °C, before the precipitate was filtered and washed with methanol (3 x 100 mL). The solvent was removed under vacuum and the slightly beige TREN-hydrochloride salt was dried (yield: 6.84 g). This intermediate (6.84 g) was added to a mixture of water (12.0 mL), formic acid (56.0 mL, 1.40 mol) and formaldehyde solution (56.0 mL) and were heated to 120 °C for 6 h. The residue was obtained by removing the volatile component via rotary evaporation and aqueous solution of NaOH (5 M, 100 mL) was added until complete dissolution was achieved. Solid KOH (50.0 g, 900 µol) was slowly added until the solution had a pH value of 14. The aqueous phase was extracted with ethyl acetate (5 x 75 mL). The combined organic phases were dried over solid KOH and the solvent was removed under vacuum, followed by fractioning vacuum distillation (52 °C, 5.7 x 10^{-2} mbar) under a nitrogen atmosphere to furnish product **10** (6.96 g, 30.2 mmol, 83%, Lit.:[2] 91%) as a colorless oil.

^{1}H NMR (500 MHz, $CDCl_3$): δ = 2.50 – 2.18 (m, 12 H, H-a, H-b), 2.08 (m, 18 H, H-c) ppm.

^{13}C{^{1}H} NMR (126 MHz, $CDCl_3$): δ = 57.3 (C-b), 52.9 (C-a), 45.8 (C-c) ppm.

IR (ATR): $\tilde{\nu}$ = 2940 (m), 2850 (w), 2814 (m), 2762 (s), 1455 (s), 1263 (w), 1153 (s), 1122 (m), 1030 (s) cm^{-1}.

[4] As the molecule fragments during the mass measurement, the [M$^+$] could not be measured.

Polymerization Procedures

To conduct the polymerization with Cu(0), copper wire was wrapped around a stirring bar, cleaned with concentrated HCl (12 M) for 10 min, rinsed with water and acetone and transferred into the glovebox. The stirring bar was added to the reaction mixture to start the polymerization. To irradiate the reaction vial with light during the reaction, the LED light source was switched on just before the stirring bar was added. A solution of $CuBr_2$ in DMSO (67 mg/3 mL, 0.1 M) was prepared in the glovebox.

*Typical procedure (TP1) for the polymerization of methyl acrylate **3a–3d** with initiators **2a–2d***

Methyl acrylate (1.72 g, 20.0 mmol, 1000 equiv), initiators **2a–2d** (20.0 µmol/40.0 µmol, 1.00 equiv/2.00 equiv), and DMSO (1.9 mL) were added to a microwave vial and degassed by purging with argon for 10 min. The sealed vial was transferred into a glovebox, opened and AA (35 mg, 22.2 µmol, 50 equiv), $CuBr_2$ solution in DMSO (40.0 µL, 4.00 µmol, 0.1 M, 0.2 equiv) and Me$_6$TREN (**10**, 6.40 µL, 24.0 µmol, 1.2 equiv) were added within 20 s. The vial was sealed, transferred out of the glovebox and stirred at 20 °C for 2 h. Samples were taken periodically and conversions were measured using ^{1}H NMR spectroscopy. Then, the vial was opened and the reaction mixture was precipitated dropwise in stirring methanol (25 mL). The resulting solid was collected, redissolved in THF (2.5 mL) and re-precipitated in methanol (25 mL) twice before the solid residue **3a–3d** was dried in vacuum (50 °C, 48 h).

The reaction was performed according to the typical procedure (TP1) using the reagent **2a** (10.7 mg, 20.0 µmol), leading to the corresponding product **3a** (244 mg, 14%) as a yellow solid.

The reaction was performed according to the typical procedure (TP1) using the reagent **2b** (10.7 mg, 20.0 µmol), leading to the corresponding product **3b** (401 mg, 23%) as a yellow solid.

The reaction was performed according to the typical procedure (TP1) using the reagent **2c** (11.3 mg, 20.0 µmol), leading to the corresponding product **3c** (395 mg, 23%) as a yellow solid.

The reaction was performed according to the typical procedure (TP1) using the reagent **2d** (18.7 mg, 40.0 µmol), leading to the corresponding product **3d** (325 mg, 19%) as a yellow solid.

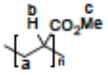

^{1}H NMR (600 MHz, CDCl$_3$): δ = 3.62 (s, 3H, H-c), 2.27 (s, 1H, H-b), 1.96 – 1.37 (m, 2H, H-a) ppm.

*Typical procedure (TP2) for the polymerization of methyl methacrylate **4a–4d** with initiators **2a–2d***

Methyl methacrylate (2.00 g, 20.0 mmol, 1000 equiv), initiators **2a–2d** (20.0 µmol/40.0 µmol, 1.00 equiv/2.00 equiv), and anisole (2.2 mL) were added to a microwave vial and degassed by purging with argon for 10 min. The sealed vial was transferred into the glovebox, opened and AA (3.5 mg, 20 µmol, 1 equiv), $CuBr_2$ solution in DMSO (20.0 µL, 2.00 µmol, 0.1 M, 0.1 equiv) and PMDETA (4.20 µL, 53.0 µmol, 1 equiv) were added within 20 s. The vial was sealed, transferred out of the glovebox and stirred at 90 °C for the given time. Samples were taken periodically and conversions were measured using ^{1}H NMR spectroscopy. Then, the vial was opened and to the reaction mixture was added THF (2.5 mL) and precipitated dropwise in stirring methanol (25 mL). The resulting solid was collected, redissolved in THF (5 mL) and re-precipitated in methanol (25 mL) twice before the solid residue **4a–4d** was dried in vacuum (50 °C, 48 h).

The reaction was performed according to the typical procedure (TP2) with the reagent **2a** (10.7 mg, 20.0 µmol), leading to the corresponding product **4a** (986 mg, 49%) as a yellow solid.

The reaction was performed according to the typical procedure (TP2) with using the reagent **2b** (10.7 mg, 20.0 µmol), leading to the corresponding product **4b** (1.104 g, 55%) as a yellow solid.

The reaction was performed according to the typical procedure (TP2) with 3using the reagent **2c** (11.3 mg, 20.0 µmol), leading to the corresponding product **4c** (1.274 g, 63%) as a yellow solid.

The reaction was performed according to the typical procedure (TP2) with 3using the reagent **2d** (18.7 mg, 40.0 µmol), leading to the corresponding product **4d** (1.219 g, 61%) as a yellow solid.

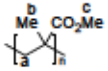

^{1}H NMR (600 MHz, CDCl$_3$): δ = 3.56 (s, 3H, H-c), 2.07 – 1.32 (m, 2H, H-a), 1.25 – 0.72 (m, 3H, H-b) ppm.

For the synthesis of the polymethyl methacrylate negative control, the reaction was performed according to the typical procedure (TP2) with 3 h of reaction time using ethyl α-bromoisobutyrate (EBiB) (5.9 µL, 40.0 µmol) as initiator, after which 100 µL of the reaction solution was precipitated in methanol (1 mL) and the solid residue was dissolved in THF (1 mL) for GPC analysis.

Polymerization Results

The conversion at a certain reaction time was determined by the integral relations of monomer and combined monomer/polymer signals of the methyl ester groups in the ^{1}H NMR spectrum. The theoretical degree of polymerization (DP) and the theoretical molar mass are determined by:

$$DP = \text{conversion} \frac{[\text{monomer}]}{[\text{initiator}]}$$

$$M_{n,theo} = M_{initiator} + DP\, M_{monomer}$$

Finally, the dispersity $Đ$ was calculated from GPC data and is defined as: $Đ = \frac{M_w}{M_n}$

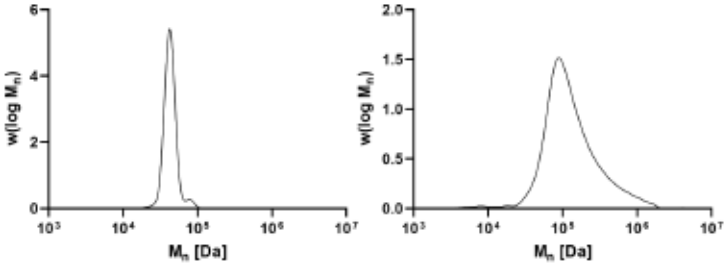

Figure S1. Molar mass distributions of entry 1 (left) and entry 2 (right).

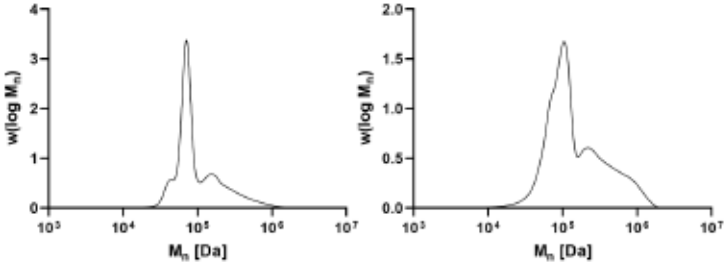

Figure S2. Molar mass distributions of entry 3 (left) and 4 (right).

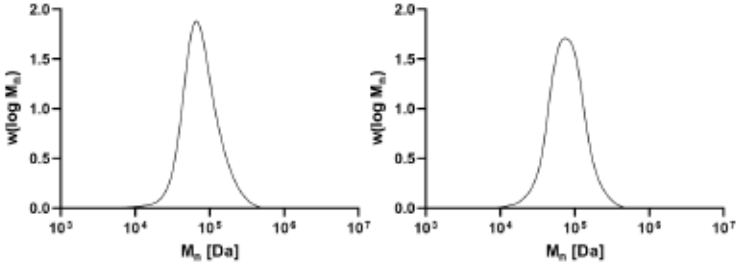

Figure S3. Molar mass distributions of entry 5 (left) and 6 (right).

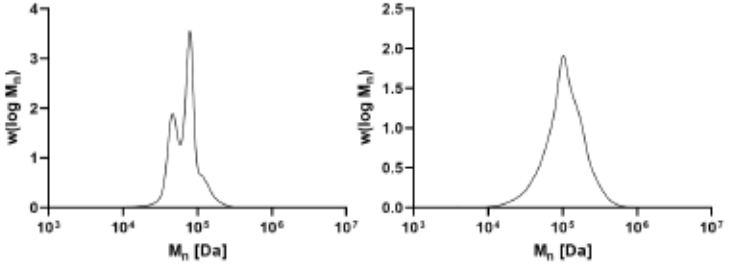

Figure S4. Molar mass distributions of entry 7 (left) and 8 (= **3a**, right).

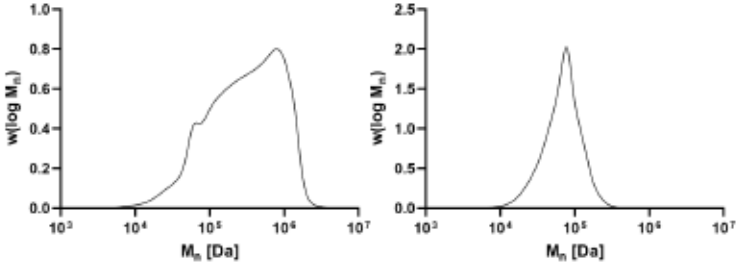

Figure S5. Molar mass distributions of entry 9 (left) of Table S1 and **3b** (right).

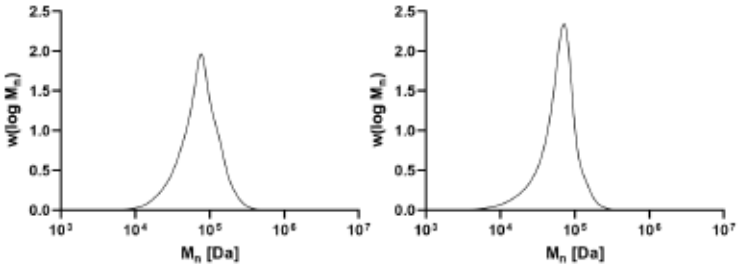

Figure S6. Molar mass distributions of entry **3c** (left) and **3d** (right).

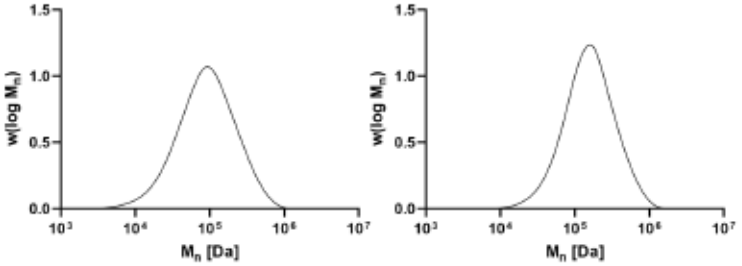

Figure S7. Molar mass distributions of entry **4a** (left) and **4b** (right).

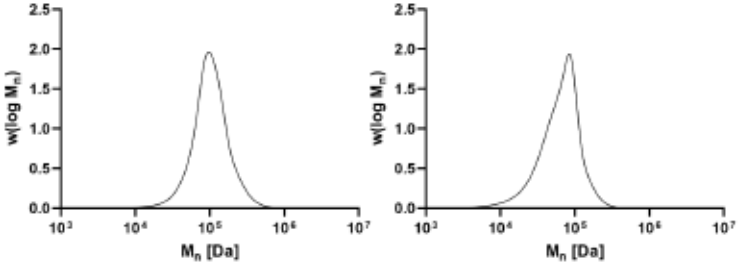

Figure S8. Molar mass distributions of entry **4c** (left) and **4d** (right).

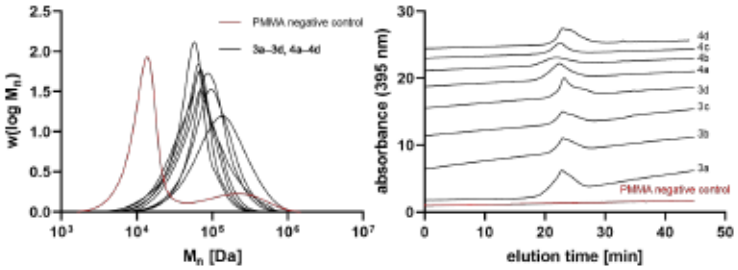

Figure S9. Molar mass distributions (left) and GPC elugrams of entries **3a–3d** and **4a–4d** (black) in comparison with a polymethyl methacrylate (PMMA) negative control (red).

Absorption Maxima, Kinetics and Photostationary States of Compounds 2–4

The photostationary states (PSS) of compounds **2a–2d** were determined by ^{1}H NMR spectroscopy (5 mM in MeCN-d_3) at 25 °C. The NMR tubes were irradiated with light at 405 nm and 525 nm wavelength for 2 min each before the NMR spectra were recorded. Absorption maxima at wavelengths $\lambda_{max}(E)$ and $\lambda_{max}(Z)$ of compounds **2–4** were determined by UV-vis spectroscopy (1 mM in THF for **2a–2d**, 10 mg/mL in THF for **3a–3d** and **4a–4d**) at 25 °C. The cuvettes were irradiated with light at 405 nm and 525 nm wavelength for 2 min each before the absorption spectra were measured. Thermal relaxation kinetics of compounds **2–4** were monitored by UV-vis spectroscopy (1 mM in THF for **2a–2d**, 10 mg/mL in THF and as drop-casted thin films for **3a–3d** and **4a–4d**) at 25 °C. After the photostationary state (PSS) at 405 nm was reached, 19 spectra were recorded in the dark in 10 min intervals. The absorptions at $\lambda_{max}(E)$ were plotted against the reaction time before the rate constant **k** and the half-life $t_{1/2}$ were determined via first-order kinetics. Kinetic measurements for every sample were conducted three times to determine the mean and the standard deviation of **k** and $t_{1/2}$.

Integrated rate law for the first-order reaction from reactant (*E*) to product (*Z*): $\ln\frac{[E]}{[E]_0} = k\,t$

With Lambert-Beer's law $A \propto [E]$ for the absorption A at λ_{max}: $\ln\frac{A-A_\infty}{A_0-A_\infty} = k\,t$

First-order reaction half-life: $t_{1/2} = \frac{\ln 2}{k}$

Table S1. *Z*/*E* ratios of initiators **2a–2d** at PSS at 405 and 525 nm wavelengths obtained from ^{1}H NMR results

Initiator	PSS (405 nm) [%] (*E*)	PSS (525 nm) [%] (*Z*)
2a	63	>99
2b	55	>99
2c	69	>99
2d	67	>99

Table S2. Maximum absorption wavelengths of the diazocine products **2a–2d**, **3a–3d** and **4a–4d** obtained from UV-vis results

Diazocine product	2a	2b	2c	2d	3a	3b	3c	3d	4a	4b	4c	4d
$\lambda_{max}(E)$ [nm]	495	483	487	491	499	487	492	495	500	488	491	494
$\lambda_{max}(Z)$ [nm]	406	400	403	407	406	403	405	408	410	401	404	407

Table S3. $E \rightarrow Z$ thermal relaxation rate constants **k** of the diazocine products **2a–2d**, **3a–3d** and **4a–4d** in THF and as solid films determined from UV-vis spectroscopy.

Diazocine product	2a–2d in THF [10^{-3} min^{-1}]	3a–3d in THF [10^{-3} min^{-1}]	3a–3d as solid film [10^{-3} min^{-1}]	4a–4d in THF [10^{-3} min^{-1}]
a	4.874±0.435	6.126±0.099	4.566±0.54	6.574±0.096
b	2.084±0.067	2.268±0.152	0.839±0.027	1.567±0.198
c	2.926±0.007	4.003±0.099	1.888±0.096	3.088±0.071
d	10.002±0.017	9.225±0.113	17.737±2.241	13.770±0.718

UV-Vis Spectra of Diazocines and Diazocine-Centered Polymers 2–4

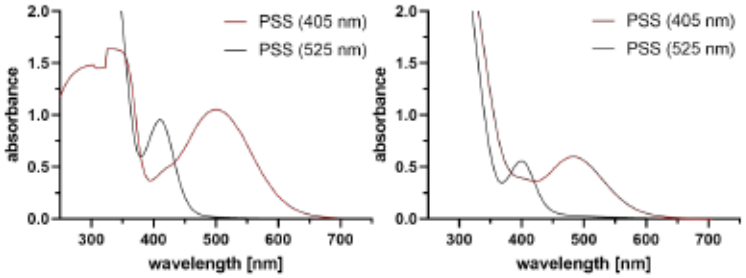

Figure S10. UV-vis spectra of compounds **2a** (left) and **2b** (right) after light irradiation at 405 (red) and 525 nm wavelength (black) in THF.

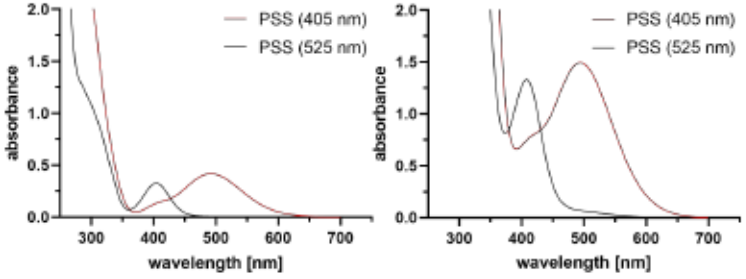

Figure S11. UV-vis spectra of compounds **2c** (left) and **2d** (right) after light irradiation at 405 (red) and 525 nm wavelength (black) in THF.

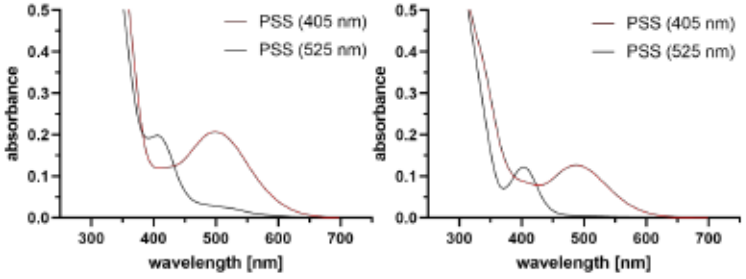

Figure S12. UV-vis spectra of compounds **3a** (left) and **3b** (right) after light irradiation at 405 (red) and 525 nm wavelength (black) in THF.

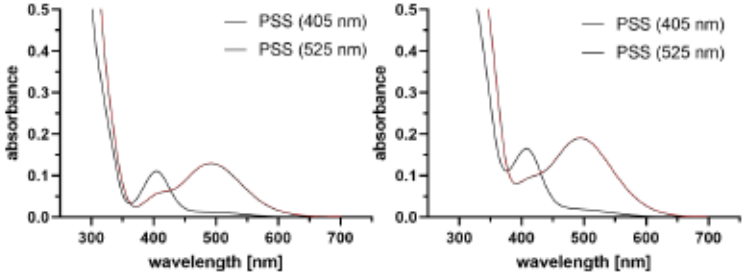

Figure S13. UV-vis spectra of compounds **3c** (left) and **3d** (right) after light irradiation at 405 (red) and 525 nm wavelength (black) in THF.

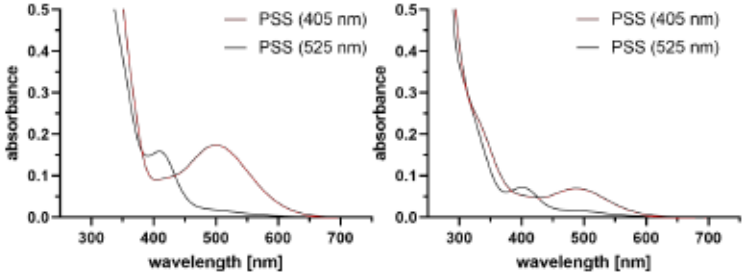

Figure S14. UV-vis spectra of compounds **4a** (left) and **4b** (right) after light irradiation at 405 (red) and 525 nm wavelength (black) in THF.

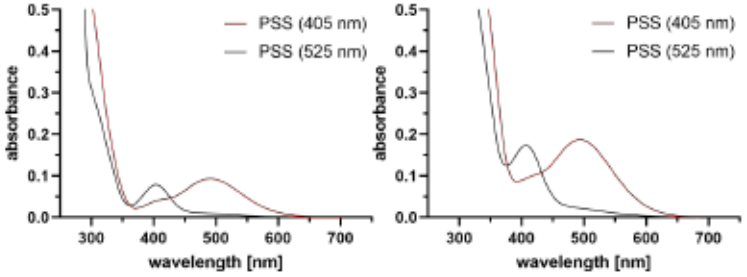

Figure S15. UV-vis spectra of compounds **4c** (left) and **4d** (right) after light irradiation at 405 (red) and 525 nm wavelength (black) in THF.

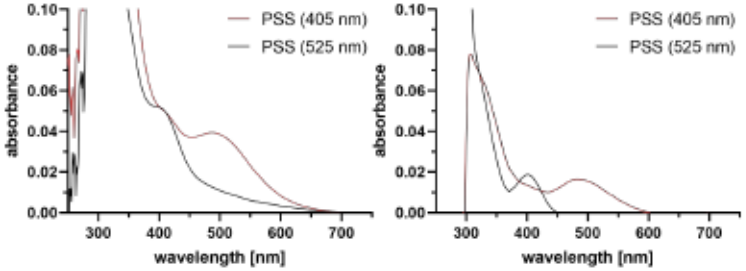

Figure S16. UV-vis spectra of compounds **3a** (left) and **3b** (right) after light irradiation at 405 (red) and 525 nm wavelength (black) as solid film.

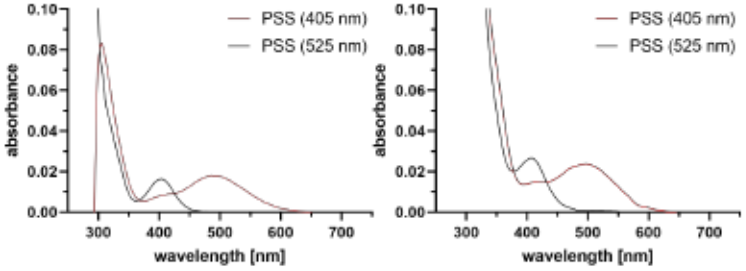

Figure S17. UV-vis spectra of compounds **3c** (left) and **3d** (right) after light irradiation at 405 (red) and 525 nm wavelength (black) as solid film.

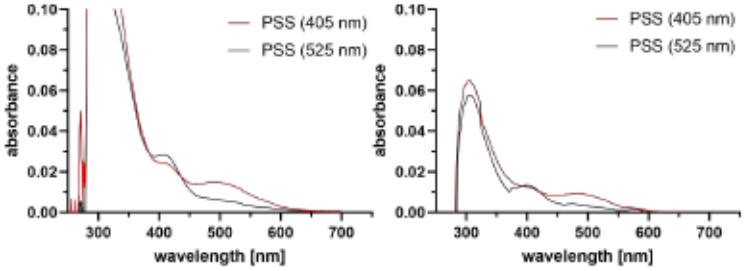

Figure S18. UV-vis spectra of compounds **4a** (left) and **4b** (right) after light irradiation at 405 (red) and 525 nm wavelength (black) as solid film.

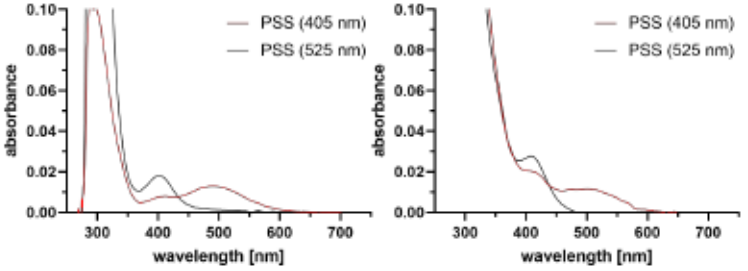

Figure S19. UV-vis spectra of compounds **4c** (left) and **4d** (right) after light irradiation at 405 (red) and 525 nm wavelength (black) as solid film.

First-Order Kinetic Plots of Diazocine-Containing Products 2–4

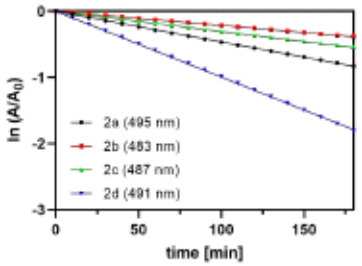

Figure S20. First-order thermal relaxation kinetic plots of compounds **2a–2d** from PSS (405 nm) at $\lambda_{max}(E)$ in THF.

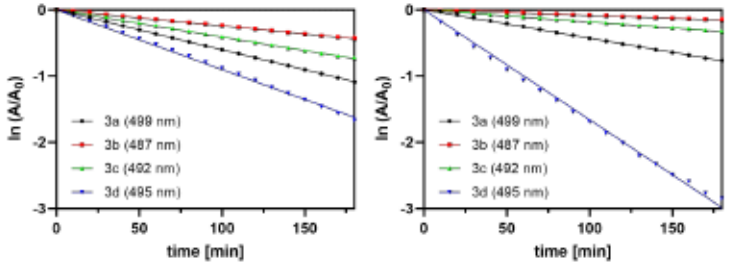

Figure S21. First-order thermal relaxation kinetic plots of compounds **3a–3d** (left) from the PSS (405 nm) at $\lambda_{max}(E)$ in THF (left) and as thin films (right).

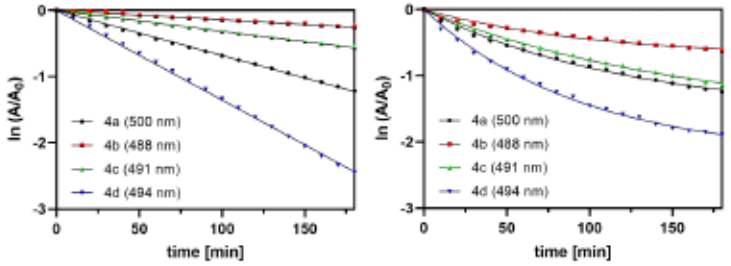

Figure S22. First-order thermal relaxation kinetic plots of compounds **4a–4d** (left) from the PSS (405 nm) at $\lambda_{max}(E)$ in THF (left) and as thin films (right).

^{1}H and $^{13}C\{^{1}H\}$ NMR Spectra of the Products

(*Z*)-*N*,*N*'-(11,12-Dihydrodibenzo[*c*,*g*][1,2]diazocine-2,3-diyl)bis(2-bromo-2-methylpropanamide) (2a)

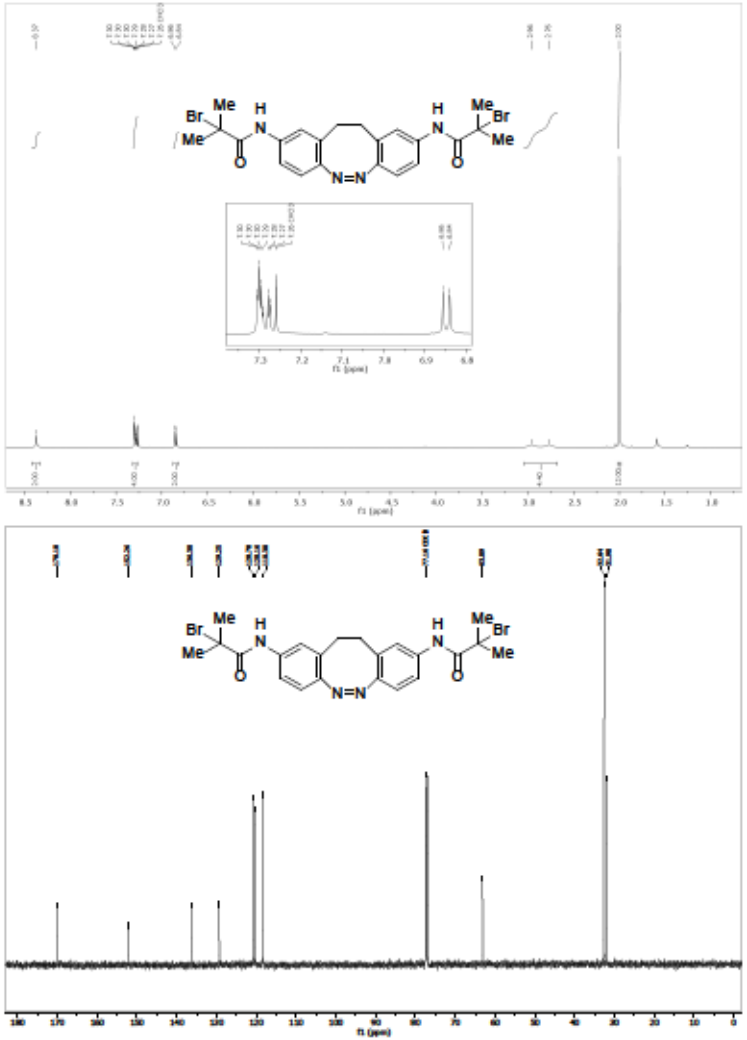

(*Z*)-*N*,*N*'-(11,12-Dihydrodibenzo[*c*,*g*][1,2]diazocine-3,8-diyl)bis(2-bromo-2-methylpropanamide) (2b)

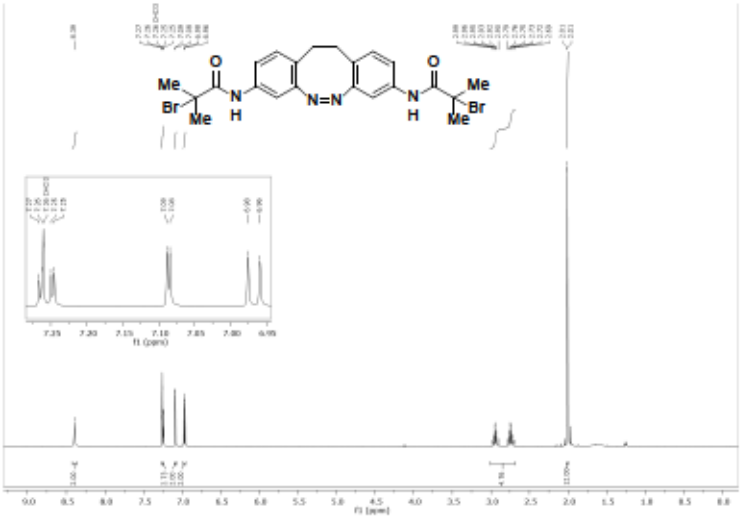

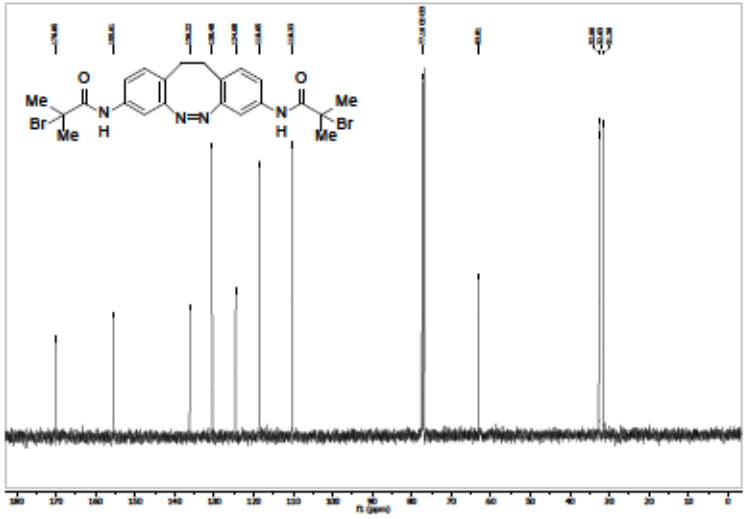

(*Z*)-(11,12-Dihydrodibenzo[*c*,*g*][1,2]diazocine-2,9-diyl)bis(methylene) bis(2-bromo-2-methylpropanoate) (2c)

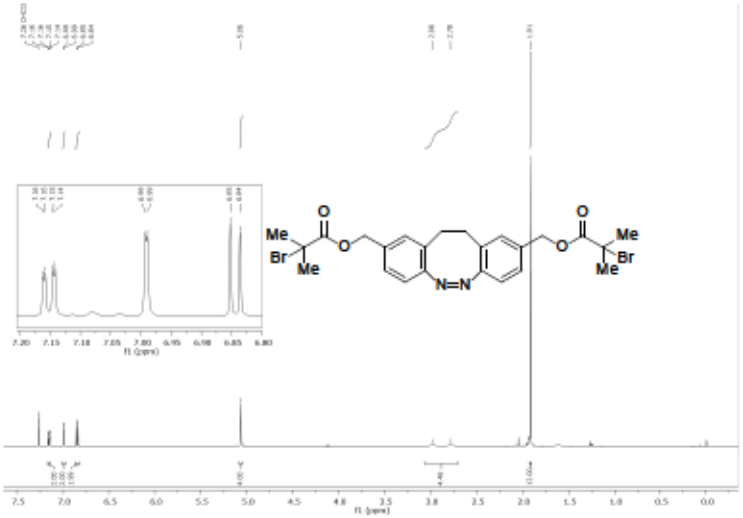

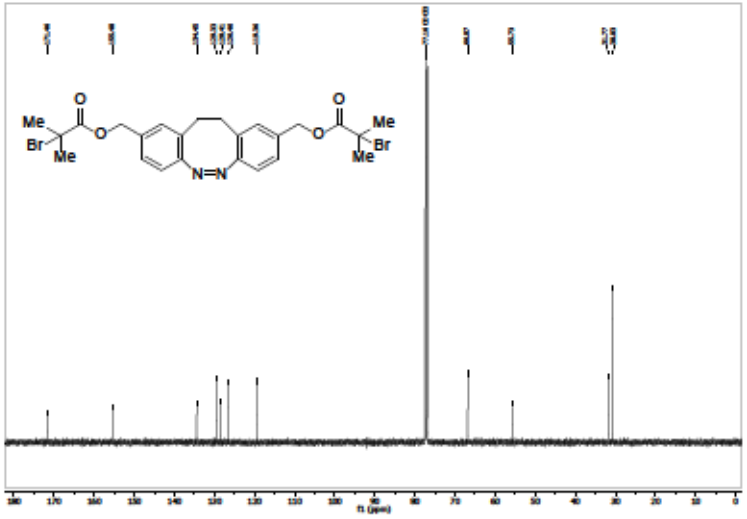

2-Bromo-5-butoxybenzaldehyde (6)

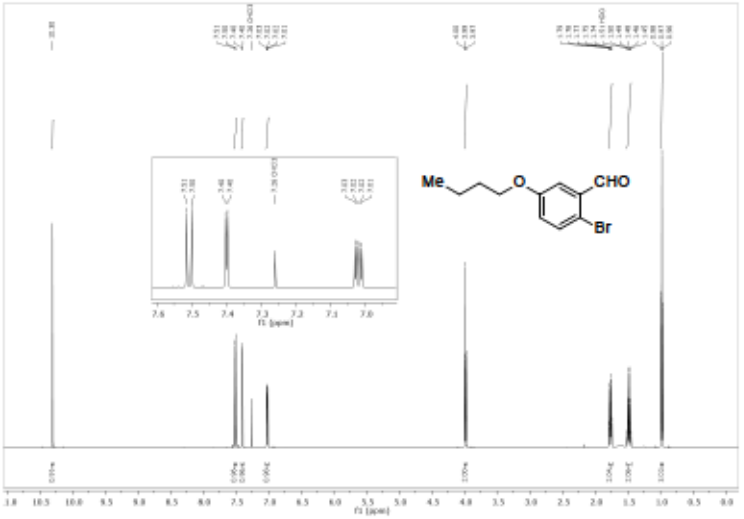

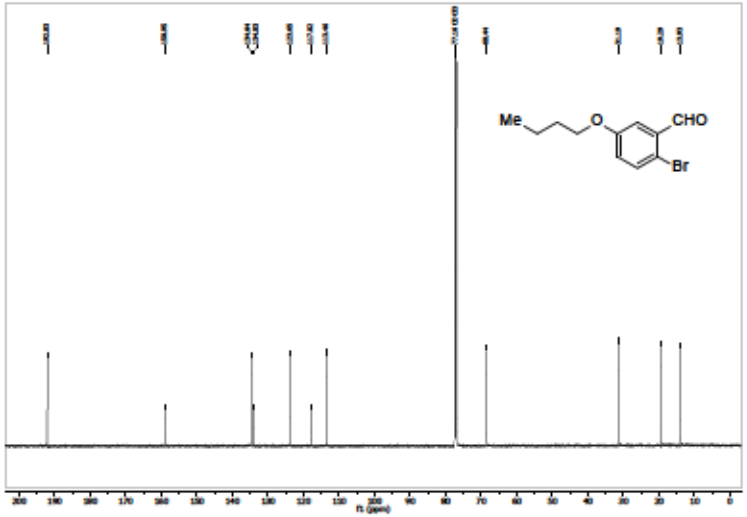

Methyl (Z)-4-bromo-3-(2-bromo-5-butoxystyryl)benzoate (7)

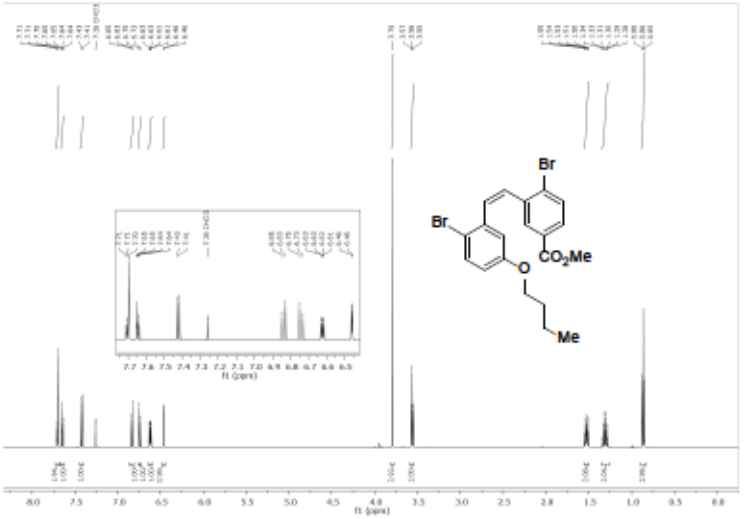

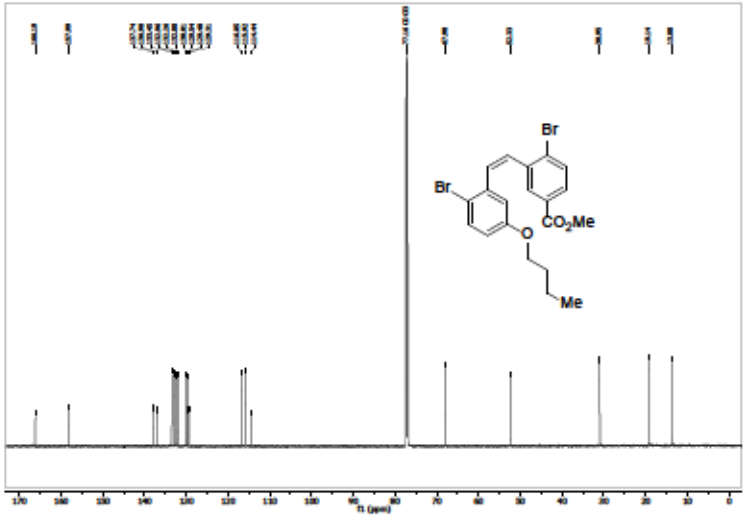

5,6-Di-tert-butyl 2-methyl 9-butoxy-11,12-dihydrodibenzo[c,g][1,2]diazocine-2,5,6-tricarboxylate (8)

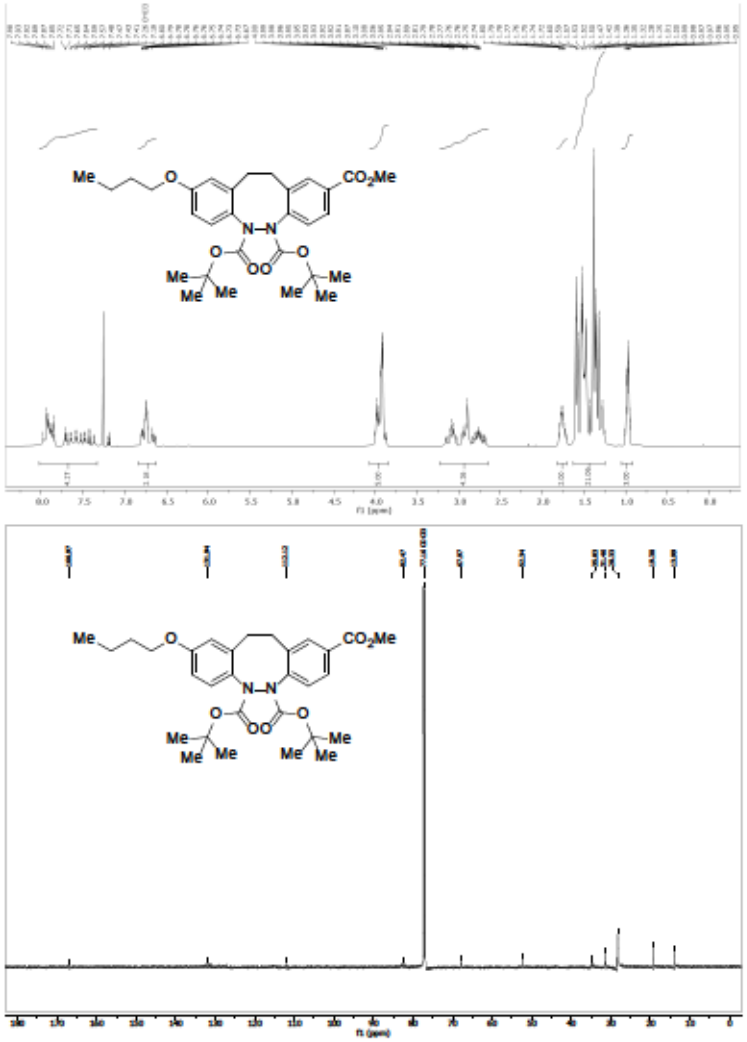

Methyl (Z)-9-butoxy-11,12-dihydrodibenzo[c,g][1,2]diazocine-2-carboxylate (9)

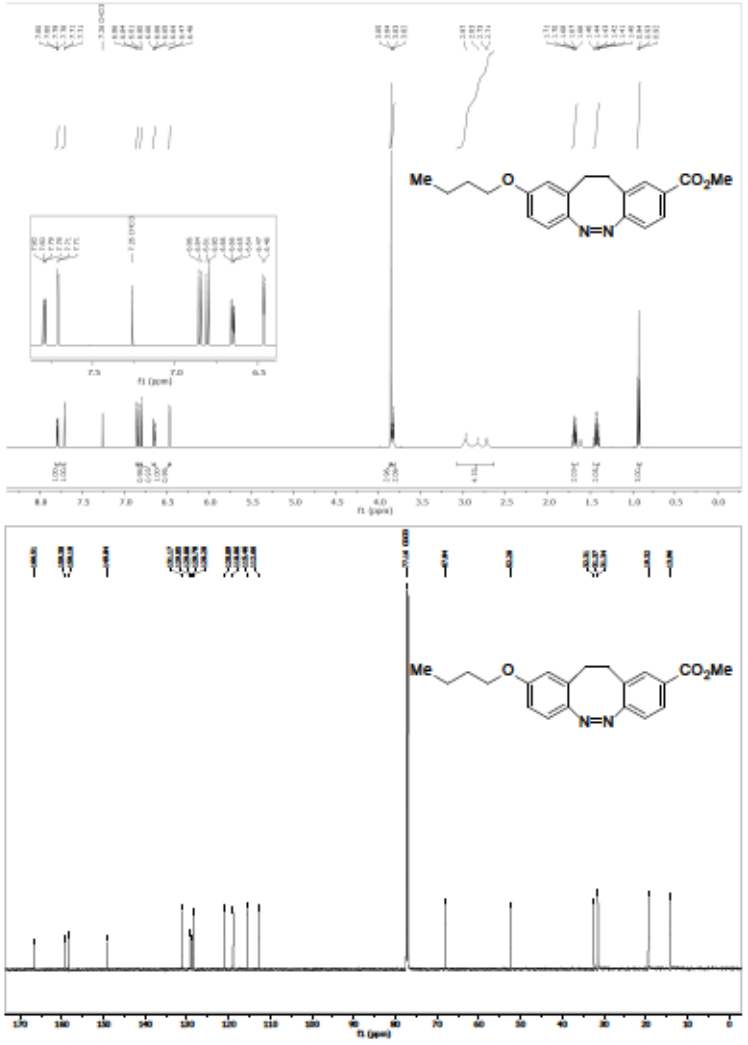

(Z)-(9-Butoxy-11,12-dihydrodibenzo[c,g][1,2]diazocin-2-yl)methanol (1d)

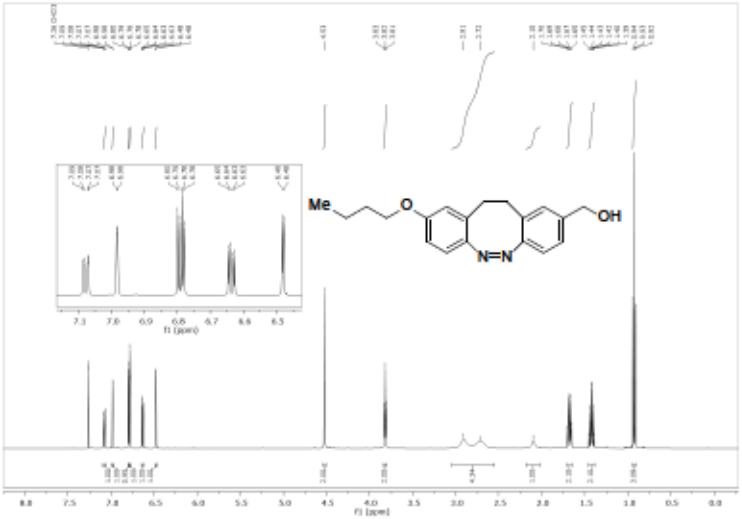

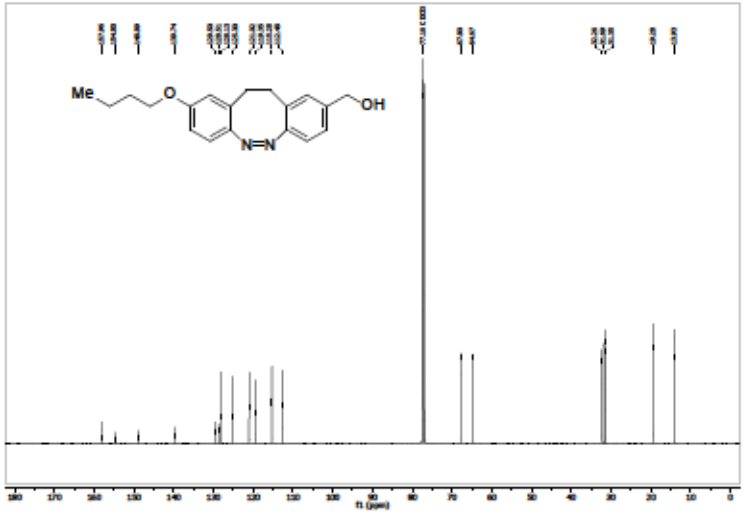

(Z)-(9-Butoxy-11,12-dihydrodibenzo[c,g][1,2]diazocin-2-yl)methyl 2-bromo-2-methylpropanoate (2d)

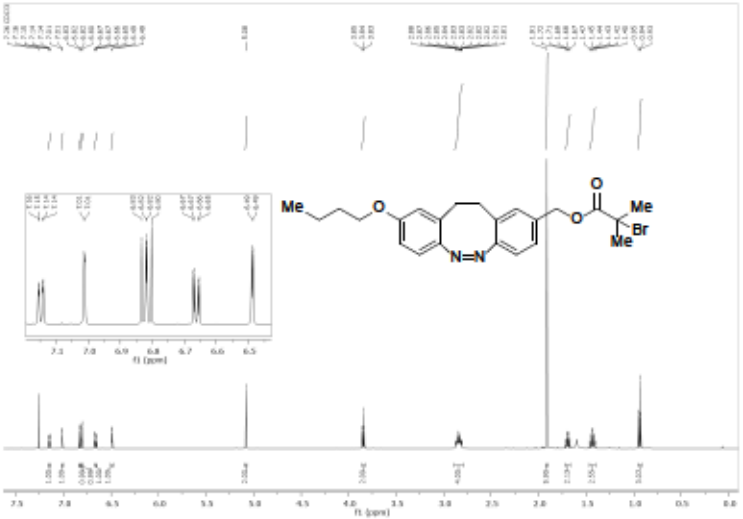

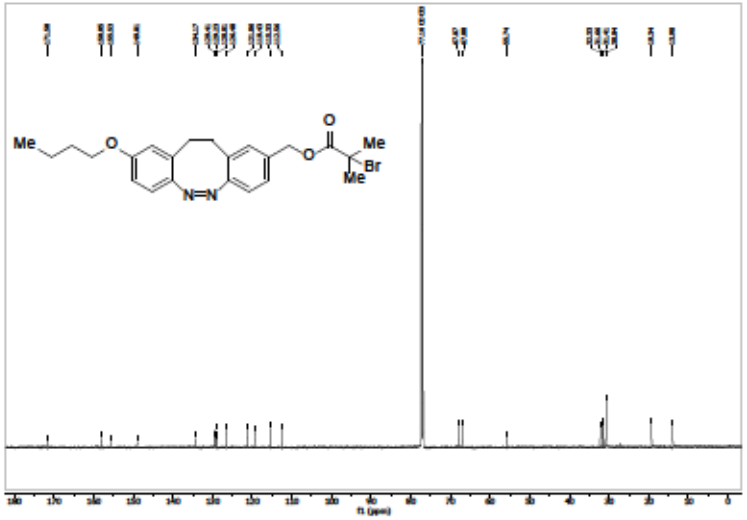

Tris[2-(dimethylamino)ethyl]amine (10)

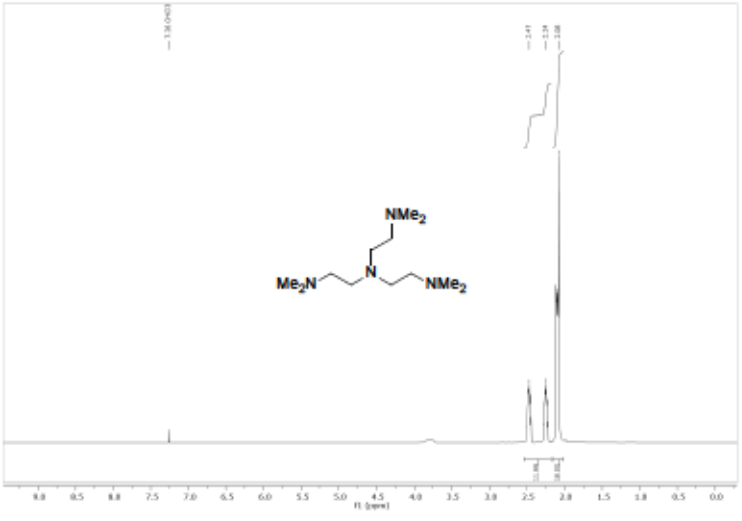

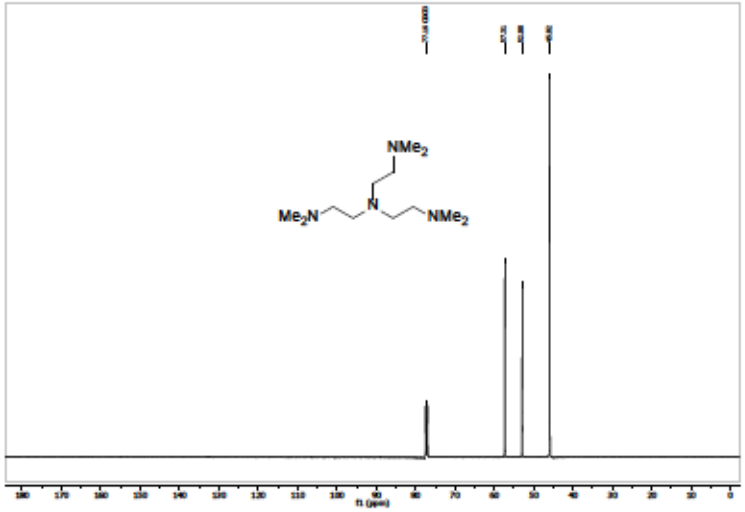

Polymethyl acrylate (3a)

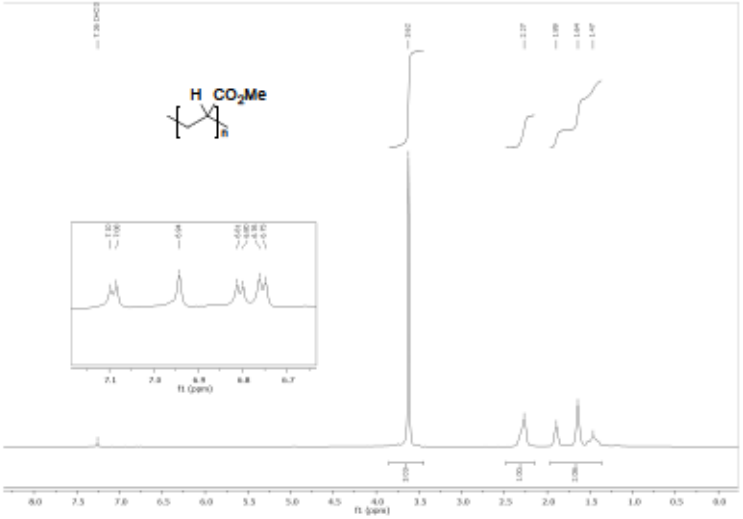

Polymethyl acrylate (3b)

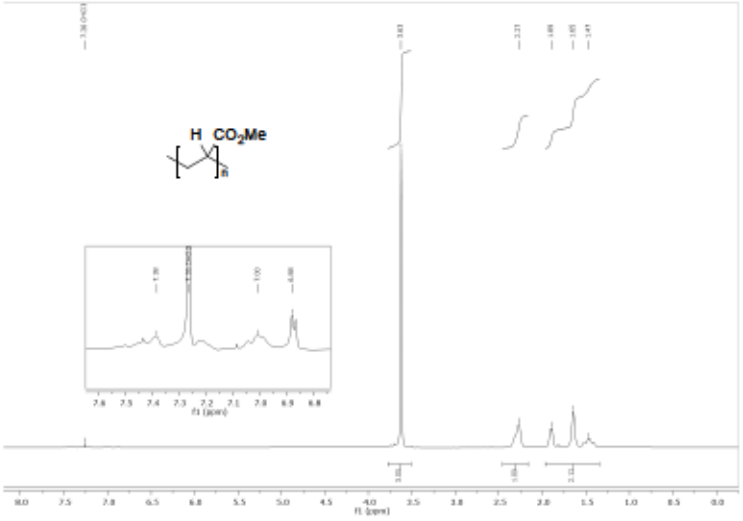

Polymethyl acrylate (3c)

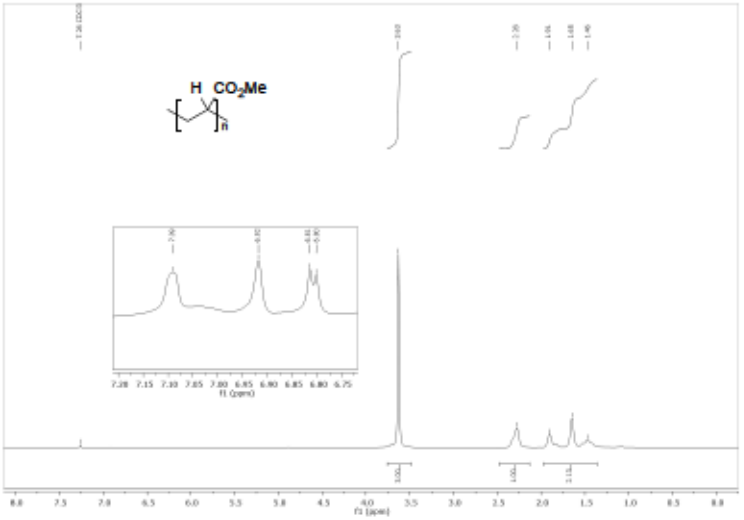

Polymethyl acrylate (3d)

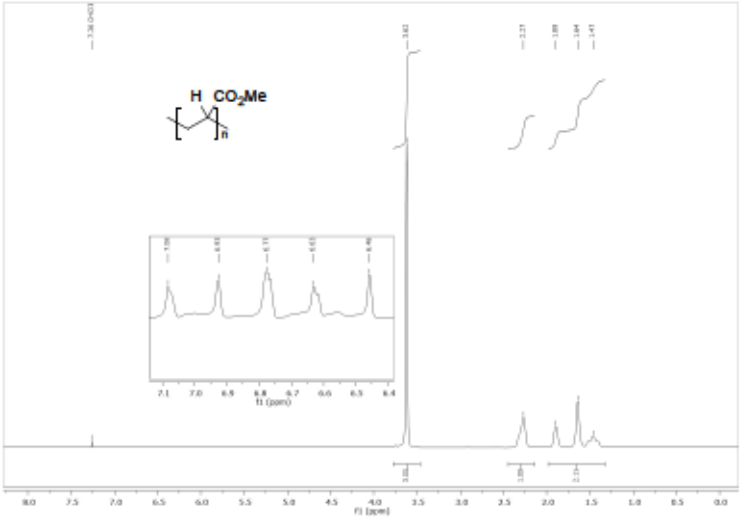

Polymethyl methacrylate (4a)

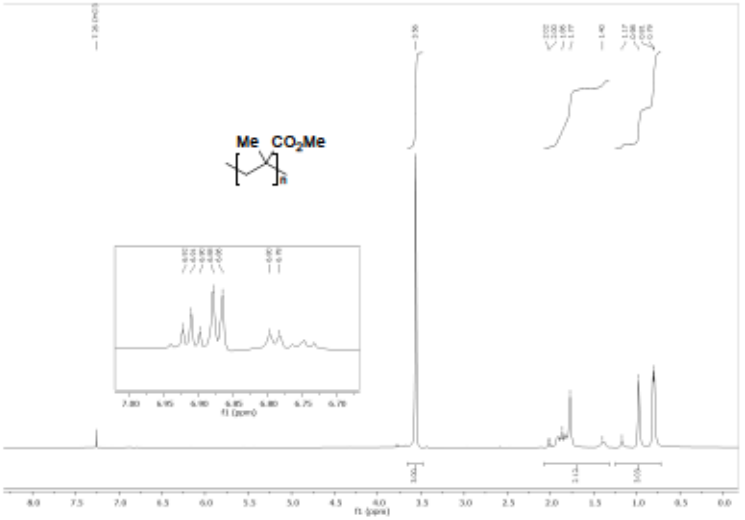

Polymethyl methacrylate (4b)

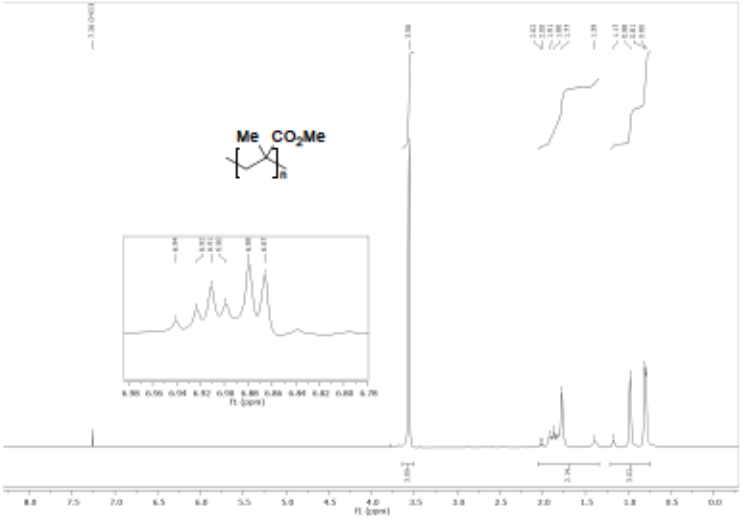

Polymethyl methacrylate (4c)

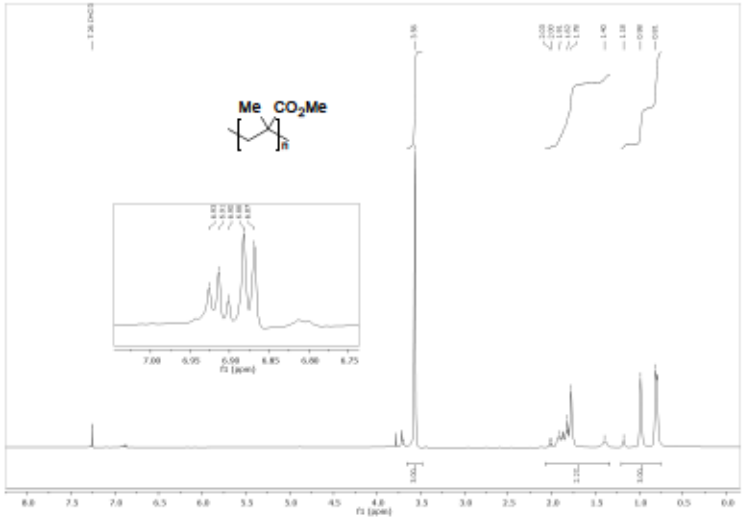

Polymethyl methacrylate (4d)

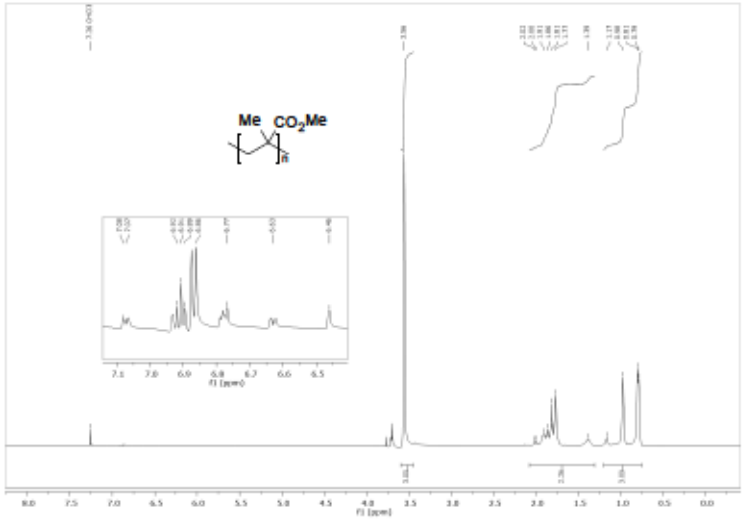

^{1}H NMR Spectra of **2a**–**2d** in the PSS at 405 and 525 nm

(*Z*)-*N*,*N*′-(11,12-Dihydrodibenzo[*c*,*g*][1,2]diazocine-2,9-diyl)bis(2-bromo-2-methylpropanamide) (2a)

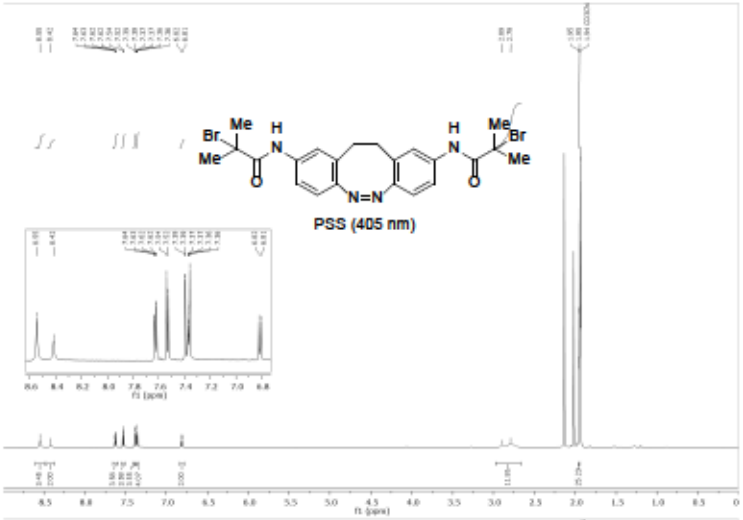

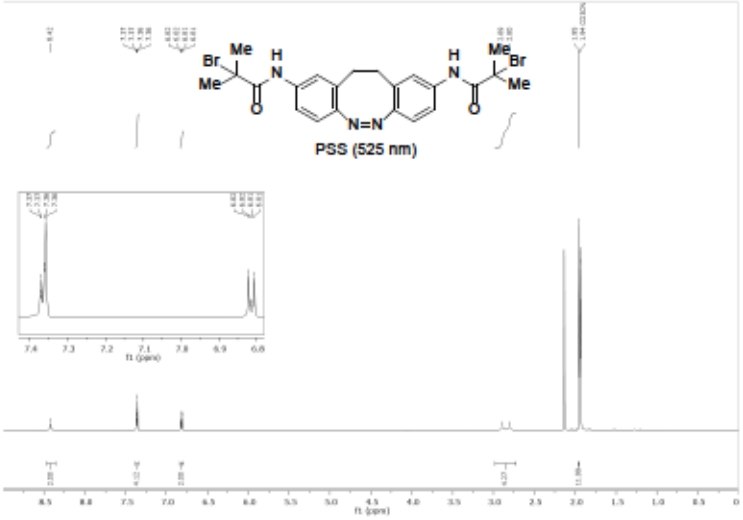

(*Z*)-*N*,*N*'-(11,12-Dihydrodibenzo[*c*,*g*][1,2]diazocine-3,8-diyl)bis(2-bromo-2-methylpropanamide) (2b)

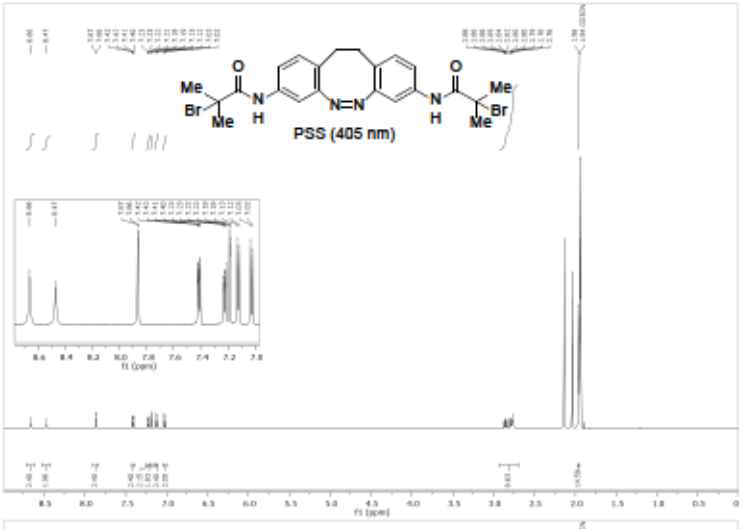

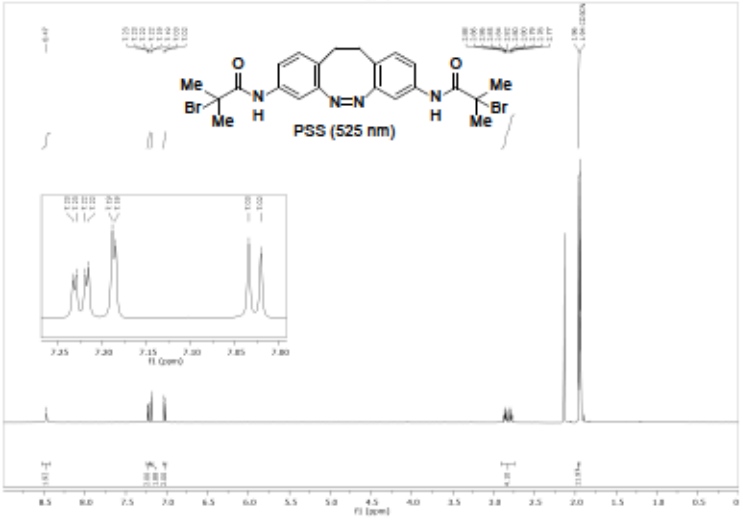

(*Z*)-(11,12-Dihydrodibenzo[*c*,*g*][1,2]diazocine-2,9-diyl)bis(methylene) bis(2-bromo-2-methylpropanoate) (2c)

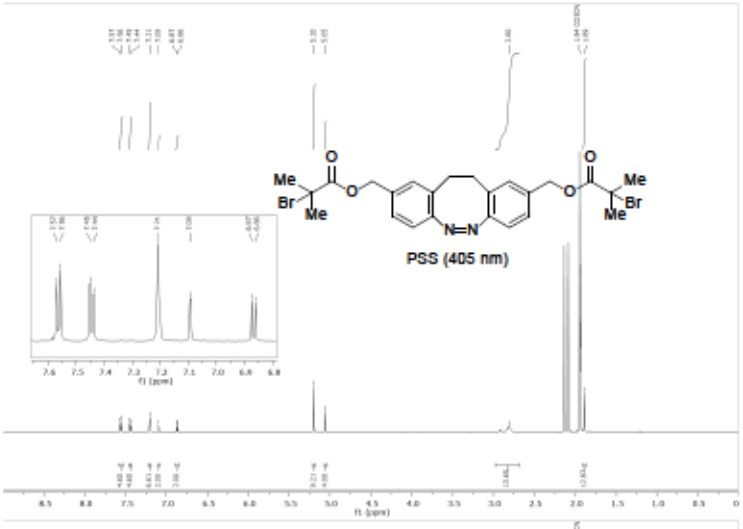

(*Z*)-(9-Butoxy-11,12-dihydrodibenzo[*c*,*g*][1,2]diazocin-2-yl)methyl 2-bromo-2-methylpropanoate (2d)

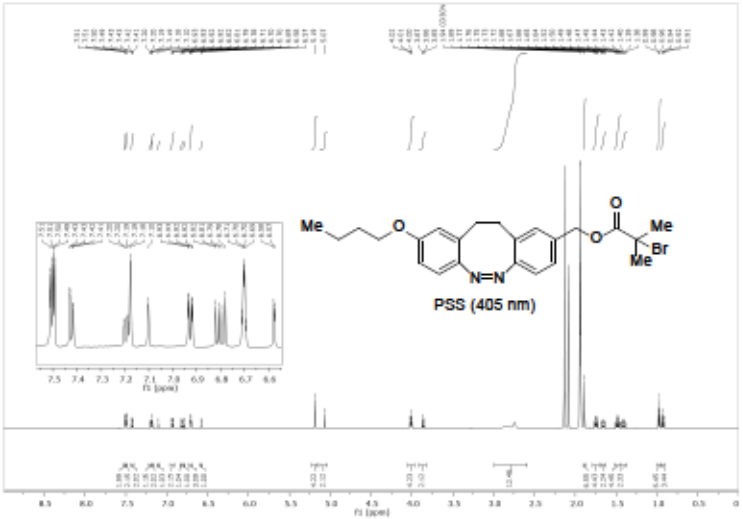

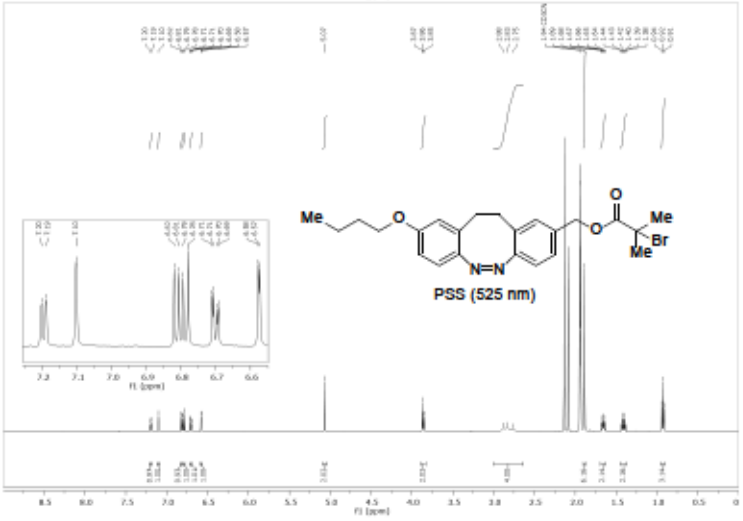

References

(1) Li, S.; Eleya, N.; Staubitz, A. *Org. Lett.* **2020**, *22*, 1624–1627.

(2) Ciampolini, M.; Nardi, N. *Inorg. Chem.* **1966**, *5*, 41–44.

polymers

MDPI

Supporting Information for

Facile Synthesis of a Light Switchable Polymers with Diazocine Units in the Main Chain

- Experimental Data -

Shuo Li [1,2], Katrin Bamberg [3], Yuzhou Lu [1,2], Frank D. Sönnichsen [3] and Anne Staubitz [1,2,*]

[1]University of Bremen, Institute for Organic and Analytical Chemistry Leobener Str. 7, 28359 Bremen, Germany
[2]University of Bremen, Center for Materials and Processes, MAPEX Bibliothekstr. 1, 28359 Bremen, Germany
[3]Kiel University, Otto-Diels-Institute for Organic Chemistry, Otto-Hahn-Platz 4, D-24098 Kiel, Germany
*staubitz@uni-bremen.de

Table of Contents

The use of abbreviations follows the conventions from the ACS Style guide [1]:

1. *The ACS Style Guide: Effective Communication of Scientific Information*; Coghill, A.M., Garson, L.R., American Chemical Society, Eds.; 3rd ed.; American Chemical Society ; Oxford University Press: Washington, DC : Oxford ; New York, 2006; ISBN 9780841239999 9780841274006.

UV-Vis Spectra of the Products

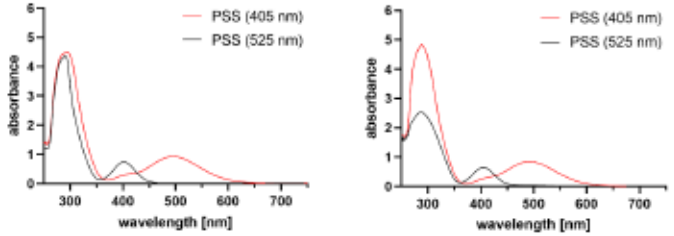

Figure S1. UV-vis spectra of compounds **M1** (left) and **M2** (right) after light irradiation at 405 nm (red) and 525 nm wavelength (black) at a concentration of 1 mM in THF.

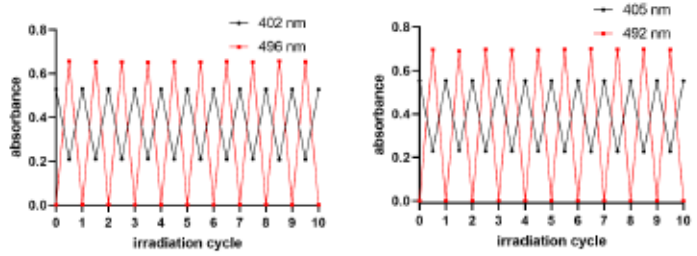

Figure S2. Cyclic UV-vis measurements of polymers **P1** (left) and **P2** (right) after light irradiation at 405 nm and 525 nm wavelength monitoring the absorption at $\lambda_{max}(Z)$ (black) and $\lambda_{max}(E)$ (red) at a concentration of 0.5 mg/mL in THF.

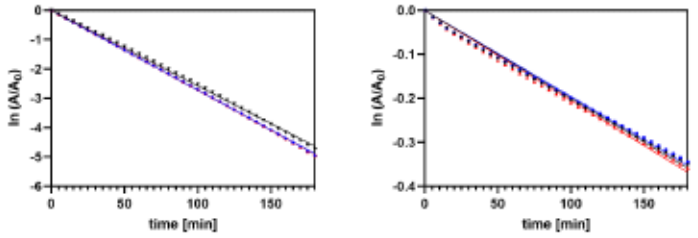

Figure S3. First-order thermal relaxation kinetics of **M1** (left) and **M2** (right) from PSS (405 nm) wavelength at $\lambda_{max}(E)$ at a concentration of 3 mg/mL in THF.

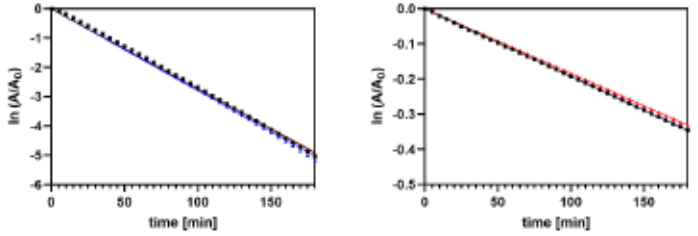

Figure S4. First-order thermal relaxation kinetics of **P1** (left) and **P2** (right) from PSS (405 nm) wavelength at $\lambda_{max}(E)$ at a concentration of 3 mg/mL in THF.

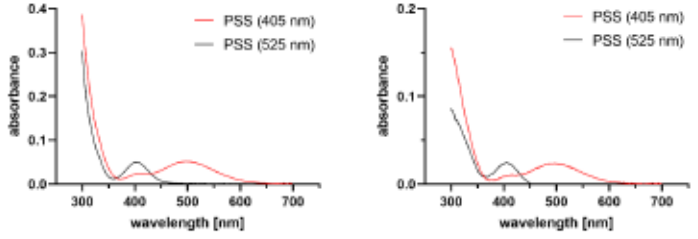

Figure S5. UV-vis spectra of polymers **P1** (left) and **P2** (right) after light irradiation at 405 (red) and 525 nm wavelength (black) as spin-coated thin films.

DSC Plots of Polymers P1 and P2

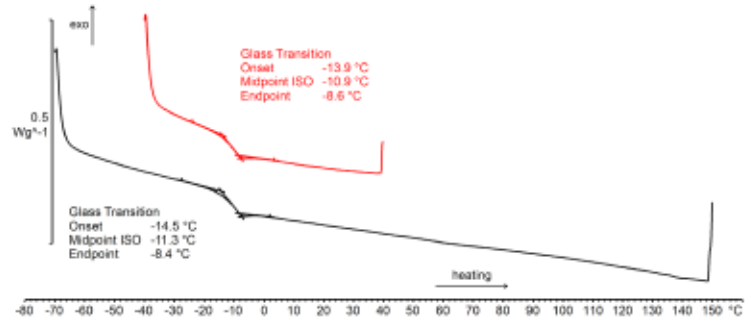

Figure S6. DSC plots of polymer **P1** at PSS (525 nm) (black) and PSS (405 nm) (red) indicating the glass transition temperature T_g. The DSC measurements were cycled between -70 to 150 ° and -40 to 40 °C, respectively.

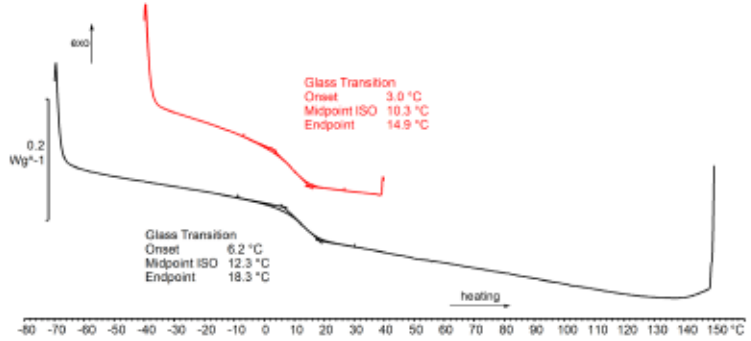

Figure S7. DSC plots of polymer **P2** at PSS (525 nm) (black) and PSS (405 nm) (red) indicating the glass transition temperature Tg. The DSC measurements were cycled between and -70 to 150 °C and -40 to 40 °C, respectively.

^{1}H DOSY NMR Correction Factors and Fitting Graphs

Bis(9-(acryloyloxy)nonyl) (*Z*)-11,12-dihydrodibenzo[*c*,*g*][1,2]diazocine-2,9-dicarboxylate (M1)

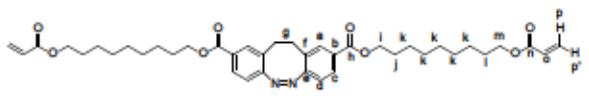

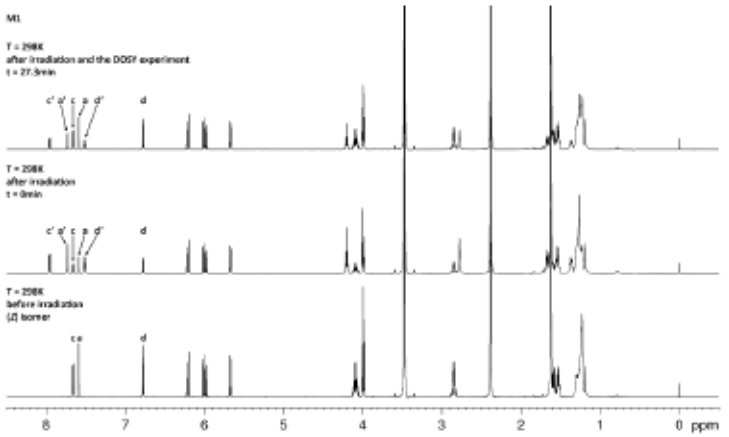

Figure S8. Stacked plot of the 1D ^{1}H NMR spectra of **M1** from 8.5 to -0.5 ppm at T = 298 K. Bottom: before irradiation, centre: after irradiation at t = 0 min and top: after irradiation and the DOSY experiment at t = 27.3 min.

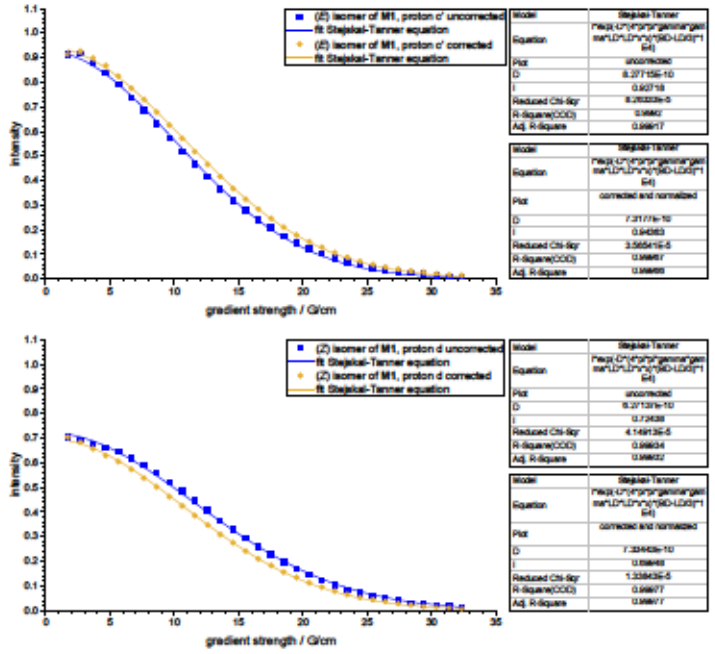

Figure S9. Example graphs are presented to highlight the effect of data intensity correction of one peak of the (E) (top) and (Z) isomer (bottom) after light irradiation at 405 nm wavelength of **M1**. Fit statistics are shown for the individual fits of these resonances.

Poly[3,3′-hexane-1,6-diylbis(sulfanediyl) bis(propionyloxynonyl) (*Z*)-(11,12-dihydrodibenzo[*c*,*g*][1,2]diazocine-2,9-diacarboxylate] (P1)

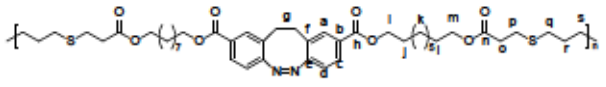

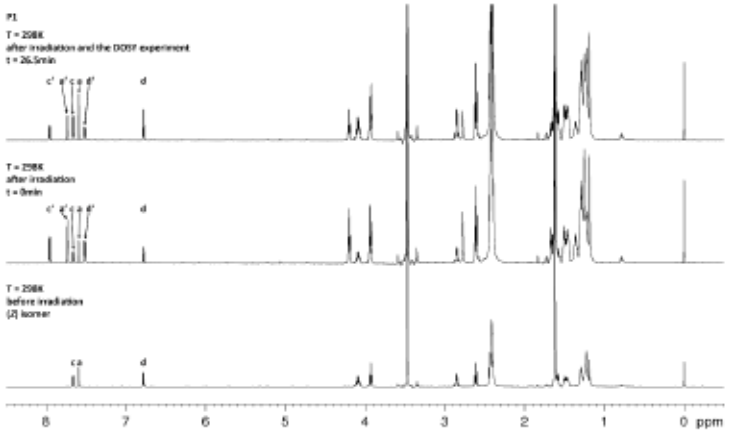

Figure S10. Stacked plot of the 1D ^{1}H NMR spectra of polymer P1 from 8.5 to -0.5 ppm at T = 298 K. Bottom: before irradiation, centre: after irradiation at t = 0 min and top: after irradiation and the DOSY experiment at t = 26.5 min.

Aromatic proton assignments of **M1, P1, M2, P2** for ^{1}H DOSY NMR:

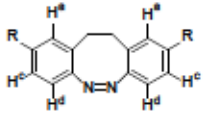

Table S1. Corrected diffusion coefficients D [10^{-6} cm^2 s^{-1}] of the (Z) and (E) isomers of **M1, P1, M2, P2** after light irradiation at 405 and 525 nm wavelength from ^{1}H DOSY NMR measurements.

		PSS (405 nm)			PSS (525 nm)	
	Z (average)	*Z* (c; a; d)	*E* (average)	*E* (c'; a'; d')	*Z* (average)	*Z* (c; a; d)
M1[1]	7.45±0.14	7.60±0.04 7.43±0.05 7.33±0.04	7.39±0.07	7.32±0.04 7.41±0.06 7.45±0.03	7.46±0.11	7.58±0.03 7.42±0.02 7.37±0.03
P1[2]	1.90±0.03	1.90±0.03 1.87±0.03 1.92±0.03	1.91±0.02	1.89±0.03 1.93±0.03 1.91±0.03	1.96±0.05	2.00±0.03 1.91±0.03 1.98±0.03
M2	10.4±0.16	10.3±0.26 10.3±0.10 10.6±0.06	11.0±0.26	11.3±0.04 10.8±0.04 10.8±0.11	10.6±0.09	10.7±0.05 10.5±0.04 10.7±0.06
P2	2.72±0.21	2.91±0.03 2.74±0.03 2.49±0.02	2.75±0.07	2.79±0.03 2.79±0.03 2.67±0.03	2.84±0.08	2.84±0.02 2.93±0.03 2.76±0.03

[1]Amount of (*E*) at t = 0: 68.5%; f = 22.93 min. [2]Amount of (*E*) at t = 0: 67.2%; f = 17.20 min.

^{1}H and $^{13}C\{^{1}H\}$ NMR Spectra of the Products

9-Hydroxynonyl acrylate

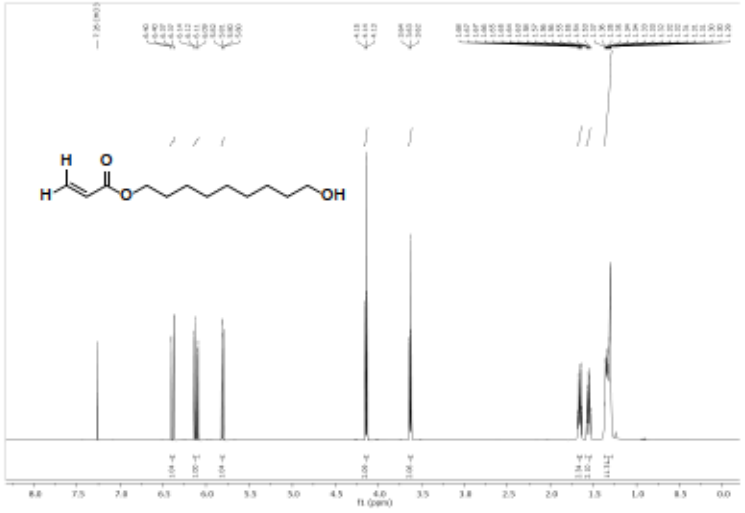

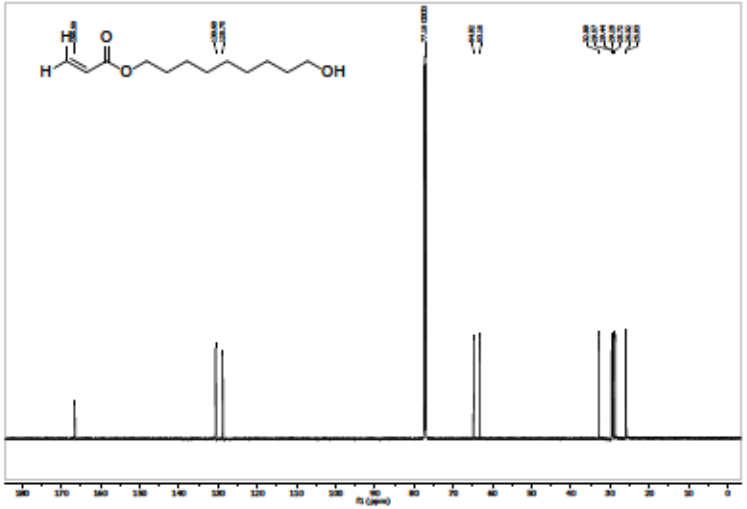

Bis(9-(acryloyloxy)nonyl) (*Z*)-11,12-dihydrodibenzo[*c*,*g*][1,2]diazocine-2,9-dicarboxylate (M1)

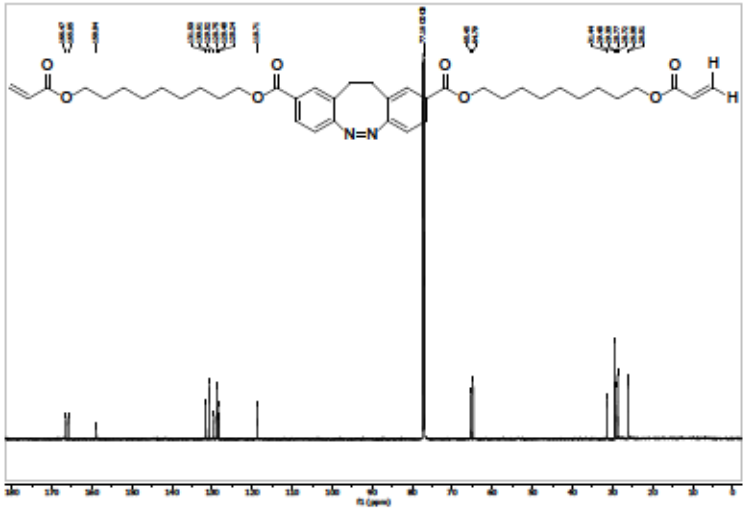

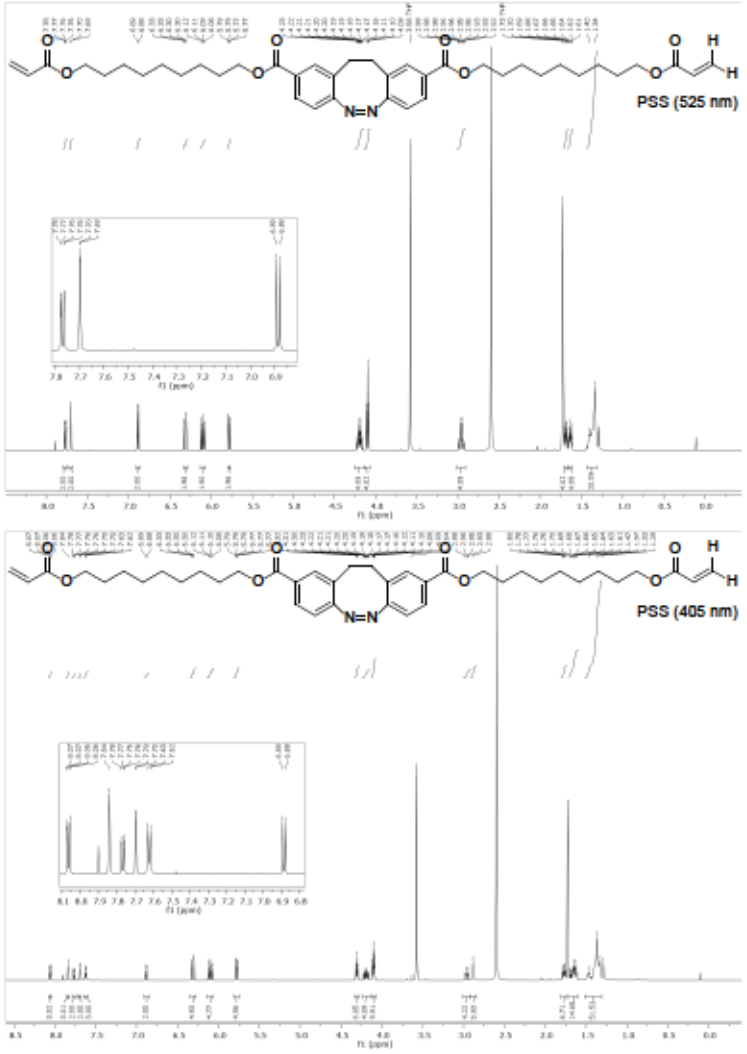

(Z)-(11,12-Dihydrodibenzo[*c*,*g*][1,2]diazocine-2,9-diyl)bis(methylene) diacrylate (M2)

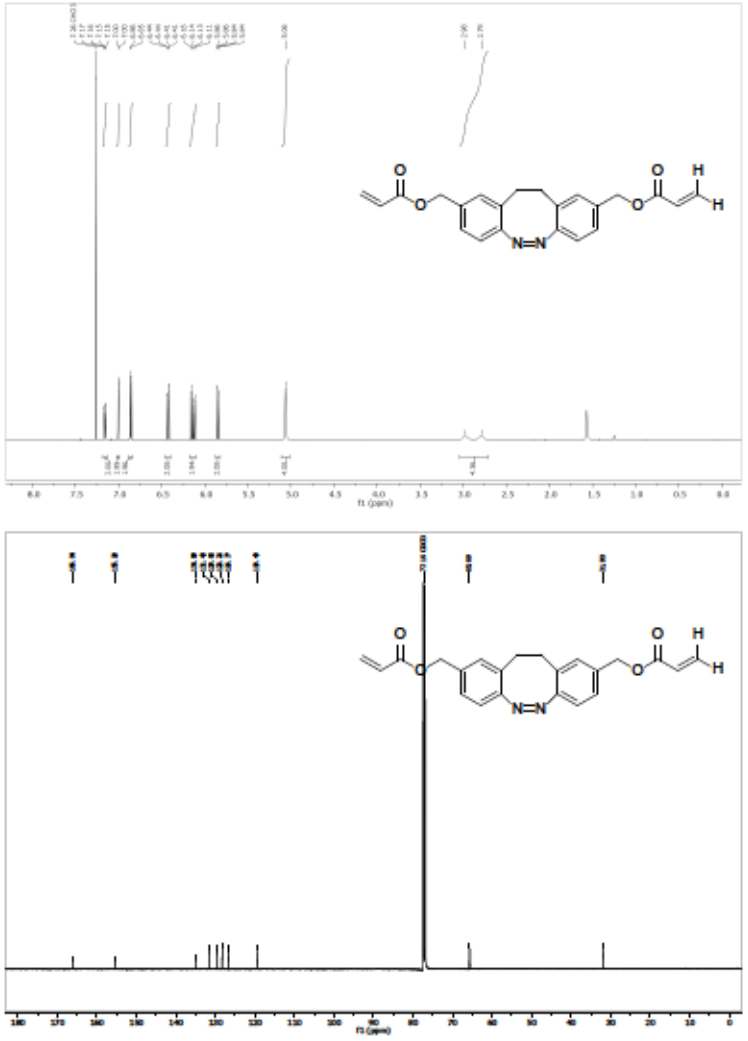

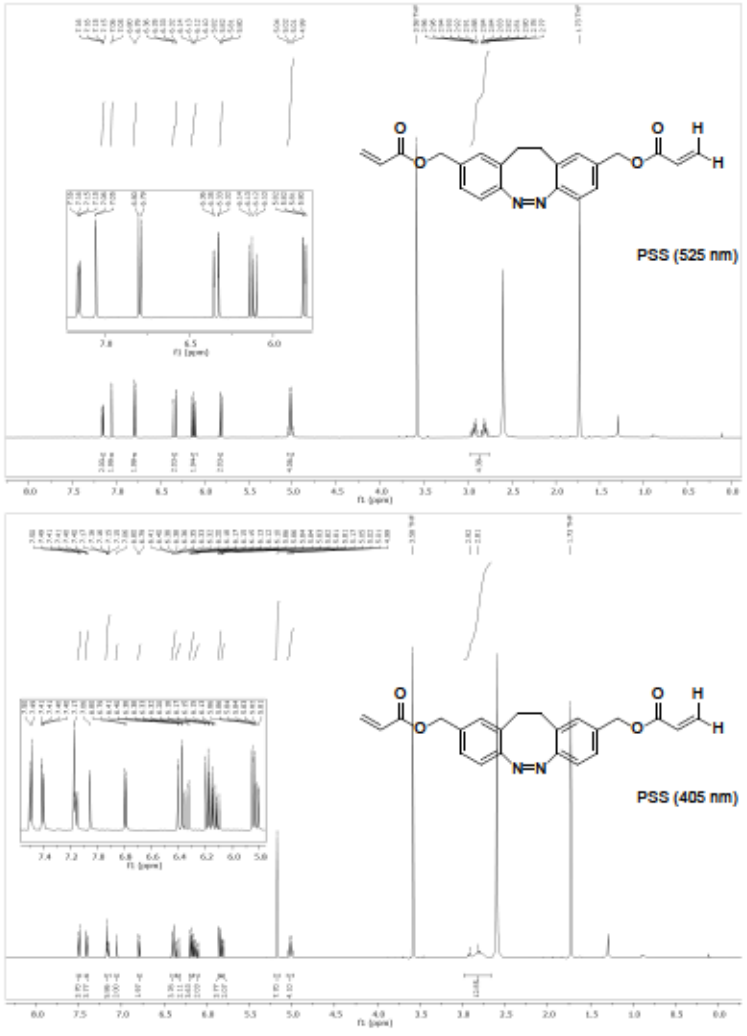

Poly[3,3′-hexane-1,6-diylbis(sulfanediyl) bis(propionyloxynonyl) (Z)-(11,12-dihydrodibenzo[*c*,*g*][1,2]diazocine-2,9-diacarboxylate] (P1)

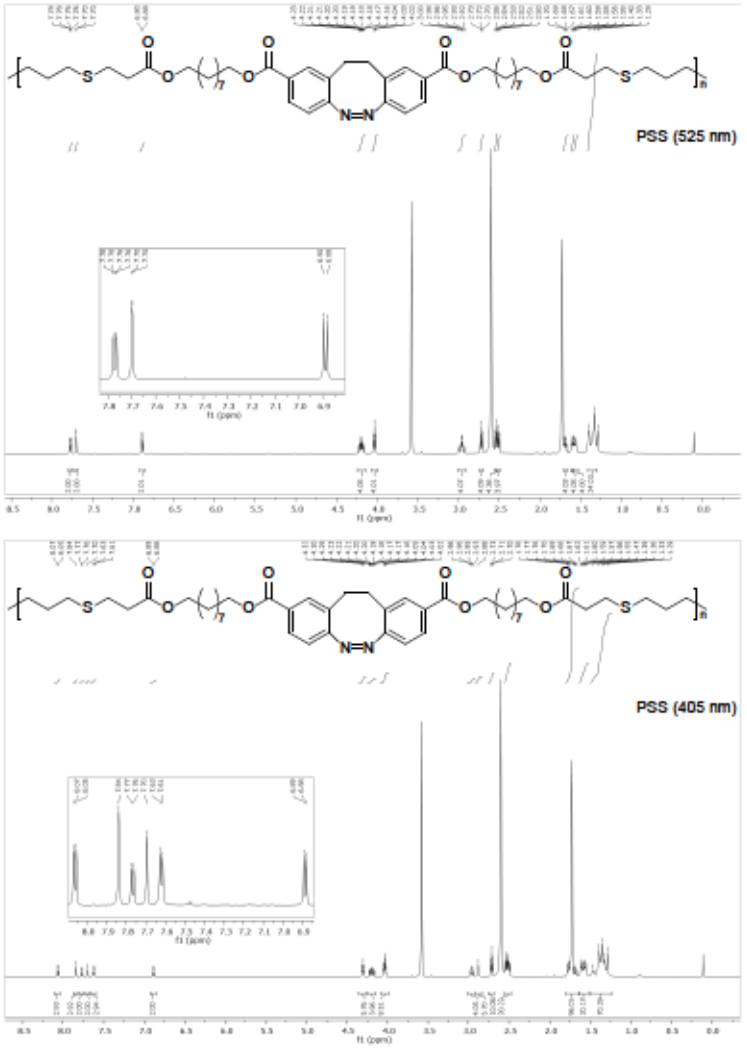

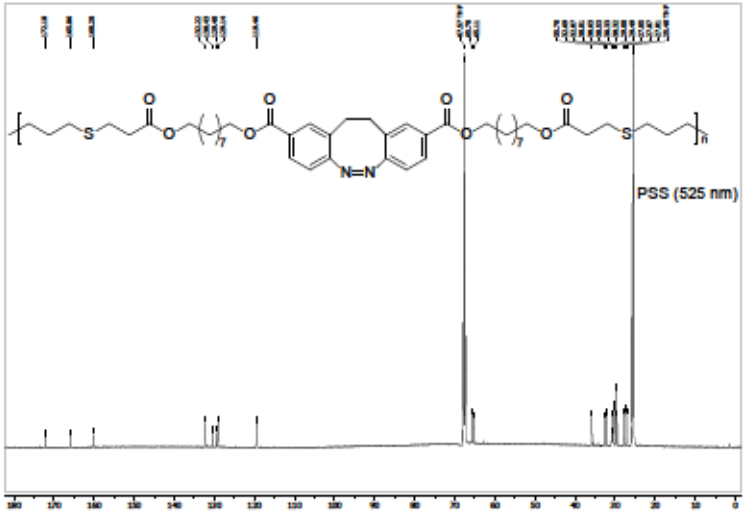

Poly[(Z)-(11,12-dihydrodibenzo[*c*,*g*][1,2]diazocine-2,9-dimethyl-3,3′-(hexane-1,6-diylbis(sulfanediyl))dipropionate] (P2)

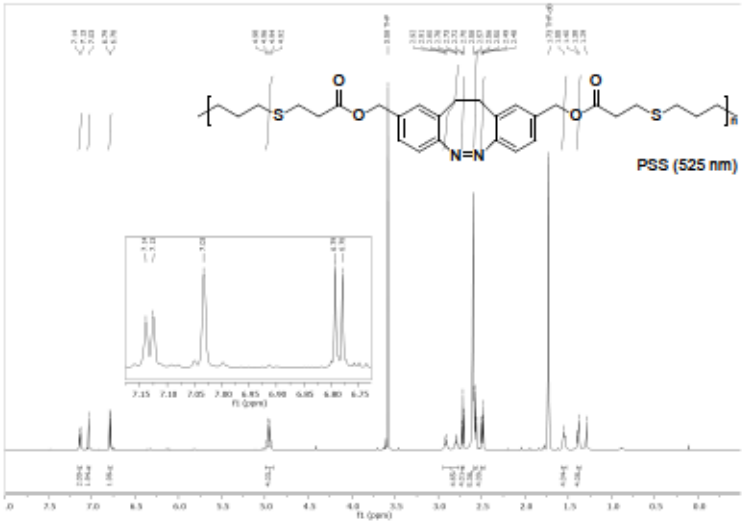

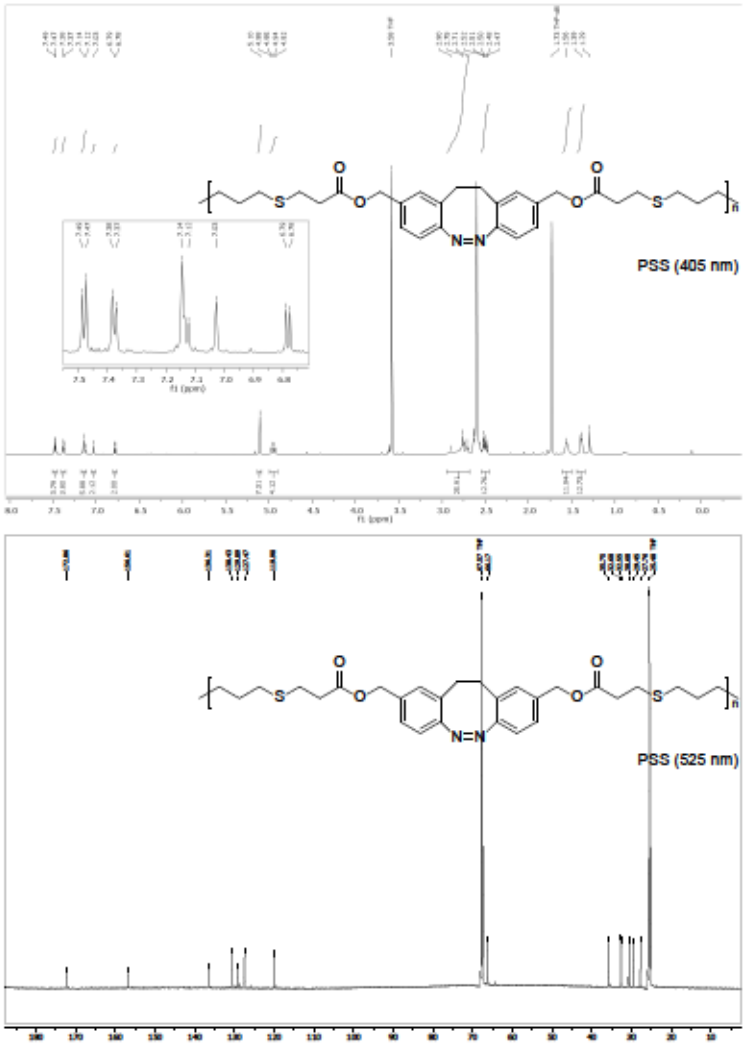

^{1}H DOSY NMR Spectra of M2 and P2

(Z)-(11,12-Dihydrodibenzo[*c*,*g*][1,2]diazocine-2,9-diyl)bis(methylene) diacrylate (M2)

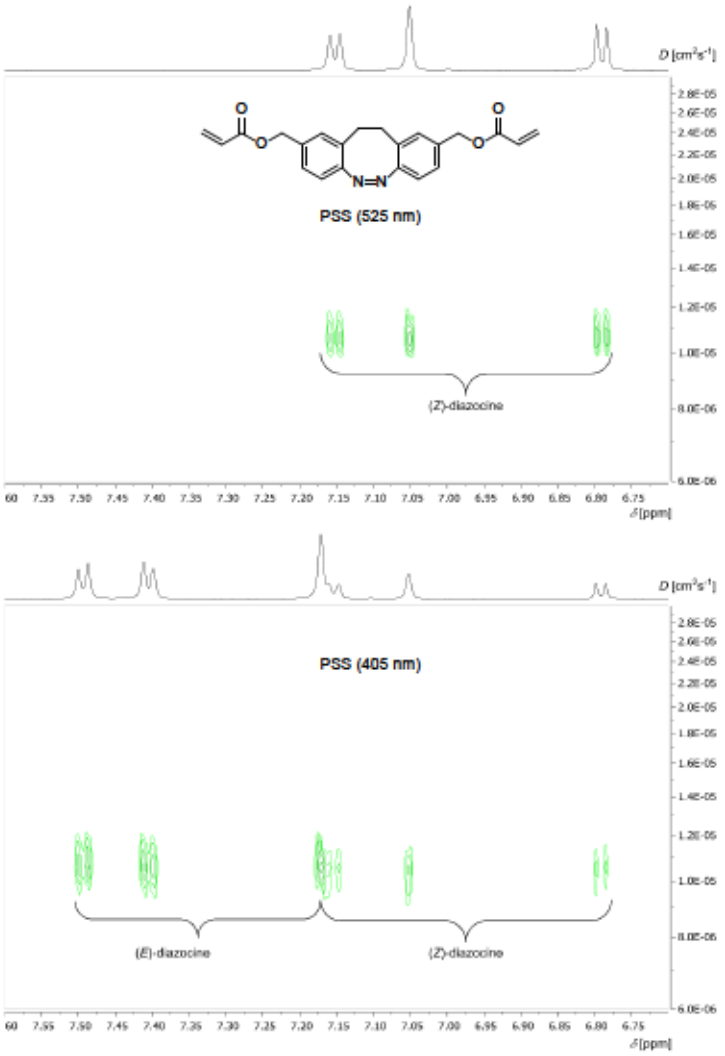

Poly[(*Z*)-(11,12-dihydrodibenzo[*c*,*g*][1,2]diazocine-2,9-dimethyl-3,3′-(hexane-1,6-diylbis(sulfanediyl))dipropionate] (P2)

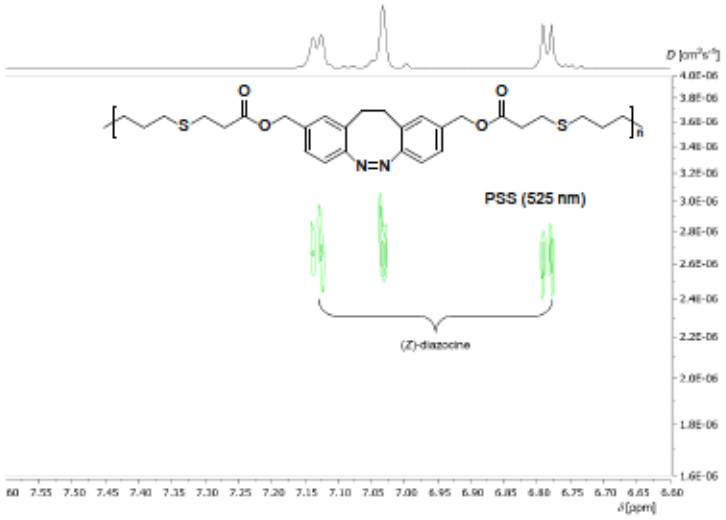

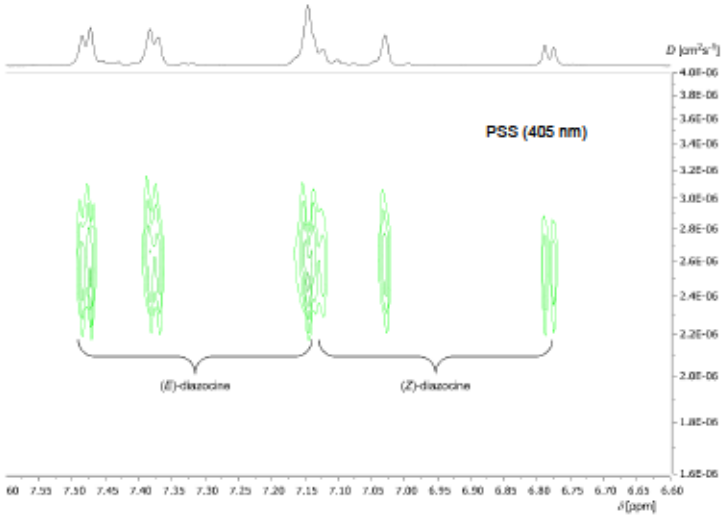

Supporting Information

for

Project 3, Part B

- Experimental Data -

General information about analytical methods, reagents and solvents were adopted from the previous projects. 4-Bromo-1-butene was purchased from Apollo. The photostationary states (PSS) of compounds **M3** and **M4** were determined by ^{1}H NMR spectroscopy (5 mM in MeCN-d_3) at 25 °C. The NMR tubes were irradiated with light at 405 nm and 525 nm wavelength for 2 min each before the NMR spectra were recorded. Absorption maxima at wavelengths λ_{max}(*E*) and λ_{max}(*Z*) of compounds **M3** and **M4** were determined by UV-vis spectroscopy (5 mM in MeCN) at 25 °C. The cuvettes were irradiated with light at 405 nm and 525 nm wavelength for 2 min each before the absorption spectra were measured. Polymer **P2a** was dissolved in THF (1 mg/mL) and the GPC elugrams were recorded at an elution flow rate of 1 mL/min. The vial was irradiated with light at 405 nm or 565 nm wavelength for 2 min before the polymer solution was injected into the GPC system.

(*Z*)-(9-Butoxy-11,12-dihydrodibenzo[*c*,*g*][1,2]diazocin-2-yl)methyl acrylate (M3)

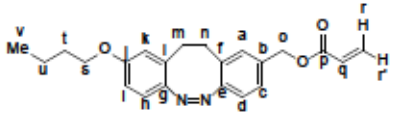

In a glovebox, compound **1d from Project II** (3.17 mmol), dry DMF (16 mL) and dry TEA (900 µL, 6.35 mmol) were added into a microwave vial. The vial was capped with a crimp cap equipped with a PTFE septum, transferred out of the glovebox and cooled down to 0 °C. Acryloyl chloride (400 µL, 4.76 mmol) was dissolved in dry DMF (5 mL) and added dropwise within 5 min. The mixture was stirred at 0 °C for 1 h, then warmed up to 20 °C and stirred for a further 24 h. The solution was diluted and extracted with ethyl acetate (50 mL), washed with H_2O (2 x 15 mL), brine (10 mL) and dried over Na_2SO_4. After filtration, the organic phase was concentrated under reduced pressure and the crude residue was purified by silica gel column chromatography (cyclohexane/ethyl acetate 70/30) to furnish product **M3** as a yellow solid (300 mg, 800 µmol, 28%).

^{1}H NMR (601 MHz, $CDCl_3$): δ = 7.15 (dd, *J* = 8.1, 1.8 Hz, 1H, H-c), 7.01 (d, *J* = 1.8 Hz, 1H, H-a), 6.83 (d, *J* = 8.0 Hz, 1H, H-d), 6.82 (d, *J* = 8.6 Hz, 1H, H-h), 6.67 (dd, *J* = 8.7, 2.6 Hz, 1H, H-l), 6.50 (d, *J* = 2.6 Hz, 1H, H-k), 6.43 (dd, *J* = 17.3, 1.4 Hz, 1H, H-r'), 6.14 (dd, *J* = 17.3, 10.4 Hz, 1H, H-q), 5.85 (dd, *J* = 10.4, 1.4 Hz, 1H, H-r'), 5.07 (s, 2H, H-o), 3.85 (t, *J* = 6.5 Hz, 2H, H-s), 3.08 – 2.62 (m, 4H, H-m, H-n), 1.74 – 1.66 (m, 2H, H-t), 1.44 (h, *J* = 7.4 Hz, 2H, H-u), 0.94 (t, *J* = 7.4 Hz, 3H, H-v) ppm.

^{13}C{^{1}H} NMR (151 MHz, $CDCl_3$): δ = 166.1 (C-p), 158.0 (C-j), 155.4 (C-e), 149.0 (C-g), 134.6 (C-b), 131.4 (C-r), 129.5 (C-a), 129.4 (C-f), 128.7 (C-l), 128.3 (C-q), 126.7 (C-c), 121.1 (C-h), 119.5 (C-d), 115.4 (C-k), 112.6 (C-l), 67.9 (C-s), 65.8 (C-o), 32.3 (C-m/n), 31.7 (C-m/n), 31.4 (C-t), 19.3 (C-u), 14.0 (C-v) ppm.

HRMS (ESI) *m/z* for $C_{22}H_{25}N_2O_3$ $[M+H]^+$: calcd 365.18597, found: 365.18575.

IR (ATR): $\tilde{\nu}$ = 2948 (w), 2870 (w), 1716 (m), 1609 (w), 1577 (w), 1486 (w), 1406 (s), 1307 (m), 1263 (s), 1177 (s), 1111 (w), 978 (m), 892 (m), 799 (s), 746 (m), 688 (w) cm^{-1}.

mp: 46 °C.

Rf: 0.53 (cyclohexane/ethyl acetate = 80/20)

2-Bromo-5-(but-3-en-1-yloxy)benzaldehyde (b1)

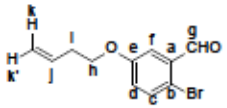

2-Bromo-5-hydroxybenzaldehyde (2.100 g, 10.45 mmol), K_2CO_3 (3.610 g, 26.12 mmol), acetonitrile (40 mL) and 4-bromo-1-butene (2.12 mL, 20.89 mmol) were added to a round-bottomed flask. The reaction mixture was stirred at 80 °C for 12 h before it was concentrated under reduced pressure. Water (30 mL) and diethyl ether (100 mL) was added and the mixture was washed with aq NaOH (2 x 30 mL, 1 M) and dried over Na_2SO_4. After filtration, the organic phase was concentrated under reduced pressure and the residue was dried in vacuum to furnish the product **b1** (1.768 g, 6.93 mmol, 66%) as a colorless oil.

^{1}H NMR (601 MHz, $CDCl_3$): δ = 10.30 (s, 1H, H-g), 7.52 (d, J = 8.7 Hz, 1H, H-c), 7.41 (d, J = 3.2 Hz, 1H, H-f), 7.03 (dd, J = 8.8, 3.2 Hz, 1H, H-d), 5.88 (ddt, J = 17.0, 10.3, 6.7 Hz, 1H, H-j), 5.17 (dq, J = 17.2, 1.5 Hz, 1H, H-k), 5.12 (dd, J = 10.3, 1.6 Hz, 1H, H-k'), 4.04 (t, J = 6.6 Hz, 2H, H-j), 2.55 (qt, J = 6.7, 1.4 Hz, 2H, H-l) ppm.

^{13}C{^{1}H} NMR (151 MHz, $CDCl_3$): δ = 191.9 (C-g), 158.7 (C-e), 134.7 (C-c), 134.1 (C-a), 134.0 (C-j), 123.7 (C-d), 118.1 (C-b), 117.6 (C-k), 113.5 (C-f), 67.9 (C-h), 33.5 (C-l) ppm.

HRMS (EI) m/z for $C_{11}H_{11}{}^{79}BrO_2$ [M]$^+$: calcd 253.99424, found: 253.99402 (5); 55 (100).

IR (ATR): $\tilde{\nu}$ = 3076 (w), 2871 (w), 2749 (w), 1690 (s), 1590 (m), 1568 (w), 1464 (s), 1418 (w), 1386 (m), 1309 (s), 1271 (s), 1229 (s), 1165 (s), 1110 (w), 1017 (m), 918 (m), 867 (m), 822 (m), 748 (m) cm^{-1}.

Rf: 0.62 (cyclohexane/ethyl acetate = 90/10)

1-Bromo-2-(bromomethyl)-4-(but-3-en-1-yloxy)benzene (b2)

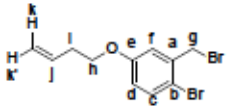

A dry, nitrogen flushed Schlenk-flask equipped with a magnetic stirring bar and septa was charged with **b1** (426 mg, 1.67 mmol) and anhydrous methanol (6 mL). After cooling to 0 °C, $NaBH_4$ (109 mg, 2.87 mmol) was portionwise over the course of 1 min added and the reaction mixture was stirred at 0 °C for 2 h. Then, the reaction mixture was allowed to warm slowly to 20 °C and quenched by dropwise addition of saturated aq NH_4Cl (30 mL), extracted with ethyl acetate (3 x 30 mL), washed with brine (30 mL) and dried over Na_2SO_4. After filtration, the organic phase was concentrated under reduced pressure.

A dry, nitrogen flushed Schlenk-flask equipped with a magnetic stirring bar and a septum was charged with the residue, anhydrous CH_2Cl_2 (2.5 mL) and the flask was cooled to 0 °C prior to the dropwise addition of PBr_3 (100 µL, 835 µmol) over the course of 30 s. The reaction mixture was stirred at 0 °C for 2 h. Then, the reaction mixture was allowed to warm slowly to 20 °C and quenched by dropwise addition of saturated aq $NaHCO_3$ (30 mL), extracted with $CHCl_3$ (3 x 30 mL), washed with brine (30 mL) and dried over Na_2SO_4. After filtration, the organic phase was concentrated under reduced pressure and the crude residue was purified by silica gel column chromatography (cyclohexane/ethyl acetate 80/20) to furnish the product **b2** as a colorless oil (343 mg, 1.07 mmol, 64%).

^{1}H NMR (601 MHz, $CDCl_3$): δ = 7.44 (d, J = 8.8 Hz, 1H, H-c), 7.00 (d, J = 3.0 Hz, 1H, H-f), 6.73 (dd, J = 8.8, 3.0 Hz, 1H, H-d), 5.89 (ddt, J = 17.0, 10.3, 6.7 Hz, 1H, H-j), 5.17 (dq, J = 17.2, 1.6 Hz, 1H, H-k), 5.12 (dq, J = 10.3, 1.2 Hz, 1H, H-k'), 4.54 (s, 2H, H-g), 3.99 (t, J = 6.7 Hz, 2H, H-h), 2.54 (qt, J = 6.7, 1.4 Hz, 2H, H-l) ppm.

^{13}C{^{1}H} NMR (151 MHz, $CDCl_3$): δ = 158.6 (C-e), 137.9 (C-a), 134.2 (C-j), 134.0 (C-c), 117.5 (C-k), 117.4 (C-f), 116.8 (C-d), 114.8 (C-b), 67.7 (C-h), 33.6 (C-l), 33.6 (C-g) ppm.

HRMS (EI) m/z for $C_{11}H_{12}{}^{79}Br_2O$ [M]$^+$: calcd 317.92549, found: 317.92535 (5); 55 (100).

IR (ATR): $\tilde{\nu}$ = 3077 (w), 2927 (w), 1641 (w), 1590 (w), 1570 (m), 1466 (s), 1407 (w), 1280 (s), 1239 (s), 1214 (m), 1174 (s), 1018 (m), 988 (m), 917 (m), 803 (m), 711 (m) cm^{-1}.

Rf: 0.68 (cyclohexane/ethyl acetate = 90/10)

1,2-Bis(2-bromo-5-(but-3-en-1-yloxy)phenyl)ethane (b3)

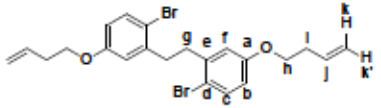

Compound **b2** (6.00 g, 18.75 mmol) and THF (56 mL) were added into a pre-dried two-necked Schlenk flask. After cooling to -78 °C, *n*-butyllithium (3.75 mL, 9.37 mmol, 2.5 M in hexanes) was added dropwise over the course of 30 s under stirring. After completion of the addition and stirring at -78 °C for 5 min, the reaction mixture was warmed to 20 °C. The reaction mixture was quenched with water (30 mL), extracted with $CHCl_3$ (3 x 30 mL) and washed with brine (30 mL) and dried over Na_2SO_4. After filtration, the organic phase was concentrated under reduced pressure and the crude residue was washed with hexane (20 mL) and dried under vacuum (0.1 mbar) to furnish the product **b3** as a colorless solid (2.96 mg, 5.1 mmol, 78%).

^{1}H NMR (601 MHz, $CDCl_3$): δ = 7.41 (d, J = 8.7 Hz, 1H, H-c), 6.73 (d, J = 3.0 Hz, 1H, H-f), 6.64 (dd, J = 8.7, 3.0 Hz, 1H, H-b), 5.88 (ddt, J = 17.0, 10.3, 6.7 Hz, 1H, H-j), 5.16 (dq, J = 17.2, 1.6 Hz, 1H, H-k), 5.11 (dd, J = 10.3, 1.7 Hz, 1H, H-k'), 3.94 (t, J = 6.7 Hz, 2H, H-h), 2.96 (s, 2H, H-f), 2.51 (qt, J = 6.6, 1.2 Hz, 2H, H-l) ppm.

^{13}C{^{1}H} NMR (151 MHz, $CDCl_3$): δ = 158.4 (C-a), 141.6 (C-e), 134.4 (C-j), 133.4 (C-c), 117.3 (C-l), 117.0 (C-f), 115.0 (C-d), 114.3 (C-b), 67.5 (C-h), 36.7 (C-g), 33.7 (C-l) ppm.

HRMS (EI) m/z for $C_{22}H_{24}{}^{79}Br_2O_2$ [M]$^+$: calcd 478.01431, found: 478.01401 (5); 55 (100).

IR (ATR): $\tilde{\nu}$ = 3080 (w), 2938 (w), 2912 (w), 2868 (w), 2359 (w), 1857 (w), 1741 (w), 1643 (w), 1597 (w), 1568 (m), 1465 (m), 1389 (w), 1294 (m), 1248 (s), 1169 (m), 1151 (m), 1118 (m), 1047 (s), 1012 (m), 927 (s), 873 (s), 817 (s) cm^{-1}.

mp: 56 °C.

Rf: 0.68 (cyclohexane/ethyl acetate = 90/10)

Di-tert-butyl 2,9-bis(but-3-en-1-yloxy)-11,12-dihydrodibenzo[c,g][1,2]diazocine-5,6-dicarboxylate (b4)

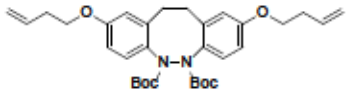

In a glovebox, compound **b3** (1.544 g, 3.22 mmol), di-*tert*-butyl hydrazine-1,2-dicarboxylate (897 mg, 3.86 mmol), CuI (610 mg, 3.22 mmol), K_3PO_4 (2.05 g, 9.65 mmol), acetonitrile (16 mL) and 1,2-dimethylethylenediamine (70 µL, 650 µmol) were added sequentially to a microwave vial. The vial was capped with a crimp cap equipped with a PTFE septum, transferred out of the glovebox and stirred at 82 °C for 18 h. After cooling to 20 °C, the reaction mixture was quenched with water (60 mL), washed with aq NH_3 (60 mL, 25%), extracted with $CHCl_3$ (3 x 20 mL), washed with brine (30 mL) and dried over Na_2SO_4. After filtration, the organic phase was concentrated under reduced pressure and the crude residue was purified by silica gel column chromatography to furnish the product **b4** (846 mg, 1.54 mmol, 48%) as a colorless solid.

^{1}H NMR (600 MHz, $CDCl_3$): δ = 7.75 – 7.06 (m, 3H), 6.83 – 6.65 (m, 4H), 6.00 – 5.84 (m, 2H), 5.25 – 5.09 (m, 4H), 4.09 – 3.93 (m, 4H), 3.08 – 2.70 (m, 4H), 2.61 – 2.49 (m, 4H), 1.63 – 1.31 (m, 20H) ppm.

HRMS (EI) *m/z* for $C_{32}H_{42}N_2O_8$ $[M]^+$: calcd 550.30429, found: 550.30386 (5); 57 (100).

IR (ATR): $\tilde{\nu}$ = 2977 (w), 2930 (w), 1713 (s), 1604 (s), 1502 (m), 1366 (m), 1306 (m), 1237 (s), 1151 (s), 1040 (m), 1004 (m), 913 (m), 854 (m), 754 (m) cm^{-1}.

R_f: 0.58 (cyclohexane/ethyl acetate = 80/20)

(*Z*)-2,9-Bis(but-3-en-1-yloxy)-11,12-dihydrodibenzo[*c*,*g*][1,2]diazocine (M4)

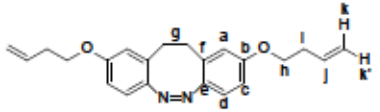

In a glovebox, compound **b4** (1.895 g, 1.18 mmol), CH_2Cl_2 (12 mL) and trimethylsilyl iodide (350 µL, 2.37 mmol) were added sequentially to a round-bottomed flask equipped with a magnetic stirring bar. The reaction mixture was stirred at 20 °C for 10 min before it was treated with triethylamine (350 µL, 2.37 mmol). The flask was capped, transferred out of the glovebox where the reaction mixture was quenched with water (5 mL), extracted with $CHCl_3$ (3 x 5 mL), washed with brine (5 mL) and dried over Na_2SO_4. After filtration, the organic phase was concentrated under reduced pressure. The resulting residue, CH_2Cl_2 (12 mL) and pyridine (120 µL, 1.5 mmol) were added sequentially to a round-bottomed flask. NBS (252 mg, 1.42 mmol) was added portionwise over the course of 2 min under stirring and the reaction mixture was stirred at 20 °C for 30 min. The reaction mixture was concentrated under reduced pressure and the residue was purified by silica gel column chromatography (applied gradient from pentane to pentane/ethyl acetate = 70/30) to furnish the product **M4** (172 mg, 0.49 mmol, 37%) as a red oil.

^{1}H NMR (601 MHz, $CDCl_3$): δ = 6.79 (d, *J* = 8.6 Hz, 2H, H-d), 6.67 (dd, *J* = 8.7, 2.6 Hz, 2H, H-c), 6.52 (d, *J* = 2.6 Hz, 2H, H-a), 5.85 (ddt, *J* = 17.0, 10.3, 6.7 Hz, 2H, H-j), 5.13 (dq, *J* = 17.2, 1.6 Hz, 2H, H-k), 5.08 (dq, *J* = 10.3, 1.1 Hz, 2H, H-k'), 3.91 (t, *J* = 6.7 Hz, 4H, H-h), 2.80 (s, 4H, H-g), 2.48 (qt, *J* = 6.6, 1.2 Hz, 4H, H-i) ppm.

^{13}C{^{1}H} NMR (151 MHz, $CDCl_3$): δ = 157.6 (C-b), 149.1 (C-e), 134.4 (C-j), 129.8 (C-f), 121.1 (C-d), 117.2 (C-i), 115.3 (C-a), 112.5 (C-c), 67.3 (C-h), 33.7 (C-i), 32.2 (C-g) ppm.

HRMS (EI) *m/z* for $C_{22}H_{24}N_2O_2$ $[M]^+$: calcd 348.18378, found: 348.18274 (5); 55 (100).

IR (ATR): $\tilde{\nu}$ = 3075 (w), 2929 (w), 1640 (w), 1600 (s), 1573 (m), 1469 (m), 1429 (w), 1278 (m), 1239 (s), 1162 (m), 1104 (m), 1034 (m), 988 (w), 913 (m), 796 (m) cm^{-1}.

R_f: 0.54 (cyclohexane/ethyl acetate = 80/20)

(Z)-(9-Butoxy-11,12-dihydrodibenzo[c,g][1,2]diazocin-2-yl)methyl acrylate (M3)

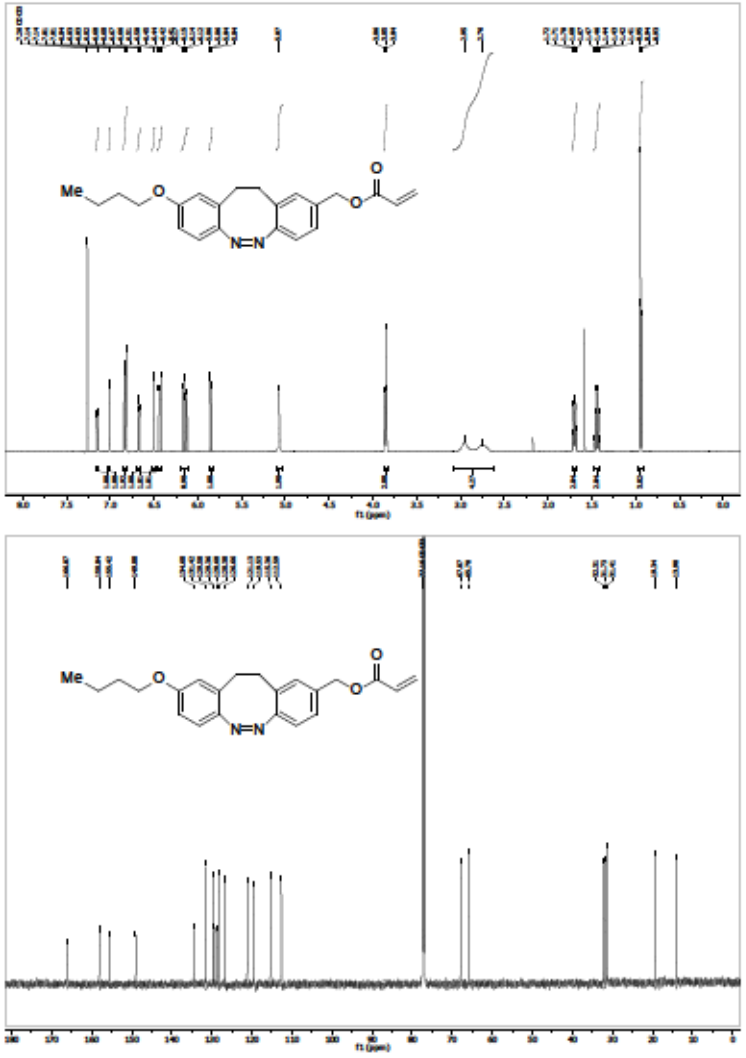

2-Bromo-5-(but-3-en-1-yloxy)benzaldehyde (b1)

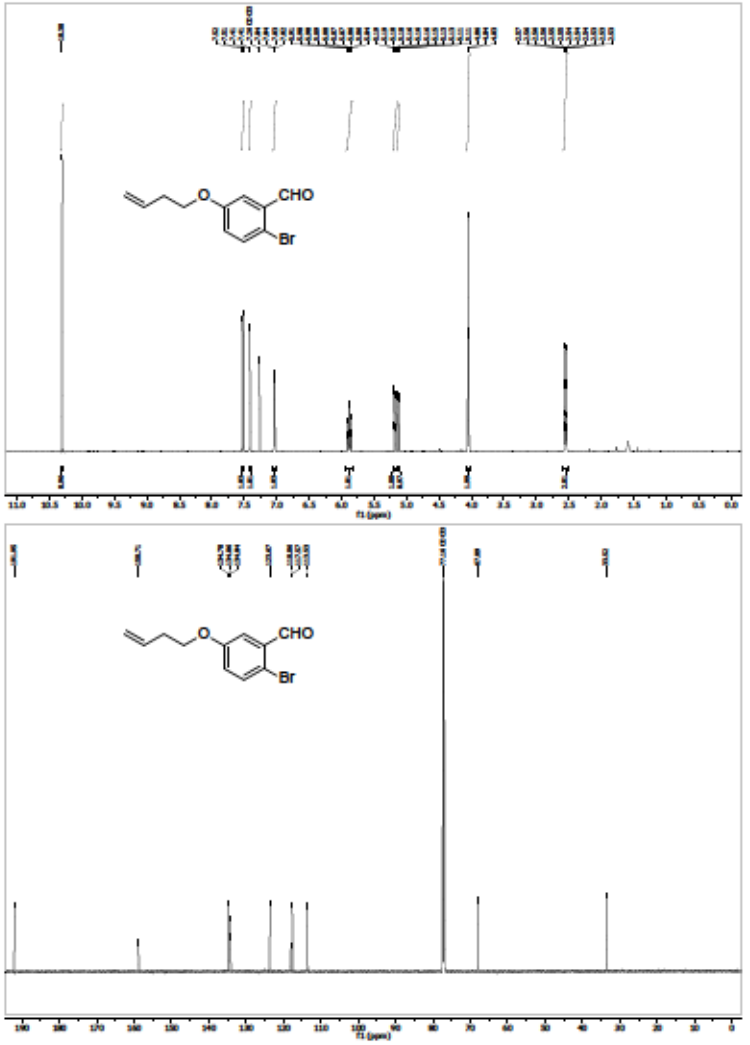

1-Bromo-2-(bromomethyl)-4-(but-3-en-1-yloxy)benzene (b2)

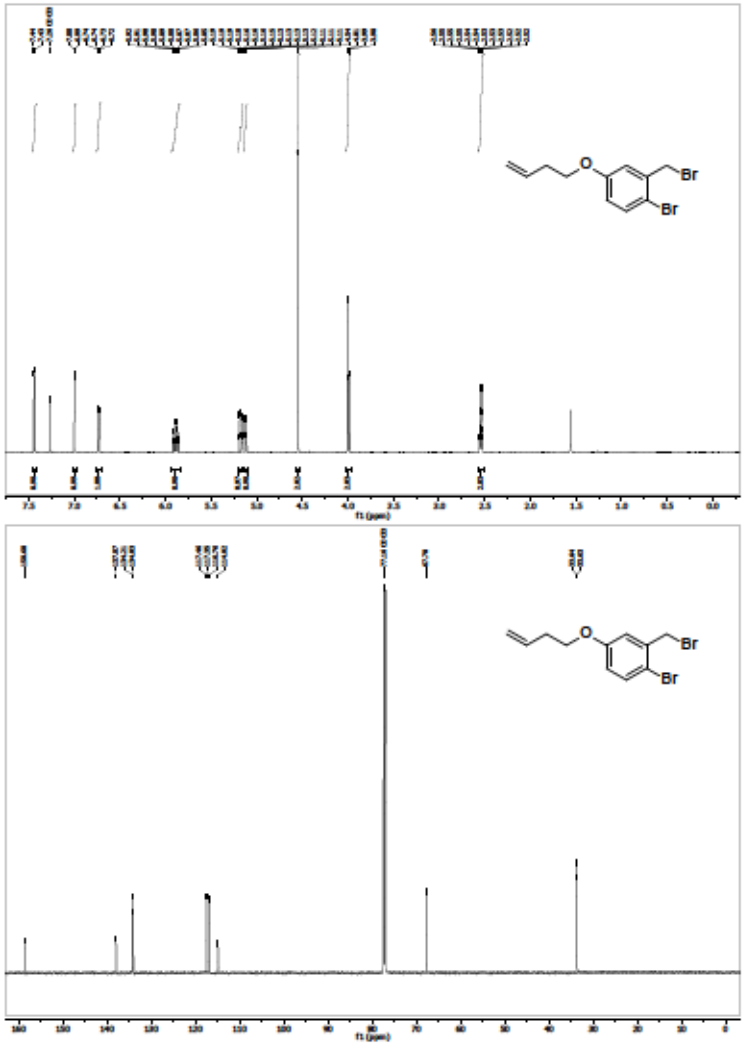

1,2-Bis(2-bromo-5-(but-3-en-1-yloxy)phenyl)ethane (b3)

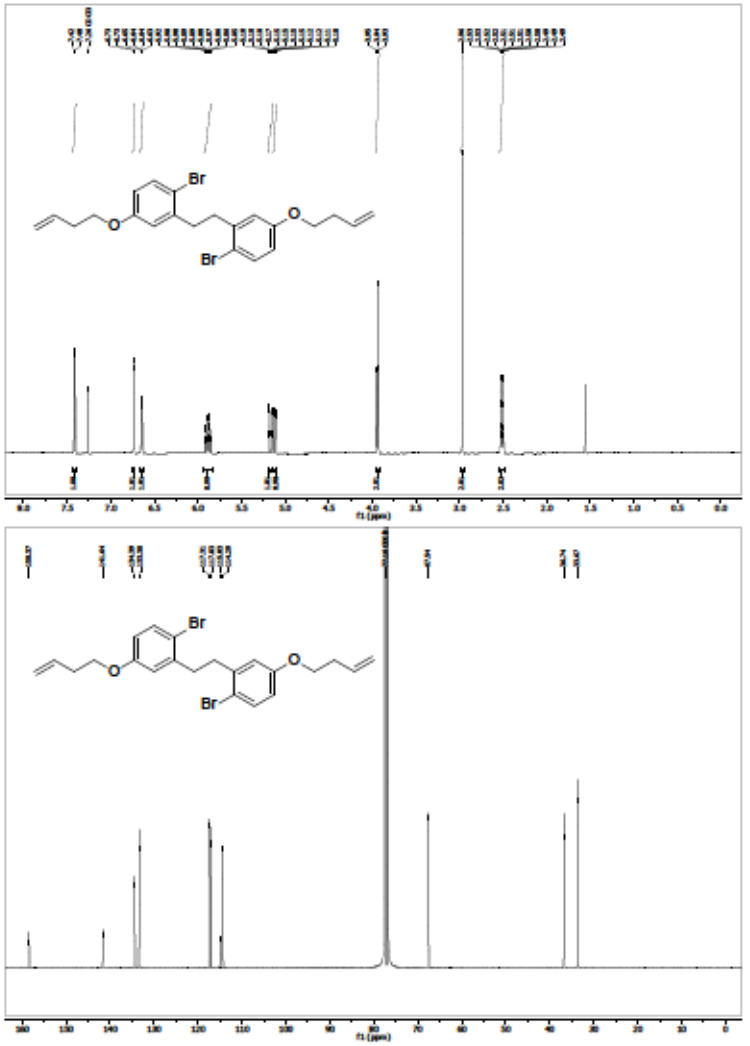

Di-tert-butyl 2,9-bis(but-3-en-1-yloxy)-11,12-dihydrodibenzo[*c*,*g*][1,2]diazocine-5,6-dicarboxylate (b4)

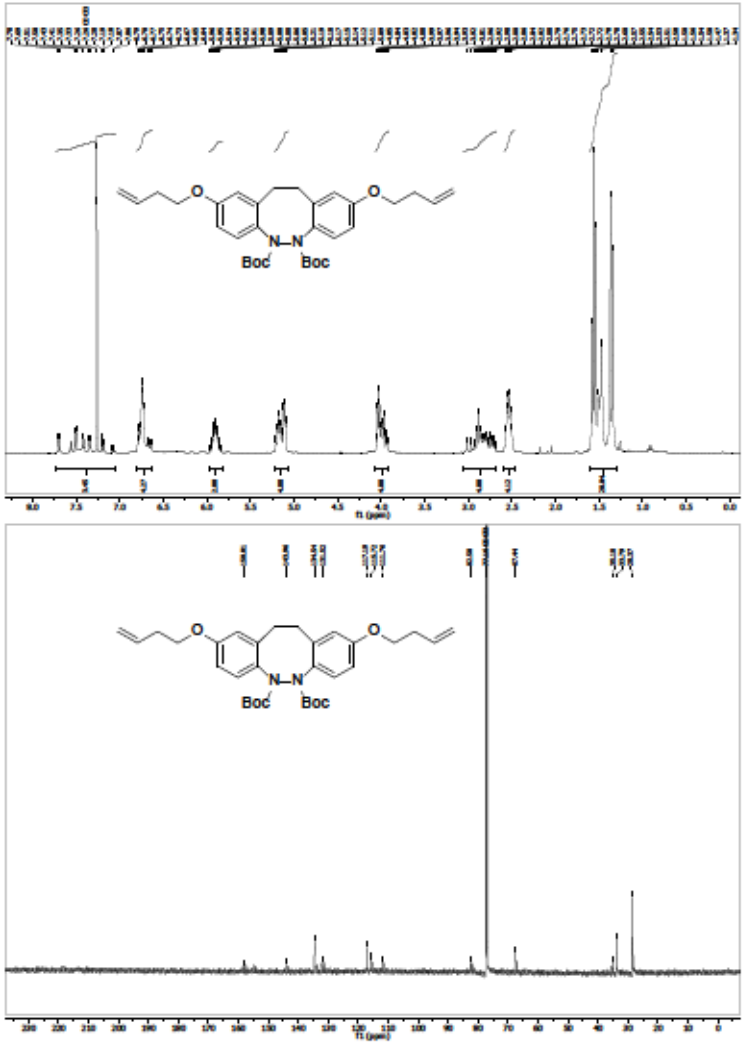

(Z)-2,9-Bis(but-3-en-1-yloxy)-11,12-dihydrodibenzo[*c*,*g*][1,2]diazocine (M4)

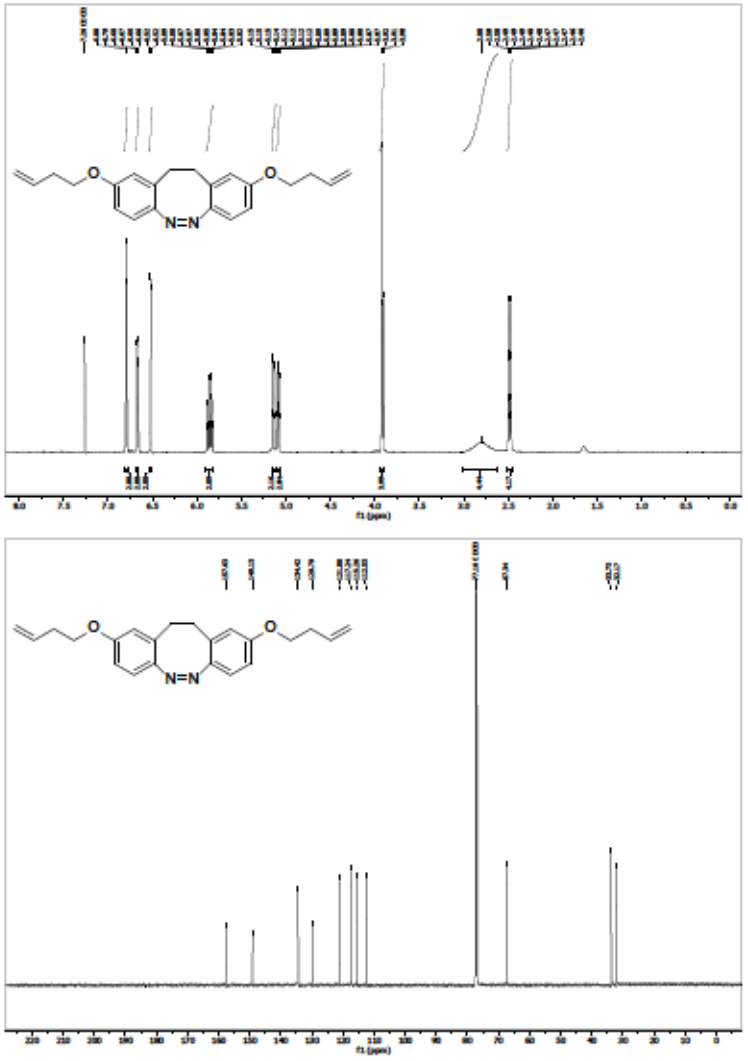

^{1}H NMR Spectra of **M3 and M4** in the PSS at 405 and 525 nm

(Z)-(9-Butoxy-11,12-dihydrodibenzo[c,g][1,2]diazocin-2-yl)methyl acrylate (M3)

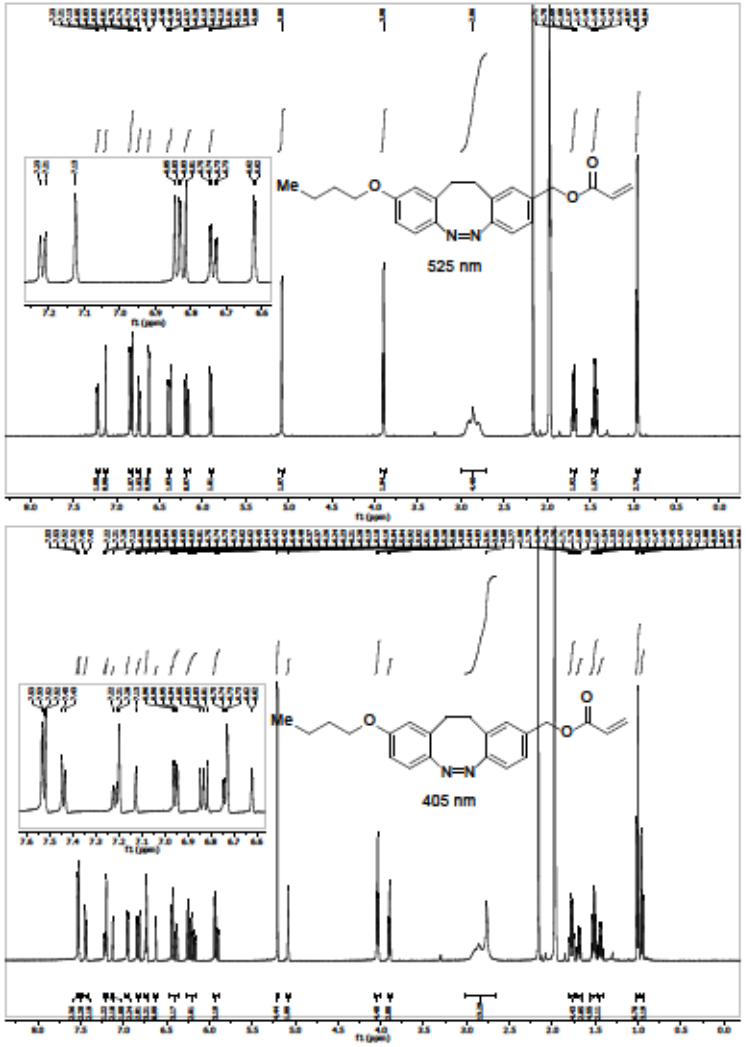

(Z)-2,9-Bis(but-3-en-1-yloxy)-11,12-dihydrodibenzo[c,g][1,2]diazocine (M4)

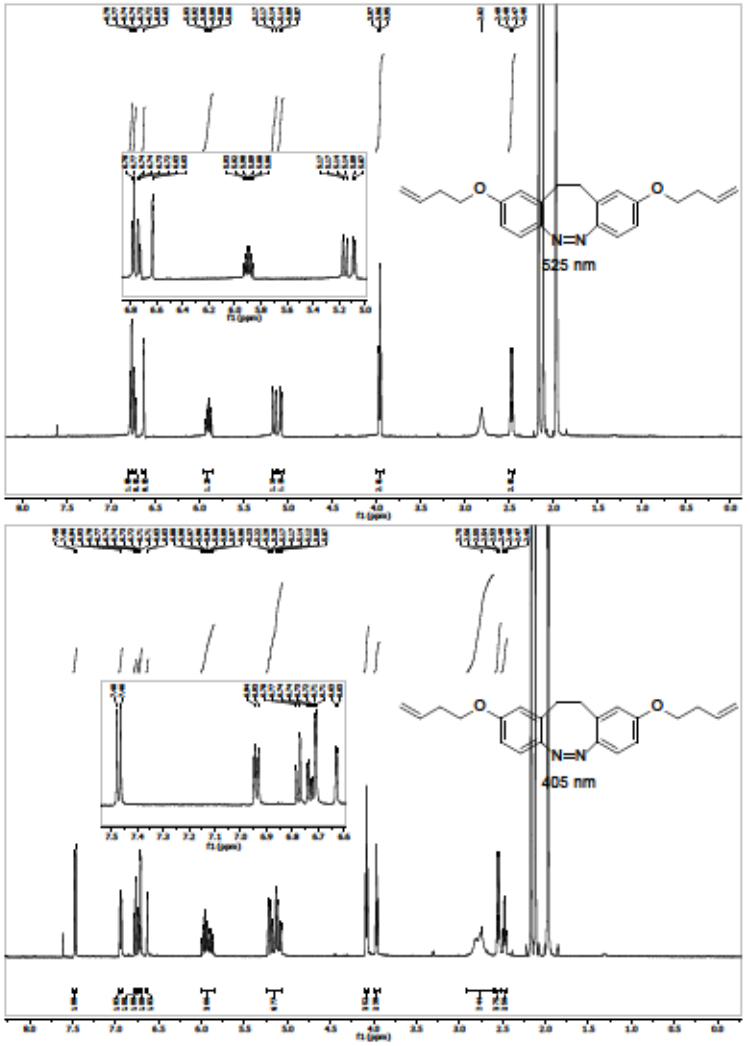

List of Figures

List of Schemes

List of Tables

Abbreviations

AcOH	Acetic acid
Adoc	Adamantyl-oxycarbonyl
AFM	Atomic force microscopy
AGET	Activators generated by electron transfer
ARGET	Activators regenerated by electron transfer
ATRP	Atom transfer radical polymerization
Boc	*tert*-Butyloxycarbonyl
BIBB	α-Bromoisobutyryl bromide
$\mathbf{C_b}$	Bridged carbon atom
$\boldsymbol{\Delta L}$	Maximum length change
$\boldsymbol{Đ}$	Dispersity
$\mathbf{DBADH_2}$	Di-*tert*-butyl hydrazine-1,2-dicarboxylate
dmeda	1,2-Dimethylethylenediamine
DMPP	Dimethylphenylphosphine
DMT	Dimethoxytrityl
DOSY	Diffusion-ordered spectroscopy
EBiB	Ethyl α-bromoisobutyrate
fs	Femtosecond
$\boldsymbol{k_{act}}$	Activation rate constant
$\boldsymbol{K_{\mathrm{ATRP}}}$	Atom transfer radical polymerization equilibrium constant
$\boldsymbol{k_{deact}}$	Deactivation rate constant
$\boldsymbol{k_p}$	Polymerization rate
kcal	Kilocalorie
kDa	Kilodalton
kJ	Kilojoule
$\boldsymbol{\lambda_{max}}$	Maximum absorption wavelength

***m*CPBA**	*meta*-Chloroperoxybenzoic acid
Me_6TREN	Tris[2-(dimethylamino)ethyl]amine
NIS	*N*-Iodosuccinimide
nN	Nanonewton
OMRP	Organometallic mediated radical polymerization
p	Monomer conversion
photoATRP	Photocontrolled atom transfer radical polymerization
PMA	Poly(methyl acrylate)
ps	Picosecond
PSS	Photostationary state
RAFT	Reversible addition-fragmentation chain-transfer polymerization
SARA	Supplemental activator and reducing agent
TEA	Triethylamine
TMSI	Trimethylsilyl iodide
Tr	Trityl